Universitat Autònoma de Barcelona
Facultat de Ciències
Departament de Química

New Azobenzene-based Photoswitches for Two-Photon Optical Control of Neuronal Receptors

Marta Gascón Moya

Ph.D. Thesis

Ph.D. in Chemistry

2014

Supervisors:
Dr. Ramon Alibés Arqués
Dr. Felix Busqué Sánchez
Dr. Jordi Hernando Campos

Memòria presentada per aspirar al Grau

de Doctor per Marta Gascón Moya

Marta Gascón Moya

Vist i plau

Dr. Ramon Alibés Arqués | Dr. Félix Busqué Sánchez | Dr. Jordi Hernando Campos

Bellaterra, 7 de Maig del 2014

Part of the results of this thesis is described in the following scientific publication:

- “Two-photon celular stimulation of azobenzene-based photoswitches” Gascón-Moya M.; Izquierdo-Serra, M.; Hirtz, J. J.; Pittolo, S.; Poskanzer, E. K.; Ferrer, E.; Alibés, R.; Busque, F.; Yuste, R.; Hernando, J.; Gorostiza, P. (submitted)

Table of Contents

TABLE OF CONTENTS

ABBREVIATIONS

AcOH	Acetic acid
AMPA	2-amino-3-(5-methyl-3-hydroxyisoxasol-4-yl)propanaoic acid
ATD	Amino-terminal domain
Boc	*tert*-butyl carbamate
Boc_2O	Di-*tert*-butyl dicarbonate
c	Concentration
CLs	Caged Ligands
CNS	Central Nervous System
COSY	Correlation Spectroscopy
CTD	Carboxy-terminal domain
DAPI	2-(4-amidinophenyl)-1*H*-indole-6-carboxamidine
DEPT	Distortionless Enhancement by Polarisation Transfer
DIAD	Diisopropyl azodicarboxylate
DIPEA	*N,N*-diisopropylethylamine
DMAP	4-dimethylaminopyridine
DMEM/F12	Dulbecco's Modified Eagle's Medium/Nutrient Mixture F-12 Ham
DMF	Dimethylformamide
DMSO	Dimethylsulfoxide
DTE	Dithientylethene
EDCI	*N*-ethyl-*N'*-(3-dimethyldiamino propyl)-carbodiimide HCl
EDG	Electron-donating group
em	Emission
ESI	Electrospray Ionization
Et	Ethyl
EtOH	Ethanol
EtOAc	Ethyl acetate
EWG	Electron-withdrawing
exc	excitation
FBS	Fetal Bovine Serum
Fl	Fluorescence
Fl,D	Fluorescence of the donor
Fmoc	Fluorenylmethyl carbamate
GluK	Ionotropic glutamate receptor subtype 6
HATU	*O*-(7-azabenzotriazol-1-yl)-*N,N,N',N'*-tetramethyluronium hexafluorophosphate
HEPES	4-(2-hydroxyethyl)-1-piperazineethanesulfonic acid
HEK293	Human Embryonic Kidney
HRMS	High Resolution Mass Spectrometry
HMBC	Heteronuclear Multiple Bond Correlation
HSQC	Heteronuclear Single Quantum Coherence
HOBt	1-hydroxibenzotriazole
iGluRs	Ionotropic Glutamate Receptors
IR (ATR)	Infrared Spectroscopy in Attenuated Total Reflection

LBD	Ligand-binding domain
LiHMDS	Lithium bis(trimethylsilyl)amide
LiGluR	Light-gated ionotropic Glutamate Receptor
max	Maxima
MeOH	Methanol
Mp	Melting point
nAChRs	Ionotropic Acetylcholine Receptors
NIR	Near-infrared
NMDA	*N*-methyl-D-aspartate
NMM	*N*-methylmorpholine
NMR	Nuclear Magnetic Resonance
P	pore
PBS	Phosphate Buffer Solution
PCLs	Photochromic Ligands
Ph	Phenyl
PSS	Photostationary state
PTLs	Photochromic Tethered Ligands
py	pyridine
PyBOP	(Benzotriazol-1-yloxy)tripyrrolidino phosphonium hexafluorophosphate
pyr	pyrene
ref	reference
rt	room temperature
RET	Resonance Energy Transfer
s.e.m	standard error of mean
sm	starting material
TBAB	Tetrabutylammonium bromide
^{t}Bu	*tert*-butyl
^{t}BuOAc	*tert*-butyl acetate
^{t}BuOK	potassium *tert*-butoxide
TFA	Trifluoroacetic acid
THF	Tetrahydrofuran
TLC	Thin Layer Chromatography
TMD	Transmembrane domain
Tot	total
TPA	Two-photon absorption
TSTU	*N*,*N*,*N′*,*N′*-tetramethyl-*O*-(*N*-succinimidyl)uronium tetrafluoroborate)
UV	Ultraviolet
vis	visible
1P	One-photon
2P	Two-photon

Chapter I

Introduction

Memories, feelings, thoughts and movement are mediated by the brain, which is an incredibly complicated circuit made out of zillions of cells called neurons. Understanding how neurons control physiological functions and how their malfunction correlates with mental disorders, such as depression or schizophrenia, has long been a priority in basic and clinical neuroscience. However, such a deep knowledge of the brain has been challenging to achieve with traditional methods relying on its local stimulation with tiny electrodes, which make impossible neither to distinguish between different cell types nor to turn neurons on and off with precision. Unravelling the complexity of neural circuits therefore requires the development of new techniques allowing specific types of cells in the brain to be controlled remotely with high spatial and time resolution. By enabling accurate manipulation of neuronal signalling upon irradiation with light, the recent emergence of optogenetic[1] and optochemical genetic[2] tools promise to revolutionise this field.

The interest of this dissertation falls into this new area of research. In particular, this work aims to the synthesis of new azobenzene-based molecular photoswitches with which selected ion channels in neurons could be optically controlled using, for the first time, two-photon excitation with near-infrared light (NIR, λ = 750-1100 nm). Hence, the first part of this chapter will introduce the fundamentals of optogenetics and optochemical genetics as well as the specific neuronal ion channels targeted in this work. The second part will be devoted to provide basic notions of molecular photoswitches and, particularly, of azobenzenes, our system of choice, whose previous applications to the light-driven manipulation of neural activity will be overviewed. Finally, the last section will outline a few general principles about two-photon excitation processes and other photophysical phenomena involved in our strategy to attain control of optochemical genetic tools by means of NIR radiation.

I.1. CONTROLLING NEURONS WITH LIGHT: FROM OPTOGENETICS TO OPTOCHEMICAL GENETICS

In 1979 Nobel laureate Francis Crick suggested that the major challenge facing neuroscience was controlling one type of cell in the brain while leaving others unaltered. At that time, electrodes (which have a poor spatial resolution) and drugs (whose time window of action is much larger than the timescale of brain processes) were the only methods used. Thus, Crick speculated that light might have the ideal properties to serve as external stimulus for the modulation of cellular activity in neuroscience studies,[3] since (i) it can be manipulated with very high spatial (in the sub-micrometer range) and time (down to femtoseconds) precision, (ii) it can be projected onto a tissue from afar, and (iii) it is non-invasive and does not interfere with most native biological processes.

Inspired by Crick's prophetic vision, research in neuroscience has seen an explosion of strategies during the last decade devoted to optically manipulate the activity of neurons. As sketched in Figure I-1, these strategies can be classified into different groups depending on the way chemistry and/or genetics are combined to achieve light-induced control. On the one hand, this can be directly accomplished by insertion of exogenous photosensitive proteins into the membrane of neurons, the so-called optogenetic approach.[4,5] Alternatively, optochemical genetics proposes the use of small light-responsive synthetic molecules,[2] which may require or not the genetic modification of native cells. The former case is called optogenetic pharmacology, while the latter is referred to as optopharmacology.[6]

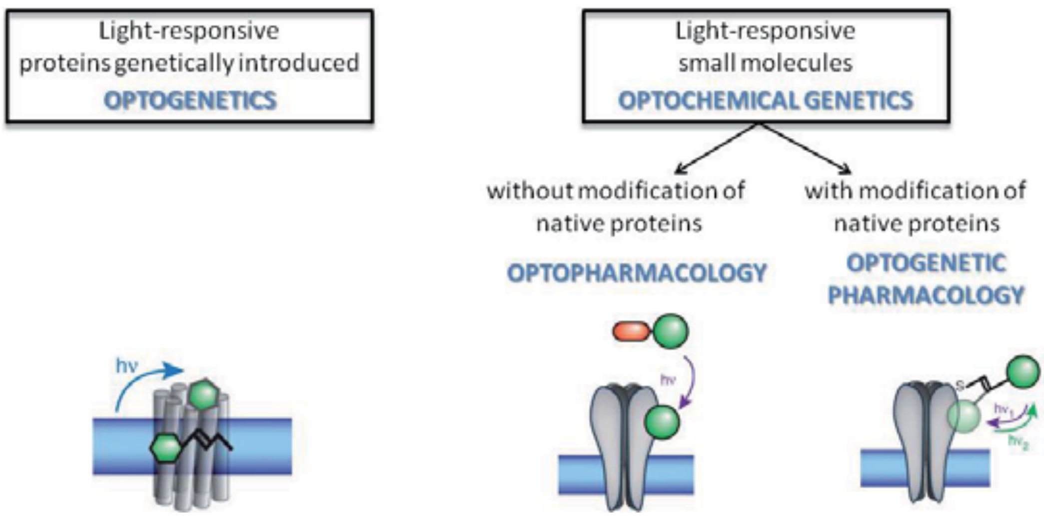

Figure I-1. Tools to optically manipulate neural activity. Light-induced control can be achieved by means of natural photosensitive proteins (optogenetics) or small synthetic molecules (optochemical genetics). Those small molecules can target both native and genetically modified proteins, thus giving rise to the fields of optopharmacology and optogenetic pharmacology.[6]

The field of **optogenetics** was pioneered by Deisseroth and co-workers in 2005, when they demonstrated for the first time that mammalian neurons could become responsive to light upon introduction of a single microbial opsin gene.[7] This type of genes is naturally found in microorganisms such as prokaryotes, algae, and fungi and it encodes the production of seven-transmembrane rhodopsin proteins containing retinal photoswitches (e.g. Channelrhodopsin-2). As such, these proteins are intrinsically light sensitive and they control diverse biological functions under visible light illumination, among them the regulation of the flow of electrical charges across the plasma membrane.[8] Although microbial opsins had been known by biologists for more than 40 years, it was not until Deisseroth's seminal work that their potential to optically manipulate neural signalling was unveiled. Since then, an increasing amount of studies in this field have been reported, and by 2010 the major classes of ion-conducting microbial opsins had all proven to function as optogenetic tools which, upon expression in mammalian neurons, allow their activity to be switched on and off in response to diverse colours of light.[9,10] In this year, optogenetics was chosen "Method of the Year" by the Nature Methods journal[11] and highlighted as one of the "Breakthroughs of the Decade" by the Science journal.[12] In addition, optogenetics has not only been shown of relevance to basic neuroscience, but it has also found preliminary applications in clinical research.[13]

In spite of its enormous success and rapid spread through many laboratories worldwide, optogenetics does present several weaknesses.[14,15] Some have to do with the technical limitations of the process of expression of light-sensitive proteins *in vivo*, which lacks specificity and does not allow accurate control of the level of genetic modification. Furthermore, the neuronal response generated by means of light-responsive microbial opsins might not perfectly match the actual endogenous behaviour and, in fact, the development of new rhodopsin mutants capable of triggering faster action potentials similar to those observed in wild type mammalian neurons is currently pursued. Finally, issues are raised about the therapeutic applications of optogenetics, since the need to overexpress exogenous proteins may provoke functional and even morphological distortions in many cell types and, eventually, it will involve the use of the still developing gene therapy. Most of these problems can be tackled by means of **optochemical genetics**, an alternative approach making use of small photoactive synthetic molecules to directly target the endogenous, or slightly genetically modified, receptors and ion channels in neurons.[2] Since this is the strategy used in this work, a deeper discussion on optochemical genetics is done in the following section.

I.1.1. Optochemical genetics

Optochemical genetics is an alternative light-based strategy to optogenetics that also holds great promise for mapping brain activity. It exploits the combined use of intrinsic neuronal receptor and ion channel proteins with synthetic photoactive molecules and light. As discussed above, such proteins can be endogenous or genetically modified, thus giving rise to the fields of optopharmacology and optogenetic pharmacology. In both cases, however, the bottom line remains the same: to use light-responsive pharmacologically active substances whose interaction with the target proteins can be modulated upon irradiation.[2,16,17] In this way, native neural signalling processes can be triggered (by photoactive receptor agonists) or blocked (by photoactive receptor antagonists and channel blockers) without the need of introducing exogenous opsins into the cell membrane. Together with the feasibility to validate and approve the pharmacological activity of these molecules using standard drug development procedures, this allows overcoming some of the main drawbacks of optogenetics, especially on the route towards therapeutic applications. Actually, optochemical genetics and, in particular, optopharmacological tools are expected to contribute to the development of personalised medicine in which treatments can be adapted to each patient, limiting the time given regions are treated and thereby reducing undesired effects.

Three main methods have emerged in optochemical genetics for remote control of cell signalling with small photoactive synthetic molecules: caged ligands,[2,18,19] photochromic ligands,[2,18,20–22] and photoswitched tethered ligands.[2,18,19,23,24] Whereas the two first types of systems are strictly optopharmacological, photoswitched tethered ligands are used both in optopharmacology and optogenetic pharmacology.

Caged ligands (CLs) are the simplest and oldest approach employed in optochemical genetics. Here, a biologically active molecule (an ion, a neurotransmitter or an intracellular signalling molecule) is endowed with a photolabile protecting group, or “caging group”, which renders it pharmacologically inactive. Upon exposure to light, photocleavage of the protecting group releases the active substrate and triggers the desired biological effect (Figure I-2a). Therefore, the performance of CLs depends on two main aspects: (i) the inertness and chemical stability of the system in the absence of light; and (ii) the efficiency and rate of release of the active ligand upon illumination.

Caged ligands have been applied to great effect in neuroscience to cage agonists for neurotransmitter receptors. The first caged neurotransmitter agonists reported were 2-nitrobenzyl derivatives of carbamoylcholine, an activator of acetylcholine receptors that was released in response to ultraviolet (UV) light exposure (Figure I-2b).[19] But it was the development of caged ligands based on glutamate, one of the main neurotransmitters in the central nervous system, which truly revolutionised the field and, to this day, continues to have major impact on neurobiology (Figure I-2c).[25]

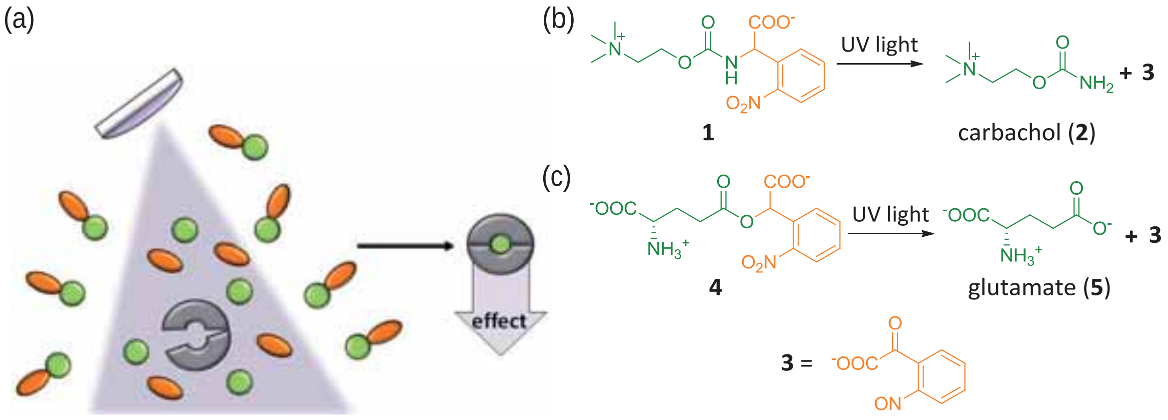

Figure I-2. (a) Schematic representation of the caged ligand approach. Upon illumination, the photolabile protecting group (orange) releases the active substrate (green) causing the desired biological effect. A common caging group is the α-carboxyl-2-nitrobenzyl used in (b) caged carbamoylcholine (**1**) and (c) caged glutamate (**4**). This group photocleaves by irradiation with UV light.[19,26]

Despite their broad use as optochemical genetic tools, CLs present several disadvantages, associated with the photolysis process of the caging group. On the one hand, by-products are generated upon photocleavage, which might be toxic or present undesired biological effects. On the other hand, it is an irreversible process, which implies that the released ligand will remain active after diffusing out of the illuminated volume and into non-target areas where its pharmacological activity is to be prevented. These two shortcomings can be overcome with the use of **photochromic ligands** (PCLs) and **photochromic tethered ligands** (PTLs). In both cases, a biologically active ligand is attached to a photoswitch, a photoisomerisable group that undergoes rapid and reversible interconversion between two different states upon illumination (see § I.2). The electronic and/or geometrical changes occurring during the isomerisation process modulate the efficiency of the ligand-protein interaction between the two states of the system, thus leading to light-induced manipulation of the resulting biological effect in a reversible and repetitive manner, at lower intensities and without generating any undesired by-product.

As caged ligands, photochromic ligands are freely diffusing optopharmacological tools that directly target the endogenous form of cell receptors and ion channels (Figure I-3a). To date PCLs have been explored for various classes of target proteins, such as enzymes,[27] ligand-gated ion channels,[22,28] and G-protein-coupled receptors.[29] For instance, photochromic agonists and antagonists of the nicotinic acetylcholine receptor, a ligand-gated ion channel, were described more than thirty years ago. More recently, Trauner, Isacoff and co-workers have reported a PCL based on glutamate that acts on kainate receptors and can be used to efficiently trigger neuronal firing with light (Figure I-3b).[22]

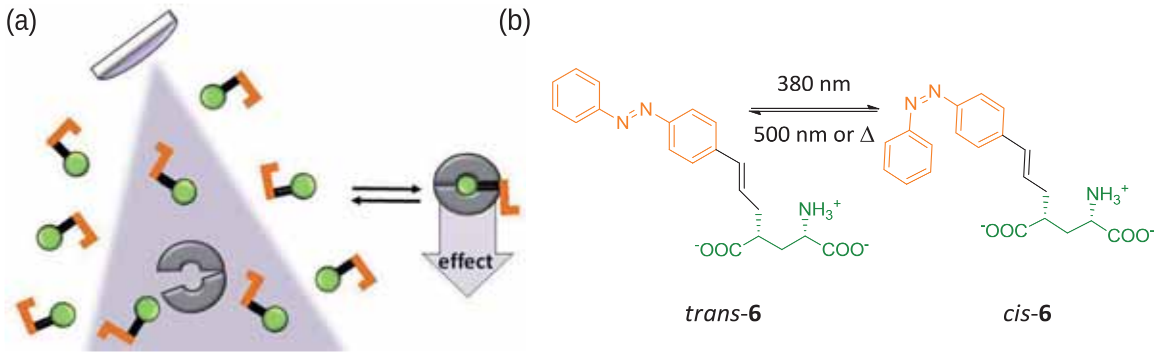

Figure I-3. (a) Schematic representation of the photochromic ligand approach, where the pharmacological active unit (green) is tethered to a photoisomerisable group (orange) through a short spacer (black). In its folded state, the ligand cannot interact with the binding site of the receptor due to steric hindrance. However, it is converted into an extended state upon illumination, for which the ligand-receptor recognition process and, therefore, the corresponding biological effect occur. (b) Example of PCL that acts as reversible caged glutamate upon photoisomerisation of its azobenzene group with UV-vis light. In this case, the *trans* state of the system binds to the receptor preferentially over the *cis* isomer.[22]

Although PCLs improve some of the properties of CLs, they still present certain limitations: (i) they can also diffuse out of the illumination volume in their active form, thus inducing biological responses in non-target areas; (ii) they are rather unspecific, since different types of receptor proteins are often sensitive to the same agonist or antagonist molecules (e.g. ionotropic and metabotropic glutamate receptors); and (iii) they are normally active in their initial state, and they only become inactive upon photoisomerisation within the irradiated region. Most of these deficiencies could be overcome if the photoisomerisable molecule with optopharmacological activity was directly attached to the protein of interest. This is the main idea behind the use of photoswitched tethered ligands, which must therefore be composed of at least three different functional units: the biologically active unit, a photoisomerisable moiety and a reactive group with which the whole system can be covalently tethered to the target protein. By proper choice of the anchoring point, the geometrical changes induced by the reversible isomerisation of the photoswitch moves the ligand closer to or away from the binding site, thus allowing the ligand-receptor interaction to be light-controlled selectively on the functionalised proteins (Figure I-4a).

Because of its modular design, PTLs can be tuned and their applicability broadened by careful selection of the nature of the biologically active unit, the optical properties of the photoswitch and the chemical behaviour of the reactive group. This has allowed the successful development of a number of PTL systems for different membrane-bound receptors, including ionotropic acetylcholine receptors (nAChRs)[28] and ionotropic glutamate receptors,[30] and even soluble proteins.[31] Although other photoswitches such as spiropyran[32] have been used, azobenzene has been chosen as photoisomerisable unit in most PTLs due to its excellent photochemical stability and fatigue resistance, and the large geometric change between its *trans* and *cis* states (see § I.2.1). The first example of such azobenzene-based PTLs was reported in the early 1970s and it was applied to the nicotinic acetylcholine receptor.[28] It consisted of a quaternary ammonium ion tethered to an azobenzene group bearing a bromomethylene moiety (QBr (**7**)), which was used to covalently attach the ligand to a native cysteine residue located near the nAChR binding site. Once attached, the agonist could bind to the receptor and activate the channel in its *trans* configuration; on the contrary, the tether was too short in the *cis* state for the agonist to bind, thus leading to light-induced operation of the receptor (Figure I-4b).

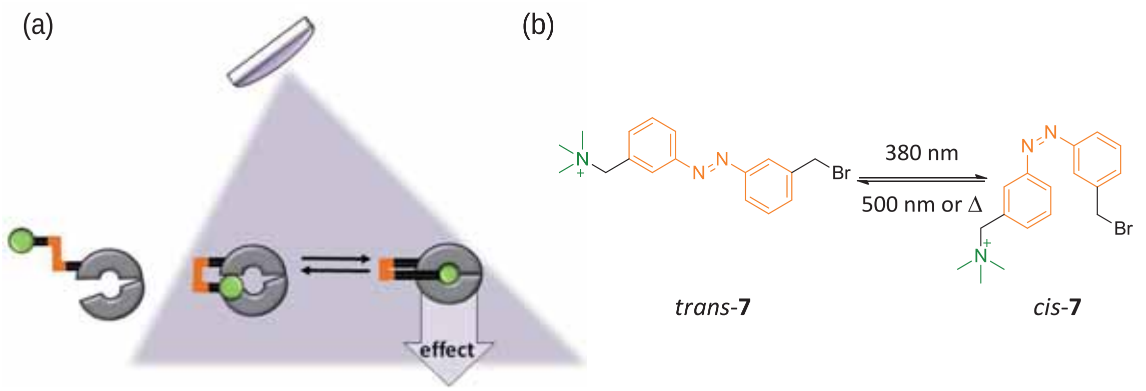

Figure I-4. (a) Schematic representation of the operation of a photoswitched tethered ligand, which is covalently attached to the target protein. In the initial extended configuration of its photoswitch unit (orange), the ligand (green) is localised far away from the binding site and no ligand-receptor interaction takes place. However, this interaction and the corresponding biological effect are enabled upon photoisomerisation to its folded configuration, which brings the ligand into close proximity to the binding site. (b) The first example of PTL reported, which was designed for the light-induced control of an ionotropic acetylcholine receptor. In this case, a quaternary ammonium ion is the biologically active group, which was attached to the protein via a bromomethylene moiety and moved towards/away from the binding site in a controlled manner by exploiting *trans*-*cis* azobenzene photoisomerisation.[28]

A key factor in the development of PTLs is the selection of the anchoring point to the target protein. Two different approaches can be followed: to covalently attach the ligand to any of the groups around the binding site of the wild type form of the protein (such as in the example given in Figure I-4b) or to selectively conjugate it to a genetically engineered chemical motif. As for the other optopharmacological tools discussed (i.e. caged ligands and photochromic ligands), no genetic modification of the endogenous material is required in the first case, which results in non-specific functionalisation of both target and non-target proteins. In the second case, however, the target proteins must be mutated to express the selected anchoring group at the desired position, a requirement that is overly compensated by the enormous gain in selectivity achieved. As discussed above, this approach is called optogenetic pharmacology, and it combines the absolute specificity that genetics can provide with the unique precision that only light can give. As such, optogenetic pharmacology is one of the most powerful methods to attain optical control of neuronal receptor and ion channel proteins. This work particularly deals with this field of research and it aims at developing a new family of azobenzene-based PTLs devoted to the optical control of ionotropic glutamate receptors.

I.1.2. Ionotropic glutamate receptors

Ionotropic glutamate receptors (iGluRs) are a family of ligand-gated channels that allow the permeation of monovalent cations (sometimes even calcium) through cell membranes with little selectivity and in response to changes in the concentration of the neurotransmitter glutamate (**5**). Located in the brain and spinal cord, these ligand-gated channels are responsible for most fast excitatory signalling in the central nervous system, and they are thought to contribute to the synaptic plasticity that is related to our ability to learn and form memories.[33]

Pharmacologically distinct subfamilies of iGluR have been identified and they can be classified into NMDA (*N*-methyl-D-aspartate (**8**), GluNs) and non-NMDA types according to their affinities for this synthetic agonist (Figure I-5). The latter can be further divided into two main subgroups, the so-called AMPA (GluAs) and kainate (Gluks) receptors.[34] AMPA receptors (named for their agonist 2-amino-3-(5-methyl-3-hydroxyisoxazol-4-yl)propanoic acid (**9**)) are mostly found in the centre of the postsynaptic density, and they are in charge of the major rapid excitatory transmission in the central nervous system (CNS). By contrast, kainate receptors (named for their agonist kainic acid (**10**)) are placed on the periphery of the synaptic cleft. Although their function is not perfectly well defined, it is generally considered that they play a modulatory role at both presynaptic and postsynaptic sites. In this work, our attention will be mainly focused on such kainate receptors.

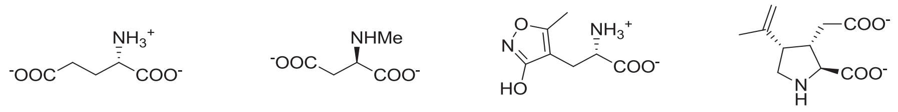

5 8 9 10

Figure I-5. The universal agonist glutamate (**5**) and the three subtype-selective agonists of iGluRs: *N*-methyl-D-aspartate (NMDA, **8**), carboxylates of 2-amino-3-(5-methyl-3-hydroxyisoxazol-4-yl)propanoic acid (AMPA, **9**), and kainic acid (**10**).

High-resolution crystal structures of the ligand binding cores of individual iGluR subunits have made possible a detailed understanding of agonist recognition in a diverse family of ionotropic glutamate receptors. As illustrated in Figure I-6, these receptors are composed of four individual subunits, each of which is made of four well-conserved domains: (i) the extracellular amino-terminal domain (ATD), which is involved in the subfamily-specific assembly and modulation of the receptor; (ii) the ligand-binding domain (LBD), which provides the binding site for agonists and antagonists through the clamshell-like arrangement of lobes D1 and D2; (iii) the transmembrane domain (TMD), composed of three transmembrane helices between which the cation-selective pore (P) is formed; and (iv) the intracellular carboxy-terminal domain (CTD), which plays a major role in channel localisation, stabilisation and targeting (Figure I-6b).[2,33,34]

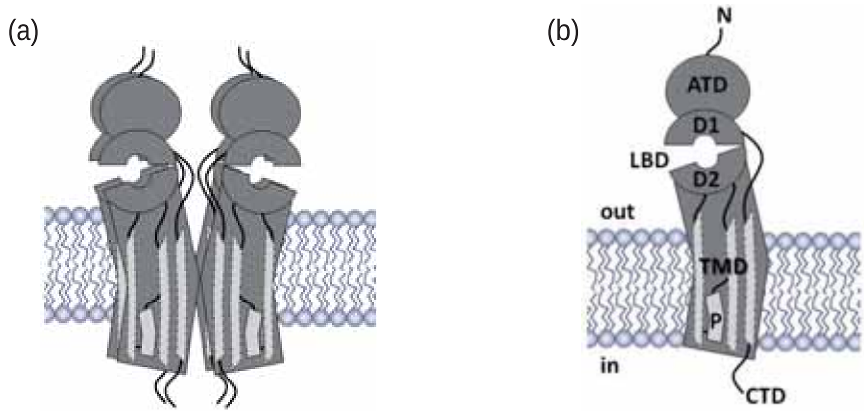

Figure I-6. (a) iGluR structure, which is made of four individual subunits. (b) Structure of each one these individual subunits (ATD = amino-terminal domain, LBD = ligand-binding domain, D1 = upper lobe of the LBD, D2 = lower lobe of the LBD, TMD = transmembrane domain, P = pore helix, CTD = carboxy-terminal domain).

The activation cycle of glutamate receptors upon ligand binding comprises three different states--namely, an inactive resting state, an active state, and an inactive desensitised state (Figure I-7). The active state is formed after the binding of glutamate or other agonists to the LBD of the receptor, which induces an allosteric conformational change in the TMD that allows a pore to be opened in the membrane. This aperture evokes a flux of sodium, potassium and/or calcium ions, thus causing a depolarising current whose rise time and duration varies for each type of iGluR. If a large enough number of glutamate receptors are activated, such excitatory current triggers an action potential in the postsynaptic neuron. In any case, and after a certain period of time, the channel undergoes a process of desensitization, which results in a further conformational change in the TMD that closes the channel and, eventually, leads to agonist unbinding.[2]

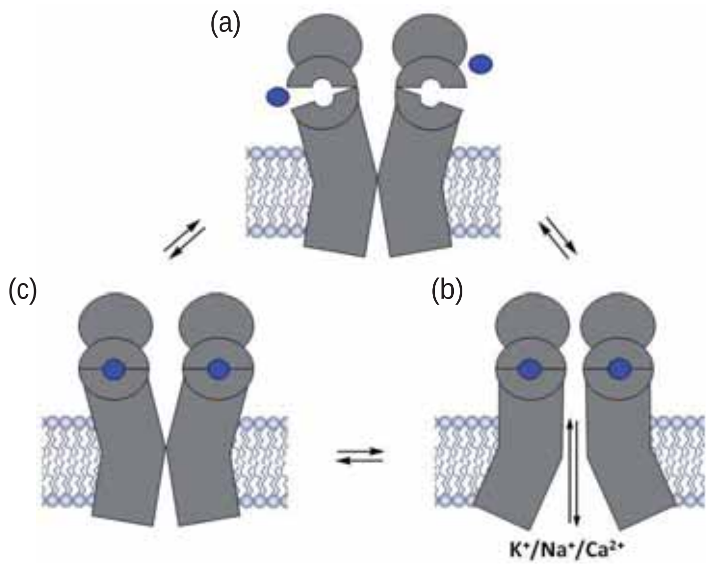

Figure I-7. Schematic representation of the (a) resting, (b) activated, and (c) desensitised states of the activation cycle of iGluRs upon ligand (blue) binding. Only two of the four subunits of the receptor are shown for clarity.

To date, several strategies have been reported to enable optical manipulation of glutamate receptors, which involve the use of caged ligands,[25] photochromic ligands[22] or photoswitched tethered ligands.[30] As noted above, this dissertation is focused on the development of new PTLs to achieve light-control of kainate-type glutamate receptors. For this reason, the next section is devoted to introduce the type of photoswitches used in our design (i.e. azobenzene) as well as to overview previous PTL approaches applied to the optical control of iGluRs.

I.2. MOLECULAR PHOTOSWITCHES

Extensive research has been recently dedicated to the study of molecules whose physico-chemical properties can be reversibly switched as response to an external stimulus. These systems are called molecular switches due to their ability to interconvert between an *"Off"* and an *"On"* states (Scheme I-1).

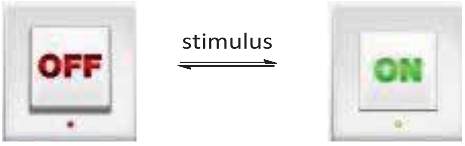

Scheme I-1. Operation of a molecular switch.

In general, molecular switches may respond to a large variety of stimuli, such as thermal,[35] electronic,[36] optical,[37] magnetic,[38] or chemical stimuli.[39] Among them, the use of photons to promote the interconversion process is of special interest. On the one hand, it enables remote operation of the system. Moreover, the development of ultrafast pulsed lasers and the capability to focus light onto localised sub-micrometer sized areas allows very precise control of the switch both in terms of time and space. As such, a wealth of research has been devoted to the design, synthesis and characterisation of light-responsive molecular switches, the so-called photoswitches. The most widely studied of these compounds are photochromes.[40]

Photochromism is defined as the reversible transformation of a chemical species between two forms with different absorption spectra that is induced by the absorption of electromagnetic radiation (Scheme I-2).[40] Although the term "photochromism" strictly indicates a change of colour, the difference in optical properties between the two states of a photochrome is always accompanied by variations in other physical and chemical properties, such as molecular geometries, redox potentials, refractive indexes or dielectric constants. All these changes are the result of chemical transformations, which for the majority of photochromic systems are reversible unimolecular photoisomerisation reactions.

$$A \underset{h\nu_2 \text{ or } \Delta}{\overset{h\nu_1}{\rightleftharpoons}} B$$

Scheme I-2. Photochromism as the reversible transformation between two forms of a molecular system displaying different colours, which must be photoinduced at least in one direction.

Photochromic systems are classified into two major groups according to the thermal stability of the photochemically generated state. If it is thermally unstable, the back reaction can also occur thermally on the ground electronic state and the photochrome is then called of T-type (**thermally reversible type**). Most of the known photochromic compounds belong to this group, azobenzenes being probably the most extensively studied.[41] As shown in Figure I-8a, azobenzenes undergo a reversible photochemical *trans-cis* isomerisation, which can also be reverted thermally owing to the limited stability of their *cis* state. When the photochemically generated form of the photochrome is thermally stable, the initial state can only be recovered photochemically and the system is then called of P-type (**photochemically reversible type**). One of the most popular P-type photochromic switches are dithienylethenes (DTEs), which interconvert between their open and closed states via photoinduced electrocyclic reactions (Figure I-8b).[41]

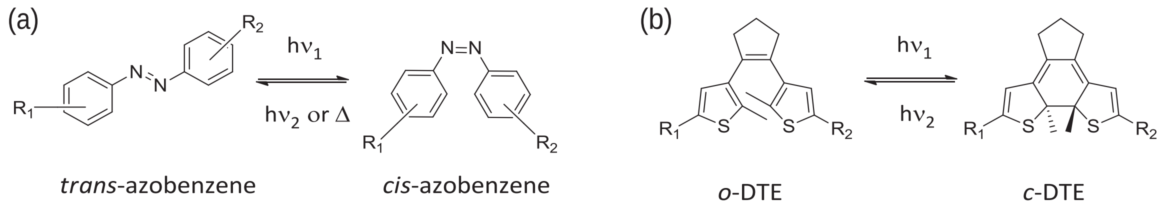

Figure I-8. Examples of (a) T-type (azobenzene) and (b) P-type (dithienylethene) photochromic compounds. Azobenzenes undergo reversible *trans-cis* photoisomerisation, while DTEs photoconvert between their open and closed states.

Molecular photoswitches show very relevant properties that make them promising candidates for an extensive variety of applications. For instance, these molecular systems are proposed for the construction of data storage devices,[37] logic operators,[42] photoprotective coatings,[43] and security printing.[44] In addition, molecular photoswitches are also of relevance in the field of biosciences, where they have been applied to the optical control of the structure and activity of a wide range of biomolecules.[45–47] This is the case of the photoswitched tethered ligands for the light-induced manipulation of glutamate receptors that we aim to develop in this thesis by exploiting azobenzene photochromes.

I.2.1. Azobenzene-based photoswitches

The discovery of *trans*-azobenzene dates back to 1834 and since then azobenzene compounds have been extensively used as synthetic colouring agents in the dye industry. By observing changes in the absorbance of a *trans*-azobenzene solution exposed to light, Hartley reported first evidence for the photochemical formation of *cis*-azobenzene in 1937, which he was able to isolate using careful solvent extraction methods.[48] More than 70 years later, azobenzenes have become some of the most used organic compounds for optical switching applications both in materials science and biosciences[46,47,49,50] owing to their excellent photochemical properties and their facile synthetic accessibility and versatility.

Azobenzenes are organic molecules composed of two phenyl rings linked by an azo bond. As such, they can present two different geometric isomers around the -N=N- bond, the thermally stable *trans* isomer and the metastable *cis* isomer (Figure I-9a). *Trans*-azobenzene has a nearly planar structure and no dipole moment, whereas the *cis* isomer presents a dipole moment of 3.0

D and a bent geometry with its phenyl rings twisted ~ 55º out of plane. Such configurational change results in a large variation in the end-to-end distance between the two isomers (~ 3.5 Å for the carbon atoms at the *para* positions of the phenyl rings), which is one of the most important features accounting for the widespread application of azobenzenes as photoswitches.[46]

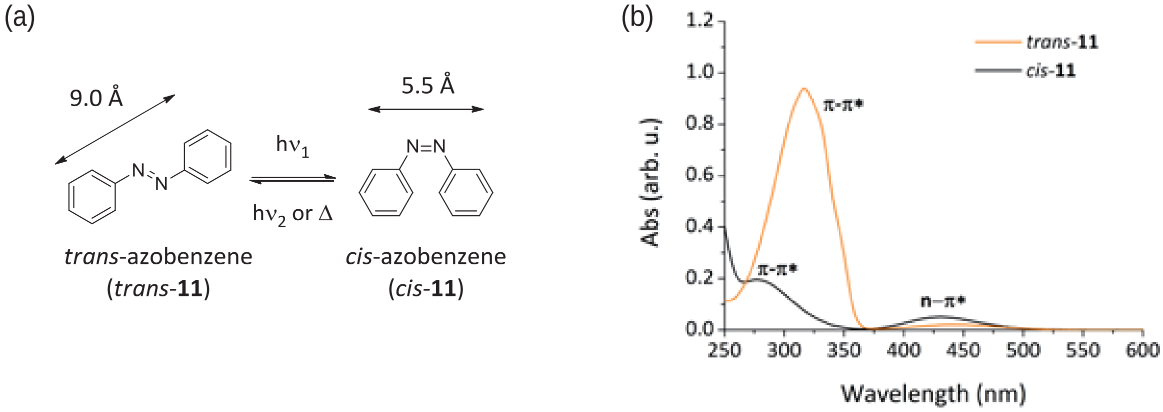

Figure I-9. (a) Photochemical and thermal isomerisation of azobenzene (**11**). (b) UV-vis absorption spectra of *trans*- and *cis*-azobenzene in acetonitrile, in which the two characteristic absorption bands of each isomer are observed ($\pi \rightarrow \pi^*$ and $n \rightarrow \pi^*$).

The *trans* isomer of azobenzene is ~ 12 kcal/mol more stable than its *cis* isomer and the energy barrier between them is ~ 23 kcal/mol on the ground electronic state. As a result, *trans*-azobenzene is the predominant isomer at equilibrium in the dark. As illustrated in Figure I-9b, the UV-vis absorption spectrum of *trans*-azobenzene presents two characteristic absorption bands: (i) a very intense band around λ = 320 nm corresponding to a $\pi \rightarrow \pi^*$ electronic transition; and (ii) a weaker band around λ = 440 nm arising from the symmetry-forbidden $n \rightarrow \pi^*$ electronic transition.[51] Excitation of the allowed $\pi \rightarrow \pi^*$ transition leads to photoisomerisation towards the *cis* isomer with a rather high isomerisation quantum yield ($\Phi_{trans \rightarrow cis}$ ~ 0.14 in acetonitrile)[52] and without generation of by-products. However, since the absorption spectra of the *trans* and *cis* isomers substantially overlap, the photoisomerisation process is not quantitative and an equilibrium state is reached, which is highly enriched in the *cis* isomer (~ 95% of *cis*-azobenzene in acetonitrile at λ_{exc} = 365 nm).[52] This is called a photostationary state (PSS), whose composition depends on a number of parameters, such as the extinction coefficients of both isomers at the excitation wavelength, the isomerisation quantum yields in both directions and the thermal back isomerisation rate constant ($k_{cis \rightarrow trans}$).

As for *trans*-azobenzene, the UV-vis absorption spectrum of *cis*-azobenzene displays a low intensity band around λ = 440 nm, which corresponds to the symmetry-forbidden $n \rightarrow \pi^*$

electronic transition. In what regards to the $\pi\rightarrow\pi^*$ transition, a blue-shifted and weaker band at λ = 280 nm is observed for this isomer (Figure I-9b). Since the intensity of the $n\rightarrow\pi^*$ band is slightly higher for the *cis* state, photoexcitation of this transition allows the isomerisation process to be reverted ($\Phi_{cis\rightarrow trans}$ ~ 0.46 in acetonitrile),[53] thus leading to a new photostationary state enriched essentially with the *trans* isomer. In addition, the *cis* isomer is thermally unstable, which opens up an alternative back isomerisation process evolving through the ground electronic state ($k_{cis\rightarrow trans}$ = 4.3 x 10^{-6} s^{-1} at 22 ºC in acetonitrile).[52] Therefore, quantitative formation of *trans*-azobenzene is eventually observed in the dark.

The mechanism of photoisomerisation of azobenzene has been a subject of debate for many years. As depicted in Scheme I-3, two different mechanisms were originally proposed to take place depending on the excitation wavelength: an inversion mechanism under excitation of the $n\rightarrow\pi^*$ transition, and a rotational mechanism similar to that reported for stilbene upon photoexcitation of the $\pi\rightarrow\pi^*$ band.[54,55] However, recent investigations have revealed that other hybrid mechanisms can occur, such as a concerted inversion or an inversion-assisted rotation.[56]

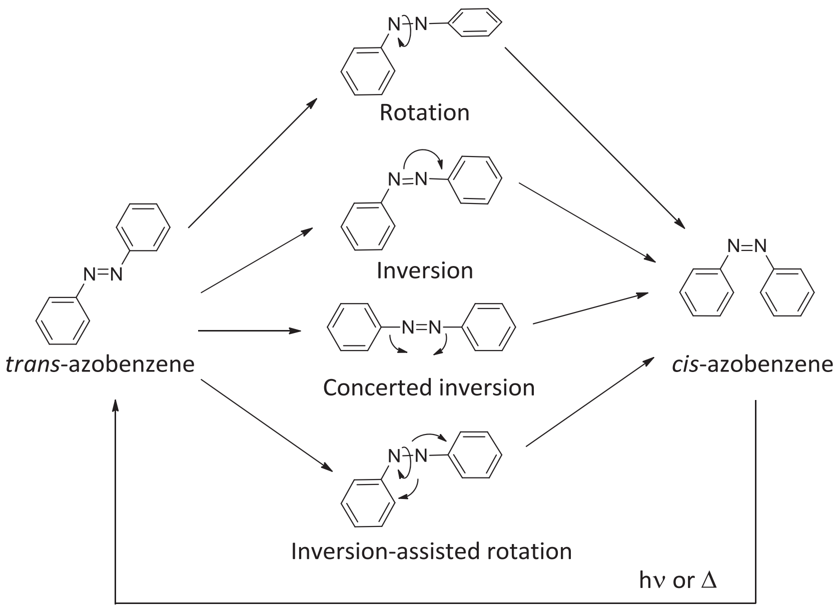

Scheme I-3. Rotation and inversion mechanisms proposed for the *trans-cis* isomerisation process of azobenzene.[56]

The photophysical and photochemical properties of azobenzenes can be finely tuned by introduction of proper substituents into the aromatic rings.[41,57] This has motivated the development of a range of synthetic methodologies to prepare and functionalise azobenzene photochromes, such as diazonium coupling reactions, Mills reaction between aromatic nitroso derivatives and anilines, and transition-metal-catalysed cross-coupling reactions.[58] The resulting azobenzene derivatives can be divided into three main categories based on their photochemical behaviour, which is closely related to their substitution pattern.[59] Table I-1 summarises some of the properties of these three types of azobenzene photochromes.

Table I-1. Photochemical properties of three representative compounds of azobenzene-type, aminoazobenzene and pseudo-stilbene photochromes.

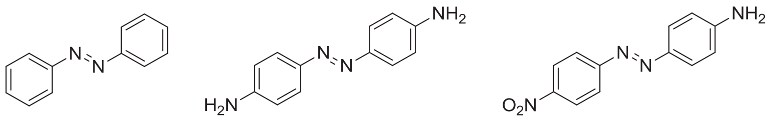

11 **12** **13**

Entry	Azobenzene	λ_{max} (*trans*)	$k_{cis \rightarrow trans}$ (s^{-1})	$t_{1/2}$
1	**11**[a]	316 nm	4.3×10^{-6} (22 ºC)[52]	45 h
2	**12**[a]	382 nm	1.7×10^{-4} (22 ºC)[52]	66 min
3	**13**[b]	410 nm	6.9×10^{-1} (20 ºC)[60]	1 s

(a) In acetonitrile; (b) in methylcyclohexane.

- Azobenzene-type molecules (Figure I-10a), which present similar properties to those of the parent azobenzene compound--namely, a $\pi \rightarrow \pi^*$ transition in the UV region that is well separated from the less energetic $n \rightarrow \pi^*$ transition, and a slow thermal *cis*→*trans* back isomerisation rate, which usually takes place in the timescale of hours at room temperature (Table I-1, entry 1).

- Aminoazobenzenes (Figure I-10b), which are obtained by introducing electron-donating groups (EDG, e.g. amino groups) at the *ortho*- and/or *para*-positions of the aromatic rings. This causes the $\pi \rightarrow \pi^*$ transition to bathochromically shift to the visible region of the spectrum, where it partially overlaps the $n \rightarrow \pi^*$ absorption band. In addition, the thermal *cis*→*trans* back isomerisation rate is accelerated, and the lifetime of the *cis* isomer in the dark at room temperature is reduced to the minute timescale (Table I-1, entry 2).

- Pseudo-stilbenes (Figure I-10c), which feature a strong asymmetric charge distribution arising from the substitution at the 4 and 4′ positions of their aromatic rings with an electron-withdrawing (EWG) and an electron-donor groups (the so-called push-pull substitution).[61] As a result, the $\pi \rightarrow \pi^*$ and $n \rightarrow \pi^*$ electronic absorption bands become nearly degenerate and they further bathochromically shift with respect to aminoazobenzenes. This effect is ascribed to the larger dipolar character of the excited state of these systems due to the push-pull subtitution.[62–65] Another consequence of this is a dramatic increase of the thermal *cis*→*trans* back isomerisation rate (Table I-1, entry 3). As a result, the lifetime of the *cis* isomer in the dark at room temperature drops down to the second or even sub-second timescale, a situation that is strongly accentuated in solvents of increasing polarity (e.g. for **13**, $t_{1/2}$ varies from 1 s in methylcyclohexane[60] to 252 ms in acetone[66]).

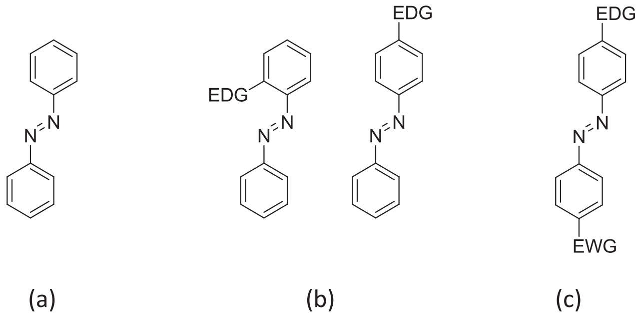

Figure I-10. Spectroscopic classes of azobenzenes depending on their substitution patterns: (a) azobenzenes; (b) aminoazobenzenes; and (c) pseudo-stilbenes.

Aside from these types of azobenzene photochromes, new systems displaying novel properties are being currently developed that cannot be classified into any of these three traditional categories. For instance, the introduction of bulky or bridging groups at the *ortho*-positions of the aromatic rings allows the preparation of azobenzene derivatives with (i) different, non-overlapping $n \rightarrow \pi^*$ bands that can be exploited to induce effective *trans*→*cis* photoisomerisation with visible light,[67–69] (ii) very long-lived *cis* states (up to several years at room temperature),[68] or (iii) even inverted thermal stability of their two isomers.[69] These changes and those described above arising from different substitution patterns must be carefully considered when designing azobenzene-based photochromes for specific applications, since they will ultimately determine both their performance and operation conditions. This is the case of: (i) the wavelength at which *trans*→*cis* photoisomerisation will take place, which can be tuned along the UV and visible regions; (ii) the extent of isomerisation attained upon irradiation of the *trans* isomer, which will be dramatically limited in systems displaying large thermal *cis*→*trans* back isomerisation rates; and (iii) the need for a second excitation source to revert back the process, which could be ignored for photochromes with very short-lived *cis* isomer.

In summary, azobenzene derivatives are photoresponsive compounds whose optical properties can be precisely tailored to fulfill the requirements of specific applications. Together with their synthetic accessibility, their excellent photo- and chemical stabilities and the remarkable variation in their geometry, polarity and electro-optical properties upon isomerisation, this makes azobenzene-based systems promising candidates to enable the photocontrol of molecular processes in diverse fields. In optochemical genetics, the use of azobenzene photoswitches has been extensively used and it has led to the development of different photochromic ligands and photoswitched tethered ligands for the light-control of neuronal ion channels. This is the case of the ionotropic glutamate receptors whose photoinduced operation with NIR light is pursued in this work.

I.2.2. Azobenzene photoswitches for the light-control of ionotropic glutamate receptors

Azobenzene-mediated photocontrol of ion channels has been substantially improved, extended and generalised by Trauner, Isacoff and co-workers.[22,30,70–72] In 2005, they pioneered the development of the first light-controlled ionotropic glutamate receptor, which they accomplished by exploiting the PTL strategy.[30] Among all the subtypes of iGluRs, they particularly focused on kainate receptors owing to the well-defined architecture of their clamshell-like ligand binding domain and their readily interpretable pharmacology. For these receptors a tethered analogue of glutamate was designed containing a photoisomerisable azobenzene moiety that was selectively anchored to a specific site of the upper lobe of the LBD clamshell. The drastic change in geometry between the two states of this azobenzene-based system allowed light-control of the glutamate-binding site interaction, which was only observed to take place for the *cis* isomer of the photoswitch. This resulted in a clamshell-like movement of the LBD around the tethered agonist upon illumination, which was demonstrated to allosterically trigger the opening and closing of the channel pore.

The design of the tethered agonist was based both on the extensive pharmacology of iGluRs and on the X-ray structure of the ionotropic glutamate receptor subtype 6 (iGluR6, now named Gluk2) containing the agonist (2*S*,4*R*)-4-methyl glutamate bound. After evaluation of the stereochemistry and accessibility of several candidates, they decided to focus on a PTL called MAG-1 (**14**). This compound is composed of three different units: (i) a maleimide moiety for conjugation to a cysteine on the exterior of the LBD (M); (ii) an azobenzene photoswitch undergoing *trans-cis* photoisomerisation (A); and (iii) a glutamate analogue as ligand (G) (Figure I-11a). Simultaneously, they prepared a series of single cysteine mutants of Gluk2 by site-directed mutagenesis to find a suitable attachment site for the maleimide group of the PTL. The positions screened were chosen to form a perimeter around the exit channel of the receptor where the maleimide end of the tether was predicted to stick out upon ligand-binding site interaction with the *cis* state of the system (Figure I-11b). In addition, they avoided altering residues of the protein whose interactions could contribute to the stability of the closed state of the pore. Of all the Gluk2 mutants tested, that with a cysteine introduced at position 439 was shown to display the largest biological responses and it was selected for further studies. This assembly of the cysteine-mutated Gluk2 and the tethered MAG-1 ligand was named light-gated ionotropic glutamate receptor (LiGluR) and it has been demonstrated to allow current to be rapidly and briefly injected into cells upon photoirradiation.[22,30,71]

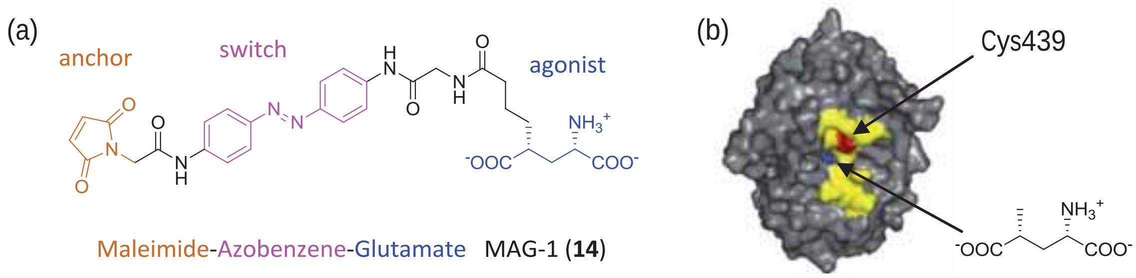

Figure I-11. (a) Structure of molecular switch MAG-1 (**14**). (b) View of the cleft of Gluk2 LBD in association with agonist (2*S*,4*R*)-4-methyl glutamate (in blue). All the positions where cysteine residues were introduced are shown in yellow, while position 439 is depicted in red.[30]

A schematic representation of how LiGluR works under illumination is given in Figure I-12. This light-gated ion channel is prepared by expression of the cysteine-mutated Gluk2 receptor into the cells of interest and subsequent incubation with a UV-irradiated solution of MAG-1 to induce conjugation of the photoswitch. This process is considered to be strongly favoured by affinity labelling, whereby docking of the glutamate group of MAG-1 at the binding site of the receptor takes place first and thus places the reactive maleimide unit near to the cysteine conjugation position.

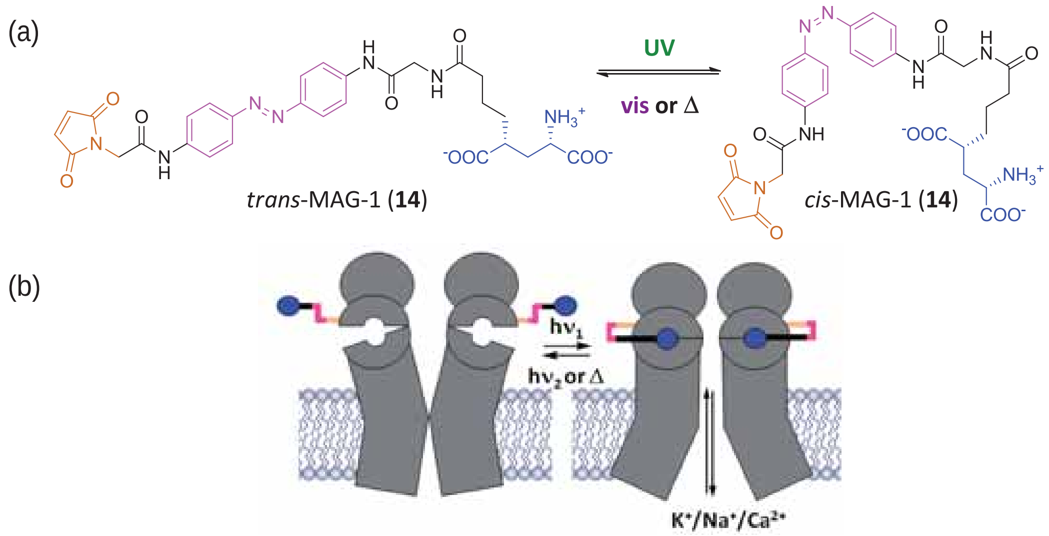

Figure I-12. (a) *Trans-cis* isomerisation of MAG-1 (**14**). (b) Schematic representation of the light-induced operation of LiGluR.[30]

In the dark, the photoswitch of LiGluR is in *trans* configuration, which is the most extended form and moves the glutamate ligand far away from the binding pocket. As a consequence, the ion channel pore remains closed. Upon irradiation with UV light (~ 380 nm), the azobenzene group of the switch photoisomerises towards its *cis* configuration. In this bent form, glutamate is brought into close proximity to the binding site, where it can be bound to induce the aperture of the channel and the transport of cations across the pore. This situation can be finally reverted back either by *cis*→*trans* photoisomerisation with visible light (~ 500 nm), or thermally in the dark ($t_{1/2}^{cis}$ ~ 17 min).[70]

The capability of LiGluR to optically evoke ion currents through the cell membrane was first tested in the well-established Human Embryonic Kidney (HEK293) cell line,[22,30,70,71] which can be easily grown and transfected. The biological response of these cells under illumination was evaluated using common electrophysiological (whole-cell patch clamp, see § IV.5.2)[22,30,71,72] and fluorescence measurements (calcium imaging, see § III.4.1).[30,71] The whole-cell patch clamp technique allows registering the differences in current or potential across the cell membrane caused by light-induced aperture of LiGluR channels and the concomitant transport of ions between the extra- and intracellular media (Figure I-13a). On the other hand, calcium imaging enables the detection of the influx of Ca^{2+} ions into the cell upon channel opening by monitoring the fluorescence signal of a Ca^{2+}-sensitive intracellular indicator (Figure I-13b). With both techniques, the robust, repetitive and reproducible light-induced aperture and closure of LiGluR channels was successfully demonstrated by illumination at 380 nm and 500 nm, respectively.

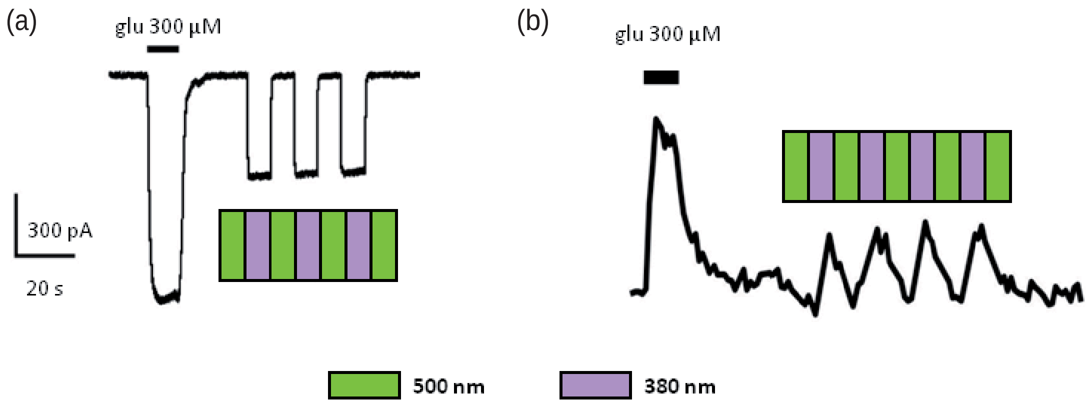

Figure I-13. Examples of (a) a whole-cell patch clamp current trace and (b) a calcium imagining fluorescence measurement for HEK293 cells transfected with LiGluR.[30] Whereas the first signal observed in both traces arises from the injection of free glutamate to the sample (c = 300 µM), the rest of them are induced by sequential irradiation at 380 nm and 500 nm. As discussed in the text, photoexcitation with UV light results in activation of the channel upon *trans*→*cis* photoisomerisation, thus leading to changes in current (a) and fluorescence intensity (b). Subsequent photoexcitation with visible light allows the process to be reverted back, and the overall photochemical cycle can be repeated several times without apparent degradation.

In view of the good results obtained *in vitro*, Trauner, Isacoff and co-workers investigated the ability of LiGluR to manipulate the firing of neurons *in vivo*. The first experiments were performed on zebrafish larvae, which are fully transparent at this growth stage. To introduce LiGluR channels into this organism, cysteine-mutated Gluk2 was encoded in the neurons that are involved in touch sensation of embryonic zebrafish. Regular behaviour was observed for genetically-modified zebrafish larvae in the dark after incubation in an aqueous solution of MAG-1--namely, they retained their ability to swim out after a gentle touch with a glass pipette. However, 28% of the larvae surprisingly lost this intrinsic escape behaviour upon irradiation with UV light inducing *trans→cis* photoisomerisation of the LiGluR photoswitch (Figure I-14a). Subsequent photoexcitation with visible light to revert this process allowed 81% of the non-responding larvae to recover their normal touch response (Figure I-14b). These results demonstrate that LiGluR can be exploited to reversibly interfere with neuronal signalling *in vivo*.[72]

(a)

(b)

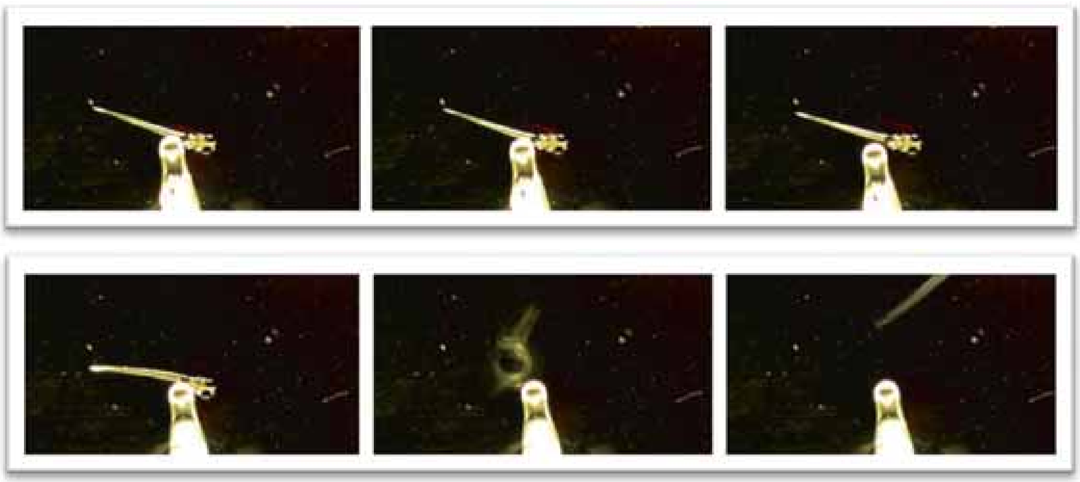

Figure I-14. Zebrafish larvae expressing LiGluR channels in their touch sensory neurons. (a) Upon 365 nm illumination, the regular escape behaviour is lost, and (b) it is restored by irradiation at 488 nm.[72]

Inspired by the pioneering work of Trauner, Isacoff and co-workers, new versions of LiGluR channels have been developed during the last years. This has involved both the modification of the photoswitch structure as well as of the sub-type of glutamate receptor targeted. For instance, MAG derivatives MAG-0 (**15**) and MAG-2 (**16**) were synthesised and conjugated to cysteine-mutated Gluk2 to investigate the effect of the spacer length between the glutamate and azobenzene units on the light-induced activity of LiGluR (Figure I-15).[71] More recently, this approach has been expanded to metabotropic glutamate receptors.[73]

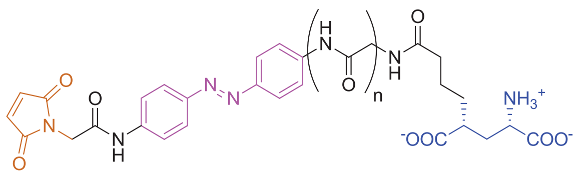

n= 0: MAG-0 (**15**)
n= 1: MAG-1 (**14**)
n= 2: MAG-2 (**16**)

Figure I-15. Three MAG variants studied: MAG-1 (**14**) and the two homologous compounds with shorter (MAG-0 (**15**)) and longer linkers (MAG-2 (**16**)).

In spite of their successful performance, the azobenzene-based PTLs so far developed to optically control the response of glutamate receptors suffer from several limitations, especially when applied *in vivo*. The most severe of them is the need for UV irradiation to induce *trans*→*cis* photoisomerisation, which (i) can produce cellular apoptosis or other photodamage processes upon prolonged exposure, and (ii) is strongly scattered and absorbed by biological media, thus significantly reducing the penetration depth in tissues (e.g. less than 300 μm in human white brain matter[74]). Therefore, bathochromically shifting the excitation wavelength into the near-infrared region would tremendously enhance the performance of azobenzene-based PTLs, since much larger penetration depths are achieved in this spectral area (e.g. more than 1 mm in human white brain matter[74]) with no biological photodamage. An effort towards this objective has been very recently reported by Isacoff, Trauner and co-workers, who described the synthesis, characterisation and application to the light-control of Gluk2 of a red-shifted MAG derivative (**17**, Figure I-16) during the writing period of this manuscript.[75] By introducing an amino group at the 4′ position of the azobenzene unit of MAG-0, it was possible to induce the *trans*→*cis* photoisomerisation of **17** with blue-green visible light (λ_{max} = 460 nm). In this spectral region, however, the penetration depths attained in neural tissues are still 2-3 times lower than those achievable with NIR radiation.

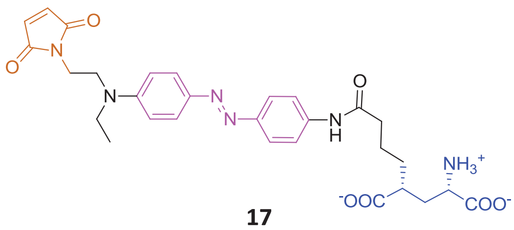

17

Figure I-16. Structure of the first red-shifted photoswitched tethered ligand for LiGluR.[75]

An additional limitation of the parent MAG-1 photoswitch and its derivatives reported so far is that their *trans-cis* photoisomerisation upon illumination with UV or visible light proceeds via one-photon excitation processes (i.e. via absorption of a single photon that is resonant with the energy gap between the ground and excited electronic states). This hinders exploiting the advantages of multiphoton excitation to optically address biological samples with unprecedented three-dimensional (3-D) spatial resolution (see § I.3.1). Together with deep penetration into tissues, this is a crucial requirement if optogenetic and optochemical genetic tools are to be applied to the manipulation and mapping of brain activity *in vivo*. Consequently, to achieve light-induced control of neural receptors and ion channels via **both multiphoton excitation and NIR light** is one of the main challenges in these fields, which has led to the development of two-photon IR-responsive caged ligands[76] and channelrhodopsin-2 mutants.[77–80] However, the application of this stimulation technology to photochromic ligands and photoswitched tethered ligands is yet to be demonstrated. Aiming at filling this gap, in this work we pursue the preparation of new MAG derivatives enabling the optical control of Gluk2 receptors via two-photon absorption of NIR light.

I.3. TWO-PHOTON EXCITATION OF MOLECULAR PHOTOSWITCHES WITH NIR LIGHT

I.3.1. Two-photon absorption

Two-photon absorption (TPA) is defined as a non-linear optical process whereby two photons of equal energy are simultaneously absorbed by the same molecule to raise a system into an excited state. This process was first postulated by Göppert-Mayer in 1931, but it was not until the invention of the laser in 1961 that this theory was demonstrated experimentally.[81,82] Although the effect of TPA on a molecular system might be the same as that resulting from one-photon absorption (e.g. the excitation from the ground electronic state (S_0) to the first excited singlet electronic state (S_1) of a closed-shell organic molecule), these processes proceed via noticeably different mechanisms. As schematically shown in Figure I-17, TPA is based on the absorption of two photons of equal frequency leading to the formation of an excited state with twice the excitation energy of that of the absorbed photons. Importantly, TPA does not evolve through the formation of any real intermediate eigenstate, but it is considered to emerge through the generation of a virtual state with an infinitely short lifetime; hence, the need for the nearly simultaneous absorption of the two photons involved. As discussed below, this makes TPA a very unlikely process to occur that requires high excitation power densities, since it is related to the probability that two photons are absorbed by the same molecule at the same time. Actually, TPA is an optical process several orders of magnitude weaker than one-photon absorption.

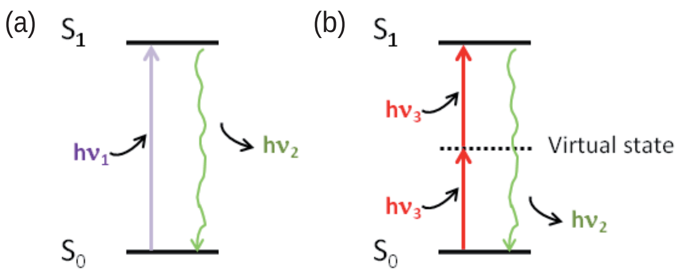

Figure I-17. Energy level diagrams for the (a) one-photon, and (b) two-photon absorption processes promoting a closed-shell molecule from its ground electronic state (S_0) to its first excited singlet electronic state (S_1). Once in the S_1 state, the system will undergo the same relaxation processes in both cases, such as the emission of fluorescence (shown in the figure), non-radiative internal conversion or energy transfer to another molecule.

Equation I.1 describes the one- and two-photon absorption contributions to the attenuation of a beam of light propagating through an absorbing material:[82]

$$-\frac{dI}{dz} = \alpha \cdot I + \beta \cdot I^2 \qquad \textbf{(I.1)}$$

In this equation I is the intensity of light, z is the propagation length inside the sample, and α and β are the probability coefficients for one- and two-photon absorption, respectively. Clearly, while the latter depends linearly on the intensity of the incident beam, TPA scales with the second-power of I. As such, it is considered to be a non-linear optical process. Since $\beta << \alpha$, the contribution of two-photon absorption only becomes of importance at very high excitation intensities, which usually requires the use of pulsed lasers. By expressing the intensity as photon flux ($F = I/h\nu$) and taking into account the concentration of absorbing molecules in the sample (c), the TPA term in Equation I.1 can be written as:[81]

$$-\left(\frac{dI}{dz}\right)_{TPA} = c \cdot \delta \cdot F \cdot I \qquad \textbf{(I.2)}$$

In Equation I.2 δ is the so-called two-photon absorption cross-section, which relates the TPA rate to the photon flux and is usually expressed in Göppert-Mayer units (1 GM = 10^{-50} cm^4 s^{-1} $photons^{-1}$ $molecule^{-1}$). This is the main parameter used to evaluate the efficiency of two-photon absorption processes for any molecular material.

In spite of its lower intrinsic probability, TPA presents several advantages over one-photon absorption, which make it very attractive for applications in biosciences, both in bioimaging[83–85] and for the photoactivation of light-responsive (bio)molecules.[77–80,82] The most outstanding of these features are listed below:

- TPA provides 3-D excitation resolution. As illustrated in Figure I-18, if a light beam is focused onto sample at a wavelength only suitable for one-photon absorption, molecules are excited throughout the beam path in the sample. By contrast, at a wavelength specific for TPA only the molecules located very close to the focus of the laser beam are excited. As discussed above, this behaviour is due to the fact that the absorption probability depends on the square of the excitation intensity. At the focal point, the power density of light is at its maximum and it decreases approximately with the square of the distance from the focal plane along the propagation direction. Consequently, TPA is only observed at the very high photon fluxes achieved in the small volume at the focus of the laser beam.

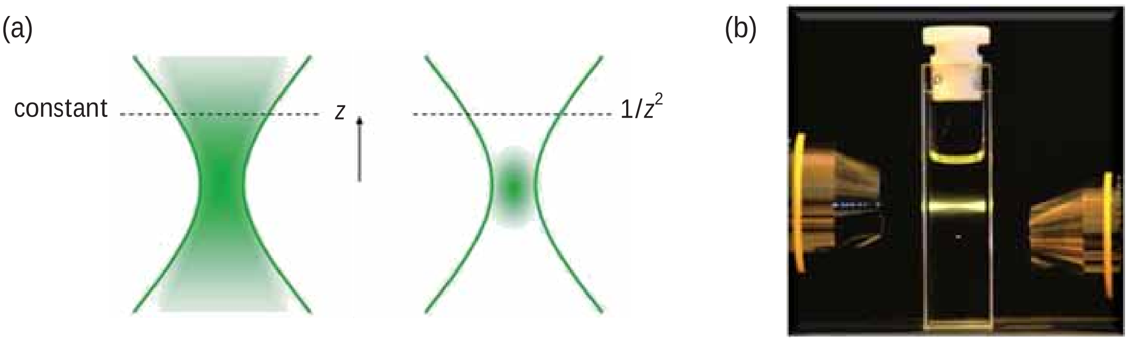

Figure I-18. (a) Schematic representation of the one- (left) and two-photon (right) absorption probability along the propagation direction (*z*) of a focused laser beam. TPA is non-linear, the fluorescence is confined to the focal centre of the laser beam, and fluorescence intensity decays as $1/z^2$. (b) Image of two different laser beams focused onto a cuvette containing a fluorescein dye solution. The top beam excites the dye via one-photon absorption and fluorescence is emitted all along the propagation path through the cuvette. The bottom beam induces two-photon excitation of these molecules, which selectively fluoresce from the focal point.[86]

- TPA improves penetration depth. On the one hand, absorption of the incident radiation takes place almost selectively at the focal point, which minimises the absorption losses throughout the material. On the other hand, two-photon absorption takes place in the NIR region for many organic chromophores, in contrast to the UV-vis one-photon absorption displayed by the same molecules. As discussed above, light absorption and scattering in biological tissues are minimised for NIR radiation, which results in longer penetration depths under these excitation conditions.
- TPA reduces photochemical damage. This is mainly due to the optical properties of most biological chromophores, which are neither strong two-photon absorbers nor absorb NIR light via one-photon processes.

Unfortunately, only a small number of organic chromophores are able to absorb light efficiently via TPA, since δ values are found to be very low for most molecules (typically, below 10 GM). After the first experimental demonstration of TPA in organic dyes in 1963, an increasing effort has been devoted to the design of chromophores with large TPA cross-sections. With this aim, the most important structural parameters enhancing TPA have been identified and investigated.[87] These are: (i) long π-conjugation in the system; (ii) the presence of strong EDGs and/or EWGs at the centre and ends of the π-conjugated system (π) to promote strong internal charge transfer upon electronic excitation; (iii) molecular symmetry, being centrosymmetric structures (e.g. EDG-π-EDG) normally preferred; (iv) molecular planarity; and (v) the incorporation of multibranched or oligomer structures. The effect of some of these parameters are clearly illustrated by the examples given in Figure I-19.[82] With respect to stilbene (**18**), a 14 fold increase in TPA cross-section is observed for derivative **19** bearing two dialkylamino substituents at 4 and 4′ positions. In addition, extension of the conjugation in derivative **20** leads to a further increase in δ_{max}.

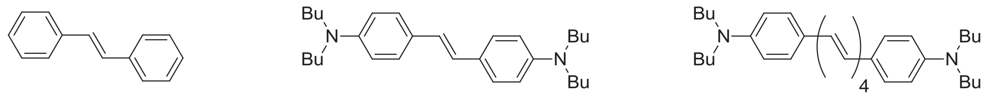

18 δ_{max} = 8 GM (at 514 nm)

19 δ_{max} = 110 GM (at 605 nm)

20 δ_{max} = 410 GM (at 695 nm)

Figure I-19. TPA cross-sections at the maximum of the TPA spectrum of stilbene (**18**), stilbene derivative **19**, and stilbene derivative **20**.[82]

In contrast to stilbene, only a limited number of studies investigating the TPA activity of azobenzenes from a fundamental point of view are found in the literature,[88–91] which is probably due to their low TPA cross-sections and the impossibility of measuring them by means of two-photon excitation fluorescence. Instead, the *z*-scan technique is normally used, which often overestimates the actual δ values.[82] Most of these studies have been reported by Mendonça and co-workers, who aimed at establishing a correlation between the molecular structure and the TPA cross-sections of azobenzenes.[88–90] For this, they investigated the influence of both the introduction of donor and acceptor groups into the azobenzene core and the increase of the conjugation path. While the latter factor seems to have little influence on the TPA cross-sections of azobenzenes, larger variations were found upon addition of EDGs and EWGs. Thus, they found that electronically symmetric azobenzene derivatives such as azobenzene and 4,4′-diaminoazobenzene (see Table I-1) do not present any peak in their TPA spectra and they display rather low TPA cross-sections in the NIR region (below 50 GM). Instead, push-pull substitution by introduction of both EDGs and EWGs resulted in clear TPA spectral peaks at twice the energy of the one-photon absorption bands of the corresponding azobenzene derivatives. For such compounds, δ values up to 500 GM have been measured in the NIR region.[88–90]

Based on these precedents, we propose in this work two different approaches to reach two-photon excitation control with NIR light of azobenzene-based photoswitched tethered ligands:

- To use azobenzene derivatives with large enough push-pull character as to present high TPA cross-sections. Although this design concept has been exploited in Chapter IV of this thesis, it presents two main drawbacks *a priori*: (i) it requires modification of the symmetrically-substituted azobenzene core of MAG-1, the most successful and investigated PTL to light-control glutamate receptors; (ii) it leads to very short-lived *cis* isomers (see § I.2.1), which may result in rather small biological responses upon *trans*→*cis* photoisomerisation owing to fast thermal back reaction.

- To induce *trans*→*cis* photoisomerisation of the PTL via two-photon excitation of a photosensitiser instead of by direct absorption of the azoaromatic group (i.e. via sensitised TPA). This would not only allow preserving the substitution pattern of the azobenzene group in reference compound MAG-1, but also to freely tune it in view of the photochemical requirements of future applications. Consequently, this novel design concept has been thoroughly explored in this thesis and it has been applied both in Chapters III and IV.

I.3.2. Sensitised azobenzene isomerisation via two-photon absorption of NIR light

Figure I-20 sketches the strategy followed in this work to achieve sensitised isomerisation of azobenzene-based PTLs via two-photon excitation with NIR light. It is based on two main concepts: (i) the use of an additional photoactive moiety, the so-called two-photon antenna or photosensitiser, which should be a strong TPA chromophore; and (ii) the ability of this group to transfer its electronic excitation energy to the azoaromatic unit upon two-photon excitation with NIR light, which will eventually undergo *trans*→*cis* isomerisation. To optimise the efficiency of such transfer process, it was devised to take place via intramolecular **resonance energy transfer** (RET).

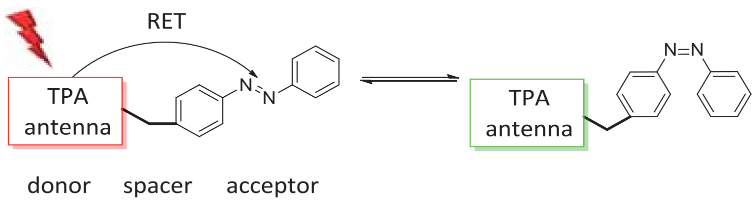

Figure I-20. Schematic representation of the sensitised photoisomerisation of azobenzene using a two-photon absorbing photo-harvesting antenna.

Resonance energy transfer was described for the first time over 70 years ago and it is an absorption-induced process whereby the excitation energy of a chromophore in an excited electronic state (the so-called energy donor) is transferred to a nearby molecule (the so-called energy acceptor).[92,93] RET is a non-radiative quantum mechanical process induced by the electrostatic interaction between the transition dipole moments of the donor and the acceptor. It is outlined in Figure I-21, where we consider the electronic excitation of the donor to proceed via two-photon absorption. If RET takes place, the excited donor does not relax back to its ground electronic state via emission of fluorescence, as shown in the figure, or internal conversion.

Instead, it decays to S_0 by transferring its excitation energy to the acceptor, which is simultaneously brought into its electronically excited state in a resonant process. From that state the acceptor will eventually relax through intrinsic photophysical processes; in the case of *trans*-azobenzene, it is meant to be the isomerisation to its *cis* state.

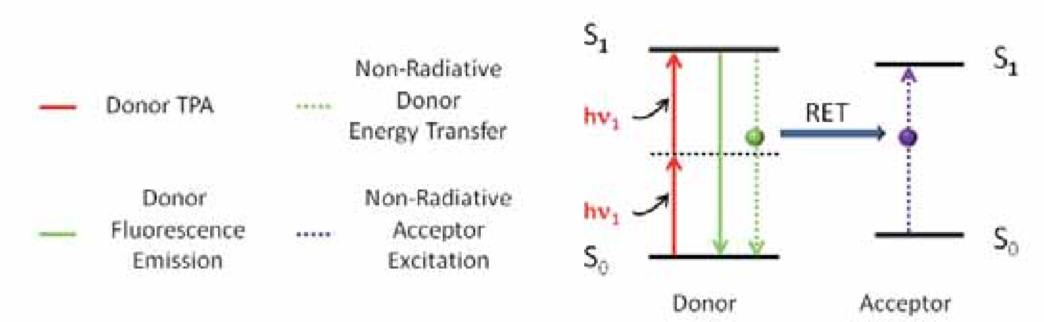

Figure I-21. Diagram illustrating the coupled transitions involved in resonance energy transfer.

Several criteria must be satisfied for resonance energy transfer to occur. As described in Equation I.3 originally derived by Förster in the 1940s,[94] the energy transfer efficiency (*E*) between the donor and acceptor moieties decreases with the sixth power of their separation distance (*r*). As such, *r* must be on the nm scale. Actually, for most molecular donor-acceptor pairs, efficient RET takes place when their separation distance is in the 1-10 nm range.[95] At very short distances (less than 1 nm), other energy transfer mechanisms may occur (e.g. Dexter energy transfer via electron exchange), while at $r > 10$ nm only radiative energy transfer is expected, which requires the emitted photons from the donor to be reabsorbed by the acceptor.

$$E = \frac{1}{1+\left(\frac{r}{R_0}\right)^6} \quad \textbf{(I.3)}$$

In Equation I.3, R_0 is the Förster critical distance or Förster radius, which corresponds to the donor-acceptor distance at which the energy transfer efficiency is 0.5. This parameter determines the actual dependence of RET efficiency with donor-acceptor distance, and it can be calculated from Equation I.4:

$$R_0 = \left(8.88 \times 10^{-25} K^2 n^{-4} \Phi_{Fl,D} J\right)^{1/6} \quad \text{(in cm}^{-1}\text{)} \quad \textbf{(I.4)}$$

As observed in this equation, R_0 depends on the overlap integral (*J*) of the donor emission spectrum with the acceptor absorption spectrum, the orientation parameter between the emission transition dipole of the donor and the absorption transition dipole of the acceptor (k^2), the fluorescence quantum yield of the donor ($\Phi_{Fl,D}$) and the refractive index of the medium (*n*). This allows identifying additional requirements for efficient RET to occur: (i) the transition dipole moments of the donor and acceptor should not be orthogonally oriented, since $k^2 = 0$ in this case; (ii) the donor must be strongly fluorescent ($\Phi_{Fl,D} > 0$); and (iii) its emission spectrum should overlap with the absorption of the acceptor, as shown in Figure I-22. The overlap integral can be calculated from Equation I.5:

$$J = \int [F(\bar{\nu})\varepsilon(\bar{\nu})/\bar{\nu}^4]d\bar{\nu} \quad \textbf{(I.5)}$$

Where $F(\bar{\nu})$ is the normalised emission spectrum of the donor, and $\varepsilon(\bar{\nu})$ is the wavelength-dependent molar extinction coefficient of the acceptor.

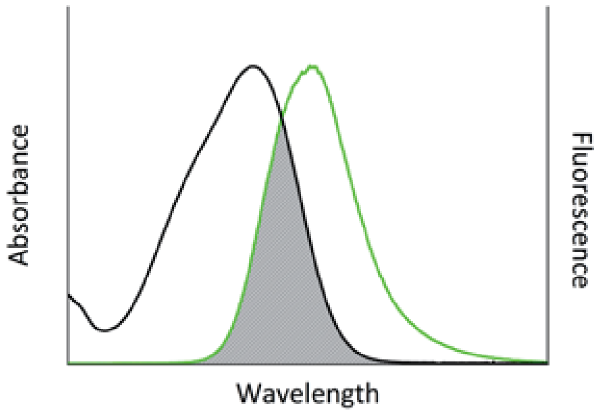

Figure I-22. Spectral overlap between the emission spectrum of the donor (green) and the absorption spectrum of the acceptor (black) required for resonance energy transfer.

Resonance energy transfer processes have already been exploited to induce the sensitised photoisomerisation of azobenzenes. However, most examples reported proceed via one-photon excitation of the sensitiser.[96,97] To our knowledge, only two precedents on TPA sensitisation of azobenzene isomerisation have previously been described. On the one hand, Jiang and co-workers designed highly-branched dendrimers composed of an azobenzene core functionalised with polyaryl ether groups, whose two-photon excitation with IR light resulted in *trans-cis* photoisomerisation of the central azoaromatic group.[98] On the other hand, Zink and co-workers very recently reported azobenzene-based nanovalves for controlled drug delivery in cancer cells, which can be triggered by sensitised two-photon *trans-cis* isomerisation at 760 nm using a paracyclophane fluorophore.[99] Herein we explore for the first time the use of sensitised azobenzene isomerisation to achieve control of optochemical genetic tools by means of two-photon excitation with NIR light. As a proof of principle, we have chosen the light-gated ionotropic glutamate receptor as the model system to demonstrate the viability of this novel stimulation methodology. Based on the well-established MAG-type scheme developed to optically control this type of receptor, we propose in this work the synthesis of analogous photoswitches bearing an additional functional unit: a photo-harvesting antenna with which we intend to sensitise the *trans*→*cis* isomerisation of the system by strong two-photon absorption of NIR radiation and subsequent resonant electronic energy transfer to the *trans*-azobenzene group (Figure I-23).

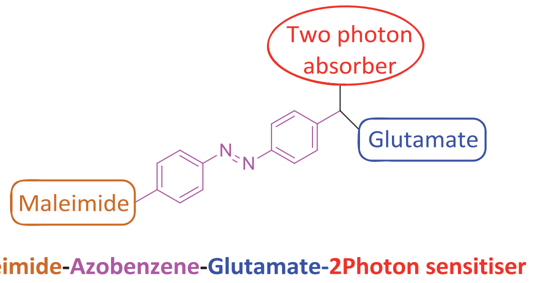

Figure I-23. General structure of the new azobenzene-based PTLs devised in this work to achieve light-control of ionotropic glutamate receptors via two-photon excitation of a photosensitiser. With this aim, an additional two-photon absorber unit will be introduced into the well-known MAG scheme.

I.4. REFERENCES

(1) Fenno, L.; Yizhar, O.; Deisseroth, K. *Annu. Rev. Neurosci.* **2011**, *34*, 389–412.

(2) Fehrentz, T.; Schönberger, M.; Trauner, D. *Angew. Chem. Int. Ed.* **2011**, *50*, 12156–12182.

(3) Crick, F. H. *Sci. Am.* **1979**, *241*, 219–232.

(4) Deisseroth, K. *Sci. Am.* **2010**, *303*, 48–55.

(5) Deisseroth, K. *Nat. Methods* **2011**, *8*, 26–29.

(6) Kramer, R. H.; Mourot, A.; Adesnik, H. *Nat. Neurosci.* **2013**, *16*, 816–823.

(7) Boyden, E. S.; Zhang, F.; Bamberg, E.; Nagel, G.; Deisseroth, K. *Nat. Neurosci.* **2005**, *8*, 1263–1268.

(8) Zhang, F.; Vierock, J.; Yizhar, O.; Fenno, L. E.; Tsunoda, S.; Kianianmomeni, A.; Prigge, M.; Berndt, A.; Cushman, J.; Polle, J.; Magnuson, J.; Hegemann, P.; Deisseroth, K. *Cell* **2011**, *147*, 1446–1457.

(9) Nagel, G.; Brauner, M.; Liewald, J. F.; Adeishvili, N.; Bamberg, E.; Gottschalk, A. *Curr. Biol.* **2005**, *15*, 2279–2284.

(10) Li, X.; Gutierrez, D. V; Hanson, M. G.; Han, J.; Mark, M. D.; Chiel, H.; Hegemann, P.; Landmesser, L. T.; Herlitze, S. *Proc. Natl. Acad. Sci. U. S. A.* **2005**, *102*, 17816–17821.

(11) Pastrana, E. *Nat. Methods* **2010**, *8*, 24–25.

(12) Staff, N. *Science* **2010**, *330*, 1612–1613.

(13) Gradinaru, V.; Mogri, M.; Thompson, K. R.; Henderson, J. M.; Deisseroth, K. *Science* **2009**, *324*, 354–359.

(14) Kasparov, S.; Herlitze, S. *Exp. Physiol.* **2013**, *98*, 971–972.

(15) Packer, A. M.; Roska, B.; Häusser, M. *Nat. Neurosci.* **2013**, *16*, 805–815.

(16) Tochitsky, I.; Banghart, M. R.; Mourot, A.; Yao, J. Z.; Gaub, B.; Kramer, R. H.; Trauner, D. *Nat. Chem.* **2012**, *4*, 105–111.

(17) Mourot, A.; Tochitsky, I.; Kramer, R. H. *Front. Mol. Neurosci.* **2013**, *6*, 5–5.

(18) Gorostiza, P.; Isacoff, E. Y. *Science* **2008**, *322*, 395–399.

(19) Gorostiza, P.; Isacoff, E. *Mol. Biosyst.* **2007**, *3*, 686–704.

(20) Stawski, P.; Sumser, M.; Trauner, D. *Angew. Chem. Int. Ed.* **2012**, *51*, 5748–5751.

(21) Banghart, M. R.; Mourot, A.; Fortin, D. L.; Yao, J. Z.; Kramer, R. H.; Trauner, D. *Angew. Chem. Int. Ed.* **2009**, *48*, 9097–9101.

(22) Volgraf, M.; Gorostiza, P.; Szobota, S.; Helix, M. R.; Isacoff, E. Y.; Trauner, D. *J. Am. Chem. Soc.* **2007**, *129*, 260–261.

(23) Chambers, J. J.; Kramer, R. H. *Photosensitive Molecules for Controlling Biological Function*; Humana Pre.; Springer, 2011.

(24) Gorostiza, P.; Isacoff, E. Y. *Physiology* **2008**, *23*, 238–247.

(25) Wieboldt, R.; Gee, K. R.; Niu, L.; Ramesh, D.; Carpenter, B. K.; Hess, G. P. *Proc. Natl. Acad. Sci. U. S. A.* **1994**, *91*, 8752–6.

(26) Corrie, J. E. T.; Munasinghe, V. R. N.; Trentham, D. R.; Barth, A. *Photochem. Photobiol. Sci.* **2008**, *7*, 84–97.

(27) Engstrom, H.; Ades, H. W.; Sataloff, J.; Vassallo, L.; Igarashi, M.; Gacek, R. R.; Kirbourne, E. D. *Science* **1968**, *162*, 1487–1489.

(28) Bartels, E.; Wassermann, N. H.; Erlanger, B. F. *Proc. Natl. Acad. Sci. U. S. A.* **1971**, *68*, 1820–1823.

(29) Nargeot, J.; Lester, H. A.; Birdsall, N. J.; Stockton, J.; Wassermann, N. H.; Erlanger, B. F. *J. Gen. Physiol.* **1982**, *79*, 657–678.

(30) Volgraf, M.; Gorostiza, P.; Numano, R.; Kramer, R. H.; Isacoff, E. Y.; Trauner, D. *Nat. Chem. Biol.* **2006**, *2*, 47–52.

(31) Harvey, J. H.; Trauner, D. *ChemBioChem* **2008**, *9*, 191–193.

(32) Koçer, A.; Walko, M.; Meijberg, W.; Feringa, B. L. *Science* **2005**, *309*, 755–758.

(33) Madden, D. R. *Nat. Rev. Neurosci.* **2002**, *3*, 91–101.

(34) Stawski, P.; Janovjak, H.; Trauner, D. *Bioorg. Med. Chem.* **2010**, *18*, 7759–7772.

(35) Van Delden, R. A.; Hurenkamp, J. H.; Feringa, B. L. *Chem. Eur. J.* **2003**, *9*, 2845–2853.

(36) Guirado, G.; Coudret, C.; Hliwa, M.; Launay, J.-P. *J. Phys. Chem. B* **2005**, *109*, 17445–17459.

(37) Irie, M. *Chem. Rev.* **2000**, *100*, 1683–1684.

(38) Dierking, I.; San, S. E. *Appl. Phys. Lett.* **2005**, *87*, 233507.

(39) Callan, J. F.; de Silva, A. P.; Magri, D. C. *Tetrahedron* **2005**, *61*, 8551–8588.

(40) Rau, H. *Photochromism: Molecules and System*; Bouas-Laurent, H.; Dürr, H., Eds.; Elsevier Amsterdam, 1990; Vol. 73, pp. 639–665.

(41) García-Amorós, J.; Velasco, D. *Beilstein J. Org. Chem.* **2012**, *8*, 1003–1017.

(42) Andréasson, J.; Pischel, U.; Straight, S. D.; Moore, T. A.; Moore, A. L.; Gust, D. *J. Am. Chem. Soc.* **2011**, *133*, 11641–11648.

(43) Vázquez-Mera, N.; Roscini, C.; Hernando, J.; Ruiz-Molina, D. *Adv. Opt. Mater.* **2013**, *1*, 631–636.

(44) Nigel Corns, S.; Partington, S. M.; Towns, A. D. *Color. Technol.* **2009**, *125*, 249–261.

(45) Jurt, S.; Aemissegger, A.; Güntert, P.; Zerbe, O.; Hilvert, D. *Angew. Chem. Int. Ed.* **2006**, *45*, 6297–6300.

(46) Beharry, A. A.; Woolley, G. A. *Chem. Soc. Rev.* **2011**, *40*, 4422–4437.

(47) Beierle, J. M.; Kistemaker, H. A. V; Velema, W. A.; Feringa, B. L. *Chem. Rev.* **2013**, *113*, 6114–6178.

(48) Hartley, G. S. *Nature* **1937**, *140*, 281–281.

(49) Tomiki, I.; Tsutsumi, O. *Science* **1995**, *268*, 1873–1875.

(50) Dalton, L. R.; Harper, A. W.; Ghosn, R.; Steier, W. H.; Ziarj, M.; Fetterman, H.; Shi, Y.; Mustacich, R. V; Shea, K. J. *Chem. Mater.* **1995**, *7*, 1060–1081.

(51) Merino, E.; Ribagorda, M. *Beilstein J. Org. Chem.* **2012**, *8*, 1071–1090.

(52) Bassotti, E.; Carbone, P.; Credi, A.; Di Stefano, M.; Masiero, S.; Negri, F.; Orlandi, G.; Spada, G. P. *J. Phys. Chem. A* **2006**, *110*, 12385–94.

(53) Bortolus, P.; Monti, S. *J. Phys. Chem.* **1979**, *83*, 648–652.

(54) Tamai, N.; Miyasaka, H. *Chem. Rev.* **2000**, *100*, 1875–1890.

(55) Altoè, P.; Bernardi, F.; Conti, I.; Garavelli, M.; Negri, F.; Orlandi, G. *Theor. Chem. Acc.* **2006**, *117*, 1041–1059.

(56) Bandara, H. M. D.; Burdette, S. C. *Chem. Soc. Rev.* **2012**, *41*, 1809–1825.

(57) Renner, C.; Moroder, L. *ChemBioChem* **2006**, *7*, 868–878.

(58) Merino, E. *Chem. Soc. Rev.* **2011**, *40*, 3835–3853.

(59) Halabieh, R. El; Mermut, O.; Barrett, C. *Pure Appl. Chem.* **2004**, *76*, 1445–1465.

(60) King, N. R.; Whale, E. A.; Davis, F. J.; Gilbert, A.; Mitchell, G. R. *J. Mater. Chem.* **1997**, *7*, 625–630.

(61) Yager, K. G.; Barrett, C. J. *J. Photochem. Photobiol. A Chem.* **2006**, *182*, 250–261.

(62) Hallas, G.; Jalil, M. A. *Dyes and Pigments* **1992**, *20*, 13–23.

(63) Hallas, G.; Jalil, M. A. *Dyes and Pigments* **1996**, *32*, 129–133.

(64) Hallas, G.; Marsden, R.; Hepworth, J. D.; Mason, D. *J. Chem. Soc. Perkin Trans. II* **1984**, 149–153.

(65) Hallas, G.; Marsden, R.; Hepworth, J. D.; Mason, D. *J. Chem. Soc. Perkin Trans. II* **1986**, 123–126.

(66) Wildes, P. D.; Pacifici, J. G.; Irick, G.; Whitten, D. G. *J. Am. Chem. Soc.* **1971**, *1192*, 2004–2008.

(67) Beharry, A. A.; Sadovski, O.; Woolley, G. A. *J. Am. Chem. Soc.* **2011**, *133*, 19684–19687.

(68) Bléger, D.; Schwarz, J.; Brouwer, A. M.; Hecht, S. *J. Am. Chem. Soc.* **2012**, *134*, 20597–20600.

(69) Siewertsen, R.; Neumann, H.; Buchheim-Stehn, B.; Herges, R.; Näther, C.; Renth, F.; Temps, F. *J. Am. Chem. Soc.* **2009**, *131*, 15594–15595.

(70) Gorostiza, P.; Volgraf, M.; Numano, R.; Szobota, S.; Trauner, D.; Isacoff, E. Y. *Proc. Natl. Acad. Sci. U. S. A.* **2007**, *104*, 10865–10870.

(71) Numano, R.; Szobota, S.; Lau, A. Y.; Gorostiza, P.; Volgraf, M.; Roux, B.; Trauner, D.; Isacoff, E. Y. *Proc. Natl. Acad. Sci. U. S. A.* **2009**, *106*, 6814–6819.

(72) Szobota, S.; Gorostiza, P.; Del Bene, F.; Wyart, C.; Fortin, D. L.; Kolstad, K. D.; Tulyathan, O.; Volgraf, M.; Numano, R.; Aaron, H. L.; Scott, E. K.; Kramer, R. H.; Flannery, J.; Baier, H.; Trauner, D.; Isacoff, E. Y. *Neuron* **2007**, *54*, 535–545.

(73) Levitz, J.; Pantoja, C.; Gaub, B.; Janovjak, H.; Reiner, A.; Hoagland, A.; Schoppik, D.; Kane, B.; Stawski, P.; Schier, A. F.; Trauner, D.; Isacoff, E. Y. *Nat. Neurosci.* **2013**, *16*, 507–516.

(74) Yaroslavsky, A. N.; Schulze, P. C.; Yaroslavsky, I. V; Schober, R.; Ulrich, F.; Schwarzmaier, H. J. *Phys. Med. Biol.* **2002**, *47*, 2059–2073.

(75) Kienzler, M. A.; Reiner, A.; Trautman, E.; Yoo, S.; Trauner, D.; Isacoff, E. Y. *J. Am. Chem. Soc.* **2013**, *135*, 17683–17686.

(76) Judkewitz, B.; Roth, A.; Häusser, M. *Neuron* **2006**, *50*, 177–180.

(77) Rickgauer, J. P.; Tank, D. W. *Proc. Natl. Acad. Sci. U. S. A.* **2009**, *106*, 15025–15030.

(78) Andrasfalvy, B. K.; Zemelman, B. V; Tang, J.; Vaziri, A. *Proc. Natl. Acad. Sci. U. S. A.* **2010**, *107*, 11981–11986.

(79) Mohanty, S. K.; Reinscheid, R. K.; Liu, X.; Okamura, N.; Krasieva, T. B.; Berns, M. W. *Biophys. J.* **2008**, *95*, 3916–3926.

(80) Packer, A. M.; Peterka, D. S.; Hirtz, J. J.; Prakash, R.; Deisseroth, K.; Yuste, R. *Nat. Methods* **2012**, *9*, 1202–1205.

(81) Pawlicki, M.; Collins, H. A.; Denning, R. G.; Anderson, H. L. *Angew. Chem. Int. Ed.* **2009**, *48*, 3244–3266.

(82) Bort, G.; Gallavardin, T.; Ogden, D.; Dalko, P. I. *Angew. Chem. Int. Ed.* **2013**, *52*, 4526–4537.

(83) Kim, M. K.; Lim, C. S.; Hong, J. T.; Han, J. H.; Jang, H.-Y.; Kim, H. M.; Cho, B. R. *Angew. Chem. Int. Ed.* **2010**, *49*, 364–367.

(84) Kim, H. M.; Cho, B. R. *Acc. Chem. Res.* **2009**, *42*, 863–872.

(85) Hu, M.; Li, L.; Wu, H.; Su, Y.; Yang, P.-Y.; Uttamchandani, M.; Xu, Q.-H.; Yao, S. Q. *J. Am. Chem. Soc.* **2011**, *133*, 12009–12020.

(86) Andrade, C. D.; Yanez, C. O.; Rodriguez, L.; Belfield, K. D. *J. Org. Chem.* **2010**, *75*, 3975–3982.

(87) Peticolas, L. W.; Goldsborough, J. P.; Rieckhoff, K. E. *Phys. Rev. Lett.* **1963**, 43–45.

(88) Boni, L. De; Jr, J. J. R.; Jr, D. S. S.; Silva, C. H. T. P.; Balogh, D. T.; Jr, O. N. O.; Zilio, S. C.; Misoguti, L.; Mendonça, C. R. *Chem. Phys. Lett.* **2002**, *361*, 209–213.

(89) Andrade, A. A.; Yamaki, S. B.; Misoguti, L.; Zilio, S. C.; Atvars, T. D. Z.; Oliveira, O. N.; Mendonça, C. R. *Opt. Mater.* **2004**, *27*, 441–444.

(90) De Boni, L.; Misoguti, L.; Zílio, S. C.; Mendonça, C. R. *ChemPhysChem* **2005**, *6*, 1121–1125.

(91) Antonov, L.; Kamada, K.; Ohta, K.; Kamounah, F. S. *Phys. Chem. Chem. Phys.* **2003**, *5*, 1193–1197.

(92) Saini, S.; Singh, H.; Bagchi, B. *J. Chem. Sci.* **2006**, *118*, 23–35.

(93) Wu, P.; Brand, L. *Anal. Biochem.* **1994**, *218*, 1–13.

(94) Förster, T. *Ann. Physik* **1948**, *248*, 55–75.

(95) Lakowicz, J. R. *Principles of Fluorescence Spectroscopy*; Springer. New York (USA), 2006.

(96) Venkataramani, S.; Jana, U.; Dommaschk, M.; Sönnichsen, F. D.; Tuczek, F.; Herges, R. *Science* **2011**, *331*, 445–448.

(97) Sakamoto, R.; Kume, S.; Sugimoto, M.; Nishihara, H. *Chem. Eur. J.* **2009**, *15*, 1429–1439.

(98) Jiang, D.; Aida, T. *Nature* **1997**, *388*, 454–456.

(99) Croissant, J.; Chaix, A.; Mongin, O.; Wang, M.; Clément, S.; Raehm, L.; Durand, J.-O.; Hugues, V.; Blanchard-Desce, M.; Maynadier, M.; Gallud, A.; Gary-Bobo, M.; Garcia, M.; Lu, J.; Tamanoi, F.; Ferris, D. P.; Tarn, D.; Zink, J. I. *Small* **2014**, 1–4.

Chapter II

Objectives

Azobenzene-based photoswitches so far used in optochemical genetics require one-photon excitation with UV-vis light to control neural receptors and ion channels. To unleash the full potential of these tools, their photoactivity must be regulated via multiphoton excitation with near-infrared light, which would provide unprecedented 3-D stimulation resolution and penetration depths while minimising biological photodamage. Hence, the aim of this work is to synthesise, characterise and apply *in vitro* for the first time photoswitched tethered ligands devised to modulate neural activity upon two-photon absorption of NIR radiation. As a proof of concept, our attention has focused on the light-control of ionotropic glutamate receptors, which are responsible of most excitatory signalling in the central nervous system.

Because of the low two-photon absorption cross-sections of most azobenzene derivatives, different strategies have been explored to attain this goal, which have given rise to the two main objectives of this work:

- **Objective 1:** Synthesis, characterisation and application *in vitro* of photoswitched tethered ligands for the light-control of ionotropic glutamate receptors via **two-photon sensitised photoisomerisation of their azobenzene switch**. This novel strategy requires the introduction of a photo-harvesting antenna into the system, which will efficiently absorb NIR light via a two-photon process and subsequently transfer its excitation energy to the azoaromatic group to induce its *trans-cis* isomerisation (Figure II-1a). Two different target compounds have been designed to explore this concept:

  (a) Photoswitched tethered ligand **21** (*objective 1a*, Figure II-1b), which mimics the structure of MAG-1, the very first PTL developed to optically control ionotropic glutamate receptors. Consequently, it presents an azobenzene core symmetrically substituted with amido groups at 4 and 4’ positions, a glutamate unit and a cysteine-reactive maleimide moiety. In addition, a pyrene chromophore has been added as two-photon absorber to sensitise azobenzene isomerisation. Pyrene was chosen in this case because of its spectral properties, which should allow efficient resonant energy transfer to the azoaromatic group in MAG-1. In this way, the optimal biological response described for this system is expected to be preserved in new compound **21**. The synthesis and results obtained for this PTL are described in Chapter III.

(b) Photoswitched tethered ligand **22** (*objective 1b*, Figure II-1c), which is also based on a maleimide-azobenzene-glutamate-antenna scheme. In this case, a naphthalene derivative was used as sensitiser owing to its lower hydrophobicity, larger two-photon absorption cross-section and red-shifted emission spectrum with respect to pyrene. Because of the latter, we modified the substitution pattern of the azobenzene core in order to ensure efficient resonance energy transfer between this moiety and the sensitiser. Thus, a *para*-amino group was introduced, which should significantly decrease the stability of the *cis* isomer of the system with respect to MAG-1 and **21**. As such, we expect new compound **22** to act as a single-wavelength photoswitched tethered ligand that rapidly returns to the initial state in the absence of illumination. The synthesis and results obtained for this system are described in Chapter IV.

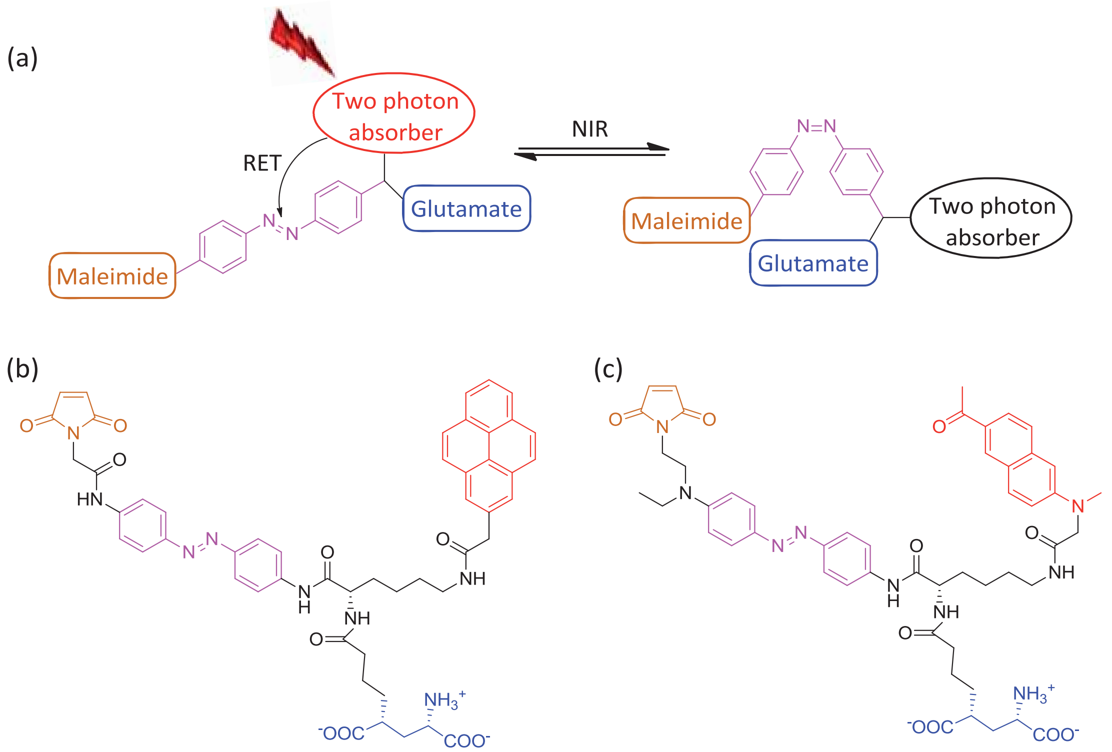

21 **22**

Figure II-1. (a) The two-photon sensitised approach to induce *trans-cis* isomerisation of MAG-type photoswitched tethered ligands with NIR light. Structures target of PTLs (b) **21** and (c) **22** based in this scheme.

- **<u>Objective 2</u>**: Synthesis, characterisation and application *in vitro* of photoswitched tethered ligands for the light-control of ionotropic glutamate receptors via **direct two-photon photoisomerisation of their azobenzene switch** (Figure II-2a). In principle, this strategy is not suitable for symmetrically-substituted azobenzenes, such as that in reference compound MAG-1. Instead, it requires push-pull substitution of the azoaromatic group to enhance the intrinsic two-photon absorption cross-section of the system. To explore whether this design concept can be applied to the optical control of ionotropic glutamate receptors, photoswitched tethered ligand **23** was devised (Figure II-2b). No photo-harvesting antenna is required in this case and, therefore, the target compound only presents maleimide, azobenzene and glutamate groups. To introduce push-pull character into the system, a *para*-amino substituent was introduced into the azobenzene core. As for compound **22**, this should lead to a dramatic decrease of the thermal stability of *cis*-**23**, thus enabling single-wavelength operation of the photoswitch. Because of its structural similarity to **22**, the synthesis and results for this new PTL are given in Chapter IV as well.

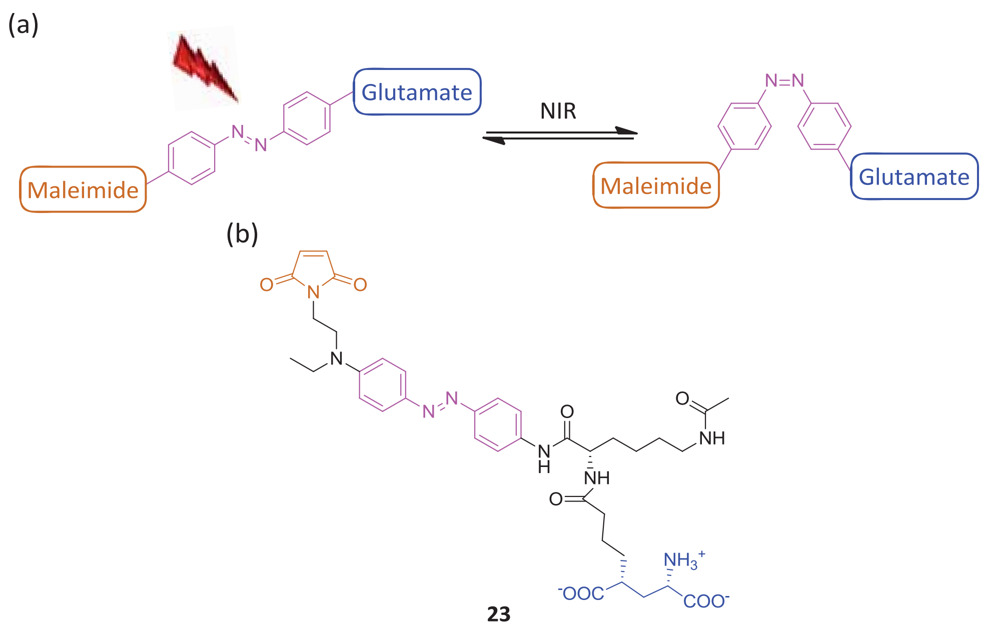

Figure II-2. (a) Direct two-photon photoisomerisation of azobenzene-based photoswitched tethered ligands with NIR light. Structure of target PTL **23** to be synthesised in this work to explore this strategy.

Chapter III

Two-Photon Optical Control of Azobenzene-based Photoswitched Tethered Ligands Using a Pyrene Sensitiser

Herein we describe our initial efforts towards the optical control of the light-gated ionotropic glutamate receptor via sensitised two-photon excitation with NIR light, an approach that requires the use of a photo-harvesting antenna. Our first sensitiser of choice was a pyrene derivative, which was introduced to the well-established MAG-type structure originally developed by Trauner, Isacoff and co-workers. The synthesis, characterisation and biological application *in vitro* of the resulting photoswitched tethered ligand are reported in this chapter.

III.1. INTRODUCTION

In the attempt of preserving the optimal biological behaviour displayed by the photoswitched tethered ligand MAG-1 (see § I.2.2),[1] we took this compound as reference for the design of the new PTLs aiming at two-photon sensitised control of LiGluR. Consequently, our strategy relied on introducing the minimal number of changes required to MAG-1 structure. As a first approach, we therefore decided not to modify the 4,4'-diamido substitution pattern of the azobenzene core of this compound. This had a direct implication in the choice of the photo-harvesting antenna, since its fluorescence emission spectrum should overlap with the $\pi\rightarrow\pi^*$ absorption band of the *trans* isomer of the azoaromatic group, thus enabling selective sensitised *trans*$\rightarrow$*cis* photoisomerisation. Unfortunately, there are only few two-photon fluorophores that emit in the absorption range of *trans*-MAG-1 (λ_{max} ~ 375 nm for its $\pi\rightarrow\pi^*$ transition). Among them, we chose pyrene derivative **24** as photosensitiser because (i) it is commercially available, (ii) it can be easily incorporated to MAG structure via its carboxylic acid moiety, and (iii) it presents rather small dimensions (Figure III-1). The latter is a key issue in our design, since the introduction of bulky sensitisers into the MAG backbone could hinder the ligand-binding site recognition process in LiGluR owing to steric hindrance.

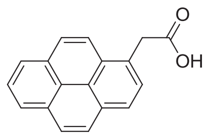

24

Figure III-1. Structure of 2-(pyren-1-yl)acetic acid (**24**), the pyrene derivative used in this chapter as photo-harvesting antenna.

As depicted in Figure III-2, the emission spectrum of pyrene derivative **24** shows bands at λ_{max} = 398, 418 and 438 nm, which correspond to different vibronic transitions of the fundamental electronic transition $S_1 \rightarrow S_0$. These bands largely overlap with the $\pi \rightarrow \pi^*$ absorption band of the *trans*-azobenzene group found in MAG-1, thus ensuring efficient energy transfer upon electronic excitation. Actually, there are several examples in the literature of RET systems for biological applications where pyrene derivatives are used as energy donors;[2,3] to our knowledge, however, none of them exploit azobenzene as energy acceptor.

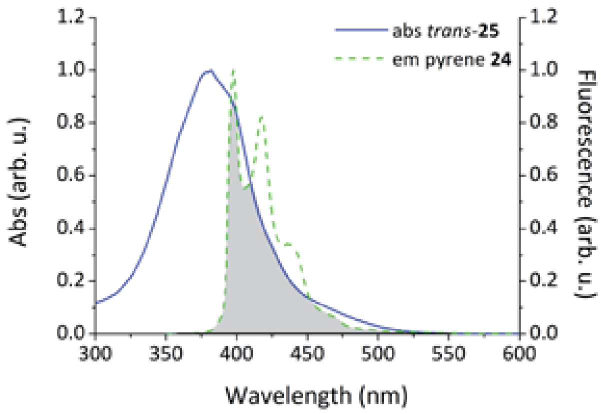

Figure III-2. Spectral overlap in DMSO between the fluorescence emission spectrum of pyrene derivative **24** and the absorbance spectrum of a *trans*-azobenzene group analogous to that found in MAG-1 (compound *trans*-**25** in Figure III-4).

The one-photon absorption spectrum of **24** is shown in Figure III-3a, which displays different vibronic bands at λ_{max} = 315, 329 and 346 nm. Although highly substituted pyrene derivatives can be designed to display very high two-photon absorption cross-sections (Figure III-3b),[4] smaller, mono-alkylated pyrenes such as **24** present moderate to low δ values in the NIR region (δ < 50 GM).[5] Nevertheless, they are often used as two-photon fluorescent probes for labelling cell membranes in confocal fluorescence microscopy studies[5] and it has even been possible to detect them on the single-molecule level upon two-photon excitation.[6] Together with its small size, chemical accessibility and fluorescence spectral properties, this encouraged us to use pyrene derivative **24** as photo-harvesting antenna in the design of the new PTLs.

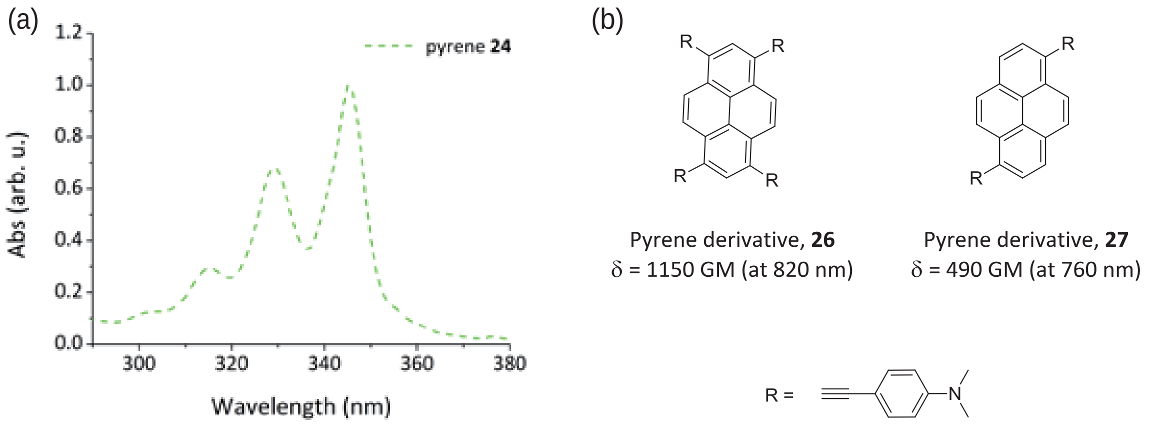

Figure III-3. (a) Absorption spectrum of **24** in DMSO. (b) Highly substituted pyrene derivatives displaying high two-photon absorption cross-sections.[4]

Figure III-4 shows the structure of the photoswitched tethered ligand **21** devised in this work to achieve two-photon optical control of LiGluR by means of a pyrene sensitiser. It is composed of different fragment units, three of which are equivalent to those found in MAG-1 (i.e. maleimide, glutamate and 4,4'-diamidoazobenzene groups). Moreover, it incorporates two additional fragments: (i) pyrene derivative **24** as photo-harvesting antenna; and (ii) L-lysine as central scaffold, to which the different functional units of the target compound would be tethered. The synthesis of **21** is described in the next section. In addition, the preparation of compound **25** is also reported, an analogous azobenzene derivative that will be used as reference in the subsequent optical studies (Figure III-4).

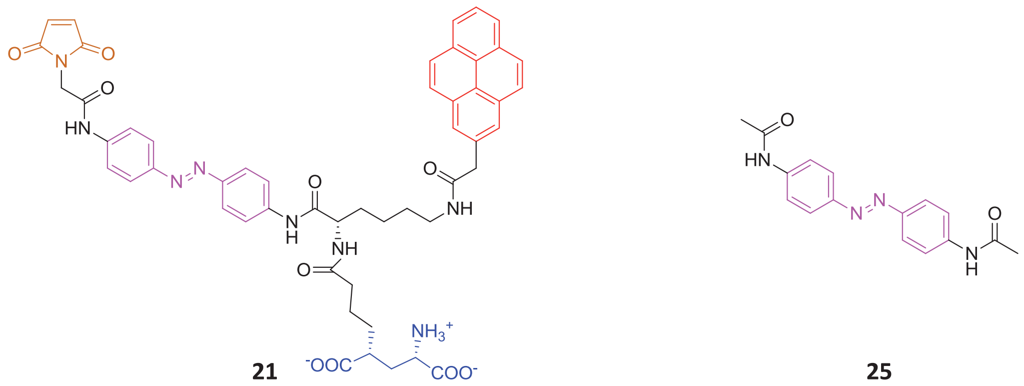

Figure III-4. Structures of target PTL **21** and reference compound **25**. The distinct functional units of these compounds are shown in different colours (blue: glutamate, pink: azobenzene; brown: maleimide; red: pyrene).

III.2. SYNTHESIS OF PHOTOSWITCHED TETHERED LIGAND 21 AND REFERENCE COMPOUND 25

III.2.1. Synthesis of reference compound 25

Because of its simple structure, the first synthetic target of our work was the preparation of reference compound **25**. This was achieved following the diacylation procedure of azobenzene derivative **11** reported by Blevins and Blanchard.[7,8]

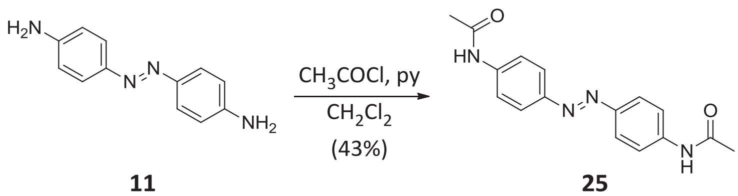

Scheme III-1. Synthesis of compound **25**.

As shown in Scheme III-1, commercially available azobenzene derivative **11** and acetyl chloride were reacted to obtain diamide **25**, using dichloromethane as solvent and pyridine to scavenge the hydrochloric acid formed as by-product. The reaction was carried out under an inert atmosphere to prevent the hydrolysis of the acid chloride and, in this way, diamide **25** was obtained in moderate yield (43%). In the ^{1}H-NMR spectrum of **25**, characteristic singlet signals were observed both for the amide protons (δ 10.27) and the methyl groups (δ 2.09).

III.2.2. Preparation of target compound 21: first approach

Scheme III-2 depicts the synthetic pathway designed for the synthesis of target photoswitch **21**. The synthesis of compound **21** would start with the coupling reaction of azobenzene derivative **11** with orthogonally commercially available *N,N*-diprotected L-lysine (**28**). Such lysine fragment plays a central role in our synthetic approach, since it should allow sequential tethering of the azobenzene, glutamate and maleimide units. Thus, selective removal of the *tert*-butyl carbamate (Boc) protecting group followed by introduction of a glutamate derivative obtained from commercial L-pyroglutamic acid would lead to intermediate **30**. Afterwards, cleavage of the fluorenylmethyl carbamate (Fmoc) protecting group and coupling reaction of the resulting amine with commercially available pyrene **24** would furnish amide **31**. Finally, opening of the glutamate ring moiety, removal of the ethyl ester protecting group and introduction of the maleimide moiety would afford intermediate **32**, whose deprotection would eventually lead to target compound **21**. Next, all these different synthetic steps are described in detail.

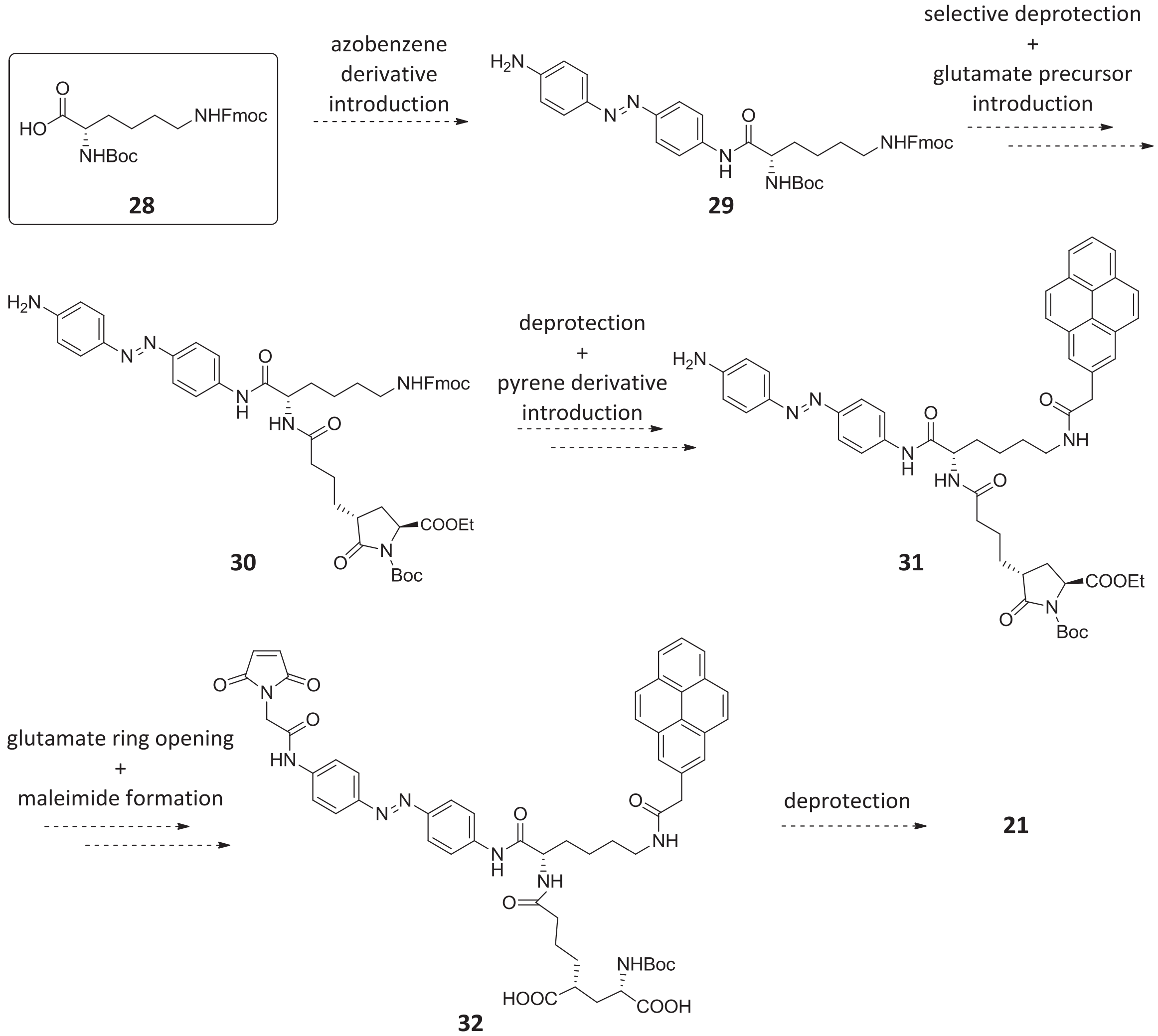

Scheme III-2. Synthetic pathway designed for the preparation of PTL **21**.

III.2.2.1. Coupling reaction between 4,4'-diaminoazobenzene and L-lysine derivative 28

As noted above, our synthetic approach to compound **21** started with the peptide coupling reaction between azobenzene derivative **11** and L-lysine **28**. This type of process has been widely used in this dissertation, as already shown for the preparation of reference compound **25**, where a traditional amine-acyl halide reaction was applied (see § III.2.1). However, many other methods and reagents for peptide coupling have been assayed along this work. Accordingly, some basic concepts on this class of reaction are now overviewed.

In a typical peptide coupling reaction, the carboxylic acid moiety is first activated by an appropriate coupling agent, and then reacted with the amine moiety to produce the desired amide bond (Scheme III-3). This synthetic strategy has been successfully applied to the formation of amides (and also esters bonds) in different molecular contexts beyond peptide synthesis.[9–12]

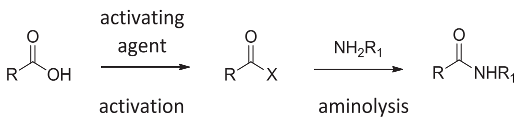

Scheme III-3. Principle of the activation process for amide bond formation.[10]

There is a widespread variety of peptide coupling reagents (phosponium, aminium, immonium, and uronium salts, carbodiimides, etc), some of which are shown in Figure III-5. As the efficiency of these reagents largely depends on the nature of the amine and carboxylic acid precursors, the choice of the coupling agent is determined by them, thus making impossible the existence of a general method for the preparation of amides in good yields.

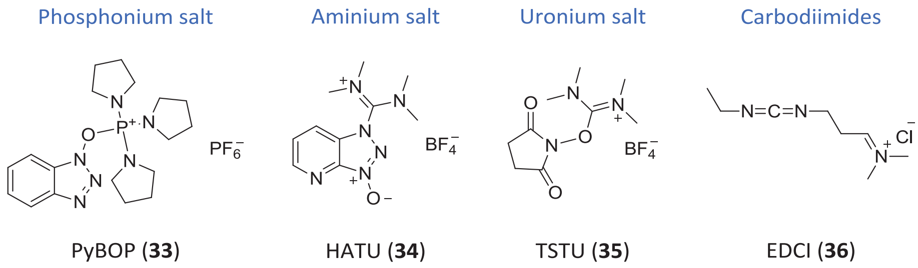

Figure III-5. Representative examples of different kinds of coupling agents for amide bond formation. PyBOP, (Benzotriazol-1-yloxy)tripyrrolidino phosphonium hexafluorophosphate; HATU, *O*-(7-azabenzotriazol-1-yl)-*N*,*N*,*N'*,*N'*-tetramethyluronium hexafluorophosphate; TSTU, *N*,*N*,*N'*,*N'*-tetramethyl-*O*-(*N*-succinimidyl)uronium tetrafluoroborate); and EDCI, *N*-ethyl-*N'*-(3-dimethyldiaminopropyl)-carbodiimide HCl.

Together with coupling agents, other reagents are typically used in peptide coupling reactions. On the one hand, a stable organic base must be added to the reaction medium as proton scavenger. Tertiary amines such as *N*,*N*-diisopropylethylamine (DIPEA, Hünig's Base) and *N*-methylmorpholine (NMM) are normally chosen owing to their non-nucleophilic character. On the other hand, it is often necessary to carry out the amide bond formation in the presence of a so-called additive, whose function is to inhibit side reactions (e.g. undesired racemisation processes) and to enhance the reaction rate. Noteworthy, most additives contain hydroxyl groups that can form active esters by reaction with the acylating moiety resulting from activation of the carboxylic acid with the coupling agent.

Once selected the reagents for the peptide coupling reaction, different strategies can be followed to achieve amide bond formation: (i) the activated form of the carboxylic acid is first generated, isolated and purified, and subsequently reacted with the amine; (ii) the activated acid is formed in a separated step and then reacted with the amine without neither isolation nor purification; and (iii) the acylating agent is generated *in situ* by addition of the coupling agent to a mixture of the carboxylic acid and amine precursors.[10] In the present research work, these three strategies have been employed together with different coupling agents and DIPEA as base. 1-hydroxibenzotriazole (HOBt) has been used as additive when required.

*III.2.2.1.a Preparation of compound **29***

Among all possible strategies, the first step towards the synthesis of target compound **21** was carried out employing EDCI as coupling agent and HOBt as additive.[13] EDCI (**36**) is a carbodiimide commonly employed to prepare amides, esters and acid anhydrides from carboxylic acids because of its moderate activity and affordable price. However, the use of this coupling reagent can often cause partial racemisation of the stereogenic centres in the final product as well as the formation of by-products, being then necessary the addition of an additive (typically, HOBt). The mechanism of action of HOBt is illustrated in Scheme III-4.[9] Firstly, the carboxylic acid reacts with EDCI to form the corresponding *O*-acylurea, which could lead both to the desired compound and to some by-products (i.e. epimerisation or *N*-acylurea). However, if HOBt is added, it rapidly reacts with the *O*-acylurea intermediate to give the OBt activated ester, which presents a higher reactivity as acylating agent by favouring the approach of the amine via hydrogen bonding.

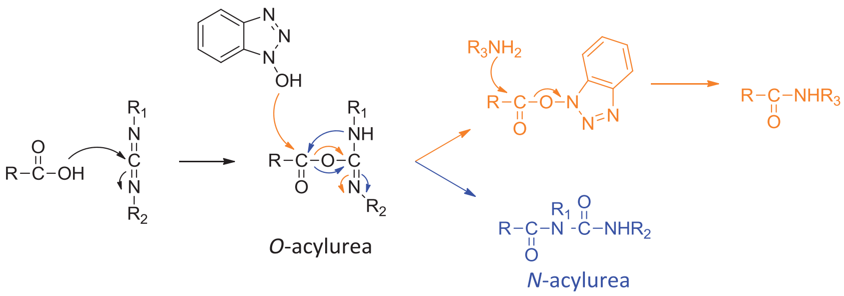

Scheme III-4. Mechanism of amide bond formation using EDCI and HOBt. In blue it is shown one of the undesired by-products that can be formed in absence of HOBt.

Hence, in this work azobenzene derivative **29** was prepared by coupling compound **11** to *N,N*-orthogonally diprotected L-lysine **28** using EDCI and HOBt (Scheme III-5).[14] After 12 h, the crude consisted of a mixture of the starting material and the desired monoacylate **29**. Subsequent purification of the crude by column chromatography afforded amine **29** in 53% yield. In the ^{1}H-NMR spectrum of **29**, the desymmetrisation of the protons of the azobenzene core as well as the appearance of new signals corresponding to the diprotected L-lysine fragment introduced were observed. Similar features were also found in the ^{13}C-NMR spectrum, thus confirming the formation of **29**.

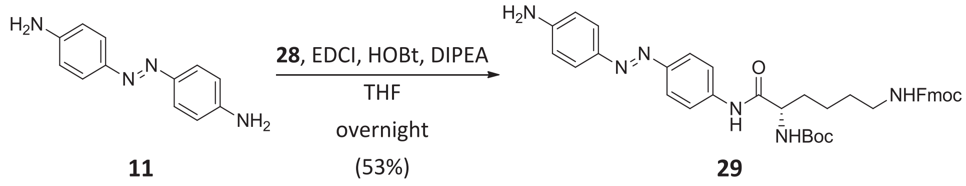

Scheme III-5. Synthesis of compound **29**.

III.2.2.2. Preparation and introduction of glutamate precursor 43. Synthesis of intermediate 30

According to the synthetic pathway proposed, the next step towards the preparation of photoswitched tethered ligand **21** is the introduction of glutamate precursor **43**. This compound was prepared following the sequence of reactions outlined in Scheme III-6.

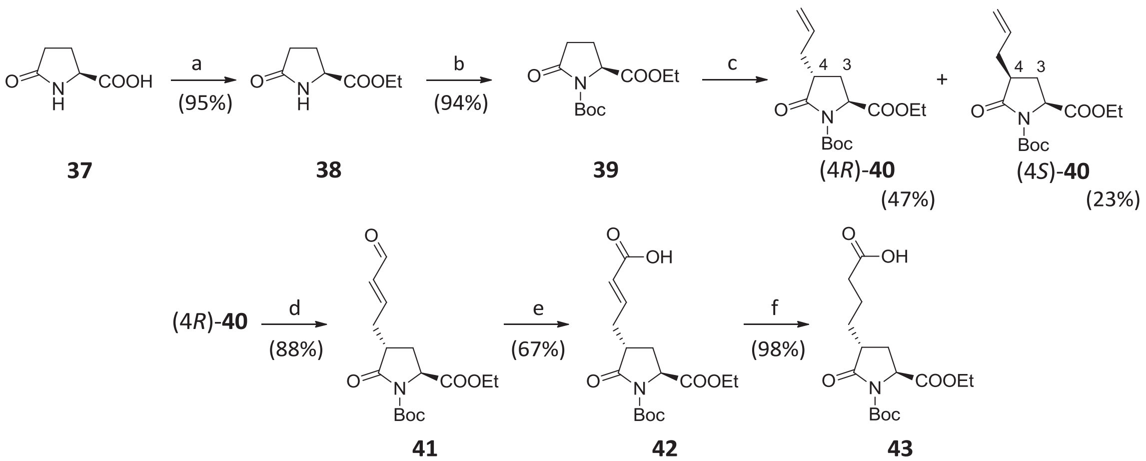

Reagents and conditions: (a) $SOCl_2$, EtOH; (b) Boc_2O, DMAP, CH_3CN; (c) i) LiHMDS, THF; ii) allyl bromide; (d) Hoveyda-Grubbs II, crotonaldehyde, reflux, CH_2Cl_2; (e) $NaClO_2$, NaH_2PO_4, 2-methyl-2-butene, $^tBuOH/H_2O$; (f) H_2, Pd/C (10% w/w), EtOAc.

Scheme III-6. Synthesis of glutamate derivative **43**.

The synthesis of **43** started with the protection of the carboxylic acid group and the nitrogen atom of the lactam moiety of commercially available compound **37** as the corresponding ethyl ester and *tert*-butyl carbamate groups using standard procedures. The resulting protected pyroglutamate **39** was treated with LiHMDS in THF at -78 ºC, and the enolate formed was then reacted with allyl bromide to provide a 2:1 mixture of allyls (4*R*)- and (4*S*)-**40** in 70% yield. The two diastereoisomers were isolated by column chromatography and identified by comparison of the value of the coupling constant between H-4 and H-3 with those found in the literature.[15] Then, the major isomer (4*R*)-**40** was used in a cross-metathesis reaction with crotonaldehyde in reflux of dichloromethane and in the presence of 1% of Hoveyda-Grubbs II catalyst obtaining essentially the *E*-enone **41**.[16] Next, this intermediate was oxidised to the corresponding acid **42** using the Pinnick protocol,[17,18] which was eventually converted into desired glutamate precursor **43** by hydrogenation under palladium catalyst[1] (6 steps, 24% overall yield from L-pyroglutamic acid **37**). The spectral data of the synthesised pyroglutamate **43** matched that reported in the literature.[1]

Then, glutamate precursor **43** was coupled to the azobenzene-lysine intermediate **29**. This first required removal of the *tert*-butyl carbamate protection of this intermediate by treatment with 37% HCl in methanol, which furnished amine **44** as an orange solid in 98% yield (Scheme III-7).[19] Reaction time had to be carefully controlled in this case, because prolonged exposure of this product and precursor **29** (t > 1 h) to the acidic conditions used was found to lead to partial cleavage of their peptide bond. In the ^{1}H-NMR spectrum of **44**, the characteristic singlet signal around 1.60 ppm corresponding to the Boc group cleaved was observed to disappear.

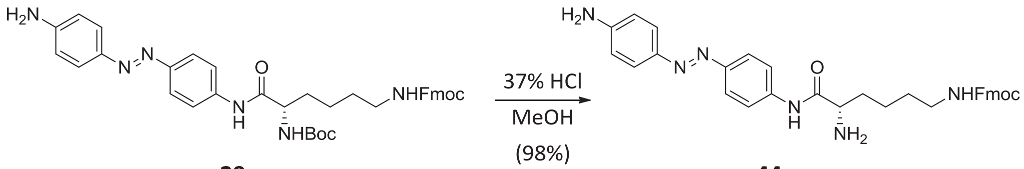

29 **44**

Scheme III-7. Removal of Boc protecting group of **29** under acidic conditions.

In the next step, acid **43** was treated with EDCI, DIPEA and HOBt, and then added over a solution of azobenzene derivative **44** in THF (Scheme III-8). The resulting crude was purified by column chromatography, delivering intermediate **30** in good yield (84%). This was confirmed by analysis of its ^{1}H-NMR and ^{13}C-NMR spectra, where new signals were observed corresponding to the glutamate moiety introduced and H-1^{ii} and C-1^{ii} signals were found to shift downfield and upfield, respectively (H-1^{ii}: from 3.49 ppm in **44** to 4.60 ppm in **30**; C-1^{ii}: from 55.5 ppm in **44** to 54.1 ppm in **30**).

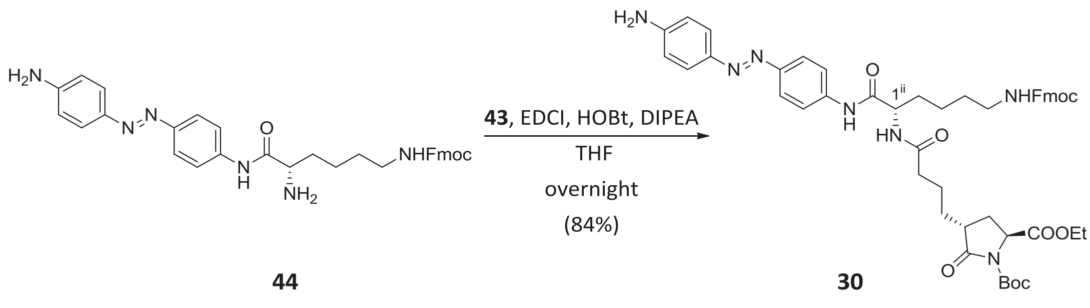

44 **30**

Scheme III-8. Synthesis of compound **30**.

III.2.2.3. Incorporation of the pyrene unit. Preparation of intermediate 31

To achieve the synthesis of intermediate **31**, removal of the Fmoc protecting group of **30** was first required. This was accomplished by treatment with 20% piperidine in DMF at rt for 30 min.[20] Under these conditions, amine **45** was obtained in 87% yield after purification by column chromatography (Scheme III-9). The disappearance of the signals corresponding to the Fmoc group in its ^{1}H-NMR and ^{13}C-NMR spectra confirmed the formation of compound **45**. Furthermore, the upfield shift of H-5^{ii} signal from 3.18 ppm in **30** to 2.84 ppm in **45** was also observed.

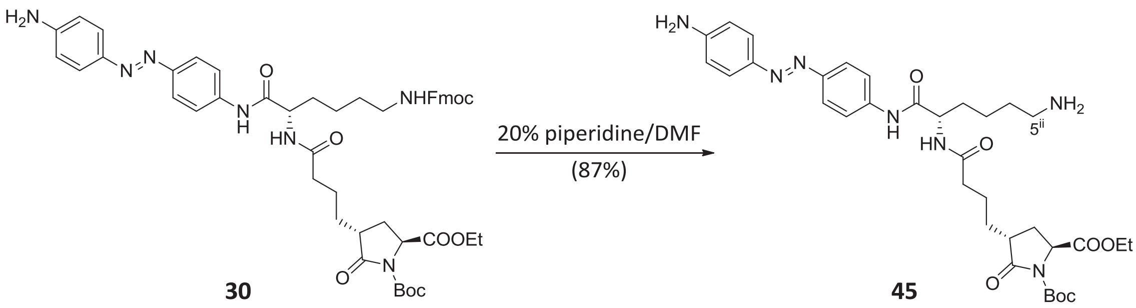

Scheme III-9. Fmoc deprotection of **30** in basic conditions.

Subsequent coupling of commercial pyrene derivative **24** to amine **45** provided advanced intermediate **31**. Similar reaction conditions to those used in previous synthetic steps were applied, although in this case the reaction was carried out without the presence of the HOBt additive (Scheme III-10). The reaction mixture was stirred at rt during 12 h and after subsequent treatment, the crude was purified by column chromatography to isolate product **31** as an orange solid in 76% yield.

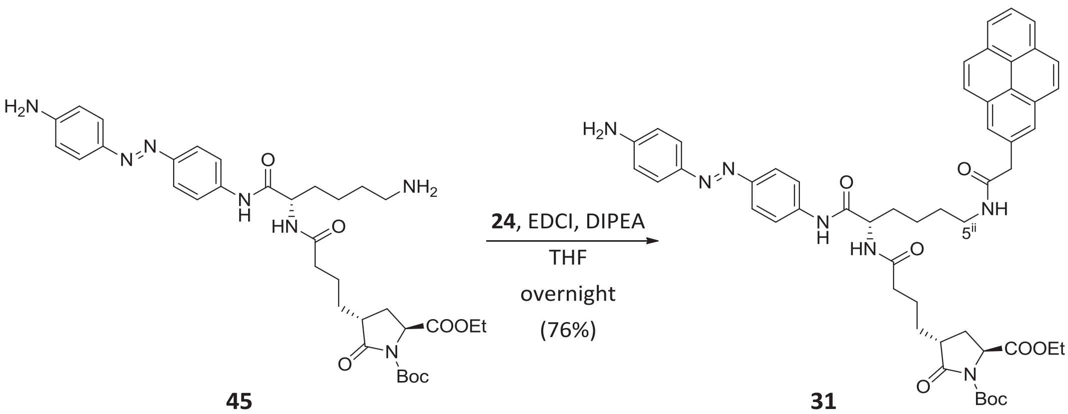

Scheme III-10. Coupling of amine **45** with 2-(pyren-1-yl)acetic (**24**) acid to obtain intermediate **31**.

The introduction of the pyrene group was clearly confirmed by the presence of its distinctive signals in the ^{1}H-NMR (new aromatic signals within the 8.37-7.98 ppm region as well as 1 new aliphatic signal between 4.21-4.08 ppm) and ^{13}C-NMR (16 new aromatic signals between 131.1-123.9 ppm as well as 1 new aliphatic signal at 40.1 ppm) spectra of **31**. In addition, downfield and upfield shifts were observed for H-5^{ii} and C-5^{ii} signals, respectively (H-5^{ii}: from 2.84 ppm in **45** to 3.09 ppm in **31**; C-5^{ii}: from 41.9 ppm in **45** to 38.6 ppm in **31**).

III.2.2.4. Glutamate ring opening. Preparation of compound 46

Next, azobenzene derivative **31** was subjected to glutamate ring opening by exposure to 1 M LiOH in THF/H_2O and subsequent treatment with 1 M HCl (Scheme III-11).[21] The resulting solid was highly insoluble in organic solvents, which made its purification by column chromatography impossible. Instead, **46** was purified by repetitive washing with diethyl ether and finally isolated in 79% yield. The aperture of the glutamate ring was clearly evidenced by the disappearance of the characteristic signals of the ethoxy group in the ^{1}H-NMR spectrum of **46**.

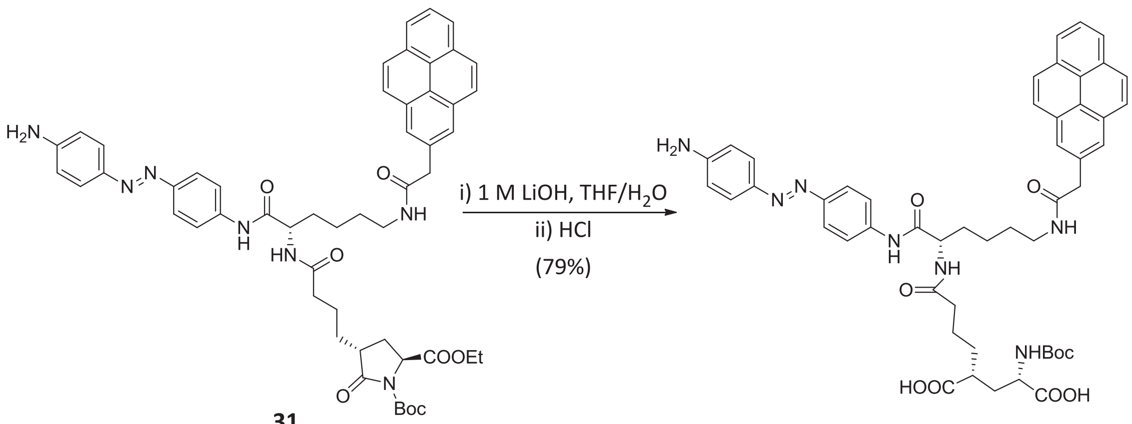

31 **46**

Scheme III-11. Pyroglutamate ring opening to afford **46**.

At this stage, we had already covalently assembled three of the four functional units of the target photoswitched tethered ligand **21**. Our final efforts were therefore devoted to the introduction of the maleimide unit.

III.2.2.5. Introduction of the maleimide moiety. Preparation of compound 21

To culminate the synthesis of target compound **21**, the maleimide moiety had to be incorporated to intermediate **46** and the Boc protecting group of the glutamate fragment had to be finally removed. With this aim, we decided to introduce the maleimide group by joining new fragment **49** to **46**. Compound **49** was synthesised by refluxing an acetic acid solution of commercially available β-alanine (**47**) and maleic anhydride (**48**) following a procedure previously described in the literature (Scheme III-12).[22] After purification by column chromatography, compound **49** was obtained in 45% yield and chemically characterised, with identical results to those already reported.[22]

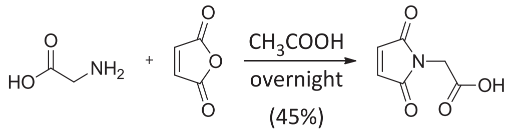

47 **48** **49**

Scheme III-12. Synthesis of compound **49**.

Next, carboxylic acid **49** was activated by formation *in situ* of the corresponding acid chloride upon treatment with oxalyl chloride and DMF in dichloromethane. After 1 h, the solvent was evaporated and the resulting product was added to an ice-cooled mixture of amine **46** and DIPEA in THF (Scheme III-13). The reaction mixture was warmed up slowly to rt and stirred overnight.

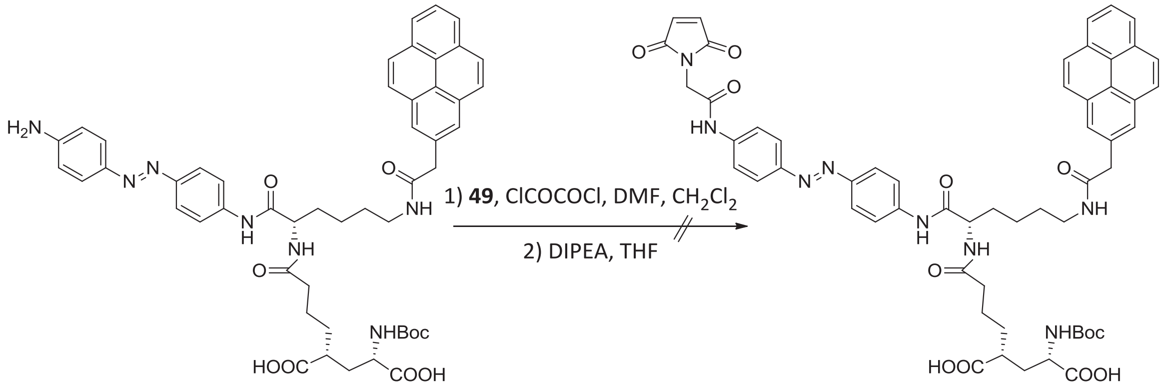

46 **32**

Scheme III-13. First attempted introduction of maleimide moiety to form **32**.

Unfortunately, no reaction was observed to take place by ^{1}H-NMR spectroscopy and starting amine **46** was recovered. This was ascribed to the poor nucleophilic character of the aromatic amine used as well as to the low solubility of the precursor in the reaction medium, which probably arose from the presence of both highly hydrophobic (i.e. pyrene) and hydrophilic (i.e. glutamate) moieties in its structure. As an alternative, we explored the synthetic procedure described by Trauner, Isacoff and co-workers, who applied a two-step protocol to attach the maleimide unit to the azobenzene core (Scheme III-14).[1] Thus, commercially available Fmoc-protected glycine **50** was activated with oxalyl chloride and then added to a solution of amine **46** and DIPEA in THF. However, the formation of amide **51** was not observed by ^{1}H-NMR spectroscopy and the starting material was once again recovered.

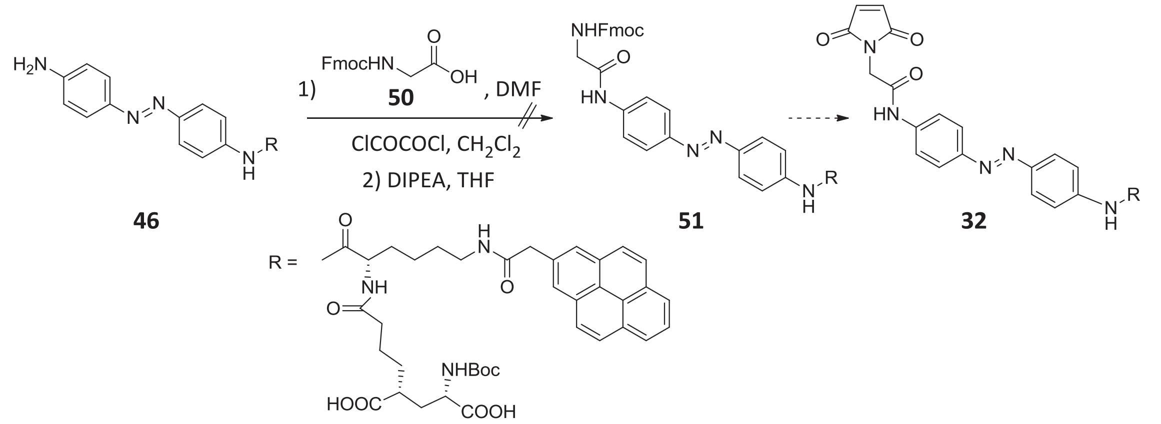

Scheme III-14. Alternative synthetic sequence attempted for the introduction of the maleimide moiety.

In view of these results, we decided to reconsider our synthetic strategy and to introduce the maleimide group into the earlier intermediate **31**, where the pyroglutamate ring had not been opened yet. In this way, we expected to prevent the solubility problems observed when manipulating compound **46**. However, it must be anticipated that this will probably cause some difficulties in the later stages of the synthesis, since the maleimide group introduced might not resist the basic conditions required for glutamate ring opening.[23]

Thus, we decided to apply the same methodology reported by Trauner, Isacoff and co-workers for maleimide introduction into intermediate **31**.[1] Accordingly, the acyl chloride of glycine derivative **50** was generated *in situ* by treatment with oxalyl chloride, then added to a solution of amine **31**, DIPEA and DMAP in THF to form the corresponding amide, and its Fmoc protecting group finally cleaved to furnish product **52** in low yield (36%) (Scheme III-15). In its ^{1}H-NMR spectrum, the most significant changes found with respect to the starting material were the presence of the glycine proton signals (H-2^{vi}) at 3.25 ppm and the downfield shifts observed for H-3^v, H-5^v (from 6.67 ppm in **31** to 7.84 ppm in **52**) and H-2^v, H-6^v (from 7.62 ppm in **31** to 7.84 ppm in **52**).

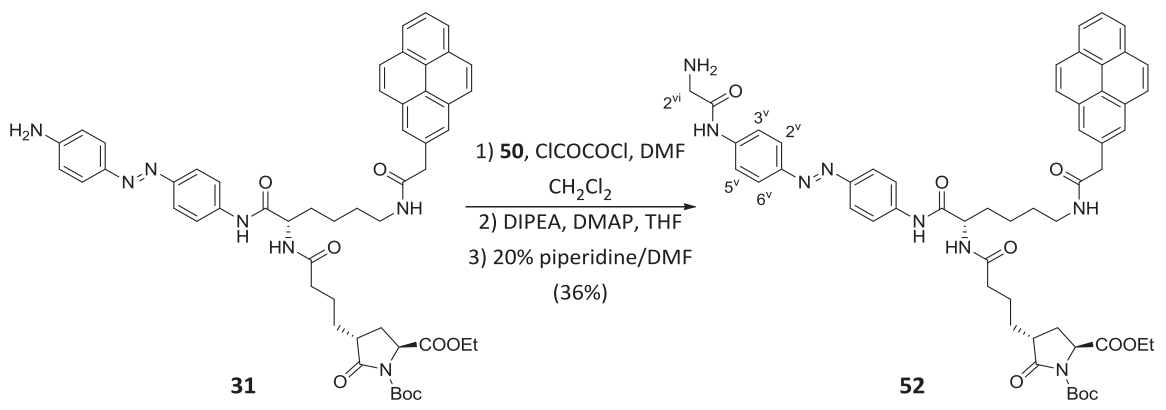

Scheme III-15. Peptide coupling of **31** with glycine derivative **50** followed by removal of its Fmoc protecting group.

To finally introduce the maleimide group, intermediate **52** was treated with a $NaHCO_3$ saturated solution and *N*-methoxycarboxylmaleimide (**53**) (Scheme III-16).[1] Unfortunately, only the starting material was recovered. Alternatively, we explored the possibility of coupling the free amine moiety of **52** to the carboxylic acid of the previously prepared maleimide derivative **49**. With this aim, the acyl chloride of **49** was generated *in situ* by treatment with oxalyl chloride and then added to a solution of **52** in THF. Nevertheless, the signals expected for amide **55** were not observed in the ^{1}H-NMR spectrum of the corresponding reaction mixture, which only showed signals of starting amine **52**.

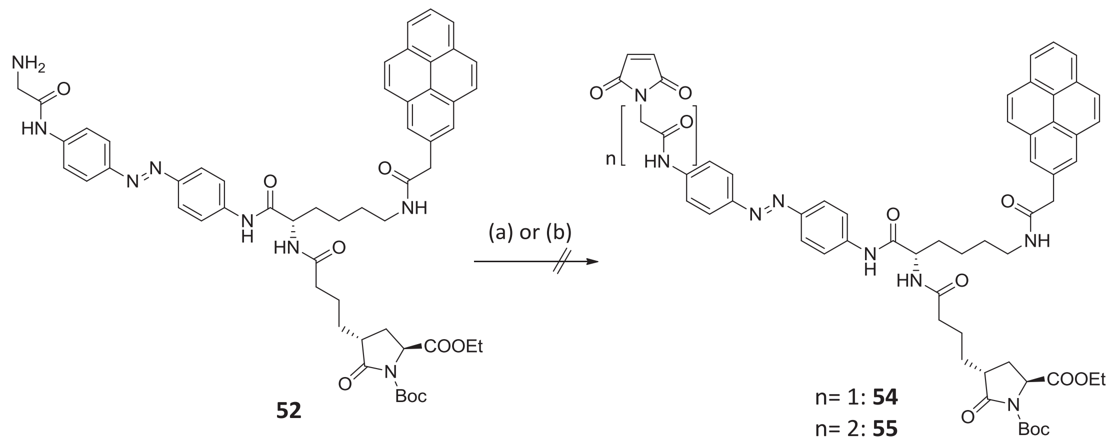

Reagents and conditions: (a) **53**, $NaHCO_3$, THF; (b) **49**, ClCOCOCl, DMF, THF and then DIPEA.

Scheme III-16. Attempted reactions to introduce the maleimide group to intermediate **52**.

After these unsuccessful attempts to introduce the maleimide group, we decided to completely redesign the synthetic pathway to obtain target compound **21**.

III.2.3. Synthesis of target compound 21: second approach

A new strategy to prepare compound **21** was devised to avoid the main obstacles faced in our first synthetic approach, namely: (i) the solubility issues arising from the incorporation of the pyrene fragment and the ring opening of the pyroglutamate group; and (ii) the chemical instability of the maleimide moiety in basic conditions,[23] which requires this group to be the last to be incorporated to the system. With that in mind, our second approach for the preparation of photoswitched tethered ligand **21** was designed to present the following advantages (Scheme III-17):

- The glutamate derivative would be introduced in its open form, thus avoiding the basic conditions needed for the ring opening of pyroglutamate.

- The amine and carboxylic acid moieties of the new glutamate precursor used in the synthesis would be protected with groups that can be cleaved under acidic conditions, at which the maleimide unit is expected to be stable. Therefore, the cleavage of such protecting groups could take place in the last step of the synthesis, which allowed us to prevent the solubility problems related to the presence of free carboxylate/carboxylic acid moieties in advanced synthetic intermediates.
- The introduction of the pyrene fragment would be postponed to the later stages of the synthetic sequence in a further attempt to avoid solubility issues.

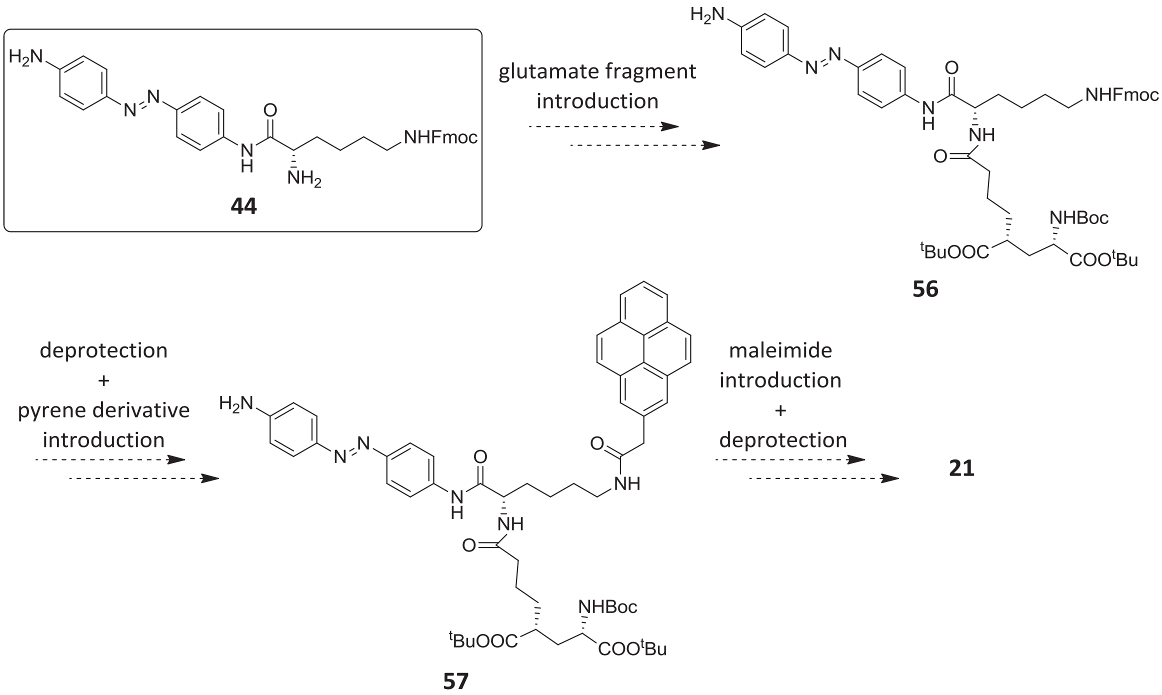

Scheme III-17. Alternative synthetic pathway designed to prepare the PTL **21**.

As shown in Scheme III-17, our new synthetic strategy would start from intermediate **44** of the previous approach, which bears the azobenzene core and the *N*,*N*-diprotected L-lysine fragment. In a first step, this compound would be assembled to a new fully protected glutamate derivative to deliver **56**. Then, the Fmoc group of **56** would be removed to enable the peptide coupling reaction with the pyrene derivative to yield amide **57**. Finally, introduction of the maleimide moiety followed by acid removal of the *tert*-butyl carbamate and *tert*-butyl ester protections of the glutamate unit would afford target compound **21**.

III.2.3.1. Preparation and introduction of glutamate derivative 65. Synthesis of compound 56

Our research group has recently developed a multistep synthetic sequence to obtain the new open glutamate derivative **65** (Scheme III-18).[24] This synthetic route is partially based on the procedure previously described for the synthesis of cyclic glutamate fragment **43**. However, with respect to such cyclic group, compound **65** provides a more robust and versatile way to introduce glutamate moieties in the synthesis of MAG derivatives.

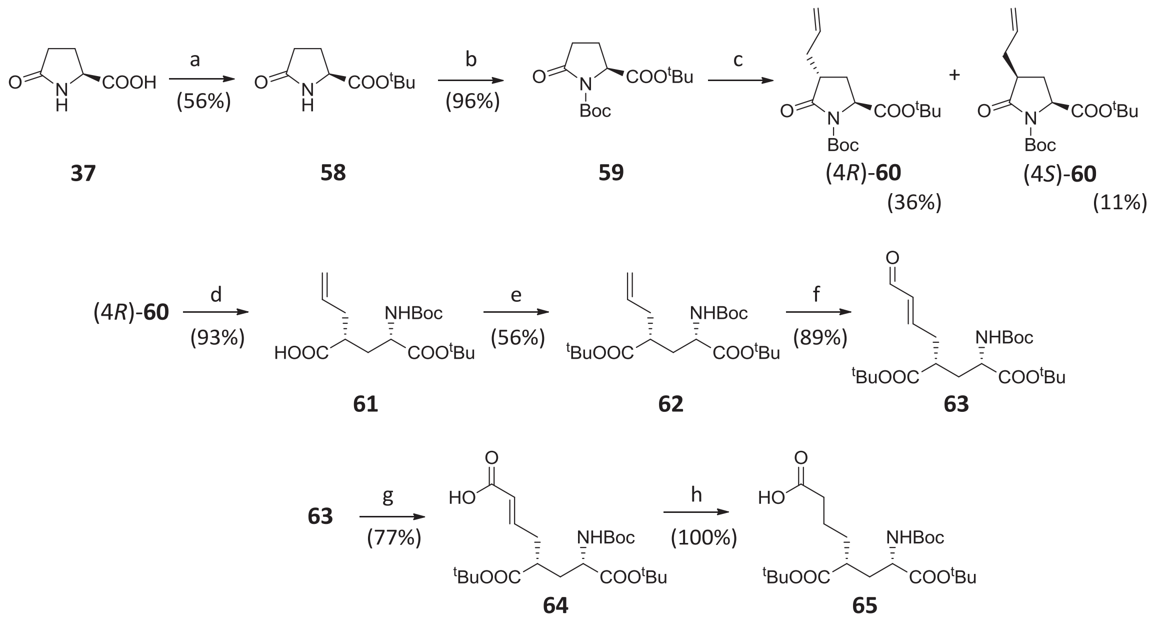

Reagents and conditions: (a) H_2SO_4, ^tBuOAc; (b) Boc_2O, DMAP, CH_3CN; (c) i) LiHMDS, THF; ii) allyl bromide; (d) i) 1 M LiOH, THF/H_2O; ii) 1 M HCl; (e) *tert*-butyl 2,2,2-trichloroacetimidate, $BF_3{\cdot}OEt_2$, CH_2Cl_2; (f) Hoveyda-Grubbs II, crotonaldehyde, reflux, CH_2Cl_2; (g) $NaClO_2$, NaH_2PO_4, 2-methyl-2-butene, $^tBuOH/H_2O$; (h) H_2, Pd/C (10% w/w), EtOAc.

Scheme III-18. Synthesis of new fully protected glutamate derivative **65.**

The synthetic sequence towards compound **65** started from L-pyroglutamic acid (**37**), whose carboxylic acid group and the nitrogen atom of the lactam moiety were first protected using standard procedures as *tert*-butyl ester and *tert*-butyl carbamate groups, respectively. The protected pyroglutamate **59** was treated with LiHMDS in THF at -78 ºC, and the enolate formed was then reacted with allyl bromide to provide a 3:1 mixture of allyls (4*R*)- and (4*S*)-**60** in 47% yield. The configuration assignment of these two diastereisomers was performed by NMR comparison with the values found in the literature.[25] Next, ring opening of the major isomer (4*R*)-**60** was carried out by treatment with LiOH, which furnished carboxylic acid **61** after subsequent acidification with 5% HCl.[21] Further *tert*-butyl protection of the carboxylic acid of this compound led to glutamate derivative **62**,[26] which was submitted to a cross-metathesis reaction with crotonaldehyde in reflux of dichloromethane and in the presence of 1% of Hoveyda-Grubbs II catalyst. *E*-enone **63** was obtained in good yield from this reaction, and it was then oxidised to the corresponding carboxylic acid **64** using the Pinnick protocol. This intermediate was eventually converted into the desired glutamate derivative **65** by hydrogenation under palladium catalyst (8 steps, 7% overall yield from L-pyroglutamic acid (**37**)).

Once prepared, carboxylic acid **65** was coupled to amine **44** to obtain intermediate **56** applying the same conditions previously established for the synthesis of compound **29** (Scheme III-19). After 12 h of reaction and purification by column chromatography, product **56** was obtained in 88% yield. New signals corresponding to the glutamate fragment introduced were observed in the ^{1}H-NMR and ^{13}C-NMR spectra of this compound. In addition, the downfield shift of H-1^{ii} NMR signal from 3.49 ppm in **44** to 4.56 ppm in **56** was also observed.

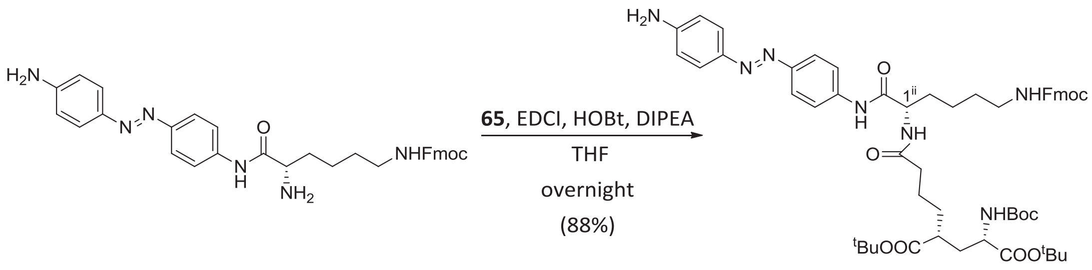

44 **56**

Scheme III-19. Peptide coupling for the synthesis of compound **56**.

III.2.3.2. Incorporation of the pyrene unit. Preparation of compound 57

The next transformation of our synthetic route was to remove the Fmoc protecting group of intermediate **56**. Thus, compound **56** was treated with 20% piperidine in DMF affording amine **66** in 76% yield after purification by column chromatography (Scheme III-20). Deprotection of the amino group was clearly evidenced by the ^{1}H-NMR spectrum of **66**, which shows the disappearance of the characteristic aromatic Fmoc signals as well as the upfield shift of H-5^{ii} signal from 3.22 ppm to 2.82 ppm.

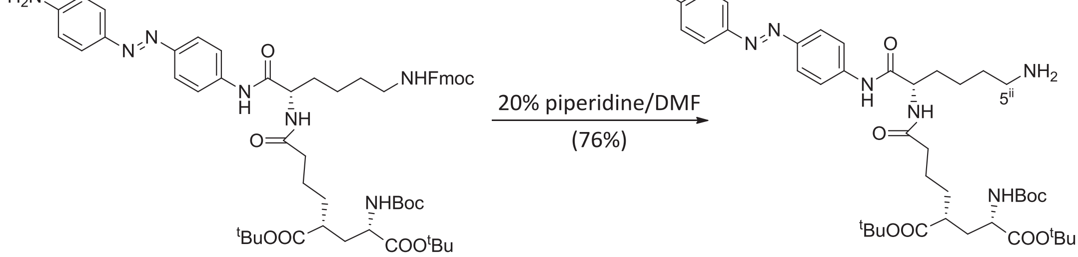

56 **66**

Scheme III-20. Fmoc deprotection of **56** in basic conditions.

To carry out the coupling reaction between 2-(pyren-1-yl)acetic acid and amine **66**, we applied the same methodology previously used for the synthesis of analogous compound **29** (Scheme III-21). Under the above conditions and subsequent purification by column chromatography, product **57** was obtained in 84% yield. The incorporation of the pyrene fragment was confirmed by the new aromatic (δ 8.37-7.99) and aliphatic signals (δ 4.17) found in the ^{1}H-NMR spectrum.

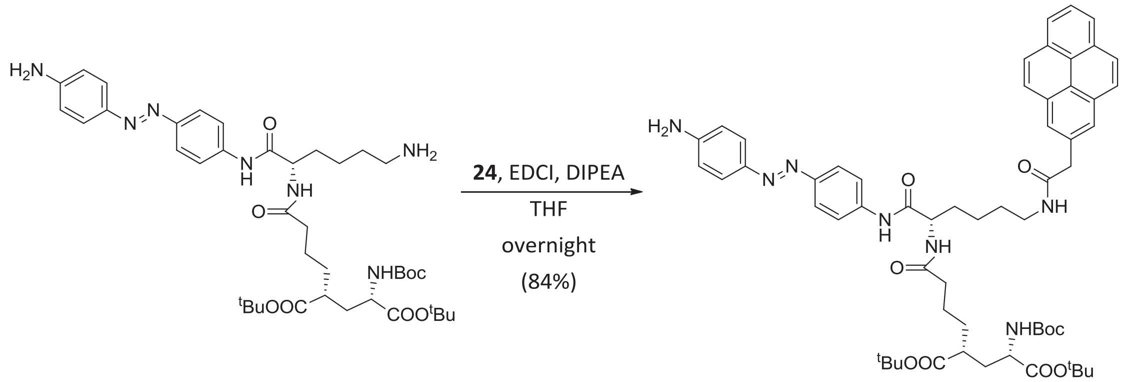

66 **57**

Scheme III-21. Preparation of compound **57**.

At this point we had prepared an advanced intermediate containing three of the four functional units of the target compound, which closely resembles compound **46** from our first synthetic approach (see § III.2.2.4). However, two main important differences must be noted. First, the glutamate derivative in **57** was introduced in its open form and it presents fully protected carboxylic acid groups, thus facilitating the subsequent coupling reaction with the maleimide unit. Second, the pyrene moiety was incorporated in a later stage of the synthesis, with which we pretended to minimise the manipulation and purification problems arising from the low solubility of this fragment in most organic solvents.

III.2.3.3. Introduction of the maleimide moiety. Preparation of target compound 21

In order to introduce the maleimide fragment into intermediate **57**, we followed one of the two strategies already attempted in our previous synthetic approach. This strategy made use of maleimide derivative **49** (see § III.2.2.5), which was activated by treatment with oxalyl chloride in dichloromethane and then added onto an ice-cooled solution of amine **57** and DIPEA in THF (Scheme III-22). After 4 h of reaction, the desired amide product **67** was isolated in 74% yield after purification by column chromatography. This was clearly evidenced by the appearance of two new singlet signals at 7.16 ppm and 4.33 ppm in the ^{1}H-NMR spectrum of **67**, which correspond to the olefinic (H-3^{vii} and H-4^{vii}) and methylene (H-2^{vi}) protons of the assembled maleimide moiety, respectively.

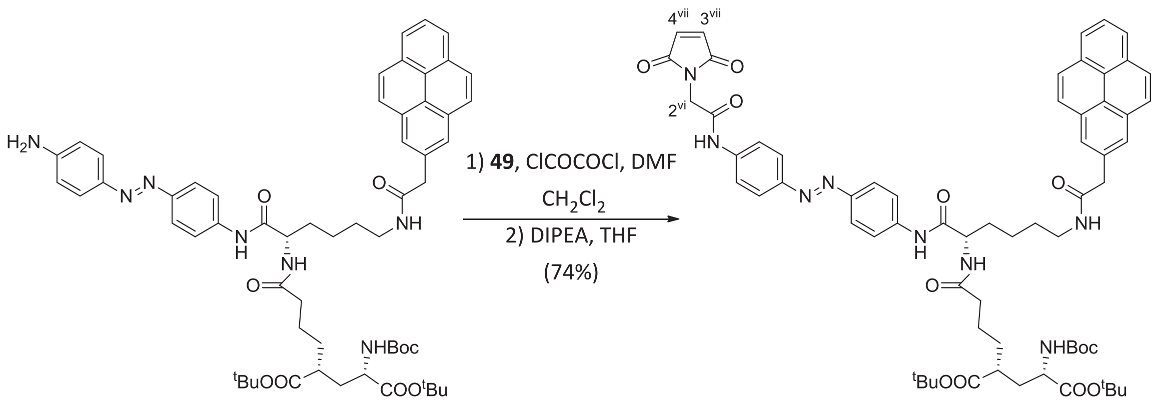

57 **67**

Scheme III-22. Synthesis of **67** via coupling with the acyl chloride of **49**.

The final step of the synthesis consisted in the removal of both the *tert*-butyl carbamate and *tert*-butyl ester protecting groups of the glutamate moiety. This was carried out in a one-step process by exposure of product **67** to a 1:2 mixture of trifluoroacetic acid (TFA) and dichloromethane, which finally afforded a lilac solid in 79% yield that was unambiguously identified as target compound **21** from its spectroscopic data (Scheme III-23). Thus, the ^{1}H-NMR signal of the *tert*-butyl groups at 1.50 ppm disappeared from the spectrum of **21**. In addition, downfield shifts were observed for H-1 and H-3 NMR signals (H-1: from 3.76 ppm in **67** to 4.19 ppm in **21**; H-3: from 2.31 ppm in **67** to 2.68 ppm in **21**).

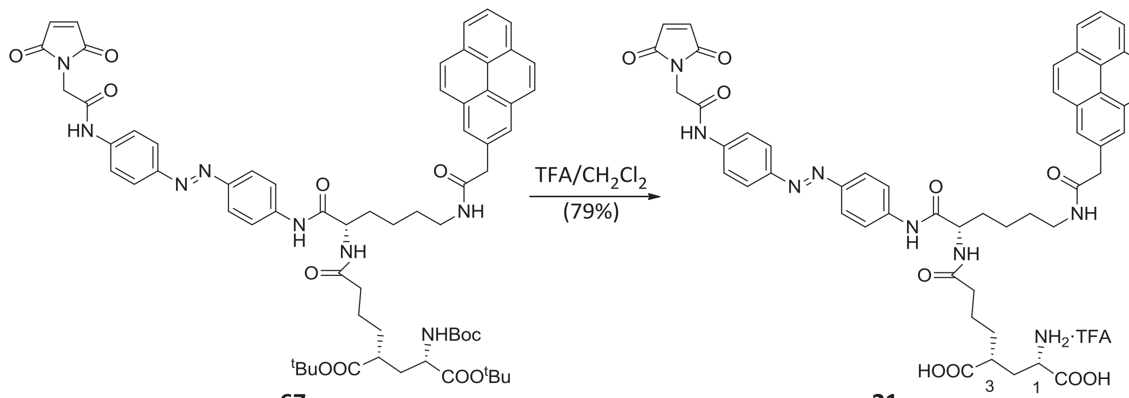

67 **21**

Scheme III-23. Final synthetic step of the preparation of PTL **21**.

In summary, a new MAG derivative with potential activity as two-photon NIR-responsive photoswitched tethered ligand was prepared through a modular 7-step convergent synthesis from *N,N*-diprotected L-lysine **28** in 17% overall yield. Our synthetic approach relied on the sequential introduction of the different functional fragments to this lysine scaffold: azobenzene core **11**, glutamate derivative **65**, which was prepared in 8 steps and 7% global yield from L-pyroglutamic acid (**37**), 2-(pyren-1-yl)acetic acid (**24**) and maleimide derivative **49**, which was obtained from maleic anhydride in 1 step and 45% yield.

III.3. PHOTOCHEMICAL CHARACTERISATION OF PHOTOSWITCHED TETHERED LIGAND 21

As depicted in Scheme III-24, both target ligand **21** and reference compound **25** are azobenzene-based switches that should present two states with different structural and physico-chemical properties resulting from reversible photoinduced *trans-cis* isomerisation upon direct excitation of their azoaromatic units. Furthermore, sensitised isomerisation is also expected for compound **21** by irradiation of its pyrene photo-harvesting antenna and subsequent resonance energy transfer towards its azobenzene group. Once synthesised and chemical characterised, we therefore focused our attention on the investigation of the photochemical behaviour in solution of potential molecular switch **21**, eventually aiming to demonstrate the pyrene-sensitised pathway for the *trans-cis* photoisomerisation of this compound. Since a NIR tunable pulsed laser is not available in our laboratories, it must be noted that our photochemical study has only been conducted under one-photon excitation conditions. Two-photon experiments with near-infrared light irradiation will only be carried out on biological samples.

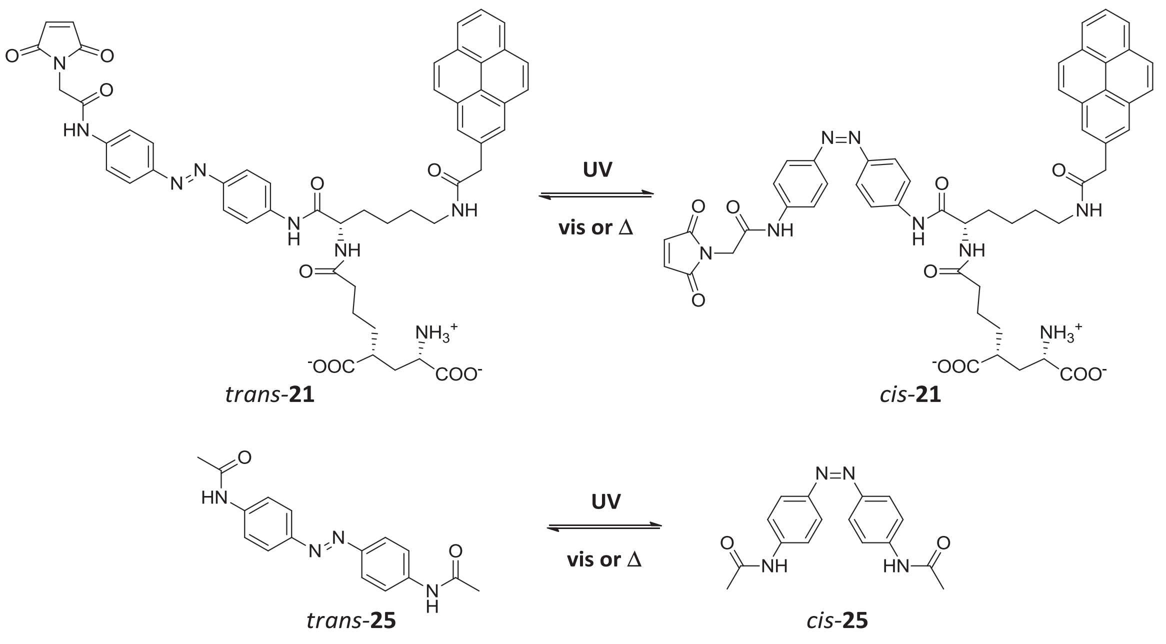

Scheme III-24. Photoinduced *trans-cis* isomerisation of PTL **21** and reference compound **25** upon one-photon excitation with UV-vis light. *Cis*→*trans* back isomerisation can also take place thermally.

III.3.1. Absorption and fluorescence spectra

To start with, the absorption and fluorescence properties of the thermally stable *trans* isomer of target ligand **21** were investigated. Figure III-6 displays the absorption spectrum of this compound in DMSO, which is compared to those of their constitutive chromophore units: reference azobenzene derivative **25** and pyrene derivative **24**.

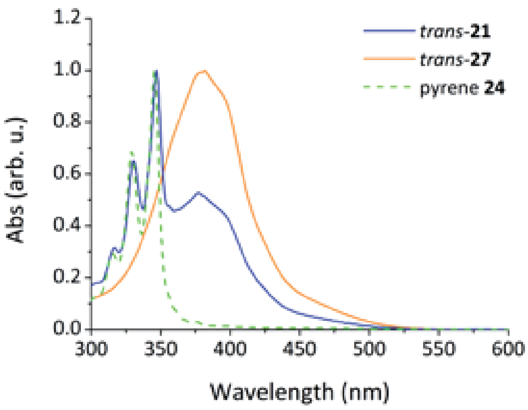

Figure III-6. Normalised absorption spectra of compounds **21**, **25** and pyrene derivative **24** in DMSO. Measurements were carried out at low concentrations ($c \sim 10^{-5}$ M) to minimise aggregation processes driven by π-stacking of the pyrene units.

The absorption spectrum of pyrene shows peaks at λ_{max} = 314, 328 and 345 nm corresponding to different vibronic bands of its $S_0 \rightarrow S_1$ electronic transition. Regarding to reference compound *trans*-**25**, it displays a broad spectrum arising from the partial overlap of its $\pi \rightarrow \pi^*$ (λ_{max} = 381 nm) and $n \rightarrow \pi^*$ (λ > 450 nm) absorption bands. Clearly, the absorption spectrum of compound *trans*-**21** is indeed similar to those of its constituent units, since it both presents the narrow and broad absorption bands arising from its pyrene and azobenzene groups, respectively. This demonstrates that these units are not electronically coupled in the ground state of **21**.

Figure III-7 shows the fluorescence spectra and fluorescence quantum yield (Φ_{Fl}) of *trans*-**21** and pyrene derivative **24** in DMSO. The emission spectra of these two compounds present similar shapes and they display distinct vibronic bands corresponding to their fundamental $S_1 \rightarrow S_0$ electronic transition (for pyrene **24**, at λ_{max} = 383, 401 and 423 nm). However, a dramatic difference is observed in emission intensity. While pyrene derivative has a rather high fluorescence quantum yield in DMSO (Φ_{Fl} = 0.30), a ~ 43 fold decrease is observed for *trans*-**21** (Φ_{Fl} = 0.007). This point towards the occurrence of efficient resonance energy transfer processes from the photoexcited pyrene group to the azobenzene moiety of *trans*-**21**, which would therefore result in fluorescence quenching. As discussed above, such RET processes are crucial for the photosensitised isomerisation of **21** to take place, a process that will be investigated in detail in section § III.3.3.

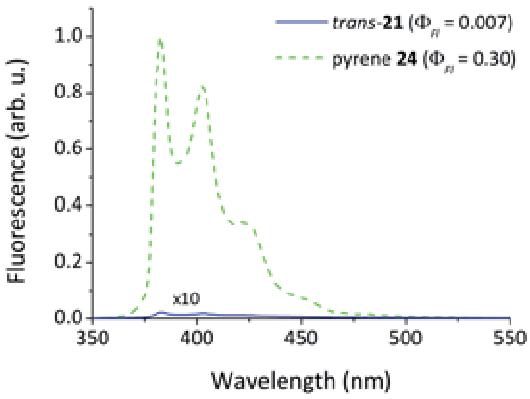

Figure III-7. Fluorescence emission spectra of *trans*-**21** and pyrene derivative **24** in DMSO at λ_{exc} = 320 nm and λ_{exc} = 305 nm, respectively. All emission spectra were normalised relative to the absorption at the excitation wavelength. Measurements were carried out at low concentrations ($c \sim 10^{-7}$ M) to minimise aggregation processes driven by π-stacking of the pyrene units.

III.3.2. Direct *trans-cis* photoisomerisation

As discussed in Chapter I, azobenzene derivatives can undergo *trans*→*cis* isomerisation upon irradiation of the $\pi\rightarrow\pi^*$ absorption band of the *trans* isomer, while this process can be reverted back by photoexcitation of the $n\rightarrow\pi^*$ absorption transition of the *cis* isomer with visible light.[27] Moreover, the thermal instability of the *cis* isomer results in spontaneous back isomerisation to the more stable *trans* state, a thermally induced process whose kinetics depends on the substitution pattern of the azobenzene core.[27] All these photo- and thermally driven processes have been investigated in detail for target ligand **21** and reference compound **25**.

III.3.2.1. *Trans*→*cis* photoisomerisation

As commented earlier, *trans*-azobenzene derivatives present a very intense $\pi\rightarrow\pi^*$ absorption band in the UV or blue region of the spectrum and a much weaker $n\rightarrow\pi^*$ absorption band in the blue-green region of the visible spectrum. On the other hand, the absorption spectrum of the corresponding *cis* isomer displays two noticeable differences: (i) hypsochromical shift and intensity decrease of the $\pi\rightarrow\pi^*$ electronic transition band, which are ascribed to the loss of planarity of the azobenzene moiety; and (ii) a slight increase of the $n\rightarrow\pi^*$ transition absorption band. As a consequence, the *trans*-*cis* photoisomerisation reaction of azobenzenes can be monitored in a straightforward manner by means of UV-vis absorption measurements. In this way, the typical spectral features accounting for *trans*→*cis* photoisomerisation could be observed when irradiating compounds *trans*-**21** and *trans*-**25** at 365 nm in DMSO, an excitation wavelength that lies close to the maximum of their $\pi \rightarrow \pi^*$ absorption bands (Figure III-8). Thus, a clear decrease of their broad $\pi \rightarrow \pi^*$ band at $\lambda_{max} \sim 380$ nm was observed in both cases, while a slight increase of the $n \rightarrow \pi^*$ absorption band was found at $\lambda > 470$ nm. On the contrary, the narrow pyrene absorption bands of compound **21** did not suffer an appreciable change upon irradiation, thus indicating that this group is not affected by the azobenzene photoisomerisation process.

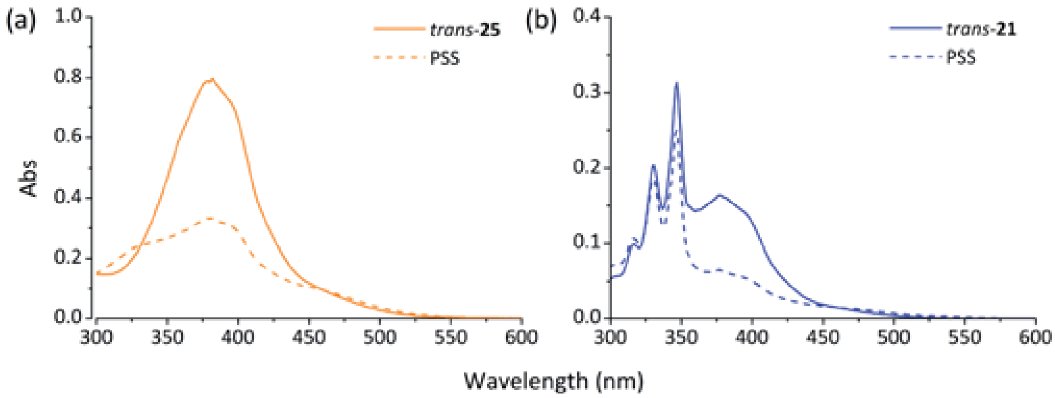

Figure III-8. (a) Absorption spectra of *trans*-**25** and the PSS mixture obtained upon irradiation at 365 nm in DMSO. (b) Absorption spectra of *trans*-**21** and the PSS mixture obtained upon irradiation at 365 nm in DMSO.

As commented in Chapter I, *trans*→*cis* photoconversion of azobenzene derivatives is not quantitative due to the competition with both photo- and thermally induced *cis*→*trans* back isomerisation. Instead, a photostationary state is reached after a certain irradiation time. This was observed both for compounds **21** and **25**, as shown in Figure III-8. From ^{1}H-NMR analysis of the PSS mixtures obtained in DMSO-d_6, the following compositions were determined for the photostationary states: 65% of *cis*-**21** and 35% of *trans*-**21**, and 63% of *cis*-**25** and 37% of *trans*-**25** (Table III-1). Clearly, similar results were obtained for both azobenzene-based switches, which reveal that their direct *trans*→*cis* photoisomerisation is not affected by the introduction of a pyrene photosensitiser and bulkier substituents into the azobenzene core of target ligand **21**. This was further demonstrated by determining the *trans*→*cis* photoisomerisation quantum yields ($\Phi_{trans \rightarrow cis}$) of **21** and **25**, for which we used both spectroscopic and ^{1}H-NMR data and compared the experimental behaviour of these compounds with that of azobenzene (**11**) ($\Phi_{trans \rightarrow cis} = 0.15$ in acetonitrile)[28] as reference. As shown in Table III-1, equal $\Phi_{trans \rightarrow cis}$ were obtained for photoswitches **21** and **25**, thus confirming the equivalent *trans*→*cis* photoisomerisation properties of their azobenzene moieties.

Table III-1. PSS conversions and *trans*→*cis* photoisomerisation quantum yields of compounds **21** and **25**.[a]

Compound	^{cis}PSS (%)[b]	$\Phi_{trans\rightarrow cis}$
21	65	0.28[c]
25	63	0.28[d]

(a) Values determined in DMSO at 25 ºC. (b) λ_{exc} = 365 nm. (c) λ_{exc} = 380 nm. (d) λ_{exc} = 340 nm.

III.3.2.2. *Cis*→*trans* isomerisation

Cis→*trans* back isomerisation of compounds *cis*-**21** and *cis*-**25** was observed to occur both photochemically and thermally. Thus, irradiation of the n-π* absorption band of these species with blue light resulted in nearly quantitative conversion to their *trans* isomers, as observed for most azobenzene derivatives. The corresponding *cis*→*trans* photoisomerisation quantum yields were also measured, obtaining identical results for both compounds ($\Phi_{cis\rightarrow trans}$ = 0.03, Table III-2). Although this value is significantly lower than those measured for other azobenzene-type derivatives,[28] the similar behaviour observed for both *cis*-**21** and *cis*-**25** evidences that the direct *cis*→*trans* photoisomerisation of these compounds is negligibly influenced by the different size of the amide substituents of their azobenzene groups.

Table III-2. Parameters of the photoinduced and thermal *cis*→*trans* isomerisation of compounds **21** and **25**.[a]

Compound	$\Phi_{cis\rightarrow trans}$[b]	$k_{cis\rightarrow trans}$ (s^{-1})[c]	$t_{1/2}^{cis}$ (h)[c]
21	0.03	3.2 x 10^{-5}	6.0
25	0.03	4.1 x 10^{-5}	4.6

(a) Values determined in DMSO at 25 ºC. (b) $\Phi_{cis\rightarrow trans}$ values measured under excitation at 473 nm. Determined using azobenzene (**11**) ($\Phi_{cis\rightarrow trans}$ = 0.35 in acetonitrile)[28] as reference. (c) Thermal *cis*→*trans* isomerisation rate constants and *cis* isomer half-lives determined from monoexponential fits of the experimental data.

Concerning the thermal *cis*→*trans* isomerisation process, it was investigated by monitoring the spectral changes of a photoinduced mixture of the *trans* and *cis* isomers of **21** and **25** over time in the dark by UV-vis absorption spectroscopy. As shown in Figure III-9a and b, the intensity of the $\pi\rightarrow\pi^*$ absorption band of *trans*-**21** and *trans*-**25** clearly increases in time even in the absence of blue light illumination, which unambiguously indicates that thermal *cis*→*trans* isomerisation took place. Figure III-9c and d plot the absorption recovery time traces at 382 nm, a wavelength that lies close to the absorption maximum of the $\pi\rightarrow\pi^*$ transition for both *trans*-**21** and *trans*-**25**. These two traces can be fitted with a monoexponential growth function, which demonstrates that thermal *cis*→*trans* isomerisation follows a first order kinetics and allows the rate constant of this process and the half-lives of *cis*-**21** and *cis*-**25** to be determined (Table III-2).

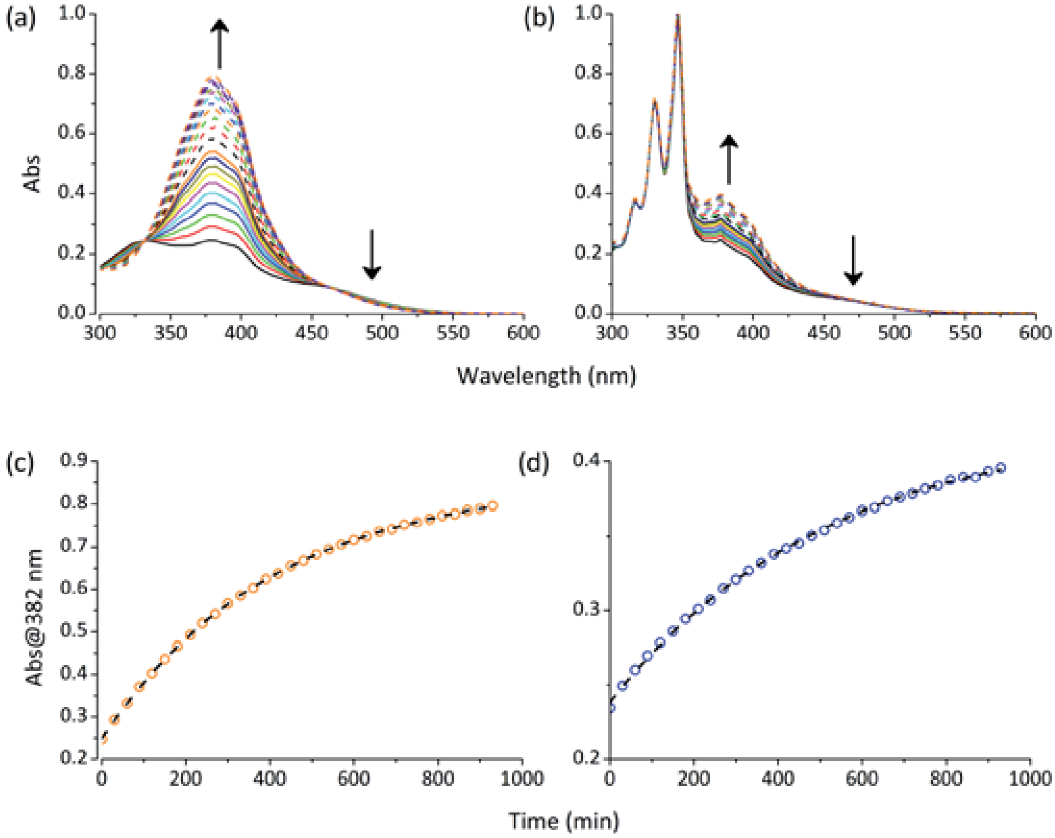

Figure III-9. (a-b) Variation of the absorption of the *trans/cis* photostationary state mixtures of (a) **25** and (b) **21** in the dark at 25 ºC in DMSO. The arrows indicate the direction of the changes observed in time. (c-d) Time dependence of the absorption at λ_{abs} = 382 nm under these conditions, which reports on the recovery of the concentration of (c) *trans*-**25** and (d) *trans*-**21** upon thermal *cis*→*trans* isomerisation. Points correspond to the experimental data, while dashed lines were obtained from monoexponential fits.

Notably, the thermal *cis*→*trans* back isomerisation process of compounds **21** and **25** takes place in the timescale of hours at rt ($t_{1/2}^{cis}$ = 6.0 h and 4.6 h for *cis*-**21** and *cis*-**25**, respectively), as expected for azobenzene-type molecules.[29] The difference observed in $t_{1/2}^{cis}$ values might be ascribed to the distinct sizes of the amide substituents of the azobenzene cores of these products, the bulkier groups introduced into target ligand **21** slowing down the thermal *cis*→*trans* isomerisation. More importantly, the long lifetime measured for the *cis* isomer of this compound has an important implication in its use for the optical control of neural receptors and ion channels. Namely, fast gating of these biological systems will require two-wavelength excitation, with which sequential *trans*→*cis* and *cis*→*trans* photoisomerisations could be induced. This might be a limitation in our work, since photoswitched tethered ligand **21** was only designed to undergo two-photon sensitised *trans*→*cis* isomerisation with NIR light. As such, subsequent illumination with visible radiation will be needed to revert back this process via one-photon excitation. To tackle this problem, the use of azobenzene-based photoswitched tethered ligands that could be operated under single-wavelength excitation conditions will be proposed in Chapter IV.

III.3.3. Sensitised *trans*→*cis* photoisomerisation

Target ligand **21** was designed to also operate under sensitised *trans*→*cis* photoisomerisation through irradiation of its pyrene photo-harvesting antenna and intramolecular resonance energy transfer towards its azobenzene core. Therefore, our next step was to demonstrate the occurrence of this process.

As mentioned above, the fluorescence emission of the pyrene group in *trans*-**21** is strongly quenched (see § III.3.1), which can be ascribed to efficient energy transfer from the electronic excited state of this moiety to the azoaromatic group. The efficiency of this process can be predicted from the Förster radius (R_0) of this donor-acceptor pair in DMSO, which can be calculated from Equation I.4. In this case, the following parameters were used in the calculation of R_0: (i) J = 4.32 x 10^{-14} cm^{-1}, which is the spectral overlap integral between the absorption spectrum of the antenna-less *trans*-**25** molecule and the emission spectrum of the pyrene group in DMSO (see Figure III-2); (ii) $\Phi_{Fl,D}$= 0.30, which is the fluorescence quantum yield of pyrene reference compound in DMSO; (iii) k^2 = 2/3, which assumes random orientation between the donor and acceptor units owing to the flexible alkyl chain linking them together in *trans*-**21**; and (iv) n = 1.479, which is the refractive index of DMSO at rt. In this way, a value of R_0 = 34.2 Å for *trans*-**21** was determined, which is higher than the centre-to-centre distance between its antenna and azobenzene groups according to a molecular mechanics calculation with a MM2 force field (r = 11.8 Å). By introducing these parameters into Equation I.3, the efficiency of the RET process in *trans*-**21** was found to be higher than 99%, which would account for the nearly complete suppression of the fluorescence emission from the pyrene sensitiser of this compound.

To investigate whether the occurrence of such RET processes enable sensitised *trans*→*cis* photoisomerisation in **21**, DMSO solutions of this compound and reference product **25** were irradiated at 347 nm and the formation over time of the corresponding *cis* isomers ($\%_{cis}$) was monitored by UV-vis absorption spectroscopy. It must be noted that at this excitation wavelength the pyrene photo-harvesting antenna absorbs light more efficiently than the *trans*-azobenzene groups of **21** and **25**. Thus, from the spectroscopic data registered for these two compounds we determined that $\varepsilon^{347\text{ nm}}_{\text{pyrene}} / \varepsilon^{347\text{ nm}}_{trans\text{-azo}} \sim 2$ and $\varepsilon^{347\text{ nm}}_{\text{pyrene}} / \varepsilon^{347\text{ nm}}_{cis\text{-azo}} \sim 4$. Therefore, if compound **21** reaches a faster or/and more *cis*-enriched PSS than **25** under such irradiation conditions, this would mean that sensitised *trans*→*cis* isomerisation is taking place. The results of these experiments are plotted in Figure III-10a. Clearly, *trans*→*cis* photoisomerisation occurs both for **21** and **25** at λ_{exc} = 347 nm, the photostationary mixtures obtained containing ~ 40% (**21**) and ~ 55% (**25**) of the corresponding *cis* isomers. However, these states are achieved at different velocities under equivalent irradiation intensities. Thus, illumination for at least 175 min is required for **25** to reach its PSS. Instead, the photostationary state of **21** is attained after just ~ 75 min of irradiation. Additionally, larger photoconversions are achieved for this compound at times well below those needed to reach the equilibrium state (e.g. $\%_{cis}$ = 32 and 26 for **21** and **25** after 25 min of irradiation). These results unambiguously indicate that the *trans*→*cis* photoisomerisation rate of our target ligand is enhanced upon excitation of the pyrene group, which must be related to the occurrence of a sensitised isomerisation pathway.

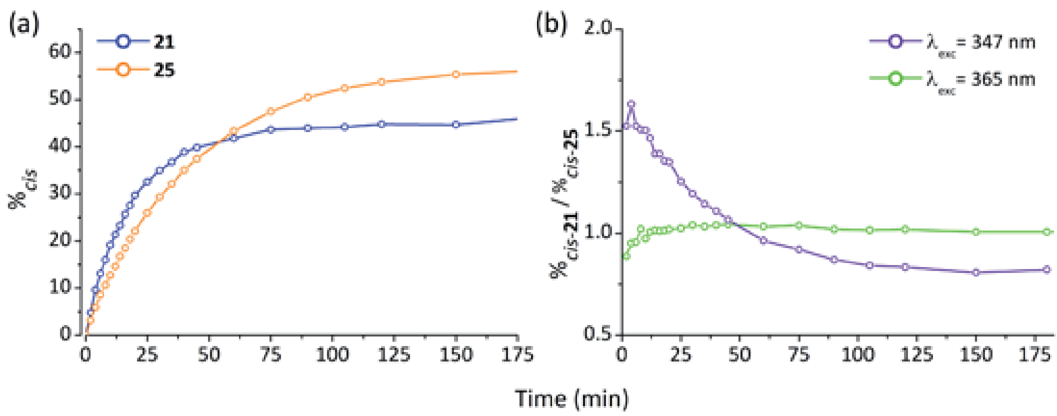

Figure III-10. (a) Percentage of *cis*-**21** and *cis*-**25** photogenerated upon continuous irradiation at 347 nm of DMSO solutions of their *trans* isomers. (b) Photogenerated ratio of *cis*-**21** and *cis*-**25** ($\%_{cis\text{-}\mathbf{21}} / \%_{cis\text{-}\mathbf{25}}$) versus irradiation time at 347 nm and 365 nm in DMSO.

Further evidence for the implication of such process was provided by additional measurements conducted at an excitation wavelength where the pyrene group of target ligand **21** does not absorb (λ_{exc} = 365 nm). Under this irradiation condition, only direct *trans*→*cis* photoisomerisation should therefore take place, a photoswitching mechanism that was demonstrated to yield identical results for the analogous azobenzene groups in **21** and **25** (see section III.3.2). Figure III-10b plots the time profile of the concentration ratio between *cis*-**21** and *cis*-**25** ($\%_{cis\text{-}\mathbf{21}} / \%_{cis\text{-}\mathbf{25}}$) photogenerated in these experiments and in those carried out at λ_{exc} = 347 nm. Aside from the values measured at very short irradiation times where significant errors in the determination of $\%_{cis}$ might be committed due to low photoconversion efficiencies, a straight line around $\%_{cis\text{-}\mathbf{21}}$ / $\%_{cis\text{-}\mathbf{27}}$ = 1 was obtained at λ_{exc} = 365 nm. This indicates that equivalent photostationary states were produced at the same rates for both **21** and **25** at this excitation wavelength. As discussed above, this is the expected result since only the direct *trans*→*cis* photoisomerisation mechanism operates in this case.

On the contrary, a more complex time profile was obtained at λ_{exc} = 347 nm. At short irradiation times (t < 50 min), we found $\%_{cis\text{-}\mathbf{21}}$ / $\%_{cis\text{-}\mathbf{25}}$ to be larger than 1, which indicates that *trans*→*cis* photoisomerisation takes place faster for target ligand **21**. Together with the results in Figure III-10a, this clearly demonstrates that sensitisation via pyrene excitation is accelerating the isomerisation process under such irradiation conditions. Nevertheless, lower photoconversion efficiencies are eventually measured for compound **21** when reaching the equilibrium state ($\%_{cis\text{-}\mathbf{21}}$ / $\%_{cis\text{-}\mathbf{25}}$ = 0.8 at t = 175 min). We ascribe this result to the fact that the photo-harvesting antenna in this compound does not only sensitise *trans*→*cis* isomerisation, but also the reverse reaction. As such, the PSS composition achieved at λ_{exc} = 347 nm for ligand **21** depends on the complex balance between the rates of both direct and sensitised *trans*→*cis* and *cis*→*trans* isomerisation processes.

In conclusion, the photochemical characterisation of target compound **21** has unequivocally revealed that it behaves as a reversible photoswitch that can be triggered both via direct irradiation of its azobenzene group or via sensitised excitation of its pyrene photo-harvesting antenna, as originally devised in our design.

III.4. EVALUATION OF THE LIGHT-INDUCED BIOLOGICAL ACTIVITY OF PHOTOSWITCHED TETHERED LIGAND 21

Having demonstrated the successful photochemical operation of photoswitched tethered ligand **21** in solution, we then turned our attention to test the capability of this compound to light-control ionotropic glutamate receptors in cells. To start with, these experiments were conducted via one-photon excitation with UV-vis light and they were carried out in the laboratories of the research group of Prof. Pau Gorostiza at *Institut de Bioenginyeria de Catalunya* (IBEC).

In particular, our biological measurements consisted in illuminating LiGluR-expressing cells incubated with compound **21**. As described in § I.2.2, when the azobenzene group of the photoswitch tethered to LiGluR is in its *trans* configuration, the ion channel should remain closed because the glutamate ligand lies far away from the binding site. However, upon illumination with UV light inducing *trans*→*cis* photoisomerisation, glutamate should be brought into close proximity to the binding pocket, where it must bind and cause the aperture of the channel and the transport of cations across the cell membrane. Finally, this flux of ions should be stopped by irradiation with visible light, which restores the initial state via *cis*→*trans* photoisomerisation.

Different techniques have been applied to monitor such light-controlled operation of ion channels, which normally measure physico-chemical signals related to the flux of ions between the extra- and intracellular media. Among these methods, fluorescence imaging techniques are especially popular because they are relatively simple and enable simultaneous recordings from many individual cells at the same time. As such, one of these fluorescence imaging methodologies has been exploited in this chapter to evaluate the biological activity of photoswitched tethered ligand **21**.

III.4.1. Fluorescence imaging of LiGluR operation

Live cell fluorescent imaging is based on the use of fluorescent dyes with which biologically relevant compounds can be specifically labelled and/or targeted. In this study, we chose calcium ions as the analyte of interest because: (i) kainate-type ionotropic glutamate receptors such as LiGluR allow the transport of not only monovalent ions, but also Ca^{2+} across the cell membrane; and (ii) it is a major second intracellular messenger mediating neural activity.[30] Therefore, the light-controlled operation of LiGluR can be followed by monitoring the changes in intracellular calcium ion concentration arising from the aperture of this channel. This can be achieved by the so-called calcium imaging technique, which measures the emission signal from fluorescent calcium indicators loaded into the cells of interest.

Among all different types of calcium indicators, fura-2 (**68**) was selected to perform our experiments. As shown in Figure III-11a, this compound is composed of a Ca^{2+} chelating group and a fluorophore unit. However, fura-2 can hardly cross the cell membrane owing to the negative charges of its carboxylate groups at physiological pH. For this reason, it is not directly loaded into cells, but they are incubated with its ester derivative **69** (fura-2 AM, Figure III-11b). Thus, derivatisation of the carboxylate groups of fura-2 as acetoxymethyl esters converts it into a non-polar compound that is permeable to cell membrane. Once inside the cell, the ester protecting groups are hydrolysed by intracellular esterases, thus rendering the active form of the indicator.

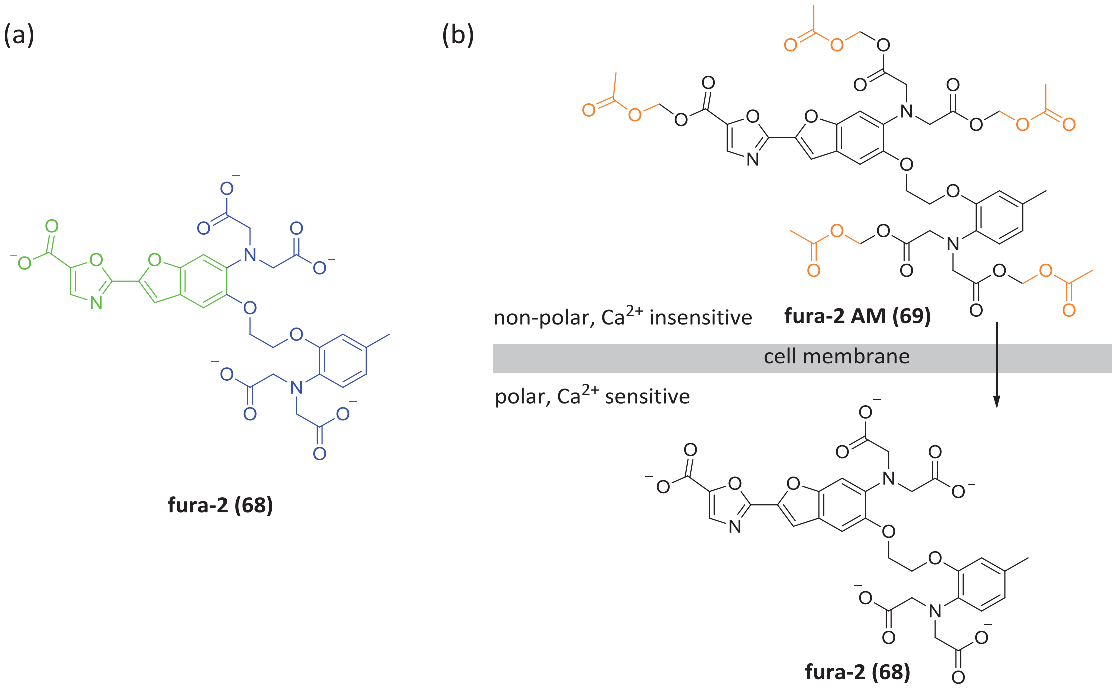

Figure III-11. (a) Structure of fura-2, which contains a high affinity Ca^{2+} ligand (in blue) and an oxazole-benzofuran fluorophore (in green). (b) Fura-2 AM ester derivative is a non-polar calcium insensitive compound that freely crosses the cell membrane. Once inside the cell, ubiquitous cellular esterases hydrolyse the protecting ester groups to yield the calcium ion sensitive, negatively charge fura-2 indicator.

Fura-2 is a green-emitting indicator that binds to calcium ions via its free carboxylate groups, which changes the ionization state of the chromophore and concomitantly modifies its UV-vis absorption spectrum. This is clearly shown by the fluorescence excitation spectra plotted in Figure III-12.

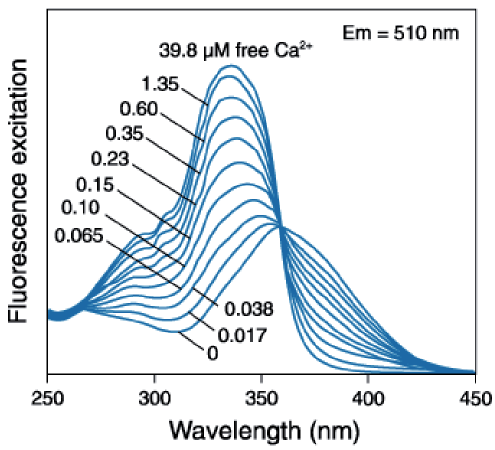

Figure III-12. Fluorescence excitation spectra at λ_{em} = 510 nm of fura-2 in solutions containing 0-39.8 μM of calcium ions.[31]

In the absence of Ca^{2+}, the absorption spectrum of fura-2 peaks at 365 nm and maximum emission intensity is therefore measured at this excitation wavelength. Upon complexation of

Ca^{2+}, the absorption spectrum of the indicator blue-shifts and maximum emission is detected at λ_{exc} = 340 nm. As a result, ratiometric fluorescence measurements are usually performed with fura-2, the difference in emission intensity at λ_{exc} = 340 nm and 380 nm being directly correlated to the ratio of complexed/uncomplexed fura-2 molecules and, therefore, the amount of intracellular calcium ions.[30]

III.4.1.1. Calcium imaging measurements of 21

To evaluate the efficiency of compound **21** to light-control ionotropic glutamate receptors, cells must overexpress the target LiGluR channel, which incorporates a genetically-encoded cysteine residue at position 439 as anchoring site for the tethered ligand. This was achieved by transfecting HEK293 cells with Gluk2-L439C for 48 hours. Afterwards, these cells were incubated with buffer solutions of **21** to induce ligand tethering and fura-2 AM to load the calcium ion indicator into them. Finally, they were subjected to calcium imaging experiments upon UV-vis irradiation. In addition, control measurements were performed on wild type HEK293 cells equivalently treated with **21** and fura-2 AM, and by measuring the response of these and the transfected cells to free glutamate.

Figure III-13a shows typical calcium imaging traces recorded for both wild type and LiGluR-expressing cells in the dark upon addition of free glutamate. As discussed above, the emission intensity ratio between λ_{exc} = 340 nm and 380 nm ($R_{f340/f380}$) is plotted in these traces as a measure of the intracellular calcium ion concentration. Thus, if $[Ca^{2+}]$ grows due to LiGluR channel opening, $R_{f340/f380}$ should automatically increase, and it will gradually recover its initial value as basal calcium ion levels are restored by regular removal and/or storage processes. In the experiments shown in Figure III-13a, two consecutive additions of free glutamate were carried out at t = 0.5 and 9.5 min. None of them had any effect on wild type HEK293 cells owing to the lack of LiGluR channels in their cell membrane that could be opened by glutamate ligand recognition. As such, $R_{f340/f380}$ remained constant in time. On the contrary, LiGluR-expressing cells were repetitively activated by free glutamate, which resulted in an influx of calcium ions and, therefore, an increase of the $R_{f340/f380}$ ratio. This demonstrates the success of the transfection process of HEK293 cells, which turned them sensitive to glutamate-induced changes in intracellular Ca^{2+} concentration.

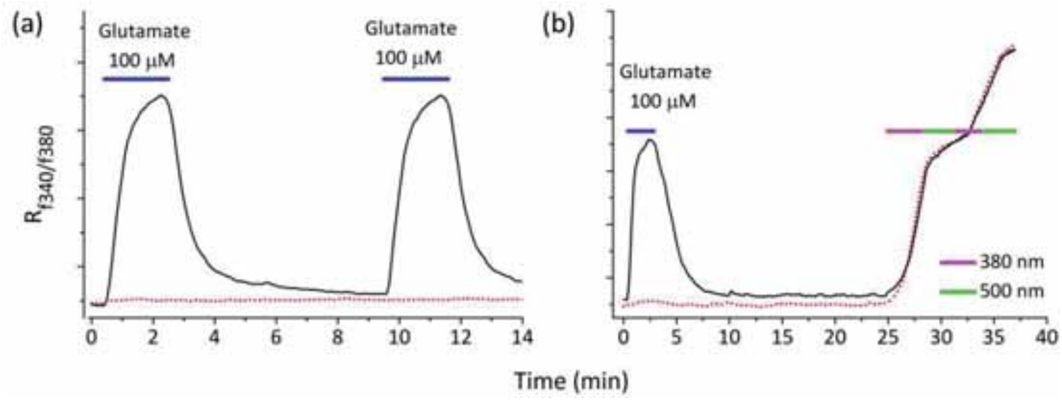

Figure III-13. (a) Calcium imaging traces measured for wild type (red dotted line) and LiGluR-expressing HEK293 cells upon repetitive free glutamate addition (c = 100 μM) at t = 0.5 and 9.5 min. (b) Calcium imaging traces measured for wild type (red dotted line) and LiGluR-expressing HEK293 cells upon one initial addition of free glutamate (c = 100 μM, t = 0.4 min) and subsequent sequential illumination with UV (λ_{exc} = 380 nm, t = 25-28 and 31-34 min) and green light (λ_{exc} = 500 nm, t = 28-31 and 34-37 min).

Next, the light-induced response of those cells was investigated. With this aim, they were sequentially illuminated at λ_{exc} = 380 and 500 nm. Excitation with UV radiation should induce the aperture of the cellular LiGluR channels via *trans*→*cis* isomerisation of photoswitched tethered ligand **21**, thus resulting in an increase of $R_{f340/f380}$ similar to that observed upon free glutamate addition. Subsequent irradiation with green light should revert back this process and lead to channel closure. Consequently, basal calcium ion levels and $R_{f340/f380}$ values should be eventually restored. The results obtained in such experiments for both transfected and wild type cells are given in Figure III-13b.

In both cases, measurements started with one single addition of free glutamate at t = 0.4 min. This was intended to demonstrate the proper functioning of the cells at the beginning of the experiment, as unambiguously proven by the initial part of the fluorescence traces in Figure III-13b. Then, cells were subjected to sequential and repetitive irradiation at λ_{exc} = 380 (t = 25-28 and 31-34 min) and 500 nm (t = 28-31 and 34-37 min). As expected, illumination of LiGluR-expressing cells with UV light resulted in a large $R_{f340/f380}$ increase, thus indicating that the cell membrane had become permeable to calcium ions. However, subsequent irradiation with green light did not allow the initial $R_{f340/f380}$ value to be restored, but it slightly increased in time. Worse still, the same behaviour was observed for wild type cells, which did not present glutamate-sensitive channels in their plasmatic membrane. Therefore, the light-induced effect measured was clearly unspecific and did not seem to be related to the *trans*-*cis* isomerisation of the LiGluR-ligand **21** tether.

To shed more light into this issue, additional experiments were performed. First, measurements were carried out for cells that had not been incubated with ligand **21**. No changes in $R_{f340/f380}$ values were observed upon illumination in this case, which suggests that the unspecific and irreversible calcium imaging signals have to be related to the photoinduced behaviour of this compound. This was further confirmed by new calcium imaging measurements on incubated cells where the initial excitation wavelength was tuned from 340 to 530 nm. The intensity of the irreversible $R_{f340/f380}$ increase registered was found to correlate with the absorption spectrum of *trans*-**21**. Thus, large signals were measured for irradiation wavelengths around the absorption maximum of the $\pi \rightarrow \pi^*$ transition of this compound, while minor or even no changes in $R_{f340/f380}$ were observed for both shorter and longer wavelengths. Finally, additional calcium imaging measurements were conducted by varying other experimental parameters, with which we aimed to detect specific and reversible $R_{f340/f380}$ peaks for LiGluR-expressing cells (Table III-3). In particular, we tested the following conditions: (i) lowering the extracellular Ca^{2+} concentration to ensure that irreversible signals were not arising from cell damage caused by excessive calcium ion influx (entries 2-6); (ii) decreasing the amount of *trans*-**21** molecules incorporated to the cell membrane by halving the incubation time (entry 3) and concentration (entries 4-6); (iii) reducing the UV light dose (entries 5 and 6) and increasing the irradiation time with the restoring green light (entry 6). Although variations in the intensity of the light-induced $R_{f340/f380}$ increments were measured in these experiments, they were found to be unspecific and irreversible in all cases, which eventually led to cell death.

Table III-3. Different experimental conditions assayed in the calcium imaging measurements.

Entry	Extracellular [Ca^{2+}]	[Compound 21]	Incubation time[a]	Time irradiation λ_{exc} = 380 nm	Time irradiation λ_{exc} = 500 nm
1	10 mM	200 μM	1 h	3 min	3 min
2	2 mM	200 μM	1h	3 min	3 min
3	2 mM	200 μM	30 min	3 min	3 min
4	2 mM	100 μM	1 h	3 min	3 min
5	2 mM	100 μM	1 h	1 min	3 min
6	2 mM	100 μM	1 h	1 min	4 min

(a) In the dark at 37 ºC.

From all these results we conclude that the light-induced calcium ion permeability observed in our experiments was due to *trans*→*cis* photoisomerisation of compound **21**, which had to be unspecifically incorporated to the cell membrane of wild type and LiGluR-expressing cells. Since this behaviour had not been previously reported for other MAG derivatives, we ascribe it to the introduction of the pyrene photo-harvesting antenna into the photoswitched tethered ligand. We believe that the hydrophobic nature of this group should favour the accumulation of this compound in the lipophilic domains of the plasmatic membrane instead of selective attachment to LiGluR channels. Subsequent *trans*→*cis* photoisomerisation upon UV irradiation of the inserted molecules must then irreversibly alter the structure of those membrane domains, rendering them permeable to Ca^{2+} ions regardless of the presence or not of glutamate sensitive ion channels. As a consequence, compound **21** is not a good candidate to light-control ionotropic glutamate receptors and for that reason, further biological experiments to explore the two-photon activity of this switch were not conducted.

III.5. CONCLUSIONS

In this chapter, we described the synthesis, characterisation and biological application of the novel photoswitched tethered ligand **21**, which was designed to control the operation of ionotropic glutamate receptors via two-photon excitation with NIR light. As depicted Figure III-14, compound **21** contains the three characteristic building blocks of the original MAG-1 switch (maleimide, azobenzene and glutamate groups), but it additionally incorporates a fourth functional unit (pyrene fluorophore). This new fragment was devised to act as sensitiser, by absorbing NIR light via two-photon excitation and then transferring its excited state energy to the azobenzene group, which should eventually undergo *trans-cis* photoisomerisation. As reference for the photochemical studies, model azobenzene compound **25** was also designed and synthesised.

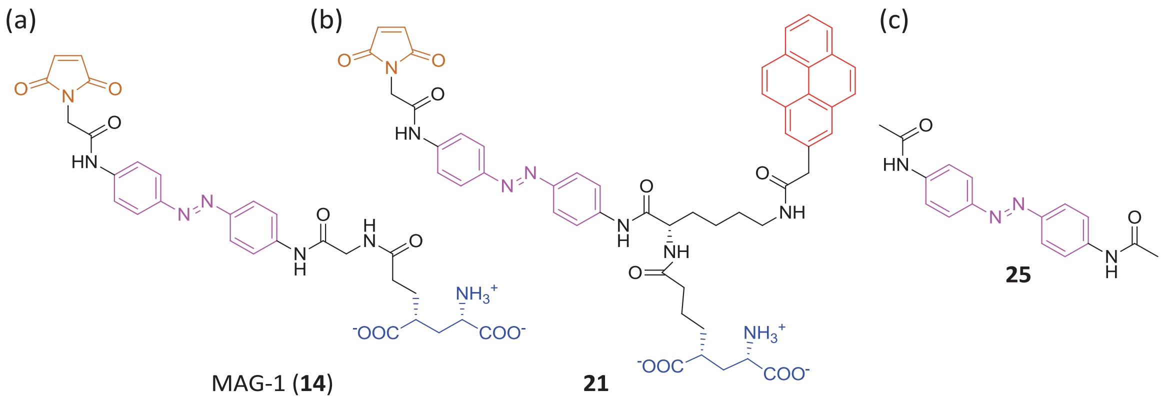

Figure III-14. Structures of: (a) the most representative compound of MAG-type photoswitches (MAG-1 (**14**));[1] (b) PTL **21** synthesised in this work; and (c) model azobenzene compound **25**.

Compound **21** was prepared in 7 steps and 17% overall yield by convergent synthesis from *N*,*N*-orthogonally diprotected L-lysine **28**. The different functional units of the target ligand were sequentially introduced into this scaffold: 4,4'-diaminoazobenzene (**11**); glutamate derivative **65**, which was obtained in 8 steps and 7% global yield from L-pyroglutamic acid (**37**); 2-

(pyren-1-yl)acetic acid (**24**); and maleimide derivative **49**, which was prepared from β-alanine (**47**) and maleic anhydride (**48**) in 1 step and 45% yield (Scheme III-25). Importantly, the novel glutamate derivative **65** described in this work provides a more versatile and robust way to introduce this group in the synthesis of future MAG-type derivatives. On the other hand, reference compound **25** was synthesised in 1 step and 43% yield via direct acylation of **11**.

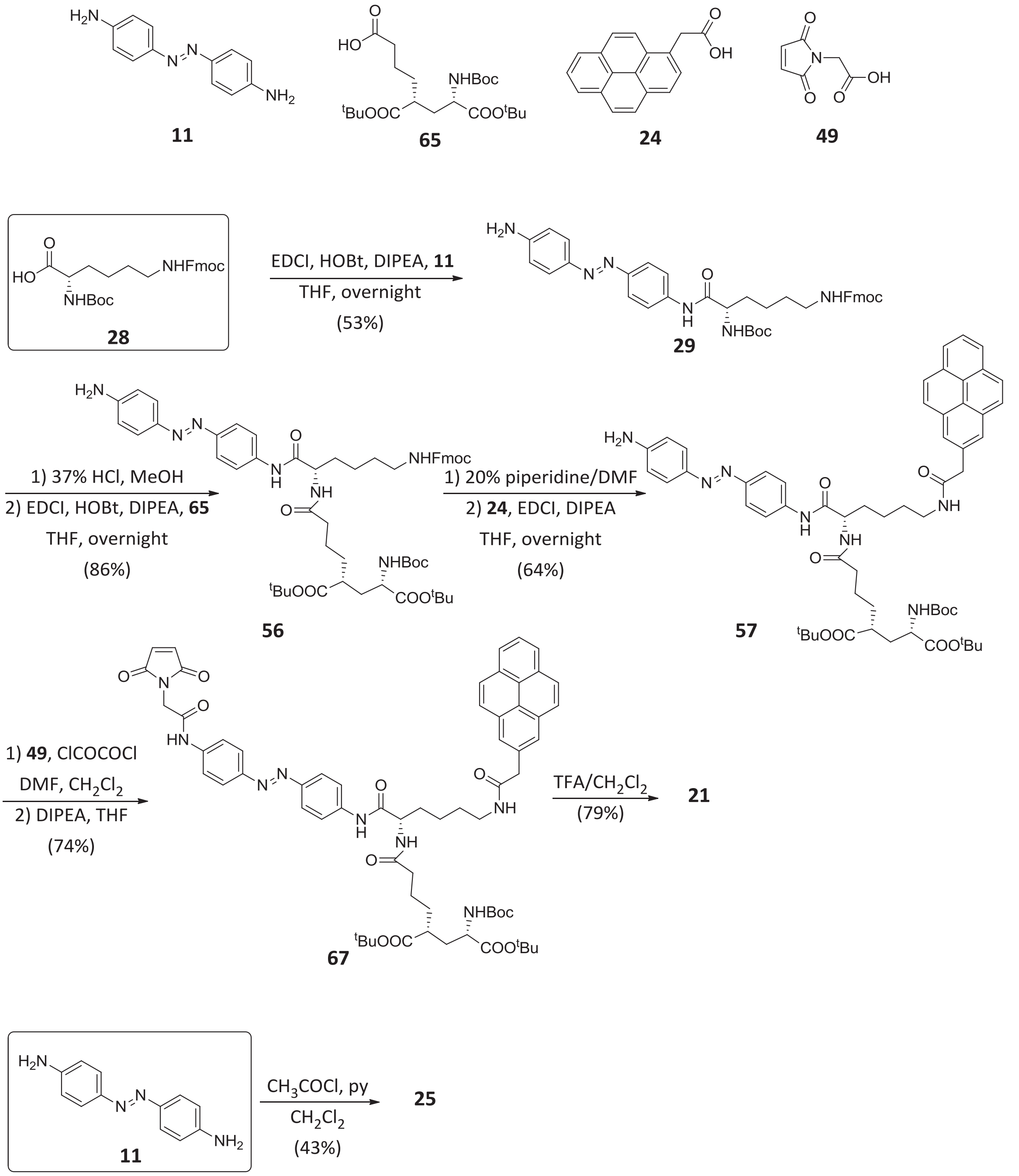

Scheme III-25. Synthesis of molecular photoswitch **21** and reference compound **25**.

The comparative study of the photochemical properties of **21** and **25** revealed that the incorporation of the pyrene photosensitiser to the MAG structure does not significantly alter the intrinsic light-induced behaviour of its azobenzene core, whose *trans-cis* photoisomerisation quantum yields, photostationary states and *cis* isomer lifetime resemble those of the antenna-less compound. However, additional photochemical features were observed for target ligand **21** arising from its novel design. Thus, it displays new absorption bands corresponding to its pyrene fragment, which opens up a novel photoinduced *trans-cis* isomerisation pathway evolving via excitation of the sensitiser and subsequent intramolecular energy transfer towards the azobenzene group. This was corroborated by different experiments and simulations: (i) extensive fluorescence quenching of the pyrene moiety was observed in compound **21**; (ii) large resonance energy transfer efficiencies were determined for the pyrene-azobenzene pair; and (iii) faster *trans*→*cis* photoconversions were measured for **21** with respect to model azobenzene compound **25** upon excitation of the sensitiser group.

Finally, the activity of photoswitched tethered ligand **21** to light-control ionotropic glutamate receptors in cells was tested *in vitro* by means of calcium imaging measurements. These experiments showed that incorporation of **21** to the plasmatic membrane does not evoke selective and reversible Ca^{2+} influxes for LiGluR-expressing cells. Instead, irreversible and unspecific light-induced signals were measured that were not related to the presence of glutamate sensitive ion channels. We ascribe this result to the massive accumulation of this compound into the lipophilic domains of the cell membrane owing to the hydrophobic character of its pyrene group. Subsequent *trans*→*cis* photoisomerisation of the inserted molecules opened pores for Ca^{2+} transport across the membrane that could not be fully closed by light-induced back isomerisation of **21**.

In conclusion, we have demonstrated in this chapter that novel MAG derivatives bearing two-photon photo-harvesting antennas are synthetically accessible and do display sensitised azobenzene photoisomerisation if their spectral properties are properly selected. Nevertheless, other factors may limit the overall biological activity of the resulting switch, such as its unspecific affinity towards the lipophilic domains of the cell membrane, which might prevent selective attachment to the target ionotropic glutamate receptors. To overcome this obstacle, two different approaches are explored in the next chapter: (i) the use of other, less hydrophobic photo-harvesting antennas; and (ii) direct two-photon excitation of MAG photoswitches with NIR light.

III.6. REFERENCES

(1) Volgraf, M.; Gorostiza, P.; Numano, R.; Kramer, R. H.; Isacoff, E. Y.; Trauner, D. *Nat. Chem. Biol.* **2006**, *2*, 47–52.

(2) Banerjee, S.; Goswami, N.; Pal, S. K. *ChemPhysChem* **2013**, *14*, 3581–3593.

(3) Masuko, M.; Ohuchi, S.; Sode, K.; Ohtani, H.; Shimadzu, A. *Nucleic Acids Res.* **2000**, *28*, E34.

(4) Kim, H. M.; Lee, Y. O.; Lim, C. S.; Kim, J. S.; Cho, B. R. *J. Org. Chem.* **2008**, 5127–5130.

(5) Xu, C.; Williams, R. M.; Zipfel, W.; Webb, W. W. *Bioimaging* **1996**, *4*, 198–207.

(6) Chirico, G.; Cannone, F.; Baldini, G.; Diaspro, A. *Biophys. J.* **2003**, *84*, 588–598.

(7) Blevins, A. A.; Blanchard, G. J. *J. Phys. Chem. B* **2004**, *108*, 4962–4968.

(8) Sørensen, T. J.; Kjaer, K.; Breiby, D. W.; Laursen, B. W. *Langmuir* **2008**, *24*, 3223–3227.

(9) Joullié, M. M.; Lassen, K. M. *Arkivoc* **2010**, *2010*, 189–250.

(10) Montalbetti, C. a. G. N.; Falque, V. *Tetrahedron* **2005**, *61*, 10827–10852.

(11) Valeur, E.; Bradley, M. *Chem. Soc. Rev.* **2009**, *38*, 606–631.

(12) Kvsrg, P.; Bharathi, K.; B, H. B. *Int. J. Pharm. Sci. Rev. Res.* **2011**, *8*, 108–119.

(13) Boger, D. L.; Miyazaki, S.; Kim, S. H.; Wu, J. H.; Castle, S. L.; Loiseleur, O.; Jin, Q.; Scripps, T.; Torrey, N.; Road, P.; Jolla, L. *J. Am. Chem. Soc.* **1999**, *121*, 10004–10011.

(14) Xu, H.; Baidoo, K.; Gunn, A. J.; Boswell, C. A.; Milenic, D. E.; Choyke, P. L.; Brechbiel, M. W. *J. Med. Chem.* **2007**, *50*, 4759–4765.

(15) Ezquerra, J.; Pedregal, C.; Rubio, A.; Yruretagoyena, B.; Escribano, A.; Sánchez-Ferrando, F. *Tetrahedron* **1993**, *49*, 8665–8678.

(16) Andrade, R. B.; Martin, S. F. *Org. Lett.* **2005**, *7*, 5733–5735.

(17) Eal, B. S.; Childers, W. E.; Pinnick, H. W. *Tetrahedron* **1981**, *11*, 2091–2096.

(18) Liu, D.; Acharya, H. P.; Yu, M.; Wang, J.; Yeh, V. S. C.; Kang, S.; Chiruta, C.; Jachak, S. M.; Clive, D. L. J. *J. Org. Chem.* **2009**, *74*, 7417–7428.

(19) Shendage, D. M.; Fröhlich, R.; Haufe, G. *Org. Lett.* **2004**, *6*, 3675–3678.

(20) Campo, V. L.; Martins, M. B.; da Silva, C. H. T. P.; Carvalho, I. *Tetrahedron* **2009**, *65*, 5343–5349.

(21) Avent, A. G.; Duggan, H. M. E.; Young, D. W. *Org. Biomol. Chem.* **2005**, 2327–2332.

(22) Pearson, R. J.; Kassianidis, E.; Slawin, A. M. Z.; Philp, D. *Org. Biomol. Chem.* **2004**, *2*, 3434–3441.

(23) Kauffman, J. M.; Moyna, G. *J. Org. Chem.* **2003**, *68*, 839–853.

(24) Pejoan, A. Màster en Experimentació en Química, Universitat Autònoma de Barcelona, 2012.

(25) Steger, M.; Young, D. W. *Tetrahedron* **1999**, *55*, 7935–7956.

(26) Ten Brink, H. T.; Rijkers, D. T. S.; Liskamp, R. M. J. *J. Org. Chem.* **2006**, *71*, 1817–1824.

(27) Yager, K. G.; Barrett, C. J. *J. Photochem. Photobiol. A Chem.* **2006**, *182*, 250–261.

(28) Bandara, H. M. D.; Burdette, S. C. *Chem. Soc. Rev.* **2012**, *41*, 1809–1825.

(29) Halabieh, R. El; Mermut, O.; Barrett, C. *Pure Appl. Chem.* **2004**, *76*, 1445–1465.

(30) Grienberger, C.; Konnerth, A. *Neuron* **2012**, *73*, 862–885.

(31) Life Technology, http://www.b2b.invitrogen.com/site/us/en/home/References/Molecular-Probes-The-Handbook/Indicators-for-Ca2-Mg2-Zn2-and-Other-Metal-Ions/Fluorescent-Ca2-Indicators-Excited-with-UV-Light.html.

Chapter IV

Direct *vs* Sensitised Two-Photon Excitation of Photoswitched Tethered Ligands Based on Red-Shifted Azobenzene Derivatives

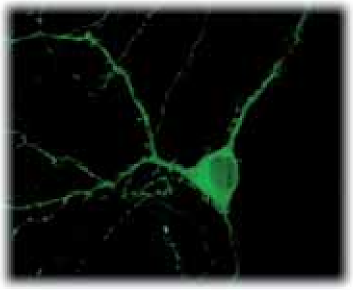

In the previous chapter we described the synthesis, characterisation and biological evaluation of a novel MAG-type photoswitched tethered ligand featuring a pyrene moiety as two-photon sensitiser. Despite the good photochemical results obtained in solution, this compound failed to provide light-control over ionotropic glutamate receptors because it unspecifically binds to the hydrophobic domains of the cell membrane. To overcome this limitation, two different approaches are investigated in this chapter: (i) to replace the pyrene photo-harvesting antenna with a naphthalene derivative, an alternative two-photon absorber that should not interfere with the ligand-binding site recognition process of the resulting PTL; and (ii) to achieve *trans-cis* isomerisation of the photoswitch via direct two-photon excitation of its azobenzene group upon irradiation with NIR light. Both strategies require the use of red-shifted azoaromatic units with respect to that employed in Chapter III, either to ensure efficient energy transfer from the new naphthalene sensitiser to the azobenzene core or to enhance its intrinsic two-photon absorption cross-section. Hence, this chapter reports the synthesis, characterisation and biological application *in vitro* of two new PTLs based on red-shifted azobenzene derivatives.

IV.1. INTRODUCTION

Aiming at two-photon sensitised control of LiGluR by means of the maleimide-azobenzene-glutamate-antenna scheme developed in Chapter III, herein we propose the use of naphthalene derivative **70** as photo-harvesting antenna instead of a pyrene moiety. This group was selected as sensitiser because of: (i) its high two-photon absorption cross-section ($\delta \sim 200$ GM at 780 nm);[1] (ii) its relatively small size, which might minimise sterical hindrance effects hampering ligand-binding site interaction upon *trans-cis* photoisomerisation; (iii) its wide use as two-photon fluorescence indicator for monitoring free intracellular ions in live tissues, which reveals its ability to cross cell membranes;[2,3] and (iv) the presence of a free carboxylic acid moiety that can be exploited to incorporate this photo-harvesting antenna to the MAG structure in a simple and straightforward manner (Figure IV-1).

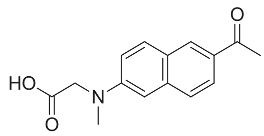

70

Figure IV-1. Structure of [(6-acetyl-2-naphthyl)(methyl)amino]acetic acid (**70**), the naphthalene derivative used in this chapter as photo-harvesting antenna for the sensitised approach to attain two-photon photoswitch operation.

The one-photon absorption spectrum of naphthalene derivative **70** is shown in Figure IV-2a, which exhibits a single band at λ_{max} = 362 nm. As depicted in Figure IV-2b, its fluorescence emission spectrum peaks at λ_{max} = 512 nm and it is therefore clearly red-shifted with respect to that of the pyrene sensitiser used in the previous chapter (λ_{max} = 315, 329 and 346 nm). Because of this, it only overlaps with the $n\rightarrow\pi^*$ absorption band of the *trans*-4,4′-diamidoazobenzene group found in MAG-1. Since sensitisation of azobenzene *trans*→*cis* isomerisation requires spectral overlap with its more intense $\pi\rightarrow\pi^*$ absorption band, the optical properties of the azoaromatic core must therefore be adapted to the new photo-harvesting antenna selected. Namely, its absorption spectrum must be red-shifted. As previously commented (see § I.2.I), this can be easily achieved by properly varying the substitution pattern of the azoaromatic group. For instance, introduction of *para*-amino substituents is known to bathochromically shift azobenzene absorption spectrum.[4] Accordingly, in this chapter we pursue the preparation of a novel photoswitched tethered ligand based on the maleimide-azobenzene-glutamate-antenna scheme developed by us, where naphthalene derivative **70** is to be used as antenna and a red-shifted aminoazobenzene as core (Figure IV-3a).

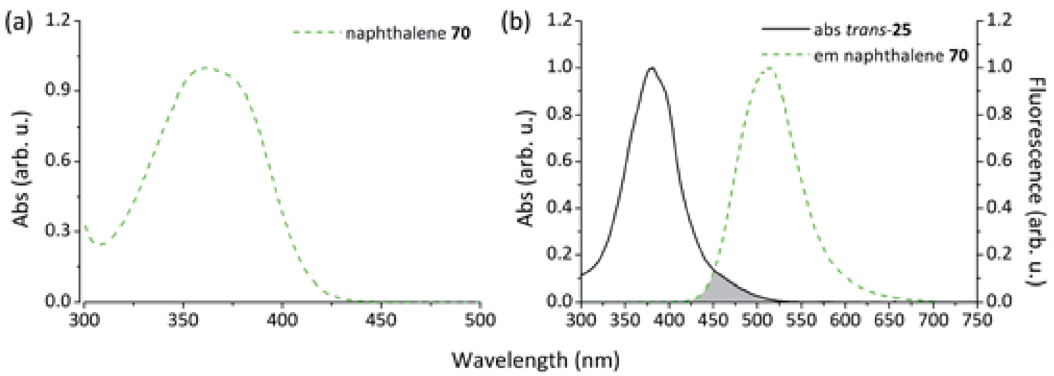

Figure IV-2. (a) Normalised absorption spectrum of naphthalene derivative **70** in DMSO. (b) Spectral overlap in DMSO between the fluorescence emission spectrum of **70** and the absorbance spectrum of a *trans*-azobenzene group analogous to that found in MAG-1 (compound *trans*-**25**, see § III.1).

Regarding to the second strategy explored in this chapter, efficient two-photon excitation of azobenzene chromophores also requires the use of red-shifted derivatives bearing a strong electro-donating substituent at *para*-position, such as an amino group. In this case, however, they must additionally display a strong asymmetrical electronic distribution, which should increase their two-photon absorption cross-section according to model push-pull azobenzenes.[5–8] Therefore, to investigate whether LiGluR can be light-controlled upon direct two-photon photoisomerisation of azobenzene-based compounds, a second type of photoswitched tethered ligand was synthesised in this chapter. This compound was designed on the basis of the maleimide-azobenzene-maleimide scheme originally described by Trauner, Isacoff and co-workers,[9] where an asymmetric, red-shifted azobenzene derivative was chosen as core to enhance its intrinsic non-linear optical response (Figure IV-3b).

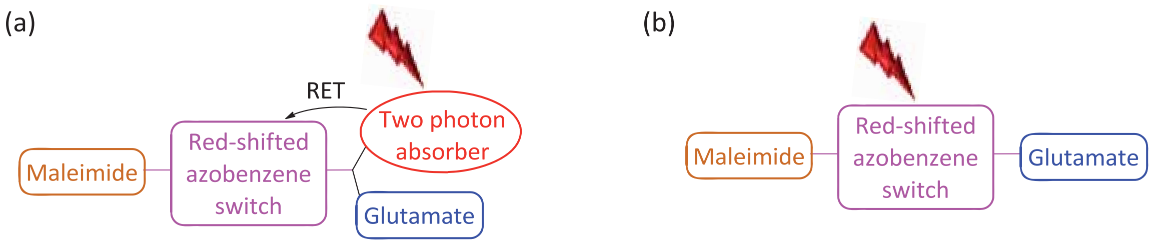

Figure IV-3. Schematic representation of the two new types of PTLs investigated in this chapter, both of which bear a red-shifted azobenzene core.

It is important to note that the use of red-shifted azobenzene switches should dramatically decrease the thermal stability of the *cis* state of the system.[10] Consequently, fast spontaneous *cis*→*trans* back isomerisation under physiological conditions is expected for the new photoswitched tethered ligands developed herein, in striking contrast to MAG-1 and potential PTL **21** synthesised in Chapter III. When applied to LiGluR, this should therefore result in channel closure immediately after stopping light irradiation and without requiring further excitation at other frequencies to revert the process, thus enabling single-wavelength gating of the receptor. In spite of this advantage, the low thermal stability of their *cis* isomers could also be a limitation for the biological application of the new switches, since a smaller population of open-state channels will be built up upon continuous irradiation. As a result, lower biological responses are expected to be elicited by these compounds. Consequently, it is of high importance to properly choose the suitable substitution pattern of the azobenzene core of the new PTLs, which should allow maximising the processes governing their photochemical operation (i.e. two-photon sensitisation or direct excitation) without compromising their overall biological activity. For this reason, we decided to prepare and photochemically characterise four model red-shifted azobenzene chromophores, which were designed as potential candidates for the construction of the new photoswitched tethered ligands. The following section is devoted to this study.

IV.2. SYNTHESIS AND PHOTOCHEMICAL CHARACTERISATION OF RED-SHIFTED AZOBENZENE MODEL PHOTOSWICTHES

Figure IV-4 shows the structure of the four azoaromatic model compounds devised in this work as potential building blocks for the synthesis of the new photoswitched tethered ligands. Two families of azobenzene derivatives were prepared: (i) symmetrically-substituted 4,4'-diaminoazobenzenes (**71** and **72**, Figure IV-4a); and (ii) asymmetrically-substituted azobenzenes (**73** and **74**, Figure IV-4b), which are characterised by an asymmetric charge distribution arising from the introduction of acetamido and amino groups at 4 and 4' positions, respectively. The first group of these compounds was devised to maximise energy transfer processes from the new naphthalene sensitiser owing to the larger degree of red-shifting arising from the two *para*-amino substituents. On the other hand, the asymmetric electronic distribution of the second type should increase the two-photon absorption cross-section of the system sufficiently as to enable efficient direct excitation of the azobenzene switch with NIR light.

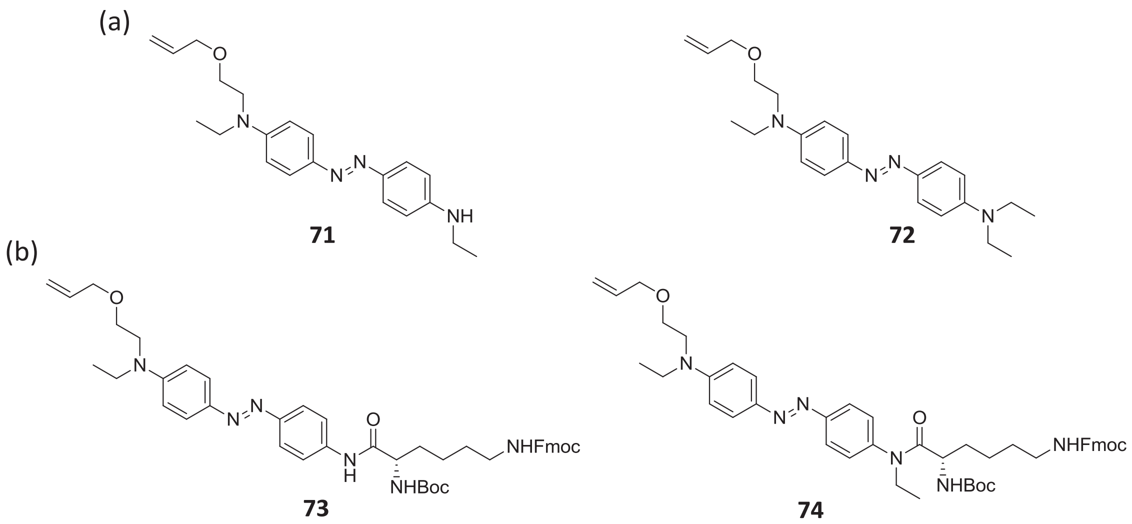

Figure IV-4. Structures of azobenzene model photoswitches.

Taking into account that the best of these model compounds were to be chosen as azobenzene cores to prepare the new two PTLs, their structures were designed to allow further synthetic modification on route towards the target ligands. For this reason, all bear an alcohol group masked as an allyl ether, which is a suitable orthogonal protection with respect to the others used in the synthesis due to its relative stability towards both acidic and basic conditions.

In addition, the carboxylic acid moiety introduced in compounds **73** and **74** would be L-lysine derivative **28**. As already carried out in Chapter III, this fragment is to be used as the central scaffold for the preparation of the new target PTLs.

Scheme IV-1 depicts the synthetic strategy designed for the synthesis of the four red-shifted azobenzene model compounds. The synthesis would begin with the protection of the primary alcohol of the commercially available azobenzene derivative **75** as an allyl ether. Next, reduction of the aromatic nitro group would provide the common intermediate **76**, from which the synthetic pathway would diverge. On the one hand, alkylation of amine **76** would lead to model photoswitches **71** and **72**. On the other hand, introduction of lysine derivative **28** into intermediate **76** and monoalkylated product **71** via peptide coupling would deliver azobenzene model **73** and **74**, respectively. The preparation of these compounds is outlined in the following section.

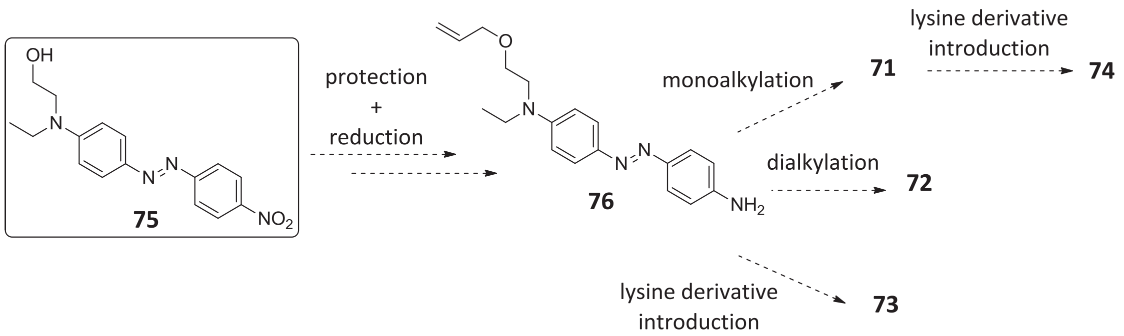

Scheme IV-1. Planned synthetic strategy for the preparation of the red-shifted azobenzene model photoswitches **71-74**.

IV.2.1. Synthesis of model azobenzene compounds 71-74

IV.2.1.1. Reduction of the aromatic nitro group. Preparation of intermediate 76

As noted above, our synthetic approach towards the model red-shifted azobenzene compounds starts with the protection of the hydroxyl group of the commercially available Disperse Red 1 dye (**75**) followed by the reduction of its aromatic nitro group (Scheme IV-2).

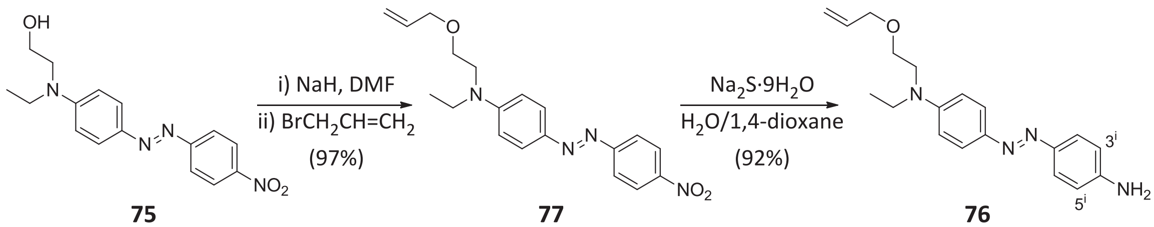

Scheme IV-2. Synthesis of amine **76**.

Thus, treatment of Disperse Red 1 with sodium hydride afforded the corresponding alkoxide ion, which was subsequently alkylated with allyl bromide rendering allyl ether **77** nearly in a quantitative yield.[11] The appearance of the signals corresponding to the allyl group in the ^{1}H-NMR and ^{13}C-NMR spectra of compound **77** indicated that the incorporation of this group had effectively occurred.

Subsequent exposure of **77** to sodium sulphide in H_2O/1,4-dioxane at 100 ºC provided a red oil identified as **76** in 92% yield.[12] The reduction of the nitro group was confirmed by the upfield shift of H-3^{i} and H-5^{i} signals from 8.30 ppm in **77** to 6.73 ppm in **76**. This amine is a key intermediate to obtain the model azobenzenes designed either by alkylation and/or peptide coupling reaction.

IV.2.1.2. Alkylation of amine 76. Preparation of compounds 71 and 72

To achieve the synthesis of model compounds **71** and **72** the next transformation required was the alkylation of amine **76**.

The monoalkylation of primary amine **76** to obtain **71** was first attempted under reductive amination conditions. Thus, **76** was treated with acetaldehyde in THF followed by *in situ* reduction with $NaBH(OAc)_3$, delivering the alkylated amine **71** albeit in very low yield (26%) (Scheme IV-3).[13] In order to improve this yield and also to concomitantly obtain model compound **72**, we decided to employ another alkylation methodology. This consisted in using ethyl bromide, ^{t}BuOK and tetrabutylammonium bromide (TBAB) to furnish a mixture of the mono- and dialkylated products.[14] The resulting crude was purified by column chromatography, affording separate fractions of compounds **71** (51% yield) and **72** (7% yield). In spite of the lower yield obtained for **72**, enough quantity of this compound was isolated as to conduct the subsequent photochemical characterisation.

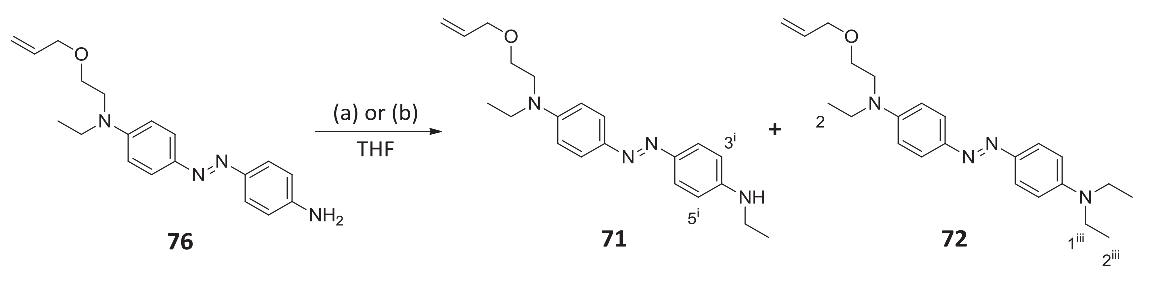

Reagents and conditions: (a) CH_3CHO, AcOH, $NaBH(OAc)_3$ (26%, only **71**); (b) CH_3CH_2Br, ^{t}BuOK, TBAB (51% for **71**, 7% for **72**).

Scheme IV-3. Alkylation of amine **76**.

The ^{1}H-NMR spectrum of **71** shows a new quartet at 3.24 ppm and a new triplet at 1.29 ppm corresponding to the ethyl group incorporated, while the H-3^{i} and H-5^{i} NMR signals shift upfield from 6.72 ppm in **76** to 6.64 ppm in **71**. For compound **72**, the most significant change found with respect to the starting material was the emergence of a quartet at 3.43 ppm corresponding to H-1^{iii}, whereas the signal from H-2^{iii} overlapped with that of H-2 at 1.21 ppm.

IV.2.1.3. L-lysine incorporation. Preparation of compounds 73 and 74

Once prepared the diaminosubstituted model compounds, we turned our attention to the synthesis of asymmetrically-substituted azobenzenes **73** and **74.** Hence, the next step consisted in the incorporation of lysine fragment **28**, which had to be attached to intermediate **76** to obtain **73** and to alkylated product **71** to furnish **74**.

We decided to start with the synthesis of azobenzene-lysine derivative **74,** because it was anticipated to be more difficult to prepare it owing to the steric hindrance of secondary amine **71**. Thus, peptide coupling reaction of amine **71** with *N,N*-orthogonally diprotected L-lysine **28** was expected to deliver compound **74** (Scheme IV-4).

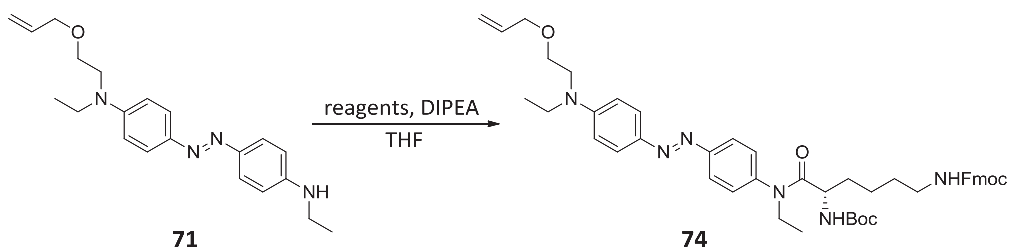

71 74

Scheme IV-4. Peptide coupling reaction for the preparation of model compound **74.**

Four different methodologies were explored to achieve the preparation of compound **74**, which involved the use of different peptidic coupling agents: TSTU, HATU, PyBOP and EDCI. In all cases, DIPEA was used as base and THF as solvent. It must be noted that only when TSTU was used as coupling agent, the activated ester was formed in a separated step, isolated and purified. In this case, commercially available lysine **28** was transformed into active ester **78** by reaction with TSTU in THF (Scheme IV-5).[15] After 12 h, the crude was purified by column chromatography providing compound **78** in 73% yield. This was confirmed by analysis of its ^{1}H-NMR and ^{13}C-NMR spectra, where new signals were found for the succinimide group introduced. In all the other cases, the active ester was prepared *in situ* as intermediate and subsequently reacted with amine **71** (one-pot coupling).

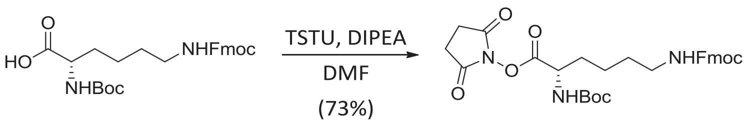

28 78

Scheme IV-5. Formation of active ester **78**.

Table IV-1 shows the results obtained for the different synthetic conditions assayed. Clearly, the desired compound **74** could only be afforded using the conditions of entry 2, whereas in the other cases the starting material (sm) was recovered unaltered. The successful methodology started by activating lysine **28** with the coupling agent HATU and DIPEA in THF. Then, amine **71** was added and the reaction mixture was stirred at rt for 7 days. Purification by column chromatography furnished compound **74** in 25% yield. New signals corresponding to the lysine fragment introduced were observed in the ^{1}H-NMR and ^{13}C-NMR spectra of this compound.

Table IV-1. Methodologies tested for the peptidic coupling reaction leading to compound **74**.[a]

Entry	Reagents	Time	Yield (%)
1	**78**/DMF	7 days	sm
2	HATU/**28**	7 days	25
4	PyBOP/HOBt/**28**	5 days	sm
5	EDCI/HOBt/**28**	5 days	sm

(a) DIPEA was used as base and THF as solvent.

Azobenzene derivative **73** was prepared applying the best conditions previously found for analogous compound **74**. Thus, treatment of lysine derivative **28** with HATU and DIPEA and subsequent addition over a solution of azobenzene derivative **76** in THF delivered azobenzene-lysine tether **73** in 81% yield (Scheme IV-6). The less steric hindrance of primary amine **76** most probably accounts for the significantly better yield obtained in this case. In the ^{1}H-NMR and ^{13}C-NMR spectra of new product **73**, the appearance of new signals corresponding to the diprotected lysine fragment introduced were observed.

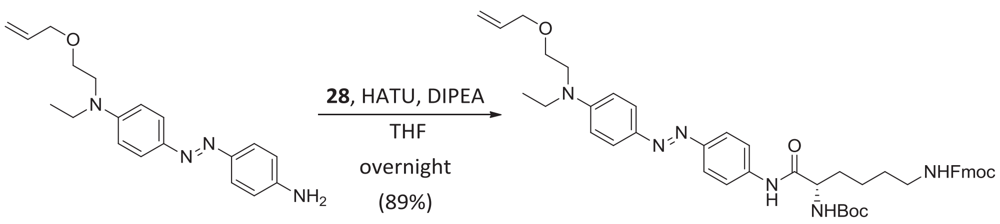

76 73

Scheme IV-6. Synthesis of compound **73**.

IV.2.2. Photochemical characterisation of model compounds 71-74

Red-shifted azobenzene model photoswitches **71-74** should present two states with different structural and physico-chemical properties resulting from the reversible photoinduced *trans-cis* isomerisation of their azobenzene units (Scheme IV-7). Once synthesised and chemically characterised, we focused on the investigation of their photochemical behaviour in solution, eventually aiming to determine the most suitable substitution pattern of the azoaromatic system for: (i) achieving sensitised *trans*→*cis* isomerisation with the naphthalene photo-harvesting antenna; and (ii) increasing the rate of thermal *cis*→*trans* back isomerisation for enabling single-wavelength operation of LiGluR.

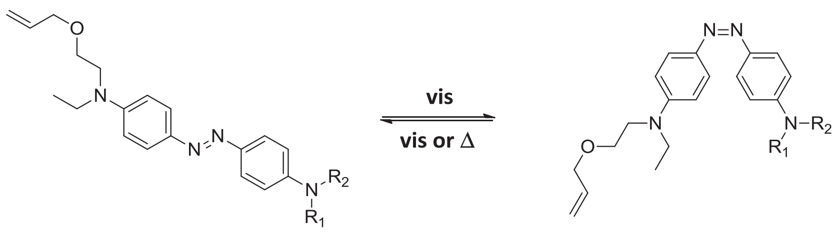

trans-**71**: R_1 = H; R_2 = CH_2CH_3 *cis*-**71**: R_1 = H; R_2 = CH_2CH_3
trans-**72**: R_1 = CH_2CH_3; R_2 = CH_2CH_3 *cis*-**72**: R_1 = CH_2CH_3; R_2 = CH_2CH_3
trans-**73**: R_1 = H; R_2 = Boc-Lys(Fmoc) *cis*-**73**: R_1 = H; R_2 = Boc-Lys(Fmoc)
trans-**74**: R_1 = CH_2CH_3; R_2 = Boc-Lys(Fmoc) *cis*-**74**: R_1 = CH_2CH_3; R_2 = Boc-Lys(Fmoc)

Scheme IV-7. Photoinduced *trans-cis* isomerisation of model red-shifted azobenzene compounds **71-74** upon one-photon excitation with visible light. *Cis*→*trans* back isomerisation can also take place thermally.

IV.2.2.1. Absorption spectra and sensitised *trans*→*cis* photoisomerisation

Initially, the absorption properties of the thermally stable *trans* isomer of the azobenzene model photoswitches were investigated. Figure IV-5 plots the absorbance spectra of these compounds in DMSO solution, which are compared to that of the 4,4'-diamidoazobenzene group found in MAG-1 (compound *trans*-**25**, see § III.1).

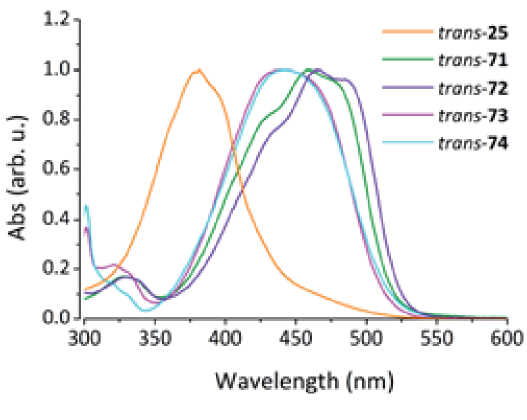

Figure IV-5. Normalised absorption spectra of compounds *trans*-**25**, **71-74** in DMSO ($c \sim 10^{-5}$ M).

In contrast to *trans*-**25**, the electronic absorption spectra of *trans*-**71**-**74** in DMSO only show a broad single band above 350 nm arising from the overlap of their $\pi\rightarrow\pi^*$ and $n\rightarrow\pi^*$ electronic transitions. As previously discussed (see § I.2.1), this is ascribed to the electron-donating character of the amino substituent introduced at the 4′ position of the azobenzene unit of these compounds. The maxima of this band are shown in Table IV-2, which report on the excitation energy of their strongly allowed $\pi\rightarrow\pi^*$ electronic transition. Noticeably, it shows a large dependence on the substitution pattern of the azobenzene core. Compared to *trans*-**25**, all model azobenzenes exhibit substantial bathochromical shifts of their $\pi\rightarrow\pi^*$ band (~ 60 nm in DMSO) owing to the introduction of an electro-donating tertiary amine at their *para*-position. On the other hand, the presence of an additional *para*-amino substituent further red-shifts the $\pi\rightarrow\pi^*$ electronic transition by ~ 20 nm, thus accounting for the spectral differences observed between compounds **71**-**72** and **73**-**74**. Contrarily, *N*-ethyl substitution of the 4′-amino and 4-amido groups of **71**-**72** and **73**-**74** only has a minor influence on the absorption spectra of these compounds.

Table IV-2. Absorption maxima of the $\pi\rightarrow\pi^*$ electronic transition of *trans*-**25**, **71**-**74** in DMSO.

Compound	λ_{max} (nm)
trans-**25**	381
trans-**71**	459
trans-**72**	465
trans-**73**	439
trans-**74**	441

To evaluate whether the degree of red-shifting achieved in the model compounds would enable sensitised *trans*→*cis* isomerisation by RET from the photoexcited naphthalene unit to the azobenzene group, the Förster radius of this donor-acceptor pair in aqueous buffer was calculated for *trans*-**71**-**74** by means of Equation I.4. In this calculation, the following parameters were used for all four compounds: (i) $\Phi_{Fl,D}$= 0.43, which is the fluorescence quantum yield of the naphthalene model antenna **100** in a PBS-DMSO 4:1 mixture (see Figure IV-11 and § IV.4.1); (ii) k^2= 2/3, which was calculated assuming that the donor and acceptor would be randomly oriented; and (iii) n = 1.365, which is the refractive index of PBS-DMSO 4:1 at rt. The overlap integrals determined between the absorption spectrum of *trans*-**71**-**74** and the emission spectrum of naphthalene derivative **100** are collected in Table IV-3 together with the R_0 values calculated from them.

Table IV-3. Overlap integrals and Förster radii for the resonant energy transfer process between *trans*-**71**-**74** and naphthalene antenna **100** in PBS-DMSO 4:1.

Compound	*J* (cm^{-1})	R_0 (Å)
trans-**71**	1.03 x 10^{-13}	44.3
trans-**72**	8.77 x 10^{-14}	43.1
trans-**73**	5.38 x 10^{-14}	39.7
trans-**74**	5.63 x 10^{-14}	40.0

In all cases, the values of R_0 obtained are larger than the center-to-center distance expected in the target ligands between the antenna and azobenzene groups according to our previous calculation for the analogous compound **21** (r = 11.8 Å, see § III.3.3). By introducing these parameters into Equation I.3, the efficiency of the RET process between *trans*-**71**-**74** and the naphthalene group is predicted to be higher than 99% in all cases. Consequently, the *trans*→*cis* isomerisation of all these azobenzene derivatives should be efficiently sensitised by means of the photo-harvesting antenna selected in this chapter.

IV.2.2.2. Direct *trans-cis* photoisomerisation

The study of the photochromic behaviour of model azobenzenes **71**-**74** was done by analyzing the direct *trans*→*cis* photoisomerisation of all these compounds under one-photon excitation conditions as well as the kinetics of their *cis*→*trans* thermal back isomerisation.

When irradiating DMSO solutions of *trans*-**71**-**74** with blue light, noticeable changes in the absorption spectra of these samples were observed, which are consistent with the occurrence of their *trans*→*cis* photoisomerisation reaction (Figure IV-6). Thus, upon irradiation at 473 nm all compounds showed a significant decrease of their broad absorption maxima at ~ 450 nm associated to their $\pi\rightarrow\pi^*$ electronic transition and a slight increase of the red tail of their absorption band corresponding to their $n\rightarrow\pi^*$ transition.

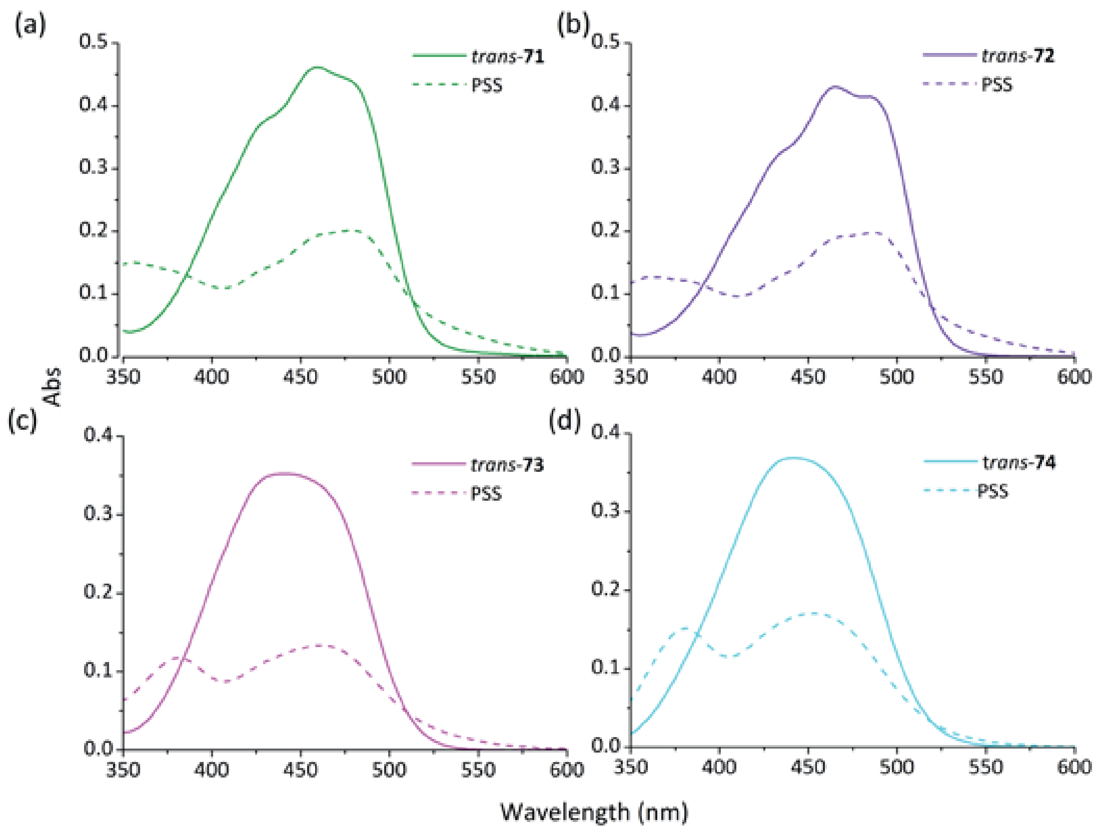

Figure IV-6. (a) Absorption spectra of the initial *trans* state and the PSS mixture obtained upon irradiation of (a) **71**, (b) **72**, (c) **73** and (d) **74** at 473 nm in DMSO.

On the other hand, *cis*→*trans* isomerisation of compounds **71-74** was observed to occur both photochemically and thermally. As expected, irradiation of the *cis* state of these species with green light induced nearly quantitative conversion to their *trans* isomer. Concerning the *cis*→*trans* thermal isomerisation process, it was investigated in detail for all compounds in DMSO solution by means of UV-vis absorption spectroscopy measurements. As shown in Figure IV-7, the intensity of the $\pi \rightarrow \pi^*$ absorption component of *trans/cis* mixtures of **71-74** clearly increased in time in the absence of light illumination, while a slight decrease of the $n \rightarrow \pi^*$ absorption band was also observed. These results clearly indicate that thermal *cis*→*trans* isomerisation took place.

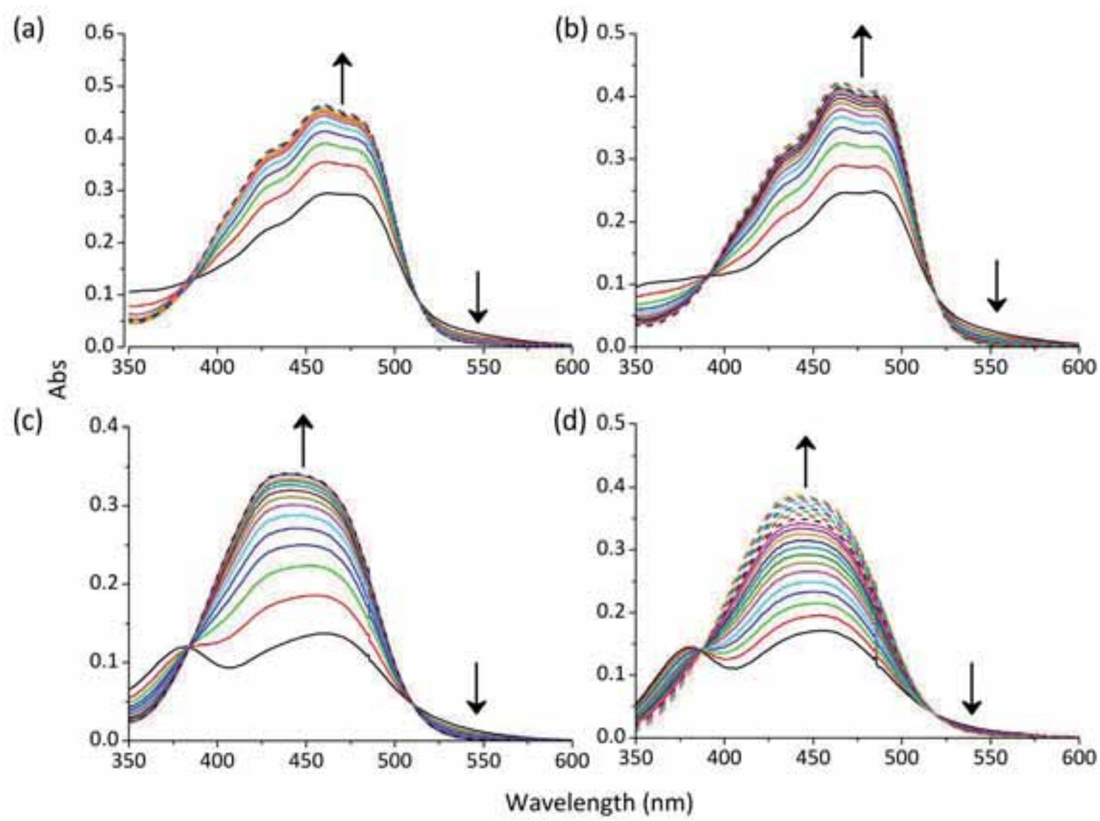

Figure IV-7. Variation of the absorption of the *trans/cis* photostationary state mixtures of (a) **71**, (b) **72**, (c) **73** and (c) **74** in the dark at 25 ºC in DMSO. The arrows indicate the direction of the changes observed in time.

The absorption recovery time traces at the absorption maximum of the *trans* isomer of each compound can be fitted with a monoexponential growth function (Figure IV-8), which allows to determine the rate constant of the thermal back isomerisation reaction and the half-lives of *cis*-**71**-**74** (Table IV-4). Clearly, no significant differences were observed between the *cis* state lifetime of the two azobenzene compounds with similar substitution patterns ($t_{1/2}^{cis}$ = 2.5 and 1.8 min for 4,4′-diamino derivatives **71** and **72**, respectively; $t_{1/2}^{cis}$ = 38 and 46 min for 4-amido-4′-amino photoswitches **73** and **74**, respectively). This indicates that the introduction of an ethyl group into the amino substituent at the *para*-position does not have a large influence on the thermal stability of the *cis* isomer. In contrast, a ~ 16 fold increase in thermal back isomerisation rate was observed when turning the asymmetrical 4-amido-4′-amino derivatives **73** and **74** into 4,4′-diamino substituted azobenzenes **71** and **72** displaying symmetrical electronic distribution. In addition, it must be noted that the lifetime of the *cis* isomer of the four model compounds designed drops off down to the minute timescale at rt, in stark contrast to the much larger thermal stability of the *cis*-azobenzene group of MAG-1 and the potential PTL **21** developed in Chapter III (e.g. $t_{1/2}^{cis}$= 6.0 h for **21** in DMSO). This can be unambiguously ascribed to the *para*-

amino substituent introduced into the azobenzene core of all these compounds, which does not only red-shifts their absorption spectra but also dramatically reduces their *cis* isomer lifetime.

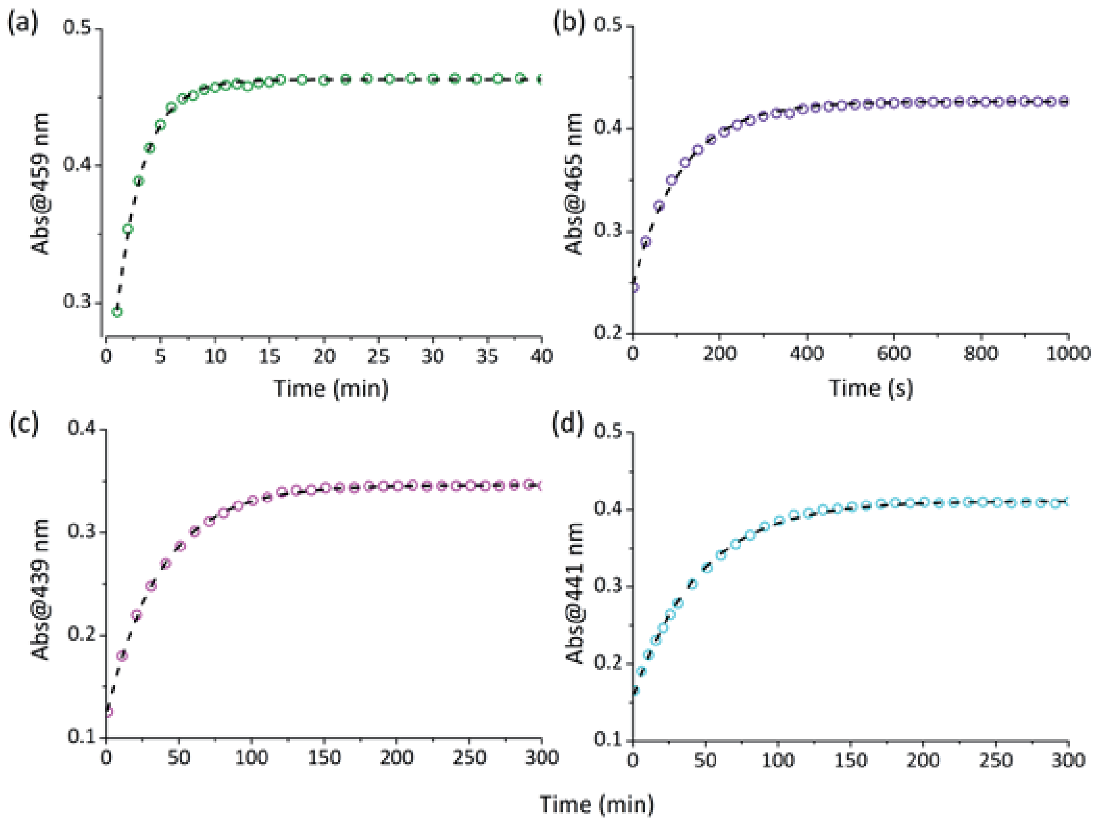

Figure IV-8. Kinetics of the *cis*→*trans* thermal isomerisation of (a) **71**, (b) **72**, (c) **73** and (d) **74** monitored at the absorption maximum of the *trans* isomer of each compound in the dark at 25 ºC in DMSO**.** Points correspond to the experimental data, while dashed lines were obtained from monoexponential fits.

To check whether such enhancement of the *cis*→*trans* thermal isomerisation rate could enable single-wavelength control of LiGluR, further measurements were conducted in phosphate buffer solution (PBS) to mimic the conditions of the biological experiments. In particular, these measurements had to be carried out in a PBS-DMSO 4:1 mixture because of the poor solubility of the compounds in aqueous solution. In this medium, a much faster thermal back isomerisation rate was observed, which could not be studied by steady-state absorption spectroscopy. Instead, we investigated the formation and lifetime of the *cis* isomer of model compounds **71-74** by means of transient absorption spectroscopy with ns-time resolution. In these experiments, the absorbance at the maximum wavelength of the $\pi\rightarrow\pi^*$ transition of each *trans* isomer was measured as function of time after pulsed laser excitation at 475 nm and then subtracted from that of the initial non-irradiated sample to derive the corresponding transient absorption values (ΔAbs). The resulting transient absorption time traces are plotted in Figure IV-9. In all cases, pulsed blue-light irradiation of *trans*-**71-74** immediately resulted in a dramatic decrease of the absorption signal associated to their π→π* transition (i.e. ΔAbs < 0 at t = 0 s). This is ascribed to the depletion of the *trans* ground electronic state due to the photoinduced formation of the corresponding *cis* isomer, which presents a smaller absorption coefficient at the detection wavelength (see e.g. Figure IV-6). However, this negative signal rapidly decays in time and the initial absorption values (i.e. ΔAbs = 0) are recovered in less than 200 ms in all cases. This is due to the *cis*→*trans* thermal back isomerisation process restoring the initial concentration of *trans* state molecules, whose rate can be determined by a monoexponential fit of the transient absorption signal (Table IV-5).

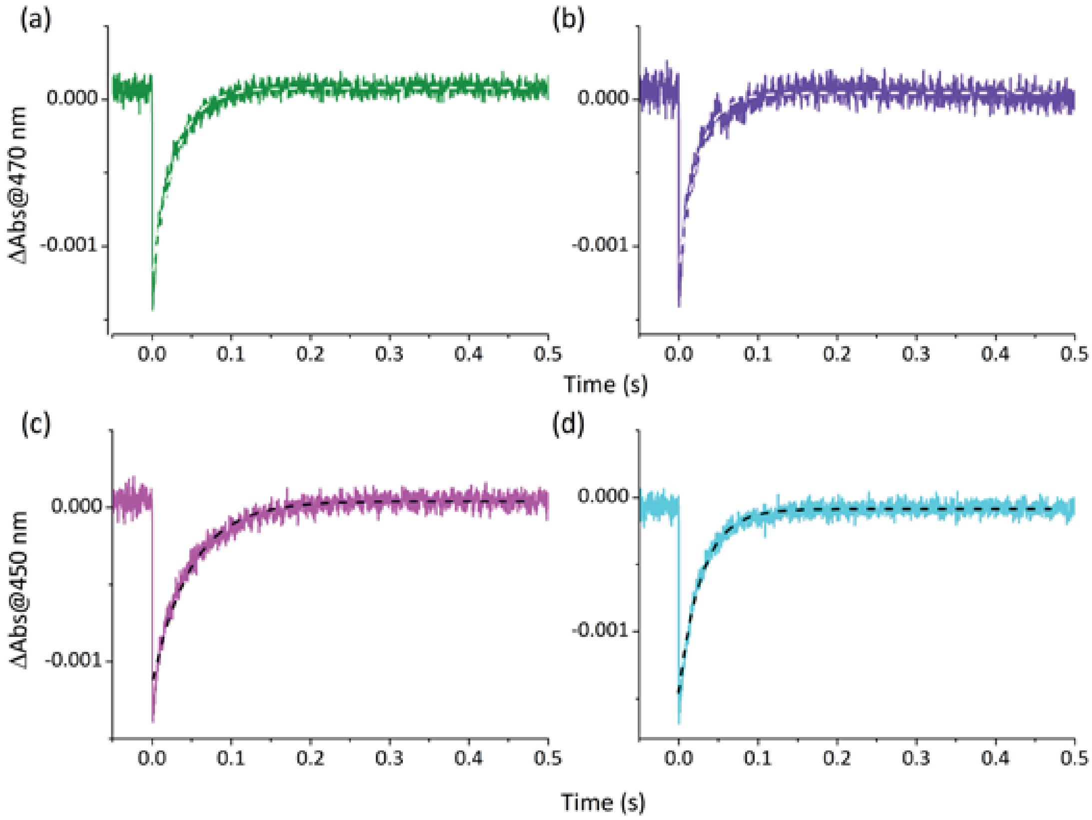

Figure IV-9. Transient absorption time traces measured at 470 nm for (a) *trans*-**71** and (b) *trans*-**72** and 450 nm for (c) *trans*-**73** and (d) *trans*-**74** upon excitation at 475 nm (0.5 mJ/pulse) in the dark at 25 ºC in PBS-DMSO 4:1. Solid lines correspond to the experimental data, while dashed lines were obtained from monoexponential fits.

Notably, the thermal stability of the *cis* isomer of **71**-**74** falls down to the millisecond timescale in aqueous buffer at rt, as previously reported for other aminoazobenzene derivatives.[16] Actually, the half-life of the *cis* state of the four model compounds is shorter than 50 ms, and minor differences are found between them. As such, all of them would allow fast gating of LiGluR using a single irradiation source to induce *trans*→*cis* isomerisation. As soon as illumination ceases, this process should be reverted back spontaneously in the millisecond scale due to rapid thermal *cis*→*trans* isomerisation.

Table IV-4. Thermal *cis*→*trans* isomerisation rate constants and *cis* isomer half-lives determined from monoexponential fits of the experimental data measured for compounds **71-74** in DMSO and PBS-DMSO 4:1.[a]

Compound	$k_{cis\rightarrow trans}$ (s^{-1}) in DMSO	$t_{1/2}^{cis}$ (min) in DMSO	$k_{cis\rightarrow trans}$ (s^{-1}) in PBS-DMSO 4:1	$t_{1/2}^{cis}$ (ms) in PBS-DMSO 4:1
71	6.7×10^{-3}	2.5	59	17
72	8.8×10^{-3}	1.9	59	17
73	4.4×10^{-4}	38	29	34
74	3.6×10^{-4}	46	53	19

(a) Values determined at 25 ºC.

Once characterised the four red-shifted azobenzene models prepared, compound **73** was selected as the azobenzene core for the preparation of the two types of photoswitched tethered ligands targeted in this chapter. The features that made it the best candidate for our purposes are the following: (i) it meets the criteria required for favouring both the sensitised (i.e. efficient RET with the naphthalene antenna chosen) and direct (i.e. asymmetrical electronic distribution) excitation strategies to be explored to attain two-photon control of LiGluR; (ii) it presents a fast spontaneous *cis*→*trans* back isomerisation rate, which should enable single-wavelength operation of the ion channel; and (iii) its easier synthetic accessibility, since no alkylation of the 4-amido group is needed.

Based on the substitution pattern of the selected red-shifted azobenzene model compound **73** and aiming at preserving the main structural features of MAG-1, two new target photoswitched tethered ligands were designed to pursue the objectives of this chapter (Figure IV-10): (i) compound **22**, which incorporates a naphthalene photo-harvesting antenna to enable two-photon sensitised operation of the switch; and (ii) compound **23**, which is devised to operate via direct two-photon photoisomerisation of its azobenzene core. Furthermore, as compound **22** would present the same azoaromatic substitution pattern as **23**, this ligand would be able to also operate via direct irradiation of its azobenzene group as well.

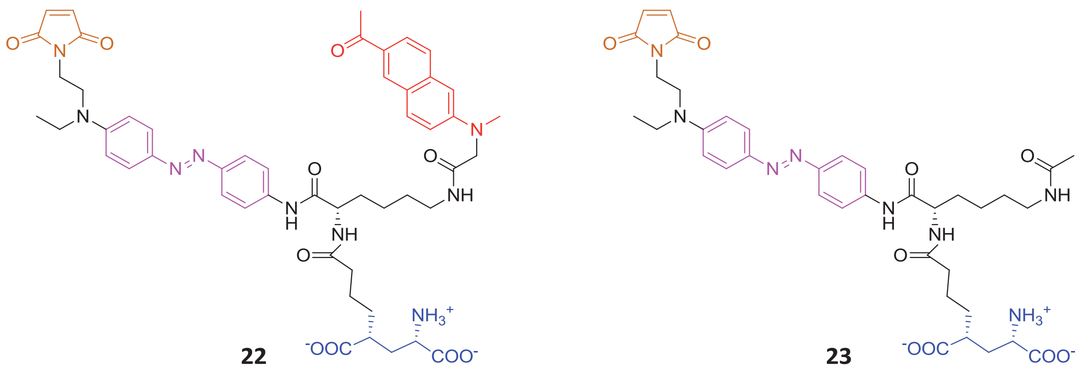

Figure IV-10. Structures of the target PTLs **22** and **23**. The distinct functional units of these compounds are shown in different colours (blue: glutamate, pink: azobenzene; brown: maleimide; red: naphthalene).

As illustrated in Figure IV-10 both compounds are composed of different fragments, three of which are equivalent to those found in MAG-1 (i.e. maleimide, glutamate and azobenzene groups). Moreover, product **22** incorporates two additional units: (i) naphthalene derivative **70** as photo-harvesting antenna; and (ii) L-lysine as central scaffold, to which the different functional units of the target compound would be tethered. For sake of comparison, photoswitch **23** also bears this lysine derivative, which will ensure that the intramolecular distances between the maleimide, azobenzene and glutamate fragments are preserved for both target ligands. To prevent side-reactions during the synthesis of PTL **23**, its free amino residue will be protected with an acetyl group. The preparation of the two photoswitched tethered ligands is described in the following section. In addition, we report the synthesis of photo-harvesting antenna model **100** as well (see § IV.3.3).

IV.3. SYNTHESIS OF PHOTOSWITCHED TETHERED LIGANDS 22 AND 23

IV.3.1. Preparation of target compound 22

The first target ligand of this chapter could be prepared via the modular synthetic sequence depicted in Scheme IV-8, which followed a similar strategy to that devised in Chapter III for the preparation of potential PTL **21**. Thus, L-lysine **28** was taken as scaffold, to which the azobenzene, naphthalene and glutamate moieties would be directly attached.

The synthetic pathway would start by coupling *O*-protected aminoazobenzene **76** to *N*,*N*-diprotected L-lysine **28** to yield tether **73**, whose preparation has already been described in § IV.2.1.3. Then, selective removal of the Fmoc protecting group followed by introduction of a naphthalene derivative obtained from commercial 1-(6-methoxy-2-naphthyl)ethanone would provide intermediate **79**. Afterwards, acid removal of the Boc protection of **79** and subsequent coupling reaction of the resulting amine with the glutamate derivative obtained from L-pyroglutamic acid would furnish amide **80**. Deprotection of the alcohol group of **80** and further introduction of the maleimide moiety would deliver advanced compound **81**. Finally, the desired ligand **22** would be obtained after removal of the protecting groups of the maleimide and glutamate moieties. Next, all these different synthetic steps are described in detail.

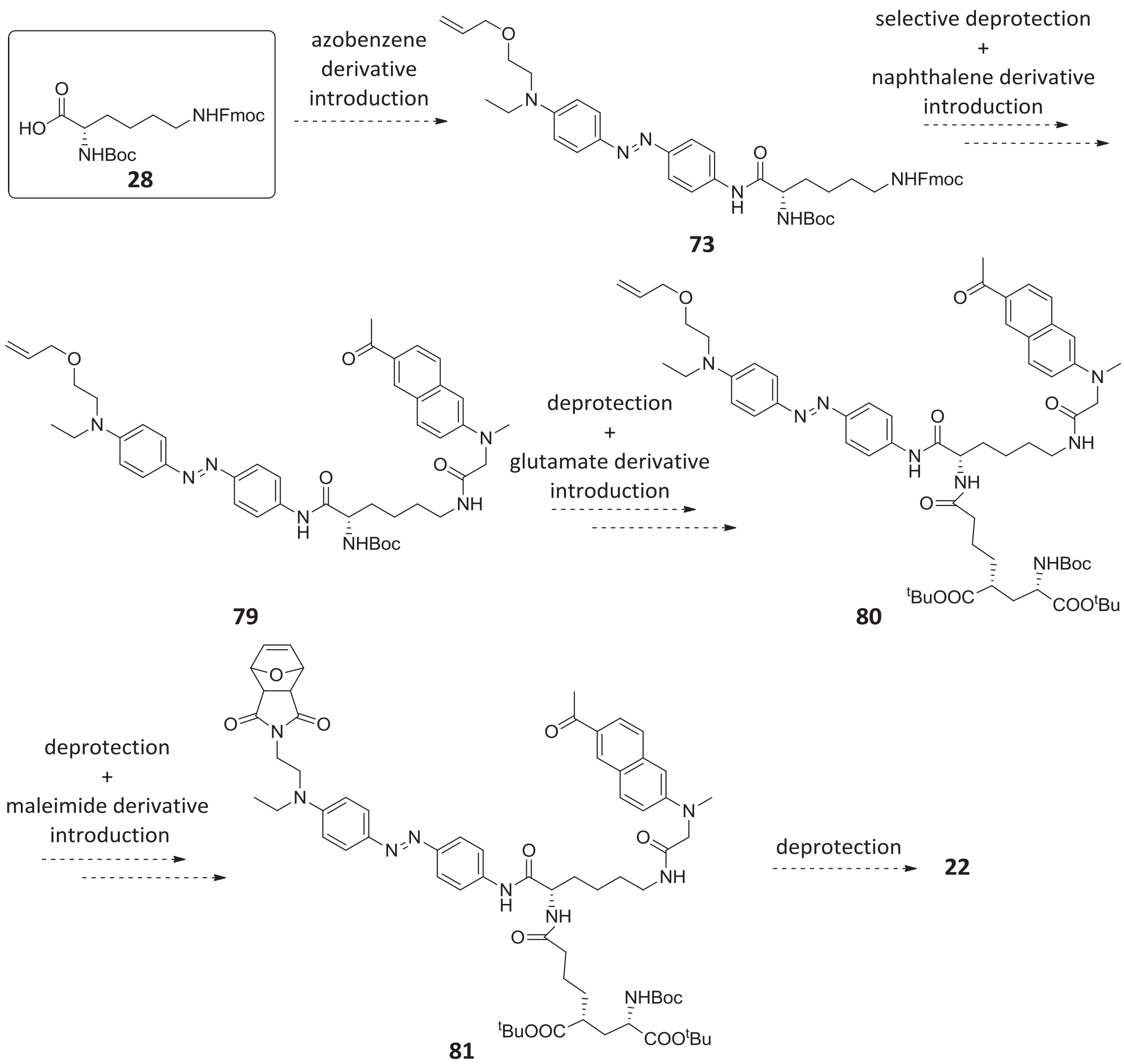

Scheme IV-8. Planned strategy designed for the preparation of PTL **22**.

IV.3.1.1. Preparation and introduction of naphthalene derivative 70. Synthesis of intermediate 79

According to the synthetic pathway proposed, the second step towards the preparation of target photoswicth **22** was the introduction of naphthalene derivative **70** into already synthesised model azobenzene **73**. Compound **70** was prepared following the sequence of reactions outlined in Scheme IV-9, which are based on a previously reported procedure by Cho and co-workers.[3]

This methodology allows its synthesis on a multi-gram scale and in satisfactory yield from 1-(6-methoxy-2-naphthyl)ethanone (**82**).

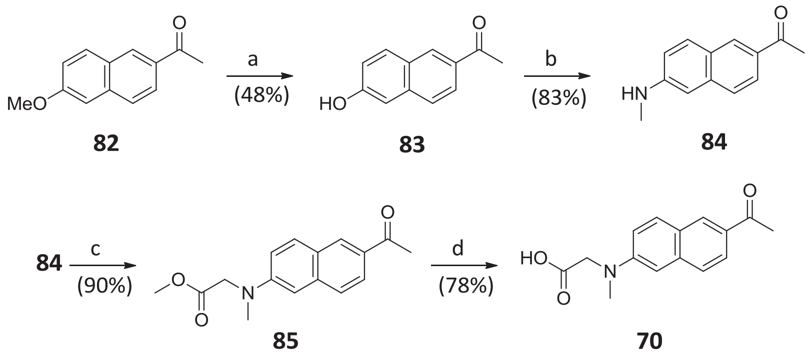

Reagents and conditions: (a) CH_3COOH glacial, 48% HBr, 100 ºC, overnight; (b) $MeNH_2$·HCl, $Na_2S_2O_5$, NaOH, H_2O, 140 ºC, 7 days; (c) methyl 2-bromoacetate, Na_2HPO_4, NaI, CH_3CN, 18 h; (d) KOH, EtOH/H_2O.

Scheme IV-9. Synthesis of naphthalene derivative **70**.

The synthesis of **70** started with the cleavage of the methyl ether protection of naphthalene derivative **82** with HBr in CH_3COOH glacial at 100 ºC to afford alcohol **83.** Reaction of the resulting primary alcohol with $MeNH_2$ in the presence of $Na_2S_2O_5$ and NaOH gave amine **84** in 83% yield. Next, this intermediate was alkylated with methyl 2-bromoacetate and subsequent hydrolysis of the methyl ester group rendered the desired naphthalene derivative **70** (4 steps, 28% overall yield from **82**). The spectroscopic data collected for naphthalene derivative **70** matched that reported in the literature.[3]

Then, naphthalene derivative **70** was attached to azobenzene-lysine tether **73**. This first required removal of the Fmoc protection of this intermediate by treatment with 20% piperidine in DMF (Scheme IV-10). Under these conditions, amine **86** was obtained in 87% yield after purification by column chromatography. In the ^{1}H-NMR and ^{13}C-NMR spectra of **86**, the characteristic signals corresponding to the Fmoc group cleaved were observed to disappear.

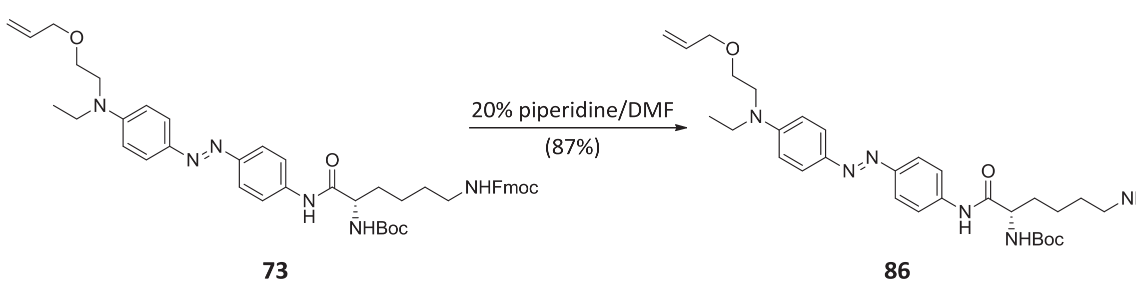

Scheme IV-10. Fmoc deprotection of **73** in basic conditions.

In the next step, acid **70** was treated with EDCI, DIPEA and HOBt, and then added over a solution of azobenzene derivative **86** in THF (Scheme IV-11). After 12 h of reaction and purification by column chromatography, product **79** was obtained in 81% yield. The incorporation of the naphthalene fragment was clearly confirmed by the presence of its distinctive signals in the ^{1}H-NMR (6 new aromatic signals within the 8.31-6.93 ppm region as well as 3 new aliphatic signals between 4.01-2.65 ppm) and in the ^{13}C-NMR spectra of this compound (2 new carbonyl signals at 197.9 ppm and 170.2 ppm, 10 new aromatic signals between 148.9-106.9 ppm as well as 3 new aliphatic signals at 58.4, 39.9 and 26.6 ppm). In addition, downfield and upfield shifts were observed for H-5 and C-5 NMR signals, respectively (H-5: from 2.80 ppm in **86** to 3.33 ppm in **79**; C-5: from 41.3 ppm in **86** to 38.4 ppm in **79**).

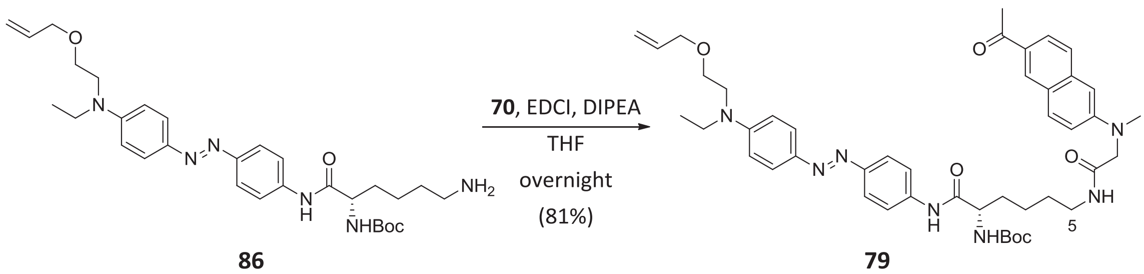

Scheme IV-11. Coupling of [(6-acetyl-2-naphthyl)(methyl)amino]acetic acid (**70**) to amine **86**.

IV.3.1.2. Incorporation of glutamate derivative 65. Synthesis of intermediate 80

To achieve the synthesis of intermediate **80**, removal of the Boc protecting group of **79** was first needed. This was accomplished by treatment with 37% HCl in methanol, which furnished amine **87** as an orange solid in 93% yield (Scheme IV-12). The disappearance of the signals corresponding to the Boc protecting group in its ^{1}H-NMR and ^{13}C-NMR spectra confirmed the formation of amine **87**.

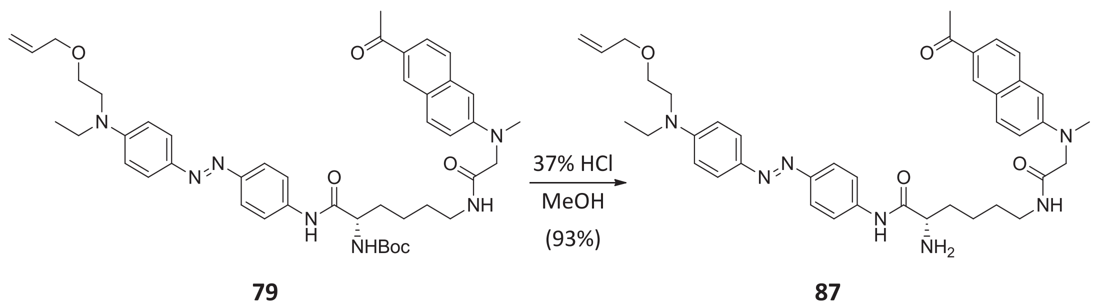

Scheme IV-12. Removal of the Boc protecting group of **79** under acidic conditions.

Subsequent coupling of glutamate derivative **65** (see § III.2.3.1) to amine **87** provided advanced intermediate **80**. Similar reaction conditions to those used in previous similar synthetic steps were applied (i.e. EDCI as coupling agent, DIPEA as base, HOBt as additive and THF as solvent, Scheme IV-13). The reaction mixture was stirred at rt during 12 h and after subsequent work-up, the crude was purified by column chromatography to isolate product **80** as an orange solid in 71% yield. New signals corresponding to the glutamate fragment introduced were observed in the ^{1}H-NMR and ^{13}C-NMR spectra of this compound.

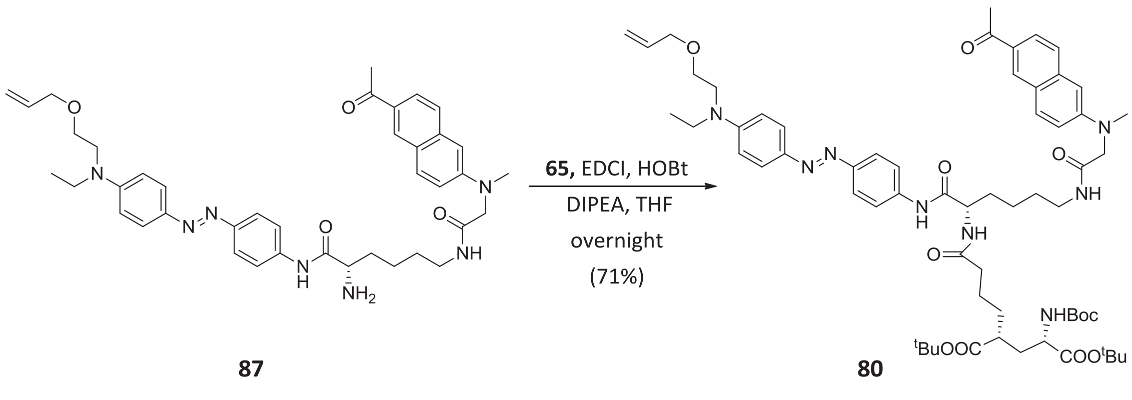

Scheme IV-13. Peptide coupling reaction for the synthesis of compound **80**.

IV.3.1.3. Preparation and introduction of furan-protected maleimide 89. Synthesis of compound 81

Having covalently attached three of the four functional units of the desired photoswitchable tethered ligand **22** to the L-lysine scaffold, we next aimed at the introduction of the maleimide unit group. To this end, the allyl protecting group was first cleaved and then the maleimide moiety was coupled.

Allyl ether deprotection can be accomplished in a step-wise manner: first, this moiety is isomerised to propenyl ether under mild conditions using a transition metal catalyst and, in a second step, the resulting ether group is hydrolysed upon addition of a Lewis acid.[17,18] Thus, the rearrangement of allyl ether **80** was achieved by treatment with Wilkinson's catalyst ($RhCl(PPh_3)_3$) in reflux of aqueous ethanol (Scheme IV-14). The resulting propenyl ether was removed directly with a mixture of $HgCl_2$ and HgO in aqueous acetone, furnishing alcohol **88** in 88% for the two steps.[19] This was confirmed by analysis of its ^{1}H-NMR spectrum, where the signals of the allyl protecting group disappeared.

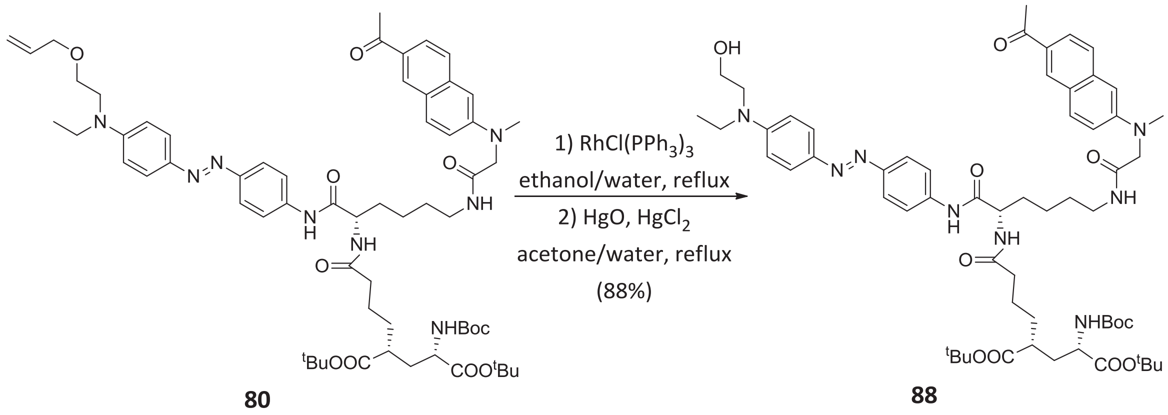

Scheme IV-14. Two-step sequence to cleave the allyl protecting group of **80**.

Direct functionalisation of the primary alcohol in **88** with the maleimide moiety could be achieved using Mitsunobu conditions. The Mitsunobu reaction, one of the most useful and specific reactions in organic chemistry, converts primary or secondary alcohols into excellent leaving groups that can be displaced with a wide range of nucleophiles both intra- and intermolecularly.[20,21] Unfortunately, the maleimide group would probably not resist the basic conditions needed in this process. This problem could be solved by using a furan-protected maleimide during the functionalisation step instead, which could be easily diprotected afterwards via retro-Diels-Alder reaction (Scheme IV-15).

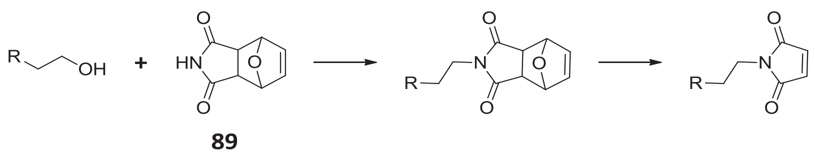

Scheme IV-15. Mitsunobu reaction between a primary alcohol and furan-protected maleimide followed by maleimide deprotection.

The protection of maleimide -C=C- bond was achieved according to the procedure described in the literature (Scheme IV-16).[22] Thus, Diels-Alder reaction between commercially available maleimide (**90**) and furan (**91**) delivered the furan-masked maleimide **89** in 60% yield. Its chemical characterisation was in agreement with the selective formation of the more stable *exo* isomer of the adduct, according to the spectroscopic data reported in the bibliography.[22]

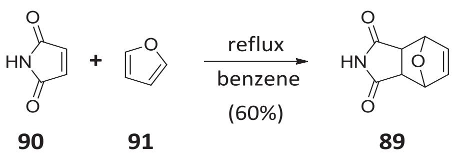

Scheme IV-16. Protection of the maleimide -C=C- bond.

Next, alcohol **88** was treated with **89**, triphenylphosphine and diisopropyl azodicarboxylate (DIAD) in THF to afford the corresponding product **81** in low yield (32%) after purification by column chromatography (Scheme IV-17).[23]

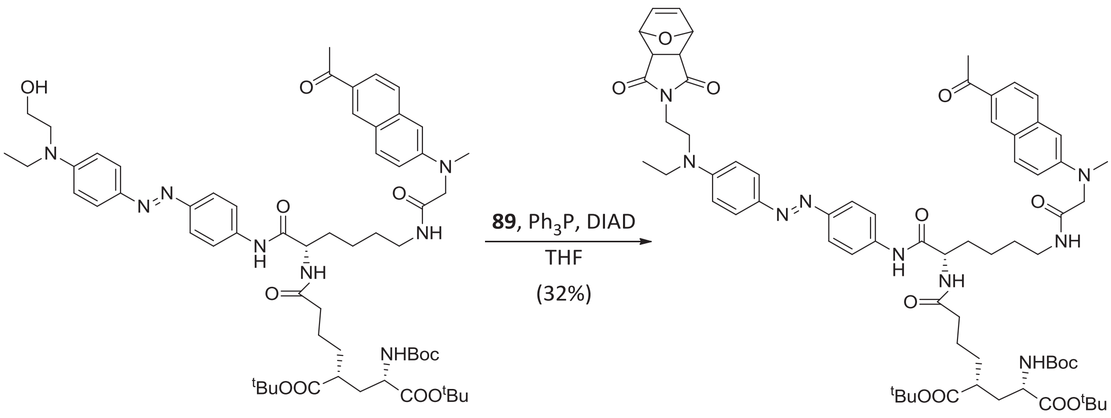

Scheme IV-17. Introduction of the furan-masked maleimide **88** through Mitsunobu methodology.

The presence of the maleimide derivative on substrate **81** was established by the appearance of new signals on its ^{1}H-NMR and ^{13}C-NMR spectra. Thus, 3 additional ^{1}H-NMR signals were found at 6.52, 5.26 and 2.76 ppm arising from the furan-masked maleimide fragment introduced, while the corresponding ^{13}C-NMR signals were observed at 176.3, 136.7, 81.0 and 47.7 ppm.

IV.3.1.4. Removal of protecting groups. Preparation of target compound 22

The last transformation to complete the synthesis of PTL **22** was the deprotection of both maleimide and glutamate fragments. Retro-Diels Alder deprotection of furan-masked maleimide was accomplished by heating **81** in refluxing toluene for 5 h (Scheme IV-18).[24] The resulting crude was purified by column chromatography, obtaining **92** in quantitative yield. The formation of **92** was clearly evidenced by the absence of the signals corresponding to the furan group in their ^{1}H-NMR and ^{13}C-NMR spectra. Additionally, a new signal at 6.66 ppm corresponding to the olefinic protons of the free maleimide group (H-3^{vi} and H-4^{vi}) was observed by ^{1}H-NMR.

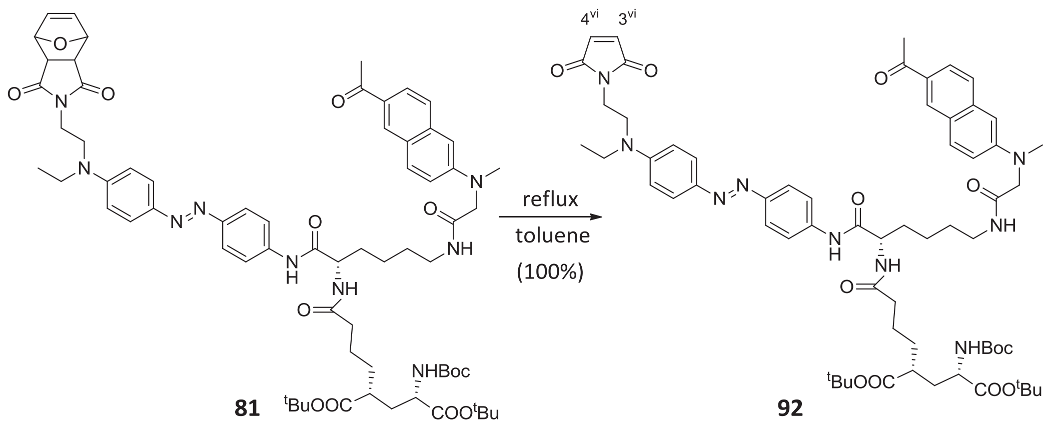

Scheme IV-18. Release of the maleimide moiety via retro-Diels-Alder reaction.

Next, simultaneous removal of the *tert*-butyl ester and Boc protecting groups of **92** was achieved by exposure to a 1:2 mixture of trifluoroacetic acid and dichloromethane. Under these conditions, target compound **22** was obtained in 86% yield (Scheme IV-19). As expected, the ^{1}H-NMR signal of the *tert*-butyl ester and Boc groups at 1.43 ppm disappeared from the spectrum of **22**. In addition, upfield and downfield shifts were observed for H-1 and H-3 signals, respectively (H-1: from 4.16 ppm in **92** to 3.99 ppm in **22**; H-3: from 2.36 ppm in **92** to 2.67 ppm in **22**).

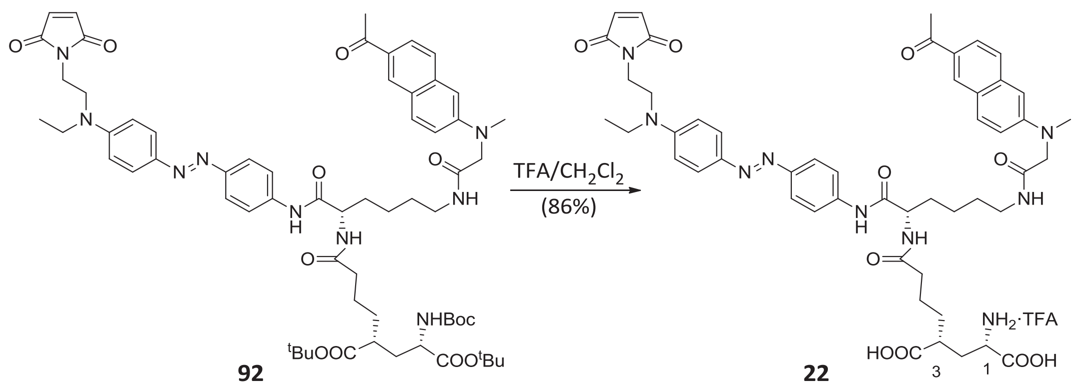

Scheme IV-19. Final synthetic step to obtain PTL **22**.

To sum up, a new MAG derivative bearing a naphthalene sensitiser was prepared by a convergent synthesis of 9 steps starting from *N,N*-diprotected L-lysine **28** in 10% overall yield. Our synthetic approach relied on the sequential introduction of the different functional fragments of the target compound to this lysine scaffold: *O*-protected aminoazobenzene **76**, naphthalene derivative **70** (obtained from 1-(6-methoxy-2-naphthyl) ethanone (**82**) in 4 steps and 28% yield), glutamate derivative **65** (prepared in 8 steps and 7.0% global yield from L-pyroglutamic acid (**37**)) and furan-protected maleimide **89** (prepared in 1 step and 60% yield from furan (**91**) and maleimide (**90**)).

IV.3.2. Preparation of target compound 23

After completing the synthesis of PTL **22**, we focused on the preparation of the second target compound of this chapter: photoswitched tethered ligand **23.** This compound could be obtained following the sequence of reactions depicted in Scheme IV-20, which are based on those previously used for the synthesis of **22**. However, in this case no naphthalene sensitiser had to be incorporated into the ligand and the free amino residue of the L-lysine scaffold was converted into an acetamide group instead. Since the Boc protecting group of the L-lysine fragment does not support the conditions of this acetylation step, the glutamate derivative would be introduced in an earlier stage than in the case of **22**.

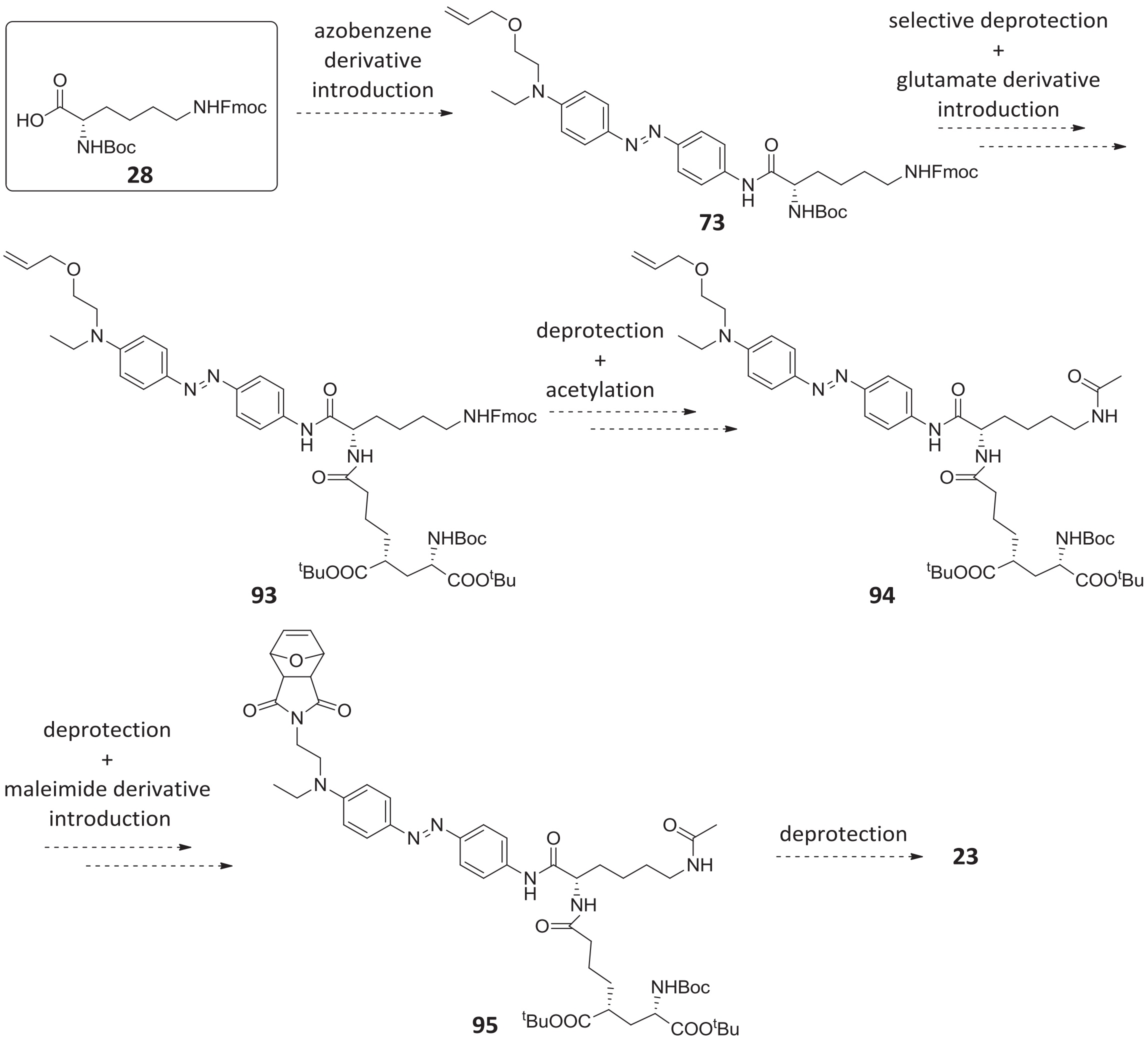

Scheme IV-20. Planned strategy designed for the preparation of PTL **23**.

Once again, the synthetic strategy would start by preparing azobenzene-lysine tether **73**, which is one of the model chromophores already investigated and a common intermediate of the synthesis of target ligand **22** (see § IV.2.1.3). Selective cleavage of the Boc protecting group and subsequent coupling reaction of the resulting amine with a glutamate derivative would render

93. Afterwards, cleavage of the Fmoc protecting group followed by acetylation of the corresponding amine would provide amide **94**. From amide **94** the synthetic steps proposed are analogous to those exploited in the preparation of **22**. Thus, removal of the allyl ether protecting group would enable the introduction of furan-protected maleimide to deliver advanced intermediate **95**. Finally, deprotection of both maleimide and glutamate moieties would afford the target photoswitched tethered ligand **23**. All these different synthetic steps are described in detail in the following sections.

IV.3.2.1. Incorporation of glutamate derivative 65. Preparation of intermediate 93

The synthesis of **93** started with the selective cleavage of the Boc protecting group of the already prepared azobenzene-lysine tether **73**. This compound was treated with 37% HCl in methanol, thus delivering amine **96** in 93% yield after purification by column chromatography (Scheme IV-21). Deprotection of the amino group was confirmed by the absence of the signals corresponding to the Boc protecting group in the ^{1}H-NMR and ^{13}C-NMR spectra of **96**.

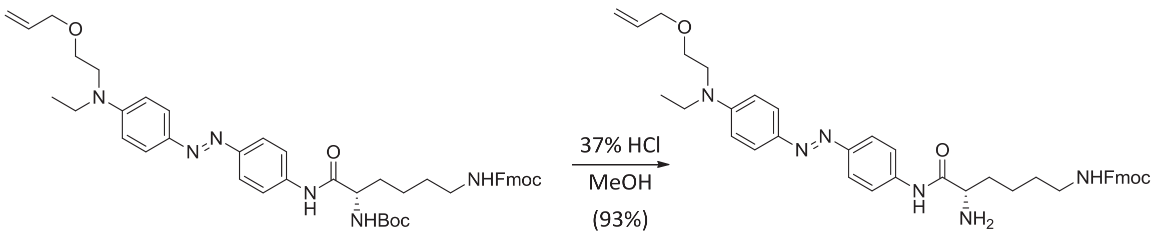

73 **96**

Scheme IV-21. Removal of Boc protecting group of **73** under acidic conditions.

In the next step, acid **65** was activated with EDCI, DIPEA and HOBt, and then added over a solution of amine **96** (Scheme IV-22). After 12 h of reaction and subsequent purification by column chromatography, product **93** was obtained in 88% yield. Glutamate derivative attachment could be corroborated by the ^{1}H-NMR spectrum of this compound, where new signals corresponding to this fragment appeared.

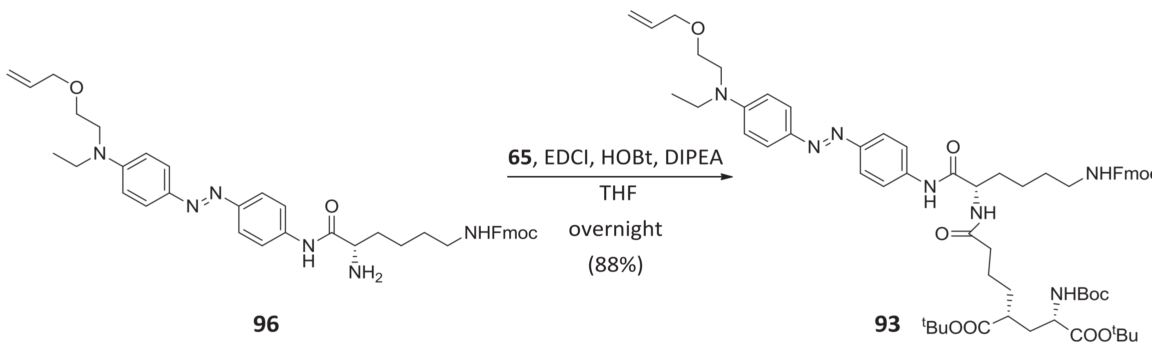

Scheme IV-22. Synthesis of compound **93**.

IV.3.2.2. Acetylation of intermediate 93. Synthesis of compound 94

The next transformation of our synthetic route was the cleavage of the Fmoc protecting group of intermediate **93**. With this aim, this compound was treated with 20% piperidine in DMF providing amine **97** in 64% yield (Scheme IV-23). In its ^{1}H-NMR spectrum, the most significant changes found with respect to the starting material were the absence of the characteristic signals of the Fmoc group and a downfield shift for H-5^{ii} NMR signal from 2.76 ppm to 3.19 ppm. Similar features were observed in its ^{13}C-NMR spectrum.

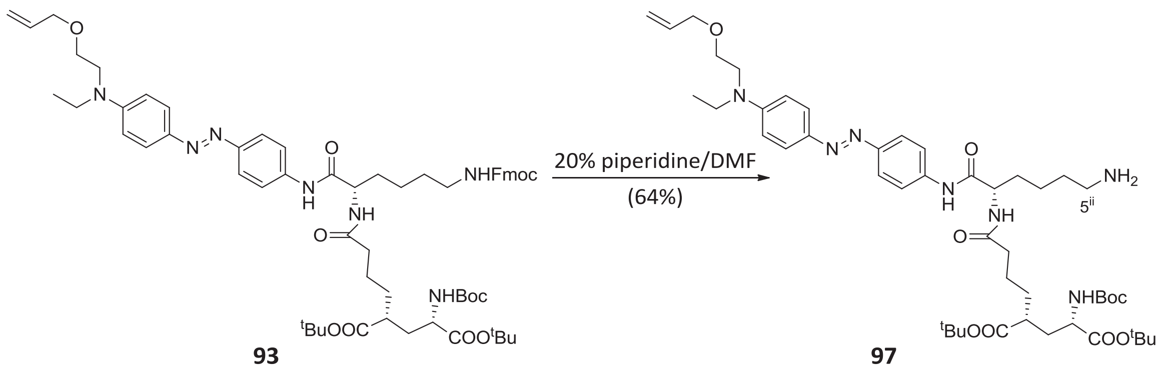

Scheme IV-23. Fmoc deprotection of **93** in basic conditions.

As mentioned above, the free amino group of the lysine residue should be masked in order to avoid solubility problems and side-reactions in the following steps of the synthetic route towards target ligand **23**. To overcome these issues in a simple manner, we decided to acetylate amine **97** by treatment with acetyl chloride and pyridine as base in dichloromethane, which delivered amine **94** in 69% yield (Scheme IV-24). The incorporation of the new acetyl group could be easily confirmed by ^{1}H-NMR and ^{13}C-NMR. Thus, a new ^{1}H-NMR signal arising from the methyl group introduced appeared at 2.15-1.88 ppm, while the corresponding carbonyl and methyl ^{13}C-NMR signals were found at 170.5 and 23.4 ppm, respectively.

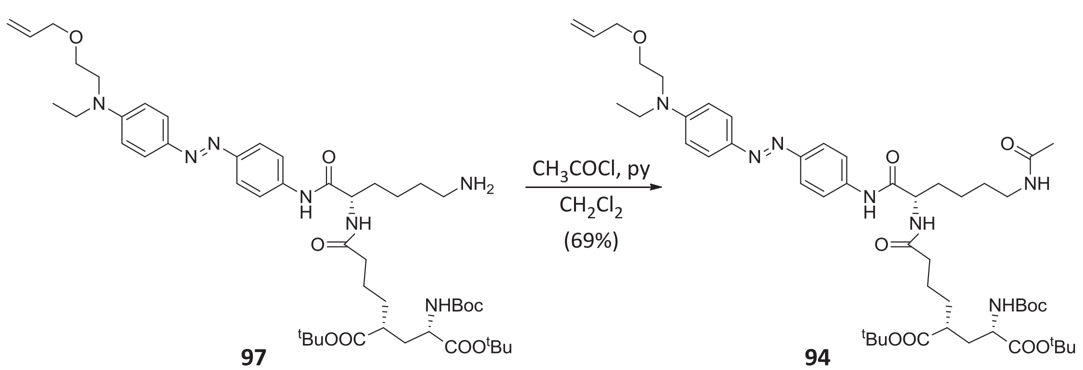

Scheme IV-24. Synthesis of compound **94**.

IV.3.2.3. Introduction of furan-protected maleimide 89. Preparation of intermediate 95

Maleimide derivative was expected to be attached to advanced intermediate **94** using Mitsunobu methodology. First, removal of the allyl protecting group through a two-step protocol was required. Thus, compound **94** was treated with Wilkinson's catalyst at reflux of aqueous ethanol and, when allyl ether isomerisation to propenyl ether had occurred, the solvent was evaporated. Then, the crude was treated with a mixture of $HgCl_2$ and HgO in aqueous acetone furnishing primary alcohol **98** in 48% yield (Scheme IV-25). The ^{1}H-NMR spectrum of **98** shows the absence of the characteristic signals of the allyl protecting group.

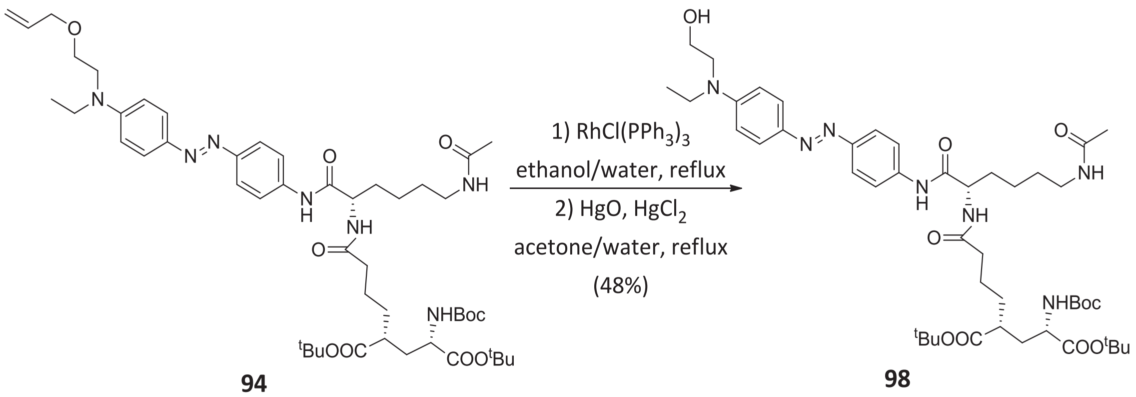

Scheme IV-25. Allyl ether deprotection of **94**.

For the conversion of alcohol **98** into advanced intermediate **95** the same procedure was used as in the case of compound **81**. Namely, the furan-protected maleimide moiety **89** was introduced via Mitsunobu reaction. Thus, treatment of alcohol **98** with **89**, Ph_3P and DIAD in THF delivered product **95** in 92% yield after purification by column chromatography (Scheme IV-26). In its ^{1}H-NMR spectrum, the most significant changes found with respect to precursor **98** were the presence of the furan-masked maleimide ^{1}H-NMR signals at 6.38, 5.25 and 2.75 ppm and the upfield shift observed for H-2^v (from 3.84 ppm in **98** to 3.70 ppm in **95**).

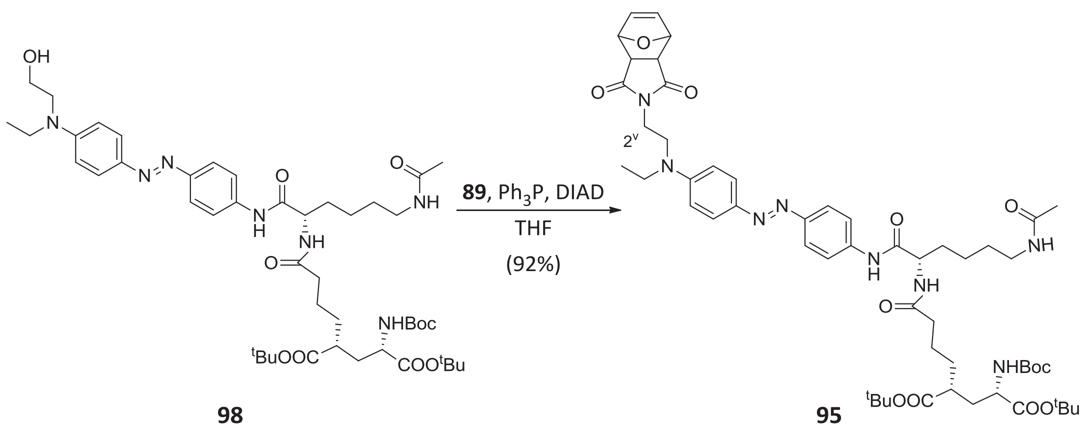

Scheme IV-26. Introduction of the furan-protected maleimide **89** through Mitsunobu methodology.

IV.3.2.4. Removal of protecting groups. Preparation of target compound 23

To culminate the synthesis of photoswitched tethered ligand **23**, the last transformations required were the removal of the protecting groups of both maleimide and glutamate moieties, which we undertook using the same methodology established for the synthesis of PTL **22**. Thus, heating intermediate **95** in refluxing toluene afforded maleimide **99** in 90% yield after purification by column chromatography (Scheme IV-27). The deprotection of the maleimide moiety was clearly evidenced in the ^{1}H-NMR spectrum of **99** by the absence of the typical furan signals and the appearance of a new signal at 6.66 ppm corresponding to the olefinic protons H-3^{vii} and H-4^{vii} of the maleimide unit.

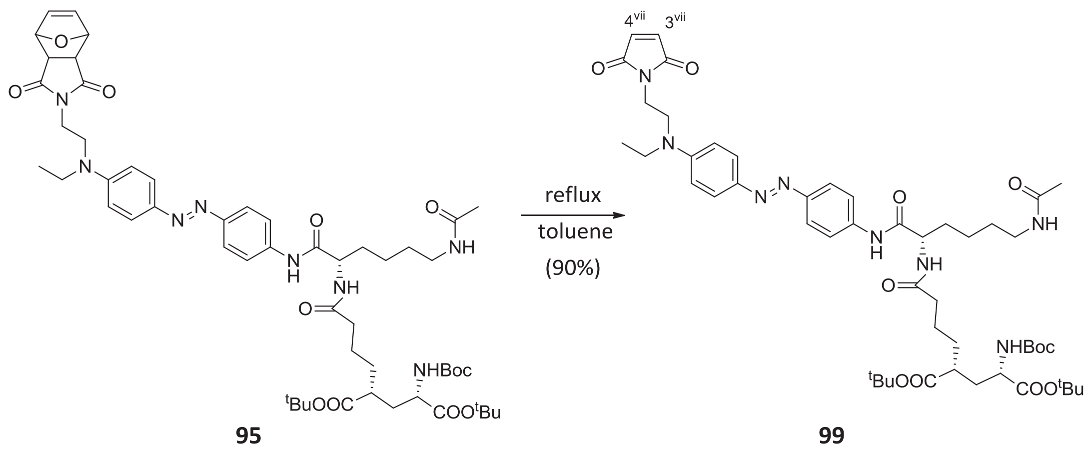

Scheme IV-27. Release of the maleimide moiety via retro-Diels Alder reaction.

Further cleavage of the *tert*-butyl ester and Boc protecting groups of the glutamate moiety with a 1:2 mixture of trifluoroacetic acid and dichloromethane delivered the target PTL **23** in 92% yield after purification by column chromatography (Scheme IV-28). This was confirmed by the disappearance of the signals corresponding to the *tert*-butyl ester and Boc protecting groups in the ^{1}H-NMR and ^{13}C-NMR spectra of **23**.

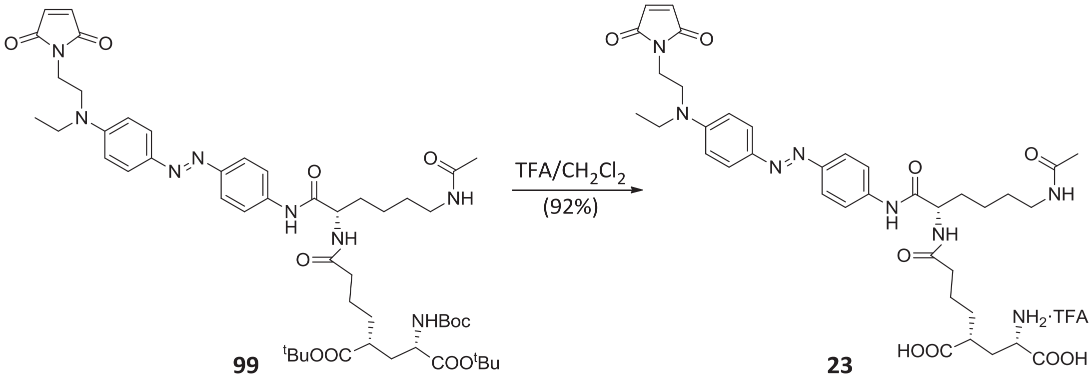

Scheme IV-28. Final synthetic step of the preparation of PTL **23**.

In summary, a new red-shifted MAG derivative devised to isomerise under direct two-photon excitation with NIR light was prepared by a convergent synthesis of 9 steps in 12% overall yield. Starting from L-lysine derivative **28**, the different functional fragments of the compound were sequentially introduced: *O*-protected aminoazobenzene **76**, glutamate derivative **65** (prepared in 8 steps and 7.0% global yield from L-pyroglutamic acid (**37**)) and furan-protected maleimide **89** (prepared in 1 step and 60% yield from furan (**91**) and maleimide (**90**)).

IV.3.3. Preparation of photo-harvesting antenna model 100

Having successfully prepared the two new MAG derivatives, we finally turned our attention to the synthesis of photo-harvesting antenna model **100**, which will be used as reference in the photochemical characterisation of target ligand **22**. As illustrated in Figure IV-11, compound **100** is composed of the naphthalene derivative used as sensitiser and a glutamate moiety that should render it soluble in aqueous media.

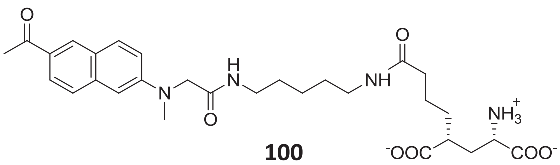

Figure IV-11. Structure of photo-harvesting antenna model **100**.

As shown in Scheme IV-29, the synthetic route towards **100** would start with the coupling reaction of commercially available *N*-protected cadaverine **101** with naphthalene derivative **70**, which had already been obtained during the preparation of photoswitched tethered ligand **22** (see § IV.3.1.1). Acid removal of the Boc protecting group of **102** followed by the introduction of glutamate derivative **65** would lead to advanced intermediate **103**. Finally, the desired compound **100** would be obtained after removal of the *tert*-butyl carbamate and ethyl ester protections of this intermediate.

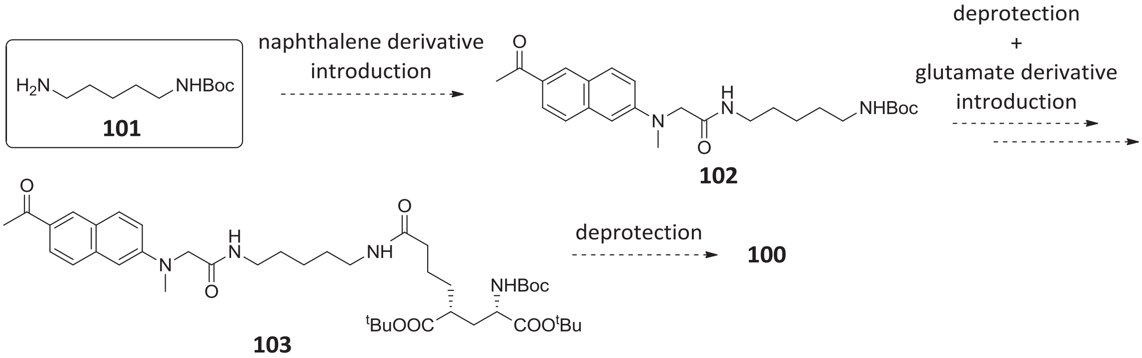

Scheme IV-29. Synthetic strategy for the preparation of photo-harvesting antenna model **100**.

IV.3.3.1. Coupling reaction between naphthalene derivative 70 and cadaverine derivative 101

According to the synthetic route described, the first step towards photo-harvesting antenna model **100** was the preparation of naphthalene-cadaverine compound **102**. To this end, naphthalene derivative **70** was treated with EDCI and DIPEA, and then added over a solution of commercially available *N*-protected cadaverine **101** in THF (Scheme IV-30). The resulting crude was purified by column chromatography, which delivered intermediate **102** in moderate yield (61%). This was confirmed by analysis of its ^{1}H-NMR and ^{13}C-NMR spectra, where new signals were observed corresponding to the assembled cadaverine moiety.

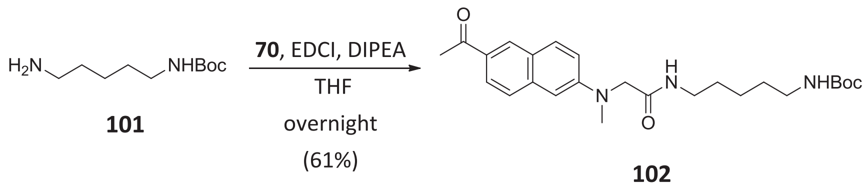

101 **102**

Scheme IV-30. Synthesis of compound **102**.

IV.3.3.2. Introduction of glutamate derivative 65. Synthesis of intermediate 103

In the next step, glutamate derivative **65** had to be coupled to the naphthalene-cadaverine intermediate **104**. This first required removal of the *tert*-butyl carbamate protection of **102** by treatment with trifluoroacetic acid, which furnished amine **104** in 97% yield after purification by column chromatography (Scheme IV-31).[9] In its ^{1}H-NMR and ^{13}C-NMR spectra, the absence of the characteristic signals corresponding to the Boc protecting group corroborated the formation of **104**.

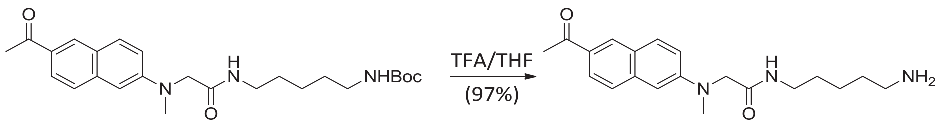

102 **104**

Scheme IV-31. Removal of Boc protecting group of **102** under acidic conditions.

Subsequent coupling of glutamate derivative **65** to amine **104** provided advanced intermediate **103**. Similar reaction conditions to those used in previous synthetic steps were applied (i.e. EDCI as coupling agent, DIPEA as base and HOBt as additive, Scheme IV-32). The reaction mixture was stirred at rt during 12 h and after subsequent treatment, the crude was purified by column chromatography on silica gel to isolate product **103** in 38% yield. The ^{1}H-NMR and ^{13}C-NMR spectra showed the expected signals attributed to the incorporation of the glutamate fragment.

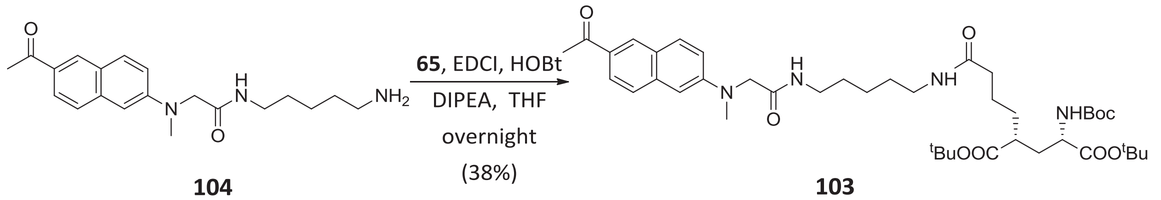

104 **103**

Scheme IV-32. Peptide coupling reaction for the synthesis of compound **103**.

IV.3.3.3. Removal of protecting groups. Preparation of target compound 100

The last step to prepare compound **100** was the cleavage of its *tert*-butyl ester and Boc protecting groups. This was accomplished using a 1:2 mixture of trifluoroacetic acid and dichloromethane, which delivered photo-harvesting antenna model **100** in quantitative yield (Scheme IV-33). The disappearance of the ^{1}H-NMR and ^{13}C-NMR signals corresponding to the *tert*-butyl ester and Boc protecting groups confirmed the formation of compound **100**.

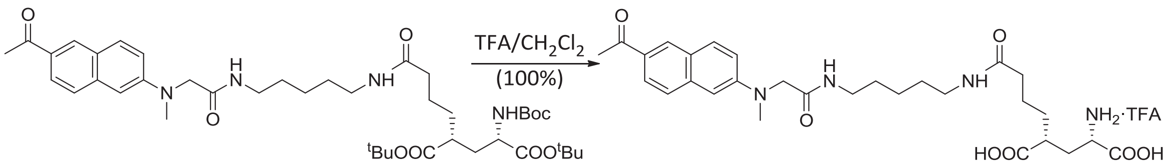

103 **100**

Scheme IV-33. Final synthetic step of the preparation of reference sensitiser **100**.

To sum up, photo-harvesting antenna model **100** was prepared by a convergent synthesis of 4 steps starting from *N*-protected cadaverine **101** in 22% overall yield. *N*-protected cadaverine **101** was used as scaffold to which the different functional fragments of the target compound were sequentially introduced: the previously prepared naphthalene derivative **70** (obtained from 1-(6-methoxy-2-naphthyl)ethanone (**82**) in 4 steps and 28% yield) and glutamate derivative **65** (prepared in 8 steps and 7.0% global yield from L-pyroglutamic acid (**37**)).

IV.4. PHOTOCHEMICAL CHARACTERISATION OF PHOTOSWITCHED TETHERED LIGANDS 22 AND 23

As illustrated in Scheme IV-34, compounds **22** and **23** should present two different stable states resulting from the reversible photoinduced *trans-cis* isomerisation of their azobenzene moieties.

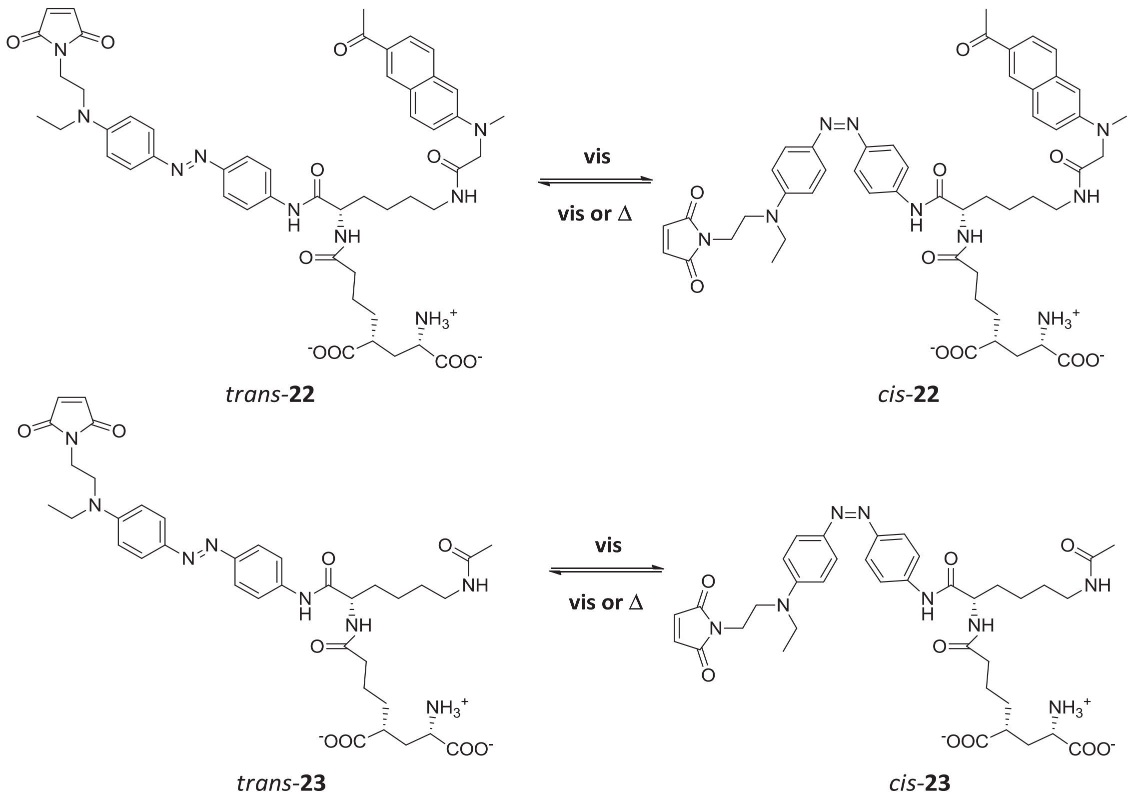

Scheme IV-34. Photoinduced *trans-cis* isomerisation of PTLs **22** and **23** upon one-photon excitation with visible light. *Cis*→*trans* back isomerisation can also take place thermally.

Both compounds are devised to undergo *trans*→*cis* isomerisation upon direct two-photon excitation with NIR light of their azoaromatic groups, owing to the introduction of asymmetric aminoazobenzene cores with sufficiently strong push-pull character as to enhance their two-photon absorption cross-section. In addition, two-photon sensitised photoisomerisation is also expected for ligand **22** upon irradiation of its naphthalene photo-harvesting antenna, which will subsequently transfer its electronic excitation energy to the central *trans*-azobenzene unit. On the other hand, the presence of the electron-donating tertiary amine at the 4′ position of their azoaromatic groups should dramatically decrease the thermal stability of the *cis* state of both **22** and **23** at physiological conditions. This should result in fast spontaneous *cis*→*trans* back isomerisation and, as such, enable single-wavelength operation of these switches. Therefore, once the synthesis and chemical characterisation of these compounds was achieved, their photochemical characterisation was performed in order to demonstrate: (i) sensitised *trans*→*cis* photoisomerisation of **22** upon selective photoexcitation of the naphthalene antenna; and (ii) fast *cis*→*trans* thermal isomerisation at rt. As previously commented, these experiments were carried out under one-photon excitation conditions with visible light since a NIR tunable pulsed laser is not available in our laboratories.

IV.4.1. Absorption and fluorescence spectra

In a first step, the absorption and fluorescence properties of the thermally stable *trans* isomer of target ligands **22** and **23** were investigated. Figure IV-12 plots the absorption spectra of *trans*-**22** and *trans*-**23** in DMSO and PBS-DMSO 4:1 solutions, which are compared to those of the model naphthalene photo-harvesting antenna **100**.

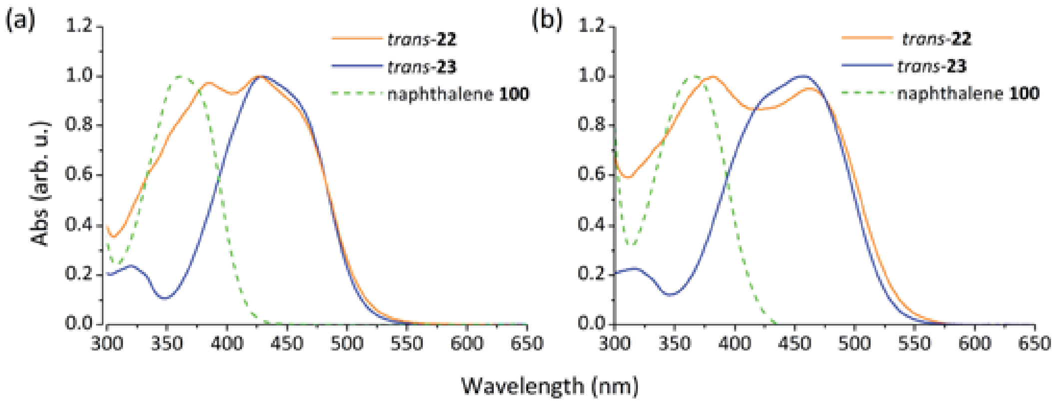

Figure IV-12. Normalised absorption spectra of *trans*-**22**, *trans*-**23** and photo-harvesting antenna model **100** in (a) DMSO and (b) PBS-DMSO 4:1.

The absorption spectrum of *trans*-**23** shows a broad band at λ_{max} ~ 450 nm, which arises from the overlap of its allowed $\pi\rightarrow\pi^*$ and forbidden $n\rightarrow\pi^*$ electronic transitions. Concerning naphthalene derivative **100**, it presents an absorption band at λ_{max} ~ 360 nm that is attributed to its fundamental electronic transition $S_0\rightarrow S_1$. In the case of *trans*-**22**, both the absorption bands corresponding to its azobenzene and naphthalene units are observed. This indicates that no electronic interaction takes place between the ground states of these groups in target ligand **22**.

Figure IV-13 shows the fluorescence spectra and fluorescence quantum yields (Φ_{Fl}) of *trans*-**22** and photo-harvesting antenna model **100** in a PBS-DMSO 4:1 mixture. As expected, the emission spectrum of compound **22** is identical to that of its naphthalene fluorophore (λ_{max} = 512 nm in PBS-DMSO 4:1 for both **22** and **100**). However, its fluorescence emission is strongly quenched upon incorporation into the *trans*-**22** backbone, with a ~ 20 fold decrease in fluorescence quantum yield (from Φ_{Fl} = 0.43 for **100** to Φ_{Fl} = 0.02 for **22**). This suggests the occurrence of efficient RET processes from the photoexcited naphthalene antenna to the azobenzene moiety of *trans*-**22**. The additional measurements performed to investigate this behaviour are described in § IV.4.3.

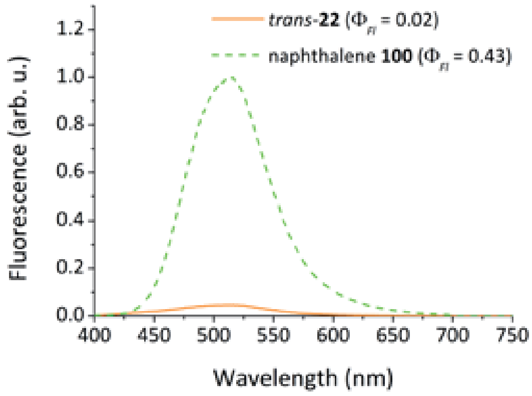

Figure IV-13. Fluorescence emission spectra of *trans*-**22** and the photo-harvesting antenna model **100** in a PBS-DMSO 4:1 mixture. The spectra are normalized relative to the excitation intensity and the absorption at the excitation wavelength (λ_{exc} = 355 nm).

IV.4.2. Direct *trans-cis* photoisomerisation

As explained in Chapter I, azobenzene derivatives can undergo efficient *trans*→*cis* photoisomerisation upon irradiation of the $\pi\rightarrow\pi^*$ absorption band of the *trans* isomer. The photogenerated *cis* isomer can be reverted back to the *trans* state either by excitation of the $n\rightarrow\pi^*$ transition and/or spontaneously due to its thermal instability. All these processes have been studied in detail for ligands **22** and **23**.

IV.4.2.1. *Trans*→*cis* photoisomerisation

Figure IV-14 shows the changes in absorption spectrum induced by direct irradiation of the azobenzene $\pi\rightarrow\pi^*$ band of *trans*-**22** and *trans*-**23** with blue light in DMSO. Clearly, both compounds experienced a significant decrease of the typical $\pi\rightarrow\pi^*$ absorption of their t*rans*-isomers (λ_{max} ~ 450 nm) and a slight increase of the $n\rightarrow\pi^*$ absorption of their *cis* states (λ > 525 nm). These changes are clear signatures of the occurrence of *trans*→*cis* photoisomerisation. Regarding to the naphthalene absorption band of compound **22,** it did not suffer any noticeable change upon irradiation, thus indicating that the azobenzene photoisomerisation process does not have any influence on this group.

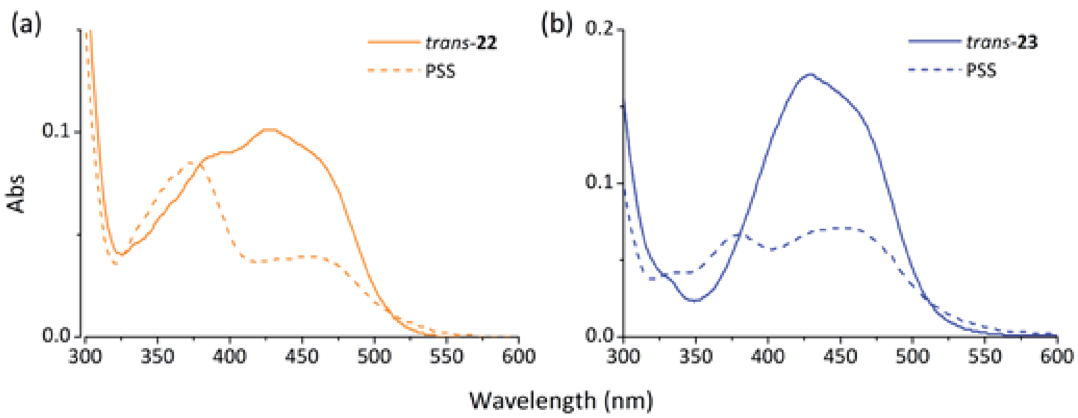

Figure IV-14. Absorption spectra in DMSO of (a) *trans*-**22** and (b) *trans*-**23** and of the PSS mixtures obtained upon photoexcitation of these compounds at λ_{exc} = 473 nm.

As expected, *trans*→*cis* isomerisation was found not to be quantitative and a PSS was reached upon irradiation of both *trans*-**22** and *trans*-**23**. From ^{1}H-NMR analysis of the PSS mixtures obtained in DMSO-d_6, the composition of the photostationary states mixtures was found to be: 58% of *cis*-**22** and 42% of *trans*-**22**, and 58% of *cis*-**23** and 42% of *trans*-**23** (Table IV-5). Indeed, identical values were obtained for both azobenzene-based switches, which indicate that their direct *trans*→*cis* photoisomerisation processes are not significantly altered by the introduction of a naphthalene substituent into the azobenzene core of target ligand **23**. Analogously, rather similar *trans*→*cis* photoisomerisation quantum yields were determined for both compounds using spectroscopic and ^{1}H-NMR data (Table IV-5).

Table IV-5. PSS conversions and *trans*→*cis* photoisomerisation quantum yields of compounds **22** and **23**.[a]

Compound	^{cis}PSS (%)[b]	$\Phi_{trans\rightarrow cis}$[c]
22	58	0.52[d]
23	58	0.39[e]

(a) Values determined in DMSO at 25 ºC. (b) λ_{exc} = 473 nm. (c) $\Phi_{cis\rightarrow trans}$ values measured under excitation at (d) 426 nm and (e) 400 nm and determined using compound **25** ($\Phi_{trans\rightarrow cis}$ = 0.28 in DMSO) as reference.

IV.4.2.2. *Cis*→*trans* isomerisation

Cis→*trans* back isomerisation of compounds *cis*-**22** and *cis*-**23** was observed to occur both photochemically and thermally. Thus, irradiation of the PSS solutions of these compounds with green light afforded the corresponding *trans* isomers nearly quantitatively. On the other hand, the thermal *cis*→*trans* isomerisation of *cis*-**22** and *cis*-**23** in DMSO was analysed in more detail by means of UV-vis absorption spectroscopy measurements. As depicted in Figure IV-15a and b, noticeable changes in the absorption spectra of *trans/cis* mixtures of these compounds were observed in time in the dark, which are consistent with *trans* state formation via thermal *cis*→*trans* isomerisation.

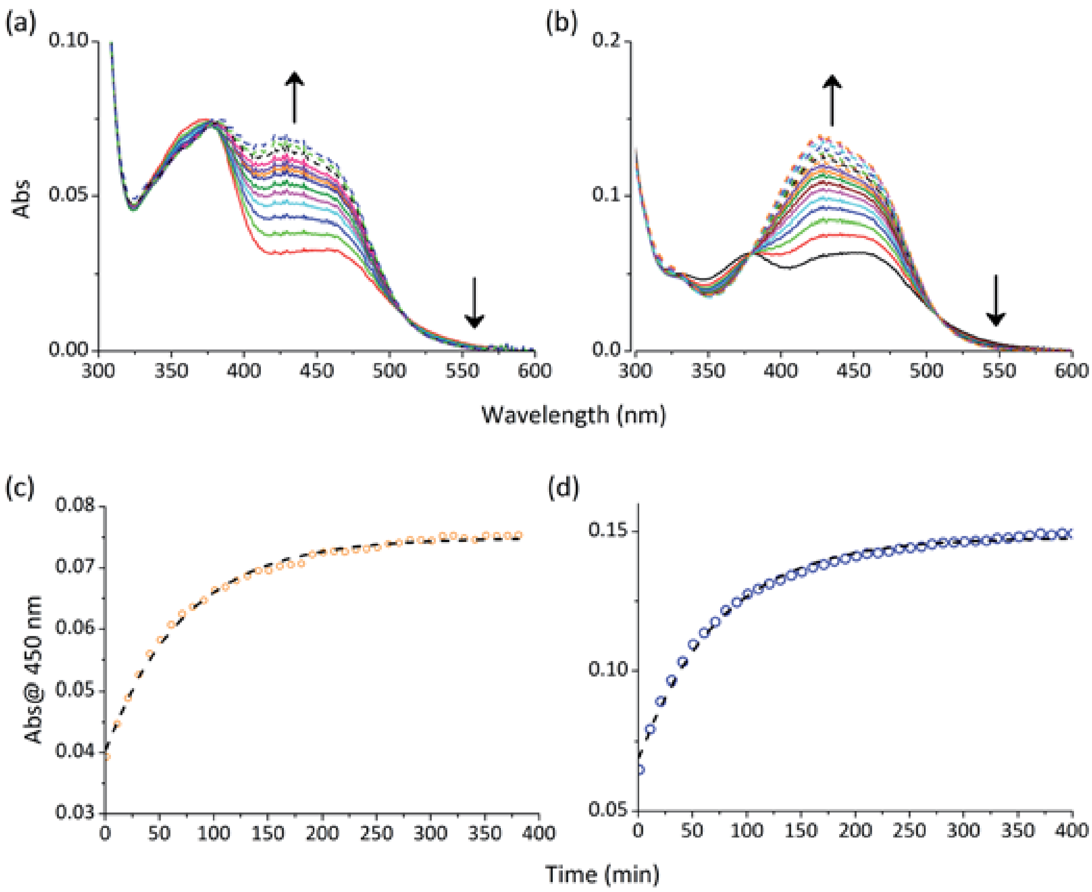

Figure IV-15. (a-b) Variation of the absorption of the *trans/cis* photostationary state mixtures of (a) **22** and (b) **23** in the dark at 25 ºC in DMSO. The arrows indicate the direction of the changes observed in time. (c-d) Time dependence of the absorption at λ_{abs} = 450 nm under these conditions, which reports on the recovery of the concentration of (c) *trans*-**22** and (d) *trans*-**23** upon thermal *cis*→*trans* isomerisation. Points correspond to the experimental data, while dashed lines were obtained from monoexponential fits.

The recovery kinetics of *trans*-**22** and *trans*-**23** in the dark follows a monoexponential growth function that allows the rate constant of this process and the half-lives of *cis*-**22** and *cis*-**23** to be determined (Table IV-6). As previously observed for the red-shifted azobenzene model compounds investigated, the thermal *cis*→*trans* isomerisation process of these compounds was found to take place in the timescale of minutes in DMSO ($t_{1/2}^{cis}$ = 73 min and 76 min for *cis*-**22** and *cis*-**23**, respectively). Clearly, similar results were obtained for both switches bearing analogous azobenzene substitution patterns, thus confirming that they display equivalent photochromic properties.

Since PTLs are devised to operate under physiological conditions and the *cis*→*trans* thermal isomerisation rate of azobenzenes largely depends on solvent polarity, the half-lives of *cis*-**22** and *cis*-**23** were also determined in aqueous buffer. As commented earlier, this should lead to faster thermal back isomerisation rates, whose characterisation would therefore require the use of spectroscopic techniques with better time resolution than steady-state UV-vis absorption spectroscopy.[25] For this reason, we characterised the spontaneous *cis*→*trans* kinetics of **22** and **23** in aqueous media by measuring the time-resolved transient absorption spectra of these compounds upon pulsed laser excitation at rt. These spectra are given in Figure IV-16.

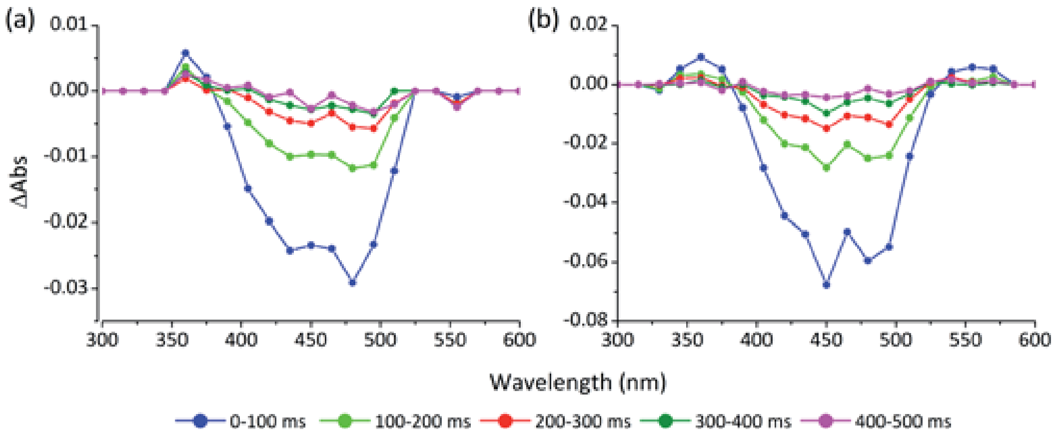

Figure IV-16. Transient absorption spectra of (a) *trans*-**22** and (b) *trans*-**23** in PBS-DMSO 4:1. All spectra were measured upon pulsed irradiation at λ_{exc} = 475 nm and integrating the wavelength-dependent transient signal at different intervals of time.

Clearly, similar features are encountered for the transient absorption spectra of the two compounds investigated. In both cases, a large negative signal is found in the absorption region of the π→π* electronic transition of the irradiated *trans* isomer (see Figure IV-12), whose minimum is located around 465 nm. As discussed for the model azobenzene photoswitches, this indicates that the concentration of *trans*-**22** and *trans*-**23** decreases right after pulsed excitation at 475 nm, which is accompanied by the formation of the corresponding *cis* isomers with lower absorption extinction coefficients in the ~ 370-520 nm range. Interestingly, no differences are observed in the transient absorption spectra of *trans*-**22** and *trans*-**23** despite the presence of an additional naphthalene chromophore in the former compound. This is due to the fact that differential absorption values are plotted in Figure IV-16, in contrast to the absolute values measured in steady-state absorption spectroscopy. As a result, the contribution of the species that are not involved in the photochemical process under investigation are washed out from transient absorption spectra. This must therefore be the case of the naphthalene photo-harvesting antenna of **22**, which does not seem to play any role in the direct *trans*→*cis* photoisomerisation of this compound.

Figure IV-16 also shows that the negative transient signal measured upon pulsed excitation of *trans*-**22** and *trans*-**23** rapidly decays in time without any apparent spectral variation. This demonstrates that the transient species formed by irradiation (i.e. *cis* isomer) returns to the initial *trans* state in a fast, single-step process. In particular, the initial absorption signal was recovered after ~ 0.4 s for both compounds, as clearly shown by the transient absorption time traces depicted in Figure IV-17. Therefore, very short-lived species are formed via photoisomerisation of *trans*-**22** and *trans*-**23**, whose half-lives can be determined from monoexponential fits of the decays of the negative ΔAbs signals (Table IV-6). Indeed, the thermal stability of the *cis* isomers of the target ligands decreases down to the millisecond timescale in aqueous media ($t_{1/2}^{cis}$ = 67 ms and $t_{1/2}^{cis}$ = 82 ms for *cis*-**22** and *cis*-**23**, respectively). This should open up the door for single-wavelength control of ionotropic glutamate receptors with these compounds.

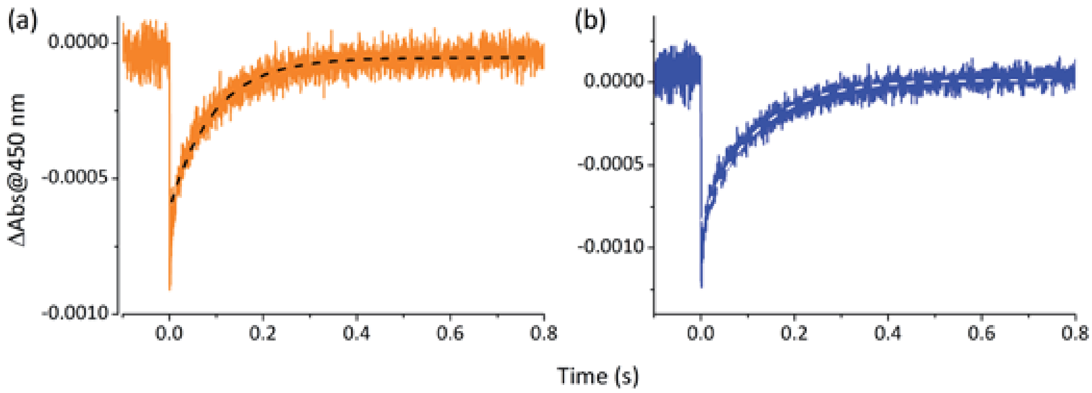

Figure IV-17. Variation of the transient absorption at λ_{abs} = 450 nm of (a) *trans*-**22** and (b) *trans*-**23** at 25 ºC in PBS-DMSO 4:1 upon pulsed excitation at 475 nm. Solid lines correspond to the experimental data, while dashed lines were obtained from monoexponential fits.

Table IV-6. Parameters of the thermal *cis*→*trans* isomerisation of compounds **22** and **23** in DMSO and PBS-DMSO 4:1 at 25 ºC.[a]

Compound	$k_{cis\rightarrow trans}$ (s^{-1}) in DMSO	$t_{1/2}^{cis}$ (min) in DMSO	$k_{cis\rightarrow trans}$ (s^{-1}) in PBS-DMSO 4:1	$t_{1/2}^{cis}$ (ms) in PBS-DMSO 4:1
22	2.3 x 10^{-4}	73	15	67
23	2.2 x 10^{-4}	76	12	82

(a) Values determined from monoexponential fits of the experimental data.

IV.4.3. Sensitised *trans*→*cis* photoisomerisation

So far it has been shown that both **22** and **23** are able to isomerise under direct one-photon excitation of their azobenzene units. However, target ligand **22** was designed to undergo sensitised *trans-cis* photoisomerisation upon naphthalene excitation as well. Therefore, our next step was to demonstrate the occurrence of this process.

As previously commented, the fluorescence emission of the naphthalene group in *trans*-**22** is strongly quenched (see § IV.4.1), which points towards the occurrence of efficient resonance energy transfer processes from this photoexcited moiety to the azoaromatic group. To evaluate RET probability, the Förster radius (R_0) of the naphthalene-azobenzene donor-acceptor pair in a PBS-DMSO 4:1 mixture was calculated using Equation I.4. In this case, the following parameters were used: (i) J = 3.99 x 10^{-14} cm^{-1}, which is the spectral overlap integral between the absorption spectrum of the antenna-less *trans*-**23** molecule and the emission spectrum of the model antenna group **100** in PBS-DMSO 4:1 (see Figure IV-18); (ii) $\Phi_{Fl,D}$= 0.43, which is the fluorescence quantum yield of **100** in PBS-DMSO 4:1; (iii) k^2 = 2/3, which assumes random orientation between the donor and acceptor units owing to the flexible alkyl chain linking them together in *trans*-**22**; and (iv) n = 1.365, which is the refractive index of PBS-DMSO 4:1 at rt. In this way, a value of R_0 = 37.8 Å was obtained for *trans*-**22**, which is higher than the centre-to-centre distance between its antenna and azobenzene groups in this compound according to a molecular mechanics calculation with a MM2 force field (r = 10.1 Å). By introducing these parameters into Equation I.3, the efficiency of the RET process in *trans*-**22** was found to be higher than 99%, which would account for the nearly complete suppression of the fluorescence emission from the naphthalene sensitiser of this compound.

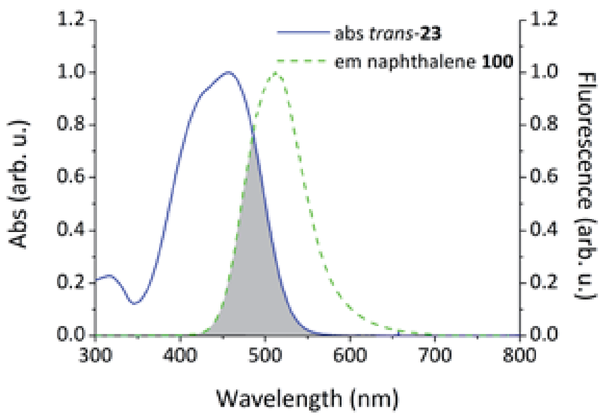

Figure IV-18. Spectral overlap in PBS-DMSO 4:1 between the fluorescence emission spectrum of photo-harvesting antenna model **100** and the absorbance spectrum of *trans*-**23**.

To reveal whether sensitised *trans-cis* photoisomerisation in **22** takes place due to resonance energy transfer from the naphthalene photo-harvesting antenna, DMSO solutions of this compound and ligand **22** were irradiated at 355 nm and the formation over time of the corresponding *cis* isomers ($\%_{cis}$) was monitored by UV-vis absorption spectroscopy. At these excitation conditions, the photo-harvesting antenna model **100** absorbs light more efficiently than the *trans*-azobenzene groups of **22** and **23** ($\varepsilon^{355\,nm}_{naphthalene} / \varepsilon^{355\,nm}_{trans\text{-}azo} \sim 3$). Therefore, nearly selective excitation of the photo-harvesting antenna should be expected for *trans*-**22** and as a consequence, a faster or/and more *cis*-enriched photostationary state should be produced under such irradiation conditions for this compound. The results of these experiments are shown in Figure IV-19.

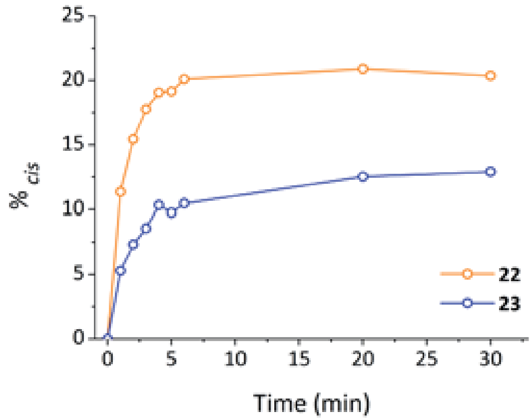

Figure IV-19. *trans-cis* photoconversion efficiency of *trans*-**22** and *trans*-**23** upon irradiation at λ = 355 nm in DMSO, which allows nearly selective excitation of *trans*-**22** sensitiser (see Figure IV-12).

Noticeably, *trans*→*cis* photoisomerisation occurs for **22** and **23** at λ_{exc} = 355 nm. In both cases, a photostationary state was achieved after several minutes of irradiation, which was determined to consist of ~ 20% of *cis*-**22** and ~ 13% of *cis*-**23**. Indeed, the *trans*→*cis* photoconversion of **22** is ~ 60% higher than that of **23** at equivalent photoexcitation conditions. Such increase in photoconversion can be unambiguously ascribed to photosensitised *trans-cis* isomerisation of the azobenzene moiety of PTL **22**.

In conclusion, we have demonstrated that target compounds **22** and **23** behave as reversible photoswitches that can be operated via direct irradiation of their azobenzene groups. Additionally, photoswitched tethered ligand **22** also undergoes *trans*→*cis* photoisomerisation via sensitised excitation of its naphthalene photo-harvesting antenna. Finally, these compounds have been shown to present fast spontaneous *cis*→*trans* back isomerisation, thus enabling the use of a single irradiation source to control the operation of the switch at physiological conditions.

IV.5. EVALUATION OF THE LIGHT-INDUCED BIOLOGICAL ACTIVITY OF PHOTOSWITCHED TETHERED LIGANDS 22 AND 23

Once analysed the photochemical properties of photoswitched tethered ligands **22** and **23**, we finally investigated the capability of these compounds to light-control ionotropic glutamate receptors in living cells using one- (1P) and two-photon (2P) stimulation. These experiments were conducted on cells transfected with cysteine-mutated LiGluR channels and they were carried out in the laboratories of the research groups of Prof. Pau Gorostiza at *Institut de Bioenginyeria de Catalunya* (IBEC) and Prof. Rafael Yuste at *Columbia University*.

As described in § I.2.2, LiGluR channels must remain closed when the conjugated photoswitches are on their thermodynamically stable *trans* state, which makes the glutamate group of the ligand lie far away from the binding pocket. Upon *trans*→*cis* isomerisation, the glutamate-binding site distance is shortened, ligand recognition takes place and the channels must open, thereby allowing monovalent and calcium ions to cross the cell membrane. Subsequently, this process can be reverted back by photo- and/or thermally induced *cis*→*trans* back isomerisation, which breaks the glutamate-binding site complex apart and leads to channel closing. Because of their ability to monitor ion fluxes across the cell membrane, two different techniques have been applied in this chapter to study the photoinduced operation of LiGluR channels tethered to compounds **22** and **23**: calcium imaging and whole-cell patch-clamp.

IV.5.1. Calcium imaging measurements of LiGluR-22 and LiGluR-23 tethers

To start with, calcium imagining experiments were performed on LiGluR-**22** and LiGluR-**23** tethers upon one-photon excitation with blue light. Hence, HEK293 cells transfected with cysteine-mutated iGluk2 channels (see § III.4.1) were loaded with the fluorescent calcium indicator fura-2 AM (**69**) and incubated with the PTLs **22** and **23**. As reference, wild type HEK293 cells equivalently treated with **22** and **23** and fura-2 AM were also investigated.

As explained in § III.4.1.1, calcium imaging experiments with fura-2 measure the ratiometric fluorescence response of this indicator at two different excitation wavelengths ($R_{f340/f380}$), a signal that must increase with intracellular Ca^{2+} concentration. Therefore, if LiGluR-**22** and LiGluR-**23** tethers undergo *trans*→*cis* isomerisation upon excitation and channel opening occurs, the $R_{f340/f380}$ ratio should increase due to calcium ion influx. Because of the short lifetime of *cis*-**22** and *cis*-**23** at physiological conditions, this process must be rapidly reverted back in the absence of illumination, which should lead to thermal channel closing and recovery of basal calcium ion levels and $R_{f340/f380}$ signals. In view of this, calcium imaging traces were registered for both wild type and LiGluR-expressing cells incubated with **22** and **23** upon exposure to intermittent blue-light irradiation (λ_{exc} = 435 nm, Figure IV-20). At this excitation wavelength direct *trans*→*cis* photoisomerisation of the two photoswitched tethered ligands prepared should take place (see Figure IV-12).

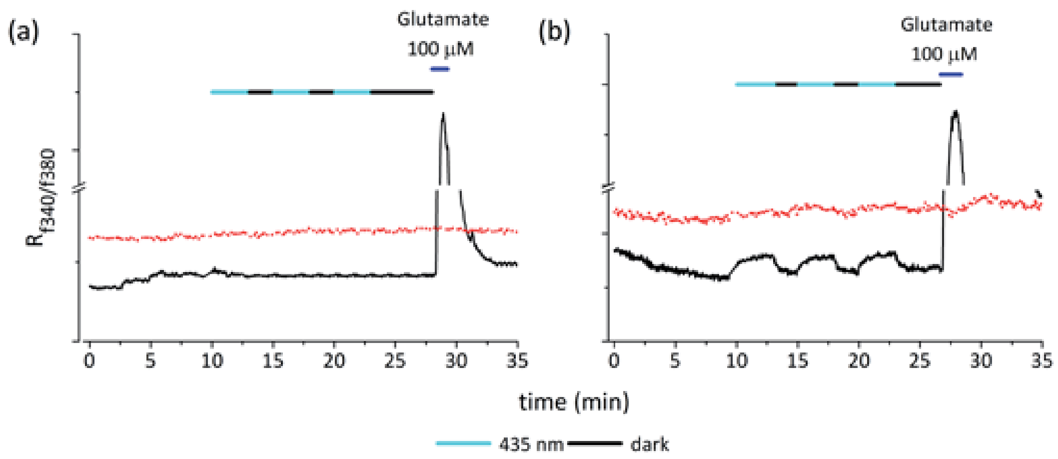

Figure IV-20. Calcium imaging traces measured for wild type (red dotted line) and LiGluR-expressing HEK293 cells (black line) incubated with (a) **22** and (b) **23**. Bars indicate the duration of the blue-light illumination (λ_{exc} = 435 nm, *t* = 10-13, 15-18 and 20-23 min, cyan line) and dark periods (*t* = 13-15, 18-20 and 23-28 min). At the end of each experiment, free glutamate (*c* = 100 μM) was added (*t* = 27 and 28 min for (a) and (b), respectively).

As expected, no changes in $R_{f340/f380}$ were observed upon irradiation of wild type cells owing to the lack of glutamate-responsive LiGluR channels (red traces in Figure IV-20). This was further confirmed by perfusing an external solution containing 100 μM of free glutamate at the end of each measurement, which did not lead to any increase in fluorescence emission ratio either. In contrast, different results were obtained when monitoring LiGluR-expressing cells (black traces in Figure IV-20). For both **22**- and **23**-incubated cells, a large rise in $R_{f340/f380}$ was measured upon free glutamate addition (*t* = 27 or 28 min). This clearly demonstrates the successful transfection of the cells with LiGluR channels, which allows extensive Ca^{2+} influx upon glutamate recognition. In spite of this, smaller or even no $R_{f340/f380}$ increments were observed upon blue-light irradiation at *t* = 10-13, 15-18 and 20-23 min. In the case of LiGluR-**23** tethers, sequential excitation at 435 nm reproducibly led to a slight increase in $R_{f340/f380}$, which unambiguously demonstrates photoinduced channel opening (Figure IV-20b). Moreover, this process was found to rapidly revert back in the dark due to the short lifetime of *cis*-**23** in aqueous media, thus explaining the fast recovery of initial $R_{f340/f380}$ values as soon as blue-light irradiation was stopped. Actually, we ascribe the minor photoinduced signals measured for LiGluR-**23** tethers to such fast thermal *cis*→*trans* isomerisation process, which must result in poorly *cis*-enriched photostationary states at physiological conditions. As such, a very small fraction of light-responsive glutamate channels are expected to be opened in the steady state upon continuous illumination, thereby ensuing low influxes of calcium ions. Unfortunately, this produced $R_{f340/f380}$ increments that are close to the limit of detection of our calcium imaging experiments. For comparison, $R_{f340/f380}$ signals measured for LiGluR-MAG-1 tethers under similar experimental conditions are about ~ 5 fold larger, as a consequence of the higher thermal stability of the *cis* state of this photoswitch.[27]

A worse scenario was encountered for LiGluR-**22** tethers (Figure IV-20a). In this case, no photoinduced calcium imaging signals could be detected upon blue-light irradiation. Since similar *trans*→*cis* photoisomerisation efficiencies were expected for **22** and **23** at λ_{exc} = 435 nm according to our previous photochemical measurements (see § IV.4.2.1), other factors should account for the results obtained: (i) lower LiGluR-**22** conjugation efficiencies, and/or (ii) steric hindrance effects hampering proper glutamate-binding site interaction arising from the additional naphthalene unit attached to the photoswitch structure. Taking into account that no improvements were observed when increasing the time and PTL concentration of the incubation process of transfected cells with **22**, the latter seems to be the most plausible explanation. As such, the light-induced response of LiGluR-**22** tethers is expected to be even smaller than that measured for PTL **23**, which would therefore require the use of more sensitive detection techniques. This is the case of whole-cell patch-clamp.

IV.5.2. Patch-clamp measurements of LiGluR-22 and LiGluR-23 tethers

Patch-clamp is a neurophysiology technique that allows measuring the electrical currents and potentials arising from ion transport across a small patch or even the overall cell membrane.[26]

As illustrated in Figure IV-21a, patch-clamp measurements rely on the use of a thin electrode (normally, a chloride silver electrode) located in the interior of a glass micropipette filled with a buffer solution resembling the intracellular medium. The pipette has an open tip diameter of about one micrometre, with which a small membrane surface area or "patch" containing just one or few ion channels can be enclosed. In the most typical operation mode called **cell-attached patch-clamp**, the pipette is pressed against the cell membrane and a small amount of suction is applied to assist in the formation of a high-resistance seal between the glass and the cell membrane (a "gigaohm seal" or "gigaseal", Figure IV-21b). In this way, the electrode detects the electrical potential within the pipette relative to an extracellular reference electrode and the small changes stemming from ion transport across the enclosed cell membrane area can be measured with the use of an ultrasensitive electronic amplifier.

Several variations can be applied to this basic configuration depending on the experimental requirements. These include excised inside-out patch, whole-cell patch and outside-out patch. In our case, **whole-cell patch-clamp** measurements have been performed since they allow the activity of multiple ion channels to be measured at once over the membrane of the entire cell (Figure IV-21c). In this configuration, the membrane patch is disrupted by briefly applying strong suction, thus providing access to the intracellular space of the cell and, therefore, increasing the sensitivity of the experiment. Two different operation modes can be used in whole-cell patch-clamp: (i) the voltage-clamp mode, in which the voltage is kept constant and the electrical current between the intra- and extracellular media is recorded; or (ii) the current-clamp mode, in which the current is maintained invariant and changes in the membrane potential can be monitored.

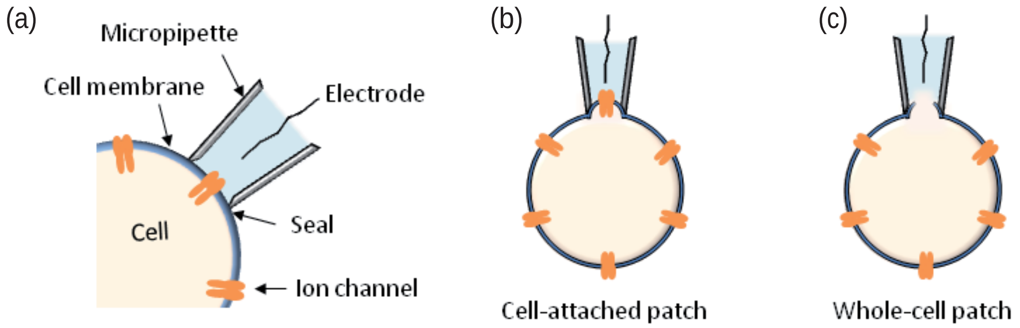

Figure IV-21. (a) General principles of patch-clamp measurements. A glass micropipette containing an electrolyte solution is tightly sealed onto the cell membrane, thus isolating a membrane patch electrically. Currents fluxing through the ion channels in this patch are recorded by the electrode located in the interior of the pipette, which is connected to a highly sensitive differential amplifier. When a tight seal is formed between the pipette and the membrane, the technique is called cell-attached patch-clamp (b). Alternatively, the membrane can be ruptured and the electrical measurements take place over all the remaining ion channels in the cell (c, whole-cell patch-clamp).

IV.5.2.1. Whole-cell patch-clamp measurements of LiGluR-22 and LiGluR-23 tethers

While all the previous biological experiments described in this dissertation were conducted directly by myself, the whole-cell patch-clamp measurements on PTLs **22** and **23** were carried out by Dr. Mercè Izquierdo from Prof. Gorostiza's group at IBEC. There she performed the patch-clamp experiments under one-photon stimulation conditions. Further measurements under two-photon excitation conditions were undertaken in the laboratories of Prof. Yuste's group at Columbia University during a research exchange stay. Since the results from these experiments successfully demonstrate the capability of the photoswitched tethered ligands developed in this chapter to light-control the operation of ionotropic glutamate receptors upon multiphoton excitation with NIR radiation, a brief summary is given below. A more detailed description of these measurements and the experimental procedures followed can be found elsewhere.[27]

As for previous calcium imaging experiments already discussed, most whole-cell path-clamp measurements were carried out in HEK293 cells expressing cysteine-mutated Gluk2 channels, which were incubated with **22** and **23** and recorded 24-48 h after transfection. The resulting biological samples containing LiGluR-**22** and LiGluR-**23** tethers were exposed to intermittent illumination with UV, visible or NIR light to sequentially induce (i) 1P or 2P *trans*→*cis* photoisomerisation and channel opening, and (ii) fast thermal *cis*→*trans* isomerisation and channel closing. The concomitant changes in electrical current stemming from ion transport across LiGluR channels were measured by means of whole-cell patch-clamp running in voltage-clamp mode.

IV.5.2.1.a One-photon stimulation

To start with, the light-induced operation of LiGluR channels conjugated to **22** and **23** was investigated under one-photon stimulation with UV and visible light. Figure IV-22 plots the changes in electrical current measured upon excitation of cells containing LiGluR-**22** and LiGluR-**23** with a single 500 ms-pulse of blue light, for which direct *trans*→*cis* photoisomerisation of the PTLs is expected to occur. For sake of comparison, a similar current trace is given for HEK293 cells bearing LiGluR-MAG-1 tethers, which were sequentially illuminated with UV and visible light to induce *trans*→*cis* and *cis*→*trans* photoisomerisation, respectively.

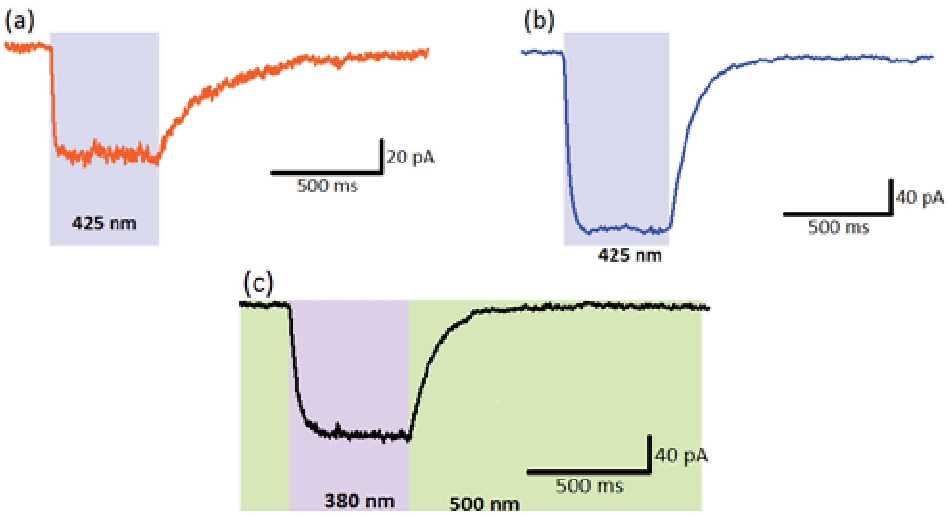

Figure IV-22. One-photon whole-cell voltage-clamp recordings on LiGluR-expressing HEK293 cells conjugated to (a) **22**, (b) **23** and (c) MAG-1 (**14**) photoswitches. Bars indicate stimulation pulses applied to open (in violet and blue) and close LiGluR (in green). Irradiation wavelengths are given in each case.

Noticeably, an increase in electrical current across the cell membrane (plotted as a negative signal for inward currents) was measured both for LiGluR-**22** and LiGluR-**23** tethers upon excitation at λ_{exc} = 425 nm, which resembles that observed for LiGluR-MAG-1 at λ_{exc} = 380 nm. As extensively discussed for MAG-1,[9] this is clear evidence of the light-induced opening of glutamate channels due to *trans*→*cis* photoisomerisation of the conjugated PTLs, which results in ion influxes into the irradiated cells and the detection of concomitant changes in electrical current. In all the cases, constant current values were obtained after less than 100 ms of irradiation, a situation ascribed to the formation of the corresponding photostationary states upon continuous illumination. Differences were however observed after the irradiation pulse. For LiGluR-MAG-1, the photoinduced current elicited remained nearly constant in the dark and it only slowly decreased in time unless irradiation with green light was applied (λ_{exc} = 500 nm). In such a case, photoinduced *cis*→*trans* isomerisation of the switch and, therefore, channel closing took place, which led to fast recovery of the basal electrical signal (less than 1 s in Figure IV-22c). Instead, rapid thermal back isomerisation and channel closing occurred for LiGluR-**22** and LiGluR-**23** tethers directly in the dark (Figure IV-22a and b), as expected on the basis of the photochemical experiments conducted in solution. As such, the initial current values were restored spontaneously in less than 1 s after stopping illumination, thus allowing fast gating of LiGluR with a single irradiation source. By fitting the one-photon current decays in the dark with monoexponential functions, the thermal half-lives of the open state of the channels were determined to be 184 ± 2 ms and 104 ± 7 ms for LiGluR-**22** and LiGluR-**23**, respectively. These values are larger than those measured in solution (see § IV.4.2.2), which suggests that the ligand-binding site interaction slows down the thermal *cis*→*trans* isomerisation of the azobenzene-based switches.

Once proven the capability of **22** and **23** to light-control ionotropic glutamate receptors in living cells, the dependence of their photoinduced activity with the excitation wavelength was investigated--namely, their action spectra were measured. With this aim, voltage-clamp registers were performed at wavelengths ranging from 325 to 575 nm and using 500 ms-excitation pulses in all cases to ensure reaching the corresponding steady states. Figure IV-23 plots the resulting action spectra determined for LiGluR-**22** and LiGluR-**23**, which display very similar features. In agreement with the absorption spectra of their *tran*s isomers (see Figure IV-12), the largest currents measured for both compounds were observed at λ_{exc} = 425 nm, which corresponds to a ~ 50 nm red-shift with respect to the maximum of the action spectrum of MAG-1.[9] As recently reported by Trauner, Isacoff and co-workers for a similar azobenzene-based PTL, this already constitutes a significant improvement of the original, UV-responsive MAG-1 photoswitch.[28]

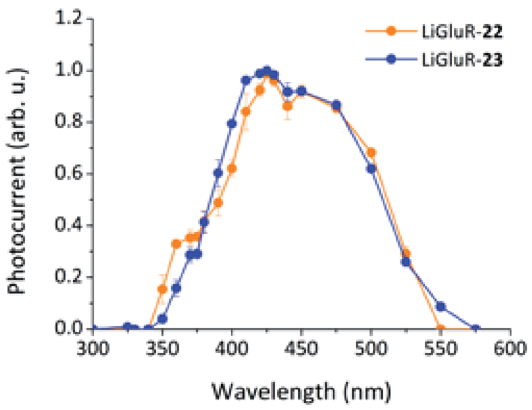

Figure IV-23. Normalised one-photon action spectra of LiGluR conjugated to **22** and **23**. Errors are s.e.m. for all cells measured.

Although the most efficient 1P response of the PTLs developed in this chapter originates from direct excitation of their *trans*-azobenzene cores with blue light, an additional component was found in the action spectrum of LiGluR-**22** at $\lambda_{exc} \sim 370$ nm. The small shoulder observed in this spectral region coincides with the absorption band of the naphthalene photo-harvesting antenna of **22** (see Figure IV-12) and it is clearly not present in the action spectrum of LiGluR-**23**. Accordingly, we ascribe this signal to the 1P sensitised *trans*→*cis* isomerisation of the conjugated PTL **22**, which can therefore be exploited to light-control ionotropic glutamate receptors.

Aside from the distinct spectral and time-dependent features observed for the photocurrents evoked by LiGluR-**22**, LiGluR-**23** and LiGluR-MAG-1, additional differences were found concerning the intensity of the light-induced signals measured. As previously mentioned, the occurrence of fast thermal *cis*→*trans* isomerisation for **22** and **23** has a direct implication on the composition of the photostationary states obtained upon continuous irradiation of these switches. In particular, lower photoconversion efficiencies are expected, which should lead to smaller light-induced electrical responses. In the case of LiGluR-**23** tethers, this does not seem to be a very critical factor and, by properly selecting the illumination conditions, 1P photocurrent intensities can be achieved that are nearly a half of those elicited by LiGluR-MAG-1.[27] Unfortunately, much worse results were obtained for LiGluR-**22**, with which 1P photocurrent intensities were evoked that are around ten times lower than for LiGluR-**23**. As discussed in § IV.5.1, steric hindrance effects arising from the presence of the additional photo-sensitiser unit in **22** may account for this situation. Nevertheless, the capability of this PTL to light-control ionotropic glutamate receptors is not fully suppressed by such effects and it could be successfully demonstrated by means of an experimental technique with higher sensitivity than calcium imaging.

IV.5.2.1.b Two-photon stimulation

Having demonstrated the ability of PTLs **22** and **23** to light-control ionotropic glutamate receptors with visible light under one-photon excitation conditions, we next investigated whether LiGluR channels can also be controlled using two-photon stimulation with NIR radiation. With this aim, further experiments were conducted on HEK293 cells transfected with cysteine-mutated Gluk2 receptors and incubated with **22** and **23**, which were subsequently studied in a custom-built patch-clamp multiphoton setup where a tightly focused fs laser is raster scanned over the cells of interest.[27]

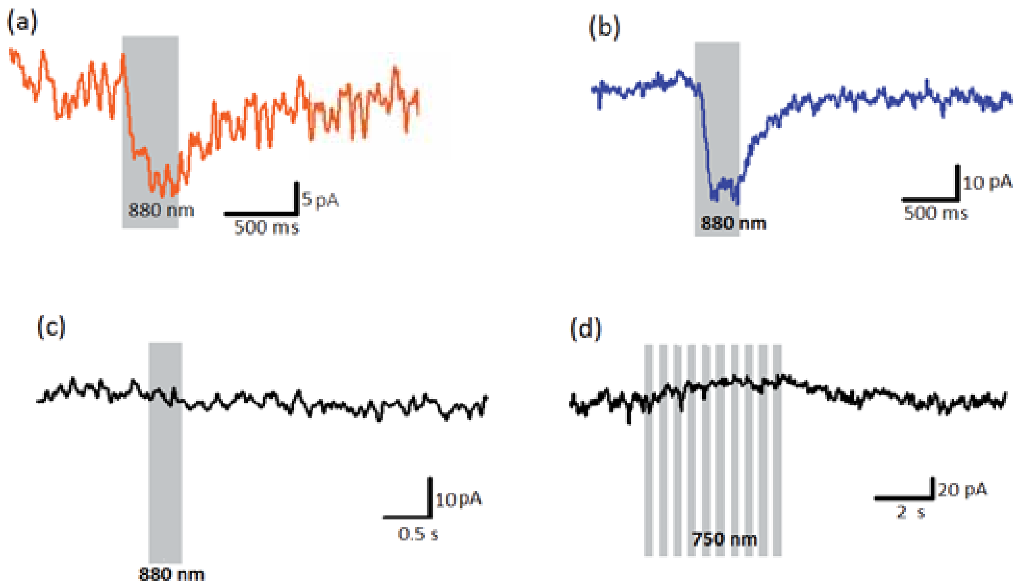

Figure IV-24. Two-photon voltage-clamp recordings on LiGluR-expressing HEK293 cells conjugated with (a) **22** and (b) **23**, and (c-d) non-conjugated. Bars indicate the duration of the stimulation periods applied, which corresponded to 1 (a-c) or 10 consecutive (d) 0.4 s-scans over the cells of interest. Irradiation wavelengths are given in each case.

Figure IV-24a and b show the whole-cell voltage-clamp traces measured for LiGluR-**22** and LiGluR-**23** upon irradiation at λ_{exc} = 880 nm, which approximately corresponds to twice the wavelength of the 1P absorption maxima of both PTLs. Therefore, direct two-photon excitation of the *trans* isomers of these photoswitches are expected under such irradiation conditions, which should lead to PTL photoisomerisation and channel opening. Indeed, similar current traces were obtained in this way to those measured upon one-photon stimulation with visible light (see Figure IV-22). Thus, a noticeable increase in electrical current was registered immediately after exciting the cells of interest with NIR radiation. A rather stable current intensity was then achieved, which rapidly decayed to the basal level as soon as illumination ceased. As discussed in the previous section, these are clear signatures of the light-induced operation of LiGluR channels, which are opened upon *trans*→*cis* photoisomerisation of the conjugated switches and spontaneously closed in the dark owing to the short thermal lifetime of their *cis* isomer. Actually, such closing process was found to take place in the ms scale (e. g. $t_{1/2}$ = 110 ± 5 ms for LiGluR-**23**), in complete agreement with our 1P excitation experiments (e. g. $t_{1/2}$ = 104 ± 7 ms for LiGluR-**23**).

To further investigate the nature of the signals measured for LiGluR-**22** and LiGluR-**23** under irradiation with NIR light, control experiments were conducted on cells transfected with cyteine-mutated Gluk2 channels that had not been incubated with the photoswitches of interest. As shown in Figure IV-24c and d, no photocurrents were registered for those cells regardless of the excitation wavelength and illumination period, which allows ruling out the occurrence of any unspecific light-induced effect caused by membrane irradiation with tightly focused fs pulses. Next, the dependence of the generated photocurrents with the excitation power was studied to corroborate the multiphoton character of the light-induced responses recorded for LiGluR-**22** and LiGluR-**23** upon irradiation with NIR light (Figure IV-25). Clearly, a non-linear correlation between the photocurrents measured and the laser intensities used was found for both PTLs. Actually, the experimental data points could be satisfactorily fitted with a square power function for low to intermediate power values (< 40 mW), which indicates that the signals measured under these conditions should arise from a two-photon absorption process. Although this quadratic dependence is lost at higher laser intensities due to saturation of the optical transition and/or cell photodamage, the results showed so far unambiguously demonstrate that we have achieved for the first time two-photon control of ionotropic glutamate receptors with NIR light.

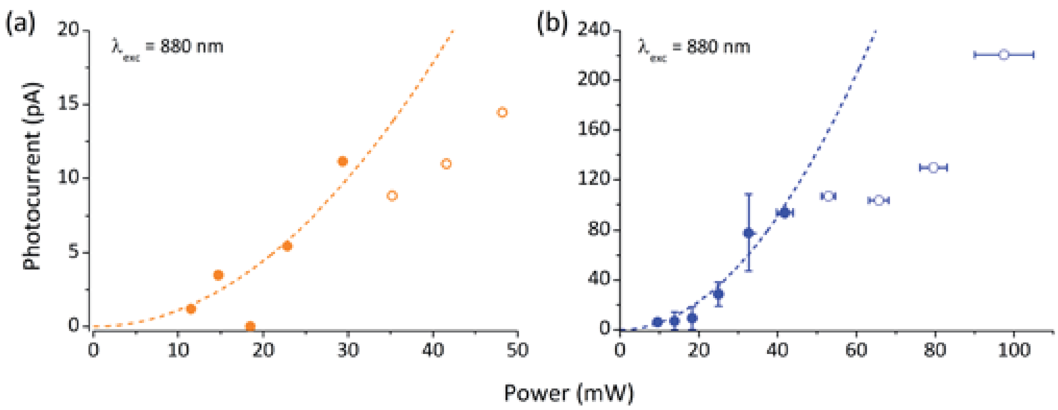

Figure IV-25. Power dependency of the photocurrents measured at λ_{exc} = 880 nm for (a) LiGluR-**22** and (b) LiGluR-**23** tethers. At low and intermediate intensities a square power function could be fitted (dotted line) to the experimental data points (full circles), while at higher intensities saturation and/or cell photodamage occurred (open circles).

Once proven the multiphoton biological activity of the two PTLs developed in this chapter, their 2P action spectra were investigated in order to (i) determine their overall spectral response under illumination with NIR light, and (ii) disentangle the two-photon sensitised and direct photoisomerisation mechanisms operating for LiGluR-**22**. Figure IV-26a plots the 2P action spectrum registered for LiGluR-**23**, which showed measurable photocurrents upon irradiation within the 780-1020 nm range. The spectrum obtained reasonably resembles that recorded under one-photon stimulation at nearly twice the excitation energy (see Figure IV-24). Thus, while maximal signal is observed in this case between 860 and 960 nm, the 1P action spectrum of LiGluR-**23** peaked between 400 and 500 nm. This is a further indication that the two-photon activity of this photoswitch proceeds via direct photoisomerisation of its azobenzene core.

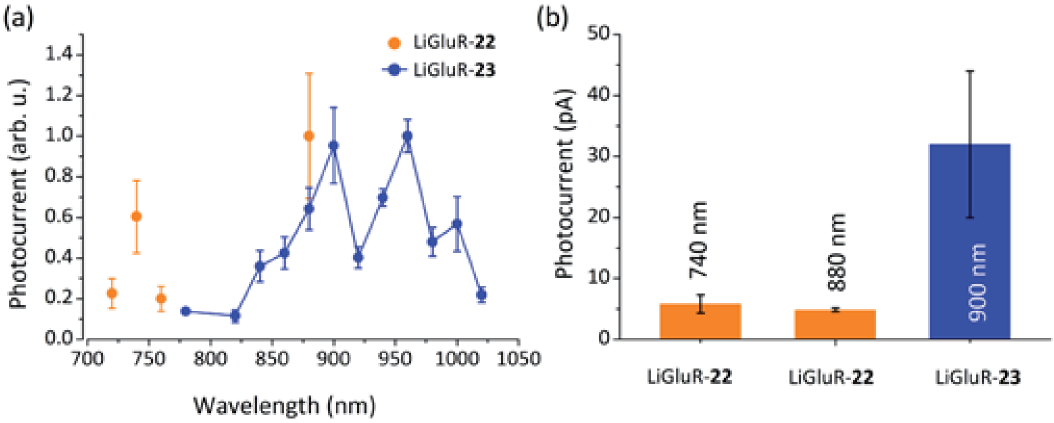

Figure IV-26. (a) Two-photon activation of LiGLuR-**22** at selected wavelengths and two-photon action spectrum of LiGluR-**23**. Photocurrents amplitudes were normalised to the spectral maximum. (b) Maximal two-photon photocurrents measured upon sensitised (λ_{exc} = 740 nm) and direct azobenzene excitation (λ_{exc} = 880 nm) of LiGluR-**22** and upon direct azobenzene excitation of LiGluR-**23** (λ_{exc} = 900 nm). Errors are s.e.m. for all cells measured.

In the case of cells bearing LiGlu-**22** tethers, it was not possible to acquire a detailed 2P action spectrum due to the reduced currents obtained for this system. Instead, photocurrent values could only be registered at selected excitation wavelengths (Figure IV-26a). In spite of this, these measurements were sufficient to identify two different spectral ranges allowing two-photon activation of LiGluR upon conjugation to **22**: (i) excitation at ~ 880 nm, which should correspond to the direct two-photon absorbance of its *trans*-azobenzene moiety, as already observed for the structural analogue **23**; and (ii) excitation at ~ 740 nm, a wavelength at which no activity was measured for the antenna-less compound **23**. It must be noted that the two-photon absorption spectrum of naphthalene derivatives similar to the photosensitiser introduced into **22** falls in this spectral region[1] and, indeed, its 1P action signal ascribed to naphthalene sensitisation was observed at half this wavelength (λ_{exc} ~ 370 nm, see Figure IV-23). From this we then conclude that the 2P photocurrents measured at λ_{exc} < 750 nm for LiGluR-**22** arise from the sensitised isomerisation of its azobenzene group, as pursued in one of the strategies explored in this chapter to achieve light-control of ionotropic glutamate receptors with NIR light.

To further investigate the two photochemical mechanisms of action of LiGluR-**22**, Figure IV-26b depicts the absolute photocurrents registered at λ_{exc} = 740 and 880 nm. Very similar current values were obtained for these two excitation wavelengths ($R_{880/740}$ = 1.2), which indicates that the 2P sensitised and direct excitation processes have nearly equivalent efficiencies. In contrast, much larger signals were registered upon direct *trans→cis* photoisomerisation of **22** via one-photon excitation with UV-vis light ($R_{425/375}$ = 3.0, see Figure IV-23). This is a clear proof that the two-photon activity in the NIR region of azobenzene-based photoswitched tethered ligands can be potentially enhanced via photosensitisation, as we aimed to demonstrate in this thesis. Nevertheless, care has to be taken when introducing a photo-harvesting antenna into the switch structure, since it can worsen the eventual light-induced efficiency of the system owing to the occurrence of undesired effects such as solubility issues (as discussed in Chapter III) or steric hindrance. The latter is considered to play a significant role in the operation of PTL **22** since lower calcium imaging signals and 1P photocurrents were measured for this compound with respect to analogue **23**. As shown in Figure IV-26b, a similar trend was also observed under two-photon stimulation, the maximal light-induced responses measured for LiGluR-**22** being around 8 times lower than for LiGluR-**23** at equivalent experimental conditions.

To finally assess the advantages of the strategies explored in this chapter to attain two-photon activation of azobenzene-based PTLs with NIR light (i.e. push-pull substitution and photosensitisation), additional experiments were performed on cells bearing LiGluR channel conjugated to MAG-1. As discussed in the introduction of this dissertation, none or low photoresponses were expected for symmetrically-substituted azobenzene-derivative MAG-1 under two-photon stimulation. In spite of this, two-photon photocurrents could be measured for those cells upon illumination with NIR radiation (Figure IV-27a). Although a more detailed description of the 2P activity of MAG-1 can be found elsewhere,[27] the main conclusions drawn when comparing the behaviour of LiGluR-**22**, LiGluR-**23** and LiGluR-MAG-1 tethers under NIR light irradiation are summarised below:

- They present clearly different 2P action spectra covering the whole NIR region. In the case of LiGluR-**23** and LiGluR-MAG-1, this arises from the different substitution pattern of their azobenzene cores, which leads to maximal 2P activity at 860-960 nm (see Figure IV-26) and 750-850 nm (Figure IV-27b), respectively. The occurrence of both sensitised and direct photoisomerisation processes for LiGluR-**22** expands its photoactivity all over these two spectral regions.

- Although LiGluR-MAG-1 channels can be opened via excitation with NIR radiation, they require the use of visible light to revert back the process under one-photon stimulation if the system is to be fully operated in the ms-to-minute scale (Figure IV-27a and c). Instead, fast gating of LiGluR-**22** and LiGluR-**23** channels with sub-second time resolution can be achieved with a single NIR irradiation source thanks to the thermal instability of the *cis* isomer of these photoswitches. As such, they behave as fully multiphoton-triggered PTLs.

- Higher absolute 2P photocurrents can be achieved with LiGluR-MAG-1 upon continuous illumination with NIR light, which are about 3.5 and 30 times larger than those obtained with LiGluR-**22** and LiGluR-**23**, respectively.[27] The different thermal stabilities of the *cis* isomers of these photoswitches mainly account for this result, which allow building up a larger population of open-state channels for MAG-1 in the long term. This is clearly demonstrated by Figure IV-27c, which plots the evolution of the 2P signal of LiGluR-**23** and LiGluR-MAG-1 upon repetitive excitation with NIR radiation. In the case of LiGluR-**23**, maximal photocurrent is attained just after four 0.16 s-scans (i.e. 640 ms of excitation in total), while it requires more than ten 0.4 s-scans (i.e. 4 s of excitation in total) for LiGluR-MAG-1. This is therefore an additional factor than makes **22** and **23** more suitable PTLs for fast gating of ionotropic glutamate receptors.

- Actually, the intrinsic 2P efficiencies of LiGluR-**23** and even LiGluR-**22** are larger than for LiGluR-MAG-1, as demonstrated by calculating the ratio between two-photon and one-photon maximal responses (Figure IV-27d). Noticeably, LiGluR-**22** (both via direct and sensitised azobenzene excitation) and LiGluR-**23** display a higher ratio than LiGluR-MAG-1, thereby demonstrating that the multiphoton activity of these new photoswitches was enhanced by the design concepts explored in this chapter.

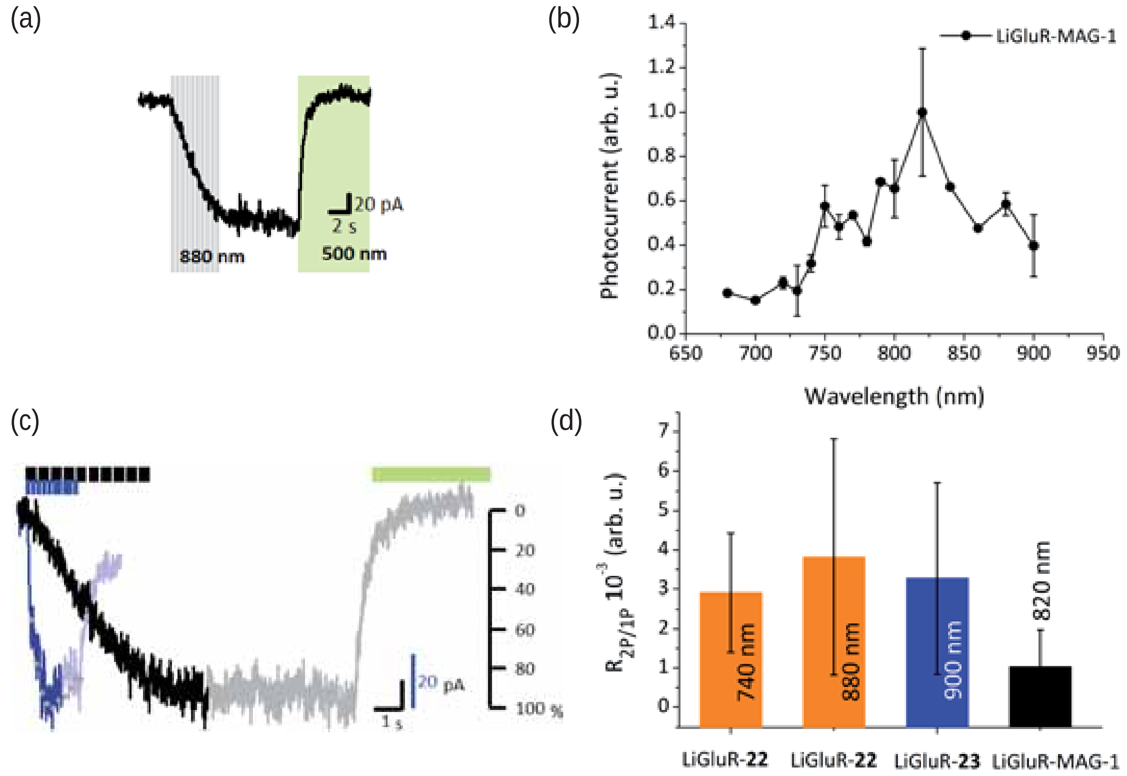

Figure IV-27. (a) Two-photon voltage-clamp recording on a LiGluR-expressing HEK293 cell conjugated with MAG-1. Bars indicate the duration of the stimulation periods applied, which corresponded to 10 consecutive 0.4 s-scans over the cell of interest with NIR light (grey) and 8 s illumination of the complete field of view with green light (green). Irradiation wavelengths are given in each case. (b) Normalised two-photon action spectrum of LiGluR-MAG-1. (c) Typical 2P photocurrent traces of LiGluR-**23** (blue) and LiGluR-MAG-1 (black). Bars indicate the stimulation scans applied and grey dots show the current values obtained at the end of each excitation scan in percentage (right axis). Excitation conditions: LiGluR-**23**: λ_{exc} = 900 nm, 10 scans of 0.16 s; LiGluR-MAG-1: λ_{exc} = 820 nm, 10 scans of 0.4 s. (d) Ratio between the two- and one-photon responses of LiGluR-**22** (sensitised and direct excitation), LiGluR-**23** and LiGluR-MAG-1. To compare between different LiGluR-tethers, two-photon responses were corrected for the distinct power densities and excitation times used. Errors are s.e.m for all cells measured.

In view of the ability of PTLs **22** and **23** to light-control LiGluR channels under two-photon stimulation faster and with a higher intrinsic efficiency than MAG-1, their application to rapidly activate neurons was finally investigated. This study was only performed for ligand **23** because of its better performance than **22**. With this aim, cysteine-mutated LiGluR channels were expressed in cultured hippocampal neurons, which were subsequently incubated with **23** and their photoactivity recorded using whole-cell patch-clamp (Figure IV-28a). As shown in Figure IV-28b and c, inward currents were elicited in these experiments not only upon irradiation with blue light (one-photon stimulation) but also upon excitation at 900 nm (two-photon stimulation). In current-clamp mode, these photocurrents triggered action potentials in two thirds of the neurons tested. Importantly, no spikes were evoked by two-photon stimulation of LiGluR-MAG-1 in the same experimental conditions, probably due to the slow photoresponses of this switch. Therefore, these results unambiguously demonstrate that it is possible to activate neurons by exploiting the two-photon activity of the synthetic photoswitchable ligands developed in this chapter.

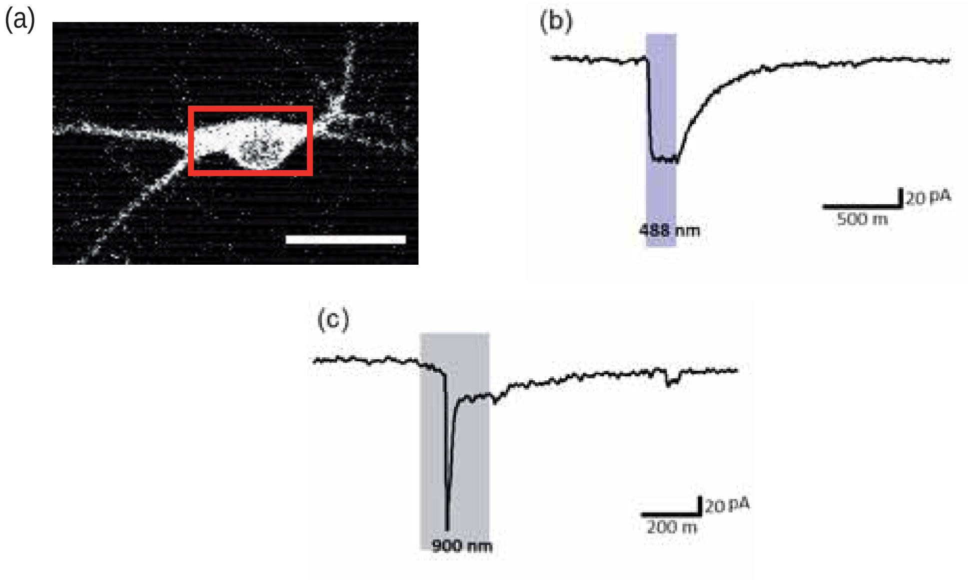

Figure IV-28. (a) Two-photon fluorescence image of a cultured LiGluR-**23** hippocampal neuron filled with Alexa Fluor 594. Red square limits the raster-scan area of two-photon stimulation. Scale bar is 20 μm. (b-c) Voltage-clamp recoding during (b) one-photon stimulation (blue bar) and (c) two-photon raster scan (grey bar).

IV.6. CONCLUSIONS

In this chapter the synthesis, characterisation and biological application of new photoswitched tethered ligands **22** and **23** have been described. As illustrated in Figure IV-29, both compounds present a different substitution pattern of their azobenzene core with respect to that of MAG-1, with which we intended to enhance their two-photon absorption cross sections and, thus, enable direct isomerisation with NIR light. In addition, compound **22** incorporates a naphthalene moiety as photosensitiser, which must efficiently absorb NIR light via two-photon excitation and then transfer its electronic energy to the central azobenzene group to induce isomerisation. As reference for the photochemical studies, photo-harvesting antenna model **100** was also designed and synthesised in this chapter.

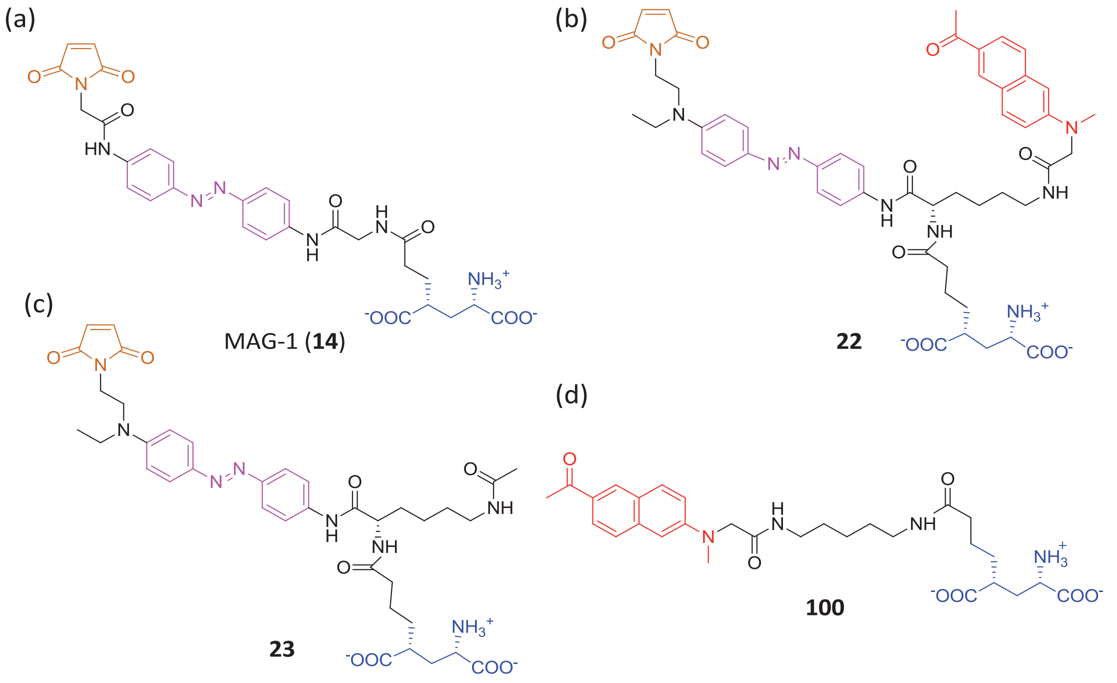

Figure IV-29. Structures of: (a) the most representative compound of MAG-type photoswitches (MAG-1 (**14**));[9] PTLs **22** (b) and **23** (c) synthesised in this work; and (d) photo-harvesting antenna model **100**.

Reference compound **100** was prepared in 4 steps and 22% overall yield from *N*-protected cadaverine **101** (Figure IV-30), to which naphthalene derivative **70** and glutamate derivative **65** were tethered in a stepwise manner.

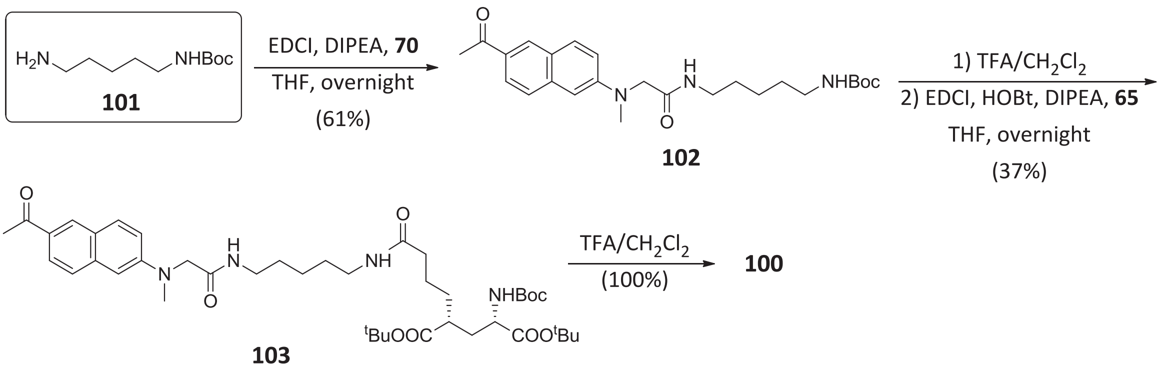

Figure IV-30. Synthesis of reference compound **100**.

As depicted in Figure IV-31, compounds **22** and **23** were obtained in 9 steps and 10% and 12% overall yield, respectively. Both PTLs were prepared following the same synthetic strategy, where *N*,*N*-orthogonally diprotected L-lysine (**28**) was used as scaffold. To this unit the three common fragments of both ligands were sequentially introduced: *O*-protected aminoazobenzene **76**, glutamate derivative **65** (prepared in 8 steps and 7.0% global yield from L-pyroglutamic acid (**37**)), and furan-protected maleimide **89** (prepared in 1 step and 60% yield from furan (**91**) and maleimide (**90**)). To obtain compound **22**, introduction of naphthalene derivative **70** was additionally required, which was obtained from 1-(6-methoxy-2-naphthyl)ethanone (**82**) in 4 steps and 28% yield.

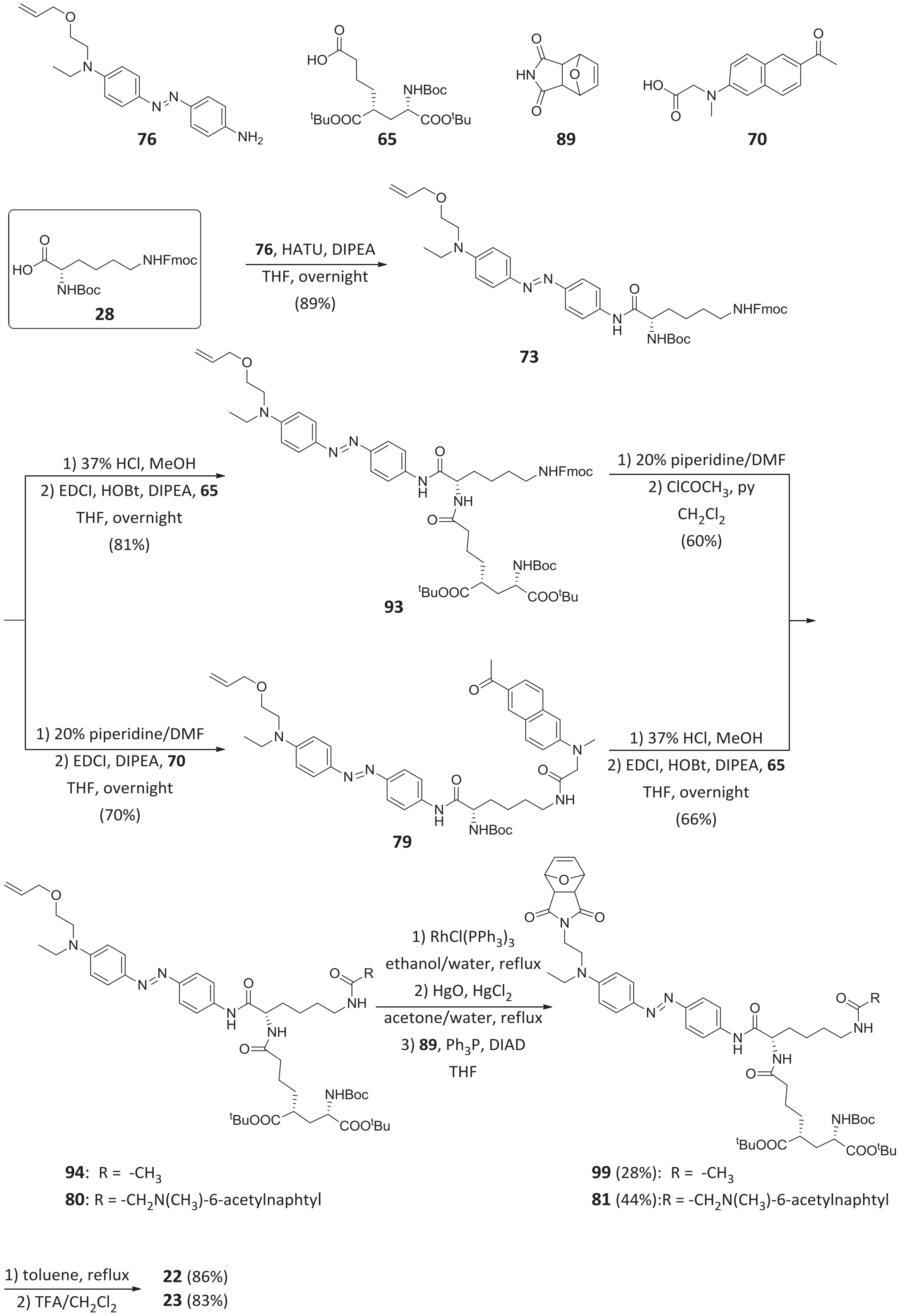

Figure IV-31. Synthesis of PTLs **22** and **23**.

The study of the photochemical properties of PTLs **22** and **23** showed that the introduction of an amino group at the *para*-position of their azoaromatic cores bathochromically shifts their absorption spectrum and substantially decreases the lifetime of their *cis* isomer. Additionally, it was demonstrated that the incorporation of the naphthalene photo-harvesting antenna to PTL **22** does not significantly influences the isomerisation quantum yields, photostationary state conversions and *cis* state lifetime of its azobenzene group. However, such structural modification alters the overall photochemical activity of **22.** Thus, it displays an additional band in the absorption spectrum corresponding to its naphthalene unit, whose photoexcitation results in sensitised *trans*→*cis* isomerisation of the ligand.

Finally, the capability of compounds **22** and **23** to light-control ionotropic glutamate receptors was tested *in vitro* using calcium imaging and whole-cell patch clamp measurements. Low sensitivity calcium imaging experiments only revealed photoactivity for PTL **23** under 1P stimulation. Instead, whole-cell patch-clamp measurements proved that both ligands are able to optically trigger LiGluR channels upon one- and two-photon excitation, which constitutes the first demonstration of multiphoton operation of ionotropic glutamate receptors with NIR light. As originally devised, this occurs through direct *trans*→*cis* azobenzene photoisomerisation in the case of **23**, while this process can also take place via sensitisation for **22**. In spite of its higher versatility, lower 1P and 2P photoresponses were evoked by **22**, which we ascribe to the occurrence of steric effects imparted by the appended photo-harvesting antenna that hinders proper glutamate-binding site interaction. It must be noted that well-established, symmetrically-substituted MAG-1 photoswitch was also observed to display 2P activity in control experiments; however, the use of PTLs **22** and **23** was shown to allow faster, single-wavelength gating of LiGluR upon NIR light irradiation with higher intrinsic efficiency. This does not only proves the viability of the design concepts explored in this chapter to attain 2P light-control of cellular ion channels, but it was also preliminary applied to successfully trigger action potentials in neurons with NIR light. Based on the promising results obtained herein, future work is to be developed to refine the properties of this new class of PTLs in order to reliably photocontrol whole neurons and individual presynaptic terminals.

IV.7. REFERENCES

(1) Kim, H. M.; Cho, B. R. *Acc. Chem. Res.* **2009**, *42*, 863–872.

(2) Kim, H. M.; Kim, B. R.; An, M. J.; Hong, J. H.; Lee, K. J.; Cho, B. R. *Chem. Eur. J.* **2008**, *14*, 2075–2083.

(3) Kim, H. M.; Jung, C.; Kim, B. R.; Jung, S.-Y.; Hong, J. H.; Ko, Y.-G.; Lee, K. J.; Cho, B. R. *Angew. Chem. Int. Ed.* **2007**, *46*, 3460–3463.

(4) Beharry, A. A.; Woolley, G. A. *Chem. Soc. Rev.* **2011**, *40*, 4422–4437.

(5) Boni, L. De; Jr, J. J. R.; Jr, D. S. S.; Silva, C. H. T. P.; Balogh, D. T.; Jr, O. N. O.; Zilio, S. C.; Misoguti, L.; Mendonça, C. R. *Chem. Phys. Lett.* **2002**, *361*, 209–213.

(6) Andrade, A. A.; Yamaki, S. B.; Misoguti, L.; Zilio, S. C.; Atvars, T. D. Z.; Oliveira, O. N.; Mendonça, C. R. *Opt. Mater.* **2004**, *27*, 441–444.

(7) De Boni, L.; Misoguti, L.; Zílio, S. C.; Mendonça, C. R. *ChemPhysChem* **2005**, *6*, 1121–1125.

(8) Antonov, L.; Kamada, K.; Ohta, K.; Kamounah, F. S. *Phys. Chem. Chem. Phys.* **2003**, *5*, 1193–1197.

(9) Volgraf, M.; Gorostiza, P.; Numano, R.; Kramer, R. H.; Isacoff, E. Y.; Trauner, D. *Nat. Chem. Biol.* **2006**, *2*, 47–52.

(10) Bandara, H. M. D.; Burdette, S. C. *Chem. Soc. Rev.* **2012**, *41*, 1809–1825.

(11) Leathen, M. L.; Rosen, B. R.; Wolfe, J. P.; Uni, V. A. V; Arbor, A.; April, R. V; Cheme, S. *J. Org. Chem.* **2009**, 5107–5110.

(12) Mourot, A.; Kienzler, M. A.; Banghart, M. R.; Fehrentz, T.; Huber, F. M. E.; Stein, M.; Kramer, R. H.; Trauner, D. *ACS Chem. Neurosci.* **2011**, *2*, 536–543.

(13) Abdel-Magid, A. F.; Carson, K. G.; Harris, B. D.; Maryanoff, C. A.; Shah, R. D. *J. Org. Chem.* **1996**, *61*, 3849–3862.

(14) Li, X.; Mintz, E. A.; Bu, X. R.; Zehnder, O.; Bosshard, C.; Gu, P. *Tetrahedron* **2000**, *56*, 5785–5791.

(15) Peschke, B.; Bak, S. *Peptides* **2009**, *30*, 689–698.

(16) Schanze, K. S.; Mattox, T. F.; Whitten, D. G. *J. Org. Chem.* **2004**, 2808–2813.

(17) Corey, E. J.; Suggs, W. J. *J. Org. Chem.* **1975**, *38*, 4899–4899.

(18) Gent, A.; Gigg, R. O. Y. *J. Chem. Soc. Chem. Commun.* **1974**, 277–278.

(19) Lahmann, M.; Thiem, J. *Tetrahedron* **2011**, *67*, 1654–1664.

(20) Elson, K. E.; Jenkins, I. D.; Loughlin, W. A. *Org. Biomol. Chem.* **2003**, *1*, 2958–65.

(21) Swamy, K. C. K.; Kumar, N. N. B.; Balaraman, E.; Kumar, K. V. P. P. *Chem. Rev.* **2009**, *109*, 2551–651.

(22) Struga, M.; Miroslaw, B.; Pakosinska-Parys, M.; Drzewiecka, A.; Borowski, P.; Kossakowski, J.; Koziol, A. E. *J. Mol. Struct.* **2010**, *965*, 23–30.

(23) Lu, Z.; Weber, R.; Twieg, R. J. *Tetrahedron Lett.* **2006**, *47*, 7213–7217.

(24) Patel, D. G.; Graham, K. R.; Reynolds, J. R. *J. Mater. Chem.* **2012**, *22*, 3004–3014.

(25) Wildes, P. D.; Pacifici, J. G.; Irick, G.; Whitten, D. G. *J. Am. Chem. Soc.* **1971**, *1192*, 2004–2008.

(26) Zhao, Y.; Inayat, S.; Dikin, D. A.; Singer, J. H.; Ruoff, R. S.; Troy, J. B. *Proc. Inst. Mech. Eng. Part N J. Nanoeng. Nanosyst.* **2008**, *222*, 1–11.

(27) Izquierda-Serra, M. Doctoral Thesis, Institut de Bioenginyeria de Catalunya,Univeristat de Barcelona 2014.

(28) Kienzler, M. A.; Reiner, A.; Trautman, E.; Yoo, S.; Trauner, D.; Isacoff, E. Y. *J. Am. Chem. Soc.* **2013**, *135*, 17683–17686.

Chapter V

General Conclusions

This thesis reports for the first time the synthesis, characterisation and biological evaluation *in vitro* of azobenzene-based photoswitched tethered ligands enabling two-photon optical control with NIR light of ionotropic glutamate receptors in living cells. Based on the well-established maleimide-azobenzene-glutamate scheme developed by Trauner, Isacoff and co-workers to trigger such receptors under one-photon stimulation conditions, two different strategies have been explored in this work to expand this approach into the multiphoton realm:

- **Two-photon sensitised photoisomerisation.** In this strategy, an additional sensitiser unit was incorporated to the original MAG structure, which should efficiently absorb NIR light via two-photon excitation and then transfer its electronic energy to the azobenzene group to induce *trans*→*cis* isomerisation. As photo-harvesting antenna, we chose a pyrene and a naphthalene derivatives, with which potential PTLs **21** and **22** were prepared following similar synthetic strategies (Figure V-1a and b). Compounds **21** was obtained in 9 steps and 12% overall yield, whereas ligand **22** was prepared in 9 steps and 10% overall yield. The photochemical characterisation of these two ligands in solution revealed that they undergo both direct and sensitised *trans*→*cis* photoisomerisation upon one-photon excitation with UV-vis light. Unfortunately, several issues were raised when applying PTLs **21** and **22** to light-control ionotropic glutamate receptors in living cells. In the case of **21**, unspecific biological responses were detected under irradiation, which were ascribed to undesired binding to the lipophilic domains of the plasmatic membrane due to the high hydrophobicity of the pyrene antenna selected. Contrarily, rather satisfactory results were obtained for **22**. When conjugated to LiGluR channels, this PTL was proven to allow light-induced transport of ions across the cell membrane under one- and two-photon stimulation, through both direct and sensitised azobenzene isomerisation, and with a single irradiation source and sub-second time resolution. Together with photoswitch **23** discussed below and MAG-1, this constitutes the first demonstration of multiphoton activation of synthetic light-responsive proteins with NIR light. However, steric hindrance effects imparted by the appended naphthalene sensitiser were found to dramatically influence the overall photoactivity of **22**, leading to two-photon biological responses about one order of magnitude lower than expected.

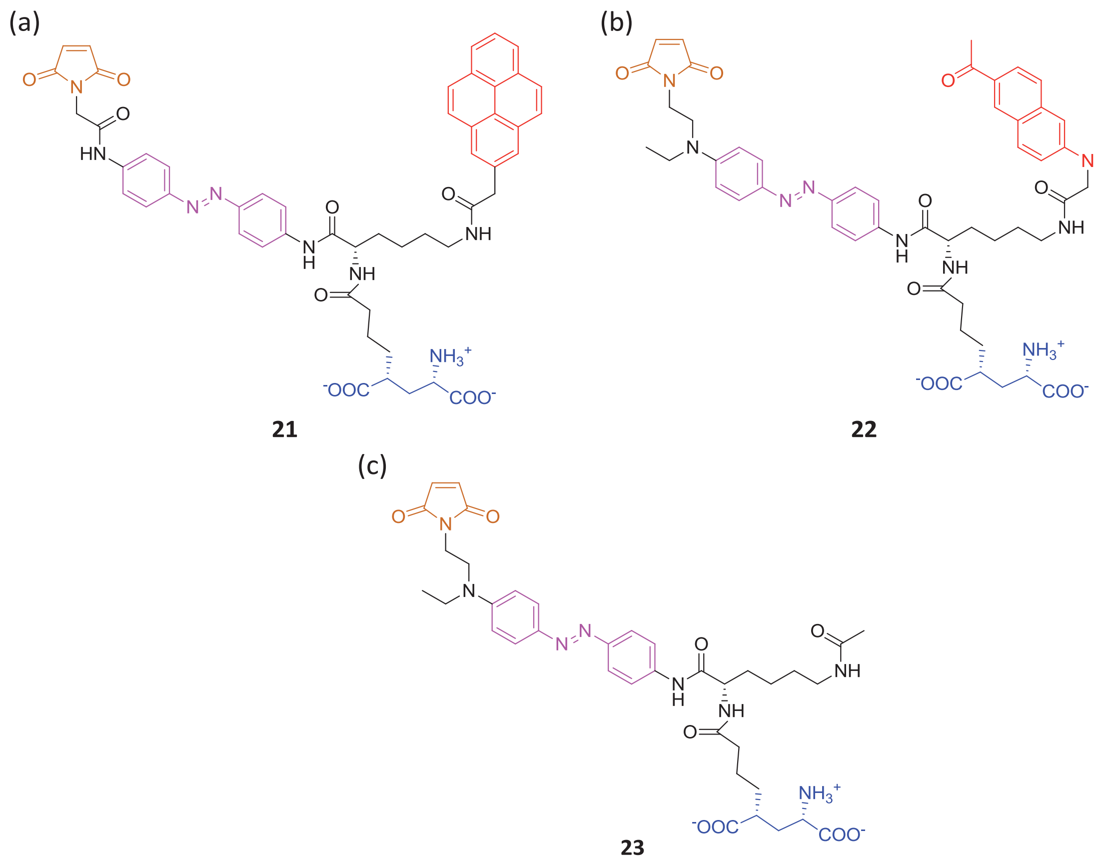

Figure V-1. Structures of the target PTLs **21**, **22** and **23** designed, synthesised and characterised in this work. The distinct functional units of these compounds are shown in different colours (blue: glutamate, pink: azobenzene; brown: maleimide; red: photo-harvesting antenna).

- **Direct two-photon photoisomerisation***.* This second strategy requires push-pull substitution of the azoaromatic group to enhance the intrinsic two-photon absorption cross-section of the system. With this aim, a 4-amido-4'-amino substitution pattern was introduced into the azobenzene core of MAG structure, thus leading to the synthesis of potential PTL **23** following a similar synthetic strategy to that used for compounds **21** and **22** (Figure V-1c). Thus, compound **23** was prepared in 9 steps and 12% overall yield. As for **22**, the photochemical characterisation and biological evaluation of this switch revealed fast, one- and two-photon gating of LiGluR channels with a single irradiation source due to the low stability of its *cis* isomer. In this case, however, light-control of ionotropic glutamate receptors solely proceeds via direct azobenzene isomerisation owing to the lack of a photosensitiser unit. Despite narrowing the action spectra of the switch, this prevents steric hindrance effects hampering glutamate-binding site interaction. As a consequence, much larger two-photon biological responses were measured for **23**, with which successful preliminary assays of triggering action potentials in neurons upon NIR light irradiation could be performed.

In summary, in this thesis we have demonstrated for the first time direct and sensitised two-photon excitation of azobenzene-based photoswitched tethered ligands with NIR radiation, which opens the door to new applications to light-control neural activity with cellular and subcellular resolution.

Chapter VI

Experimental Section

VI.1. GENERAL PROCEDURES

All commercially available reagents were used as received. Solvents were dried by distillation over the appropriate drying agents: CH_2Cl_2 (CaH_2), THF (Na^0). When needed, reactions were performed avoiding moisture by standard procedures and under N_2 atmosphere.

VI.1.1. Spectroscopy

Nuclear magnetic resonance spectra (NMR) were registered at the *Servei de Ressonància Magnètica Nuclear* of the *Universitat Autònoma de Barcelona*. ^{1}H-NMR spectra were recorded on Bruker DPX250 (250 MHz), Bruker DPX360 (360 MHz) and Bruker AR430 (400 MHz) spectrometers. Proton chemical shifts are reported in ppm (δ) ($CDCl_3$, 7.26 ppm, MeOH-d_4, 3.31 ppm and DMSO-d_6, 2.50 ppm). ^{13}C-NMR spectra were recorded with complete proton decoupling on Bruker DPX250 (62.5 MHz), Bruker DPX360 (90 MHz) and Bruker AR430 (100.6 MHz) spectrometers. Carbon chemical shifts are reported in ppm ($CDCl_3$, 77.16 ppm, MeOH-d_4, 49.00 ppm and DMSO-d_6, 39.52 ppm). NMR signals were assigned with the help of COSY, DEPT 135 HSQC, HSQCed and HMBC experiments. All spectra were measured at 298 K.

The abbreviations used to describe signal multiplicities are: s (singlet), br s (broad singlet), d (doublet), br d (broad doublet), t (triplet), q (quartet), dd (double doublet), ddd (double double doublet), dddd (double double double doublet), dt (double triplet), dq (double quartet), ddt (double double triplet), td (triple doublet), m (multiplet), br m (broad multiplet) and *J* (coupling constant).

Infrared spectra (IR) were recorded on a Bruker Tensor 27 Spectrophotometer equipped with a Golden Gate Single Refraction Diamond ATR (Attenuated Total Reflectance) accessory at *Servei d'Anàlisi Química* of the *Universitat Autònoma de Barcelona.* Peaks are reported in cm^{-1}.

Electronic absorption spectra (UV-vis) were recorded on a HP 8453 Spectrophotometer. HPLC or spectroscopy quality solvents were used.

Transient absorption measurements were carried out with a ns laser flash-photolysis system (LKII, Applied Photophysics) equipped with a Nd:YAG laser (Brilliant, Quantel) as pump source, a Xe lamp as probe source and a photomultiplier tube (PMT, R928, Hamamatsu) coupled to a spectrograph as detector.

VI.1.2. Mass Spectrometry

High resolution mass spectra (HRMS) were recorded at the *Servei d'Anàlisi Química* of the *Universitat Autònoma de Barcelona* in a Bruker micrOTOFQ spectrometer using ESIMS (QTOF).

VI.1.3. Chromatography

All reactions were monitored by analytical thin-layer chromatography (TLC) using silica gel 60 F254 pre-coated aluminium plates (0.25 mm thickness). Development was made using an UV lamp at 254 nm and/or using a $KMnO_4$/KOH aqueous solution. Flash column chromatography was performed using silica gel (230-400 mesh).

VI.1.4. Optical Rotatory Power

Specific optical rotations were measured on a Propol Automatisches Dr. Kermchen polarimeter at 20 ± 2 ºC and through a 0.05-dm optical path length or on a *J*-715 (Jasco) polarimeter with temperature regulator and using a 0.1-dm long cuvette.

VI.1.5. Melting Point

Melting points (**Mp**) were determined on a REICHERT Koffler hot stage melting point apparatus, and are uncorrected.

VI.1.6. Fluorometry

Fluorescence emission spectra were measured by means of two different spectrofluorometers: (i) a custom-made spectrofluorometer, where a Nd:YAG (Brillant, Quantel) pulsed laser emitting at 355 nm is used as excitation source and the emitted photons are detected in an Andor ICCD camera coupled to a spectrograph; and (ii) a PerkinElmer LS 55 fluorescence spectrometer. HPLC or spectroscopy quality solvents were used.

VI.1.7. Excitation Sources

Different excitation sources were used to induce *trans-cis* photoisomerisation of azobenzene-based switches: (i) a Vilber Lourmat UV lamp equipped with two 4W tubes emitting light at 254 and 365 nm; (ii) a Vilber Lourmat UV lamp equipped with a 6W tube of 312 nm light; (iii) a Nd:YAG (Brilliant, Quantel) pulsed laser emitting at 355, 532 and 430-650 nm; (iv) diode cw lasers at λ_{exc} = 473 nm (SDL-BS-300, company) and λ_{exc} = 532 nm (Z-Laser)); and (v) a Xe lamp coupled to a spectrograph (Applied Physics)

VI.1.8. Single-cell Calcium Imaging

Single-cell calcium images were measured in a fully-motorised digital inverted optical microscope (iMic 2000, Till Photonics, Gräfelfing, Germany) with a UV Apochromat 40x oil objective lens (Olympus, Tokio, Japan). A ratiometric fluorescence indicator (fura-2 AM) was used to avoid artefacts due to photobleaching during the illumination intervals needed for *trans-cis* photoisomerisation. Fura-2 AM was excited at two different wavelengths (340 and 380 nm) by means of a Polychrome V light source (Till Photonics) and a 505 nm dichroic beam splitter (Chroma Technology, Below Falls, VT, USA). The resulting emission at 510 nm was filtered by a D535/40 nm emission filter (Chroma Technology) and finally collected in a cooled CCD camera (Interline Transfer IMAGO QE, Till Photonics). The fluorescence images obtained at the two excitation wavelengths were stored by TILLvisION imaging software (Till Photonics) and the mean value of the 340:380 nm fluorescence ratio for each cell was calculated with the same software.

VI.2. EXPERIMENTAL DESCRIPTION

VI.2.1. Two-photon optical control of azobenzene-based photoswitched tethered ligands using pyrene sensitiser

Synthesis of *N*-(4-{(*E*)-2-[4-(acetylamino)phenyl]-1-diazenyl}phenyl)ethanamide, 25

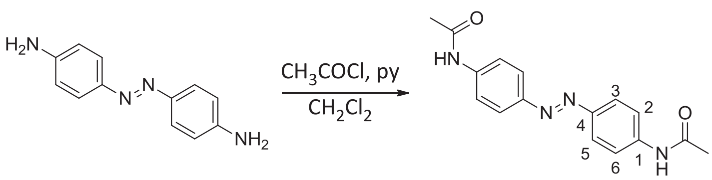

11 **25**

To an ice-cooled of 4-[(*E*)-(4-aminophenyl)-1-diazenyl]aniline (**11**) (100 mg, 0.45 mmol) and pyridine (181 µl, 0.45 mmol) in dry CH_2Cl_2 (20 ml), acetyl chloride (80 µl, 1.19 mmol) was added dropwise under N_2 atmosphere. After 2 h of stirring at rt, TLC analysis (CH_2Cl_2/EtOAc, 7:3) showed no presence of starting material. The mixture was washed with 5% HCl (10 ml), dried over $MgSO_4$ and concentrated under vacuum. Purification by column chromatography (hexanes/EtOAc, 1:1) provided a green solid identified as **25** (60 mg, 0.20 mmol, 43% yield).

Physical and spectroscopic data of **25**

Mp > 300 ºC (from hexanes/EtOAc); **^{1}H-NMR** (400 MHz, DMSO-d$_6$): δ 10.27 (s, 2H, 2xNH), 7.83 (d, $J_{3,2}$ = $J_{5,6}$ = 9.0 Hz, 4H, 2xH-3, 2xH-5), 7.78 (d, $J_{2,3}$ = $J_{6,5}$ = 9.0 Hz, 4H, 2xH-2, 2xH-6), 2.09 (s, 6H, 2xCH_3); **^{13}C-NMR** (100.6 MHz, DMSO-d$_6$): δ 168.7 (2xCO), 147.5 (2xC-4), 141.9 (2xC-1), 123.3 (2xC-3, 2xC-5), 119.1 (2xC-2, 2xC-6), 24.1 (2xCH_3); **IR** (ATR): 3299, 1660, 1595, 1538, 841 cm^{-1}; **HRMS** (ESI+) calcd. for [$C_{16}H_{16}N_4O_2$+Na]: 319.1165; found: 319.1163.

Synthesis of 9*H*-fluoren-9-ylmethyl *N*-[(5*S*)-6-{4-[(*E*)-2-(4-aminophenyl)-1-diazenyl]aniline}-5-[(*tert*-butoxycarbonyl)amino]-6-oxohexyl]carbamate, 29

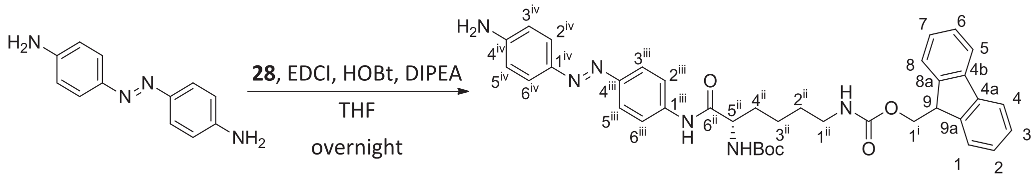

11 **29**

To a stirred solution of 4-[(*E*)-(4-aminophenyl)-1-diazenyl]aniline (**11**) (1.00 g, 4.71 mmol) in dry THF (100 ml) under N_2 atmosphere, a solution of **28** (2.43 g, 5.19 mmol), EDCI (1.17 g, 6.10 mmol), HOBt (955 mg, 7.07 mmol), DIPEA (3.3 ml, 18.8 mmol) in dry THF (100 ml) was added. The reaction mixture was stirred overnight at rt. Then, the mixture was diluted with EtOAc (200 ml) and washed with water (2x100 ml). The organic layer was dried over anhydrous $MgSO_4$ and concentrated under vacuum. The residue was purified by column chromatography (from CH_2Cl_2 to CH_2Cl_2/EtOAc, 4:1) to deliver amide **29** (1.62 g, 2.45 mmol, 53% yield) as an orange solid and starting material (388 mg).

Physical and spectroscopic data of **29**

Mp = 94-97 ºC (from CH_2Cl_2/EtOAc); **$[\alpha]_D^{20}$** = -9.70 (*c* 1.01, $CHCl_3$); **^{1}H-NMR** (250 MHz, $CDCl_3$): δ 8.73 (br s, 1H, C-1^{iii}NH), 7.77 (m, 6H, H-4, H-5, H-3^{iii}, H-5^{iii}, H-2^{iv}, H-6^{iv}), 7.65 (d, $J_{2^{iii},3^{iii}}$ = $J_{6^{iii},5^{iii}}$ = 8.0 Hz, 2H, H-2^{iii}, H-6^{iii}), 7.58 (d, $J_{1,2}$ = $J_{8,7}$ = 7.2 Hz, 2H, H-1, H-8), 7.38 (t, $J_{3,2}$ = $J_{3,4}$ = $J_{6,7}$ = $J_{6,5}$ = 7.2 Hz, 2H, H-3, H-6), 7.29 (td, $J_{2,3}$ = $J_{2,1}$ = $J_{7,8}$ = $J_{7,6}$ = 7.2 Hz, $J_{2,4}$ = $J_{7,5}$ = 1.2 Hz, 2H, H-2, H-7), 6.71 (d, $J_{3^{iv},2^{iv}}$ = $J_{5^{iv},6^{iv}}$ = 8.8 Hz, 2H, H-3^{iv}, H-5^{iv}), 5.34 (d, $J_{C\text{-}5^{ii}NH,5^{ii}}$ = 7.5 Hz, 1H, C-5^{ii}NH), 4.95 (t, $J_{C\text{-}1^{ii}NH,1^{ii}}$ = 6.0 Hz, 1H, C-1^{ii}NH), 4.41 (d, $J_{1^{i},9}$ = 6.9 Hz, 2H, H-1^{i}), 4.20 (m, 2H, H-5^{ii}, H-9), 4.06 (br s, 2H, NH_2), 3.19 (m, 2H, H-1^{ii}), 1.95 (m, 1H, H-4^{ii}), 1.72 (m, 1H, H-4^{ii}), 1.62-1.36 (m, 13H, 2xH-2^{ii}, 2xH-3^{ii}, C(CH_3)$_3$); **^{13}C-NMR** (100.6 MHz, $CDCl_3$): δ 170.8 (C-6^{ii}), 156.9 (CO, carbamate), 156.5 (CO, carbamate), 149.5 (C-4^{iii}, C-4^{iv}), 145.7 (C-1^{iv}), 144.0 (C-9a, C-8a), 141.4 (C-4a, C-4b), 139.4 (C-1^{iii}), 127.8 (C-3, C-6), 127.2 (C-2, C-7), 125.1 (C-1, C-8, C-2^{iv}, C-6^{iv}), 123.4 (C-3^{iii}, C-5^{iii}), 120.1 (C-4, C-6, C-2^{iii}, C-6^{iii}), 114.8 (C-3^{iv}, C-5^{iv}), 80.7 (*C*(CH_3)$_3$), 66.7 (C-1^{i}), 55.2 (C-5^{ii}), 47.4 (C-9), 40.3 (C-1^{ii}), 31.4 (C-4^{ii}), 29.5 (C-2^{ii}), 28.4 (C(CH_3)$_3$), 22.7 (C-3^{ii}); **IR** (ATR): 3323, 2926, 2856, 1687, 1665, 1596, 1504, 1245 cm^{-1}; **HRMS** (ESI+) calcd. for [$C_{38}H_{42}N_6O_5$+Na]: 685.3109; found: 685.3112. **COSY** and **^{1}H/^{13}C** correlation were recorded.

Synthesis of ethyl (2*S*)-5-oxotetrahydro-1*H*-pyrrolecarboxylate, 38[1]

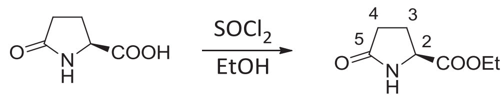

37 **38**

To an ice-cooled solution of L-pyroglutamic acid (**37**) (10.1 g, 78.1 mmol) in EtOH (150 ml), thionyl chloride (6.0 ml, 82.0 mmol) was slowly added. The resulting solution was stirred for 30 min at 0 ºC and overnight at rt. Then, water (100 ml) was added and the crude was neutralized by the addition of saturated aqueous solution of $NaHCO_3$ and extracted with $CHCl_3$ (3x200 ml). The combined organics layers were dried over anhydrous $MgSO_4$ and the solvent was removed under vacuum to furnish a colourless oil identified as **38** (11.7 g, 74.3 mmol, 95% yield).

Spectroscopic data of **38**

^{1}H-NMR (400 MHz, $CDCl_3$): δ 7.10 (m, 1H, NH), 4.17 (m, 1H, H-2), 4.16 (q, $J_{CH_2CH_3,CH_2CH_3}$ = 7.1 Hz, 2H, CH_2CH_3), 2.48-2.17 (m, 3H, H-3, 2xH-4), 2.13 (m, 1H, H-3), 1.22 (t, $J_{CH_2CH_3,CH_2CH_3}$ = 7.1 Hz, 3H, CH_2CH_3); **^{13}C-NMR** (100.6 MHz, $CDCl_3$): δ 177.7 (C-5), 171.6 (CO, ester), 60.3 (CH_2CH_3), 54.7 (C-2), 28.4 (C-4), 23.8 (C-3), 13.0 (CH_2CH_3).

Synthesis of 1-*tert*-butyl 2-ethyl (2*S*)-5-oxotetrahydro-1*H*-pyrrolecarboxylate, 39[2]

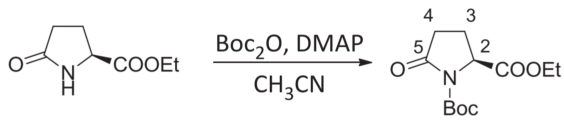

38 **39**

To an ice-cooled solution of ethyl ester **38** (10.0 g, 63.7 mmol) in CH_3CN (420 ml), 4-(dimethylamino)pyridine (DMAP) (778 mg, 6.37 mmol) and Boc_2O (20.9 g, 95.5 mmol) were added. The reaction mixture was warmed up to rt and left for 16 h. The solvent was removed under vacuum and the resulting residue was purified by column chromatography (hexanes/EtOAc, 3:1) to provide **39** (15.4 g, 51.9 mmol, 94% yield) as a brown oil.

Spectroscopic data of **39**

^{1}H-NMR (250 MHz, $CDCl_3$): δ 4.47 (dd, $J_{2,3}$ = 9.3 Hz, $J_{2,3}$ = 3.0 Hz, 1H, H-2), 4.11 (q, $J_{CH_2CH_3,CH_2CH_3}$ = 7.1 Hz, 2H, CH_2CH_3), 2.60-2.12 (m, 3H, H-3, 2xH-4), 1.91 (m, 1H, H-3) 1.37 (s, 9H, $C(CH_3)_3$), 1.18 (t, $J_{CH_2CH_3,CH_2CH_3}$ = 7.1 Hz, 3H, CH_2CH_3); **^{13}C-NMR** (100.6 MHz, $CDCl_3$): δ 172.8 (C-5), 170.8 (CO, ester), 148.6 (CO, carbamate), 82.5 ($C(CH_3)_3$), 60.9 (CH_2CH_3), 58.4 (C-2), 30.5 (C-4), 27.2 ($C(CH_3)_3$), 20.9 (C-3), 13.6 (CH_2CH_3).

Synthesis of 1-(*tert*-butyl) 2-ethyl (2*S*,4*R*)-4-allyl-5-oxo-tetrahydro-1*H*-pyrroledicarboxylate, (4*R*)-40[3]

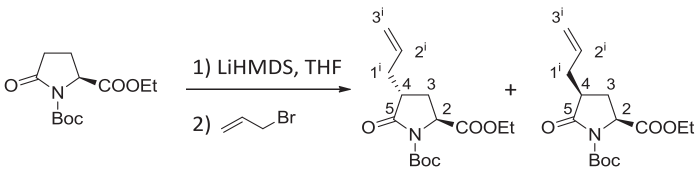

39 (4*R*)-**40** (4*S*)-**40**

To a solution of carbamate **39** (5.00 g, 19.4 mmol) in dry THF (150 ml) at -78 ºC, LiHMDS 1.0 M in THF (23 ml, 23.0 mmol) was added dropwise under N_2 atmosphere. The reaction mixture was stirred at this temperature for 1 h and allyl bromide (6.7 ml, 77.7 mmol) was slowly added. After stirring for 3 h (for more than 5 h the product decomposes), the reaction was quenched by the slow addition of NH_4Cl saturated aqueous solution at -78 ºC, washed with water (200 ml) and extracted with CH_2Cl_2 (3x100 ml). The combined organic phases were dried over anhydrous $MgSO_4$ and the solvent was evaporated under vacuum. The residue was purified by column chromatography (hexanes/Et_2O, 6:1) to give (4*S*)-**40** (1.33 g, 4.47 mmol, 23% yield) as a yellowish oil and (4*R*)-**40** (2.72 g, 9.13 mmol, 47% yield) as a brown oil.

Spectroscopic data of (4*R*)-**40**

^{1}H-NMR (250 MHz, $CDCl_3$): δ 5.72 (ddt, $J_{2^i,3^i_{trans}}$ = 16.9 Hz, $J_{2^i,3^i_{cis}}$ = 10.2 Hz, $J_{2^i,1^i}$ = 7.0 Hz, 1H, H-2^i), 5.09 (m, 2H, H-3^i), 4.52 (dd, $J_{2,3}$ = 9.5 Hz, $J_{2,3}$ = 1.8 Hz, 1H, H-2), 4.21 (q, $J_{CH_2CH_3,CH_2CH_3}$ = 7.1 Hz, 2H, CH_2CH_3), 2.78-2.55 (m, 2H, H-4, H-1^i), 2.25-2.10 (m, 2H, H-3, H-1^i), 1.99 (m, 1H, H-3), 1.48 (s, 9H, $C(CH_3)_3$), 1.27 (t, $J_{CH_2CH_3,CH_2CH_3}$ = 7.1 Hz, 3H, CH_2CH_3); **^{13}C-NMR** (90 MHz, $CDCl_3$): δ 174.5 (C-5), 171.4 (CO, ester), 149.5 (CO, carbamate), 134.5 (C-2^i), 117.8 (C-3^i), 83.6 ($C(CH_3)_3$), 61.8 (CH_2CH_3), 57.2 (C-2), 41.3 (C-4), 34.9 (C-1^i), 28.0 ($C(CH_3)_3$), 27.9 (C-3), 14.3 (CH_2CH_3).

Spectroscopic data of (4*S*)-**40**

^{1}H-NMR (400 MHz, $CDCl_3$): δ 5.68 (m, 1H, H-2^i), 4.99 (m, 2H, H-3^i), 4.44 (dd, $J_{2,3}$ = 8.9 Hz, $J_{2,3}$ = 6.6 Hz, 1H, H-2), 4.17 (q, $J_{CH_2CH_3,CH_2CH_3}$ = 7.1 Hz, 2H, CH_2CH_3), 2.58 (m, 2H, H-4, H-1^i), 2.42 (dt, J_{gem} = 13.4 Hz, $J_{3,2}$ = $J_{3,4}$ = 8.9 Hz, 1H, H-3), 2.15 (m, 1H, H-1^i), 1.66 (ddd, J_{gem} = 13.4 Hz, $J_{3,4}$ = 7.6 Hz, $J_{3,2}$ = 6.6 Hz, 1H, H-3), 1.43 (s, 9H, $C(CH_3)_3$), 1.24 (t, $J_{CH_2CH_3,CH_2CH_3}$ = 7.1 Hz, 3H, CH_2CH_3); **^{13}C-NMR** (100.6 MHz, $CDCl_3$): δ 174.6 (C-5), 171.5 (CO, ester), 149.3 (CO, carbamate), 134.6 (C-2^i), 117.6 (C-3^i), 83.6 ($C(CH_3)_3$), 61.6 (CH_2CH_3), 57.5 (C-2), 42.0 (C-4), 35.1 (C-1^i), 27.8 ($C(CH_3)_3$), 26.7 (C-3), 14.1 (CH_2CH_3).

Synthesis of 1-*tert*-butyl 2-ethyl (2*S*,4*R*)-5-oxo-4-[(2*E*)-4-oxo-2-butenyl]-tetrahydro-1*H*-pyrroledicarboxylate, 41

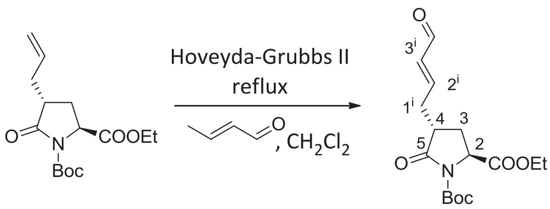

(4*R*)-**40** **41**

To a boiling solution of allyl (4*R*)-**40** (1.47 g, 4.95 mmol) and crotonaldehyde (2.1 ml, 24.7 mmol) in dry CH_2Cl_2 (20 ml), Hoveyda-Grubbs II catalyst (41 mg, 65 μmol) was added in 3 portions. The mixture was heated to reflux for 12 h. The reaction mixture was filtered off through a pad of silica gel and concentrated. The crude was purified by column chromatography (hexanes/Et_2O, from 3:1 to 1:1) to afford **41** (1.37 g, 4.21 mmol, 88% yield) as a colourless oil.

Physical and spectroscopic data of **41**

[α]$_D^{20}$ = -22.9 (*c* 0.7, $CHCl_3$); **^{1}H-NMR** (360 MHz, $CDCl_3$): δ 9.50 (d, $J_{CHO,3^i}$ = 7.8 Hz, 1H, CHO), 6.82 (dt, $J_{2^i,3^i}$ = 15.4 Hz, $J_{2^i,1^i}$ = 7.0 Hz, 1H, H-2^i), 6.14 (dd, $J_{3^i,2^i}$ = 15.4 Hz, $J_{3^i,CHO}$ = 7.8 Hz, 1H, H-3^i), 4.56 (d, $J_{2,3}$ = 9.5 Hz, 1H, H-2), 4.23 (q, $J_{CH_2CH_3,CH_2CH_3}$ = 7.1 Hz, 2H, CH_2CH_3), 2.85 (m, 2H, H-4, H-1^i), 2.47 (m, 1H, H-1^i), 2.24 (dd, J_{gem} = 13.3 Hz, $J_{3,4}$ = 8.2 Hz, 1H, H-3), 1.97 (ddd, J_{gem} = 13.3 Hz, $J_{3,4}$ = 11.7 Hz, $J_{3,2}$ = 9.8 Hz, 1H, H-3), 1.49 (s, 9H, $C(CH_3)_3$), 1.28 (t, $J_{CH_2CH_3,CH_2CH_3}$ = 7.1 Hz, 3H, CH_2CH_3); **^{13}C-NMR** (90 MHz, $CDCl_3$): δ 193.5 (CHO), 173.5 (C-5), 171.0 (CO, ester), 153.5 (C-2^i), 149.3 (CO, carbamate), 135.0 (C-3^i), 84.0 ($C(CH_3)_3$), 62.0 (CH_2CH_3), 57.1 (C-2), 40.6 (C-4), 33.3 (C-1^i), 28.2 (C-3), 28.0 ($C(CH_3)_3$), 14.3 (CH_2CH_3); **IR** (ATR): 2980, 1787, 1743, 1688, 1458, 1369, 1314, 1151 cm^{-1}; **HRMS** (ESI+) calcd. for [$C_{16}H_{23}NO_6$+Na]: 348.1418; found: 348.1413.

Synthesis of (2*E*)-4-[(3*R*,5*S*)-1-(*tert*-butoxycarbonyl)-5-(ethoxycarbonyl)-2-oxotetrahydro-1*H*-3-pyrroyl]-2-butenoic acid, 42[4]

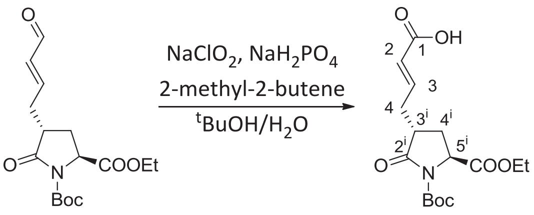

41 **42**

To an ice-cooled solution of the aldehyde **41** (1.34 g, 4.12 mmol) in a 5:1 mixture of ^{t}BuOH and water (82 ml), 2-methyl-2-butene (4.4 ml, 41.2 mmol), $NaH_2PO_4{\cdot}2H_2O$ (3.22 g, 20.6 mmol) and $NaClO_2$ (2.20 g, 24.7 mmol) were successively added. The resulting mixture was stirred at 0 ^{o}C for 1 h and warmed up to rt. The reaction mixture was stirred overnight (for more than 1 day, the product epimerizes). Then, water (47 ml) and a saturated aqueous solution of Na_2CO_3 were added until pH 8. The mixture was extracted with EtOAc (3x30 ml) and the aqueous phase was acidified to pH 3 with 5% HCl. The crude was extracted with EtOAc (3x80 ml), dried over anhydrous $MgSO_4$ and concentrated under vacuum to give **42** (942 mg, 2.76 mmol, 67% yield) as a colourless oil.

Spectroscopic data of **42**

^{1}H-NMR (360 MHz, $CDCl_3$): δ 8.22 (br s, 1H, COOH), 6.95 (ddd, $J_{3,2}$ = 15.5 Hz, $J_{3,4}$ = 7.5 Hz, $J_{3,4}$ = 6.8 Hz, 1H, H-3), 5.88 (d, $J_{2,3}$ = 15.5 Hz, 1H, H-2), 4.55 (dd, $J_{5^i,4^i}$ = 9.6 Hz, $J_{5^i,4^i}$ = 1.1 Hz, 1H, H-5^i), 4.22 (q, $J_{CH_2CH_3,CH_2CH_3}$ = 7.1 Hz, 2H, CH_2CH$_3$), 2.80 (m, 2H, H-4, H-3^i), 2.32 (m, 1H, H-4), 2.23 (ddd, J_{gem} = 13.3 Hz, $J_{4^i,3^i}$ = 8.4 Hz, $J_{4^i,5^i}$ = 1.1 Hz, 1H, H-4^i), 1.96 (ddd, J_{gem} = 13.3 Hz, $J_{4^i,3^i}$ = 11.6 Hz, $J_{4^i,5^i}$ = 9.6 Hz, 1H, H-4^i), 1.48 (s, 9H, $C(CH_3)_3$), 1.27 (t, $J_{CH_2CH_3,CH_2CH_3}$ = 7.1 Hz, 3H, CH$_2$CH_3); **^{13}C-NMR** (90 MHz, $CDCl_3$): δ 173.5 (C-2^i), 171.1/171.0 (CO, ester/C-1), 149.4 (CO, carbamate), 147.2 (C-3), 123.5 (C-2), 84.0 (*C*(CH$_3$)$_3$), 62.0 (*C*H$_2$CH$_3$), 57.1 (C-5^i), 40.7 (C-3^i), 32.9 (C-4), 28.2 (C-4^i), 28.0 (C(*C*H$_3$)$_3$), 14.3 (CH$_2$*C*H$_3$).

Synthesis of 4-[(3*R*,5*S*)-1-(*tert*-butoxycarbonyl)-5-(ethoxycarbonyl)-2-oxotetrahydro-1*H*-3-pyrroyl]butanoic acid, 43[4]

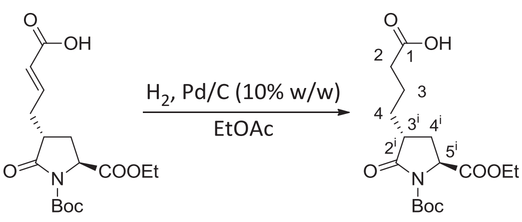

42 **43**

To a solution of olefin **42** (820 mg, 2.40 mmol) in EtOAc (99 ml), Pd/C 10% (82 mg) was added. The resulting suspension was stirred in a H_2 atmosphere for 16 h. Then, the crude was filtered through Celite® and concentrated under vacuum to furnish a brown oil identified as **43** (808 mg, 2.35 mmol, 98% yield).

Spectroscopic data of **43**

^{1}H-NMR (250 MHz, $CDCl_3$): δ 4.54 (dd, $J_{5^i,4^i}$ = 9.5 Hz, $J_{5^i,4^i}$ = 1.4 Hz, 1H, H-5^{i}), 4.21 (q, $J_{CH_2CH_3,CH_2CH_3}$ = 7.1 Hz, 2H, CH_2CH_3), 2.61 (m, 1H, H-3^{i}), 2.37 (t, $J_{2,3}$ = 7.1 Hz, 2H, H-2), 2.23 (ddd, J_{gem}= 13.2 Hz, $J_{4^i,3^i}$ = 8.6 Hz, $J_{4^i,5^i}$ = 1.4 Hz, 1H, H-4^{i}), 1.95 (m, 2H, H-4, H-4^{i}), 1.67 (m, 2H, H-3), 1.47 (m, 10H, $C(CH_3)_3$, H-4), 1.27 (t, $J_{CH_2CH_3,CH_2CH_3}$ = 7.1 Hz, 3H, CH_2CH_3); **^{13}C-NMR** (90 MHz, $CDCl_3$): δ 177.9 (C-1), 174.8 (C-2^{i}), 171.0 (CO, ester), 149.0 (CO, carbamate), 83.2 ($C(CH_3)_3$), 61.4 (CH_2CH_3), 56.9 (C-5^{i}), 41.1 (C-3^{i}), 33.3 (C-2), 29.3 (C-4), 28.0 (C-4^{i}), 27.5 ($C(CH_3)_3$), 21.6 (C-3), 13.8 (CH_2CH_3).

Synthesis of 9*H*-fluoren-9-ylmethyl *N*-((5*S*)-5-amino-6-{4-[(*E*)-2-(4-aminophenyl)-1-diazenyl]anilino}-6-oxohexyl)carbamate, 44

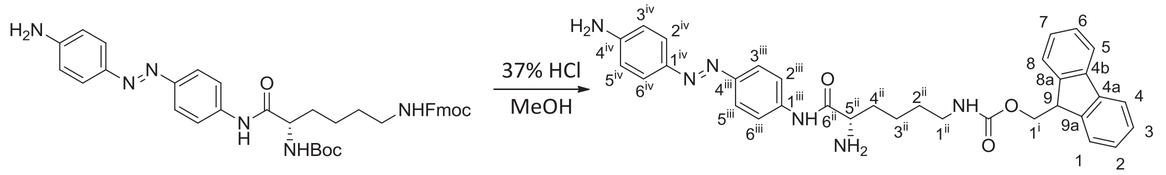

29 **44**

To a solution of amine **29** (1.07 g, 1.62 mmol) in MeOH (100 ml), 37% HCl (21 ml, 0.22 mol) was added. The reaction mixture was stirred for 1 h at room temperature until TLC (EtOAc) showed no presence of starting material. Then, the mixture was concentrated under vacuum, diluted with EtOAc (20 ml) and neutralised with a saturated aqueous solution of $NaHCO_3$. Purification by column chromatography (from EtOAc to EtOAc/MeOH, 95:5) gave **44** (890 mg, 1.58 mmol, 98% yield) as an orange solid.

Physical and spectroscopic data of **44**

Mp = 78-82 ^{o}C (from EtOAc); **$[\alpha]_D^{20}$** = -25.6 (*c* 1.19, $CHCl_3$); **^{1}H-NMR** (400 MHz, $CDCl_3$): δ 9.69 (br s, 1H, C-1^{iii}NH), 7.84 (d, $J_{3^{iii},2^{iii}} = J_{5^{iii},6^{iii}}$ = 8.7 Hz, 2H, H-3^{iii}, H-5^{iii}), 7.75 (m, 6H, H-4, H-5, H-2^{iii}, H-6^{iii}, H-2^{iv}, H-5^{iv}), 7.59 (d, $J_{1,2} = J_{8,7}$ = 7.4 Hz, 2H, H-1, H-8), 7.39 (t, $J_{3,2} = J_{3,4} = J_{6,7} = J_{6,5}$ = 7.4 Hz, 2H, H-3, H-6), 7.31 (td, $J_{2,3} = J_{2,1} = J_{7,8} = J_{7,6}$ = 7.4 Hz, $J_{2,4} = J_{7,5}$ = 0.9 Hz, 2H, H-2, H-7), 6.73 (d, $J_{3^{iv},2^{iv}} = J_{5^{iv},6^{iv}}$ = 8.7 Hz, 2H, H-3^{iv}, H-5^{iv}), 4.90 (t, $J_{C\text{-}1^{ii}NH,1^{ii}}$ = 5.4 Hz, 1H, C-1^{ii}NH), 4.40 (d, $J_{1^i,9}$ = 6.9 Hz, 2H, H-1^{i}), 4.21 (t, $J_{9,1^i}$ = 6.5 Hz, 1H, H-9), 3.49 (m, 1H, H-5^{ii}), 3.21 (m, 2H, H-1^{ii}), 1.96 (m, 1H, H-4^{ii}), 1.68-1.29 (m, 5H, 2xH-2[ii], 2xH-3[ii], H-4[ii]); **^{13}C-NMR** (100.6 MHz, $CDCl_3$): δ 173.5 (C-6[ii]), 156.7 (CO, carbamate), 149.5/ 149.4 (C-4[iii]/C-4[iv]), 145.7 (C-1[iv]), 144.1 (C-9a, C-8a), 141.4 (C-4a, C-4b), 139.4 (C-1[iii]), 127.8 (C-3, C-6), 127.2 (C-2, C-7), 125.1 (C-1, C-8, C-2[iv], C-6[iv]), 123.5 (C-3[iii], C-5[iii]), 120.1 (C-4, C-6), 119.6 (C-2[iii], C-6[iii]), 114.8 (C-3[iv], C-5[iv]), 66.7 (C-1[i]), 55.5 (C-5[ii]), 47.4 (C-9), 40.7 (C-1[ii]), 34.5 (C-4[ii]), 29.8 (C-2[ii]), 23.0 (C-3[ii]); **IR** (ATR): 3335, 2923, 1687, 1596, 1508, 1249, 1138 cm^{-1}; **HRMS** (ESI+) calcd. for [$C_{33}H_{34}N_6O_3$+H]: 563.2765; found: 563.2769.

Synthesis of 1-(*tert*-butyl) 2-ethyl (2*S*,4*R*)-4-{4-[((1*S*)-1-({4-[(*E*)-(4-aminophenyl)-1-diazenyl] anilino}carbonyl)-5-{[(9*H*-fluoren-9-ylmethoxy)carbonyl]amino}pentyl)amino]-4-oxobutyl}-5-oxotetrahydro-1*H*-1,2-pyrroledicarboxylate, 30

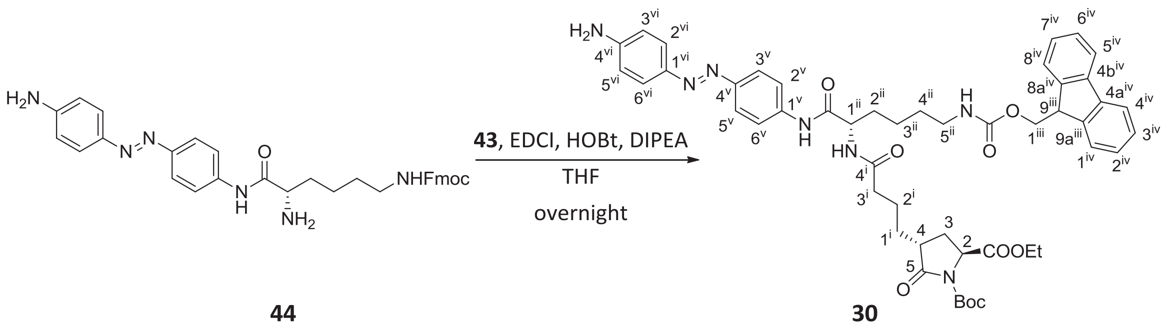

44 **30**

To a stirred solution of amine **44** (1.10 g, 1.96 mmol) in dry THF (60 ml) under N_2 atmosphere, a solution of **43** (806 mg, 2.35 mmol), EDCI (488 mg, 2.55 mmol), HOBt (397 mg, 2.94 mmol), DIPEA (1.4 ml, 8.04 mmol) in dry THF (60 ml) was added. The reaction mixture was stirred overnight at rt. Then, the mixture was diluted with EtOAc (120 ml) and washed with water (2x150 ml). The organic layer was dried over anhydrous $MgSO_4$ and concentrated under vacuum. The residue was purified by column chromatography (EtOAc/MeOH, 95:5), providing amide **30** (1.46 g, 1.64 mmol, 84% yield) as an orange solid.

Physical and spectroscopic data of **30**

Mp = 104-108 ^oC (from EtOAc); **$[\alpha]_D^{20}$** = -24.7 (*c* 0.41, $CHCl_3$); **^{1}H-NMR** (400 MHz, $CDCl_3$): δ 9.22 (br s, 1H, C-1[v]NH), 7.74 (m, 8H, H-2[v], H-6[v], H-3[v], H-5[v], H-2[vi], H-6[vi], H-4[iv], H-5[iv]), 7.57 (d, $J_{1^{iv},2^{iv}} = J_{8^{iv},7^{iv}}$ = 7.4 Hz, 2H, H-1[iv], H-8[iv]), 7.37 (t, $J_{3^{iv},2^{iv}} = J_{3^{iv},4^{iv}} = J_{6^{iv},7^{iv}} = J_{6^{iv},5^{iv}}$ = 7.4 Hz, 2H, H-3[iv], H-6[iv]), 7.31 (td, $J_{2^{iv},3^{iv}} = J_{2^{iv},1^{iv}} = J_{7^{iv},6^{iv}} = J_{7^{iv},8^{iv}}$ = 7.4 Hz, $J_{2^{iv},4^{iv}} = J_{7^{iv},5^{iv}}$ = 0.9 Hz, 2H, H-2[iv], H-7[iv]), 6.80 (d, $J_{C\text{-}1^{ii}NH,1^{ii}}$ = 7.5 Hz, 1H, C-1[ii]NH), 6.71 (d, $J_{3^{vi},2^{vi}} = J_{5^{vi},6^{vi}}$ = 7.5 Hz, 2H, H-3[vi], H-5[vi]), 5.21 (t, $J_{C\text{-}5^{ii}NH,5^{ii}}$ = 6.0 Hz, 1H, C-5[ii]NH), 4.60 (m, 1H, H-1[ii]), 4.49 (d, $J_{2,3}$ = 9.3 Hz, 1H, H-2), 4.35 (m, 2H, H-1[iii]), 4.19 (m, 3H, H-9[iv], C*H*$_2$CH$_3$), 4.07 (br s, 2H, NH_2), 3.18 (m, 2H, H-5[ii]), 2.58 (m, 1H, H-4), 2.28 (m, 2H, H-3[i]), 2.16 (m, 1H, H-3), 2.07-1.74 (m, 5H, H-3, H-1[i], 2xH-2[ii], H-4[ii]), 1.69 (m, 2H, H-2[i]), 1.54 (m, 2H, H-1[i], H-4[ii]), 1.44 (m, 11H, C(CH$_3$)$_3$, 2xH-3^{ii}), 1.26 (t, $J_{CH_2CH_3,CH_2CH_3}$ = 7.1 Hz, 3H, CH$_2$C*H*$_3$); **^{13}C-NMR** (100.6 MHz, CDCl$_3$): δ 175.3 (C-5), 173.5 (C-4^{i}), 171.4 (CO, ester), 170.5 (CO, amide), 156.9 (CO, carbamate), 149.6/149.5/ 149.4 (C-4^{v}/C-4^{vi}/CO, carbamate), 145.6 (C-1^{vi}), 144.1 (C-9a^{iv}, C-8a^{iv}), 141.4 (C-4a^{iv}, C-4b^{iv}), 139.7 (C-1^{v}), 127.8 (C-3^{iv}, C-6^{iv}), 127.2 (C-2^{iv}, C-7^{iv}), 125.2 (C-1^{iv}, C-8^{iv}), 125.1 (C-2^{vi}, C-6^{vi}), 123.4 (C-3^{v}, C-5^{v}), 120.2/120.1 (C-4^{iv}, C-5^{iv}/C-2^{v}, C-6^{v}), 114.8 (C-3^{vi}, C-6^{vi}), 83.7 (*C*(CH$_3$)$_3$), 66.8 (C-1^{iii}), 61.9 (*C*H$_2$CH$_3$), 57.3 (C-2), 54.1 (C-1^{ii}), 47.4 (C-9^{iv}), 41.5 (C-4), 40.3 (C-5^{ii}), 35.9 (C-3^{i}), 31.2 (C-2^{ii}), 29.7/29.6 (C-1^{i}/C-4^{ii}), 28.3 (C-3), 28.0 (C(*C*H$_3$)$_3$), 22.8/22.6 (C-2^{i}/C-3^{ii}), 14.3 (CH$_2$*C*H$_3$); **IR** (ATR): 3299, 2930, 1783, 1597, 1529, 1249, 1141 cm^{-1}; **HRMS** (ESI+) calcd. for [C$_{49}$H$_{57}$N$_7$O$_9$+Na]: 910.4110; found: 910.4108. **^{1}H/^{13}C** correlation were recorded.

Synthesis of 1-(*tert*-butyl) 2-ethyl (2*S*,4*R*)-4-(4-{[(1*S*)-5-amino-1-({4-[(*E*)-2-(4-aminophenyl)-1-diazenyl]anilino}carbonyl)pentyl]amino}-4-oxobutyl)-5-oxotetrahydro-1*H*-1,2-pyrroledicarboxylate, 45

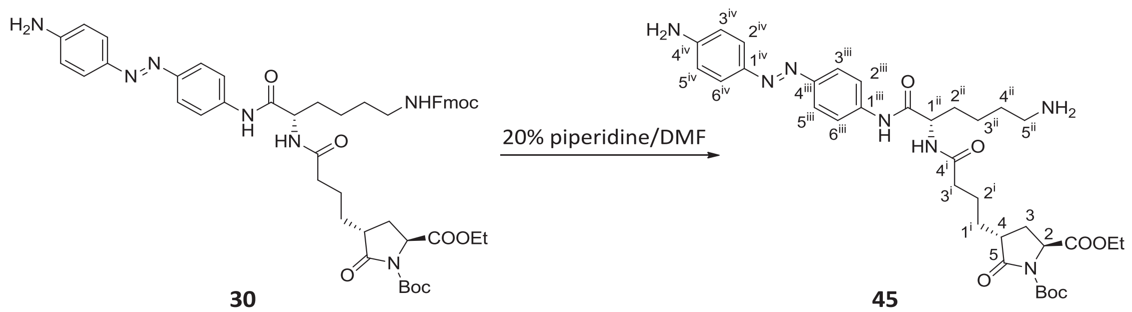

30 **45**

A commercially available solution of 20% piperidine in DMF (11 ml) was added to compound **30** (1.46 g, 1.64 mmol). After 1 h of stirring at rt, TLC analysis (EtOAc/MeOH, 95:5) showed no presence of starting material. The mixture was diluted with water (15 ml) and washed with EtOAc (3x20 ml). The combined organic extracts were dried over anhydrous MgSO$_4$ and concentrated under vacuum. The resulting solid was purified by column chromatography (from EtOAc to EtOAc/MeOH/NH$_3$, 9:2:1) to provide an orange solid identified as **45** (952 mg, 1.43 mmol, 87% yield).

Physical and spectroscopic data of **45**

Mp = 107-112 ºC (from EtOAc); **[α]$_D$^{20}** = -38.9 (*c* 0.47, CHCl$_3$); **^{1}H-NMR** (400 MHz, MeOH-d$_4$): δ 7.72 (m, 6H, H-3^{iii}, H-5^{iii}, H-2^{iii}, H-6^{iii}, H-2^{iv}, H-6^{iv}), 6.73 (d, $J_{3^{iv},2^{iv}}$ = $J_{5^{iv},6^{iv}}$ = 8.8 Hz, 2H, H-3^{iv}, H-5^{iv}), 4.61 (dd, $J_{2,3}$ = 9.8 Hz, $J_{2,3}$ = 1.4 Hz, 1H, H-2), 4.51 (dd, $J_{1^{ii},2^{ii}}$ = 8.8 Hz, $J_{1^{ii},2^{ii}}$ = 5.5 Hz, 1H, H-1^{ii}), 4.23 (m, 2H, C*H*$_2$CH$_3$), 2.84 (t, $J_{5^{ii},4^{ii}}$ = 7.5 Hz, 2H, H-5^{ii}), 2.65 (m, 1H, H-4), 2.32 (t, $J_{3^{i},2^{i}}$ = 7.1 Hz, 2H, H-3^{i}), 2.25 (m, 1H, H-3), 2.24 (ddd, J_{gem} = 13.5 Hz, $J_{3,4}$ = 11.5 Hz, $J_{3,2}$ = 9.8 Hz, 1H, H-3), 1.9-1.5 (m, 8H, 2xH-2^{ii}, 2xH-4^{ii}, 2xH-1^{i}, 2xH-2^{i}), 1.45 (m, 11H, C(CH_3)$_3$, 2xH-3^{ii}), 1.20 (t, $J_{CH_2CH_3,CH_2CH_3}$ = 7.1 Hz, 3H, CH_2CH_3); **^{13}C-NMR** (100.6 MHz, MeOH-d$_4$): δ 177.8 (C-5), 176.8 (C-4^{i}), 173.0/172.9 (CO, ester/CO, amide), 153.3/150.8/150.7 (C-4^{iii}/C-4^{iv}/CO, carbamate), 145.7 (C-1^{iv}), 140.9 (C-1^{iii}), 126.0 (C-2^{iv}, C-6^{iv}), 123.8 (C-3^{iii}, C-5^{iii}), 121.4 (C-2^{iii}, C-6^{iii}), 115.2 (C-3^{iv}, C-5^{iv}), 84.7 (*C*(CH_3)$_3$), 62.9 (*C*H_2CH_3), 58.8 (C-2), 55.5 (C-1^{ii}), 42.4 (C-4), 41.9 (C-5^{ii}), 36.2 (C-3^{i}), 32.9 (C-2^{ii}), 30.8 (C-1^{i}), 29.0/28.7 (C-4^{ii}/C-3), 28.1 (C(*C*H_3)$_3$), 24.3/23.8 (C-2^{i}/C-3^{ii}), 14.5 (CH_2CH_3); **IR** (ATR): 3350, 2929, 1779, 1595, 1501, 1298, 1247, 1139 cm^{-1}; **HRMS** (ESI+) calcd. for [$C_{34}H_{47}N_7O_7$+H]: 666.3610; found: 666.3596.

Synthesis of 1-(*tert*-butyl) 2-ethyl (2*S*,4*R*)-4-[4-({(1*S*)-1-({4-[(*E*)-2-(4-aminophenyl)-1-diazenyl]anilino}carbonyl)-5-[(2-pyrenylacetyl)amino]pentyl}amino)-4-oxobutyl]-5-oxotetrahydro-1*H*-1,2-pyrroledicarboxylate, 31

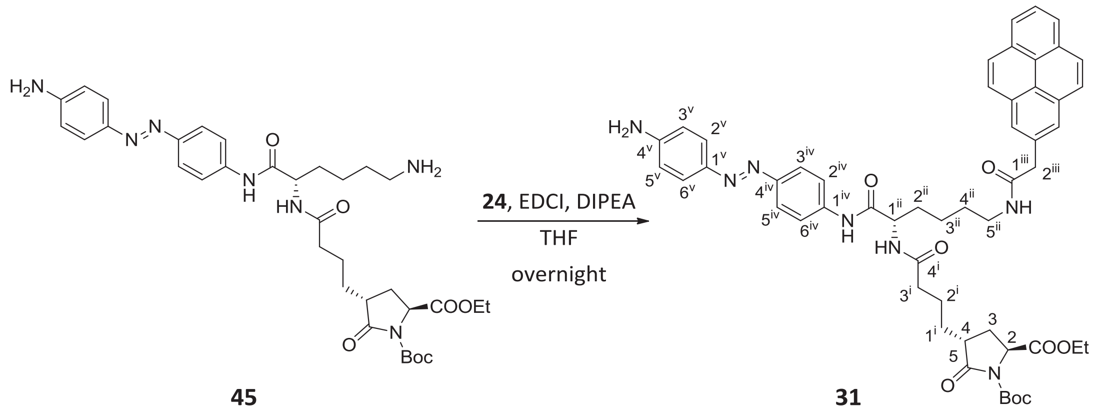

45 31

To a stirred solution of amine **45** (811 mg, 1.22 mmol) in dry THF (40 ml) under N_2 atmosphere, a solution of **24** (381 mg, 1.46 mmol), EDCI (304 mg, 1.59 mmol), DIPEA (1.1 ml, 6.09 mmol) in dry THF (60 ml) was added. The reaction mixture was stirred overnight at rt. Then, the mixture was diluted with EtOAc (100 ml) and washed with water (2x120 ml). The organic layer was dried over anhydrous $MgSO_4$ and concentrated under vacuum. The residue was purified by column chromatography (from EtOAc to EtOAc/MeOH, 95:5) to afford amide **31** (840 mg, 0.93 mmol, 76% yield) as an orange solid.

Physical and spectroscopic data of **31**

Mp = 178-183 ^oC (from EtOAc); **[α]$_D^{20}$** = 9.60 (*c* 0.82, DMSO); **^{1}H-NMR** (400 MHz, DMSO-d$_6$): δ 10.3 (s, 1H, C-1^{iv}NH), 8.37 (d, *J* = 9.3 Hz, 1H, H-pyr), 8.22 (m, 5H, C-5^{ii}NH, 4xH-pyr), 8.13 (m, 3H, C-1^{ii}NH, 2xH-pyr), 8.05 (t, *J* = 7.6 Hz, 1H, H-pyr), 7.98 (d, *J* = 7.9 Hz, 1H, H-pyr), 7.76 (d, $J_{2^{iv},3^{iv}} = J_{6^{iv},5^{iv}}$ = 9.1 Hz, 2H, H-2^{iv}, H-6^{iv}), 7.72 (d, $J_{3^{iv},2^{iv}} = J_{5^{iv},6^{iv}}$ = 9.1 Hz, 2H, H-3^{iv}, H-5^{iv}), 7.63 (d, $J_{2^{v},3^{v}} = J_{5^{v},6^{v}}$ = 8.8 Hz, 2H, H-2^{v}, H-5^{v}), 6.67 (d, $J_{3^{v},2^{v}} = J_{6^{v},5^{v}}$ = 8.8 Hz, 2H, H-3^{v}, H-5^{v}), 6.01 (s, 2H, NH_2), 4.52 (dd, $J_{2,3}$ = 9.7 Hz, $J_{2,3}$ = 1.4 Hz, 1H, H-2), 4.38 (m, 1H, H-1^{ii}), 4.21-4.08 (m, 4H, 2xH-2^{iii}, C*H*$_2CH_3$), 3.09 (m, 2H, H-5^{ii}), 2.50 (m, 1H, H-4), 2.12 (m, 3H, H-3, 2xH-3^{i}), 1.96 (m, 1H, H-3), 1.78-1.43 (m, 8H, 2xH-1^{i}, 2xH-2^{i}, 2xH-2^{ii}, 2xH-4^{ii}), 1.37 (m, 11H, C(CH$_3$)$_3$, 2xH-3^{ii}), 1.18 (t, $J_{CH_2CH_3,CH_2CH_3}$ = 7.1 Hz, 3H, CH$_2$*C*H$_3$); **^{13}C-NMR** (100.6 MHz, DMSO-d$_6$): δ 174.7 (C-5), 172.1 (C-4^{i}), 171.4/171.3 (CO, ester/CO, amide), 170.0 (C-1^{iii}), 152.5 (C-4^{v}), 148.8/146.2 (C-4^{iv}/CO, carbamate), 142.9 (C-1^{v}), 140.2 (C-1^{iv}), 131.1 (C-pyr), 130.8 (C-pyr), 130.4 (C-pyr), 129.7 (C-pyr), 129.0 (C-pyr), 128.6 (CH-pyr), 127.4 (CH-pyr), 127.2 (CH-pyr), 126.8 (CH-pyr), 126.1 (CH-pyr), 125.1 (C-2^{v}, C-6^{v}), 124.9 (CH-pyr), 124.8 (CH-pyr), 124.7 (CH-pyr), 124.1 (C-pyr), 124.0 (CH-pyr), 123.9 (C-pyr), 122.5 (C-3^{iv}, C-5^{iv}), 119.5 (C-2^{iv}, C-6^{iv}), 113.4 (C-3^{v}, C-5^{v}), 82.3 (*C*(CH$_3$)$_3$), 61.2 (*C*H$_2$CH$_3$), 56.8 (C-2), 53.5 (C-1^{ii}), 40.8 (C-4), 40.1 (C-2^{iii}), 38.6 (C-5^{ii}), 34.8 (C-3^{i}), 31.6 (C-2^{ii}), 29.5/28.8 (C-4^{ii}/C-1^{i}), 27.5 (C(*C*H$_3$)$_3$), 27.4 (C-3), 23.0/22.5 (C-2^{i}/C-3^{ii}), 14.0 (CH$_2$*C*H$_3$); **IR** (ATR): 3274, 2935, 1781, 1596, 1529, 1503, 1300, 1240, 1149 cm^{-1}; **HRMS** (ESI+) calcd. for [C$_{52}$H$_{57}$N$_7$O$_8$+Na]: 930.4161; found: 930.4160. **COSY**, **DEPT 135** and **^{1}H/^{13}C** correlation were recorded.

Synthesis of (2*R*,4*S*)-2-[4-{(1*S*)-1-({4-[(*E*)-(4-aminophenyl)-1-diazenyl]anilino}carbonyl)-5-[(2-pyrenylacetyl)amino]pentyl}amino)-4-oxobutyl]-4-[(*tert*-butoxycarbonyl)amino]pentanedioic acid, 46

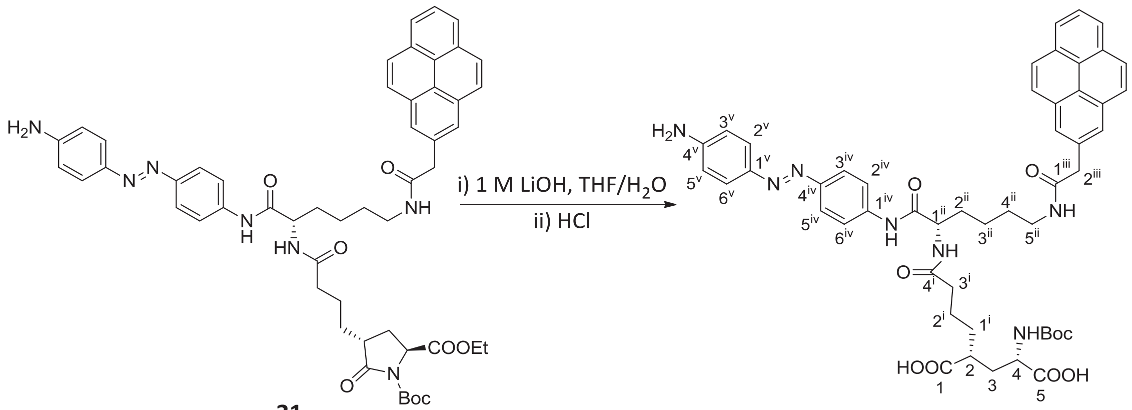

31 **46**

To an ice-cooled solution of **31** (200 mg, 0.22 mmol) in THF (17ml) was added 1 M LiOH (17 ml, 17.0 mmol) was added. After stirring for 1 h at this temperature, the mixture was acidified to pH 2 with 1 M HCl. Then, the mixture was concentrated under vacuum and the resulting purple solid was triturated with diethyl ether (2x8 ml) to furnish **46** (157 mg, 0.18 mmol, 79%) as a lilac solid.

<u>Physical and spectroscopic data of **46**</u>

Mp = 155-165 ^{o}C (from diethyl ether); **[α]$_D^{20}$** = 3.60 (*c* 0.54, DMSO); **^{1}H-NMR** (400 MHz, DMSO-d$_6$): δ 10.3 (s, 1H, C-1^{iv}NH), 8.37 (d, *J* = 9.3 Hz, 1H, H-pyr), 8.23 (m, 5H, C-5^{ii}NH, 4xH-pyr), 8.13 (m, 3H, C-1^{ii}NH, 2xH-pyr), 8.06 (t, J = 7.6 Hz, 1H, H-pyr), 7.99 (d, J = 7.8 Hz, 1H, H-pyr), 7.77 (d, $J_{2^{iv},3^{iv}}$ = $J_{6^{iv},5^{iv}}$ = 8.9 Hz, 2H, H-2^{iv}, H-6^{iv}), 7.71 (d, $J_{3^{iv},2^{iv}}$ = $J_{5^{iv},6^{iv}}$ = 8.9 Hz, 2H, H-3^{iv}, H-5^{iv}), 7.62 (d, $J_{2^{v},3^{v}}$ = $J_{6^{v},5^{v}}$ = 8.8 Hz, 2H, H-2^{v}, H-6^{v}), 7.08 (d, $J_{C\text{-}4NH,4}$ = 8.0 Hz, 1H, C-4NH) 6.67 (d, $J_{3^{v},2^{v}}$ = $J_{5^{v},6^{v}}$ = 8.8 Hz, 2H, H-3^{v}, H-5^{v}), 6.02 (br s, 2H, NH_2), 4.39 (m, 1H, H-1^{ii}), 4.18 (m, 2H, H-2^{iii}), 3.80 (m, 1H, H-4), 3.09 (m, 2H, H-5^{ii}), 2.37 (m, 1H, H-2), 2.12 (m, 3H, H-3, 2xH-3^{i}), 1.96 (m, 1H, H-3), 1.76-1.56 (m, 2H, H-2^{ii}), 1.52-1.28 (m, 17H, 2xH-1^{i}, 2xH-2^{i}, 2xH-3^{ii}, 2xH-4^{ii}, $C(CH_3)_3$); **^{13}C-NMR** (100.6 MHz, DMSO-d_6): δ 174.2 (C-1), 172.8/171.2/171.3 (C-4^{i}/C-5/CO, amide), 170.1 (C-1^{iii}), 155.7 (CO, carbamate), 152.5 (C-4^{v}), 148.2 (C-4^{iv}), 142.9 (C-1^{v}), 140.2 (C-1^{iv}), 131.1 (C-pyr), 130.8 (C-pyr), 130.4 (C-pyr), 129.7 (C-pyr), 129.0 (C-pyr), 128.6 (CH-pyr), 127.4 (CH-pyr), 127.2 (CH-pyr), 126.8 (CH-pyr), 126.3 (CH-pyr), 125.1 (C-2^{v}, C-6^{v}), 124.9 (CH-pyr), 124.8 (CH-pyr), 124.7 (CH-pyr), 124.2 (C-pyr), 124.1 (CH-pyr), 123.0 (C-pyr), 122.5 (C-3^{iv}, C-5^{iv}), 119.5 (C-2^{iv}, C-6^{iv}), 113.4 (C-3^{v}, C-5^{v}), 78.1 ($C(CH_3)_3$), 52.3 (C-4), 53.6 (C-1^{ii}), 41.6 (C-2), 40.3 (C-2^{iii}), 38.7 (C-5^{ii}), 35.0 (C-3^{i}), 33.0 (C-3), 32.1/31.7 (C-1^{i}/C-2^{ii}), 28.8 (C-4^{ii}), 28.2 ($C(CH_3)_3$), 23.0 (C-3^{ii}/C-2^{i}); **IR** (ATR): 3284, 2930, 1691, 1641, 1596, 1531 cm^{-1}; **HRMS** (ESI+) calcd. for [$C_{50}H_{55}N_7O_{89}$-H]: 896.3988; found: 896.3972. **COSY**, **DEPT 135** and **^{1}H/^{13}C** correlation were recorded.

Synthesis of 2-(2,5-dioxotetrahydro-1*H*-1-pyrrolyl)acetic acid, 49[5]

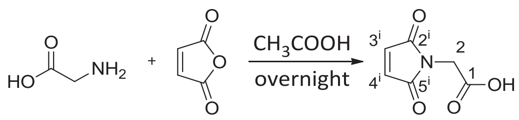

47 **48** **49**

β-alanine (**47**) (5.00 g, 66.6 mmol) and maleic anhydride (**48**) (6.53 g, 66.6 mmol) were dissolved in acetic acid (190 ml). The reaction mixture was stirred at rt overnight, under N_2 atmosphere. The resulting suspension was then warmed up to reflux for further 4 h to give a clear solution. The solvent was removed under vacuum and the residue was purified by column chromatography (CH_2Cl_2/CH_3COOH, 95:5) to afford acid **49** (4.78 g, 30.8 mmol, 45% yield) as a white powder.

Spectroscopic data of **49**

^{1}H-NMR (360 MHz, $CDCl_3$): δ 6.80 (s, 2H, H-3^{i}, H-4^{i}), 4.34 (s, 2H, H-2); **^{13}C-NMR** (100.6 MHz, $CDCl_3$): δ 172.7 (C-1), 169.8 (C-2^{i}, C-5^{i}), 134.7 (C-3^{i}, C-5^{i}), 38.4 (C-2).

Synthesis of 1-(*tert*-butyl) 2-ethyl (2*S*,4*R*)-4-[4-({(1*S*)-1-{[4-((*E*)-2-{4-[(aminoacetyl)amino] phenyl}-1-diazenyl)anilino]carbonyl}-5-[(2-pyrenylacetyl)amino]pentyl}amino)-4-oxobutyl]-5-oxotetrahydro-1*H*-1,2-pyrroledicarboxylate, 52

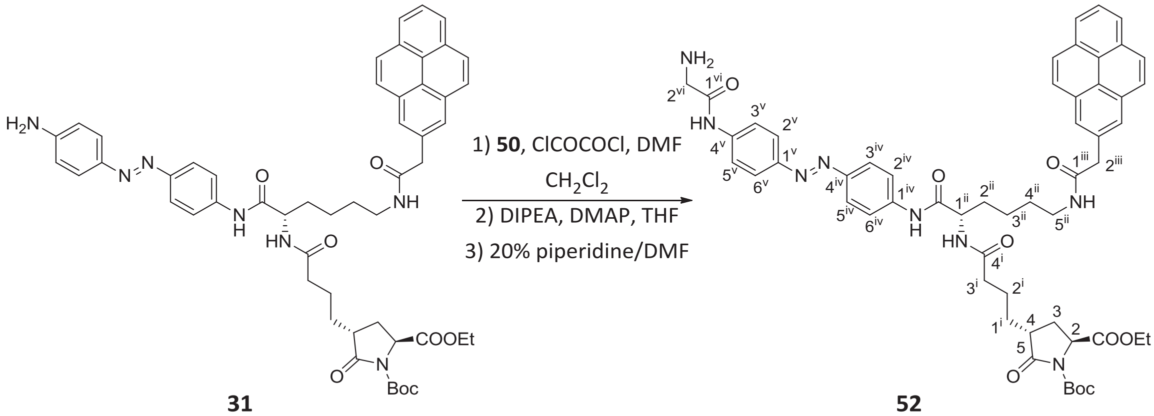

31 **52**

To a stirred solution of commercially available Fmoc-Gly-OH (**50**) (67 mg, 0.23 mmol) and oxalyl chloride (136 μl of 2.0 M solution in THF, 0.27 mmol) in dry CH_2Cl_2 (2 ml) was added one drop of DMF. After stirring for 1 h at rt the mixture was concentrated. The resulting acid chloride was taken up in dry THF (5 ml) and added to a solution of **31** (103 mg, 0.11 mmol), DIPEA (99 μl, 0.57 mmol), and DMAP (2 mg, 16 μmol) in dry THF (20 ml). After stirring 10 min at 0 ºC, the mixture was warmed to rt and stirred for 3 h. The mixture was diluted with EtOAc (25 ml) and washed with a saturated $NaHCO_3$ solution (2x75 ml) and brine (2x75 ml). The organic layer was dried over $MgSO_4$ and concentrated. Purification by column chromatography (from CH_2Cl_2 to CH_2Cl_2/MeOH, 9:1) gave the Fmoc-glycine adduct as an orange solid that was sufficiently pure for the next reaction. The resulting solid was added to a commercial available solution of 20% piperidine in DMF (1.2 ml). After stirring for 6 h at rt, the mixture was concentrated and purified by column chromatography ($CHCl_3$/MeOH, from 9:1 to 4:1) to give **52** (32 mg, 33 μmol, 36% yield) as an orange solid.

Physical and spectroscopic data of **52**

Mp = 130-137 ºC (from CH_2Cl_2); $[\alpha]_D^{20}$ = 12.5 (*c* 1.02, DMSO); **^{1}H-NMR** (400 MHz, DMSO-d$_6$): δ 10.4 (s, 1H, C-1^{iv}NH), 8.37 (d, *J* = 9.3 Hz, 1H, H-pyr), 8.22 (m, 5H, C-5^{ii}NH, 4xH-pyr), 8.14 (m, 3H, C-1^{ii}NH, 2xH-pyr), 8.05 (t, *J* = 7.6 Hz, 1H, H-pyr), 7.99 (d, *J* = 7.9 Hz, 1H, H-pyr), 7.84 (m, 8H, H-2^{iv}, H-6^{iv}, H-3^{iv}, H-5^{iv}, H-2^{v}, H-6^{v}, H-3^{v}, H-5^{v}), 4.53 (d, $J_{2,3}$ = 8.7 Hz, 1H, H-2), 4.39 (m, 1H, H-1^{ii}), 4.21-4.08 (m, 4H, 2xH-2^{iii}, CH_2CH$_3$), 3.44-3.25 (m, 4H, 2xH-2^{vi}, NH_2), 3.09 (m, 2H, H-5^{ii}), 2.50 (m, 1H, H-4), 2.13 (m, 3H, H-3, 2xH-3^{i}), 1.96 (m, 1H, H-3), 1.77-1.44 (m, 8H, 2xH-1^{i}, 2xH-2^{i}, 2xH-2^{ii}, 2xH-4^{ii}), 1.37 (m, 11H, C(CH$_3$)$_3$, 2xH-3^{ii}), 1.19 (t, $J_{CH_2CH_3,CH_2CH_3}$ = 7.1 Hz, 3H, CH$_2$CH_3); **^{13}C-NMR** (100.6 MHz, DMSO-d$_6$): δ 174.9/172.3/172.1/171.5/171.4 (C-4^{i}/C-1^{vi}/CO, amide/CO, ester), 170.2 (C-1^{iii}), 148.8 (CO, carbamate), 147.8/147.6 (C-4^{iv}/C-1^{v}), 141.6/141.5 (C-1^{iv}/C-4^{v}), 131.1 (C-pyr), 130.9 (C-pyr), 130.5 (C-pyr), 129.8 (C-pyr), 129.1 (C-pyr), 128.7 (CH-pyr), 127.5 (CH-pyr), 127.3 (CH-pyr), 126.9 (CH-pyr), 126.3 (CH-pyr), 125.2 (CH-pyr), 125.0 (CH-pyr), 124.9 (CH-pyr), 124.2 (C-pyr), 124.1 (CH-pyr), 124.0 (C-pyr), 123.5 (C-2^{v}, C-6^{v}, C-3^{iv}, C-5^{iv}), 119.63 (C-2^{iv}, C-6^{iv}, C-3^{v}, C-5^{v}), 82.4 (*C*(CH_3)$_3$), 61.2 (*C*H_2CH_3), 56.9 (C-2), 53.6 (C-1^{ii}), 45.6 (C-2^{vi}), 40.9 (C-4), 40.2 (C-2^{iii}), 38.7 (C-5^{ii}), 34.8 (C-3^{i}), 31.6 (C-2^{ii}), 29.6/28.9 (C-4^{ii}/C-1^{i}), 27.5 (C(*C*H_3)$_3$), 27.4 (C-3), 23.1/22.6 (C-2^{i}/C-3^{ii}), 14.1 (CH_2*C*H_3); **IR** (ATR): 3283, 2930, 1582, 1634, 1594, 1524, 1247, 1152 cm^{-1}; **HRMS** (ESI+) calcd. for [$C_{54}H_{60}N_8O_9$+Na]: 98.4375; found: 987.4394. **DEPT 135** and **^{1}H/^{13}C** correlation were recorded.

Synthesis of *tert*-butyl (2*S*)-5-oxotetrahydro-1*H*-pyrrolecarboxylate, 58[6]

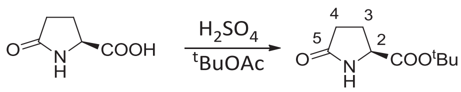

37 **58**

To a solution of L-pyroglutamic acid (**37**) (5.77 g, 43.9 mmol) in *tert*-butyl acetate (70 ml), 98% H_2SO_4 (3.7 ml, 73.1 mmol) was slowly added. The resulting solution was stirred overnight at rt. Then, the reaction mixture was slowly poured into a saturated aqueous solution of $NaHCO_3$ (250 ml) and the product was extracted with EtOAc (4x150 ml). The combined organics extracts were dried over anhydrous $MgSO_4$ and the solvent was removed under vacuum to furnish a white solid identified as **58** (4.56 g, 24.6 mmol, 56% yield).

Spectroscopic data of **58**

^{1}H-NMR (250 MHz, $CDCl_3$): δ 6.26 (br s, 1H, NH), 4.12 (m, 1H, H-2), 2.53-2.26 (m, 3H, H-3, 2xH-4), 2.26 -2.09 (m, 1H, H-3), 1.46 (s, 9H, C(CH_3)$_3$).

Synthesis of di(*tert*-butyl) (2*S*)-5-oxotetrahydro-1*H*-1,2-pyrroledicarboxylate, 59[6]

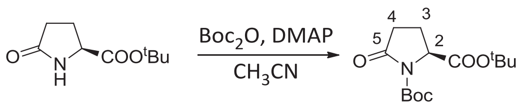

58 **59**

To an ice-cooled solution of *tert*-butyl ester **58** (3.60 g, 19.4 mmol) in dry CH_3CN (90 ml), DMAP (480 mg, 3.39 mmol) and Boc_2O (6.36 g, 29.2 mmol) were added. The solution was stirred at 0 ^oC for 30 min, warmed up to rt and left for 2 h. The solvent was removed under vacuum and the resulting residue was purified by column chromatography (hexanes/EtOAc, 2:1) to provide **59** (5.30 g, 18.6 mmol, 96% yield) as a white powder.

Spectroscopic data of **59**

^{1}H-NMR (250 MHz, $CDCl_3$): δ 4.43 (dd, $J_{2,3}$= 9.3 Hz, $J_{2,3}$ = 2.6 Hz, 1H, H-2), 2.68-2.14 (m, 3H, H-3, 2xH-4), 1.89 (m, 1H, H-3) 1.46 (s, 9H, $C(CH_3)_3$), 1.43 (s, 9H, $C(CH_3)_3$); **^{13}C-NMR** (62.5 MHz, $CDCl_3$): δ 173.5 (C-5), 170.3 (CO, ester), 149.1 (CO, carbamate), 83.1 ($\mathit{C}(CH_3)_3$), 82.1 ($\mathit{C}(CH_3)_3$), 59.5 (C-2), 31.0 (C-4), 27.9 ($C(\mathit{C}H_3)_3$), 27.8 ($C(\mathit{C}H_3)_3$), 21.5 (C-3).

Synthesis of di(*tert*-butyl) (2*S*,4*R*)-4-allyl-5-oxotetrahydro-1*H*-1,2-pyrroledicarboxylate, 60[7]

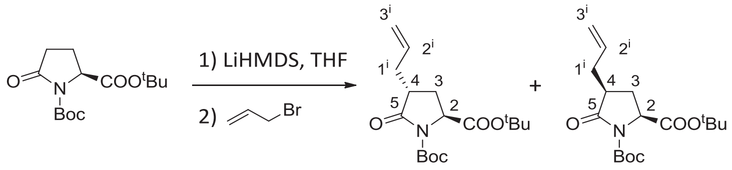

59 (4*R*)-**60** (4*S*)-**60**

To a solution of carbamate **59** (3.10 g, 10.9 mmol) in dry THF (40 ml) at -78 ^oC, LiHMDS 1.0 M in THF (12 ml, 12.0 mmol) was added dropwise under N_2 atmosphere. The reaction mixture was stirred at this temperature for 1 h and allyl bromide (2.4 ml, 43.4 mmol) was slowly added. After stirring for 4 h (for more than 5 h the product decomposes), the reaction was quenched by the slow addition of NH_4Cl saturated aqueous solution at -78 ^oC and extracted with diethyl ether (3x50 ml). The combined organic phases were dried over anhydrous $MgSO_4$ and the solvent was evaporated under vacuum. The residue was purified by column chromatography (hexanes/Et_2O, from 20:1 to 4:1) to give (4*S*)-**60** (390 mg, 0.34 mmol, 11% yield) as a tan oil and (4*R*)-**60** (1.30 g, 3.96 mmol, 36% yield) as a brown oil.

Physical and spectroscopic data of (4*R*)-**60**

$[\alpha]_D^{20}$ = -20.4 (*c* 0.97, CH_2Cl_2); **^{1}H-NMR** (360 MHz, $CDCl_3$): δ 5.74 (ddt, $J_{2^i,3^i_{trans}}$ = 17.1 Hz, $J_{2^i,3^i_{cis}}$ = 10.1 Hz, $J_{2^i,1^i}$ = 7.1 Hz, 1H, H-2^i), 5.09 (m, 2H, H-3^i), 4.42 (dd, $J_{2,3}$ = 9.6 Hz, $J_{2,3}$ = 1.6 Hz, 1H, H-2), 2.75-2.58 (m, 2H, H-4, H-1^i), 2.22-2.09 (m, 2H, H-3, H-1^i), 1.96 (ddd, J_{gem} = 13.4 Hz, $J_{3,4}$ = 11.4 Hz, $J_{3,2}$ = 9.6 Hz, 1H, H-3), 1.49 (s, 9H, $C(CH_3)_3$), 1.47 (s, 9H, $C(CH_3)_3$); **^{13}C-NMR** (90 MHz, $CDCl_3$): δ 174.6 (C-5), 170.4 (CO, ester), 149.4 (CO, carbamate), 134.5 (C-2^i), 117.8 (C-3^i), 83.6 ($\mathit{C}(CH_3)_3$), 82.3 ($\mathit{C}(CH_3)_3$), 57.5 (C-2), 41.1 (C-4), 34.5 (C-1^i), 28.0 (2x$C(\mathit{C}H_3)_3$), 27.9 (C-3); **HRMS** (ESI+) calcd. for $[C_{17}H_{27}NO_5+Na]$: 348.1781; found: 348.1787.

Physical and spectroscopic data of (4*S*)-**60**

$[\alpha]_D^{20}$ = -4.1 (*c* 2.96, CH_2Cl_2); **^{1}H-NMR** (360 MHz, $CDCl_3$): δ 5.72 (dddd, $J_{2^i,3^i_{trans}}$ = 16.5 Hz, $J_{2^i,3^i_{cis}}$ = 10.4 Hz, $J_{2^i,1^i}$ = 7.7 Hz, $J_{2^i,1^i}$ = 6.0 Hz, 1H, H-2^i), 5.05 (m, 2H, H-3^i), 4.39 (dd, $J_{2,3}$ = 9.4 Hz, $J_{2,3}$ = 5.7 Hz, 1H, H-2), 2.61 (m, 2H, H-4, H-1^{i}), 2.43 (dt, J_{gem} = 13.4 Hz, $J_{3,4}$ = $J_{3,2}$ = 9.4 Hz, 1H, H-3), 2.21 (ddd, J_{gem} = 15.3 Hz, $J_{1^i,4^i}$ = 10.7 Hz, $J_{1^i,2^i}$ = 7.6 Hz, 1H, H-1^{i}), 1.70 (m, 1H, H-3), 1.50 (s, 9H, C(CH_3)$_3$), 1.47 (s, 9H, C(CH_3)$_3$); **^{13}C-NMR** (90 MHz, $CDCl_3$): δ 174.9 (C-5), 170.7 (CO, ester), 149.5 (CO, carbamate), 134.9 (C-2^{i}), 117.7 (C-3^{i}), 83.5 (*C*(CH_3)$_3$), 82.2 (*C*(CH_3)$_3$), 58.2 (C-2), 42.1 (C-4), 35.5 (C-1^{i}), 28.0 (2xC(*C*H_3)$_3$), 26.4 (C-3); **HRMS** (ESI+) calcd. for [$C_{17}H_{27}NO_5$+Na]: 348.1781; found: 348.1775.

Synthesis of (2*R*)-2-{(2*S*)-3-(*tert*-butoxy)-2-[(*tert*-butoxycarbonyl)amino]-3-oxopropyl}-4-pentenoic acid, 61

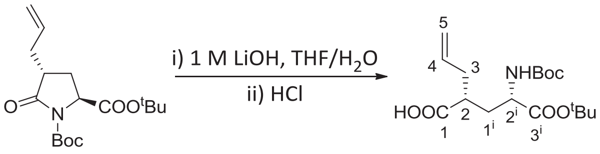

(4*R*)-**60** **61**

To an ice-cooled solution of **60** (1.80 g, 5.53 mmol) in a mixture 5:2 of THF and water (75 ml), 1 M LiOH (8.0 ml, 8.00 mmol) was added. After stirring for 1 h at this temperature, the mixture was acidified to pH 2 with 1 M HCl and extracted with EtOAc (3x50 ml). The combined organic extracts were dried over anhydrous $MgSO_4$ and the solvent was removed under vacuum. The residue was purified by column chromatography (hexanes/EtOAc, 3:1) to furnish **61** (1.78 g, 5.18 mmol, 93% yield) as a yellowish oil.

Physical and spectroscopic data of **61**

$[\alpha]_D^{20}$ = -0.8 (*c* 1.47, CH_2Cl_2); **^{1}H-NMR** (360 MHz, $CDCl_3$): δ 5.74 (m, 1H, H-4), 5.39 (br d, $J_{NH,2^i}$ = 8.5 Hz, 1H, NH), 5.08 (m, 2H, H-5), 4.22 (m, 1H, H-2^{i}), 2.49 (m, 2H, H-2, H-3), 2.31-2.04 (m, 2H, H-3, H-1^{i}), 1.66 (m, 1H, H-1^{i}), 1.46 (s, 9H, C(CH_3)$_3$), 1.45 (s, 9H, C(CH_3)$_3$); **^{13}C-NMR** (90 MHz, $CDCl_3$): δ 178.6 (C-1), 171.3 (C-3^{i}), 156.3 (CO, carbamate), 134.8 (C-4), 117.8 (C-5), 82.7 (*C*(CH_3)$_3$), 80.7 (*C*(CH_3)$_3$), 52.7 (C-2^{i}), 41.8 (C-2), 36.4 (C-3), 35.2 (C-1^{i}), 28.4 (C(*C*H_3)$_3$), 28.1 (C(*C*H_3)$_3$); **IR** (ATR): 2978, 1707, 1367, 1247, 1150 cm^{-1}; **HRMS** (ESI+) calcd. for [$C_{17}H_{29}NO_6$+Na]: 366.1887; found: 366.1893. **^{1}H/^{13}C** correlation was recorded.

Synthesis of di(*tert*-butyl) (2*R*,4*S*)-2-allyl-4-[(*tert*-butoxycarbonyl)amino]pentanedioate, 62

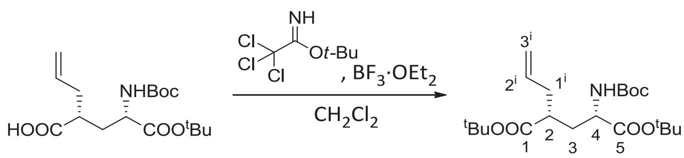

61 **62**

To a solution of compound **61** (3.50 g, 7.28 mmol) in CH_2Cl_2 (90 ml), *tert*-butyl 2,2,2-trichloroacetimidate (2.6 ml, 14.6 mmol) and $BF_3 \cdot OEt_2$ (370 µl, 2.96 mmol) were added. After 3 h of stirring, TLC analysis (hexanes/EtOAc, 2:1) indicated the complete consumption of the starting material. Then, a saturated aqueous solution of $NaHCO_3$ (20 ml) was added and the product was extracted with CH_2Cl_2 (3x50 ml). The combined organic extracts were dried over anhydrous $MgSO_4$ and the solvent was removed under vacuum. The resulting yellow oil was purified by column chromatography (hexanes/EtOAc, 3:1) to give **62** (1.64 g, 4.10 mmol, 56%) as a yellow solid.

Physical and spectroscopic data of **62**

Mp = 86-89 ºC (from hexanes/EtOAc); **$[\alpha]_D^{20}$** = 10.7 (*c* 0.59, CH_2Cl_2); **^{1}H-NMR** (250 MHz, $CDCl_3$): δ 5.70 (ddt, $J_{2^i,3^i_{trans}}$ = 17.0 Hz, $J_{2^i,3^i_{cis}}$ = 10.1 Hz, $J_{2^i,1^i}$ = 6.8 Hz, 1H, H-2^i), 5.09 (m, 3H, 2xH-3^i, NH), 4.22 (m, 1H, H-4), 2.49-2.26 (m, 2H, H-1^i, H-2), 2.26-2.03 (m, 2H, H-1^i, H-3), 1.65 (m, 1H, H-3), 1.44 (m, 27H, 3x$C(CH_3)_3$); **^{13}C-NMR** (62.5 MHz, $CDCl_3$): δ 173.9/171.7 (C-1/C-5), 155.3 (CO, carbamate), 135.0 (C-2^i), 117.2 (C-3^i), 81.8 (*C*$(CH_3)_3$), 80.7 (*C*$(CH_3)_3$), 79.5 (*C*$(CH_3)_3$), 52.7 (C-4), 42.3 (C-2), 36.8 (C-1^i), 34.1 (C-3), 28.3 (C(*C*$H_3)_3$), 28.1 (C(*C*$H_3)_3$), 28.0 (C(*C*$H_3)_3$); **IR** (ATR): 3382, 2979, 1742, 1703, 1526, 1366, 1229, 1150 cm^{-1}; **HRMS** (ESI+) calcd. for $[C_{22}H_{37}NO_6+Na]$: 422.2513; found: 422.2520.

Synthesis of di(*tert*-butyl) (2*S*,4*R*)-2-[(*tert*-butoxycarbonyl)amino]-4-[(2*E*)-4-oxo-2-butenyl] pentanedioate, 63

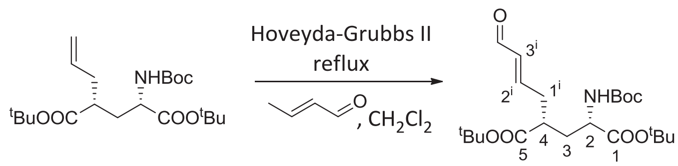

62 63

To a boiling solution of allyl (4*R*)-**62** (2.30 g, 5.75 mmol) and crotonaldehyde (2.4 ml, 28.8 mmol) in dry CH_2Cl_2 (36 ml), Hoveyda-Grubbs II catalyst (56 mg, 89 µmol) was added in 3 portions. The mixture was heated to reflux for 2.5 h, when TLC analysis (hexanes/EtOAc, 2:1) showed no starting material. The reaction mixture was filtered off through a pad of silica gel and concentrated. The crude was purified by column chromatography (hexanes/Et_2O, from 3:1 to 1:1) to provide **63** (2.19 g, 5.12 mmol, 89% yield) as a yellow oil.

Physical and spectroscopic data of **63**

$[\alpha]_D^{20}$ = 88.4 (*c* 0.48, CH_2Cl_2); **^{1}H-NMR** (250 MHz, $CDCl_3$): δ 9.46 (d, $J_{CHO,3^i}$ = 7.8 Hz, 1H, CHO), 6.73 (dt, $J_{2^i,3^i}$ = 15.7 Hz, $J_{2^i,1^i}$ = 6.7 Hz, 1H, H-2^i), 6.09 (dd, $J_{3^i,2^i}$ = 15.7 Hz, $J_{3^i,CHO}$ = 7.8 Hz, 1H, H-3^i), 5.03 (d,

$J_{NH,2}$ = 7.9 Hz, 1H, NH), 4.20 (m, 1H, H-2), 2.68-2.39 (m, 3H, H-4, 2xH-1^i), 2.15 (ddd, J_{gem} = 12.7 Hz, $J_{3,2}$ = 8.6 Hz, $J_{3,4}$ = 4.8 Hz, 1H, H-3), 1.64 (ddd, J_{gem} = 12.7 Hz, $J_{3,2}$ = 8.6 Hz, $J_{3,4}$ = 3.7 Hz, 1H, H-3), 1.44 (m, 27H, 3xC(CH_3)$_3$); **^{13}C-NMR** (90 MHz, $CDCl_3$): δ 193.6 (CHO), 173.1/171.4 (C-1/C-5), 155.3 (CO, carbamate), 154.4 (C-2^i), 134.7 (C-3^i), 82.4 (*C*(CH_3)$_3$), 81.7 (*C*(CH_3)$_3$), 79.9 (*C*(CH_3)$_3$), 52.5 (C-2), 41.6 (C-4), 35.4 (C-1^i), 34.8 (C-3), 28.4 (C(*C*H_3)$_3$), 28.2 (C(*C*H_3)$_3$), 28.1 (C(*C*H_3)$_3$); **IR** (ATR): 2977, 1699, 1392, 1367, 1251, 1150 cm^{-1}; **HRMS** (ESI+) calcd. for [$C_{22}H_{37}NO_7$+Na]: 450.2462; found: 450.2460.

Synthesis of (2*E*,5*R*,7*S*)-8-*tert*-butoxy-5-(*tert*-butoxycarbonyl)-7-[(*tert*-butoxycarbonyl)amino]-8-oxo-2-octenoic acid, 64

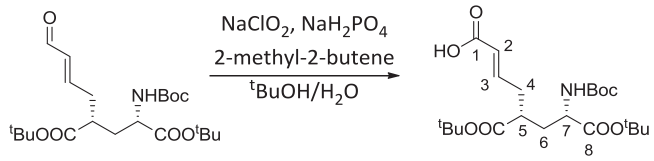

63 **64**

To an ice-cooled solution of the aldehyde **63** (2.50 g, 5.85 mmol) in a 5:1 mixture of ^{t}BuOH and water (240 ml), 2-methyl-2-butene (6.2 ml, 58.5 mmol), $NaH_2PO_4 \cdot 2H_2O$ (4.60 g, 29.2 mmol) and $NaClO_2$ (3.17 g, 35.1 mmol) were successively added. The resulting mixture was stirred at 0 ^oC for 1 h and warmed up to rt. The reaction mixture was stirred overnight. Then, water (30 ml) and a saturated aqueous solution of Na_2CO_3 were added until pH 8. The mixture was extracted with EtOAc (3x50 ml), dried over anhydrous $MgSO_4$ and concentrated under vacuum. Purification by column chromatography (hexanes/EtOAc/CH_3COOH, 4:1:0.1) gave **64** (2.00 g, 4.51 mmol, 77% yield) as a yellow oil.

Physical and spectroscopic data of **64**

[α]$_D^{20}$ = 59.8 (*c* 1.16, CH_2Cl_2); **^{1}H-NMR** (360 MHz, MeOH-d$_4$): δ 6.86 (dt, $J_{3,2}$ = 15.1 Hz, $J_{3,4}$ = 7.3 Hz, 1H, H-3), 5.84 (d, $J_{2,3}$ = 15.1 Hz, 1H, H-2), 4.06 (dd, $J_{7,6}$ = 10.6 Hz, $J_{7,6}$ = 3.8 Hz, 1H, H-7), 2.56 (m, 1H, H-5), 2.41 (m, 2H, H-4), 2.08 (m, 1H, H-6), 1.65 (m, 1H, H-6), 1.45 (m, 27H, 3xC(CH_3)$_3$); **^{13}C-NMR** (62.5 MHz, MeOH-d$_4$): δ 174.5/172.8/169.0 (C-1/C-8/CO, ester), 157.3 (CO, carbamate), 146.7 (C-3), 124.4 (C-2), 82.4 (*C*(CH_3)$_3$), 82.1 (*C*(CH_3)$_3$), 80.2 (*C*(CH_3)$_3$), 53.6 (C-7), 42.9 (C-5), 35.9 (C-4), 34.4 (C-6), 28.8 (C(*C*H_3)$_3$), 28.4 (C(*C*H_3)$_3$), 28.3 (C(*C*H_3)$_3$); **IR** (ATR): 2977, 2932, 1703, 1366, 1247, 1147 cm^{-1}; **HRMS** (ESI+) calcd. for [$C_{22}H_{37}NO_8$+Na]: 466.2411; found: 466.2417. **^{1}H/^{13}C** correlation was recorded.

Synthesis of (5*R*,7*S*)-8-*tert*-butoxy-5-(*tert*-butoxycarbonyl)-7-[(*tert*-butoxycarbonyl)amino]-8-oxooctanoic acid, 65

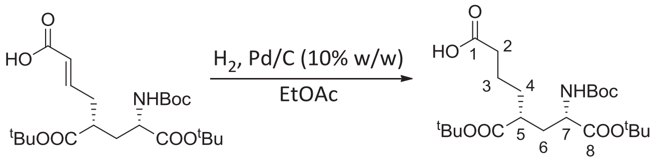

64 **65**

To a solution of compound **64** (1.50 g, 3.38 mmol) in EtOAc (60 ml), 10% Pd/C (0.15 g) was added. The resulting suspension was stirred in a H_2 atmosphere for 16 h. Then, it was filtered through Celite® and the solvent was evaporated under vacuum. The resulting oil was purified by column chromatography (hexanes/EtOAc/CH_3COOH, 5:4:1) to afford a colourless oil identified as **65** (1.50 g, 3.36 mmol, quantitative yield).

Physical and spectroscopic data of **65**

$[\alpha]_D^{20}$ = 66 (*c* 0.30, CH_2Cl_2); **^{1}H-NMR** (360 MHz, MeOH-d_4): δ 6.83 (d, $J_{NH,7}$ = 8.4 Hz, 1H, NH), 3.98 (m, 1H, H-7), 2.44 (m, 1H, H-5), 2.29 (td, $J_{2,3}$ = 6.8 Hz, $J_{2,4}$ = 3.7 Hz, 2H, H-2), 2.03 (m, 1H, H-6), 1.60 (m, 5H, 2xH-3, 2xH-4, H-6), 1.46 (m, 27H, 3x$C(CH_3)_3$); **^{13}C-NMR** (90 MHz, MeOH-d_4): δ 176.8/ 175.9/173.3 (C-1/C-8/CO, ester), 157.8 (CO, carbamate), 82.5 (*C*$(CH_3)_3$), 82.0 (*C*$(CH_3)_3$), 80.3 (*C*$(CH_3)_3$), 54.1 (C-7), 43.9 (C-5), 35.0 (C-6), 34.5 (C-2), 33.4 (C-4), 28.8 ($C(CH_3)_3$), 28.4 ($C(CH_3)_3$), 28.3 ($C(CH_3)_3$), 23.6 (C-1); **IR** (ATR): 2976, 1709, 1392, 1366, 1248, 1146 cm^{-1}; **HRMS** (ESI+) calcd. for [$C_{22}H_{39}NO_8$+Na]: 468.2568; found: 468.2570. **COSY** and **^{1}H/^{13}C** correlation were recorded.

Synthesis of di(*tert*-butyl) (2*R*,4*S*)-2-{4-[((1*S*)-1-{4-[(*E*)-(4-aminophenyl)-1-diazenyl]anilino} carbonyl-5-{[(9*H*-fluoren-9-ylmethoxy)carbonyl]amino}pentyl)amino]-4-oxobutyl}-4-[(*tert*-butoxycarbonyl)amino]pentanedioate, 56

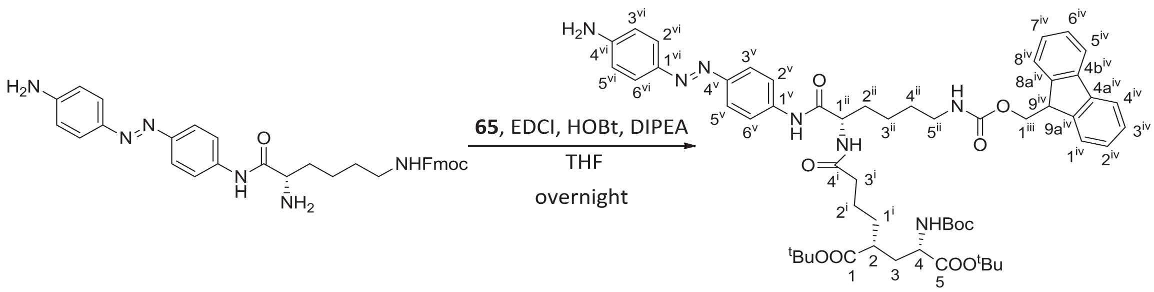

44 **56**

To a stirred solution of **44** (232 mg, 0.34 mmol) in dry THF (18 ml) under N_2 atmosphere, a solution of **65** (169 mg, 0.38 mmol), EDCI (86 mg, 0.45 mmol), HOBt (70 mg, 0.52 mmol), DIPEA (240 µl, 1.40 mmol) in dry THF (20 ml) was added. The reaction mixture was stirred overnight at rt. Then, the mixture was diluted with EtOAc (40 ml) and washed with water (2x40 ml). The organic layer was dried over anhydrous $MgSO_4$ and concentrated under vacuum. The residue was purified by column chromatography (hexanes/EtOAc, 1:9) to afford amide **56** (335 mg, 0.30 mmol, 88% yield) as an orange solid.

Physical and spectroscopic data of **56**

Mp = 98-105 °C (from hexanes/EtOAc); $[\alpha]_D^{20}$ = -22.5 (*c* 1.18, $CHCl_3$); **^{1}H-NMR** (400 MHz, $CDCl_3$): δ 8.91 (br s, 1H, C-1^{v}NH), 7.79 (m, 6H, H-4^{iv}, H-5^{iv}, H-3^{v}, H-5^{v}, H-2^{vi}, H-6^{vi}), 7.65 (d, $J_{2^v,3^v} = J_{6^v,5^v}$ = 8.7 Hz, 2H, H-2^{v}, H-6^{v}), 7.57 (d, $J_{1^{iv},2^{iv}} = J_{8^i,7^{iv}}$ = 7.4 Hz, 2H, H-1^{iv}, H-8^{iv}), 7.38 (t, $J_{3^{iv},2^{iv}} = J_{3^{iv},4^{iv}} = J_{6^{iv},5^{iv}} = J_{6^{iv},7^{iv}}$ = 7.4 Hz, 2H, H-3^{iv}, H-6^{iv}), 7.31 (t, $J_{2^{iv},3^{iv}} = J_{2^{iv},1^{iv}} = J_{7^{iv},6^{iv}} = J_{7^{iv},8^i}$ = 7.4 Hz, 2H, H-2^{iv}, H-7^{iv}), 6.73 (d, $J_{3^{vi},2^{vi}} = J_{5^{vi},6^{vi}}$ = 8.7 Hz, 2H, H-3^{vi}, H-5^{vi}), 6.48 (s, 1H, C-1^{ii}NH), 5.10 (t, $J_{C\text{-}5^{ii}NH,5^{ii}}$ = 5.4 Hz, 1H, C-5^{ii}NH), 4.56 (m, 1H, H-1^{ii}), 4.38 (d, $J_{1^{iii},9^{iv}}$ = 6.9 Hz, 2H, H-1^{iii}), 4.20 (m, 2H, H-4, H-9^{iv}), 4.05 (br s, 2H, NH_2), 3.22 (m, 2H, H-5^{ii}), 2.34 (m, 1H, H-2), 2.24 (m, 2H, H-3^{i}), 2.13-1.94 (m, 3H, H-3, H-1^{i}, H-2^{ii}), 1.86-1.37 (m, 7H, H-3, H-1^{i}, 2xH-2^{i}, H-2^{ii}, 2xH-4^{ii}), 1.44 (m, 29H, 3xC(CH_3)$_3$, 2xH-3^{ii}); **^{13}C-NMR** (100.6 MHz, $CDCl_3$): δ 174.5/173.8/171.9/170.1 (C-1/C-5/C-4^{i}/CO, amide), 157.0 (CO, carbamate), 155.5 (CO, carbamate), 149.5 (C-4^{v}/C-4^{vi}), 145.7 (C-1^{vi}), 144.1 (C-9a^{iv}, C-8a^{iv}), 141.4 (C-4a^{iv}, C-4b^{iv}), 139.5 (C-1^{v}), 127.8 (C-3^{iv}, C-6^{iv}), 127.2 (C-2^{iv}, C-7^{iv}), 125.2/125.1 (C-1^{iv}, C-8^{iv}/C-2^{vi}, C-6^{vi}), 123.4 (C-3^{v}, C-5^{v}), 120.1 (C-4^{iv}, C-5^{iv}/C-2^{v}, C-6^{v}), 114.8 (C-3^{vi}, C-5^{vi}), 82.1 (*C*(CH_3)$_3$), 81.1 (*C*(CH_3)$_3$), 79.8 (*C*(CH_3)$_3$), 66.8 (C-1^{iii}), 54.0 (C-1^{ii}), 52.8 (C-4), 47.4 (C-9^{iv}), 42.4 (C-2), 40.5 (C-5^{ii}), 36.1 (C-3^{i}), 34.9 (C-3), 32.1 (C-1^{i}), 30.7 (C-2^{ii}), 29.8 (C-4^{ii}), 28.5 (C(*C*H_3)$_3$), 28.2 (C(*C*H_3)$_3$), 28.1 (C(*C*H_3)$_3$), 23.2 (C-2^{i}), 22.6 (C-3^{ii}); **IR** (ATR): 3300, 2976, 2931, 1691, 1598, 1530, 1366, 1248, 1148 cm^{-1}; **HRMS** (ESI+) calcd. for [$C_{55}H_{71}N_7O_{10}$+H]: 990.5335; found: 990.5347. **^{1}H/^{13}C** correlation were recorded.

Synthesis of di(*tert*-butyl) (2*R*,4*S*)-2-(4-{(1*S*)-5-amino-1-({4-[(*E*)-(4-aminophenyl)-1-diazenyl]anilino}carbonyl)pentyl]amino}-4-oxobutyl)-4-[(*tert*-butoxycarbonyl)amino]pentanedioate, 66

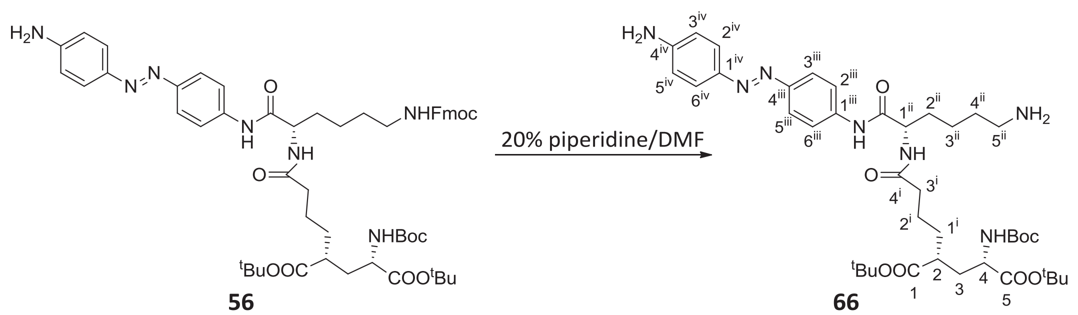

56 **66**

A commercially available solution of 20% piperidine in DMF (18 ml) was added to compound **56** (775 mg, 0.78 mmol). After 1 h of stirring at rt, TLC analysis (EtOAc/MeOH, 95:5) showed no presence of starting material. The mixture was diluted with water (18 ml) and washed with EtOAc (3x30 ml). The combined organic extracts were dried over anhydrous $MgSO_4$ and concentrated under vacuum. The resulting solid was purified by column chromatography (from EtOAc to EtOAc/MeOH/NH_3, 9:2:1) to deliver **66** (459 mg, 0.60 mmol, 76% yield) as an orange solid.

Physical and spectroscopic data of **66**

Mp = 89-96 °C (from EtOAc); **$[\alpha]_D^{20}$** = -31.1 (*c* 0.88, $CHCl_3$); **^{1}H-NMR** (400 MHz, $CDCl_3$): δ 9.56 (br s, 1H, C-1^{iii}NH), 7.81 (m, 4H, H-3^{iii}, H-5^{iii}, H-2^{iv}, H-6^{iv}), 7.70 (d, $J_{2^{iii},3^{iii}}$ = $J_{6^{iii},5^{iii}}$ = 7.7 Hz, 2H, H-2^{iii}, H-6^{iii}), 6.74 (d, $J_{3^{iv},2^{iv}}$ = $J_{5^{iv},6^{iv}}$ = 8.4 Hz, 2H, H-3^{iv}, H-5^{iv}), 6.68 (m, 1H, C-1^{ii}NH), 5.21 (m, 1H, C-4NH), 4.63 (m, 1H, H-1^{ii}), 4.19 (m, 1H, H-4), 4.06 (br s, 2H, C-4^{iv}NH_2), 2.82 (m, 2H, H-5^{ii}), 2.58-2.31 (m, 3H, H-2, C-5^{ii}NH_2), 2.27 (m, 2H, H-3^{i}), 2.20-1.90 (m, 3H, H-3, H-1^{i}, H-2^{ii}), 1.86-1.56 (m, 7H, H-3, H-1^{i}, 2xH-2^{i}, H-2^{ii}, 2xH-4^{ii}), 1.44 (m, 29H, 3x$C(CH_3)_3$, 2xH-3^{ii}); **^{13}C-NMR** (100.6 MHz, $CDCl_3$): δ 174.5/173.5/171.8/ 170.3 (C-1/C-5/C-4^{i}/CO, amide), 155.4 (CO, carbamate), 149.5 (C-4^{iii}, C-4^{iv}), 145.7 (C-1^{iv}), 139.7 (C-1^{iii}), 125.1 (C-2^{iv}, C-6^{iv}), 123.4 (C-3^{iii}, C-5^{iii}), 120.1 (C-2^{iii}, C-6^{iii}), 114.8 (C-3^{iv}, C-5^{iv}), 82.7 (*C*$(CH_3)_3$), 81.1 (*C*$(CH_3)_3$), 79.7 (*C*$(CH_3)_3$), 53.9 (C-1^{ii}), 52.8 (C-4), 42.4 (C-2), 41.2 (C-5^{ii}), 36.1 (C-3^{i}), 34.8 (C-3), 32.1 (C-1^{i}/C-2^{ii}), 31.6 (C-4^{ii}), 28.5 ($C(CH_3)_3$), 28.2 ($C(CH_3)_3$), 28.1 ($C(CH_3)_3$), 23.2 (C-2^{i}), 22.7 (C-3^{ii}); **IR** (ATR): 3343, 2977, 2933, 1701, 1598, 1506, 1368, 1249, 1150 cm^{-1}; **HRMS** (ESI+) calcd. for $[C_{40}H_{61}N_7O_8+H]$: 768.4654; found: 768.4650.

Synthesis of di(*tert*-butyl) (2*R*,4*S*)-2-(4-{(1*S*)-1-({4-[(*E*)-(4-aminophenyl)-1-diazenyl]anilino} carbonyl)-5-[(2-pyrenylacetyl)amino]pentyl}amino)-4-oxobutyl]-4-[(*tert*-butoxycarbonyl) amino]pentanedioate, 57

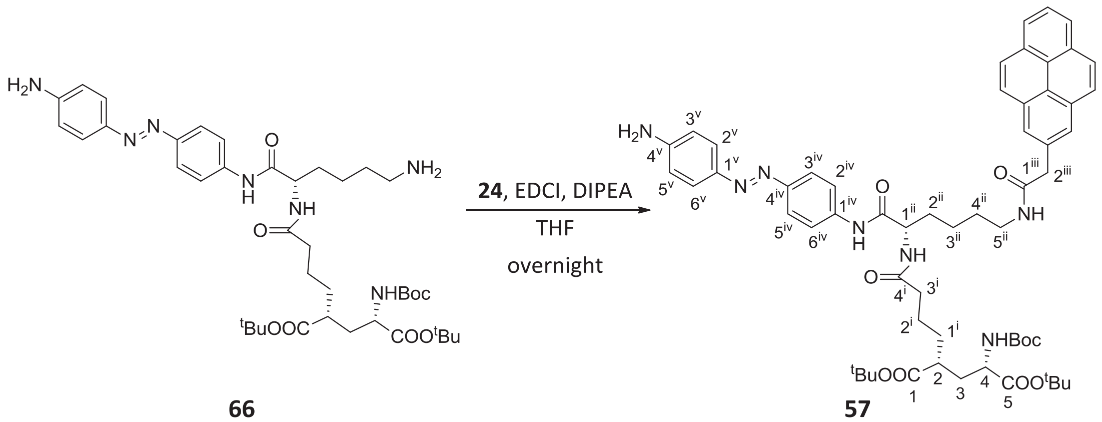

66 57

To a stirred solution of **66** (410 mg, 0.53 mmol) in dry THF (20 ml) under N_2 atmosphere, a solution of 1-pyreneacetic acid (**24**) (167 mg, 0.64 mmol), EDCI (133 mg, 0.69 mmol), DIPEA (465 μl, 2.67 mmol) in dry THF (30 ml) was added. The reaction mixture was stirred overnight at rt. Then, the mixture was diluted with EtOAc (50 ml) and washed with water (2x20 ml). The organic layer was dried over anhydrous $MgSO_4$ and concentrated under vacuum. The residue was purified by column chromatography (EtOAc) and triturated with diethyl ether (2x10 ml) to furnish an orange solid identified as **57** (458 mg, 0.45 mmol, 84% yield).

Physical and spectroscopic data of **57**

Mp = 157-161 ^{o}C (from EtOAc); **$[\alpha]_D^{20}$** = 5.30 (*c* 0.96, $CHCl_3$); **^{1}H-NMR** (400 MHz, DMSO-d_6): δ 10.3 (s, 1H, C-1^{iv}NH), 8.37 (d, *J* = 9.3 Hz, 1H, H-pyr), 8.29-8.17 (m, 5H, C-1^{ii}NH, 4xH-pyr), 8.12 (s, 2H, H-pyr), 8.08 (m, 1H, C-5^{ii}NH), 8.05 (t, *J* = 7.6 Hz, 1H, H-pyr), 7.99 (d, *J* = 7.9 Hz, 1H, H-pyr), 7.76 (d, $J_{2^{iv},3^{iv}}$ = $J_{5^{iv},6^{iv}}$ = 9.1 Hz, 2H, H-2^{iv}, H-6^{iv}), 7.71 (d, $J_{3^{iv},2^{iv}}$ = $J_{5^{iv},6^{iv}}$ = 9.1 Hz, 2H, H-3^{iv}, H-5^{iv}), 7.63 (d, $J_{2^{v},3^{v}}$ = $J_{6^{v},5^{v}}$ = 8.8 Hz, 2H, H-2^{v}, H-6^{v}), 7.10 (d, $J_{C\text{-}4NH,4}$ = 8.2 Hz, 1H, C-4NH), 6.66 (d, $J_{3^{v},2^{v}}$ = $J_{5^{v},6^{v}}$ = 8.8 Hz, 2H, H-3^{v}, H-5^{v}), 6.02 (s, 2H, NH_2), 4.40 (m, 1H, H-1^{ii}), 4.17 (s, 2H, H-2^{iii}), 3.76 (m, 1H, H-4), 3.09 (dd, $J_{5^{ii},4^{ii}}$ = 12.6 Hz, $J_{5^{ii},C\text{-}5^{ii}NH}$ = 6.7 Hz, 2H, H-5^{ii}), 2.33 (m, 1H, H-2), 2.12 (m, 2H, H-3^{i}), 1.85-1.51 (m, 6H, 2xH-3, 2xH-1^{i}, 2xH-2^{ii}), 1.52-1.25 (m, 33H, 3xC(CH_3)$_3$, 2xH-2^{i}, 2xH-3^{ii}, 2xH-4^{ii}); **^{13}C-NMR** (100.6 MHz, DMSO-d_6): δ 173.8/172.1/171.7/171.2 (C-1/C-5/C-4^{i}/CO, amide), 169.9 (C-1^{iii}), 155.5 (CO, carbamate), 152.4 (C-4^{v}), 148.1 (C-4^{iv}), 142.8 (C-1^{v}), 140.2 (C-1^{iv}), 131.1 (C-pyr), 130.8 (C-pyr), 130.4 (C-pyr), 129.7 (C-pyr), 129.0 (C-pyr), 128.6 (CH-pyr), 127.4 (CH-pyr), 127.2 (CH-pyr), 126.8 (CH-pyr), 126.1 (CH-pyr), 125.1 (C-2^{v}, C-6^{v}), 124.9 (CH-pyr), 124.8 (CH-pyr), 124.7 (CH-pyr), 124.1 (C-pyr), 124.0 (CH-pyr), 123.9 (C-pyr), 122.5 (C-3^{iv}, C-5^{iv}), 119.5 (C-2^{iv}, C-6^{iv}), 113.4 (C-3^{v}, C-5^{v}), 80.3 (*C*(CH_3)$_3$), 79.7 (*C*(CH_3)$_3$), 78.0 (*C*(CH_3)$_3$), 53.4 (C-1^{ii}), 52.5 (C-4), 42.2 (C-2), 40.1 (C-1^{iii}), 38.6 (C-5^{ii}), 34.8 (C-3^{i}), 33.0 (C-3), 32.0 (C-1^{i}), 31.6 (C-2^{ii}), 28.8 (C-4^{ii}), 28.2 (C(*C*H_3)$_3$), 27.9 (C(*C*H_3)$_3$), 27.6 (C(*C*H_3)$_3$), 23.0 (C-3^{ii}, C-2^{i}); **IR** (ATR): 3277, 2975, 2935, 1720, 1638, 1599, 1531, 1506, 1368, 1251, 1151 cm^{-1}; **HRMS** (ESI+) calcd. for [$C_{58}H_{71}N_7O_9$+H]: 1010.5386; found: 1010.5377. **COSY** and **^{1}H/^{13}C** correlation were recorded.

Synthesis of di(*tert*-butyl) (2*S*,4*R*)-2-[(*tert*-butoxycarbonyl)amino]-4-[4-({(1*S*)-1-({4-[(*E*)-(4-{[2-(2,5-dioxo-2,5-dihydro-1*H*-1-pyrrolyl)-acetyl]amino}phenyl)-1-diazenyl]anilino}carbonyl)-5-[(2-pyrenylacetyl)amino]pentyl}amino)-4-oxobutyl]pentanedioate, 67

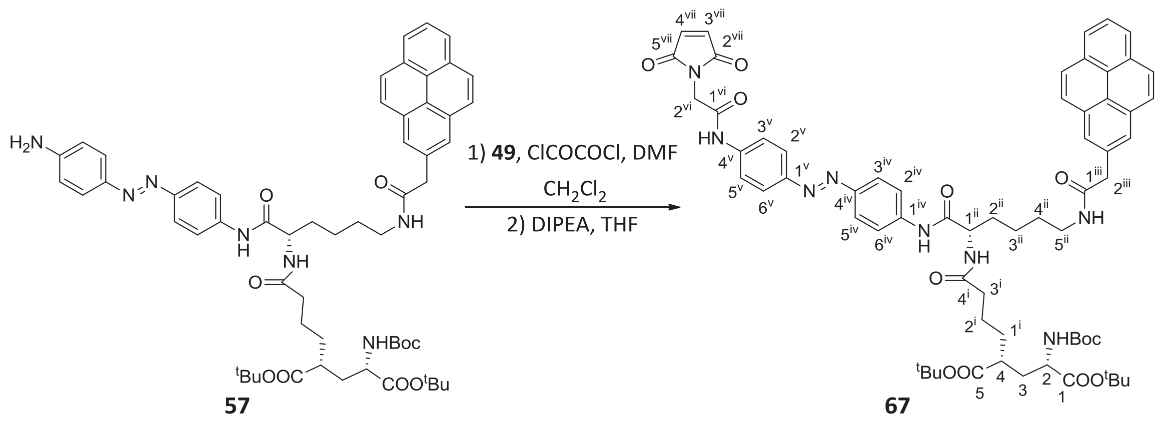

To a stirred solution of **57** (120 mg, 0.77 mmol) and oxalyl chloride 2.0 M in THF (402 µl, 0.80 mmol) in dry CH_2Cl_2 (12 ml) was added one drop of DMF. After stirring for 2 h at rt, the mixture was concentrated. The resulting acid chloride was taken up in dry THF (5 ml) and slowly added to an ice-cooled solution of **67** (200 mg, 0.20 mmol), DIPEA (207 µl, 1.19 mmol) in dry THF (25 ml). After stirring for 10 min at this temperature, the mixture was warmed up to rt and stirred for additional 4 h. Then, it was diluted with EtOAc (30 ml) and washed with water (3x10 ml). The organic extract was dried over anhydrous $MgSO_4$, concentrated under vacuum and purified by column chromatography (EtOAc/MeOH, 9:1) to provide **67** (168 mg, 0.15 mmol, 74% yield) as an orange solid.

Physical and spectroscopic data of **67**

Mp = 187-198 ºC (from EtOAc); **[α]$_D^{20}$** = 68.5 (*c* 0.70, DMSO); **^{1}H-NMR** (400 MHz, DMSO-d_6): δ 10.7 (s, 1H, C-4^{v}NH), 10.3 (s, 1H, C-1^{iv}NH), 8.37 (d, *J* = 9.3 Hz, 1H, H-pyr), 8.29-8.17 (m, 5H, C-1^{ii}NH, 4xH-pyr), 8.14 (s, 2H, H-pyr), 8.09 (m, 1H, C-5^{ii}NH), 8.07 (t, *J* = 7.8 Hz, 1H, H-pyr), 7.98 (d, *J* = 7.8 Hz, 1H, H-pyr), 7.84 (m, 6H, H-2^{iv}, H-6^{iv}, H-3^{iv}, H-5^{iv}, H-3^{v}, H-5^{v}), 7.75 (d, $J_{2^v,3^v} = J_{6^v,5^v}$ = 8.9 Hz, 2H, H-2^{v}, H-6^{v}), 7.16 (s, 2H, H-3^{vii}, H-4^{vii}), 7.09 (d, $J_{C\text{-}2NH,2}$ = 8.0 Hz, 1H, C-2NH), 4.38 (m, 1H, H-1^{ii}), 4.33 (s, 2H, H-2^{vi}), 4.16 (s, 2H, H-2^{iii}), 3.76 (m, 1H, H-2), 3.08 (dd, $J_{5^{ii},4^{ii}}$ = 12.6 Hz, $J_{5^{ii},C\text{-}5^{ii}NH}$ = 6.7 Hz, 2H, H-5^{ii}), 2.31 (m, 1H, H-4), 2.11 (m, 2H, H-3^{i}), 1.85-1.51 (m, 6H, 2xH-3, 2xH-1^{i}, 2xH-2^{ii}), 1.51-1.24 (m, 33H, 3x$C(CH_3)_3$, 2xH-2^{i}, 2xH-3^{ii}, 2xH-4^{ii}); **^{13}C-NMR** (100.6 MHz, DMSO-d_6): δ 172.8/171.1/170.7/170.5/169.7 (C-1/C-5/C-4^{i}/C-2^{vii}, C-5^{vii}/CO, amide), 168.9 (C-1^{iii}), 164.3 (C-1^{vi}), 154.5 (CO, carbamate), 146.9/146.7 (C-4^{iv}/C-1^{v}), 140.7/140.1 (C-1^{iv}/C-4^{v}), 134.0 (C-3^{vii}, C-4^{vii}), 130.1 (C-pyr), 129.8 (C-pyr), 129.4 (C-pyr), 128.7 (C-pyr), 128.0 (C-pyr), 127.6 (CH-pyr), 126.4 (CH-pyr), 126.2 (CH-pyr), 125.8 (CH-pyr), 125.1 (CH-pyr), 124.1 (CH-pyr), 123.9 (CH-pyr), 123.7 (CH-pyr), 123.1 (C-pyr), 123.0 (CH-pyr), 122.9 (C-pyr), 122.5/122.4 (C-2^{v}, C-6^{v}/C-3^{iv}, C-5^{iv}), 118.5 (C-2^{iv}, C-6^{iv}, C-3^{v}, C-5^{v}), 79.3 (C(CH$_3$)$_3$), 78.7 (C(CH$_3$)$_3$), 77.0 (C(CH$_3$)$_3$), 52.4 (C-1^{ii}), 51.6 (C-2), 41.2 (C-4), 39.5 (C-2^{iii}), 37.6 (C-5^{ii}), 33.8 (C-3^{i}), 32.0 (C-3), 31.0 (C-1^{i}), 30.6 (C-2^{ii}), 27.8 (C-4^{ii}), 27.2 (C(CH$_3$)$_3$), 26.9 (C(CH$_3$)$_3$), 26.6 (C(CH$_3$)$_3$), 22.0 (C-3^{ii}, C-2^{i}); **IR** (ATR): 3274, 2976, 2933, 1716, 1528, 1366, 1247, 1148 cm^{-1}; **HRMS** (ESI+) calcd. for [$C_{64}H_{74}N_8O_{12}$+Na]: 1169.5318; found: 1169.5350.

Synthesis of {(1*S*,3*R*)-1,3-dicarboxy-7-[((1*S*)-1-({4-[(*E*)-2-(4-{[2-(2,5-dioxo-2,5-dihydro-1*H*-1-pyrrolyl)acetyl]amino}phenyl)-1-diazenyl]anilino}carbonyl)-5-{[2-(2-pyrenyl)acetyl]amino} pentyl)amino]-7-oxoheptyl}ammonium 2,2,2-trifluoroacetate, 21

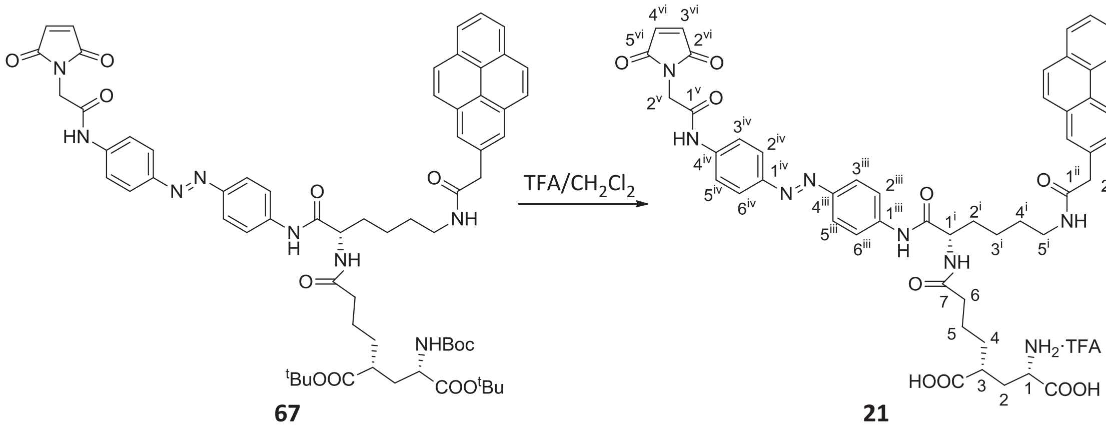

67 21

To a stirred solution of compound **67** (40 mg, 45 μmol) in CH_2Cl_2 (7.0 ml), trifluoroacetic acid (3.5 ml, 45.4 mmol) was added. The mixture was stirred at room temperature until the starting material was consumed as judged by TLC analysis (EtOAc/MeOH, 9:1). Then, the mixture was concentrated under vacuum and the resulting purple solid was triturated with diethyl ether (2x8 ml) to furnish **21** (29 mg, 28 μmol, 79%) as a brown powder.

Physical and spectroscopic data of **21**

$[\alpha]_D^{20}$ = 50.9 (*c* 0.43, DMSO); **^{1}H-NMR** (400 MHz, DMSO-d$_6$): δ 10.7 (s, 1H, C-4^{iv}NH), 10.4 (s, 1H, C-1^{iii}NH), 8.37 (d, J = 9.3 Hz, 2H, H-pyr, C-1^{i}NH), 8.30-8.17 (m, 5H, C-5^{i}NH, 4xH-pyr), 8.14 (s, 2H, H-pyr), 8.05 (t, J = 7.6 Hz, 1H, H-pyr), 7.98 (d, J = 7.6 Hz, 1H, H-pyr), 7.84 (m, 6H, H-2^{iii}, H-6^{iii}, H-3^{iii}, H-5^{iii}, H-3^{iv}, H-5^{iv}), 7.76 (d, $J_{2iv,3iv} = J_{6iv,5iv}$ = 8.6 Hz, 2H, H-2^{iv}, H-6^{iv}), 7.16 (s, 2H, H-3^{vi}, H-4^{vi}), 4.36 (m, 1H, H-1^{i}), 4.33 (s, 2H, H-2^{v}), 4.19 (s, 3H, 2xH-2^{ii}, H-1), 3.08 (m, 2H, H-5^{i}), 2.68 (m, 1H, H-3), 2.12 (m, 3H, H-2, 2xH-6), 1.80-1.26 (m, 11H, H-2, 2xH-4, 2xH-5, 2xH-4^{i}, 2xH-3^{i}, 2xH-2^{i}); **^{13}C-NMR** (100.6 MHz, DMSO-d$_6$): δ 175.9/172.3/171.7/170.7/170.0 (C-2^{vi}/C-7/C-1^{ii}/CO, acid/CO, acid/CO, amide), 165.4 (C-1^{v}), 147.9/147.6 (C-4^{iii}/C-1^{iv}), 141.8/141.1 (C-1^{iii}/C-4^{iv}), 135.0 (C-3^{vi}, C-4^{vi}), 131.1 (C-pyr), 130.8 (C-pyr), 130.4 (C-pyr), 129.7 (C-pyr), 129.0 (C-pyr), 128.6 (CH-pyr), 127.4 (CH-pyr), 127.2 (CH-pyr), 126.8 (CH-pyr), 126.1 (CH-pyr), 125.1 (CH-pyr), 124.9 (CH-pyr), 124.7 (CH-pyr), 124.1

(2xC-pyr), 123.9 (C-pyr), 123.4 (C-2^{iv}, C-6^{iv}, C-3^{iii}, C-5^{iii}), 119.5 (C-2^{iii}, C-6^{iii}, C-3^{iv}, C-5^{iv}), 53.8 (C-1^{i}), 51.6 (C-1), 40.4 (C-3), 39.5 (C-2^{ii}), 38.5 (C-5^{i}), 36.6 (C-6), 32.3 (C-2), 31.4 (C-4), 30.8 (C-2^{i}), 28.8 (C-4^{i}), 23.0/22.7 (C-3^{i}, C-5); **IR** (ATR): 3277, 3044, 2938, 1712, 1644, 1595, 1532, 1199, 1150 cm^{-1}; **HRMS** (ESI+) calcd. for [$C_{51}H_{50}N_8O_{10}$+H]: 935.3723; found: 935.3714.

VI.2.2. Direct *vs* sensitised two-photon excitation of photoswitched tethered ligands based on red-shifted azobenzene derivatives

***N*-[2-(allyloxy)ethyl]-*N*-ethyl-*N*-{4-[(*E*)-(4-nitrophenyl)-1-diazenyl]phenyl}amine, 77**

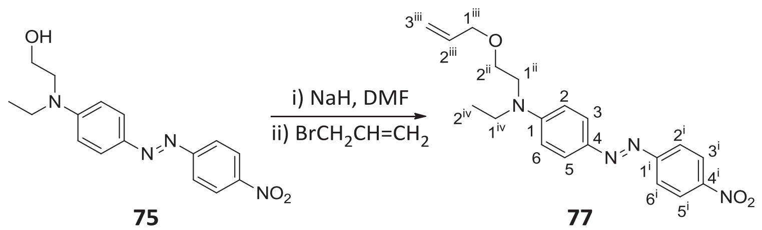

75 **77**

To an ice-cooled solution of Disperse Red 1 (5.00 g, 16.0 mmol) in dry DMF (50 ml), sodium hydride (60% dispersion in mineral oil, 840 mg, 35.1 mmol) was added. The mixture was allowed to stir 5-10 min, and then allyl bromide (2.8 ml, 33.4 mmol) was added. The mixture was stirred at rt until the starting material was consumed as judged by TLC analysis (*ca.* 5 h). The reaction was then quenched with NH_4Cl saturated solution and the two phases were separated. The aqueous one was extracted with EtOAc (3x50 ml), and the combined organic layers were washed with brine, dried over anhydrous $MgSO_4$ and concentrated under vacuum. The crude product was purified by column chromatography (hexanes/EtOAc, 1:1) to provide allyl ether **77** (5.49 g, 16.1 mmol, 97% yield) as a lilac solid.

Physical and Spectroscopic data of **77**

Mp = 65-69 ºC (from hexanes/EtOAc); **^{1}H-NMR** (400 MHz, $CDCl_3$): δ 8.30 (d, $J_{3^i,2^i} = J_{5^i,6^i}$ = 9.1 Hz, 2H, H-3^{i}, H-5^{i}), 7.90 (d, $J_{3,2} = J_{5,6}$ = 9.3 Hz, 2H, H-3, H-5), 7.88 (d, $J_{2^i,3^i} = J_{6^i,5^i}$ = 9.1 Hz, 2H, H-2^{i}, H-6^{i}), 6.76 (d, $J_{2,3} = J_{6,5}$ = 9.3 Hz, 2H, H-2, H-6), 5.90 (ddt, $J_{2^{iii},3_{trans}^{iii}}$ = 17.2 Hz, $J_{2^{iii},3_{cis}^{iii}}$ = 10.4 Hz, $J_{2^{iii},1^{iii}}$ = 5.5 Hz, 1H, H-2^{iii}), 5.28 (dq, $J_{3_{trans}^{iii},2^{iii}}$ = 17.2 Hz, $J_{3_{trans}^{iii},1^{iii}} = J_{gem}$ = 1.6 Hz, 1H, H-3$_{trans}^{iii}$), 5.19 (dq, $J_{3_{cis}^{iii},2^{iii}}$ = 10.4 Hz, $J_{3_{cis}^{iii},1^{iii}} = J_{gem}$= 1.6 Hz, 1H, H-3$_{cis}^{iii}$), 4.01 (dt, $J_{1^{iii},2^{iii}}$ = 5.5 Hz, $J_{1^{iii},3_{cis}^{iii}} = J_{1^{iii},3_{trans}^{iii}}$ = 1.6 Hz, 2H, H-1^{iii}), 3.65 (m, 4H, H-1^{ii}, H-2^{ii}), 3.55 (q, $J_{1^{iv},2^{iv}}$ = 7.1 Hz, 2H, H-1^{iv}), 1.24 (t, $J_{2^{iv},1^{iv}}$ = 7.1 Hz, 3H, H-2^{iv}); **^{13}C-NMR** (100.6 MHz, $CDCl_3$): δ 156.9 (C-1^{i}), 151.6 (C-1), 147.4 (C-4^{i}), 143.7 (C-4), 134.5 (C-2^{iii}), 126.4 (C-3/C-5), 124.8 (C-3^{i}/C-5^{i}), 122.7 (C-2^{i}/C-6^{i}), 117.3 (C-3^{iii}), 111.4 (C-2/C-6), 72.4 (C-1^{iii}), 67.8 (C-2^{ii}), 50.4 (C-1^{ii}), 46.1 (C-1^{iv}), 12.3 (C-2^{iv}); **IR** (ATR): 2920, 1646, 1599, 1508, 1081 cm^{-1}; **HRMS**

(ESI+) calcd. for $[C_{19}H_{22}N_4O_3+H]$: 355.1765; found: 355.1758. **COSY** and **^{1}H/^{13}C** correlation were recorded.

N-[2-(allyloxy)ethyl]-*N*-{4-[(*E*)-(4-aminophenyl)-1-diazenyl]phenyl}-*N*-ethylamine, 76

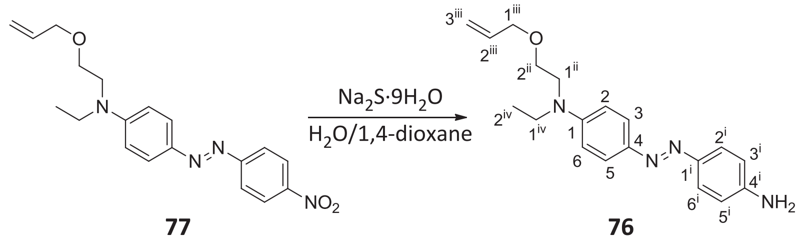

Compound **77** (5.28 g, 15.1 mmol) was dissolved in a 7:3 degassed mixture of 1,4-dioxane and water (160 ml) under N_2 atmosphere. The reaction mixture was heated to 90 ^oC and sodium sulfide (6.00 g, 25.4 mmol) was added portion-wise over 30 min. After 2 h, TLC analysis (EtOAc) of the reaction mixture revealed the absence of starting material. Then, the solution was poured on a saturated aqueous solution of $NaHCO_3$ and the crude product was extracted with CH_2Cl_2 (3x50 ml). The combined organic layers were washed with brine and dried over anhydrous $MgSO_4$. The solvent was evaporated under vacuum and the residue was purified by column chromatography (hexanes/EtOAc, 3:1) to furnish a red oil identified as **76** (4.43 g, 14.0 mmol, 92% yield).

<u>Spectroscopic data of **76**</u>

^{1}H-NMR (400 MHz, $CDCl_3$): δ 7.79 (d, $J_{3,2} = J_{5,6}$ = 9.2 Hz, 2H, H-3, H-5), 7.73 (d, $J_{2^i,3^i} = J_{5^i,6^i}$ = 8.8 Hz, 2H, H-2^i, H-6^i), 6.73 (d, $J_{2,3} = J_{6,5}$ = 9.2 Hz, 2H, H-2, H-6), 6.72 (d, $J_{3^i,2^i} = J_{6^i,5^i}$ = 8.8 Hz, 2H, H-3^i, H-5^i), 5.91 (ddt, $J_{2^{iii},3_{trans}^{iii}}$ = 17.2 Hz, $J_{2^{iii},3_{cis}^{iii}}$ = 10.4 Hz, $J_{2^{iii},1^{iii}}$ = 5.5 Hz, 1H, H-2^{iii}), 5.28 (dq, $J_{3_{trans}^{iii},2^{iii}}$ = 17.2 Hz, $J_{3_{trans}^{iii},1^{iii}} = J_{gem}$ = 1.6 Hz, 1H, H-3$_{trans}^{iii}$), 5.19 (dq, $J_{3_{cis}^{iii},2^{iii}}$ = 10.4 Hz, $J_{3_{cis}^{iii},1^{iii}} = J_{gem}$ = 1.6 Hz, 1H, H-3$_{cis}^{iii}$), 4.01 (dt, $J_{1^{iii},2^{iii}}$ = 5.5 Hz, $J_{1^{iii},3_{cis}^{iii}} = J_{1^{iii},3_{trans}^{iii}}$ = 1.6 Hz, 2H, H-1^{iii}), 3.65 (m, 4H, H-1^{ii}, H-2^{ii}), 3.50 (q, $J_{1^{iv},2^{iv}}$ = 7.1 Hz, 2H, H-1^{iv}), 1.21 (t, $J_{2^{iv},1^{iv}}$ = 7.1 Hz, 3H, H-2^{iv}); **^{13}C-NMR** (100.6 MHz, $CDCl_3$): δ 149.5 (C-1), 148.2 (C-4^i), 146.2 (C-1^i), 143.7 (C-4), 134.7 (C-2^{iii}), 124.6 (C-3, C-5), 124.2 (C-2^i, C-6^i), 117.2 (C-3^{iii}), 115.0 (C-3^i, C-5^i), 111.4 (C-2, C-6), 72.4 (C-1^{iii}), 67.9 (C-2^{ii}), 50.4 (C-1^{ii}), 45.9 (C-1^{iv}), 12.4 (C-2^{iv}); **IR** (ATR): 3354, 2865, 1590, 1508, 1147 cm^{-1}; **HRMS** (ESI+) calcd. for $[C_{19}H_{24}N_4O+H]$: 325.2023; found: 325.2025.

Synthesis of *N*-[2-(allyloxy)ethyl]-*N*-ethyl-*N*-(4-{(*E*)-[4-(ethylamino)phenyl]-1-diazenyl}phenyl) amine, 71, and *N*-[2-(allyloxy)ethyl]-*N*-(4-{(*E*)-[4-(diethylamino)phenyl]-1-diazenyl}phenyl)-*N*-ethylamine, 72

Method A

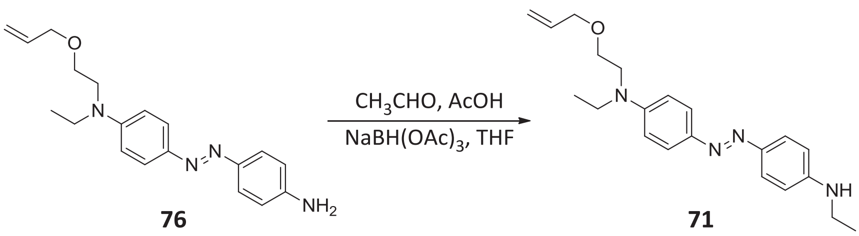

76 71

To a stirred solution of amine **76** (107 mg, 0.33 mmol) in dry THF (3.5 ml) under N_2 atmosphere, acetaldehyde (22 μl, 0.40 mmol), glacial acetic acid (21 μl, 0.37 mmol) and $NaBH(OAc)_3$ (105 mg, 0.50 mmol) were added. The mixture was stirred overnight at rt. Then, the solvent was evaporated under vacuum and the residue was purified by column chromatography (from CH_2Cl_2 to CH_2Cl_2/EtOAc, 9:1) to furnish **71** (30 mg, 85 μmol, 26% yield) as a brown solid.

Method B

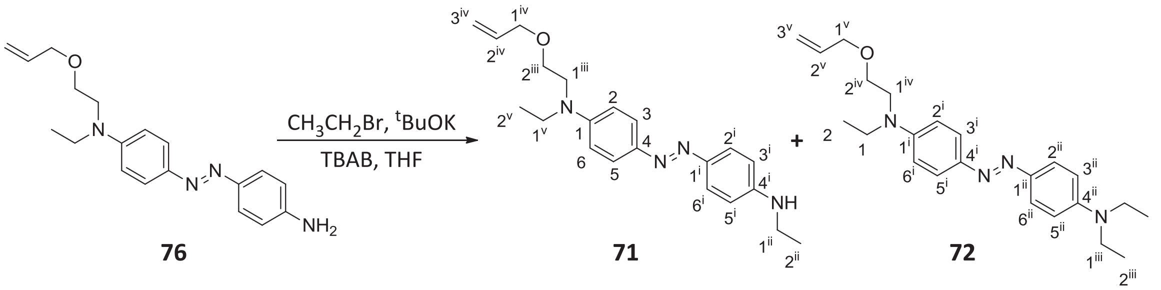

76 71 72

Ethyl bromide (320 μl, 4.28 mmol) was added to a solution of compound **76** (1.27 g, 3.91 mmol) in dry THF solution (50 ml) under N_2 atmosphere, followed by the addition of ^{t}BuOK (876 mg, 7.81 mmol) and TBAB (1.90 g, 5.89 mmol). The mixture was stirred at rt for 1 day. The mixture was poured into water (20 ml), extracted with EtOAc (3x50 ml), and the combined organic layers were dried over anhydrous $MgSO_4$ and concentrated under vacuum. The crude product was purified by column chromatography (from CH_2Cl_2 to CH_2Cl_2/EtOAc, 9:1) affording amine **71** (695 mg, 1.97 mmol, 51% yield) as a brown solid and **72** (100 mg, 0.26 mmol, 7% yield) also as a brown solid.

<u>Physical and spectroscopic data of **71**</u>

Mp = 62-65 ^oC (from CH_2Cl_2/EtOAc); **^{1}H-NMR** (250 MHz, $CDCl_3$): δ 7.77 (m, 4H, H-2^i, H-6^i, H-3, H-5), 6.73 (m, 2H, H-2, H-6), 6.64 (m, 2H, H-3^i, H-5^i), 5.91 (ddt, $J_{2^{iv},3_{trans}^{iv}}$ = 17.2 Hz, $J_{2^{iv},3_{cis}^{iv}}$ = 10.5 Hz,

$J_{2^{iv},1^{iv}}$ = 5.5 Hz, 1H, H-2^{iv}), 5.28 (dq, $J_{3_{trans}{}^{iv},2^{iv}}$ = 17.2 Hz, $J_{3_{trans}{}^{iv},1^{iv}} = J_{gem}$ = 1.7 Hz, 1H, H-3$_{trans}{}^{iv}$), 5.19 (dq, $J_{3_{cis}{}^{iv},2^{iv}}$ = 10.5 Hz, $J_{3_{cis}{}^{iv},1^{iv}} = J_{gem}$= 1.7 Hz, 1H, H-3$_{cis}{}^{iv}$), 4.01 (dt, $J_{1^{iv},2^{iv}}$ = 5.5 Hz, $J_{1^{iv},3_{cis}{}^{iv}} = J_{1^{iv},3_{trans}{}^{iv}}$ = 1.4 Hz, 2H, H-1^{iv}), 3.92 (m, 1H, NH), 3.61 (m, 4H, 2xH-1^{iii}, 2xH-2^{iii}), 3.50 (q, $J_{1^{v},2^{v}}$ = 7.0 Hz, 2H, H-1^{v}), 3.24 (q, $J_{1^{ii},2^{ii}}$ = 7.1 Hz, 2H, H-1^{ii}), 1.29 (t, $J_{2^{ii},1^{ii}}$ = 7.1 Hz, 3H, H-2^{ii}), 1.21 (t, $J_{2^{v},1^{v}}$ = 7.0 Hz, 3H, H-2^{v}); **^{13}C-NMR** (100.6 MHz, $CDCl_3$): δ 149.9 (C-1), 149.3 (C-4^{i}), 145.1 (C-1^{i}), 143.8 (C-4), 134.7 (C-2^{iv}), 124.3 (C-3, C-5, C-2^{i}, C-6^{i}), 117.1 (C-3^{iv}), 112.4 (C-3^{i}, C-5^{i}), 111.4 (C-2, C-6), 72.3 (C-1^{iv}), 67.9 (C-2^{iii}), 50.3 (C-1^{iii}), 45.9 (C-1^{v}), 38.4 (C-1^{ii}), 14.9 (C-2^{ii}), 12.4 (C-2^{v}); **IR** (ATR): 3401, 2867, 1591, 1510, 1145 cm^{-1}; **HRMS** (ESI+) calcd. for [$C_{21}H_{28}N_4O$+H]: 353.2336; found: 353.2329.

<u>Physical and spectroscopic data of **72**</u>

Mp = 38-45 ^{o}C (from CH_2Cl_2/EtOAc); **^{1}H-NMR** (400 MHz, $CDCl_3$): δ 7.78 (m, 4H, H-3^{i}, H-5^{i}, H-2^{ii}, H-6^{ii}), 6.73 (m, 4H, H-2^{i}, H-6^{i}, H-3^{ii}, H-5^{ii}), 5.91 (ddt, $J_{2^{v},3_{trans}{}^{v}}$ = 17.2 Hz, $J_{2^{v},3_{cis}{}^{v}}$ = 10.5 Hz, $J_{2^{v},1^{v}}$ = 5.5 Hz, 1H, H-2^{v}), 5.28 (dq, $J_{3_{trans}{}^{v},2^{v}}$ = 17.2 Hz, $J_{3_{trans}{}^{v},1^{v}} = J_{gem}$ = 1.6 Hz, 1H, H-3$_{trans}{}^{v}$), 5.19 (dq, $J_{3_{cis}{}^{v},2^{v}}$ = 10.5 Hz, $J_{3_{cis}{}^{v},1^{v}} = J_{gem}$= 1.6 Hz, 1H, H-3$_{cis}{}^{v}$), 4.01 (dt, $J_{1^{v},2^{v}}$ = 5.5 Hz, $J_{1^{iii},3_{cis}{}^{iii}} = J_{1^{v},3_{trans}{}^{v}}$ = 1.6 Hz, 2H, H-1^{v}), 3.62 (m, 4H, 2xH-1^{iv}, 2xH-2^{iv}), 3.50 (q, $J_{1,2}$ = 7.1 Hz, 2H, H-1), 3.43 (q, $J_{1^{iii},2^{iii}}$ = 7.1 Hz, 4H, H-1^{iii}), 1.21 (m, 9H, 3xH-2, 6xH-2^{iii}); **^{13}C-NMR** (100.6 MHz, $CDCl_3$): δ 149.1 (C-4^{ii}, C-1^{i}), 144.0/143.7 (C-1^{ii}/C-4^{i}), 134.7 (C-2^{v}), 124.4/124.2 (C-3^{i}, C-5^{i}/C-2^{ii}, C-6^{ii}), 117.1 (C-3^{v}), 111.4/111.3 (C-2^{i}, C-6^{i}/C-3^{ii}, C-5^{ii}), 72.4 (C-1^{v}), 68.0 (C-2^{iv}), 50.4 (C-1^{iv}), 45.9 (C-1), 44.8 (2xC-1^{iii}), 12.8 (2xC-2^{iii}), 12.4 (C-2); **IR** (ATR): 2966, 2923, 2854, 1731, 1592, 1510, 1136 cm^{-1}; **HRMS** (ESI+) calcd. for [$C_{23}H_{32}N_4O$+H]: 381.2649; found: 381.2654.

Synthesis of 9*H*-fluoren-9-ylmethyl *N*-{(5*S*)-6-[4-((*E*)-{4-[[2-(allyloxy)ethyl](ethyl)amino]phenyl}-1-diazenyl)(ethyl)anilino]-5-[(*tert*-butoxycarbonyl)anilino]-6-oxohexyl}carbamate, 74

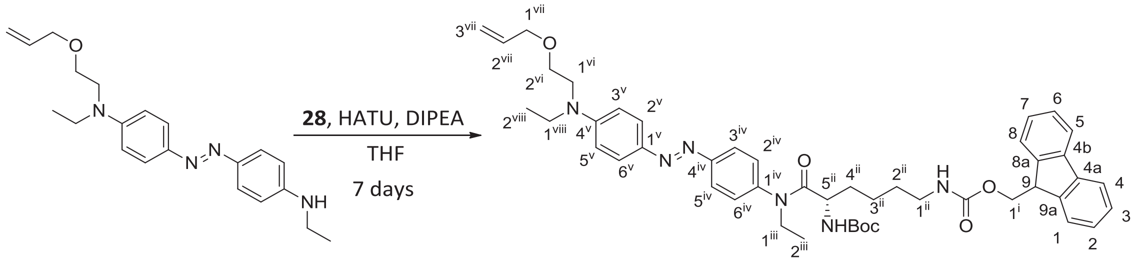

71 **74**

To a stirred solution of **71** (55 mg, 0.18 mmol) in dry THF (2.0 ml) under N_2 atmosphere, a solution of Boc-Lys(Fmoc)-OH (**28**) (81 mg, 0.17 mmol), HATU (78 mg, 0.20 mmol), DIPEA (109 μl, 0.63 mmol) in dry THF (3.0 ml) was added. The reaction mixture was stirred 24 h at rt. Then, the mixture was diluted with EtOAc (10 ml) and washed with water (2x10 ml). The organic layer was dried over anhydrous $MgSO_4$ and concentrated under vacuum. The residue was purified by column chromatography (hexanes/EtOAc, 1:1) to afford amide **74** (31 mg, 29 μmol, 25% yield) as an orange solid.

<u>Physical and spectroscopic data of **74**</u>

Mp = 49-53 °C (from hexanes/EtOAc); **$[\alpha]_D^{20}$** = -98.1 (*c* 0.62, $CHCl_3$); **^{1}H-NMR** (400 MHz, $CDCl_3$): δ 7.91 (d, $J_{3^{iv},2^{iv}} = J_{5^{iv},6^{iv}}$ = 8.4 Hz, 2H, H-3^{iv}, H-5^{iv}), 7.84 (d, $J_{2^{v},3^{v}} = J_{6^{v},5^{v}}$ = 9.1 Hz, 2H, H-2^{v}, H-6^{v}), 7.74 (d, $J_{4,3} = J_{5,6}$ = 7.6 Hz, 2H, H-4, H-5), 7.55 (dd, $J_{1,2} = J_{8,7}$ = 7.5 Hz, $J_{1,3} = J_{8,6}$ = 2.2 Hz, 2H, H-1, H-8), 7.41-7.26 (m, 6H, H-2, H-3, H-6, H-7, H-2^{iv}, H-6^{iv}), 6.69 (d, $J_{3^{v},2^{v}} = J_{5^{v},6^{v}}$ = 9.1 Hz, 2H, H-3^{v}, H-5^{v}), 5.90 (ddt, $J_{2^{vii},3_{trans}^{vii}}$ = 17.0 Hz, $J_{2^{vii},3_{cis}^{vii}}$ = 10.6 Hz, $J_{2^{vii},1^{vii}}$ = 5.5 Hz, 1H, H-2^{vii}), 5.28 (m, 2H, H-3_{trans}^{vii}, C-5^{ii}NH), 5.19 (dq, $J_{3_{cis}^{vii},2^{vii}}$ = 10.6 Hz, $J_{3_{cis}^{vii},1^{vii}} = J_{gem}$ = 1.7 Hz, 1H, H-3_{cis}^{vii}), 4.79 (m, 1H, C-1^{ii}NH), 4.37 (m, 1H, H-5^{ii}), 4.30 (d, $J_{1^{i},9}$ = 6.7 Hz, 2H, H-1^{i}), 4.13 (m, 1H, H-9), 3.99 (m, 2H, H-1^{vii}), 3.53 (m, 8H, 2xH-1^{vi}, 2xH-2^{vi}, 2xH-1^{iii}, 2xH-1^{viii}), 3.01 (m, 2H, H-1^{ii}), 1.63 (m, 2H, H-4^{ii}), 1.42 (s, 9H, $C(CH_3)_3$), 1.16 (m, 10H, 2xH-2^{ii}, 2xH-3^{ii}, 3xH-2^{iii}, 3xH-2^{viii}); **^{13}C-NMR** (100.6 MHz, $CDCl_3$): δ 172.2 (CO, amide), 156.6 (CO, carbamate), 155.6 (CO, carbamate), 152.8 (C-4^{iv}), 150.7 (C-4^{v}), 144.2 (C-9a, C-8a), 143.5 (C-1^{v}), 141.5/141.4 (C-4a, C-4b/C-1^{iv}), 134.6 (C-2^{vii}), 129.2 (C-2^{iv}, C-6^{iv}), 127.7 (C-3, C-6), 127.2 (C-2, C-7), 125.7 (C-2^{v}, C-6^{v}), 125.3 (C-1, C-8), 123.6 (C-3^{iv}, C-5^{iv}), 120.0 (C-4, C-5), 117.3 (C-3^{vii}), 111.3 (C-3^{v}, C-5^{v}), 79.6 ($\mathit{C}(CH_3)_3$), 72.4 (C-1^{vii}), 67.8 (C-2^{vi}), 66.7 (C-1^{i}), 50.7 (C-5^{ii}), 50.4 (C-1^{vi}), 47.4 (C-9), 46.0 (C-1^{viii}), 44.8 (C-1^{iii}), 40.8 (C-1^{ii}), 33.1 (C-4^{ii}), 29.8 (C-2^{ii}), 28.5 ($C(\mathit{C}H_3)_3$), 22.3 (C-3^{ii}), 13.1 (C-2^{iii}), 12.3 (C-2^{viii}); **IR** (ATR): 3321, 2932, 1705, 1597, 1241, 1132 cm^{-1}; **HRMS** (ESI+) calcd. for $[C_{47}H_{58}N_6O_6+Na]$: 825.4310; found: 825.4316. **COSY** and **^{1}H/^{13}C** correlation were recorded.

Synthesis of 9*H*-fluoren-9-ylmethyl *N*-[(5*S*)-5-[(*tert*-butoxycarbonyl)amino]-6-{(2,5-dioxo-1-pyrrolidinyloxy}-6-oxahexyl]carbamate, 78

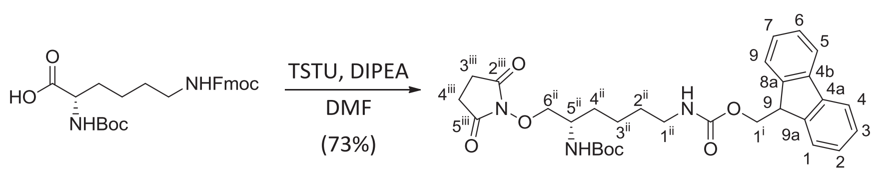

28 **78**

To a stirred solution of Boc-Lys(Fmoc)-OH (**28**) (400 mg, 0.85 mmol) in dry DMF (3 ml) was added TSTU (300 mg, 1.00 mmol) and DIPEA (208 μl, 1.20 mmol) under N_2 atmosphere. The reaction mixture was stirring overnight at rt and then water (3.0 ml) was added. The mixture was extracted with $CHCl_3$ (3x6 ml) and the combined organic extracts were dried over anhydrous $MgSO_4$ and concentrated under vacuum. The crude product was purified by column chromatography (hexanes/EtOAc, 1:1) to provide compound **78** (351 mg, 0.62 mmol, 73%) as a white solid.

Physical and spectroscopic data of **78**

Mp = 175-179 ^oC (from hexanes/EtOAc); $[\alpha]_D^{20}$ = 10.0 (*c* 1.12, $CHCl_3$); **^1H-NMR** (400 MHz, $CDCl_3$): δ 7.75 (d, $J_{4,3} = J_{5,6}$ = 7.5 Hz, 2H, H-4, H-5), 7.61 (d, $J_{1,2} = J_{8,7}$ = 7.5 Hz, 2H, H-1, H-8), 7.39 (t, $J_{3,2} = J_{3,4} = J_{6,7} = J_{6,5}$ = 7.5 Hz, 2H, H-3, H-6), 7.31 (t, $J_{2,3} = J_{2,1} = J_{7,6} = J_{7,8}$ = 7.5 Hz, 2H, H-2, H-7), 5.11 (m, 2H, C-1^{ii}NH, C-5^{ii}NH), 4.69 (m, 1H, H-5^{ii}), 4.39 (m, 2H, H-1^{i}), 4.21 (m, 1H, H-9), 3.22 (m, 2H, H-1^{ii}), 2.80 (s, 2H, H-3^{iii}, H-4^{iii}), 1.91 (m, 2H, H-4^{ii}), 1.60-1.36 (m, 13H, 2xH-2^{ii}, 2xH-3^{ii}, $C(CH_3)_3$); **^{13}C-NMR** (100.6 MHz, $CDCl_3$): δ 168.8/168.6 (C-2^{iii}/C-5^{iii}), 156.7 (CO, carbamate), 155.0 (CO, carbamate), 144.2 (C-9a, C-8a), 141.4 (C-4a, C4b), 127.8 (C-3, C-6), 127.1 (C-2, C-7), 125.3 (C-1, C-8), 120.1 (C-4, C-5), 80.7 (*C*$(CH_3)_3$), 66.7 (C-1^{i}), 51.9 (C-5^{ii}), 47.5 (C-9), 40.4 (C-1^{ii}), 32.4 (C-4^{ii}), 29.2 (C-2^{ii}), 28.4 ($C(CH_3)_3$), 25.7 (C-3^{iii}, C-4^{iii}), 21.8 (C-3^{ii}); **IR** (ATR): 3321, 2936, 1745, 1678, 1521, 1255, 1206, 1162, 1069 cm^{-1}; **HRMS** (ESI+) calcd. for $[C_{30}H_{35}N_3O_8+Na]$: 588.2316; found 588.2320.

Synthesis of 9*H*-fluoren-9-ylmethyl *N*-{(5*S*)-6-[4-((*E*)-{4-[[2-(allyloxy)ethyl](ethyl)amino]phenyl}-1-diazenyl)anilino]-5-[(*tert*-butoxycarbonyl)amino]-6-oxohexyl}carbamate, 73

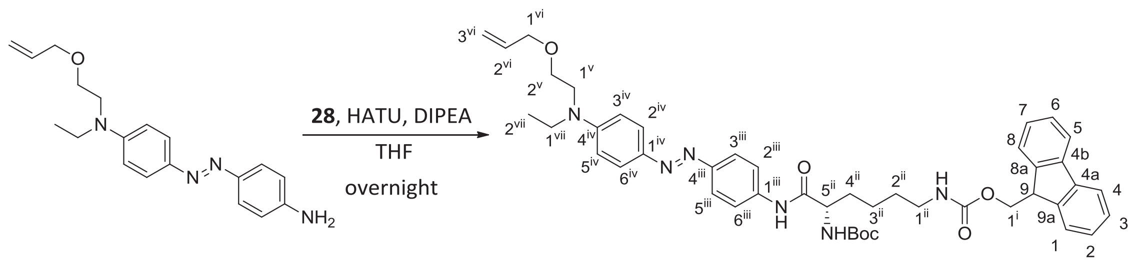

76 73

To a stirred solution of amine **76** (312 mg, 0.96 mmol) in dry THF (15 ml) under N_2 atmosphere, a solution of Boc-Lys(Fmoc)-OH (**28**) (494 mg, 1.05 mmol), HATU (476 mg, 1.25 mmol), DIPEA (668 μl, 3.85 mmol) in dry THF (10 ml) was added. The reaction mixture was stirred overnight at rt. Then, the mixture was diluted with EtOAc (30 ml) and washed with water (2x20 ml). The organic layer was dried over anhydrous $MgSO_4$ and concentrated under vacuum. The residue was purified by column chromatography (hexanes/EtOAc, 1:1), to afford amide **73** (665 mg, 0.86 mmol, 89% yield) as an orange solid.

Physical and spectroscopic data of **73**

Mp = 62-68 ^oC (from hexanes/EtOAc); $[\alpha]_D^{20}$ = -12.0 (*c* 1.86, $CHCl_3$); **^1H-NMR** (400 MHz, $CDCl_3$): δ 8.95 (br s, 1H, C-1^{iii}NH), 7.83 (d, $J_{2^{iv},3^{iv}} = J_{6^{iv},5^{iv}}$ = 9.2 Hz, 2H, H-2^{iv}, H-6^{iv}), 7.80 (d, $J_{3^{iii},2^{iii}} = J_{5^{iii},6^{iii}}$ = 8.8

Hz, 2H, H-3^{iii}, H-5^{iii}), 7.74 (d, $J_{4,3}$ = $J_{5,6}$ = 7.5 Hz, 2H, H-4, H-5), 7.67 (d, $J_{2^{iii},3^{iii}}$ = $J_{6^{iii},5^{iii}}$ = 8.8 Hz, 2H, H-2^{iii}, H-6^{iii}), 7.57 (d, $J_{1,2}$ = $J_{8,7}$ = 7.5 Hz, 2H, H-1, H-8), 7.38 (t, $J_{3,2}$ = $J_{3,4}$ = $J_{6,7}$ = $J_{6,5}$ = 7.5 Hz, 2H, H-3, H-6), 7.29 (t, $J_{2,3}$ = $J_{2,1}$ = $J_{7,6}$ = $J_{7,8}$ = 7.5 Hz, 2H, H-2, H-7), 6.72 (d, $J_{3^{iv},2^{iv}}$ = $J_{5^{iv},6^{iv}}$ = 9.2 Hz, 2H, H-3^{iv}, H-5^{iv}), 5.91 (ddt, $J_{2^{vi},3_{trans}^{vi}}$ = 17.0 Hz, $J_{2^{vi},3_{cis}^{vi}}$ = 10.8 Hz, $J_{2^{vi},1^{vi}}$ = 5.4 Hz, 1H, H-2^{vi}), 5.52 (m, 1H, C-5^{ii}NH), 5.28 (dq, $J_{3_{trans}^{vi},2^{vi}}$ = 17.0 Hz, $J_{3_{trans}^{vi},1^{vi}}$ = J_{gem} = 1.6 Hz, 1H, H-3$_{trans}^{vi}$), 5.19 (dq, $J_{3_{cis}^{vi},2^{vi}}$ = 10.8 Hz, $J_{3_{cis}^{vi},1^{vi}}$ = J_{gem}= 1.6 Hz, 1H, H-3$_{cis}^{vi}$), 5.05 (m, 1H, C-1^{ii}NH), 4.39 (m, 2H, H-1^{i}), 4.29 (m, 1H, H-5^{ii}), 4.19 (m, 1H, H-9), 4.00 (m, 2H, H-1^{vi}), 3.61 (m, 4H, 2xH-1^{v}, H-2^{v}), 3.50 (q, $J_{1^{vii},2^{vii}}$ = 7.0 Hz, 2H, H-1^{vii}), 3.18 (m, 2H, H-1^{ii}), 1.98 (m, 1H, H-4^{ii}), 1.73 (m, 1H, H-4^{ii}), 1.54-1.34 (m, 13H, 2xH-2^{ii}, 2xH-3^{ii}, $C(CH_3)_3$), 1.22 (t, $J_{2^{vii},1^{vii}}$ = 7.0 Hz, 3H, H-2^{vii}); **^{13}C-NMR** (100.6 MHz, $CDCl_3$): δ 170.9 (CO, amide), 156.8 (CO, carbamate), 156.5 (CO, carbamate), 150.1/149.7 (C-4^{iv}/C-4^{iii}), 144.0 (C-9a, C-8a), 143.5 (C-1^{iv}), 141.4 (C-4a, C-4b), 139.0 (C-1^{iii}), 134.6 (C-2^{vi}), 127.7 (C-3, C-6), 127.1 (C-2, C-7), 125.1 (C-2^{iv}, C-6^{iv}, C-1, C-8), 123.1 (C-3^{iii}, C-5^{iii}), 120.0 (C-2^{iii}, C-6^{iii}, C-4, C-5), 117.1 (C-3^{vi}), 111.3 (C-3^{iv}, C-5^{iv}), 80.5 ($\mathit{C}(CH_3)_3$), 72.3 (C-1^{vi}), 67.8 (C-2^{v}), 66.7 (C-1^{i}), 55.2 (C-5^{ii}), 50.3 (C-1^{v}), 47.3 (C-9), 45.9 (C-1^{vii}), 40.4 (C-1^{ii}), 31.6 (C-4^{ii}), 29.5 (C-2^{ii}), 28.4 ($C(\mathit{C}H_3)_3$), 22.7 (C-3^{ii}), 12.3 (C-2^{vii}); **IR** (ATR): 3297, 2928, 1668, 1594, 1511, 1242, 1135 cm^{-1}; **HRMS** (ESI+) calcd. for $[C_{45}H_{54}N_6O_6+H]$: 775.4178; found: 775.4180.

Synthesis of 1-(6-hydroxy-2-naphthyl)-1-ethanone, 83[8,9]

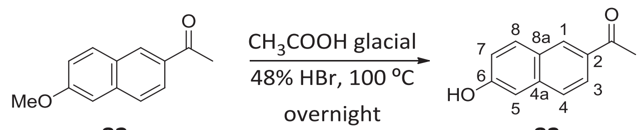

82 **83**

To a stirred solution of 1-(6-methoxy-2-naphthyl)ethanone (**82**) (1.05 g, 5.00 mmol) in glacial acetic acid (10 ml) was added 48% HBr (5.6 ml, 51.0 mmol). The mixture was stirred at 100 ºC for overnight. Excess acetic acid was removed under vacuum, and the residue was taken up in EtOAc (20 ml) and washed with saturated aqueous solution of $NaHCO_3$ and brine. The organic layer was dried over anhydrous $MgSO_4$ and the solvent was removed under vacuum. The product was purified by chromatography (hexanes/EtOAc, 1:1) to provide **83** (470 mg, 2.52 mmol, 48% yield) as a white powder.

<u>Spectroscopic data of **83**</u>

^{1}H-NMR (400 MHz, $CDCl_3$): δ 8.41 (d, $J_{1,3}$ = 1.8 Hz, 1H, H-1), 8.00 (dd, $J_{3,4}$ = 8.7 Hz, $J_{3,1}$ = 1.8 Hz, 1H, H-3), 7.88 (d, $J_{8,7}$ = 7.6 Hz, 1H, H-8), 7.72 (d, $J_{4,3}$ = 8.7 Hz, 1H, H-4), 7.19-7.17 (m, 2H, H-5, H-7), 5.44 (br s, 1H, OH), 2.70 (s, 3H, $COCH_3$); **^{13}C-NMR** (100.6 MHz, $CDCl_3$): δ 198.4 ($\mathit{C}OCH_3$), 156.0 (C-

6), 137.4 (C-4a), 132.7 (C-2), 131.9 (C-8), 130.5 (C-1), 127.9 (C-8a), 126.9 (C-4), 124.9 (C-3), 119.0 (C-7), 109.8 (C-5), 26.7 (COCH_3).

Synthesis of 1-[6-(methylamino)-2-naphthyl]-1-ethanone, 84[8]

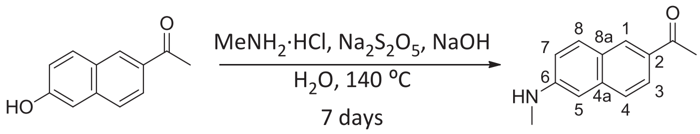

83 **84**

MeNH$_2$·HCl (766 mg, 11.3 mmol) was added to a solution of **83** (352 mg, 1.89 mmol), $Na_2S_2O_5$ (719 mg, 3.78 mmol) and NaOH (637 mg, 11.4 mmol) in water (11 ml) in a steel-bomb reactor and the mixture was stirred at 140 ºC for one week. The product was collected by filtration, washed with water, and purified by column chromatography (chloroform/EtOAc, 1:1) to give **84** (312 mg, 1.57 mmol, 83% yield) as a brown solid.

<u>Spectroscopic data of **84**</u>

^{1}H-NMR (360 MHz, $CDCl_3$): δ 8.30 (s, 1H, H-1), 7.93 (dd, $J_{3,4}$ = 8.6 Hz, $J_{3,1}$ = 1.6 Hz, 1H, H-3), 7.72 (d, $J_{8,7}$ = 8.8 Hz, 1H, H-8), 7.63 (d, $J_{4,3}$ = 8.6 Hz, 1H, H-4), 6.92 (dd, $J_{7,8}$ = 8.8 Hz, $J_{7,5}$ = 1.8 Hz, 1H, H-7), 6.80 (d, $J_{5,7}$ = 1.8 Hz, 1H, H-5), 4.50 (br m, 1H, NH), 2.97 (s, 3H, NHCH_3), 2.66 (s, 3H, $COCH_3$); **^{13}C-NMR** (90 MHz, $CDCl_3$): δ 197.9 ($COCH_3$), 149.0 (C-6), 138.1 (C-4a), 131.8 (C-2), 130.9 (C-8), 130.5 (C-1), 126.2 (C-8a, C-4), 124.9 (C-3), 118.6 (C-7), 103.6 (C-5), 30.7 ($NHCH_3$), 26.5 (COCH_3).

Synthesis of methyl 2-[(6-acetyl-2-naphthyl)(methyl)amino]acetate, 85[8]

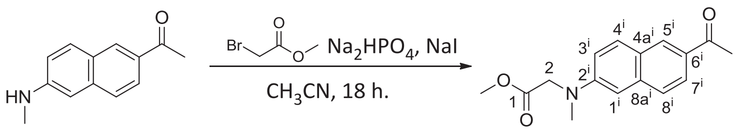

84 **85**

A mixture of amine **84** (585 mg, 2.93 mmol), methyl bromoacetate (406 μl, 4.40 mmol), Na_2HPO_4 (625 mg, 4.40 mmol), NaI (176 mg, 1.17 mmol) in CH_3CN (18 ml) was refluxed under N_2 atmosphere for 18 h. The product was extracted with EtOAc, washed with brine, and purified by column chromatography (chloroform/EtOAc, 30:1) to furnish **85** (722 mg, 2.66 mmol, 90% yield) as an orange solid.

<u>Spectroscopic data of **85**</u>

^{1}H-NMR (400 MHz, $CDCl_3$): δ 8.30 (d, $J_{5^i,7^i}$ = 1.6 Hz, 1H, H-5^i), 7.92 (dd, $J_{7^i,8^i}$ = 8.7 Hz, $J_{7^i,5^i}$ = 1.6 Hz, 1H, H-7^i), 7.78 (d, $J_{4^i,3^i}$ = 9.1 Hz, 1H, H-4^i), 7.63 (d, $J_{8^i,7^i}$ = 8.7 Hz, 1H, H-8^i), 7.07 (dd, $J_{3^i,4^i}$ = 9.1 Hz, $J_{3^i,8}$

= 2.6 Hz, 1H, H-3[i]), 6.87 (d, $J_{1^i,3^i}$ = 2.6 Hz, 1H, H-1[i]), 4.10 (s, 2H, H-2), 3.73 (s, 3H, $COOCH_3$), 3.18 (s, 3H, NCH_3), 2.64 (s, 3H, $COCH_3$); **^{13}C-NMR** (100.6 MHz, $CDCl_3$): δ 197.8 ($COCH_3$), 171.0 (C-1), 148.9 (C-2[i]), 137.6 (C-8a[i]), 131.3 (C-6[i]), 131.0 (C-4[i]), 130.3 (C-5[i]), 126.5 (C-8[i]), 125.6 (C-4a[i]), 124.6 (C-7[i]), 115.8 (C-3[i]), 106.0 (C-1[i]), 54.2 (C-2), 52.1 ($COOCH_3$), 39.7 (NCH_3), 26.4 ($COCH_3$).

Synthesis of 2-[(6-acetyl-2-naphthyl)(methyl)amino]acetic acid, 70[8]

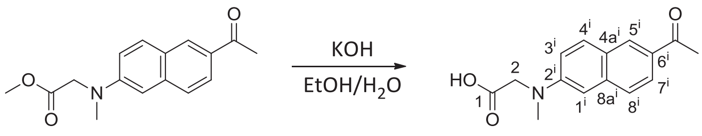

A mixture of **85** (722 mg, 2.66 mmol) and KOH (284 mg, 5.06 mmol) in a 5:1 mixture of EtOH and water (60 ml) was stirred for 5 h. The resultant solution was diluted with ice-water (36 ml) and 37% HCl was added slowly at < 5 ºC until pH 3. The resulting precipitate was collected by filtration and washed with water to provide **70** (534 mg, 2.09 mmol, 78% yield) as a green solid.

Spectroscopic data of **70**

^{1}H-NMR (400 MHz, MeOH-d_4): δ 8.41 (d, $J_{5^i,7^i}$ = 1.6 Hz, 1H, H-5[i]), 7.87 (m, 2H, H-4, H-7[i]), 7.66 (d, $J_{8^i,7^i}$ = 8.7 Hz, 1H, H-8[i]), 7.20 (dd, $J_{3^i,4^i}$ = 10.3 Hz, $J_{3^i,8}$ = 2.6 Hz, 1H, H-3[i]), 6.95 (d, $J_{1^i,3^i}$ = 2.6 Hz, 1H, H-1[i]), 4.27 (s, 2H, H-2), 3.20 (s, 3H, NCH_3), 2.65 (s, 3H, $COCH_3$); **^{13}C-NMR** (100.6 MHz, MeOH-d_4): δ 200.4 ($COCH_3$), 174.2 (C-1), 150.9 (C-2[i]), 139.3 (C-8a[i]), 131.9 (C-4[i], C-5[i], C-6[i]), 127.4 (C-8[i]), 126.8 (C-4a[i]), 125.1 (C-7[i]), 117.1 (C-3[i]), 106.6 (C-1[i]), 54.6 (C-2), 39.8 (NCH_3), 26.4 ($COCH_3$).

Synthesis of *tert*-butyl (1*S*)-1-{[4-((*E*)-{4-[[2-(allyloxy)ethyl](ethyl)amino]phenyl}diazenyl) anilino]carbonyl}-5-aminopentylcarbamate, 86

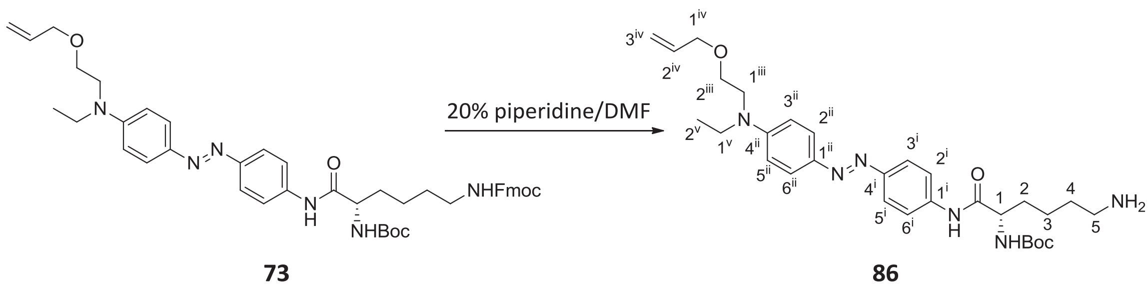

A commercially available solution of 20% piperidine in DMF (8.0 ml) was added to compound **73** (396 mg, 0.41 mmol). After 1 h of stirring at rt, TLC analysis (CH_2Cl_2/MeOH, 9:1) showed no presence of starting material. The mixture was diluted with water (8.0 ml) and washed with EtOAc (2x20 ml). The combined organic extracts were dried over anhydrous $MgSO_4$ and concentrated under vacuum. The resulting orange solid was purified by column chromatography (from CH_2Cl_2 to CH_2Cl_2/MeOH/NH_3, 95:5:1) to afford **86** (209 mg, 0.36 mmol, 87% yield) as an orange solid.

Physical and spectroscopic data of **86**

Mp = 55-61 ºC (from CH_2Cl_2); **$[\alpha]_D^{20}$** = -5.8 (*c* 0.92, $CHCl_3$); **^{1}H-NMR** (400 MHz, $CDCl_3$): δ 9.17 (br s, 1H, C-1^{i}NH), 7.81 (d, $J_{2^{ii},3^{ii}} = J_{6^{ii},5^{ii}}$ = 9.2 Hz, 2H, H-2^{ii}, H-6^{ii}), 7.80 (d, $J_{3^i,2^i} = J_{5^i,6^i}$ = 8.9 Hz, 2H, H-3^i, H-5^i), 7.67 (d, $J_{2^i,3^i} = J_{6^i,5^i}$ = 8.9 Hz, 2H, H-2^i, H-6^i), 6.73 (d, $J_{3^{ii},2^{ii}} = J_{5^{ii},6^{ii}}$ = 9.2 Hz, 2H, H-3^{ii}, H-5^{ii}), 5.92 (ddt, $J_{2^{iv},3_{trans}^{iv}}$ = 17.3 Hz, $J_{2^{iv},3_{cis}^{iv}}$ = 10.4 Hz, $J_{2^{iv},1^{iv}}$ = 5.5 Hz, 1H, H-2^{iv}), 5.38 (m, 1H, C-1NH), 5.27 (dq, $J_{3_{trans}^{iv},2^{iv}}$ = 17.3 Hz, $J_{3_{trans}^{iv},1^{iv}} = J_{gem}$ = 1.4 Hz, 1H, H-3$_{trans}^{iv}$), 5.18 (dq, $J_{3_{cis}^{iv},2^{iv}}$ = 10.4 Hz, $J_{3_{cis}^{iv},1^{iv}} = J_{gem}$= 1.4 Hz, 1H, H-3$_{cis}^{iv}$), 4.30 (m, 1H, H-1), 4.00 (dt, $J_{1^{iv},2^{iv}}$ = 5.5 Hz, $J_{1^{iv},3_{cis}^{iv}} = J_{1^{iv},3_{trans}^{iv}}$ = 1.4 Hz, 2H, H-1^{iv}), 3.61 (m, 4H, 2xH-1^{iii}, 2xH-2^{iii}), 3.51 (q, $J_{1^v,2^v}$ = 7.0 Hz, 2H, H-1^v), 2.80 (m, 4H, 2xH-5, NH_2), 1.95 (m, 1H, H-2), 1.63-1.45 (m, 5H, H-2, 2xH-3, 2xH-4), 1.50 (s, 9H, $C(CH_3)_3$), 1.21 (t, $J_{2^v,1^v}$ = 7.0 Hz, 3H, H-2^v); **^{13}C-NMR** (100.6 MHz, $CDCl_3$): δ 170.7 (CO, amide), 156.4 (CO, carbamate), 150.2/149.8 (C-4^{ii}/C-4^i), 143.5 (C-1^{ii}), 139.1 (C-1^i), 134.6 (C-2^{iv}), 125.2 (C-2^{ii}, C-6^{ii}), 123.2 (C-3^i, C-5^i), 120.1 (C-2^i, C-6^i), 117.2 (C-3^{iv}), 111.3 (C-3^{ii}, C-5^{ii}), 80.6 ($C(CH_3)_3$), 72.4 (C-1^{iv}), 67.9 (C-2^{iii}), 55.1 (C-1), 50.4 (C-1^{iii}), 46.0 (C-1^v), 41.3 (C-5), 32.2 (C-2), 31.6 (C-4), 28.5 ($C(CH_3)_3$), 22.8 (C-3), 12.4 (C-2^v); **IR** (ATR): 2923, 2853, 1671, 1593, 1510, 1244, 1153, 1135 cm^{-1}; **HRMS** (ESI+) calcd. for $[C_{30}H_{44}N_6O_4+H]$: 553.3497; found: 553.3492.

Synthesis of *tert*-butyl *N*-((1*S*)-5-({[(6-acetyl-2-naphthyl)(methyl)amino]acetyl}amino)-1-{[4-((*E*)-{4-[[2-(allyloxy)ethyl](ethyl)amino]phenyl}-1-diazenyl)anilino]carbonyl}pentyl)carbamate, 79

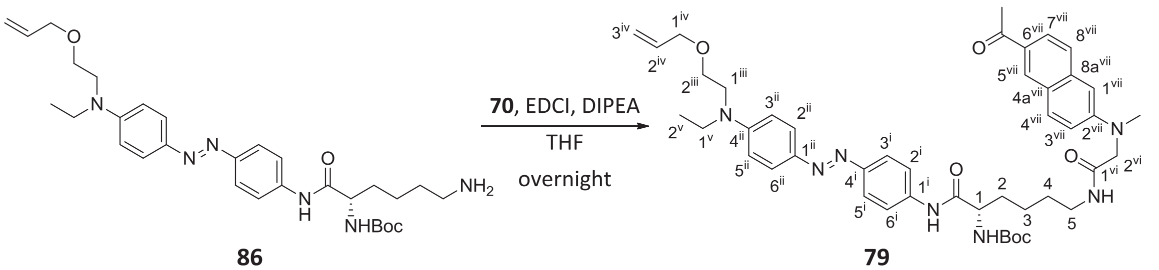

To a stirred solution of amine **86** (209 mg, 0.38 mmol) in dry THF (10 ml) under N_2 atmosphere, a solution of **70** (107 mg, 0.42 mmol), EDCI (94 mg, 0.49 mmol), DIPEA (265 μl, 1.52 mmol) in dry THF (30 ml) was added. The reaction mixture was stirred overnight at rt. Then, the mixture was diluted with EtOAc (40 ml) and washed with water (2x40 ml). The organic layer was dried over anhydrous $MgSO_4$ and concentrated under vacuum. The residue was purified by column chromatography (EtOAc) to give an orange solid identified as **79** (243 mg, 0.31 mmol, 81% yield).

<u>Physical and spectroscopic data of **79**</u>

Mp = 75-81 ºC (from EtOAc); **[α]$_D^{20}$** = -14.2 (*c* 1.01, $CHCl_3$); **^{1}H-NMR** (400 MHz, $CDCl_3$): δ 8.71 (br s, 1H, C-1^{i}NH), 8.31 (s, 1H, H-5^{vii}), 7.94 (dd, $J_{7^{vii},8^{vii}}$ = 8.7 Hz, $J_{7^{vii},5^{vii}}$ = 1.7 Hz, 1H, H-7^{vii}), 7.81 (m, 5H, H-3^i, H-5^i, H-2^{ii}, H-6^{ii}, H-4^{vii}), 7.66 (m, 3H, H-2^i, H-6^i, H-8^{vii}), 7.06 (dd, $J_{3^{vii},4^{vii}}$ = 9.1 Hz, $J_{3^{vii},1^{vii}}$ = 2.5 Hz, 1H, H-3^{vii}), 6.93 (d, $J_{1^{vii},3^{vii}}$ = 2.5 Hz, 1H, H-1^{vii}), 6.74 (d, $J_{3^{ii},2^{ii}}$ = $J_{5^{ii},6^{ii}}$ = 9.2 Hz, 2H, H-3^{ii}, H-5^{ii}), 6.59 (t, $J_{C\text{-}5NH,5}$ = 6.1 Hz, 1H, C-5NH), 5.90 (ddt, $J_{2^{iv},3_{trans}^{iv}}$ = 17.2 Hz, $J_{2^{iv},3_{cis}^{iv}}$ = 10.4 Hz, $J_{2^{iv},1^{iv}}$ = 5.5 Hz, 1H, H-2^{iv}), 5.28 (dq, $J_{3_{trans}^{iv},2^{iv}}$ = 17.2 Hz, $J_{3_{trans}^{iv},1^{iv}}$ = J_{gem} = 1.6 Hz, 1H, H-3$_{trans}^{iv}$), 5.26 (m, 1H, C-1NH), 5.18 (dq, $J_{3_{cis}^{iv},2^{iv}}$ = 10.4 Hz, $J_{3_{cis}^{iv},1^{iv}}$ = J_{gem} = 1.6 Hz, 1H, H-3$_{cis}^{iv}$), 4.17 (m, 1H, H-1), 4.01 (m, 4H, 2xH-2^{vi}, 2xH-1^{iv}), 3.62 (m, 4H, 2xH-1^{iii}, 2xH-2^{iii}), 3.51 (q, $J_{1^{v},2^{v}}$ = 7.1 Hz, 2H, H-1^v), 3.33 (m, 2H, H-5), 3.14 (s, 3H, NCH_3), 2.65 (s, 3H, $COCH_3$), 1.92 (m, 1H, H-2), 1.64 (m, 1H, H-2), 1.56-1.36 (m, 13H, $C(CH_3)_3$, 2xH-3, 2xH-4), 1.22 (t, $J_{2^{v},1^{v}}$ = 7.0 Hz, 3H, H-2^v); **^{13}C-NMR** (100.6 MHz, $CDCl_3$): δ 197.9 (*C*OCH_3), 170.5/170.2 (C-1^{vi}/CO, amide), 156.4 (CO, carbamate), 150.2/149.8 (C-4^{ii}/C-4^i), 148.9 (C-2^{vii}), 143.5 (C-1^{ii}), 139.0 (C-1^i), 137.3 (C-8a^{vii}), 134.6 (C-2^{iv}), 132.0 (C-6^{vii}), 131.4 (C-4^{vii}), 130.3 (C-5^{vii}), 126.8 (C-8^{vii}), 126.2 (C-4a^{vii}), 125.2 (C-2^{ii}, C-6^{ii}), 125.1 (C-7^{vii}), 123.2 (C-3^i, C-5^i), 120.0 (C-2^i, C-6^i), 117.2 (C-3^{iv}), 116.3 (C-3^{vii}), 111.3 (C-3^{ii}, C-5^{ii}), 106.9 (C-1^{vii}), 80.7 (*C*$(CH_3)_3$), 72.4 (C-1^{iv}), 67.9 (C-2^{iii}), 58.4 (C-2^{vi}), 55.1 (C-1), 50.4 (C-1^{iii}), 46.0 (C-1^v), 39.9 (NCH_3), 38.4 (C-5), 31.1 (C-2), 29.0 (C-4), 28.5 ($C(\mathit{C}H_3)_3$), 26.6 ($COCH_3$), 22.5 (C-3), 12.4 (C-2^v); **IR** (ATR): 3296, 2924, 2855, 1664, 1618, 1594, 1508, 1242, 1153, 1136, 1108 cm^{-1}; **HRMS** (ESI+) calcd. for $[C_{45}H_{57}N_7O_6+Na]$: 814.4263; found: 814.4275. **COSY** and **^{1}H/^{13}C** correlation were recorded.

Synthesis of (2*S*)-6-({2-[(6-acetyl-2-naphthyl)(methyl)amino]acetyl}amino)-*N*-[4-((E)-2-{4-[[2-(allyloxy)ethyl](ethyl)amino]phenyl}-1-diazenyl)phenyl]-2-aminohexanamide, 87

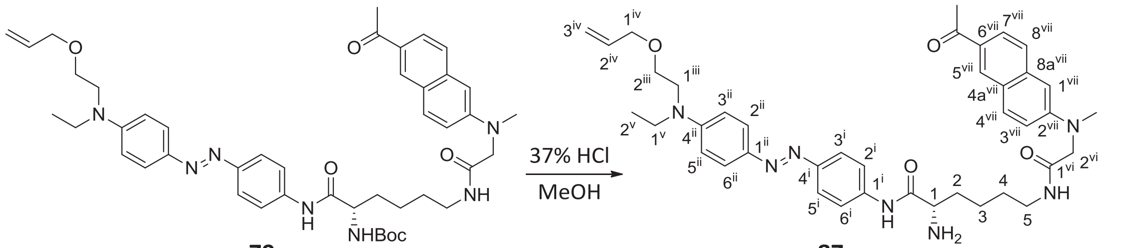

79 **87**

To a stirred solution of **79** (243 mg, 0.31 mmol) in MeOH (12 ml), 37% HCl (3.5 ml, 40.8 mmol) was added. The reaction mixture was stirred for 1 h, when TLC analysis (EtOAc/MeOH, 95:5) showed no presence of starting material, and concentrated under vacuum. The mixture was neutralized with a saturated aqueous solution of $NaHCO_3$, was extracted with EtOAc (2x20 ml) and dried over anhydrous $MgSO_4$. The solvent was evaporated under vacuum and the resulting residue was purified by column chromatography (from CH_2Cl_2 to CH_2Cl_2/MeOH/NH_3, 95:5:1) to furnish amine **87** (197 mg, 0.29 mmol, 93% yield) as an orange solid.

Physical and spectroscopic data of **87**

Mp = 138-145 ºC (from CH_2Cl_2); **$[\alpha]_D^{20}$** = -7.0 (*c* 1.02, $CHCl_3$); **^{1}H-NMR** (250 MHz, $CDCl_3$): δ 9.58 (br s, 1H, C-1^{i}NH), 8.31 (d, $J_{5^{vii},7^{vii}}$ = 1.5 Hz, 1H, H-5^{vii}), 7.94 (dd, $J_{7^{vii},8^{vii}}$ = 8.7 Hz, $J_{7^{vii},5^{vii}}$ = 1.5 Hz, 1H, H-7^{vii}), 7.83 (m, 5H, H-3^{i}, H-5^{i}, H-2^{ii}, H-6^{ii}, H-4^{vii}), 7.67 (m, 3H, H-2^{i}, H-6^{i}, H-8^{vii}), 7.06 (dd, $J_{3^{vii},4^{vii}}$ = 9.1 Hz, $J_{3^{vii},1^{vii}}$ = 2.5 Hz, 1H, H-3^{vii}), 6.92 (d, $J_{1^{vii},3^{vii}}$ = 2.5 Hz, 1H, H-1^{vii}), 6.74 (d, $J_{3^{ii},2^{ii}}$ = $J_{5^{ii},6^{ii}}$ = 9.2 Hz, 2H, H-3^{ii}, H-5^{ii}), 6.53 (t, $J_{C\text{-}5NH,5}$ = 6.1 Hz, 1H, C-5NH), 5.90 (ddt, $J_{2^{iv},3_{trans}^{iv}}$ = 17.2 Hz, $J_{2^{iv},3_{cis}^{iv}}$ = 10.4 Hz, $J_{2^{iv},1^{iv}}$ = 5.5 Hz, 1H, H-2^{iv}), 5.27 (dq, $J_{3_{trans}^{iv},2^{iv}}$ = 17.2 Hz, $J_{3_{trans}^{iv},1^{iv}}$ = J_{gem} = 1.6 Hz, 1H, H-3$_{trans}^{iv}$), 5.18 (dq, $J_{3_{cis}^{iv},2^{iv}}$ = 10.4 Hz, $J_{3_{cis}^{iv},1^{iv}}$ = J_{gem}= 1.6 Hz, 1H, H-3$_{cis}^{iv}$), 4.01 (m, 4H, 2xH-2^{vi}, 2xH-1^{iv}), 3.63 (m, 4H, 2xH-1^{iii}, 2xH-2^{iii}), 3.51 (q, $J_{1^{v},2^{v}}$ = 7.1 Hz, 2H, H-1^{v}), 3.33 (m, 3H, H-2, 2xH-6), 3.14 (s, 3H, NCH_3), 2.64 (s, 3H, $COCH_3$), 1.86 (m, 1H, H-3), 1.64-1.43 (m, 5H, H-3, 2xH-5, NH_2), 1.35 (m, 2H, H-4), 1.22 (t, $J_{2^{v},1^{v}}$ = 7.0 Hz, 3H, H-2^{v}); **^{13}C-NMR** (100.6 MHz, $CDCl_3$): δ 197.8 ($COCH_3$), 173.1 (C-1), 169.9 (C-1^{vi}), 150.2/149.6 (C-4^{ii}/C-4^{i}), 148.9 (C-2^{vii}), 143.5 (C-1^{ii}), 138.9 (C-1^{i}), 137.3 (C-8a^{vii}), 134.6 (C-2^{iv}), 131.8 (C-6^{vii}), 131.2 (C-4^{vii}), 130.2 (C-5^{vii}), 126.6 (C-8^{vii}), 126.1 (C-4a^{vii}), 125.1 (C-2^{ii}, C-6^{ii}), 124.9 (C-7^{vii}), 123.2 (C-3^{i}, C-5^{i}), 119.5 (C-2^{i}, C-6^{i}), 117.2 (C-3^{iv}), 116.2 (C-3^{vii}), 111.3 (C-3^{ii}, C-5^{ii}), 106.7 (C-1^{vii}), 72.3 (C-1^{iv}), 67.8 (C-2^{iii}), 58.3 (C-2^{vi}), 55.3 (C-2), 50.3 (C-1^{iii}), 45.9 (C-1^{v}), 40.0 (NCH_3), 38.8 (C-6), 34.3 (C-3), 29.3 (C-5), 26.6 ($COCH_3$), 22.9 (C-4), 12.3 (C-2^{v}); **IR** (ATR): 3288, 2927, 2861, 1664, 1617, 1595, 1505, 1152, 1135 cm^{-1}; **HRMS** (ESI+) calcd. for $[C_{40}H_{49}N_7O_4+H]$: 692.3919; found: 692.3931.

Synthesis of di(*tert*-butyl) (2*R*,4*S*)-2-{4-[((1*S*)-5-({[(6-acetyl-2-naphthyl)(methyl)amino]acetyl} amino)-1-{[4-((*E*)-{4-[[2-(allyloxy)ethyl](ethyl)amino]phenyl}-1-diazenyl)anilino]carbonyl} pentyl)amino]-4-oxobutyl}-4-[(*tert*-butoxycarbonyl)amino]pentanedioate, 80

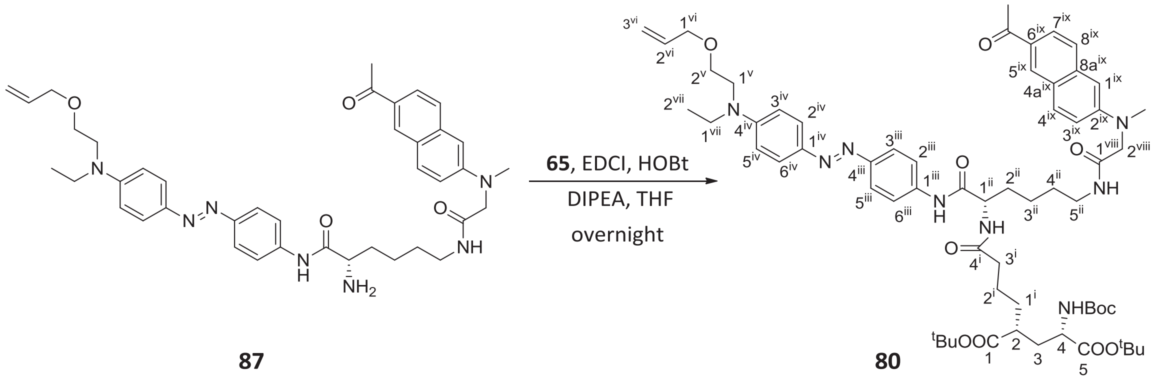

87 80

To a stirred solution of amine **87** (174 mg, 0.25 mmol) in dry THF (8.0 ml) was added a solution of **65** (123 mg, 0.28 mmol), EDCI (63 mg, 0.33 mmol), HOBt (51 mg, 0.38 mmol), DIPEA (175 μl, 1.01 mmol) in dry THF (20 ml) under N_2 atmosphere. The reaction mixture was stirred overnight at rt. Then, the mixture was diluted with EtOAc (30 ml) and washed with water (2x30 ml). The organic layer was dried over anhydrous $MgSO_4$ and concentrated under vacuum. The crude product was purified by column chromatography (EtOAc) to provide **80** (200 mg, 0.18 mmol, 71% yield) as an orange solid.

Physical and spectroscopic data of **80**

Mp = 73-80 ^oC (from EtOAc); **$[\alpha]_D^{20}$** = -54.0 (*c* 1.07, $CHCl_3$); **^{1}H-NMR** (400 MHz, $CDCl_3$): δ 9.04 (br s, 1H, C-1^{iii}NH), 8.30 (s, 1H, H-5^{ix}), 7.93 (d, $J_{7^{ix},8^{ix}}$ = 8.8 Hz, 1H, H-7^{ix}), 7.80 (m, 5H, H-3^{iii}, H-5^{iii}, H-2^{iv}, H-6^{iv}, H-4^{ix}), 7.65 (m, 3H, H-2^{iii}, H-6^{iii}, H-8^{ix}), 7.04 (dd, $J_{3^{ix},4^{ix}}$ = 8.9 Hz, $J_{3^{ix},1^{ix}}$ = 2.1 Hz, 1H, H-3^{ix}), 6.92 (s, 1H, H-1^{ix}), 6.73 (d, $J_{3^{iv},2^{iv}} = J_{5^{iv},6^{iv}}$ = 9.2 Hz, 2H, H-3^{iv}, H-5^{iv}), 6.68 (t, $J_{C\text{-}5^{ii}NH,5^{ii}}$ = 6.1 Hz, 1H, C-5^{ii}NH), 6.54 (m, 1H, C-1^{ii}NH), 5.90 (ddt, $J_{2^{vi},3_{trans}^{vi}}$ = 17.2 Hz, $J_{2^{vi},3_{cis}^{vi}}$ = 10.4 Hz, $J_{2^{vi},1^{vi}}$ = 5.5 Hz, 1H, H-2^{vi}), 5.27 (dq, $J_{3_{trans}^{vi},2^{vi}}$ = 17.2 Hz, $J_{3_{trans}^{vi},1^{vi}} = J_{gem}$ = 1.6 Hz, 1H, H-3$_{trans}^{vi}$), 5.18 (dq, $J_{3_{cis}^{vi},2^{vi}}$ = 10.4 Hz, $J_{3_{cis}^{vi},1^{vi}} = J_{gem}$= 1.6 Hz, 1H, H-3$_{cis}^{vi}$), 5.15 (m, 1H, C-3NH), 4.52 (m, 1H, H-1^{ii}), 4.16 (m, 1H, H-4), 4.01 (m, 4H, 2xH-2^{viii}, H-1^{vi}), 3.62 (m, 4H, 2xH-1^{v}, 2xH-2^{v}), 3.51 (q, $J_{1^{vii},2^{vii}}$ = 7.1 Hz, 2H, H-1^{vii}), 3.32 (m, 2H, H-5^{ii}), 3.14 (s, 3H, NCH_3), 2.64 (s, 3H, $COCH_3$), 2.35 (m, 1H, H-2), 2.24 (m, 2H, H-3^{i}), 2.13-1.89 (m, 3H, H-3, H-1^{i}, H-2^{ii}), 1.75-1.60 (m, 7H, H-3, H-1^{i}, 2xH-2^{i}, H-2^{ii}, 2xH-4^{ii}), 1.44 (m, 29H, 2xH-3^{ii}, 3x$C(CH_3)_3$), 1.21 (t, $J_{2^{vii},1^{vii}}$ = 7.1 Hz, 3H, H-2^{vii}); **^{13}C-NMR** (100.6 MHz, $CDCl_3$): δ 197.9 ($COCH_3$), 174.4/173.6/171.8/170.3/170.1 (C-1/C-5/C-4^{i}/C-1^{viii}/CO, amide), 155.5 (CO, carbamate), 150.2/ 149.8 (C-4^{iii}/C-4^{iv}), 149.0 (C-2^{ix}), 143.5 (C-1^{iv}), 138.1 (C-1^{iii}), 137.3 (C-8a^{ix}), 134.6 (C-2^{vi}), 131.9 (C-6^{ix}), 131.3 (C-4^{ix}), 130.3 (C-5^{ix}), 126.7 (C-8^{ix}), 126.2 (C-4a^{ix}), 125.2 (C-2^{iv}, C-6^{iv}), 125.0 (C-7^{ix}), 123.2 (C-3^{iii}, C-5^{iii}), 120.2 (C-2^{iii}, C-6^{iii}), 117.2 (C-3^{vi}), 116.3 (C-3^{ix}), 111.3 (C-3^{iv}, C-5^{iv}), 106.7 (C-1^{ix}), 82.0 ($\mathit{C}(CH_3)_3$), 81.0 ($\mathit{C}(CH_3)_3$), 79.7 ($\mathit{C}(CH_3)_3$), 72.4 (C-1^{vi}), 67.8 (C-2^{v}), 58.3 (C-2^{viii}), 53.8 (C-1^{ii}), 52.8 (C-4), 50.4 (C-1^{v}), 46.0 (C-1^{vii}), 42.4 (C-2), 40.0 (NCH_3), 38.4 (C-5^{ii}), 36.1 (C-3^{i}), 34.8 (C-3), 32.1 (C-1^{i}), 30.7 (C-2^{ii}), 29.8 (C-4^{ii}), 28.4 ($C(\mathit{C}H_3)_3$), 28.2 ($C(\mathit{C}H_3)_3$), 28.1 ($C(\mathit{C}H_3)_3$), 26.6 ($CO\mathit{C}H_3$), 23.4 (C-3^{ii}), 22.5 (C-2^{i}), 12.4 (C-2^{vii}); **IR** (ATR): 3276, 2928, 1718, 1595, 1150, 1138 cm^{-1}; **HRMS** (ESI+) calcd. for $[C_{62}H_{86}N_8O_{11}+Na]$: 1141.6308; found: 1141.6311. **COSY** and **^{1}H/^{13}C** correlation were recorded.

Synthesis of di(*tert*-butyl) (2*R*,4*S*)-2-{4-[((1*S*)-5-({[(6-acetyl-2-naphthyl)(methyl)amino]acetyl} amino)-1-{[4-((*E*)-{4-[ethyl(2-hydroxyethyl)amino]phenyl}-1-diazenyl)anilino]carbonyl}pentyl) amino]-4-oxobutyl}-4-[(*tert*-butoxycarbonyl)amino]pentanedioate, 88

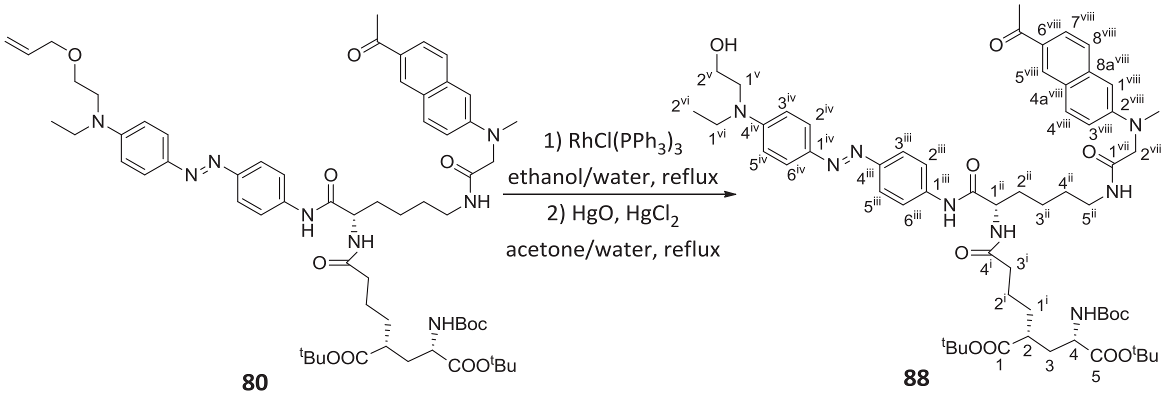

80 **88**

$RhCl(PPh_3)_3$ (16 mg, 17 μmol) was added to a solution of allyl ether **80** (155 mg, 0.14 mmol) in a 1:10 mixture of water and ethanol (17 ml) and warmed up to 100 ºC. The mixture was stirred for 2 h at this temperature, cooled, and then the solvents were removed under vacuum. The residue was dissolved in a 9:1 mixture of water and acetone (66 ml) and HgO (57 mg, 0.26 mmol) and $HgCl_2$ (56 mg, 0.21 mmol) were added. The mixture was heated at the reflux temperature during 1.5 h. Then, it was filtered through Celite© pad and concentrated under reduced pressure. The residue was dissolved in CH_2Cl_2 (50 ml), washed with aqueous 50% KI (30 ml), brine (30 ml), dried over anhydrous $MgSO_4$ and concentrated under vacuum. Purification by column chromatography (from hexanes/EtOAc, 9:1 to EtOAc/MeOH, 97:3) provided an orange solid identified as **88** (132 mg, 0.12 mmol, 88% yield).

Physical and spectroscopic data of **88**

Mp = 94-97 ºC (from EtOAc/MeOH); $[\alpha]_D^{20}$ = -13.2 (*c* 1.95, $CHCl_3$); **^{1}H-NMR** (400 MHz, $CDCl_3$): δ 9.06 (br s, 1H, C-1^{iii}NH), 8.29 (s, 1H, H-5^{viii}), 7.92 (dd, $J_{7^{viii},8^{viii}}$ = 8.7 Hz, $J_{7^{viii},5^{viii}}$ = 1.2 Hz, 1H, H-7^{viii}), 7.79 (m, 5H, H-3^{iii}, H-5^{iii}, H-2^{iv}, H-6^{iv}, H-4^{viii}), 7.64 (m, 3H, H-2^{iii}, H-6^{iii}, H-8^{viii}), 7.04 (dd, $J_{3^{viii},4^{viii}}$ = 9.1 Hz, $J_{3^{viii},1^{viii}}$ = 2.5 Hz, 1H, H-3^{viii}), 6.92 (d, $J_{1^{viii},3^{viii}}$ = 2.5 Hz, 1H, H-1^{viii}), 6.76 (d, $J_{3^{iv},2^{iv}}$ = $J_{5^{iv},6^{iv}}$ = 9.2 Hz, 2H, H-3^{iv}, H-5^{iv}), 6.69 (t, $J_{C\text{-}5^{ii}NH,5^{ii}}$ = 6.4 Hz, 1H, C-5^{ii}NH), 6.56 (m, 1H, C-1^{ii}NH), 5.15 (d, $J_{C\text{-}3NH,3}$ = 10.8 Hz, 1H, C-3NH), 4.51 (m, 1H, H-1^{ii}), 4.16 (m, 1H, H-4), 3.99 (m, 2H, H-2^{vii}), 3.85 (t, $J_{2^{v},1^{v}}$ = 6.0 Hz, 2H, H-2^{v}), 3.57 (t, $J_{3^{v},2^{v}}$ = 6.0 Hz, 2H, H-1^{v}), 3.50 (q, $J_{1^{vi},2^{vi}}$ = 7.0 Hz, 2H, H-1^{vi}), 3.32 (m, 2H, H-5^{ii}), 3.12 (s, 3H, NCH_3), 2.64 (s, 3H, $COCH_3$), 2.36 (m, 1H, H-2), 2.23 (m, 2H, H-3^{i}), 2.00-1.86 (m, 3H, H-3, H-1^{i}, H-2^{ii}), 1.78-1.56 (m, 5H, H-3, H-1^{i}, 2xH-2^{i}, H-2^{ii}), 1.52 (m, 2H, H-4^{ii}), 1.41 (m, 29H, 2xH-3^{ii}, 3x$C(CH_3)_3$), 1.21 (t, $J_{2^{vi},1^{vi}}$ = 7.0 Hz, 3H, H-2^{vi}); **^{13}C-NMR** (100.6 MHz, $CDCl_3$): δ 198.0 ($COCH_3$), 174.5/ 173.6/171.8/170.4/170.1 (C-1/C-5/C-4^{i}/C-1^{vii}/CO, amide), 155.5 (CO, carbamate), 150.5/149.7 (C-

4^{iii}/C-4^{iv}), 149.0 (C-2^{viii}), 143.7 (C-1^{iv}), 138.2 (C-1^{iii}), 137.3 (C-8a^{viii}), 131.9 (C-6^{viii}), 131.3 (C-4^{viii}), 130.3 (C-5^{viii}), 126.8 (C-8^{viii}), 126.2 (C-4a^{viii}), 125.2 (C-2^{iv}, C-6^{iv}), 125.0 (C-7^{viii}), 123.2 (C-3^{iii}, C-5^{iii}), 120.1 (C-2^{iii}, C-6^{iii}), 116.3 (C-3^{viii}), 111.7 (C-3^{iv}, C-5^{iv}), 106.9 (C-1^{viii}), 82.0 (*C*$(CH_3)_3$), 81.1 (*C*$(CH_3)_3$), 79.8 (*C*$(CH_3)_3$), 60.3 (C-2^{v}), 58.3 (C-2^{vii}), 53.8 (C-1^{ii}), 52.8 (C-4), 52.6 (C-1^{v}), 46.0 (C-1^{vi}), 42.4 (C-2), 40.0 (NCH_3), 38.4 (C-5^{ii}), 36.1 (C-3^{i}), 34.8 (C-3), 32.1 (C-1^{i}), 30.7 (C-2^{ii}), 29.1 (C-4^{ii}), 28.5 (C(*C*$H_3)_3$), 28.2 (C(*C*$H_3)_3$), 28.1 (C(*C*$H_3)_3$), 26.6 (CO*C*H_3), 23.4 (C-3^{ii}), 22.5 (C-2^{i}), 12.2 (C-2^{vi}); **IR** (ATR): 3305, 2926, 1597, 1511, 1153 cm^{-1}; **HRMS** (ESI+) calcd. for [$C_{59}H_{82}N_8O_{11}$+H]: 1079.6176; found: 1079.6186.

Synthesis of 10-oxa-4-azatricyclo[5.2.1.0^{2,6}]dec-8-ene-3,5-dione, 89[10]

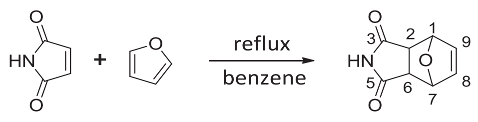

Maleimide (**90**) (500 mg, 5.15 mmol) and furan (**91**) (374 µl, 5.14 mmol) were dissolved in benzene (4.8 ml) in a sealed tube, and then heated at 90-100 ºC for 6 h. The furan-masked maleimide precipitated after cooling the mixture to rt. The product was then filtered, washed with cold diethyl ether (3x5 ml) to remove unreacted maleimide, giving rise to **89** (511 mg, 3.09 mmol, 60% yield) as a white powder. The NMR spectra indicate that the product is exclusively the *exo* isomer.

Spectroscopic data of **89**

^{1}H-NMR (400 MHz, $CDCl_3$): δ 8.48 (br s, 1H, NH), 6.53 (t, $J_{9,1}$ = $J_{8,7}$ = 0.9 Hz, 2H, H-9, H-8), 5.32 (t, $J_{1,9}$ = $J_{7,8}$ = 0.9 Hz, 2H, H-1, H-7), 2.91 (s, 2H, H-2, H-6); **^{13}C-NMR** (100.6 MHz, $CDCl_3$): δ 176.4 (C-3, C-5), 136.7 (C-9, C-8), 81.0 (C-1, C-7), 48.8 (C-2, C-6).

Synthesis of di(*tert*-butyl) (2*R*,4*S*)-2-{4-[((1*S*)-5-({[(6-acetyl-2-naphthyl)(methyl)amino]acetyl}amino)-1-{[4-((*E*)-{4-[(2-((1*R*,2*S*,6*R*,7*S*)-3,5-dioxo-10-oxa-4-azatricyclo[5.2.1.0^{2,6}]dec-8-en-4-yl]ethyl)(ethyl)amino]phenyl}-1-diazenyl)anilino]carbonyl}pentyl)amino]-4-oxobutyl}-4-[(*tert*-butoxycarbonyl)amino]pentanedioate, 81

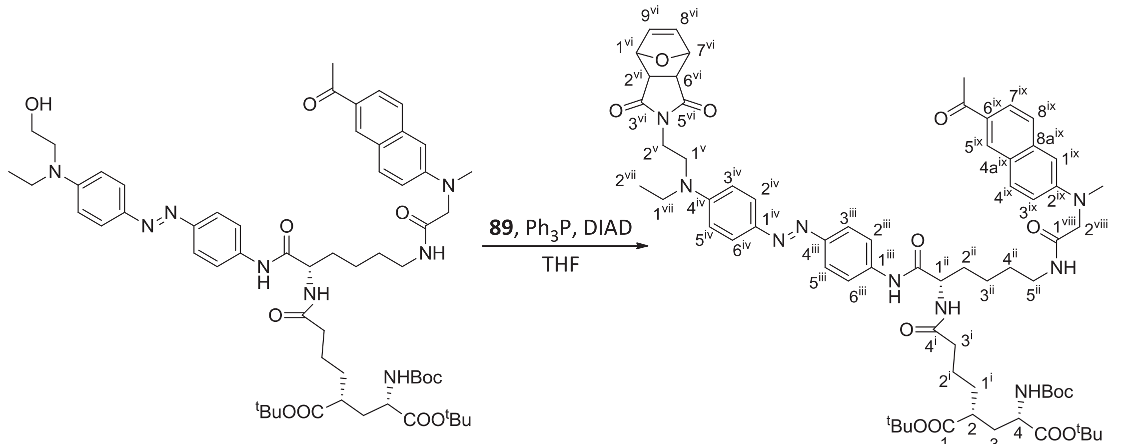

88 **81**

To an ice-cooled solution of **88** (100 mg, 93 μmol), **89** (54 mg, 0.46 mmol), Ph_3P (121 mg, 0.46 mmol) in dry THF (10 ml) was added DIAD (91 μl, 0.46 mmol) under N_2 atmosphere over 2 min. After 2 h of stirring at rt, TLC analysis (EtOAc) indicated the complete consumption of the starting material. The solvent was evaporated under vacuum and the residue was purified by column chromatography (EtOAc) to furnish compound **81** (36 mg, 29 μmol, 32% yield) as a yellowish solid.

Physical and spectroscopic data of **81**

Mp = 84-89 ^oC (from EtOAc); **$[\alpha]_D^{20}$** = -34.7 (*c* 0.32, $CHCl_3$); **^{1}H-NMR** (400 MHz, $CDCl_3$): δ 8.97 (br s, 1H, C-1^{iii}NH), 8.33 (s, 1H, H-5^{ix}), 7.95 (dd, $J_{7^{ix},8^{ix}}$ = 8.8 Hz, $J_{7^{ix},5^{ix}}$ = 1.1 Hz, 1H, H-7^{ix}), 7.81 (m, 5H, H-3^{iii}, H-5^{iii}, H-2^{iv}, H-6^{iv}, H-4^{ix}), 7.66 (m, 3H, H-2^{iii}, H-6^{iii}, H-8^{ix}), 7.06 (dd, $J_{3^{ix},4^{ix}}$ = 9.0 Hz, $J_{3^{ix},1^{ix}}$ = 2.1 Hz, 1H, H-3^{ix}), 6.94 (d, $J_{1^{ix},3^{ix}}$ = 2.1 Hz, 1H, H-1^{ix}), 6.82 (d, $J_{3^{iv},2^{iv}}$ = $J_{5^{iv},6^{iv}}$ = 9.1 Hz, 2H, H-3^{iv}, H-5^{iv}), 6.67 (t, $J_{C\text{-}5^{ii}NH,5^{ii}}$ = 5.7 Hz, 1H, C-5^{ii}NH), 6.56 (m, 1H, C-1^{ii}NH), 6.52 (s, 2H, H-8^{vi}, H-9^{vi}), 5.26 (s, 2H, H-1^{vi}, H-7^{vi}), 5.12 (d, $J_{C\text{-}3NH,3}$ = 8.7 Hz, 1H, C-3NH), 4.50 (m, 1H, H-1^{ii}), 4.16 (m, 1H, H-4), 4.02 (m, 2H, H-2^{viii}), 3.72 (t, $J_{2^{v},1^{v}}$ = 6.7 Hz, 2H, H-2^{v}), 3.53 (t, $J_{1^{v},2^{v}}$ = 6.7 Hz, 2H, H-1^{v}), 3.47 (q, $J_{1^{vii},2^{vii}}$ = 7.0 Hz, 2H, H-1^{vii}), 3.33 (m, 2H, H-5^{ii}), 3.15 (s, 3H, NCH_3), 2.76 (s, 2H, H-2^{vi}, H-6^{vi}), 2.66 (s, 3H, $COCH_3$), 2.35 (m, 1H, H-2), 2.25 (m, 2H, H-3^{i}), 2.13-1.48 (m, 10H, 2xH-3, H-1^{i}, 2xH-2^{i}, 2xH-2^{ii}, 2xH-4^{ii}), 1.41 (m, 29H, 2xH-3^{ii}, 3x$C(CH_3)_3$), 1.21 (t, $J_{2^{vii},1^{vii}}$ = 7.0 Hz, 3H, H-2^{vii}); **^{13}C-NMR** (100.6 MHz, $CDCl_3$): δ 197.9 ($COCH_3$), 176.3 (C-3^{vi}, C-3^{vi}), 174.5/173.7/171.8/170.4/170.0 (C-1/C-5/C-4^{i}/C-1^{viii}/CO, amide), 155.5 (CO, carbamate), 150.0/149.7 (C-4^{iii}/C-4^{iv}), 149.0 (C-2^{ix}), 143.9 (C-1^{iv}), 139.3 (C-1^{iii}), 137.3 (C-8a^{ix}), 136.7 (C-8^{vi}, C-9^{vi}), 132.0 (C-6^{ix}), 131.4 (C-4^{ix}), 130.3 (C-5^{ix}), 126.8 (C-8^{ix}), 126.2 (C-4a^{ix}), 125.2 (C-2^{iv}, C-

6^{iv}), 125.1 (C-7^{ix}), 123.2 (C-3^{iii}, C-5^{iii}), 120.1 (C-2^{iii}, C-6^{iii}), 116.3 (C-3^{ix}), 111.6 (C-3^{iv}, C-5^{iv}), 106.9 (C-1^{ix}), 82.0 ($C(CH_3)_3$), 81.0 ($C(CH_3)_3$, C-1^{vi}, C-7^{vi}), 79.7 ($C(CH_3)_3$), 58.4 (C-2^{vii}), 53.7 (C-1^{ii}), 52.8 (C-4), 47.7 (C-2^{vi}, C-6^{vi}), 46.9 (C-1^{v}), 45.0 (C-1^{vii}), 42.5 (C-2), 40.1 (NCH_3), 38.3 (C-5^{ii}), 36.2 (C-2^{v}, C-3^{i}), 34.8 (C-3), 32.1 (C-1^{i}), 30.5 (C-2^{ii}), 29.1 (C-4^{ii}), 28.5 ($C(CH_3)_3$), 28.2 ($C(CH_3)_3$), 28.1 ($C(CH_3)_3$), 26.6 ($COCH_3$), 23.3 (C-3^{ii}), 22.4 (C-2^{i}), 12.5 (C-2^{vii}); **IR** (ATR): 3505, 2926, 1693, 1595, 1391, 1366, 1247, 1151 cm^{-1}; **HRMS** (ESI+) calcd. for [$C_{67}H_{87}N_9O_{13}$+Na]: 1248.6316; found: 1248.6279. **^{1}H/^{13}C** correlation was recorded.

Synthesis of di(*tert*-butyl) (2*R*,4*S*)-2-{4-[((1*S*)-5-({[(6-acetyl-2-naphthyl)(methyl)amino]acetyl}amino)-1-{[4-((*E*)-{4-[[2-(2,5-dioxo-2,5-dihydro-1*H*-pyrrol-1-yl)ethyl](ethyl)amino]phenyl}-1-diazenyl)anilino]carbonyl}pentyl)amino]-4-oxobutyl}-4-[(*tert*-butoxycarbonyl)amino] pentanedioate, 92

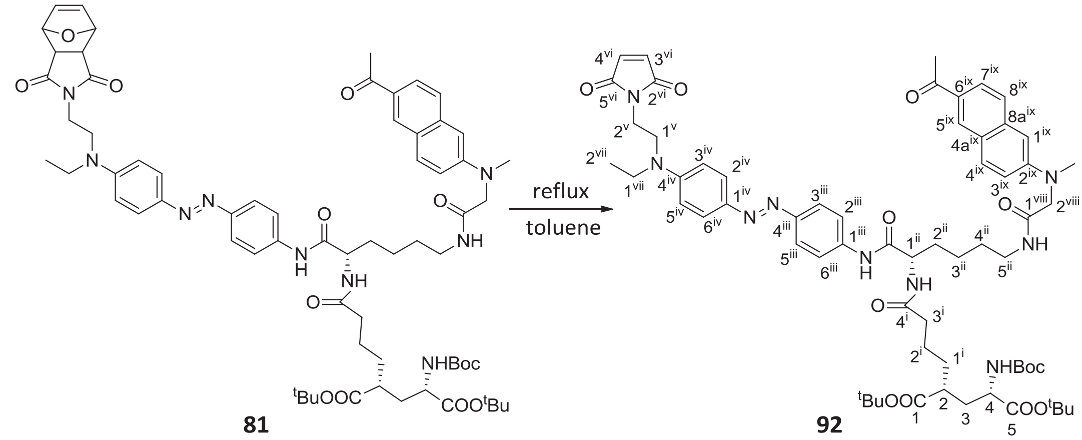

81 **92**

To a stirred solution of **81** (36 mg, 29 μmol) in toluene (2.8 ml) was heated at the reflux temperature for 5 h, when TLC analysis (EtOAc) showed no presence of starting material. The solvent was removed under vacuum and the residue was purified by column chromatography (EtOAc) to furnish compound **92** (34 mg, 29 μmol, quantitative yield) as a yellow solid.

Physical and spectroscopic data of **92**

Mp = 82-89 ºC (from EtOAc); **[α]$_D^{20}$** = -43.7 (*c* 1.60, $CHCl_3$); **^{1}H-NMR** (400 MHz, $CDCl_3$): δ 8.98 (br s, 1H, C-1^{iii}NH), 8.32 (s, 1H, H-5^{ix}), 7.94 (dd, $J_{7^{ix},8^{ix}}$ = 8.7 Hz $J_{7^{ix},5^{ix}}$ = 1.7 Hz, 1H, H-7^{ix}), 7.80 (m, 5H, H-3^{iii}, H-5^{iii}, H-2^{iv}, H-6^{iv}, H-4^{ix}), 7.66 (m, 3H, H-2^{iii}, H-6^{iii}, H-8^{ix}), 7.06 (dd, $J_{3^{ix},4^{ix}}$ = 9.1 Hz, $J_{3^{ix},1^{ix}}$ = 2.6 Hz, 1H, H-3^{ix}), 6.93 (d, $J_{1^{ix},3^{ix}}$ = 2.6 Hz, 1H, H-1^{ix}), 6.79 (d, $J_{3^{iv},2^{iv}}$ = $J_{5^{iv},6^{iv}}$ = 9.2 Hz, 2H, H-3^{iv}, H-5^{iv}), 6.66 (m, 3H, H-3^{vi}, H-4^{vi}, C-5^{ii}NH), 6.49 (m, 1H, C-1^{ii}NH), 5.13 (d, $J_{C-4NH,4}$ = 10.0 Hz, 1H, C-4NH), 4.50 (m, 1H, H-1^{ii}), 4.16 (m, 1H, H-4), 4.01 (m, 2H, H-2^{viii}), 3.75 (t, $J_{2^{v},1^{v}}$ = 7.1 Hz, 2H, H-2^{v}), 3.56 (t, $J_{1^{v},2^{v}}$ = 7.1 Hz, 2H, H-1^{v}), 3.47 (q, $J_{1^{vii},2^{vii}}$ = 7.0 Hz, 2H, H-1^{vii}), 3.33 (m, 2H, H-5^{ii}), 3.14 (s, 3H, NCH_3), 2.65 (s, 3H,

$COCH_3$), 2.36 (m, 1H, H-2), 2.24 (m, 2H, H-3^{i}), 2.05-1.48 (m, 10H, 2xH-3, 2xH-1^{i}, 2xH-2^{i}, 2xH-2^{ii}, 2xH-4^{ii}), 1.43 (m, 29H, 2xH-3^{ii}, 3xC(CH_3)$_3$), 1.22 (t, $J_{2^{vii},1^{vii}}$ = 7.0 Hz, 3H, H-2^{vii}); **^{13}C-NMR** (100.6 MHz, $CDCl_3$): δ 197.9 ($COCH_3$), 174.5/173.7/171.8 (C-1/C-5/C-4^{i}/C-1^{vii}/CO, amide), 170.7 (C-2^{vi}, C-5^{vi}), 170.4/170.0 (C-1/C-5/C-4^{i}/C-1^{viii}/CO, amide), 155.5 (CO, carbamate), 149.9/149.7 (C-4^{iii}/C-4^{iv}), 149.0 (C-2^{ix}), 143.9 (C-1^{iv}), 139.2 (C-1^{iii}), 137.3 (C-8a^{ix}), 134.3 (C-3^{vi}, C-4^{vi}), 132.0 (C-6^{ix}), 131.4 (C-4^{ix}), 130.3 (C-5^{ix}), 126.8 (C-8^{ix}), 126.2 (C-4a^{ix}), 125.2 (C-2^{iv}, C-6^{iv}), 125.1 (C-7^{ix}), 123.3 (C-3^{iii}, C-5^{iii}), 120.1 (C-2^{iii}, C-6^{iii}), 116.3 (C-3^{ix}), 111.6 (C-3^{iv}, C-5^{iv}), 106.9 (C-1^{ix}), 82.1 ($C(CH_3)_3$), 81.1 ($C(CH_3)_3$), 79.8 ($C(CH_3)_3$), 58.4 (C-2^{viii}), 53.8 (C-1^{ii}), 52.8 (C-4), 47.7 (C-1^{v}), 45.0 (C-1^{vii}), 42.4 (C-2), 40.1 (NCH_3), 38.3 (C-5^{ii}), 36.1/35.1 (C-2^{v}, C-3^{i}), 34.8 (C-3), 32.1 (C-1^{i}), 30.5 (C-2^{ii}), 29.1 (C-4^{ii}), 28.5 ($C(CH_3)_3$), 28.2 ($C(CH_3)_3$), 28.1 ($C(CH_3)_3$), 26.6 ($COCH_3$), 23.3 (C-3^{ii}), 22.4 (C-2^{i}), 12.5 (C-2^{vii}); **IR** (ATR): 3282, 2932, 1706, 1596, 1365, 1246, 1151 cm^{-1}; **HRMS** (ESI+) calcd. for [$C_{63}H_{83}N_9O_{12}$+H]: 1180.6053; found: 1180.6028.

Synthesis of (1*S*,3*R*)-7-[((1*S*)-5-({[(6-acetyl-2-naphthyl)(methyl)amino]acetyl}amino)-1-[4-((*E*)-{4-[[2-(2,5-dioxo-2,5-dihydro-1*H*-1-pyrrolyl)ethyl](ethyl)amino]phenyl}-1-diazenyl)anilino] carbonylpentyl)amino]-1,3-dicarboxy-7-oxoheptylammonium 2,2,2-trifluoroacetate, 22

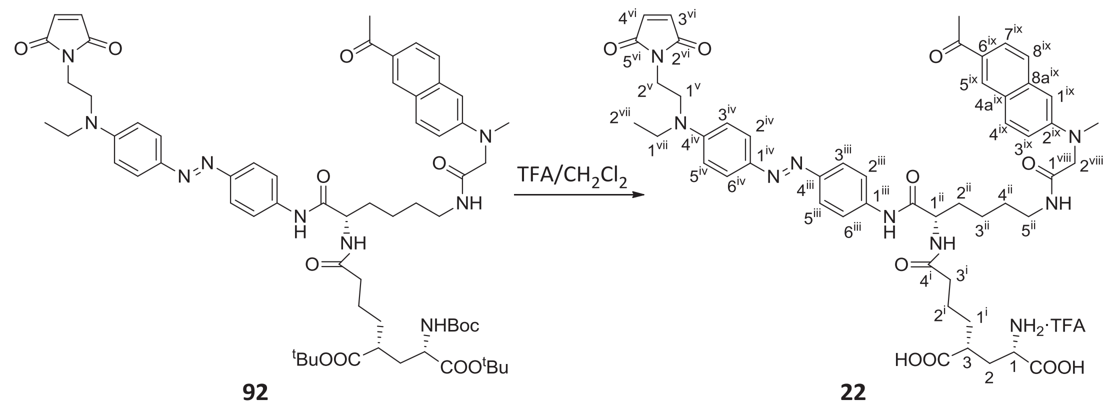

92 **22**

To a stirred solution of compound **92** (16 mg, 14 μmol) in CH_2Cl_2 (2.7 ml), trifluoroacetic acid (1.3 ml, 16.9 mmol) was added. The mixture was stirred at rt until the starting material was consumed as judged by TLC analysis (EtOAc/MeOH, 9:1). Then, the mixture was concentrated under vacuum. The resulting solid was triturated with diethyl ether (2x3 ml) to afford **22** (13 mg, 12 μmol, 86%) as a purple solid.

<u>Physical and spectroscopic data of **22**</u>

[α]$_D$^{20} = 5.1 (*c* 0.50, MeOH); **^{1}H-NMR** (400 MHz, MeOH-d$_4$): δ 8.39 (d, $J_{5^{ix},7^{ix}}$ = 1.3 Hz, 1H, H-5^{ix}), 7.86 (m, 2H, H-7^{ix}, H-4^{ix}), 7.76 (m, 4H, H-3^{iii}, H-5^{iii}, H-2^{iv}, H-6^{iv}), 7.67 (m, 3H, H-2^{iii}, H-6^{iii}, H-8^{ix}), 7.14 (dd, $J_{3^{ix},4^{ix}}$ = 9.1 Hz, $J_{3^{ix},1^{ix}}$ = 2.6 Hz, 1H, H-3^{ix}), 6.95 (d, $J_{1^{ix},3^{ix}}$ = 2.6 Hz, 1H, H-1^{ix}), 6.84 (d, $J_{3^{iv},2^{iv}}$ = $J_{5^{iv},6^{iv}}$

= 9.2 Hz, 2H, H-3^{iv}, H-5^{iv}), 6.77 (s, 2H, H-3^{vi}, H-4^{vi}), 4.40 (dd, $J_{1^{ii},2^{ii}}$ = 8.6 Hz, $J_{1^{ii},2^{ii}}$ = 5.9 Hz, 1H, H-1^{ii}), 4.07 (s, 2H, H-2^{viii}), 3.99 (dd, $J_{1,2}$ = 8.0 Hz, $J_{1,2}$ = 5.9 Hz, 1H, H-1), 3.74 (t, $J_{2^{v},1^{v}}$ = 6.8 Hz, 2H, H-2^{v}), 3.61 (t, $J_{1^{v},2^{v}}$ = 6.8 Hz, 2H, H-1^{v}), 3.49 (q, $J_{1^{vii},2^{vii}}$ = 7.0 Hz, 2H, H-1^{vii}), 3.26 (m, 2H, H-5^{ii}), 3.16 (s, 3H, NCH_3), 2.67 (m, 1H, H-3), 2.63 (s, 3H, $COCH_3$), 2.39-2.26 (m, 3H, H-2, 2xH-3^{i}), 1.95-1.79 (m, 3H, H-2, H-1^{i}, H-2^{ii}), 1.78-1.69 (m, 4H, H-1^{i}, 2xH-2^{i}, H-2^{ii}) 1.53 (m, 2H, H-4^{ii}), 1.37 (m, 2H, H-3^{ii}), 1.22 (t, $J_{2^{vii},1^{vii}}$ = 7.0 Hz, 3H, H-2^{vii}); **^{13}C-NMR** (100.6 MHz, MeOH-d$_4$): δ 200.4 ($COCH_3$), 177.7/175.8/173.0/ 172.9 (C-4^{i}/C-1^{viii}/CO, amide/CO, acid/CO, acid), 172.4 (C-2^{vi}, C-5^{vi}), 171.7 (C-4^{i}/C-1^{viii}/CO, amide/ CO, acid/CO, acid), 151.7 (C-4^{iv}), 150.9/150.8 (C-4^{iii}/C-2^{ix}), 144.8 (C-1^{iv}), 140.9 (C-1^{iii}), 139.1 (C-8a^{ix}), 135.6 (C-4^{vi}), 132.2 (C-6^{ix}), 132.1 (C-4^{ix}), 131.9 (C-5^{ix}), 127.5 (C-8^{ix}), 127.1 (C-4a^{ix}), 126.1 (C-2^{iv}, C-6^{iv}), 125.3 (C-7^{ix}), 123.8 (C-3^{iii}, C-5^{iii}), 121.4 (C-2^{iii}, C-6^{iii}), 117.4 (C-3^{ix}), 112.6 (C-3^{iv}, C-5^{iv}), 107.1 (C-1^{ix}), 57.8 (C-2^{viii}), 55.6 (C-1^{ii}), 52.7 (C-1), 48.3 (C-1^{v}), 45.9 (C-1^{vii}), 42.2 (C-3), 40.1 (NCH_3), 39.8 (C-5^{ii}), 36.1/36.0 (C-2^{v}/C-3^{i}), 33.2 (C-2), 32.6/32.4 (C-1^{i}/C-2^{ii}), 30.2 (C-4^{ii}), 26.5 ($COCH_3$), 24.1 (C-3^{ii}), 23.9 (C-2^{i}), 12.6 (C-2^{vii}); **IR** (ATR): 3269, 2933, 1704, 1595, 1509, 1248, 1136 cm^{-1}; **HRMS** (ESI+) calcd. for [$C_{50}H_{59}N_9O_{10}$+H]: 946.4458; found: 946.4492. **COSY** and **^{1}H/^{13}C** correlation were recorded.

Synthesis of 9*H*-fluoren-9-ylmethyl *N*-{(5*S*)-6-[4-((*E*)-{4-[[2-(allyloxy)ethyl](ethyl)amino]phenyl}-1-diazenyl)anilino]-5-amino-6-oxohexyl}carbamate, 96

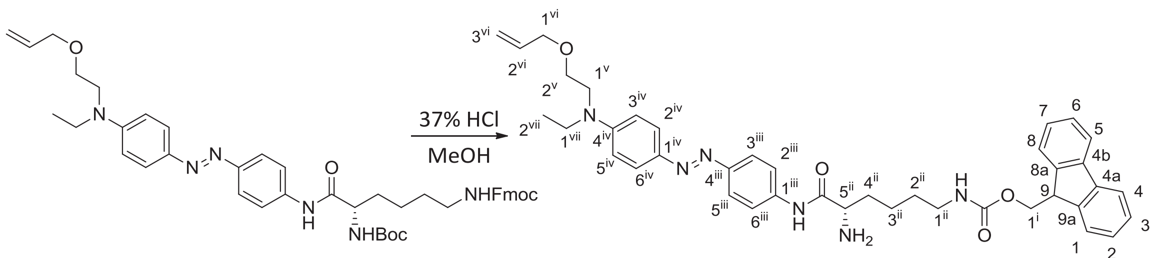

73 **96**

To a stirred solution of **73** (665 mg, 0.86 mmol) in MeOH (33 ml), 37% HCl (11 ml, 0.11 mmol) was added. The reaction mixture was stirred 1 h, when TLC analysis (hexanes/EtOAc, 1:1) showed no presence of starting material, and concentrated under vacuum. The mixture was neutralized with a saturated aqueous $NaHCO_3$ solution, was diluted with EtOAc (30 ml) and dried over anhydrous $MgSO_4$. The solvent was evaporated under reduced pressure. Purification of the residue by column chromatography (from CH_2Cl_2 to CH_2Cl_2/MeOH/NH_3, 95:5:1) furnished amine **96** (197 mg, 0.29 mmol, 93% yield) as an orange solid.

Physical and spectroscopic data of **96**

Mp = 35-42 ^{o}C (from CH_2Cl_2); **[α]$_D^{20}$** = 42.8 (*c* 0.34, $CHCl_3$); **^{1}H-NMR** (250 MHz, $CDCl_3$): δ 9.67 (br s, 1H, C-1^{iii}NH), 7.78-7.68 (m, 8H, H-2^{iv}, H-6^{iv}, H-3^{iii}, H-5^{iii}, H-2^{iii}, H-6^{iii}, H-4, H-5), 7.59 (d, $J_{1,2}$ = $J_{8,7}$ = 7.5 Hz, 2H, H-1, H-8), 7.39 (t, $J_{3,2}$ = $J_{3,4}$ = $J_{6,7}$ = $J_{6,5}$ = 7.5 Hz, 2H, H-3, H-6), 7.30 (td, $J_{2,3}$ = $J_{2,1}$ = $J_{7,8}$ = $J_{7,6}$ = 7.5 Hz, $J_{2,4}$ = $J_{7,5}$ = 1.2 Hz, 2H, H-2, H-7), 6.74 (d, $J_{3^{iv},2^{iv}}$ = $J_{5^{iv},6^{iv}}$ = 9.2 Hz, 2H, H-3^{iv}, H-5^{iv}), 5.91 (ddt, $J_{2^{vi},3_{trans}^{vi}}$ = 17.0 Hz, $J_{2^{vi},3_{cis}^{vi}}$ = 10.8 Hz, $J_{2^{vi},1^{vi}}$ = 5.4 Hz, 1H, H-2^{vi}), 5.28 (dq, $J_{3_{trans}^{vi},2^{vi}}$ = 17.2 Hz, $J_{3_{trans}^{vi},1^{vi}}$ = J_{gem} = 1.6 Hz, 1H, H-3$_{trans}^{vi}$), 5.19 (dq, $J_{3_{cis}^{vi},2^{vi}}$ = 10.4 Hz, $J_{3_{cis}^{vi},1^{vi}}$ = J_{gem} = 1.6 Hz, 1H, H-3$_{cis}^{vi}$), 4.93 (t, $J_{C\text{-}1^{iii}NH,1^{iii}}$ = 6.0 Hz, 1H, C-1^{iii}NH), 4.40 (d, $J_{1^{i},9}$ = 6.9 Hz, 2H, H-1^{i}), 4.21 (t, $J_{9,1^{i}}$ = 6.9 Hz, 1H, H-9), 4.01 (dt, $J_{1^{vi},2^{vi}}$ = 5.4 Hz, $J_{1^{vi},3_{trans}^{vi}}$ = $J_{1^{vi},3_{cis}^{vi}}$ = 1.6 Hz, 2H, H-1^{vi}), 3.66-3.44 (m, 7H, 2xH-1^{v}, 2xH-2^{v}, 2xH-1^{vii}, H-5^{ii}), 3.21 (m, 2H, H-1^{ii}), 1.96 (m, 1H, H-4^{ii}), 1.70-1.37 (m, 5H, 2xH-2^{ii}, 2xH-3^{ii}, H-4^{ii}), 1.24 (t, $J_{2^{vii},1^{vii}}$ = 7.0 Hz, 3H, H-2^{vii}); **^{13}C-NMR** (62.5 MHz, $CDCl_3$): δ 173.2 (CO, amide), 156.8 (CO, carbamate), 150.2 (C-4^{iv}), 149.4 (C-4^{iii}), 144.2 (C-9a, C-8a), 143.7 (C-1^{iv}), 141.5 (C-4a, C-4b), 139.0 (C-1^{iii}), 134.7 (C-2^{vi}), 127.8 (C-3, C-6), 127.2 (C-2, C-7), 125.2 (C-2^{iv}, C-6^{iv}, C-1, C-8), 123.3 (C-3^{iii}, C-5^{iii}), 120.1/119.6 (C-2^{iii}, C-6^{iii}/C-4, C-5), 117.2 (C-3^{vi}), 111.4 (C-3^{iv}, C-5^{iv}), 72.4 (C-1^{vi}), 67.9 (C-2^{v}), 66.7 (C-1^{i}), 55.6 (C-5^{ii}), 50.4 (C-1^{v}), 47.4 (C-9), 46.0 (C-1^{vii}), 40.8 (C-1^{ii}), 34.5 (C-4^{ii}), 30.0 (C-2^{ii}), 23.0 (C-3^{ii}), 12.4 (C-2^{vii}); **IR** (ATR): 3292, 2924, 2854, 1691, 1595, 1511, 1421, 1246, 1136 cm^{-1}; **HRMS** (ESI+) calcd. for [$C_{40}H_{46}N_6O_4$+Na]: 697.3473; found: 697.3482.

Synthesis of di(*tert*-butyl) (2*R*,4*S*)-2-{4-[((1*S*)-1-{[4-((*E*)-2-{4-[[2-(allyloxy)ethyl](ethyl)amino] phenyl}-1-diazenyl)anilino]carbonyl}-5-{[(9*H*-9-fluorenylmethoxy)carbonyl]amino}pentyl) amino]-4-oxobutyl}-4-[(*tert*-butoxycarbonyl)amino]pentanedioate, 93

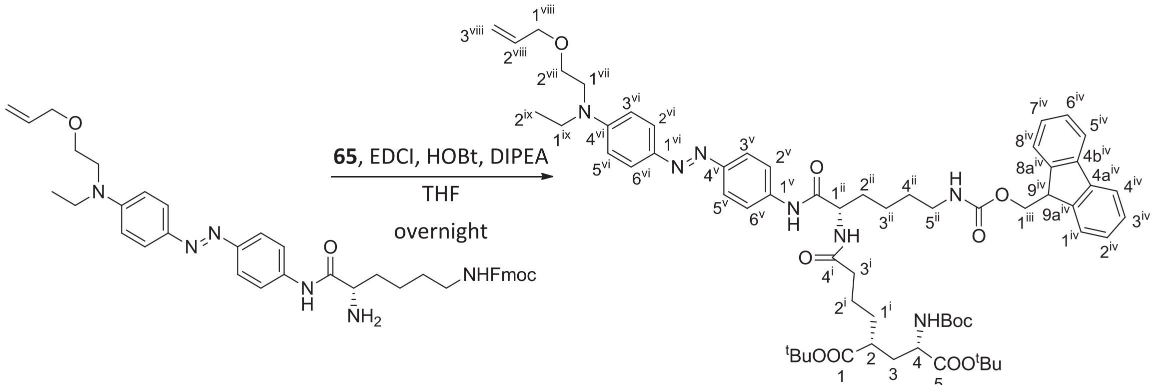

96 **93**

To a stirred solution of amine **96** (232 mg, 0.34 mmol) in dry THF (20 ml) was added a solution of **65** (169 mg, 0.38 mmol), EDCI (86 mg, 0.45 mmol), HOBt (70 mg, 0.52 mmol), DIPEA (175 μl, 1.38 mmol) in dry THF (18 ml) under N_2 atmosphere. The reaction mixture was stirred overnight at rt. Then, the mixture was diluted with EtOAc (40 ml) and washed with water (2x40 ml). The organic layer was dried over anhydrous $MgSO_4$, concentrated under vacuum and the resulting residue was purified by column chromatography (hexanes/EtOAc, 1:9) to afford **93** (335 mg, 0.30 mmol, 88% yield) as an orange solid.

Physical and spectroscopic data of **93**

Mp = 65-72 ^{o}C (from hexanes/EtOAc); $[\alpha]_D^{20}$ = -25.1 (*c* 0.95, $CHCl_3$); **^{1}H-NMR** (400 MHz, $CDCl_3$): δ 9.14 (br s, 1H, C-1^{v}NH), 7.80 (m, 4H, H-2^{vi}, H-6^{vi}, H-3^{v}, H-6^{v}), 7.74 (d, $J_{4^{iv},3^{iv}} = J_{5^{iv},6^{iv}}$ = 7.5 Hz, 2H, H-4^{iv}, H-5^{iv}), 7.66 (d, $J_{2^{v},3^{v}} = J_{6^{v},5^{v}}$ = 8.5 Hz, 2H, H-2^{v}, H-5^{v}), 7.57 (d, $J_{1^{iv},2^{iv}} = J_{8^{iv},7^{iv}}$ = 7.4 Hz, 2H, H-1^{iv}, H-8^{iv}), 7.37 (t, $J_{3^{iv},2^{iv}} = J_{3^{iv},4^{iv}} = J_{6^{iv},7^{iv}} = J_{6^{iv},5^{iv}}$ = 7.5 Hz, 2H, H-3^{iv}, H-6^{iv}), 7.30 (td, $J_{2^{iv},3^{iv}} = J_{2^{iv},1^{iv}} = J_{7^{iv},6^{iv}} = J_{7^{iv},8^{iv}}$ = 7.5 Hz, $J_{2^{iv},4^{iv}} = J_{7^{iv},5^{iv}}$ = 1.2 Hz, 2H, H-2^{iv}, H-7^{iv}), 6.73 (d, $J_{3^{vi},2^{vi}} = J_{5^{vi},6^{vi}}$ = 9.1 Hz, 2H, H-3^{vi}, H-5^{vi}), 6.68 (m, 1H, C-1^{ii}NH), 5.90 (ddt, $J_{2^{viii},3_{trans}^{viii}}$ = 17.0 Hz, $J_{2^{viii},3_{cis}^{viii}}$ = 10.8 Hz, $J_{2^{viii},1^{viii}}$ = 5.4 Hz, 1H, H-2^{viii}), 5.27 (dq, $J_{3_{trans}^{viii},2^{viii}}$ = 17.0 Hz, $J_{3_{trans}^{viii},1^{viii}} = J_{gem}$ = 1.6 Hz, 1H, H-3$_{trans}^{viii}$), 5.22 (m, 2H, C-5^{ii}NH, C-4NH), 5.18 (dq, $J_{3_{cis}^{viii},2^{viii}}$ = 10.8 Hz, $J_{3_{cis}^{viii},1^{viii}} = J_{gem}$ = 1.6 Hz, 1H, H-3$_{cis}^{viii}$), 4.62 (m, 1H, H-1^{ii}), 4.37 (m, 2H, H-1^{iii}), 4.18 (m, 2H, H-9^{iv}, H-4), 4.00 (dt, $J_{1^{viii},2^{viii}}$ = 5.4 Hz, $J_{1^{viii},3_{trans}^{viii}} = J_{1^{viii},3_{cis}^{viii}}$ = 1.6 Hz, 2H, H-1^{viii}), 3.61 (m, 4H, 2xH-2^{vii}, 2xH-1^{vii}), 3.50 (q, $J_{1^{ix},2^{ix}}$ = 7.0 Hz, 2H, H-1^{ix}), 3.19 (m, 2H, H-5^{ii}), 2.36 (m, 1H, H-2), 2.25 (m, 2H, H-3^{i}), 2.16-1.90 (m, 2H, H-3, H-2^{ii}), 1.82-1.53 (m, 8H, H-3, 2xH-1^{i}, 2xH-2^{i}, H-2^{ii}, 2xH-4^{ii}), 1.41 (m, 29H, 2xH-3^{ii}, 3x$C(CH_3)_3$), 1.21 (t, $J_{2^{ix},1^{ix}}$ = 7.0 Hz, 3H, H-2^{ix}); **^{13}C-NMR** (100.6 MHz, $CDCl_3$): δ 174.5/173.5/171.9/170.3 (C-1/C-5/C-4^{i}/CO, amide), 156.8 (CO, carbamate), 155.5 (CO, carbamate), 150.2 (C-4^{vi}), 149.8 (C-4^{v}), 144.1 (C-9a^{iv}, C-8a^{iv}), 143.7 (C-1^{vi}), 141.4 (C-4a^{iv}, C-4b^{iv}), 139.1 (C-1^{v}), 134.6 (C-2^{viii}), 127.8 (C-3^{iv}, C-6^{iv}), 127.2 (C-2^{iv}, C-7^{iv}), 125.1 (C-2^{vi}, C-6^{vi}, C-1^{iv}, C-8^{iv}), 123.2 (C-3^{v}, C-5^{v}), 120.2/120.1 (C-2^{v}, C-6^{v}/C-4^{iv}, C-5^{iv}), 117.2 (C-3^{viii}), 111.3 (C-3^{vi}, C-5^{vi}), 82.0 ($\mathit{C}(CH_3)_3$), 81.0 ($\mathit{C}(CH_3)_3$), 79.7 ($\mathit{C}(CH_3)_3$), 72.4 (C-1^{viii}), 67.8 (C-2^{vii}), 66.7 (C-1^{iii}), 53.9 (C-1^{ii}), 52.8 (C-4), 50.4 (C-1^{vii}), 47.4 (C-9^{iv}), 45.9 (C-1^{ix}), 42.4 (C-2), 40.4 (C-5^{ii}), 36.1 (C-3^{i}), 34.7 (C-3), 32.1 (C-1^{i}), 31.2 (C-2^{ii}), 29.6 (C-4^{ii}), 28.4 ($C(\mathit{C}H_3)_3$), 28.2 ($C(\mathit{C}H_3)_3$), 28.1 ($C(\mathit{C}H_3)_3$), 23.2 (C-3^{ii}), 22.6 (C-2^{i}), 12.3 (C-2^{ix}); **IR** (ATR): 3301, 2932, 1700, 1595, 1511, 1391, 1365, 1245, 1139 cm^{-1}; **HRMS** (ESI+) calcd. for [$C_{62}H_{83}N_7O_{11}$+Na]: 1124.6043; found: 1124.6028.

Synthesis of di(*tert*-butyl) (2*R*,4*S*)-2-{4-[((1*S*)-1-{[4-((*E*)-[4-[[2-(allyloxy)ethyl](ethyl)amino] phenyl}-1-diazenyl)anilino]carbonyl}-5-aminopentyl)amino]-4-oxobutyl}-4-[(*tert*-butoxy carbonyl)amino]pentanedioate, 97

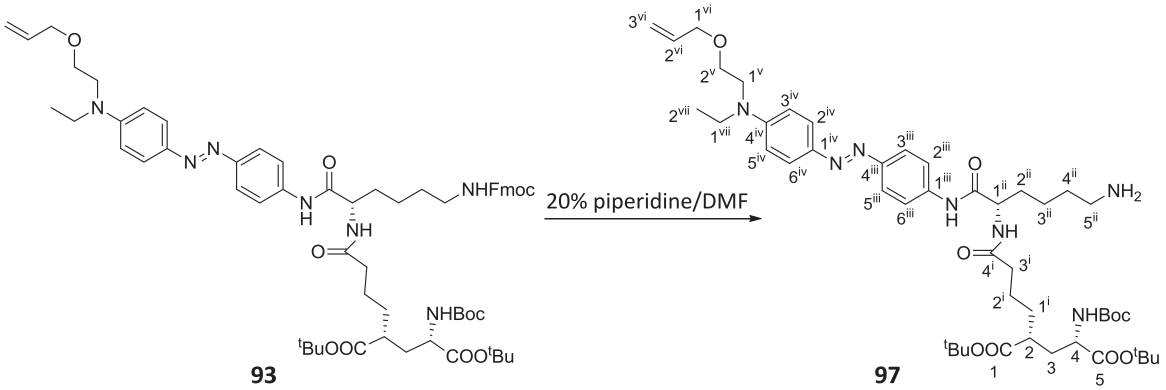

A commercially available solution of 20% piperidine in DMF (6.5 ml) was added to compound **93** (290 mg, 0.26 mmol). After 1 h of stirring at rt, TLC analysis (EtOAc/MeOH, 95:5) showed no presence of starting material. The mixture was diluted with water (8.0 ml) and washed with CH_2Cl_2 (3x5 ml). The organic extracts were dried over anhydrous $MgSO_4$ and concentrated under vacuum. The crude product was purified by column chromatography (from EtOAc to EtOAc/MeOH/NH_3, 94:5:1) to obtain amine **97** (148 mg, 0.17 mmol, 64% yield) as an orange solid.

Physical and spectroscopic data of **97**

Mp = 55-63 ºC (from EtOAc); $[\alpha]_D^{20}$ = -35.3 (*c* 1.00, $CHCl_3$); **^{1}H-NMR** (250 MHz, $CDCl_3$): δ 9.38 (br s, 1H, C-1^{iii}NH), 7.80 (m, 4H, H-2^{iv}, H-6^{iv}, H-3^{iii}, H-5^{iii}), 7.65 (d, $J_{2^{iii},3^{iii}} = J_{6^{iii},5^{iii}}$ = 8.8 Hz, 2H, H-2^{iii}, H-6^{iii}), 6.73 (d, $J_{3^{iv},2^{iv}} = J_{5^{iv},6^{iv}}$ = 9.1 Hz, 2H, H-3^{iv}, H-5^{iv}), 6.68 (m, 1H, C-1^{ii}NH), 5.90 (ddt, $J_{2^{vi},3_{trans}^{vi}}$ = 17.0 Hz, $J_{2^{vi},3_{cis}^{vi}}$ = 10.4 Hz, $J_{2^{vi},1^{vi}}$ = 5.4 Hz, 1H, H-2^{vi}), 5.58 (m, 1H, C-4NH), 5.27 (dq, $J_{3_{trans}^{vi},2^{vi}}$ = 17.0 Hz, $J_{3_{trans}^{vi},1^{vi}} = J_{gem}$ = 1.4 Hz, 1H, H-3$_{trans}^{vi}$), 5.18 (dq, $J_{3_{cis}^{vi},2^{vi}}$ = 10.4 Hz, $J_{3_{cis}^{vi},1^{vi}} = J_{gem}$ = 1.4 Hz, 1H, H-3$_{cis}^{vi}$), 4.61 (m, 1H, H-1^{ii}), 4.18 (m, 1H, H-4), 4.00 (dt, $J_{1^{vi},2^{vi}}$ = 5.4 Hz, $J_{1^{vi},3_{trans}^{vi}} = J_{1^{vi},3_{cis}^{vi}}$ = 1.4 Hz, 2H, H-1^{vi}), 3.62 (m, 4H, 2xH-2^{v}, 2xH-1^{v}), 3.51 (q, $J_{1^{vii},2^{vii}}$ = 7.0 Hz, 2H, H-1^{vii}), 2.76 (m, 2H, H-5^{ii}), 2.40 (m, 1H, H-2), 2.27 (m, 2H, H-3^{i}), 2.07-1.82 (m, 4H, H-3, H-2^{ii}, NH_2), 1.90-1.50 (m, 8H, H-3, 2xH-1^{i}, 2xH-2^{i}, 2xH-2^{ii}, 2xH-4^{ii}), 1.42 (m, 29H, 2xH-3^{ii}, 3xC(CH_3)$_3$), 1.20 (t, $J_{2^{vii},1^{vii}}$ = 7.0 Hz, 3H, H-2^{vii}); **^{13}C-NMR** (62.5 MHz, $CDCl_3$): δ 174.4/173.4/171.9/170.8 (C-1/C-5/C-4^{i}/CO, amide), 155.6 (CO, carbamate), 150.1 (C-4^{iv}), 149.6 (C-4^{iii}), 143.5 (C-1^{iv}), 139.3 (C-1^{iii}), 134.6 (C-2^{vi}), 125.1 (C-2^{iv}, C-6^{iv}), 123.0 (C-3^{iii}, C-5^{iii}), 120.2 (C-2^{iii}, C-6^{iii}), 117.0 (C-3^{vi}), 111.3 (C-3^{iv}, C-5^{iv}), 81.8 (*C*(CH_3)$_3$), 80.9 (*C*(CH_3)$_3$), 79.6 (*C*(CH_3)$_3$), 72.3 (C-1^{vi}), 67.8 (C-2^{v}), 53.9 (C-1^{ii}), 52.8 (C-4), 50.3 (C-1^{v}), 45.8 (C-1^{vii}), 42.3 (C-2), 41.2 (C-5^{ii}), 35.9 (C-3^{i}), 34.6 (C-3), 32.1 (C-1^{i}/C-2^{ii}), 29.5 (C-4^{ii}), 28.4 (C(*C*H_3)$_3$), 28.1 (C(*C*H_3)$_3$), 28.0 (C(*C*H_3)$_3$), 22.7 (C-

2^{i}, C-3^{ii}), 12.3 (C-2^{vii}); **IR** (ATR): 3276, 2928, 1715, 1595, 1512, 1365, 1246, 1138 cm^{-1}; **HRMS** (ESI+) calcd. for [$C_{47}H_{73}N_7O_9$+H]: 880.5543; found: 880.5557.

Synthesis of di(*tert*-butyl) (2*R*,4*S*)-2-{4-[((1*S*)-5-(acetylamino)-1-{[4-((*E*)-[4-[[2-(allyloxy)ethyl](ethyl)amino]phenyl}-1-diazenyl)anilino]carbonyl}pentyl)amino]-4-oxobutyl}-4-[(*tert*-butoxycarbonyl)amino]pentanedioate, 94

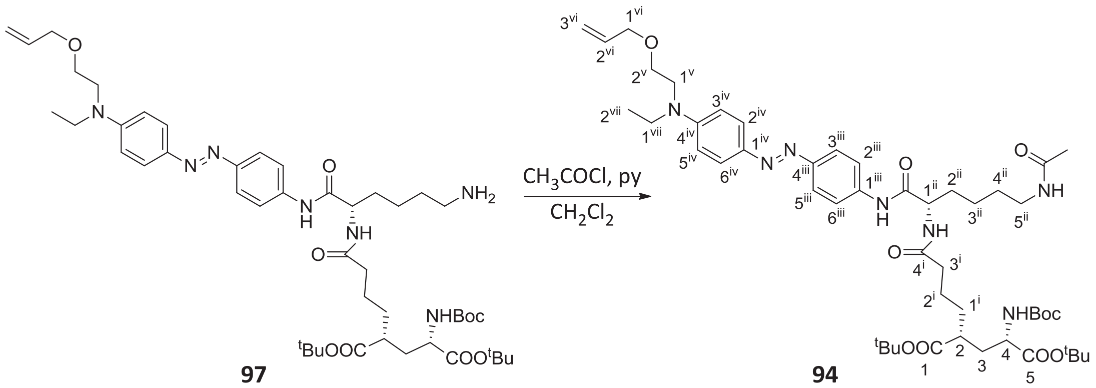

To an ice-cooled of amine **97** (128 mg, 0.15 mmol) and pyridine (11 μl, 0.13 mmol) in dry THF (33 ml), acetyl chloride (3 μl, 39 μmol) was added dropwise under N_2 atmosphere. After 2 h of stirring at rt, TLC analysis (EtOAc/MeOH, 95:5) showed no presence of starting material. The mixture was diluted with EtOAc (10 ml) and washed with 5% HCl (10 ml), dried over $MgSO_4$ and concentrated under vacuum. Purification by column chromatography (EtOAc) provided compound **94** (92 mg, 0.10 mmol, 69% yield) as an orange solid.

Physical and spectroscopic data of **94**

Mp = 62-67 ^{o}C (from EtOAc); **[α]$_D$^{20}** = -29.7 (*c* 0.83, $CHCl_3$); **^{1}H-NMR** (400 MHz, $CDCl_3$): δ 9.40 (br s, 1H, C-1^{iii}NH), 7.79 (m, 4H, H-2^{iv}, H-6^{iv}, H-3^{iii}, H-5^{iii}), 7.67 (d, $J_{2^{iii},3^{iii}} = J_{6^{iii},5^{iii}}$ = 8.8 Hz, 2H, H-2^{iii}, H-6^{iii}), 6.88 (m, 1H, C-1^{ii}NH), 6.72 (d, $J_{3^{iv},2^{iv}} = J_{5^{iv},6^{iv}}$ = 9.2 Hz, 2H, H-3^{iv}, H-5^{iv}), 6.27 (m, 1H, C-5^{ii}NH), 5.89 (ddt, $J_{2^{vi},3_{trans}^{vi}}$ = 17.0 Hz, $J_{2^{vi},3_{cis}^{vi}}$ = 10.4 Hz, $J_{2^{vi},1^{vi}}$ = 5.5 Hz, 1H, H-2^{vi}), 5.26 (dq, $J_{3_{trans}^{vi},2^{vi}}$ = 17.2 Hz, $J_{3_{trans}^{vi},1^{vi}} = J_{gem}$ = 1.4 Hz, 1H, H-3$_{trans}^{vi}$), 5.21 (m, 1H, C-4NH), 5.17 (dq, $J_{3_{cis}^{vi},2^{vi}}$ = 10.4 Hz, $J_{3_{cis}^{vi},1^{vi}} = J_{gem}$ = 1.4 Hz, 1H, H-3$_{cis}^{vi}$), 4.63 (m, 1H, H-1^{ii}), 4.15 (m, 1H, H-4), 3.99 (dt, $J_{1^{vi},2^{vi}}$ = 5.5 Hz, $J_{1^{vi},3_{trans}^{vi}} = J_{1^{vi},3_{cis}^{vi}}$ = 1.4 Hz, 2H, H-1^{vi}), 3.60 (m, 4H, 2xH-2^{v}, 2xH-1^{v}), 3.49 (q, $J_{1^{vii},2^{vii}}$ = 7.0 Hz, 2H, H-1^{vii}), 3.24 (m, 2H, H-5^{ii}), 2.37 (m, 1H, H-2), 2.40 (m, 2H, H-3^{i}), 2.15-1.88 (m, 5H, H-3, H-2^{ii}, $COCH_3$), 1.84-1.50 (m, 6H, H-3, 2xH-1^{i}, 2xH-2^{i}, H-2^{ii}), 1.56 (m, 2H, H-4^{ii}), 1.42 (m, 29H, 3xH-3^{ii}, 3x$C(CH_3)_3$), 1.20 (t, $J_{2^{vii},1^{vii}}$ = 7.0 Hz, 3H, H-2^{vii}); **^{13}C-NMR** (100.6 MHz, $CDCl_3$): δ 174.5/173.7/171.9/170.9 (C-1/C-5/C-4^{i}/CO, amide), 170.5 ($COCH_3$), 155.5 (CO, carbamate), 150.2 (C-4^{iv}), 149.7 (C-4^{iii}), 143.5 (C-1^{iv}), 139.2 (C-1^{iii}), 134.6 (C-2^{vi}), 125.1 (C-2^{iv}, C-6^{iv}), 123.1 (C-3^{iii}, C-5^{iii}), 120.2 (C-2^{iii}, C-6^{iii}), 117.2 (C-3^{vi}), 111.3 (C-3^{iv}, C-5^{iv}), 82.0 (*C*(CH_3)$_3$), 81.1 (*C*(CH_3)$_3$), 79.7 (*C*(CH_3)$_3$), 72.3 (C-1^{vi}), 67.8 (C-2^{v}), 53.8 (C-1^{ii}), 52.8 (C-4), 50.4 (C-1^{v}), 45.9 (C-1^{vii}), 42.5 (C-2), 38.8 (C-5^{ii}), 36.1 (C-3^{i}), 34.7 (C-3), 32.3/31.3 (C-1^{i}/C-2^{ii}), 29.0 (C-4^{ii}), 28.4 (C(*C*H_3)$_3$), 28.2 (C(*C*H_3)$_3$), 28.1 (C(*C*H_3)$_3$), 23.4 (CO*C*H_3, C-3^{ii}), 22.6 (C-2^{i}), 12.4 (C-2^{vii}); **IR** (ATR): 3302, 2925, 1719, 1595, 1501, 1365, 1246, 1151 cm^{-1}; **HRMS** (ESI+) calcd. for [$C_{49}H_{75}N_7O_{10}$+Na]: 944.5468; found: 944.5475. **^{1}H/^{13}C** correlation was recorded.

Synthesis of di(*tert*-butyl) (2*R*,4*S*)-2-{4-[((1*S*)-5-(acetylamino)-1-{[4-((*E*)-{4-[ethyl(2-hydroxy ethyl)amino]phenyl}-1-diazenyl)anilino]carbonyl}pentyl)amino]-4-oxobutyl}-4-[(*tert*-butoxy carbonyl)amino]pentanedioate, 98

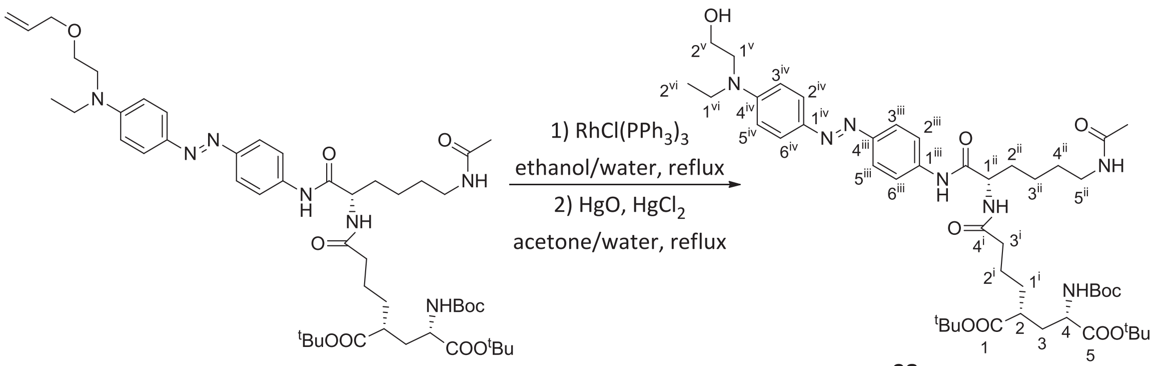

94 **98**

RhCl(PPh_3)$_3$ (19 mg, 21 μmol) was added to a solution of allyl ether **94** (160 mg, 0.17 mmol) in a 1:10 mixture of water and ethanol (18 ml) and warmed up to 100 ºC. The mixture was stirred for 2 h at this temperature, cooled, and then the solvents were removed under vacuum. The residue was dissolved in a 9:1 mixture of water and acetone (64 ml) and HgO (71 mg, 0.33 mmol) and $HgCl_2$ (71 mg, 0.26 mmol) were added. The mixture was heated at the reflux temperature during 1.5 h. Then, after cooling it was filtered through a Celite© pad and concentrated under reduce pressure. The residue was dissolved in CH_2Cl_2 (50 ml), washed with aqueous 50% KI (30 ml), brine (30 ml), dried over anhydrous $MgSO_4$ and concentrated under vacuum. Purification by column chromatography (EtOAc) gave an orange solid identified as **98** (73 mg, 83 μmol, 48% yield).

<u>Physical and spectroscopic data of **98**</u>

Mp = 75-85 ºC (from EtOAc); **[α]$_D^{20}$** = -14.7 (*c* 0.92, $CHCl_3$); **^{1}H-NMR** (400 MHz, $CDCl_3$): δ 9.27 (br s, 1H, C-1^{iii}NH), 7.78 (m, 4H, H-2^{iv}, H-6^{iv}, H-3^{iii}, H-5^{iii}), 7.65 (d, $J_{2^{iii},3^{iii}} = J_{6^{iii},5^{iii}}$ = 8.8 Hz, 2H, H-2^{iii}, H-6^{iii}), 6.81 (d, $J_{C\text{-}1^{ii}NH,1^{ii}}$ = 7.1 Hz, 1H, C-1^{ii}NH), 6.75 (d, $J_{3^{iv},2^{iv}} = J_{5^{iv},6^{iv}}$ = 9.2 Hz, 2H, H-3^{iv}, H-5^{iv}), 6.17 (t, $J_{C\text{-}5^{ii}NH,5^{ii}}$ = 5.7 Hz, 1H, C-5^{ii}NH), 5.18 (d, $J_{C\text{-}4NH,4}$ = 8.3 Hz, 1H, C-4NH), 4.59 (m, 1H, H-1^{ii}), 4.16 (m, 1H, H-4), 3.84 (t, $J_{2^{v},1^{v}}$ = 5.9 Hz, 2H, H-2^{v}), 3.55 (t, $J_{1^{v},2^{v}}$ = 5.9 Hz, 2H, H-1^{v}), 3.50 (q, $J_{1^{vi},2^{vi}}$ = 7.0 Hz, 2H, H-1^{vi}), 3.22 (m, 2H, H-5^{ii}), 2.40 (m, 1H, H-2), 2.26 (m, 2H, H-3^{i}), 2.14-1.88 (m, 5H, H-3, H-2^{ii}, $COCH_3$), 1.84-1.50 (m, 6H, H-3, 2xH-1^{i}, 2xH-2^{i}, H-2^{ii}), 1.56 (m, 2H, H-4^{ii}), 1.45 (m, 29H, 2xH-3^{ii}, 3x$C(CH_3)_3$), 1.20 (t, $J_{2^{vi},1^{vi}}$ = 7.0 Hz, 3H, H-2^{vi}); **^{13}C-NMR** (100.6 MHz, $CDCl_3$): δ 174.5/173.8/171.9/ 170.9 (C-1/C-5/C-4^{i}/CO, amide), 170.5 ($COCH_3$), 155.5 (CO, carbamate), 150.5 (C-4^{iv}), 149.7 (C-4^{iii}), 143.8 (C-1^{iv}), 139.2 (C-1^{iii}), 125.1 (C-2^{iv}, C-6^{iv}), 123.2 (C-3^{iii}, C-5^{iii}), 120.2 (C-2^{iii}, C-6^{iii}), 111.7 (C-3^{iv}, C-5^{iv}), 82.0 ($C(CH_3)_3$), 81.1 ($C(CH_3)_3$), 79.8 ($C(CH_3)_3$), 60.3 (C-2^{v}), 53.9 (C-1^{ii}), 52.9 (C-4), 52.6 (C-1^{v}), 45.9 (C-1^{vi}), 42.5 (C-2), 38.8 (C-5^{ii}), 36.1 (C-3^{i}), 34.8 (C-3), 32.3/31.0 (C-1^{i}/C-2^{ii}), 29.0 (C-4^{ii}), 28.5 ($C(CH_3)_3$), 28.2 ($C(CH_3)_3$), 28.1 ($C(CH_3)_3$), 23.4 ($COCH_3$, C-3^{ii}), 22.6 (C-2^{i}), 12.2 (C-2^{vi}); **IR** (ATR): 3288, 2930, 1699, 1650, 1513, 1366, 1248, 1152 cm^{-1}; **HRMS** (ESI+) calcd. for [$C_{46}H_{71}N_7O_{10}$+Na]: 904.5155; found: 904.5165.

Synthesis of di(*tert*-butyl) (2*R*,4*S*)-2-{4-[((1*S*)-5-(acetylamino)-1-{[4-((*E*)-{4-[(2-((1*R*,2*S*,6*R*,7*S*)-3,5-dioxo-10-oxa-4-azatricyclo[5.2.1.0^{2,6}]dec-8-en-4-yl]ethyl)(ethyl)amino]phenyl}-1-diazenyl) anilino]carbonyl}pentyl)amino]-4-oxobutyl}-4-[(*tert*-butoxycarbonyl)amino]pentanedioate, 95

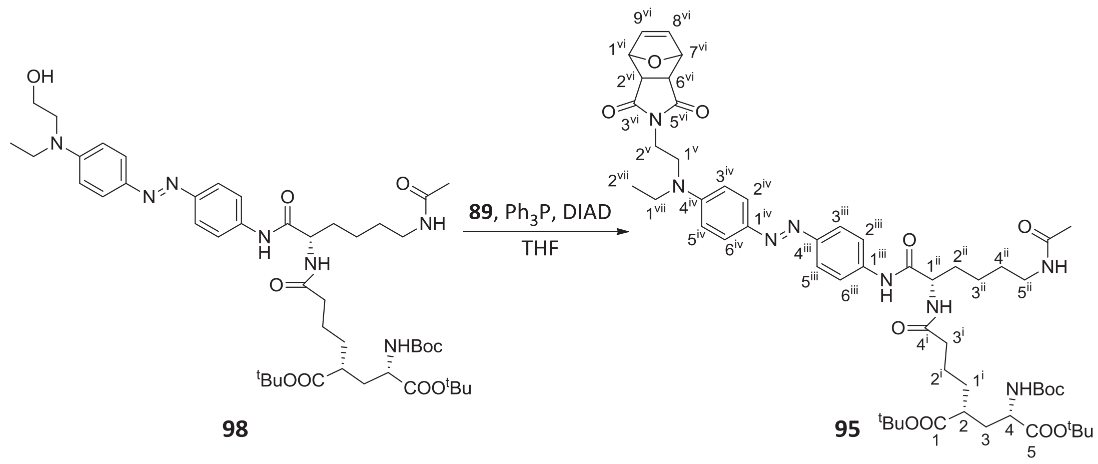

98 95

To an ice-cooled solution of alcohol **98** (75 mg, 85 μmol), **89** (70 mg, 0.42 mmol), Ph_3P (112 mg, 0.43 mmol) in dry THF (7.5 ml) was added DIAD (84 μl, 0.43 mmol) under N_2 atmosphere over 2 min. The reaction mixture was stirred overnight at rt. Then, the solvent was evaporated under vacuum and the residue was purified by column chromatography (from EtOAc to EtOAc/MeOH, 95:5) to provide compound **95** (81 mg, 79 μmol, 92% yield) as an orange solid.

Physical and spectroscopic data of **95**

Mp = 90-96 ^{o}C (from EtOAc); **[α]$_D$^{20}** = -32.9 (*c* 1.00, $CHCl_3$); **^{1}H-NMR** (400 MHz, $CDCl_3$): δ 9.42 (br s, 1H, C-1^{iii}NH), 7.80 (m, 4H, H-2^{iv}, H-6^{iv}, H-3^{iii}, H-5^{iii}), 7.67 (d, $J_{2^{iii},3^{iii}} = J_{6^{iii},5^{iii}}$ = 8.8 Hz, 2H, H-2^{iii}, H-6^{iii}), 6.91 (m, 1H, C-1^{ii}NH), 6.80 (d, $J_{3^{iv},2^{iv}} = J_{5^{iv},6^{iv}}$ = 9.0 Hz, 2H, H-3^{iv}, H-5^{iv}), 6.38 (m, 2H, H-8^{vi}, H-9^{vi}), 6.28 (m, 1H, C-5^{ii}NH), 5.25 (m, 2H, H-1^{vi}, H-7^{vi}), 4.60 (m, 1H, H-1^{ii}), 4.15 (m, 1H, H-4), 3.70 (t, $J_{2^{v},1^{v}}$ = 7.1

Hz, 2H, H-2^{v}), 3.52 (t, $J_{1^{v},2^{v}}$ = 7.1 Hz, 2H, H-1^{v}), 3.45 (q, $J_{1^{vii},2^{vii}}$ = 7.0 Hz, 2H, H-1^{vii}), 3.23 (m, 2H, H-5^{ii}), 2.75 (m, 2H, H-2^{vi}, H-6^{vi}), 2.34 (m, 1H, H-2), 2.26 (m, 2H, H-3^{i}), 2.23-1.88 (m, 5H, H-3, H-2^{ii}, $COCH_3$), 1.84-1.50 (m, 6H, H-3, 2xH-1^{i}, 2xH-2^{i}, H-2^{ii}), 1.52 (m, 2H, H-4^{ii}), 1.42 (m, 29H, 2xH-3^{ii}, 3x$C(CH_3)_3$), 1.20 (t, $J_{2^{vii},1^{vii}}$ = 7.0 Hz, 3H, H-2^{vii}); **^{13}C-NMR** (100.6 MHz, $CDCl_3$): δ 176.3 (C-3^{vi}, C-5^{vi}), 174.5/173.8/171.9/171.3 (C-1/C-5/C-4^{i}/CO, amide), 170.5 (COCH$_3$), 155.5 (CO, carbamate), 149.9 (C-4^{iv}), 149.5 (C-4^{iii}), 143.7 (C-1^{iv}), 139.3 (C-1^{iii}), 136.6 (C-8^{vi}, C-9^{vi}), 125.2 (C-2^{iv}, C-6^{iv}), 123.2 (C-3^{iii}, C-5^{iii}), 120.1 (C-2^{iii}, C-6^{iii}), 111.4 (C-3^{iv}, C-5^{iv}), 82.1 ($C(CH_3)_3$), 81.1 ($C(CH_3)_3$), 80.9 (C-1^{vi}, C-7^{vi}), 79.8 ($C(CH_3)_3$), 53.8 (C-1^{ii}), 52.7 (C-4), 47.6 (C-2^{vi}, C-6^{vi}), 46.8 (C-1^{v}), 45.0 (C-1^{vii}), 42.4 (C-2), 38.7 (C-5^{ii}), 36.1 (C-3^{i}, C-2^{v}), 34.7 (C-3), 32.0/31.0 (C-1^{i}/C-2^{ii}), 28.9 (C-4^{ii}), 28.4 ($C(CH_3)_3$), 28.2 ($C(CH_3)_3$), 28.0 ($C(CH_3)_3$), 23.4/23.3 ($COCH_3$/C-3^{ii}), 22.5 (C-2^{i}), 12.4 (C-2^{vii}); **IR** (ATR): 3286, 1774, 1595, 1512, 1392, 1366, 1247, 1151 cm^{-1}; **HRMS** (ESI+) calcd. for [$C_{54}H_{76}N_8O_{12}$+Na]: 1051.5475; found: 1051.5500.

Synthesis of di(*tert*-butyl) (2*R*,4*S*)-2-{4-[((1*S*)-5-(acetylamino)-1-{[4-((*E*)-{4-[[2-(2,5-dioxo-2,5-dihydro-*1H*-pyrrol-1-yl)ethyl](ethyl)amino]phenyl}-1-diazenyl)anilino]carbonyl}pentyl)amino]-4-oxobutyl}-4-[(*tert*-butoxycarbonyl)amino]pentanedioate, 99

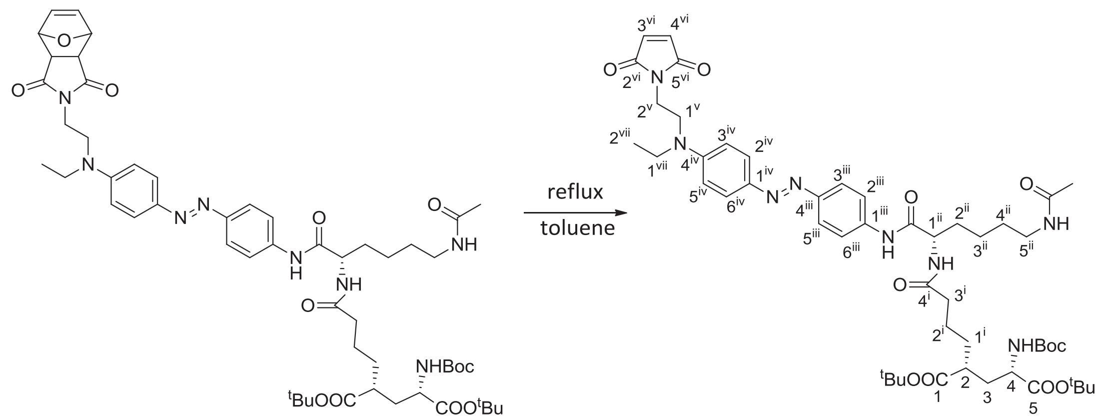

95 **99**

To a stirred solution of **95** (81 mg, 79 μmol) in toluene (4.0 ml) was heated at the reflux temperature for 5 h, when TLC analysis (EtOAc/MeOH, 95:5) showed no presence of starting material. The solvent was removed under vacuum and the residue was purified by column chromatography (from EtOAc to EtOAc/MeOH, 98:2) to provide **99** (68 mg, 71 μmol, 90%) as an orange solid.

<u>Physical and spectroscopic data of **99**</u>

Mp = 72-84 ^{o}C (from EtOAc); **$[\alpha]_D^{20}$** = -28.0 (*c* 1.20, $CHCl_3$); **^{1}H-NMR** (400 MHz, $CDCl_3$): δ 9.23 (br s, 1H, C-1^{iii}NH), 7.80 (m, 4H, H-2^{iv}, H-6^{iv}, H-3^{iii}, H-5^{iii}), 7.67 (d, $J_{2^{iii},3^{iii}} = J_{6^{iii},5^{iii}}$ = 8.8 Hz, 2H, H-2^{iii}, H-6^{iii}), 6.78 (d, $J_{3^{iv},2^{iv}} = J_{5^{iv},6^{iv}}$ = 9.0 Hz, 2H, H-3^{iv}, H-5^{iv}), 6.66 (s, 2H, H-3^{vi}, H-4^{vi}), 6.12 (m, 1H, C-5^{ii}NH), 5.16

(d, $J_{C\text{-}4NH,4}$ = 6.9 Hz, 1H, C-4NH), 4.59 (m, 1H, H-1^{ii}), 4.15 (m, 1H, H-4), 3.75 (t, $J_{2^{v},1^{v}}$ = 7.0 Hz, 2H, H-2^{v}), 3.56 (t, $J_{1^{v},2^{v}}$ = 7.0 Hz, 2H, H-1^{v}), 3.46 (q, $J_{1^{vii},2^{vii}}$ = 7.0 Hz, 2H, H-1^{vii}), 3.23 (m, 2H, H-5^{ii}), 2.37 (m, 1H, H-2), 2.30 (m, 2H, H-3^{i}), 2.14-1.88 (m, 5H, H-3, H-2^{ii}, $COCH_3$), 1.84-1.60 (m, 6H, H-3, 2xH-1^{i}, 2xH-2^{i}, H-2^{ii}), 1.56 (m, 2H, H-4^{ii}), 1.43 (m, 29H, 2xH-3^{ii}, 3x$C(CH_3)_3$), 1.21 (t, $J_{2^{vii},1^{vii}}$ = 7.0 Hz, 3H, H-2^{vii}); **^{13}C-NMR** (100.6 MHz, $CDCl_3$): δ 174.5/173.8/171.9 (C-1/C-5/C-4^{i}/CO, amide), 170.7 (C-2^{vi}, C-5^{vi}), 170.9 (C-1/C-5/C-4^{i}/CO, amide), 170.4 ($COCH_3$), 155.5 (CO, carbamate), 149.9 (C-4^{iv}), 149.7 (C-4^{iii}), 143.9 (C-1^{iv}), 139.4 (C-1^{iii}), 134.3 (C-3^{vi}, C- 4^{vi}), 125.2 (C-2^{iv}, C-6^{iv}), 123.2 (C-3^{iii}, C-5^{iii}), 120.2 (C-2^{iii}, C-6^{iii}), 111.6 (C-3^{iv}, C-5^{iv}), 82.1 ($C(CH_3)_3$), 81.1 ($C(CH_3)_3$), 79.8 ($C(CH_3)_3$), 53.8 (C-1^{ii}), 52.8 (C-4), 47.8 (C-1^{v}), 45.0 (C-1^{vii}), 42.5 (C-2), 38.6 (C-5^{ii}), 36.1 (C-3^{i}), 35.1 (C-2^{v}), 34.8 (C-3), 32.0/30.8 (C-1^{i}/C-2^{ii}), 29.0 (C-4^{ii}), 28.5 ($C(CH_3)_3$), 28.2 ($C(CH_3)_3$), 28.1 ($C(CH_3)_3$), 23.4/23.3 ($COCH_3$/C-3^{ii}), 22.5 (C-2^{i}), 12.5 (C-2^{vii}); **IR** (ATR): 3294, 2975, 2932, 1705, 1595, 1512, 1366, 1246, 1151 cm^{-1}; **HRMS** (ESI+) calcd. for [$C_{50}H_{72}N_8O_{11}$+Na]: 983.5213; found: 983.5227.

Synthesis of (1*S*,3*R*)-7-[((1*S*)-5-(acetylamino)-1-[4-((*E*)-{4-[[2-(2,5-dioxo-2,5-dihydro-1*H*-1-pyrrolyl)ethyl](ethyl)amino]phenyl-1-diazenyl)anilino]carbonylpentyl)amino]-1,3-dicarboxy-7-oxoheptylammonium 2,2,2-trifluoroacetate, 23

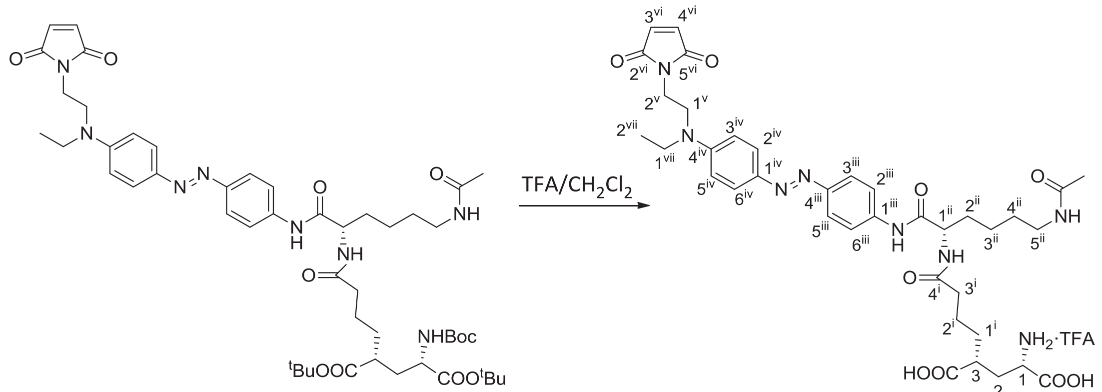

99 **23**

To a stirred solution of compound **99** (68 mg, 71 μmol) in CH_2Cl_2 (11 ml), trifluoroacetic acid (5.7 ml, 74.0 mmol) was added. The mixture was stirred at rt until the starting material was consumed as judged by TLC analysis (EtOAc/MeOH, 9:1). Then, the mixture was concentrated under vacuum. The resulting solid was triturated with diethyl ether (2x8 ml) to furnish **23** (56 mg, 65 μmol, 92%) as a purple solid.

<u>Physical and spectroscopic data of **23**</u>

$[\alpha]_D^{20}$ = -25.5 (*c* 0.50, MeOH); **^{1}H-NMR** (400 MHz, MeOH-d$_4$): δ 7.78 (m, 4H, H-3^{iii}, H-5^{iii}, H-2^{iv}, H-6^{iv}), 7.71 (d, $J_{2^{iii},3^{iii}} = J_{6^{iii},5^{iii}}$ = 9.0 Hz, 2H, H-2^{iii}, H-6^{iii}), 6.85 (d, $J_{3^{iv},2^{iv}} = J_{5^{iv},6^{iv}}$ = 9.3 Hz, 2H, H-3^{iv}, H-5^{iv}), 6.78 (s, 2H, H-3^{vi}, H-4^{vi}), 4.45 (dd, $J_{1^{ii},2^{ii}}$ = 8.7 Hz, $J_{1^{ii},2^{ii}}$ = 5.5 Hz, 1H, H-1^{ii}), 4.01 (m, $J_{1,2}$ = 8.1 Hz, $J_{1,2}$ = 5.9 Hz, 1H, H-1), 3.75 (t, $J_{2^{v},1^{v}}$ = 6.8 Hz, 2H, H-2^{v}), 3.62 (t, $J_{1^{v},2^{v}}$ = 6.8 Hz, 2H, H-1^{v}), 3.51 (q, $J_{1^{vii},2^{vii}}$ = 7.0 Hz, 2H, H-1^{vii}), 3.18 (t, $J_{5^{ii},4^{ii}}$ = 6.8 Hz, 2H, H-5^{ii}), 2.67 (m, 1H, H-3), 2.34 (m, 3H, H-2, 2xH-3^{i}), 1.95-1.84 (m, 6H, H-2, H-1^{i}, H-2^{ii}, $COCH_3$), 1.82-1.63 (m, 4H, H-1^{i}, 2xH-2^{i}, H-2^{ii}) 1.52 (m, 2H, H-4^{ii}), 1.46 (m, 2H, H-3^{ii}), 1.22 (t, $J_{2^{vii},1^{vii}}$ = 7.0 Hz, 3H, H-2^{vii}); **^{13}C-NMR** (100.6 MHz, MeOH-d$_4$): δ 177.7/ 175.8/173.3/173.1 (C-4^{i}/$COCH_3$/CO, acid/CO, acid/CO, amide), 172.4 (C-2^{vi}, C-5^{vi}), 171.7 (C-4^{i}/$COCH_3$/CO, acid/CO, acid/CO, amide), 151.7 (C-4^{iv}), 150.7 (C-4^{iii}), 144.6 (C-1^{iv}), 140.9 (C-1^{iii}), 135.5 (C-3^{vi}, C-4^{vi}), 126.2 (C-2^{iv}, C-6^{iv}), 123.8 (C-3^{iii}, C-5^{iii}), 121.4 (C-2^{iii}, C-6^{iii}), 112.7 (C-3^{iv}, C-5^{iv}), 55.6 (C-1^{ii}), 52.6 (C-1), 48.3 (C-1^{v}), 45.9 (C-1^{vii}), 42.2 (C-3), 40.1 (C-5^{ii}), 36.1/35.9 (C-2^{v}/C-3^{i}), 33.2 (C-2), 32.8/32.5 (C-1^{i}/C-2^{ii}), 30.1 (C-4^{ii}), 24.3 (C-3^{ii}), 24.0 (C-2^{i}), 22.6 ($COCH_3$), 12.6 (C-2^{vii}); **IR** (ATR): 3265, 2927, 1705, 1594, 1536, 1511, 1247, 1134 cm^{-1}; **HRMS** (ESI+) calcd. for [$C_{37}H_{48}N_8O_9$+H]: 749.3617; found: 749.3614.

Synthesis of *tert*-butyl *N*-[5-({2-[6-acetyl-2-naphthyl)(methyl)amino]acetyl}amino)pentyl carbamate, 102

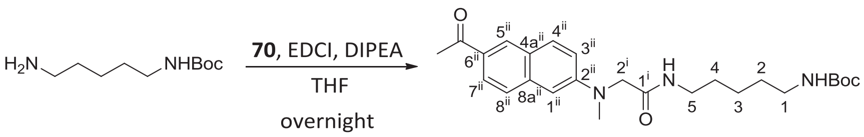

101 **102**

To a stirred solution of *tert*-Butyl *N*-(5-aminopentyl)carbamate (**101**) (89 μl, 0.45 mmol) in dry THF (5.0 ml) under N_2 atmosphere, a solution of **70** (100 mg, 0.39 mmol), EDCI (99 mg, 0.52 mmol), DIPEA (201 μl, 1.15 mmol) in dry THF (5.0 ml) was added. The reaction mixture was stirred overnight at rt. Then, the mixture was diluted with EtOAc (15 ml) and washed with water (3x5 ml). The organic layer was dried over anhydrous $MgSO_4$ and concentrated under vacuum. The residue was purified by column chromatography (from EtOAc to EtOAc/MeOH, 95:5) to give amide **102** (105 mg, 0.24 mmol, 61% yield) as a yellowish solid.

<u>Physical and spectroscopic data of **102**</u>

Mp = 112-114 ºC (from EtOAc); **^{1}H-NMR** (400 MHz, $CDCl_3$): δ 8.26 (s, 1H, H-5^{ii}), 7.88 (dd, $J_{7^{ii},8^{ii}}$ = 8.7 Hz, $J_{7^{ii},5^{ii}}$ = 1.7 Hz, 1H, H-7^{ii}), 7.78 (d, $J_{4^{ii},3^{ii}}$ = 9.1 Hz, 1H, H-4^{ii}), 7.60 (d, $J_{8^{ii},7^{ii}}$ = 8.7 Hz, 1H, H-8^{ii}), 7.04 (dd, $J_{3^{ii},4^{ii}}$ = 9.1 Hz, $J_{3^{ii},1^{ii}}$ = 2.6 Hz, 1H, H-3^{ii}), 6.89 (d, $J_{1^{ii},3^{ii}}$ = 2.6 Hz, 1H, H-1^{ii}), 6.55 (t, $J_{C\text{-}1NH,1}$ = 6.5 Hz, 1H, C-1NH), 4.57 (m, 1H, NHC-5), 3.97 (s, 2H, H-2^{i}), 3.25 (dd, $J_{5,4}$ = 13.4 Hz, $J_{5,\ C\text{-}1^{i}NH}$ = 6.8 Hz, 2H, H-5), 3.13 (s, 3H, NCH_3), 2.96 (dd, $J_{1,2}$ = 12.9 Hz, $J_{1,\ C\text{-}1NH}$ = 6.5 Hz, 2H, H-1), 2.61 (s, 3H, $COCH_3$), 1.49-1.32 (m, 4H, 2xH-2, 2xH-4), 1.40 (s, 9H, $C(CH_3)_3$), 1.20 (m, 2H, H-3); **^{13}C-NMR** (100.6 MHz, $CDCl_3$): δ

197.7 ($COCH_3$), 169.7 (C-1^{i}), 156.0 (CO, carbamate), 148.9 (C-2^{ii}), 137.3 (C-8a^{ii}), 131.8 (C-6^{ii}), 131.2 (C-4^{ii}), 130.2 (C-5^{ii}), 126.6 (C-8^{ii}), 126.1 (C-4a^{ii}), 124.9 (C-7^{ii}), 116.2 (C-3^{ii}), 106.7 (C-1^{ii}), 79.1 ($C(CH_3)_3$), 58.2 (C-2^{i}), 40.3 (C-1), 39.9 (NCH_3), 39.1 (C-5), 29.6 (C-2), 29.3 (C-4), 28.5 ($C(CH_3)_3$), 26.5 ($COCH_3$), 23.9 (C-3); **IR** (ATR): 3351, 3272, 2979, 2928, 2860, 1683, 1657, 1620, 1511, 1207, 1165 cm^{-1}; **HRMS** (ESI+) calcd. for [$C_{25}H_{35}N_3O_4$+Na]: 464.2520; found: 464.2530. **COSY** and **^{1}H/^{13}C** correlation were recorded.

Synthesis of *N*-(5-aminopentyl)-2-[(6-acetyl-2-naphthyl)(methyl)amino]acetamide, 104

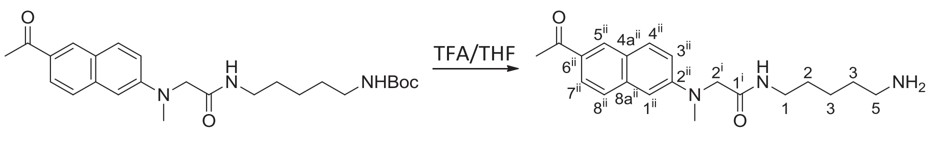

102 **104**

To a solution of compound **102** (100 mg, 0.23 mmol) in THF (1.4 ml), trifluoroacetic acid (7.3 ml, 94.8 mmol) was added. The reaction mixture was stirred overnight, when TLC analysis (EtOAc) showed no presence of starting material, and concentrated under vacuum. The mixture was neutralized with a saturated aqueous solution of Na_2CO_3, extracted with EtOAc (2x10 ml) and dried over anhydrous $MgSO_4$. The solvent was evaporated under vacuum and the residue was purified by column chromatography (from EtOAc/NH_3, 99:1 to EtOAc/MeOH/NH_3, 85:10:5) to furnish amine **104** (74 mg, 0.22 mmol, 97% yield) as a yellow solid.

Physical and spectroscopic data of **104**

Mp = 68-76 ºC (from EtOAc); **^{1}H-NMR** (250 MHz, MeOH-d$_4$): δ 8.36 (d, $J_{5^{ii},7^{ii}}$ = 1.5 Hz, 1H, H-5^{ii}), 8.07 (t, $J_{C\text{-}1^{i}NH,1}$ = 5.9 Hz, 1H, C-1^{i}NH), 7.89-7.79 (m, 2H, H-7^{ii}, H-4^{ii}), 7.62 (d, $J_{8^{ii},7^{ii}}$ = 8.8 Hz, 1H, H-8^{ii}), 7.15 (dd, $J_{3^{ii},4^{ii}}$ = 9.1 Hz, $J_{3^{ii},1^{ii}}$ = 2.6 Hz, 1H, H-3^{ii}), 6.92 (d, $J_{1^{ii},3^{ii}}$ = 2.6 Hz, 1H, H-1^{ii}), 4.08 (s, 2H, H-2^{i}), 3.28-3.20 (m, 2H, H-1), 3.18 (s, 3H, NCH_3), 2.80 (m, 2H, H-5), 2.62 (s, 3H, $COCH_3$), 1.56 (m, 4H, 2xH-2, 2xH-4), 1.32 (m, 2H, H-3); **^{13}C-NMR** (62.5 MHz, MeOH-d$_4$): δ 200.3 ($COCH_3$), 172.8 (C-1^{i}), 150.8 (C-2^{ii}), 139.0 (C-8a^{ii}), 132.1/131.9/131.8 (C-6^{ii}/C-4^{ii}/C-5^{ii}), 127.4 (C-8^{ii}), 127.0 (C-4a^{ii}), 125.3 (C-7^{ii}), 117.3 (C-3^{ii}), 107.0 (C-1^{ii}), 57.6 (C-2^{i}), 40.5 (C-5), 40.2 (NCH_3), 39.8 (C-1), 29.9 (C-4), 28.0 (C-2), 26.4 ($COCH_3$), 24.5 (C-3); **IR** (ATR): 3458, 3274, 2923, 1678, 1656, 1615, 1201, 1175, 1131 cm^{-1}; **HRMS** (ESI+) calcd. for [$C_{20}H_{27}N_3O_2$+H]: 342.2176; found: 342.2181.

Synthesis of di(*tert*-butyl) (2*R*,4*S*)-2-(4-{[5-({[(6-acetyl-2-naphthyl)(methyl)amino]acetyl}amino)pentyl]amino}-4-oxobutyl)-4-[(*tert*-butoxycarbonyl)amino]pentanedioate, 103

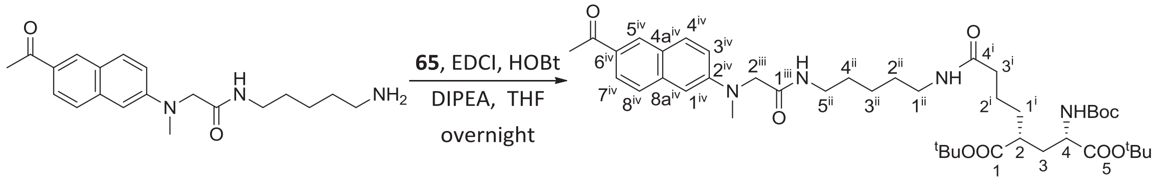

104 **103**

To a stirred solution of amine **104** (75 mg, 0.22 mmol) in dry THF (3.0 ml) under N_2 atmosphere, a solution of **65** (108 mg, 0.24 mmol), EDCI (53 mg, 0.28 mmol), DIPEA (153 μl, 0.89 mmol) in dry THF (4.5 ml) was added. The reaction mixture was stirred overnight at rt. Then, the mixture was diluted with EtOAc (15 ml) and washed with water (3x8 ml). The organic layer was dried over anhydrous $MgSO_4$ and concentrated under vacuum. The residue was purified by column chromatography (from hexanes/EtOAc, 8:2 to EtOAc), to afford amide **103** (63 mg, 82 μmol, 38% yield) as a yellowish solid.

Physical and spectroscopic data of **103**

Mp = 62-68 ^oC (from hexanes/EtOAc); **$[\alpha]_D^{20}$** = -6.6 (*c* 1.30, MeOH); **^{1}H-NMR** (400 MHz, MeOH-d_4): δ 8.40 (s, 1H, H-5^{iv}), 7.87 (m, 2H, H-7^{iv}, H-4^{iv}), 7.65 (d, $J_{8^{iv},7^{iv}}$ = 8.7 Hz, 1H, H-8^{iv}), 7.16 (dd, $J_{3^{iv},4^{iv}}$ = 9.1 Hz, $J_{3^{iv},1^{iv}}$ = 2.5 Hz, 1H, H-3^{iv}), 6.94 (d, $J_{1^{iv},3^{iv}}$ = 2.5 Hz, 1H, H-1^{iv}), 6.83 (d, $J_{C\text{-}4NH,4}$ = 8.5 Hz, 1H, C-4NH), 4.08 (s, 2H, H-2^{iii}), 3.98 (m, 1H, H-2), 3.22 (m, 2H, H-5^{ii}), 3.20 (s, 3H, NCH_3), 3.05 (t, $J_{1^{ii},2^{ii}}$ = 7.1 Hz, 2H, H-1^{ii}), 2.64 (s, 3H, $COCH_3$), 2.41 (m, 1H, H-4), 2.13 (t, $J_{3^{i},2^{i}}$ = 6.9 Hz, 2H, H-3^{i}), 2.04 (m, 1H, H-3), 1.67-1.53 (m, 5H, H-3, 2xH-1^{i}, 2xH-2^{i}), 1.52-1.35 (m, 31H, 2xH-2^{ii}, 2xH-4^{ii}, 3x($C(CH_3)_3$), 1.28 (m, 2H, H-3^{ii}); **^{13}C-NMR** (100.6 MHz, MeOH-d_4): δ 200.2 (*C*OCH_3), 176.1/175.5 (C-1/C-4^{i}), 173.5 (C-5), 172.7 (C-1^{iii}), 158.0 (CO, carbamate), 150.8 (C-2^{iv}), 139.0 (C-8a^{iv}), 132.1/132.0/131.9 (C-5^{iv}/C-6^{iv}/C-4^{iv}), 127.5 (C-8^{iv}), 127.0 (C-4a^{iv}), 125.3 (C-7^{iv}), 117.3 (C-3^{iv}), 107.0 (C-1^{iv}), 82.6 ($C(CH_3)_3$), 82.1 ($C(CH_3)_3$), 80.4 ($C(CH_3)_3$), 57.8 (C-2^{iii}), 54.1 (C-2), 44.0 (C-4), 40.2/40.1 (NCH_3/C-1^{ii}/C-5^{ii}), 36.8 (C-3^{i}), 35.0 (C-3), 33.5 (C-1^{i}), 30.1 (C-2^{ii}), 30.0 (C-4^{ii}), 28.8 ($C(CH_3)_3$), 28.4 ($C(CH_3)_3$), 28.3 ($C(CH_3)_3$), 26.5 ($COCH_3$), 25.1 (C-3^{ii}), 24.7 (C-2^{i}); **IR** (ATR): 3298, 2976, 2932, 1717, 1653, 1620, 1150 cm^{-1}; **HRMS** (ESI+) calcd. for $[C_{42}H_{64}N_4O_9+Na]$: 791.4566; found: 791.4571. **COSY** and **^{1}H/^{13}C** correlation were recorded.

Synthesis of (1*S*,3*R*)-7-{[5-({2-[(6-acetyl-2-naphthyl)(methyl)amino]acetyl}amino)pentyl]amino}-1,3-dicarboxy-7-oxoheptylammonium 2,2,2-trifluoroacetate, 100

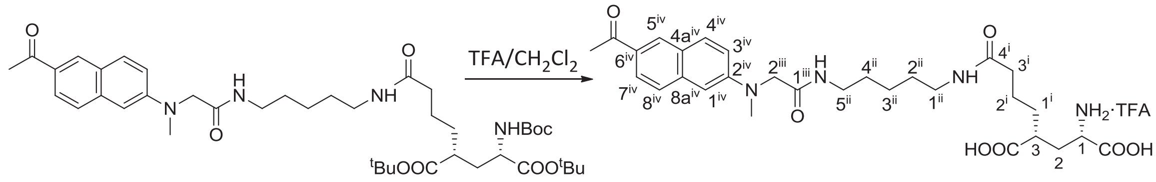

103 **100**

To a stirred solution of **103** (47 mg, 61 μmol) in CH_2Cl_2 (7.2 ml), trifluoroacetic acid (3.6 ml, 46.7 mmol) was added. After 7 h of stirring at rt, the starting material was consumed as judged by TLC analysis (EtOAc/MeOH, 9:1). Then, the mixture was concentrated under vacuum and the resulting solid was triturated with diethyl ether (2x7 ml) to provide **100** (41 mg, 61 μmol, quantitative yield) as a yellow solid.

Physical and spectroscopic data of **100**

$[\alpha]_D^{20}$ = -12.9 (*c* 0.87, MeOH); **^{1}H-NMR** (400 MHz, MeOH-d_4): δ 8.42 (d, $J_{5^{iv},7^{iv}}$ = 1.4 Hz, 1H, H-5^{iv}), 7.89 (m, 2H, H-7^{iv}, H-4^{iv}), 7.67 (d, $J_{8^{iv},7^{iv}}$ = 8.8 Hz, 1H, H-8^{iv}), 7.18 (dd, $J_{3^{iv},4^{iv}}$ = 9.1 Hz, $J_{3^{iv},1^{iv}}$ = 2.6 Hz, 1H, H-3^{iv}), 6.96 (d, $J_{1^{iv},3^{iv}}$ = 2.6 Hz, 1H, H-1^{iv}), 4.09 (s, 2H, H-2^{iii}), 3.99 (m, 1H, H-1), 3.23 (m, 2H, H-5^{ii}), 3.21 (s, 3H, NCH_3), 3.05 (t, $J_{1^{ii},2^{ii}}$ = 7.0 Hz, 2H, H-1^{ii}), 2.66 (s, 3H, $COCH_3$), 2.64 (m, 1H, H-3), 2.34 (m, 1H, H-2), 2.17 (t, $J_{3^i,2^i}$ = 6.3 Hz, 2H, H-3^i), 1.91 (m, 1H, H-2), 1.63 (m, 4H, 2xH-1^i, 2xH-2^i), 1.47 (m, 4H, 2xH-2^{ii}, 2xH-4^{ii}), 1.26 (m, 2H, H-3^{ii}); **^{13}C-NMR** (100.6 MHz, MeOH-d_4): δ 200.4 ($COCH_3$), 177.6 (CO, acid), 175.5 (C-4^i), 172.8 (C-1^{iii}), 171.6 (CO, acid), 150.8 (C-2^{iv}), 139.1 (C-8a^{iv}), 132.2/132.0/131.9 (C-5^{iv}/C-6^{iv}/C-4^{iv}), 127.5 (C-8^{iv}), 127.1 (C-4a^{iv}), 125.3 (C-7^{iv}), 117.4 (C-3^{iv}), 107.0 (C-1^{iv}), 57.8 (C-2^{iii}), 52.6 (C-1), 42.3 (C-3), 40.2 (NCH_3), 40.1 (C-1^{ii}, C-5^{ii}), 36.6 (C-3^i), 33.1 (C-2), 32.6 (C-1^i), 30.1 (C-2^{ii}), 30.0 (C-4^{ii}), 26.5 ($COCH_3$), 25.2 (C-3^{ii}), 24.1 (C-2^i); **IR** (ATR): 3308, 2925, 2857, 1615, 1182, 1135 cm^{-1}; **HRMS** (ESI+) calcd. for $[C_{29}H_{40}N_4O_7+H]$: 557.2970; found: 557.2986. **^{1}H/^{13}C** correlation was recorded.

VI.3. PHOTOCHEMICAL CHARACTERISATION

VI.3.1. Photoinduced *trans-cis* isomerisation

10^{-5} M solutions of the compounds of interest in DMSO or DMSO:PBS mixtures were degassed with nitrogen and then irradiated close to the maxima of their absorption bands with monochromatic light (**25**, λ_{exc} = 340, 347, 365 nm; **21**, λ_{exc} = 347, 365, 380 nm; **22** λ_{exc} = 355, 426, 475 nm; **23**, λ_{exc} = 355, 400, 475 nm; **71**-**74**, λ_{exc} = 475 nm). Photoinduced changes arising from *trans*→*cis* or *cis*→*trans* isomerisation were monitored by UV-Vis absorption spectroscopy.

Thermal *cis*→*trans* back isomerisation rate constants were determined by monitoring the time dependence of the absorption spectra of the sample of interest in the dark and at room temperature upon reaching their photostationary state. Depending on the *cis* isomer lifetime, these experiments were conducted by means of steady state UV-vis absorption spectroscopy (τ_{cis} > 1 min) or transient absorption spectroscopy (τ_{cis} < 1 min).

VI.3.2. Composition of the photostationary states by NMR

10^{-2} M solutions of the compounds of interest in DMSO-d_6 were degassed with nitrogen and irradiated close to the maxima of their absorption bands with monochromatic light (**21** and **25**, λ_{exc} = 365 nm; **22** and **23**, λ_{exc} = 473 nm) until no changes were observed by UV-Vis absorption spectroscopy. Then ^{1}H-NMR and UV-vis absorption spectra of the PSS mixtures were registered to determine: (i) the composition of their composition; and (ii) the absorption spectrum of the *cis* isomer.

VI.3.3. Isomerisation quantum yields

Photoisomerisation quantum yields were determined by comparison with reported reference compounds and ensuring a photoconversion lower than 15% in all cases. Equation VI.1 was employed to determine *trans*→*cis* and *cis*→*trans* isomerisation quantum yield values ($\Phi_{trans\rightarrow cis}$ and $\Phi_{cis\rightarrow trans}$) from UV-vis absorption measurements of the sample and reference of interest:[11]

$$ln\left(C_R/C_R^0\right) = \alpha \int_{t_0}^{t} \left[\left(1\text{-}10^{-Abs^{tot}}\right)/Abs^{tot}\right] dt \qquad \textbf{(VI.1)}$$

where

$$\alpha = - \Phi \cdot I_0 \cdot \varepsilon_R \cdot b \qquad \textbf{(VI.2)}$$

In this equation C_R is the concentration of the starting isomer at various illumination times t, I_0 is the incident light intensity, b is the cell path length, and Abs^{tot} and ε_R are the total absorbance and molar absorptivity of R at the irradiation wavelength. Azobenzene (**11**) ($\Phi_{trans\rightarrow cis}$ = 0.15 and $\Phi_{cis\rightarrow trans}$ = 0.35 in acetonitrile)[12] was used as reference in these measurements

VI.3.4. Fluorescence quantum yield

Equation VI.3 was employed to determine the fluorescence quantum yields of the compounds of interest (Φ_{Fl}^{sample}) from the UV-vis absorption and fluorescence measurements of this sample and of a suitable reference.

$$\Phi_{Fl}^{sample} = \frac{I_{Fl}^{sample}}{I_{Fl}^{ref}} \cdot \frac{Abs^{ref}}{Abs^{sample}} \cdot \left(\frac{n^{sample}}{n^{ref}}\right)^2 \cdot \Phi_{Fl}^{ref} \qquad \textbf{(VI.3)}$$

In this equation Φ_{Fl}^{ref} is the reported fluorescence quantum yield of the reference compound, I_{Fl}^{sample} and I_{Fl}^{ref} are the fluorescence intensities registered for the sample and reference compound at the same excitation wavelength, Abs^{ref} and Abs^{sample} are the absorbances of the reference compound and sample solutions at the excitation wavelength, and n^{ref} and n^{sample} are the refractive index of the solvents used for preparing the sample and reference compound solutions. DAPI (2-(4-amidinophenyl)-1*H*-indole-6-carboxamidine, Φ_{Fl} = 0.58 in DMSO)[13] was used as reference in these measurements.

VI.4. BIOLOGICAL EXPERIMENTS

Experimental details are only given for the experiments directly conducted in this work (cell culture, transfection and incubation, and single-cell calcium imaging measurements). Whole-cell patch clamp experiments whose results are described in Chapter IV were carried out by Dr. Mercè Izquierdo. A detailed explanation of those experiments can be found elsewhere.[14,15]

VI.4.1. Solutions and reagents

The extracellular solution used for single-cell calcium imaging contained (in mM): 140 NaCl, 5.4 KCl, 1 $MgCl_2$, 10 HEPES, 10 glucose and $CaCl_2$ (for **21**, 2 mM or 10 mM; for **22** and **23**, 2 mM); and they were titrated to pH 7.42 with NaOH. Allosteric modulators and free glutamate were stored at -20 ºC in DMSO and water, respectively, and diluted in the extracellular solution before each experiment.

Reagents for cell culture, transfection and incubation were: Dulbecco's Modified Eagle's Medium/Nutrient Mixture F-12 Ham (DMEM/F12), Fetal Bovine Serum (FBS), penicillin-streptomycin and fura-2 AM (Life Technologies); X-tremeGENE 9 Transfection Reagent (Roche Applied Science); accutase, glutamate, poly-L-Lysine and concanavalin A (Sigma-Aldrich).

VI.4.2. Cell culture and transient transfection

HEK tsA201 cells were maintained at 37 ºC and humidified atmosphere with 5% CO_2. Cells were grown in DMEM/F12 (1:1) medium and supplemented with 10% FBS and antibiotics (1% Penicillin/Streptomycin). Once at confluence, culture flasks were washed twice with PBS and harvested with 300 µl accutase.

Expression of GluK2-L439C was induced by transient transfection of the cDNA containing-plasmid with X-tremeGENE 9 DNA Transfection Reagent. For transfection, cells were seeded at a concentration of $3x10^5$ cells per well on 12-multiwell plates with a final volume of 1 ml, and immediately transfected following manufacturer's instructions (50 µl mixture of 1.5 µl:500 ng, X-tremeGENE 9 DNA TR:GluK2-L439C containing plasmid in serum-free medium for 20 minutes).

About 48 h after transfection, HEK tsA201 cells transiently overexpressing mGlu5a were seeded onto 15 mm glass coverslips pre-treated with Poly-L-Lysine to allow cell adhesion, at a concentration around $2.5·10^5$ cells in order to get pre-confluent cultures at the time of the experiment. Transfected cells were used for single-cell calcium imaging experiments between 72 and 96 h after transfection.

VI.4.3. Single-cell calcium imaging

A glass coverslip was mounted onto the recording chamber, and the cells were loaded with allosteric modulators (for **21**, 110 and 200 µM; for **22** and **23**, 200 µM. Final concentration 1-2% DMSO) in a calcium free external solution containing concanavalin A type IV (300 mg/l) to block desensitisation. After 30 minutes incubation in the dark at 37 ºC and 5% CO_2, a fura-2 AM solution (10 µM) was added and the system incubated for 30 minutes more. Then, cells were carefully rinsed with fresh external solution, three to four times, and the recording chamber was placed on an inverted fully-motorised digital microscope.

Photoisomerisation of the photochromic compounds loaded into the cell membrane was achieved by illuminating the specimen with light flashes of ultraviolet radiation (for **21**, λ_{exc} = 380 nm), and visible (for **21**, λ_{exc} = 500 nm; for **22** and **23**, λ_{exc} = 435 nm) in between each single fura-2 fluorescence measurement. Free glutamate (100 µM) was introduced into the sample at the initial and final parts of each experiment as control measurement.

VI.5. REFERENCES

(1) Williams, G. D.; Wade, C. E.; Clarkson, G. J.; Wills, M. *Tetrahedron: Asymmetry* **2007**, *18*, 664–670.

(2) Harris, P. W. R.; Brimble, M. A.; Gluckman, P. D. *Org. Lett.* **2003**, *5*, 1847–1850.

(3) Ezquerra, J.; Pedregal, C.; Rubio, A.; Yruretagoyena, B.; Escribano, A.; Sánchez-Ferrando, F. *Tetrahedron* **1993**, *49*, 8665–8678.

(4) Volgraf, M.; Gorostiza, P.; Numano, R.; Kramer, R. H.; Isacoff, E. Y.; Trauner, D. *Nat. Chem. Biol.* **2006**, *2*, 47–52.

(5) Pearson, R. J.; Kassianidis, E.; Slawin, A. M. Z.; Philp, D. *Org. Biomol. Chem.* **2004**, *2*, 3434–3441.

(6) Gross, U.; Nieger, M.; Bräse, S. *Org. Lett.* **2009**, *11*, 4740–4742.

(7) Steger, M.; Young, D. W. *Tetrahedron* **1999**, *55*, 7935–7956.

(8) Kim, H. M.; Jung, C.; Kim, B. R.; Jung, S.-Y.; Hong, J. H.; Ko, Y.-G.; Lee, K. J.; Cho, B. R. *Angew. Chem. Int. Ed.* **2007**, *46*, 3460–3463.

(9) Assié, M.; Meddour, A.; Fiaud, J.-C.; Legros, J.-Y. *Tetrahedron: Asymmetry* **2010**, *21*, 1701–1708.

(10) Struga, M.; Miroslaw, B.; Pakosinska-Parys, M.; Drzewiecka, A.; Borowski, P.; Kossakowski, J.; Koziol, A. E. *J. Mol. Struct.* **2010**, *965*, 23–30.

(11) Lees, A. J. *Anal. Chem.* **1996**, *68*, 226–229.

(12) Bandara, H. M. D.; Burdette, S. C. *Chem. Soc. Rev.* **2012**, *41*, 1809–1825.

(13) Hard, T.; Fan, P.; Kearns, R. D. *Photochem. Photobiol.* **1990**, *51*, 77–86.

(14) Izquierda-Serra, M. Doctoral Thesis, Institut de Bioenginyeria de Catalunya, Universitat de Barcelona, 2014.

(15) Izquierdo-Serra, M.; Gascón-Moya, M.; Hirtz, J. J.; Pittoloa, S.; Poskanzer, F. E.; Ferrer, E.; Alibés, R.; Busque, F.; Yuste, R.; Hernando, J.; Gorostiza, P. Submitted.

Formula Index

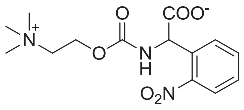

1

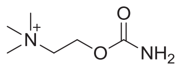

2

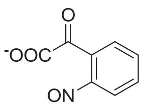

3

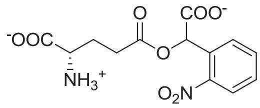

4

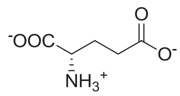

5

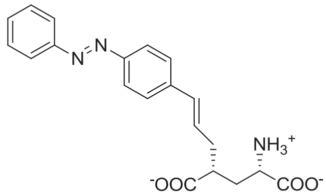

6

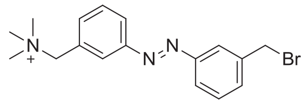

7

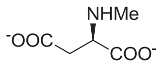

8

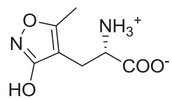

9

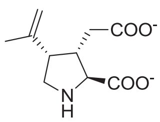

10

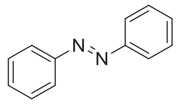

11

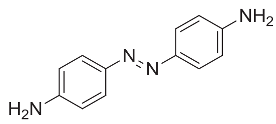

12

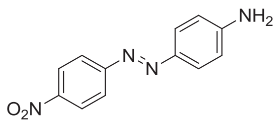

13

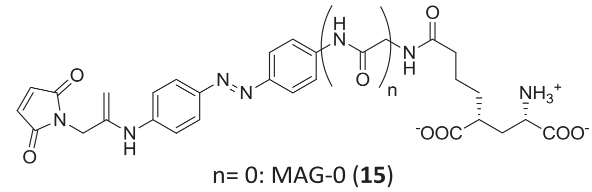

n= 0: MAG-0 (**15**)
n= 1: MAG-1 (**14**)
n= 2: MAG-2 (**16**)

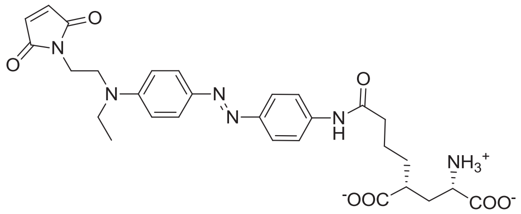

17

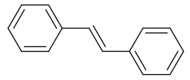

18

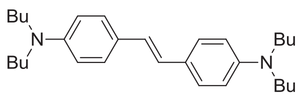

19

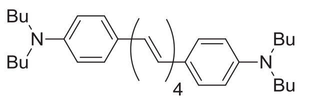

20

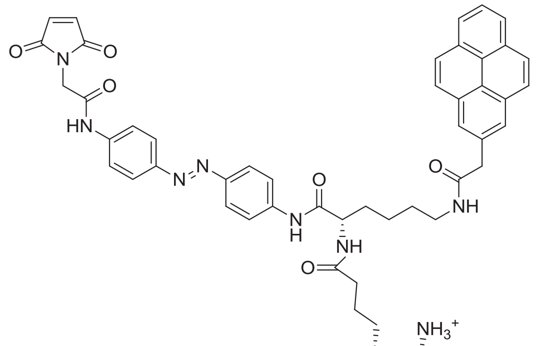

21

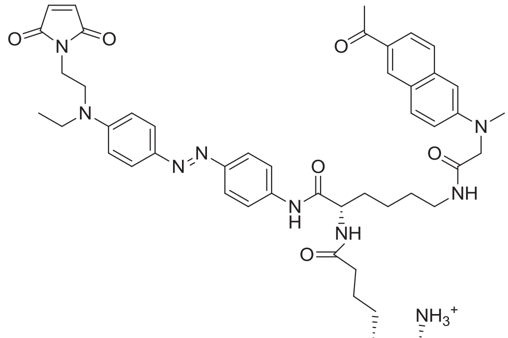

22

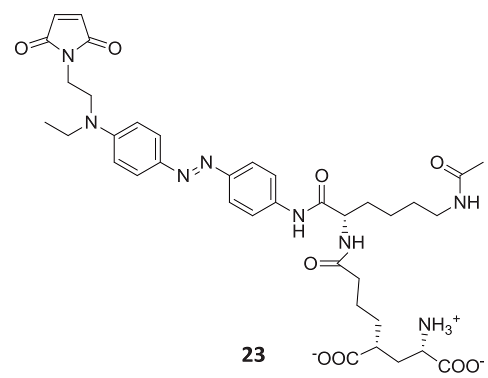

23

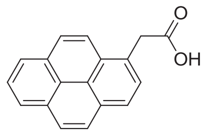

24

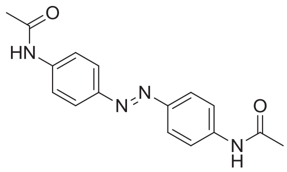

25

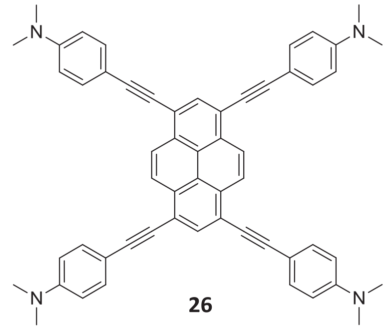

26

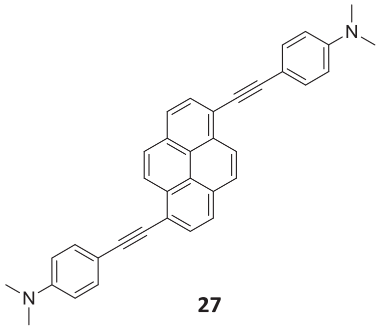

27

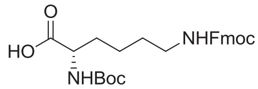

28

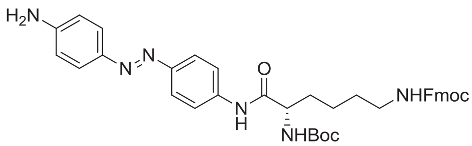

29

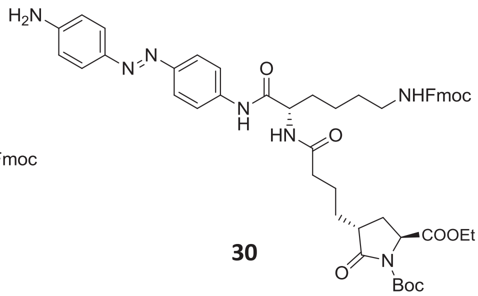

30

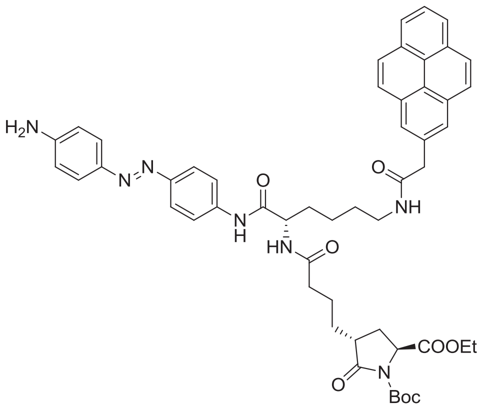

31

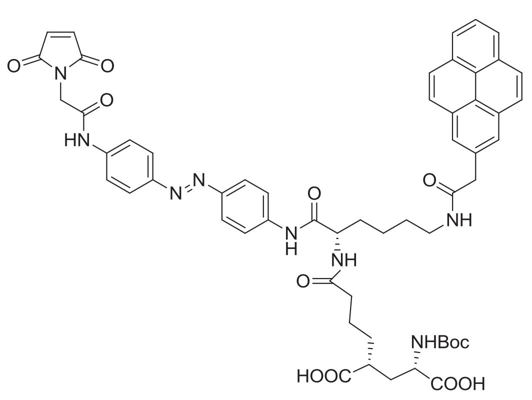

32

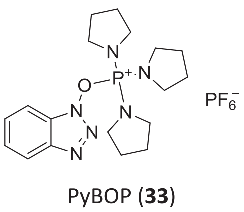

PyBOP (**33**)

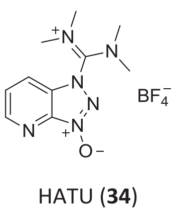

HATU (**34**)

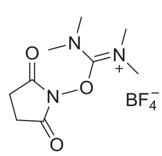

TSTU (**35**)

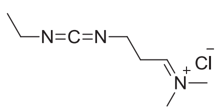

EDCI (**36**)

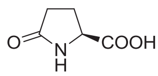

37

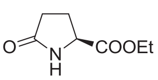
38

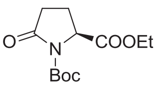
39

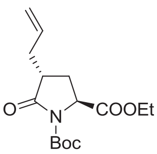
(4*R*)-**40**

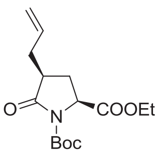
(4*S*)-**40**

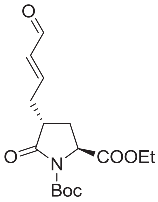
41

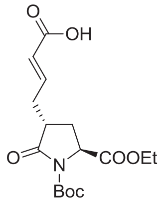
42

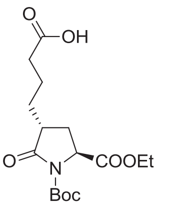
43

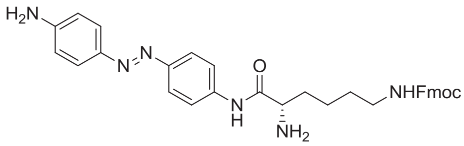
44

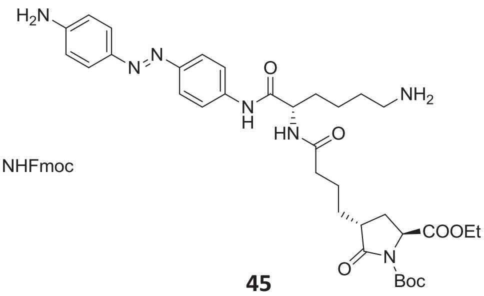
45

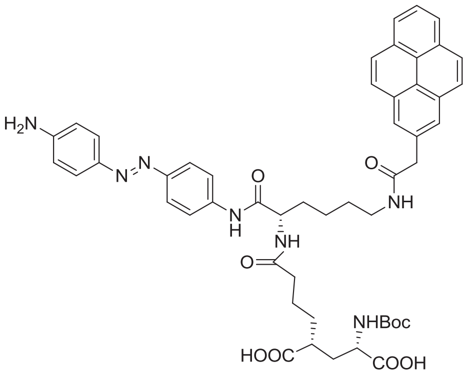
46

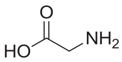
47

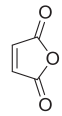
48

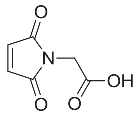
49

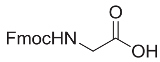
50

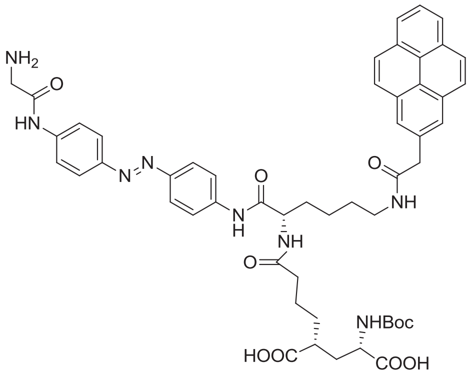
51

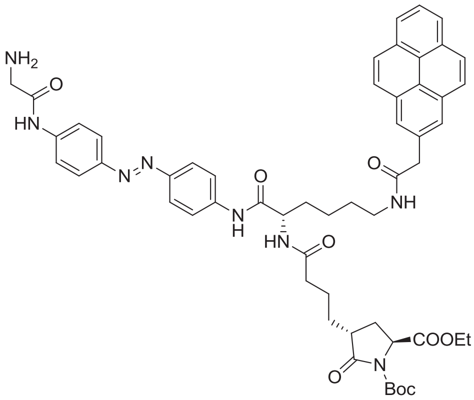
52

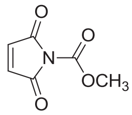
53

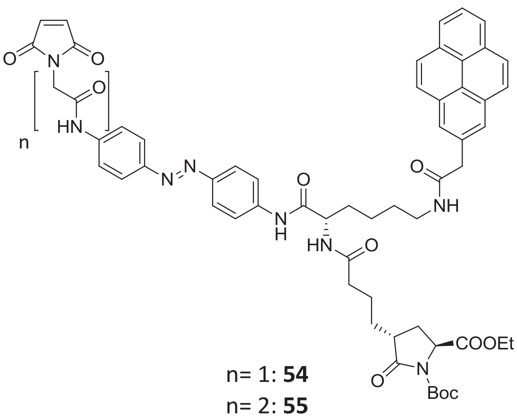
n= 1: **54**
n= 2: **55**

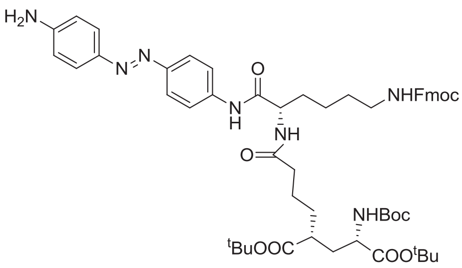
56

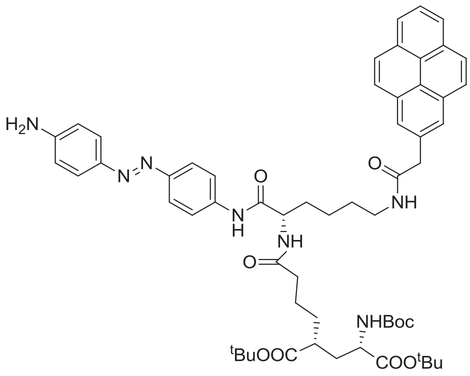

57

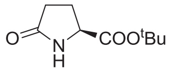

58

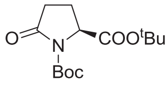

59

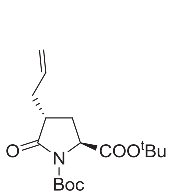

(4*R*)-**60**

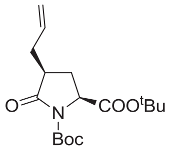

(4*S*)-**60**

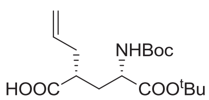

61

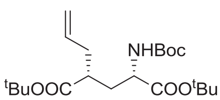

62

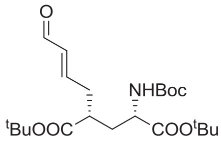

63

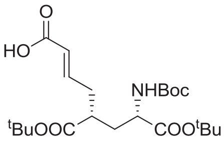

64

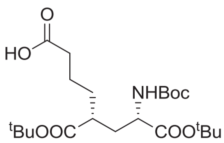

65

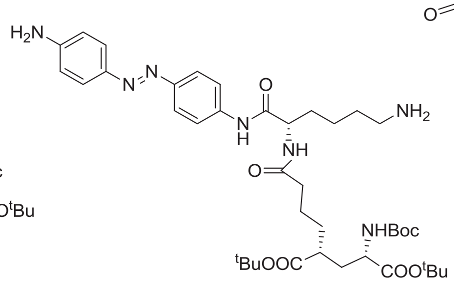

66

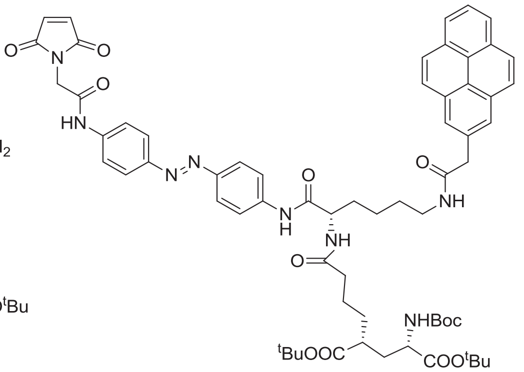

67

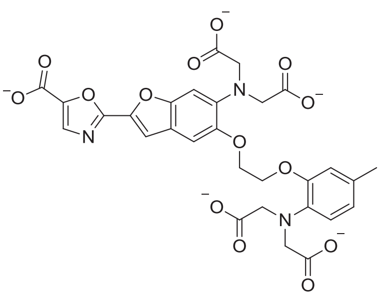

fura-2 (**68**)

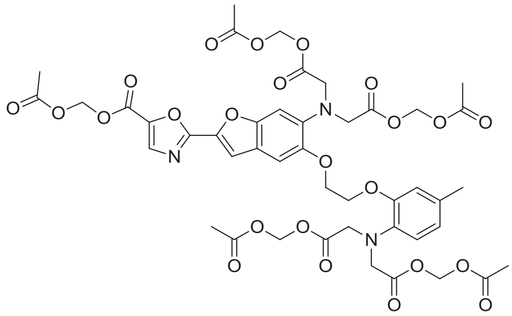

fura-2 AM (**69**)

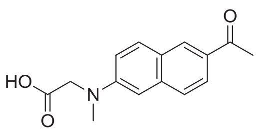

70

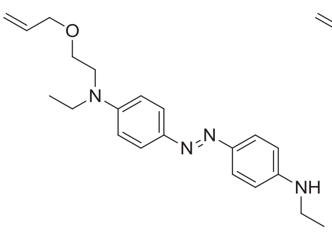

71

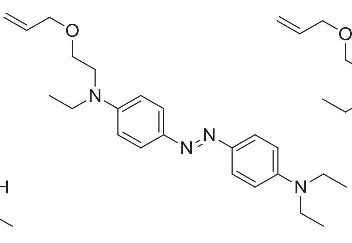

72

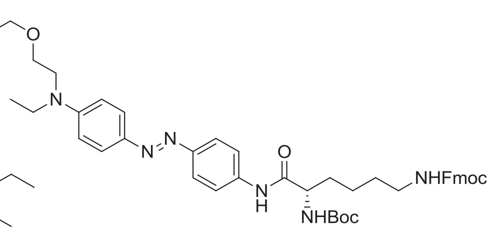

73

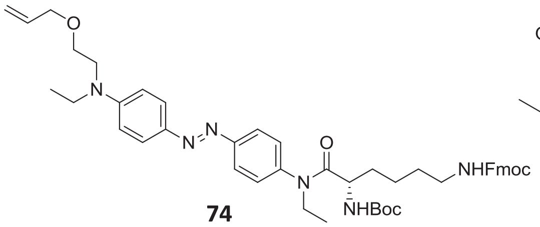

74

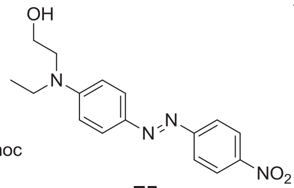

75

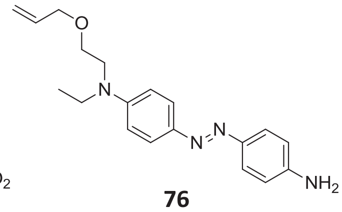

76

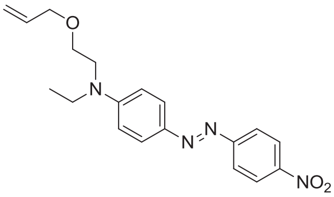

77

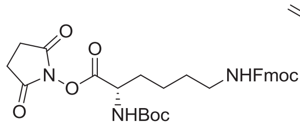

78

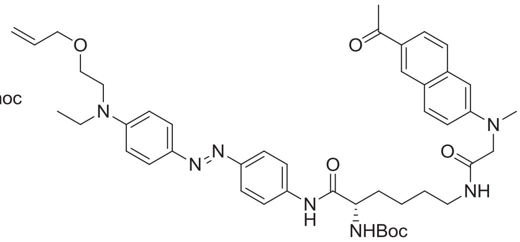

79

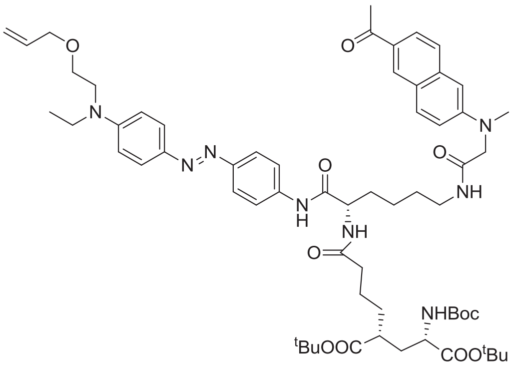

80

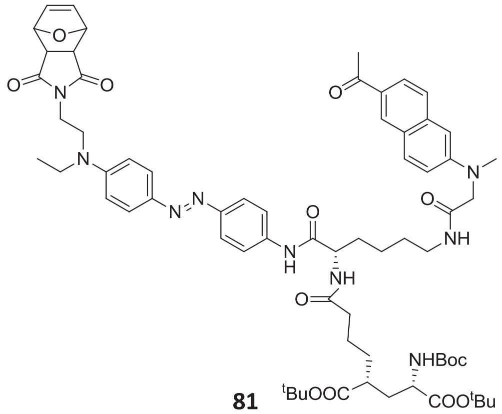

81

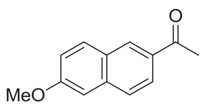

82

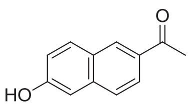

83

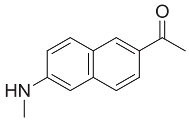

84

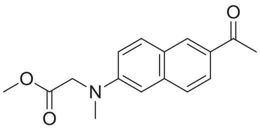

85

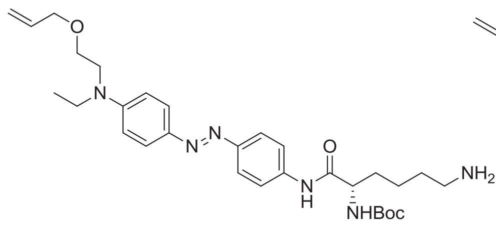

86

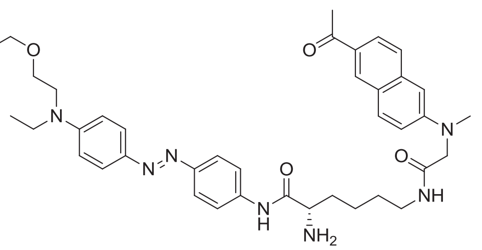

87

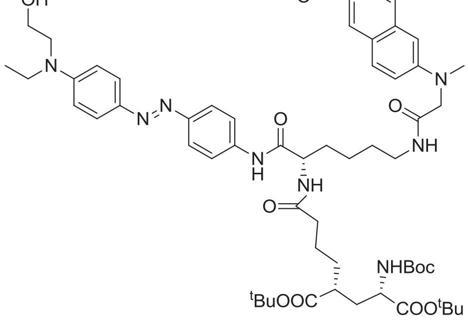

88

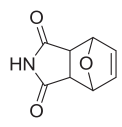

89

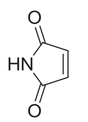

90

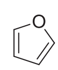

91

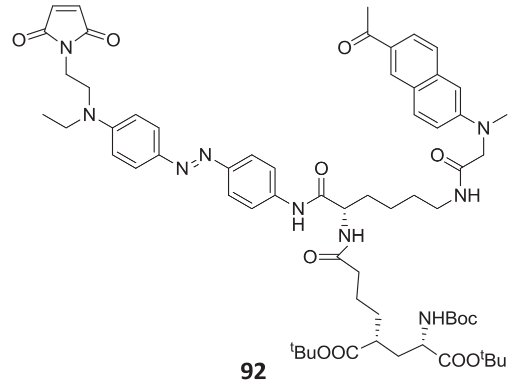

92

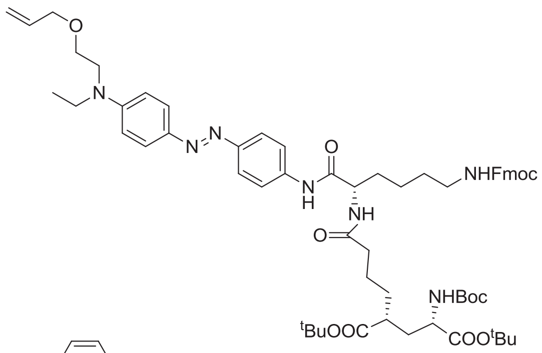

93

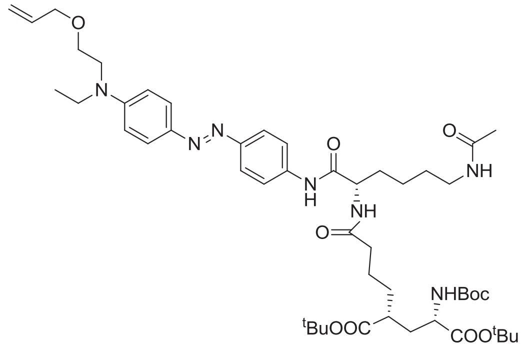

94

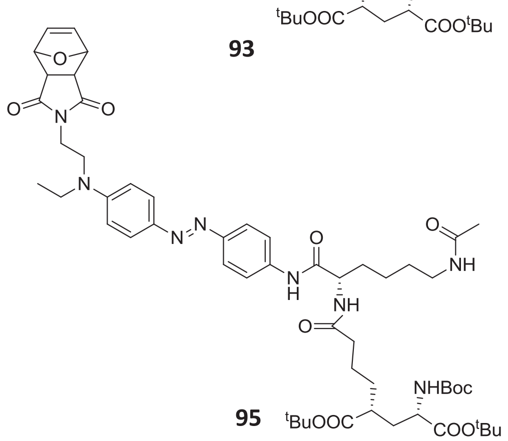

95

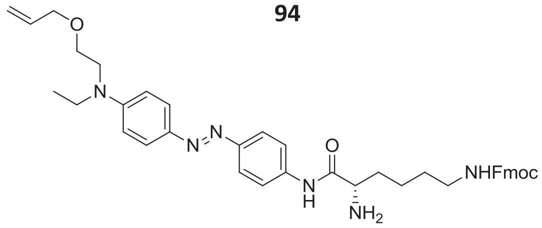

96

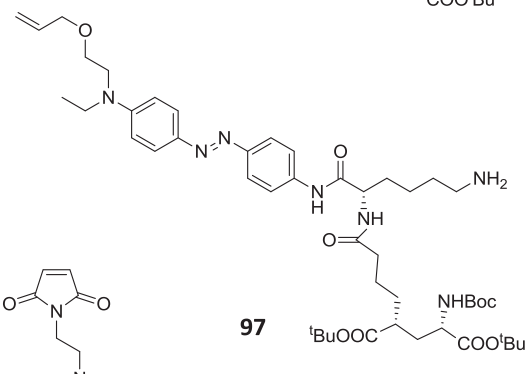

97

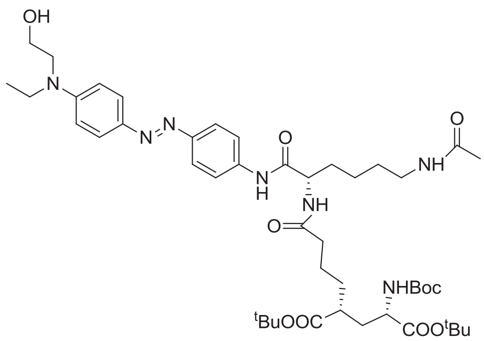

98

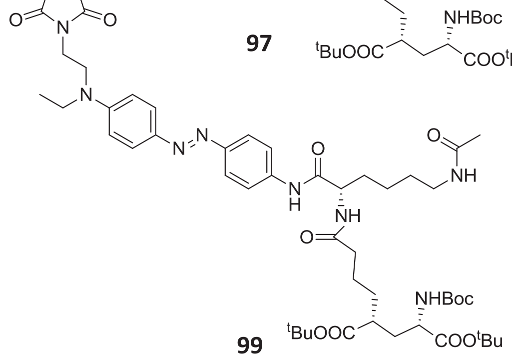

99

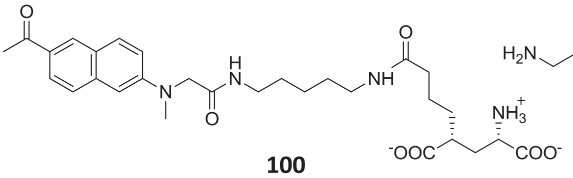

100

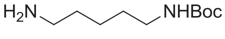

101

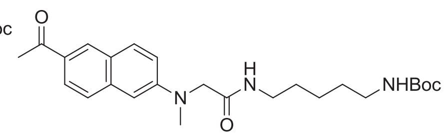

102

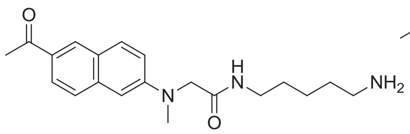

104

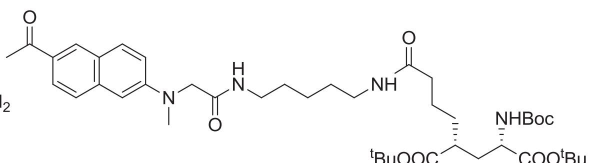

103

Annex Spectra of Selected Compounds

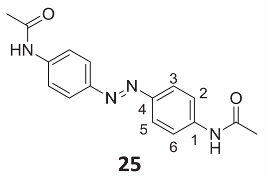

25

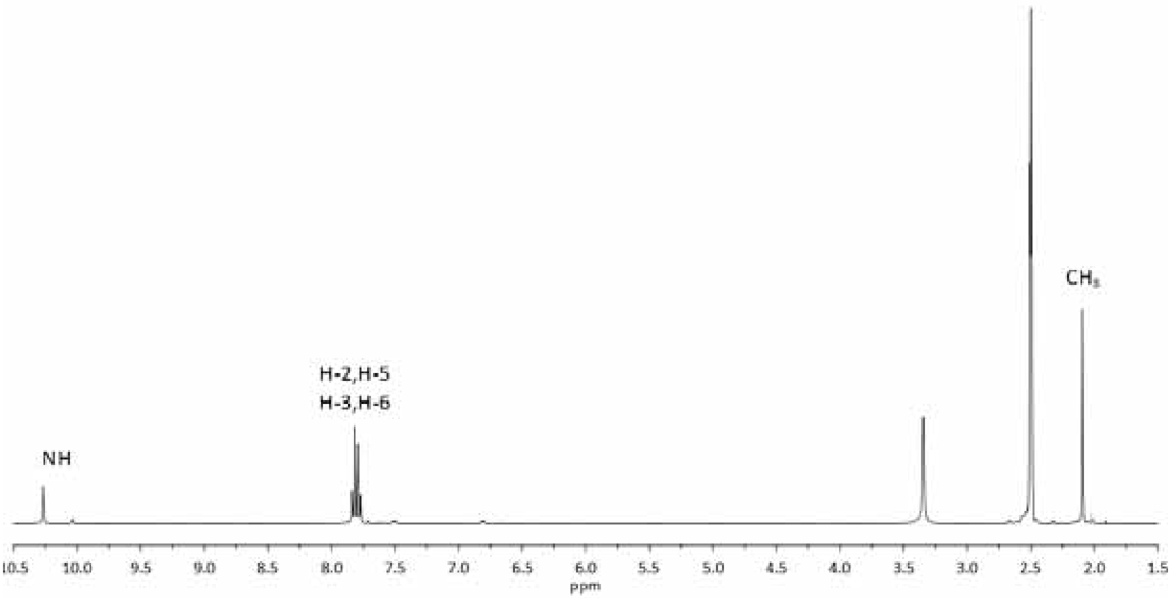

^{1}H-NMR (400 MHz, DMSO-d_6)

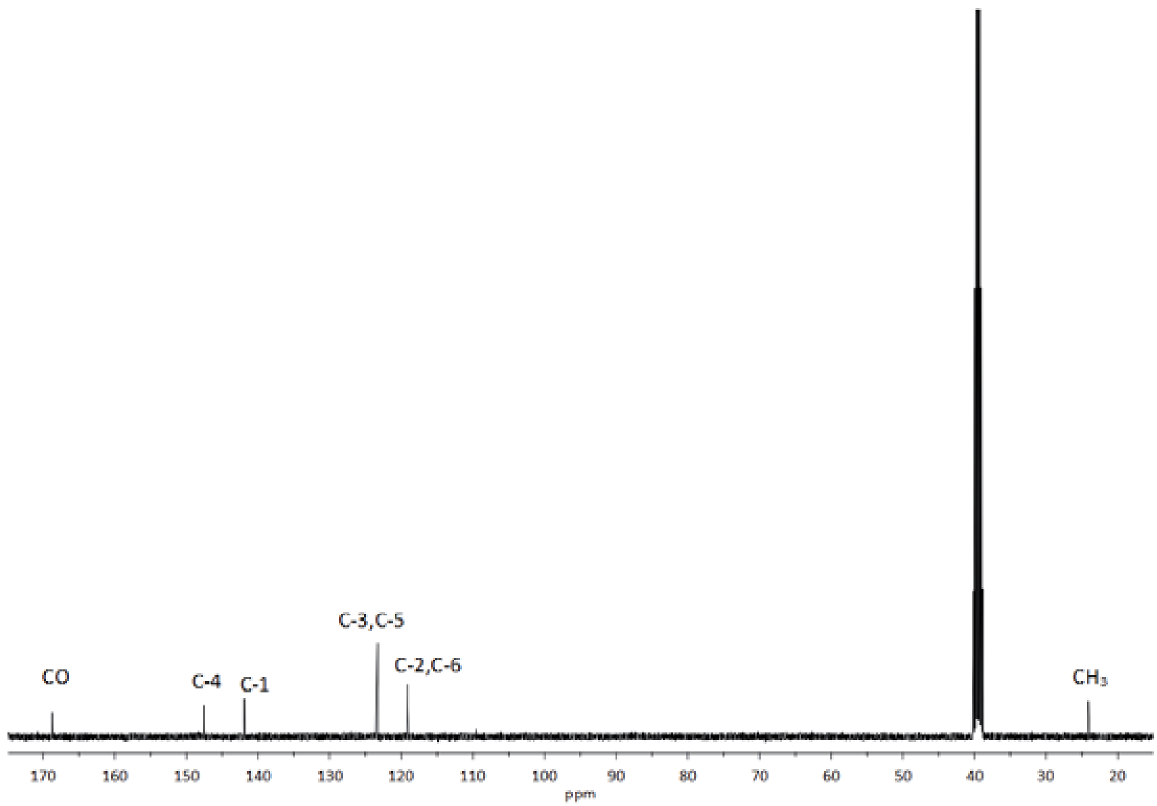

^{13}C-NMR (100.6 MHz, DMSO-d_6)

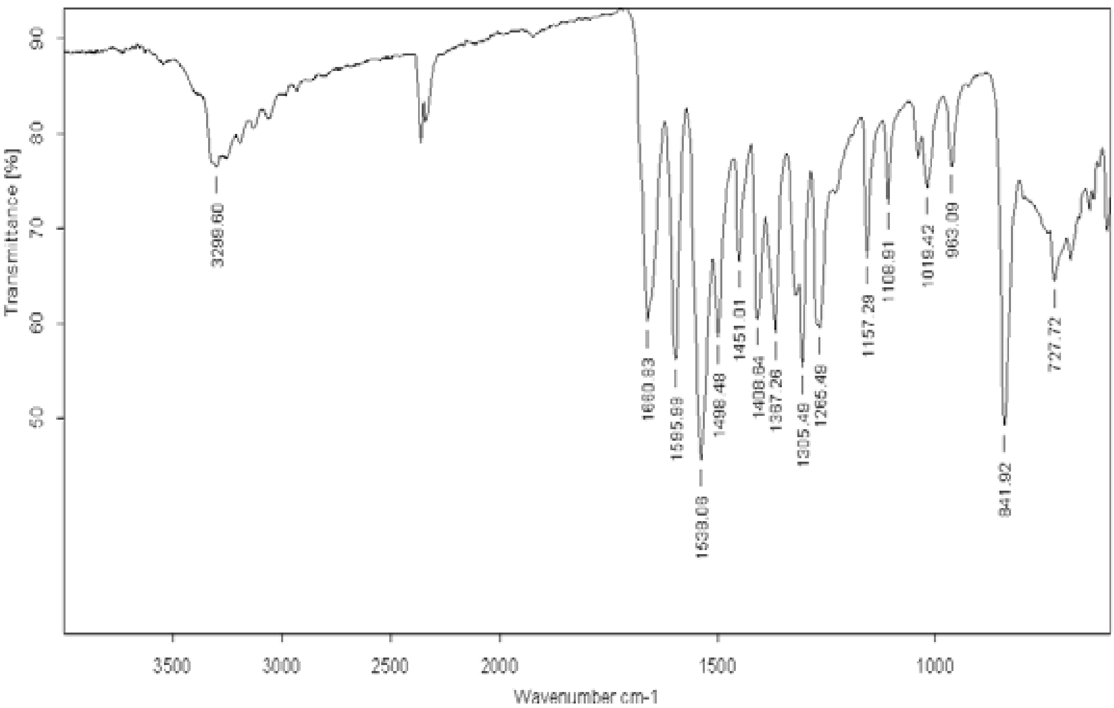

IR (ATR)

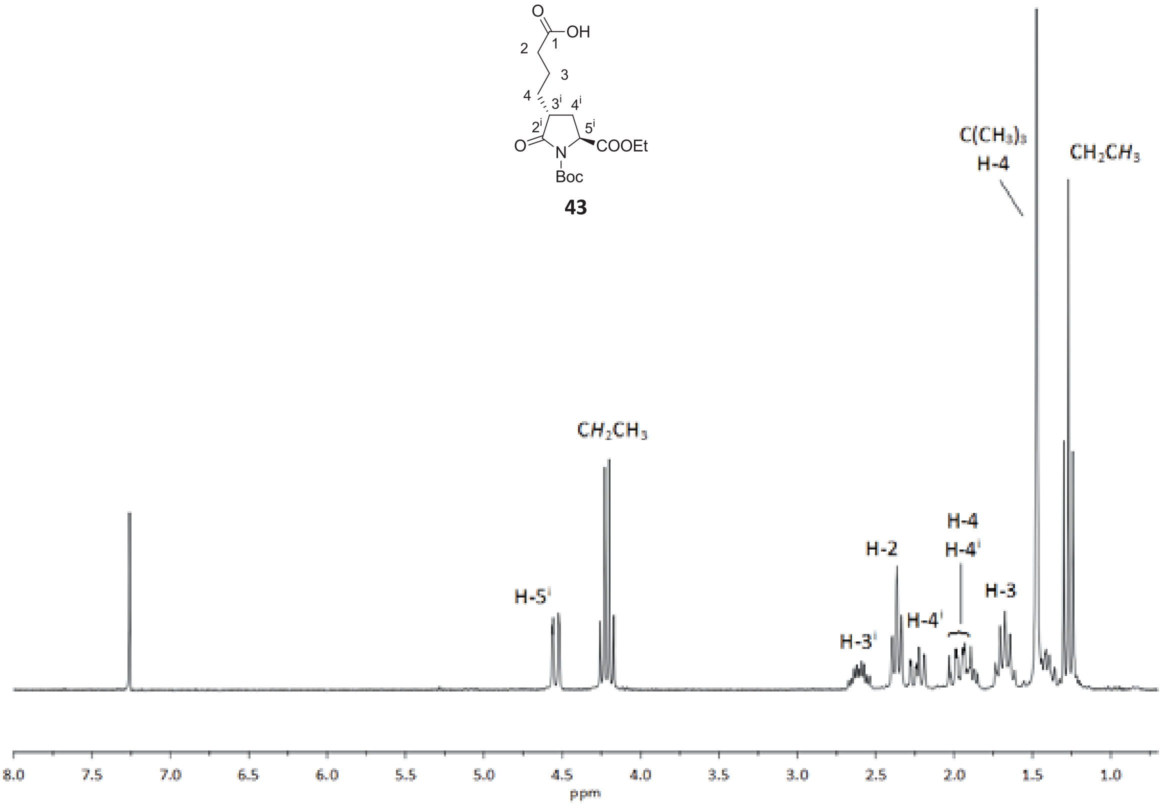

^{1}H-NMR (250 MHz, $CDCl_3$)

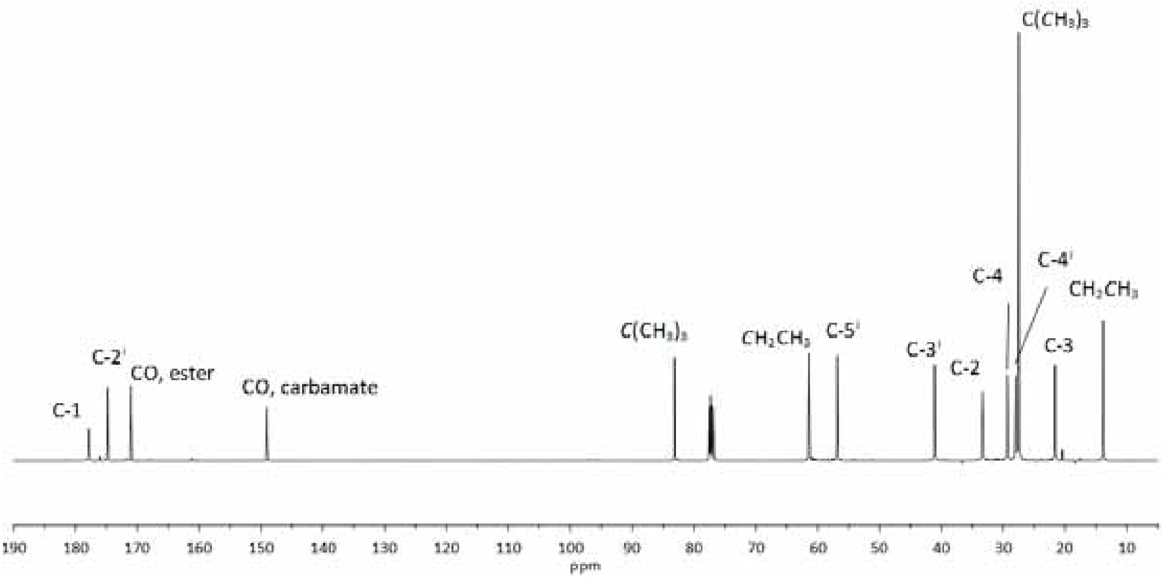

^{13}C-NMR (90 MHz, $CDCl_3$)

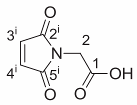

49

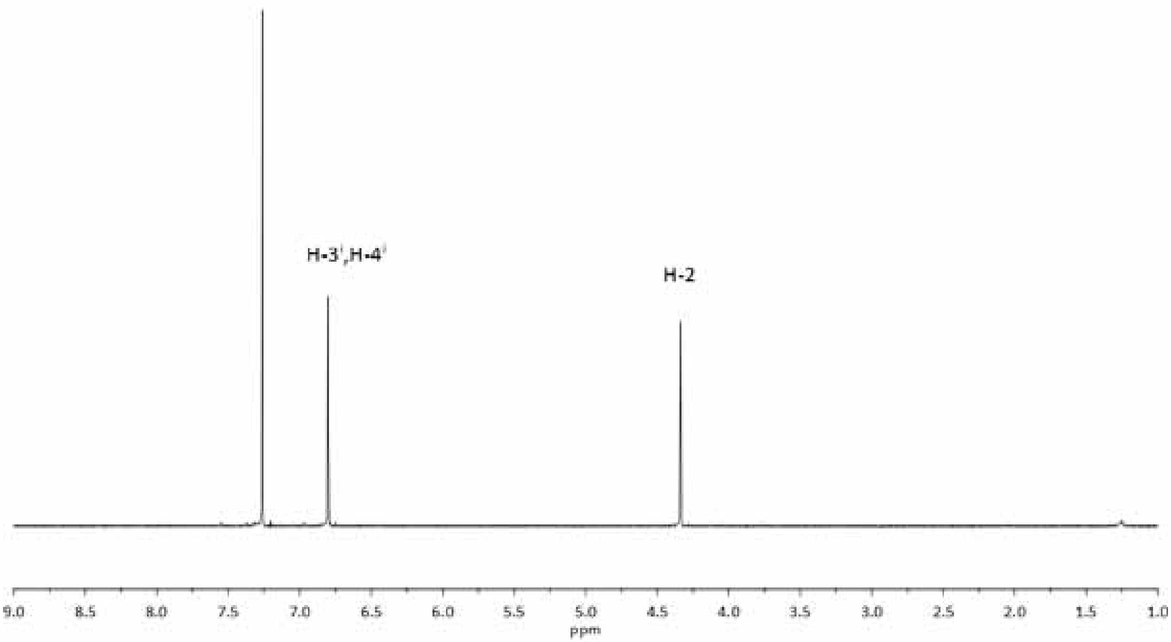

^{1}H-NMR (360 MHz, $CDCl_3$)

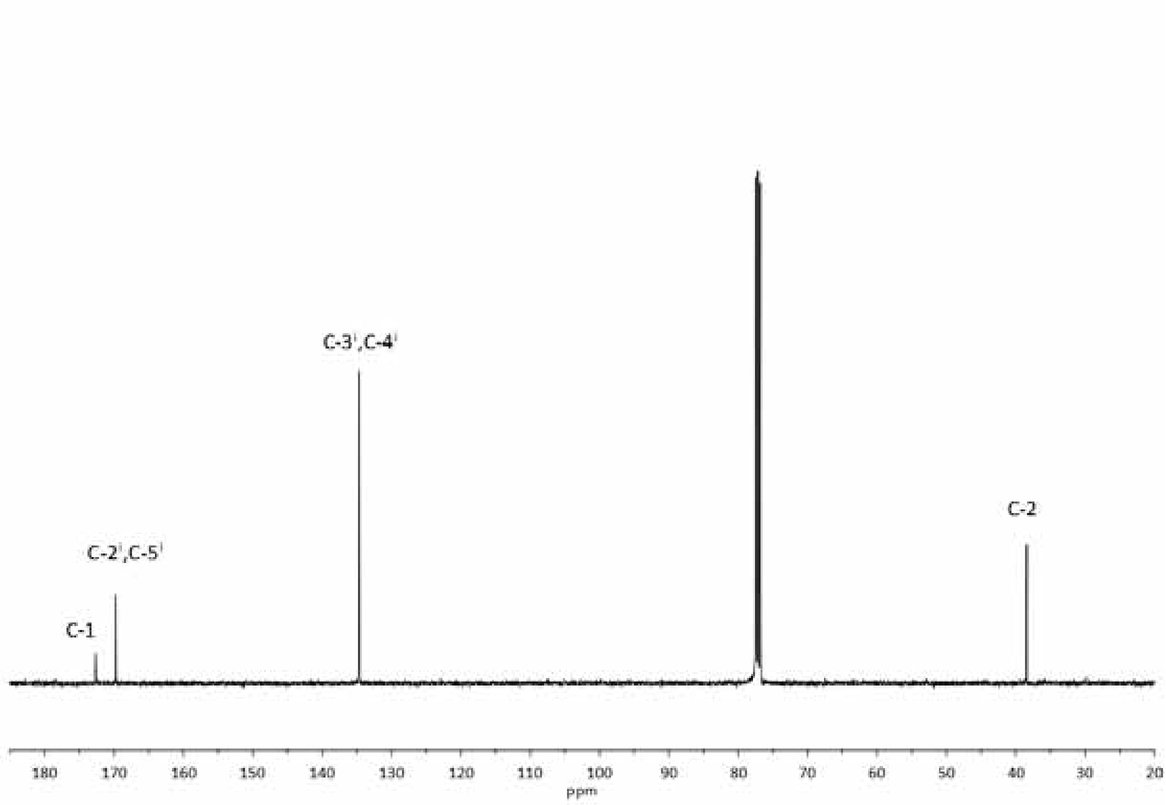

^{13}C-NMR (100.6 MHz, $CDCl_3$)

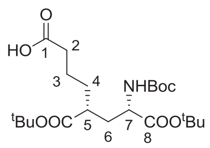

65

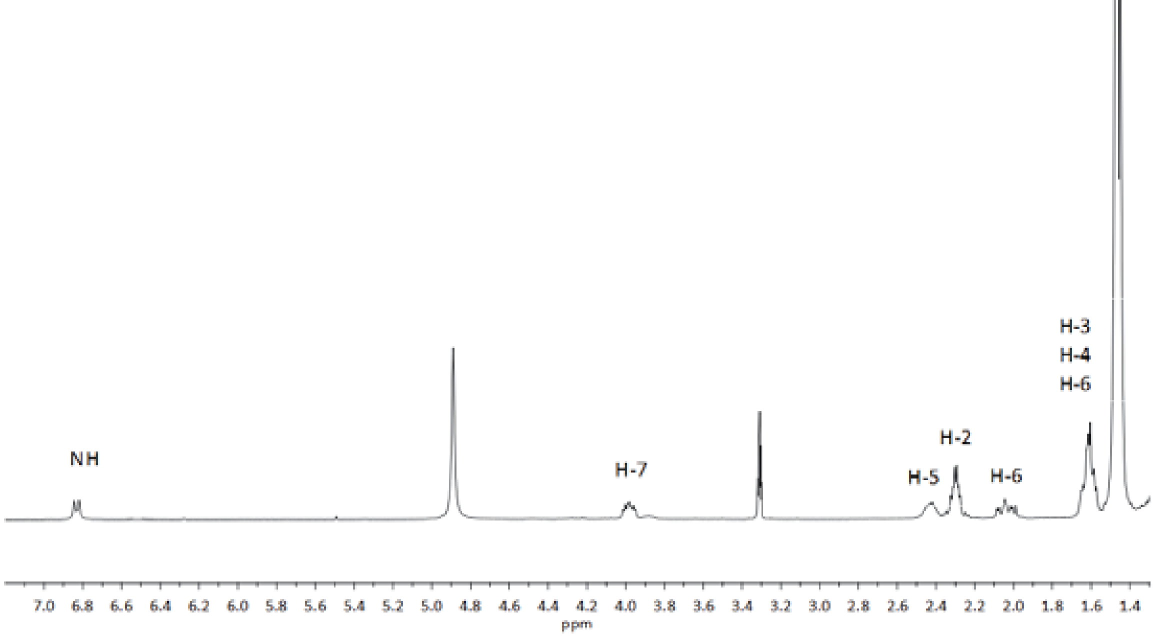

^{1}H-NMR (360 MHz, MeOH-d_4)

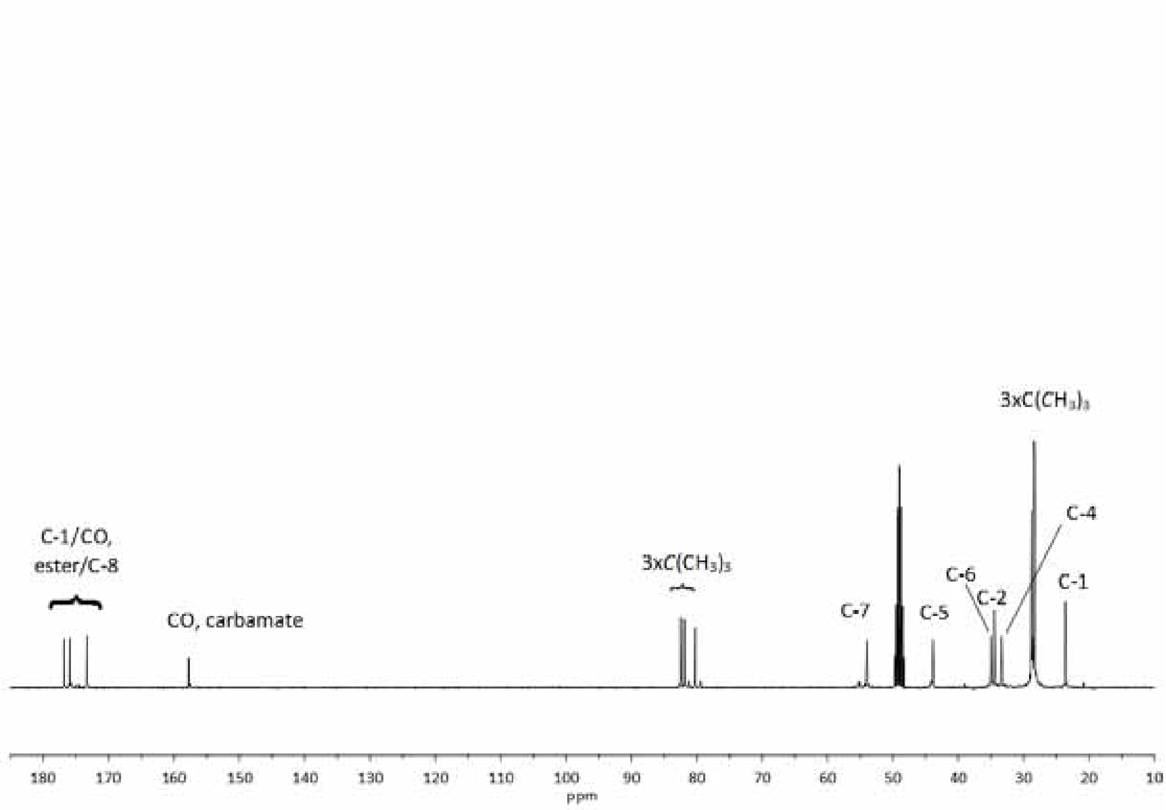

^{13}**C-NMR** (90 MHz, MeOH-d_4)

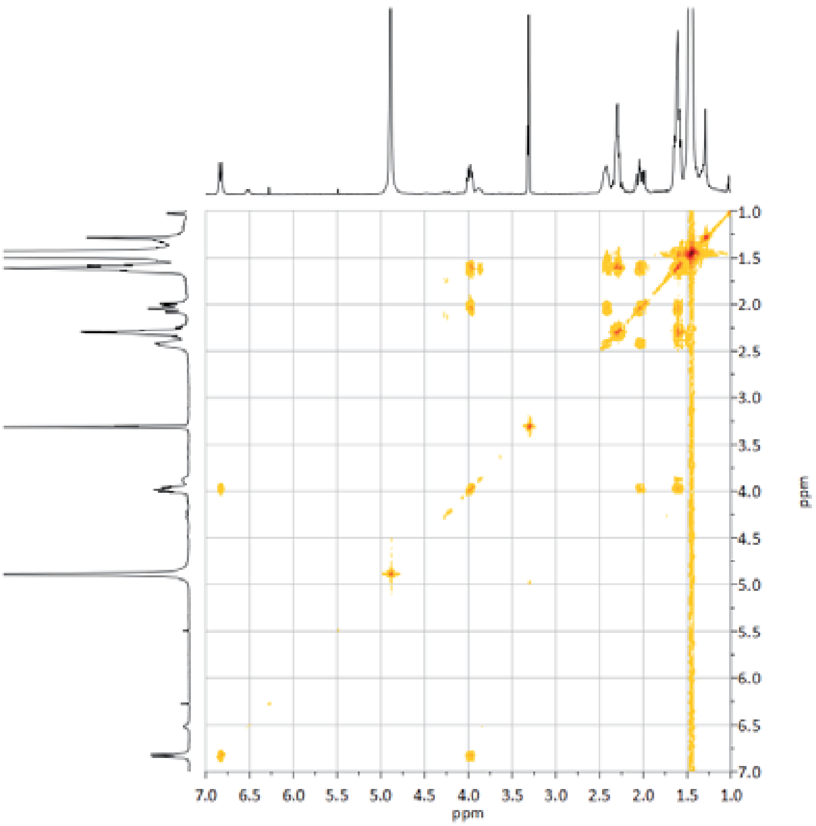

COSY (360 MHz, MeOH-d_4)

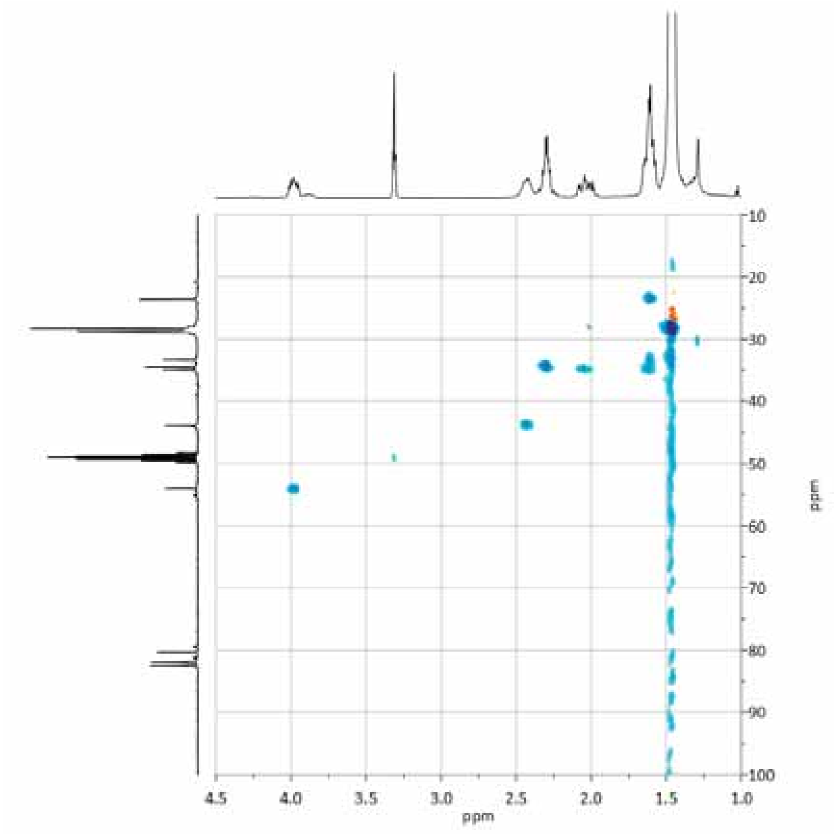

HSQC (360 MHz, MeOH-d_4)

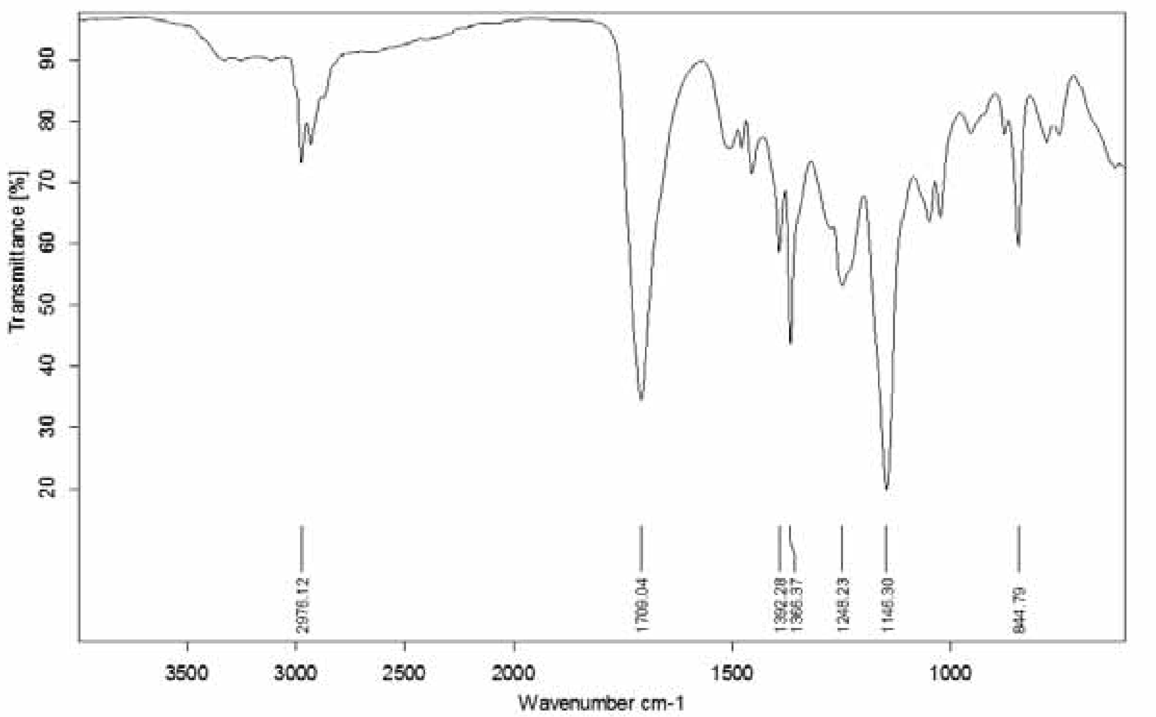

IR (ATR)

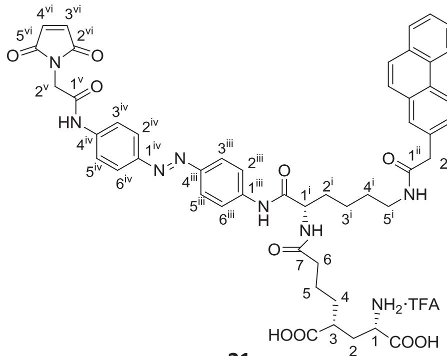

21

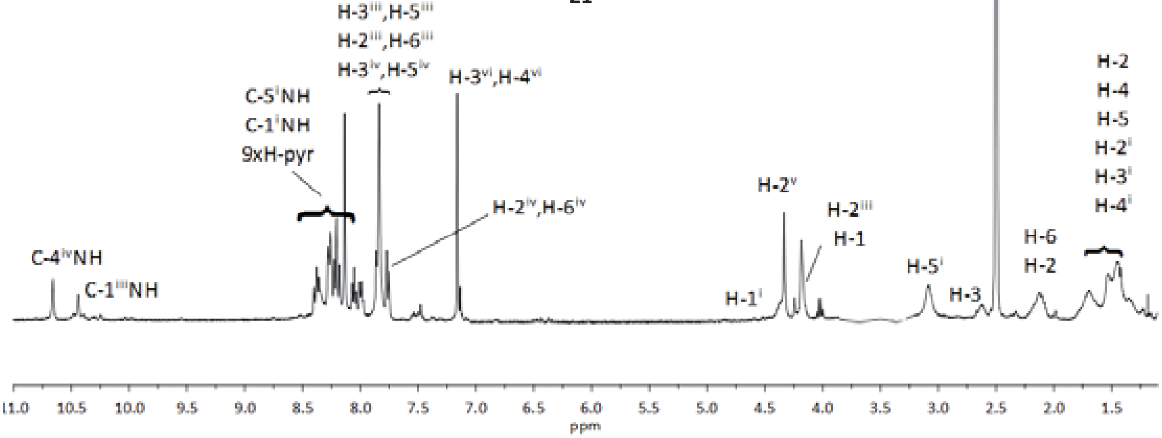

^{1}**H-NMR** (400 MHz, DMSO-d_6)

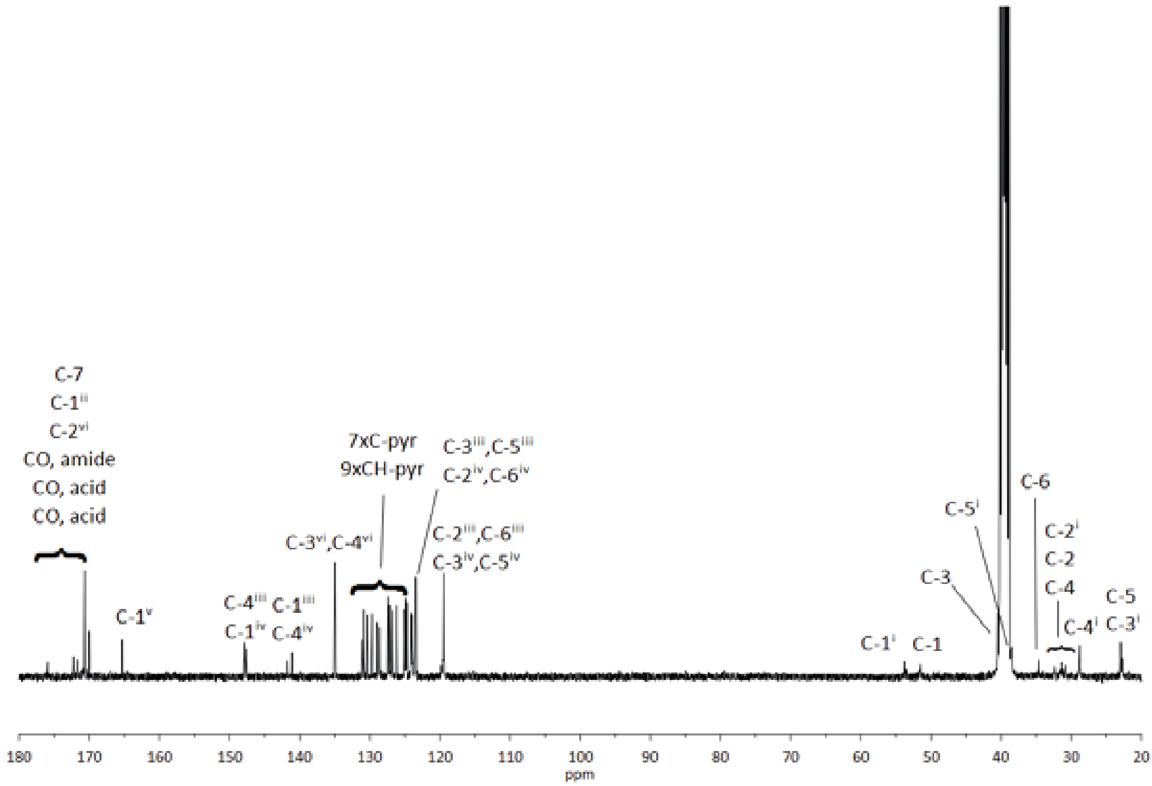

^{13}**C-NMR** (100.6 MHz, DMSO-d_6)

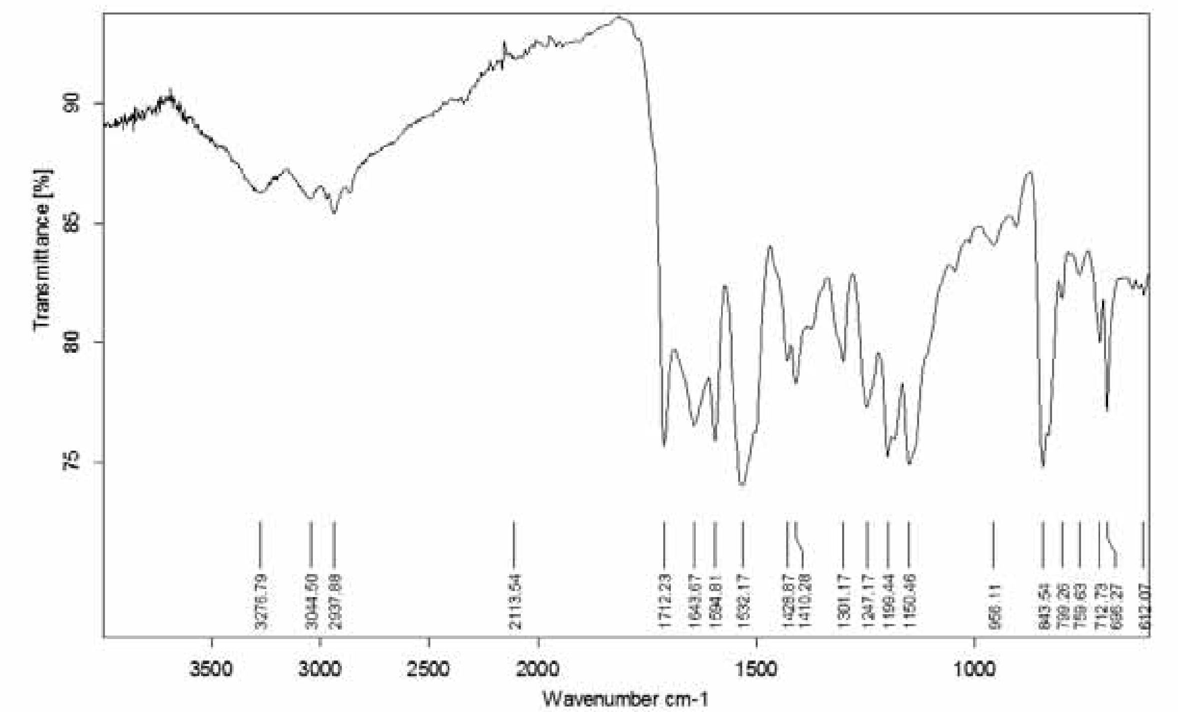

IR (ATR)

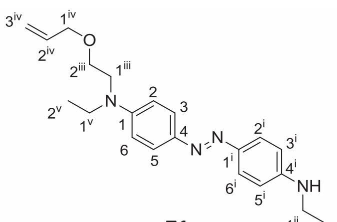

71

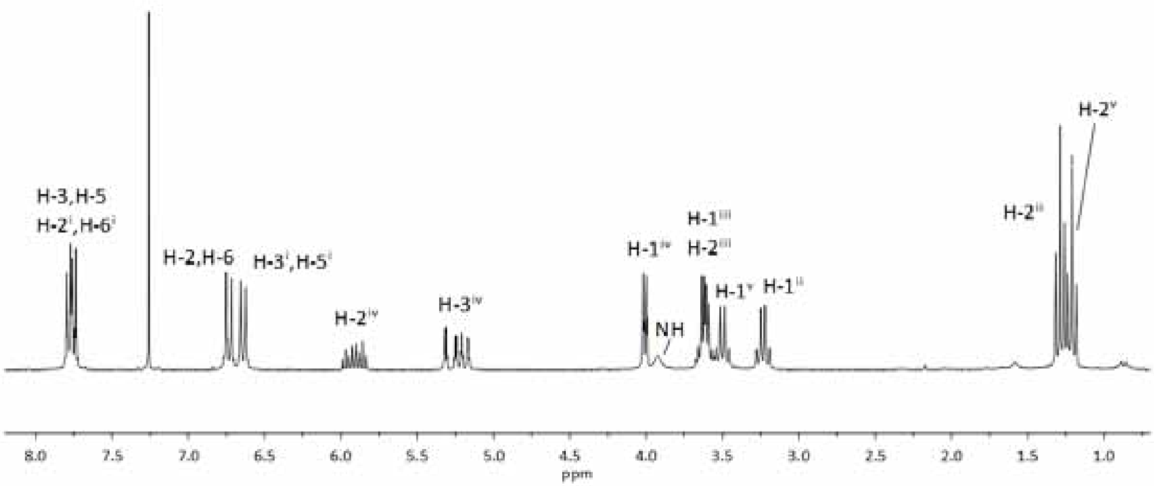

^{1}**H-NMR** (250 MHz, $CDCl_3$)

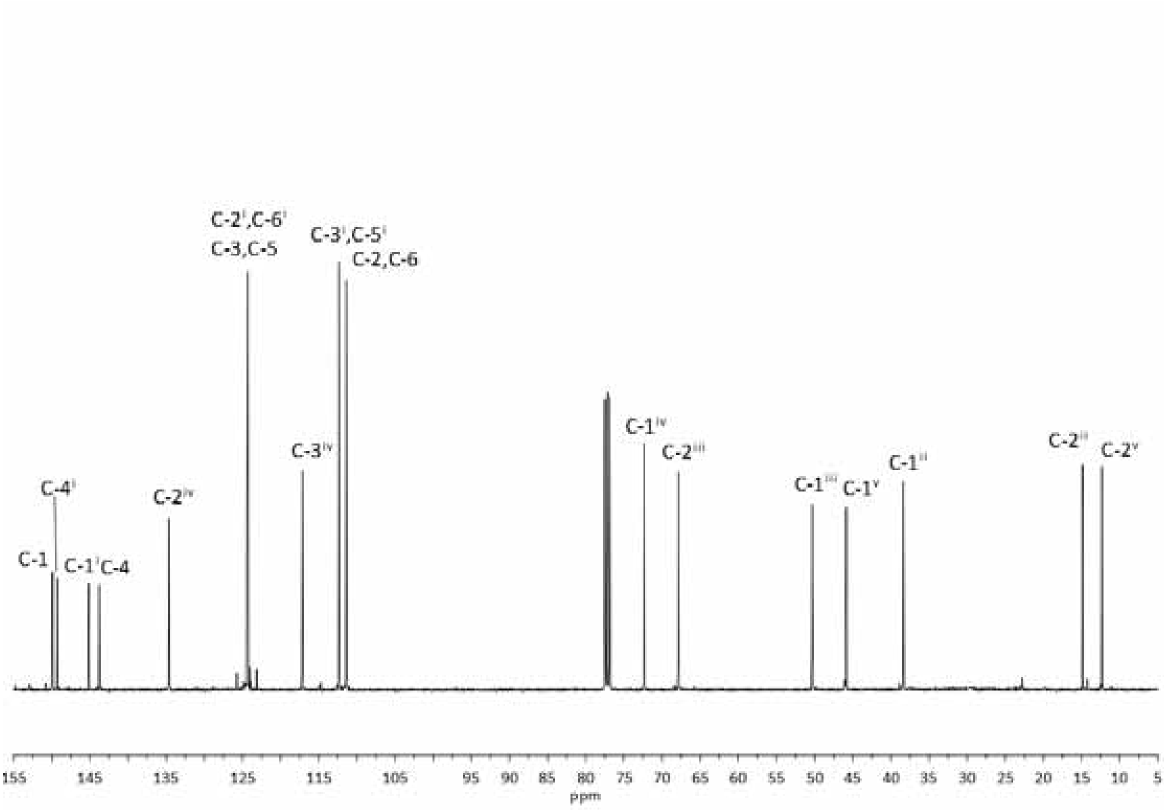

^{13}**C-NMR** (100.6 MHz, $CDCl_3$)

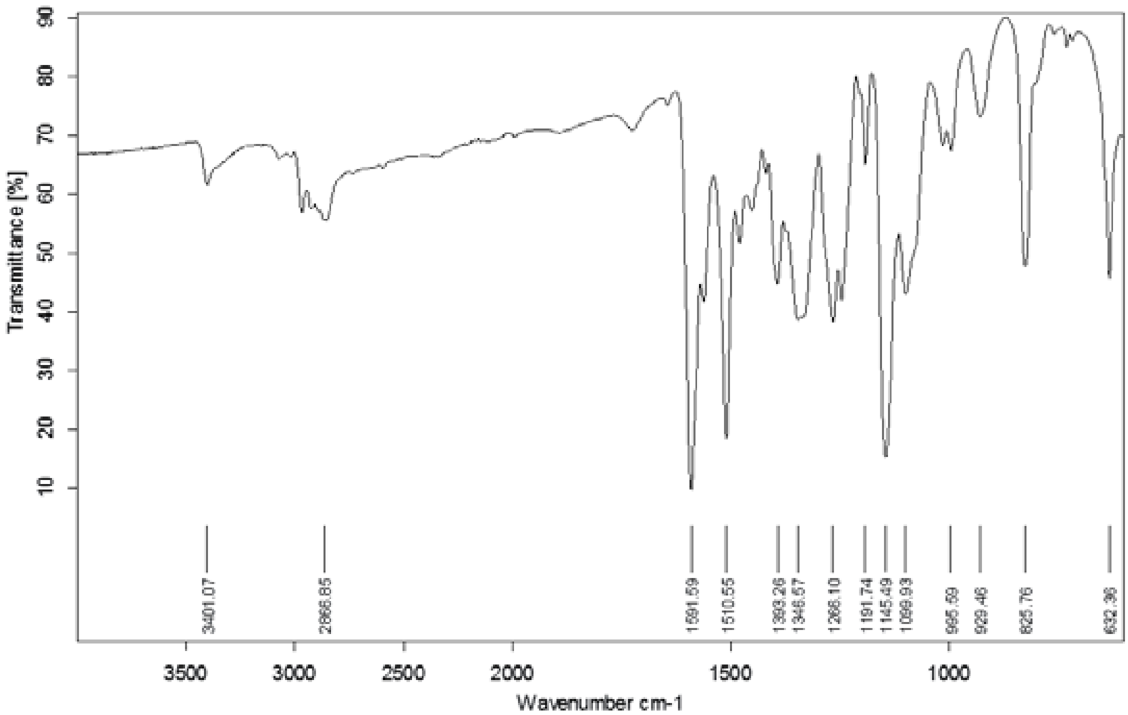

IR (ATR)

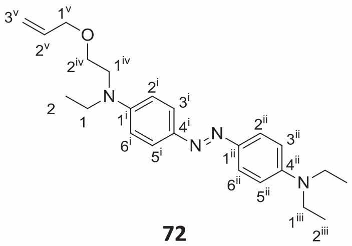

72

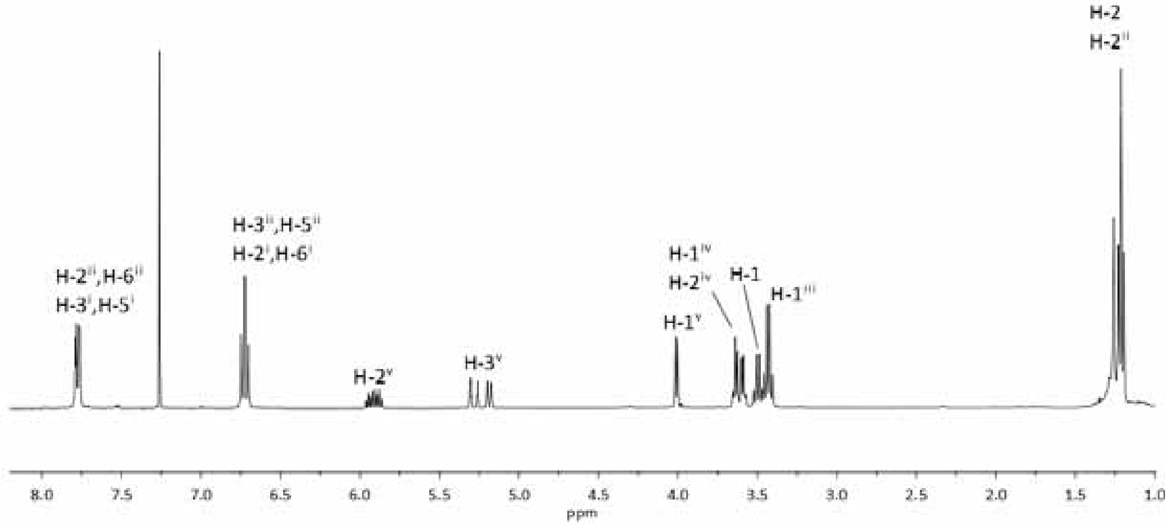

^{1}H-NMR (400 MHz, $CDCl_3$)

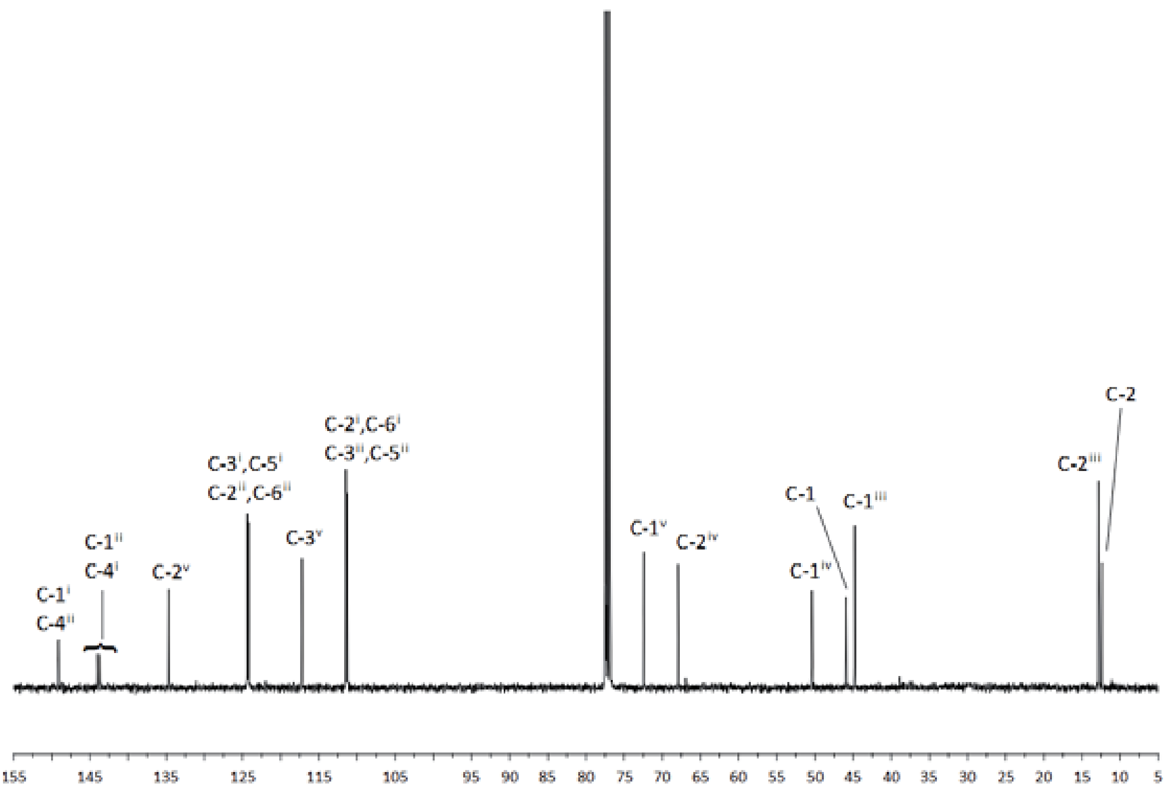

^{13}C-NMR (100.6 MHz, $CDCl_3$)

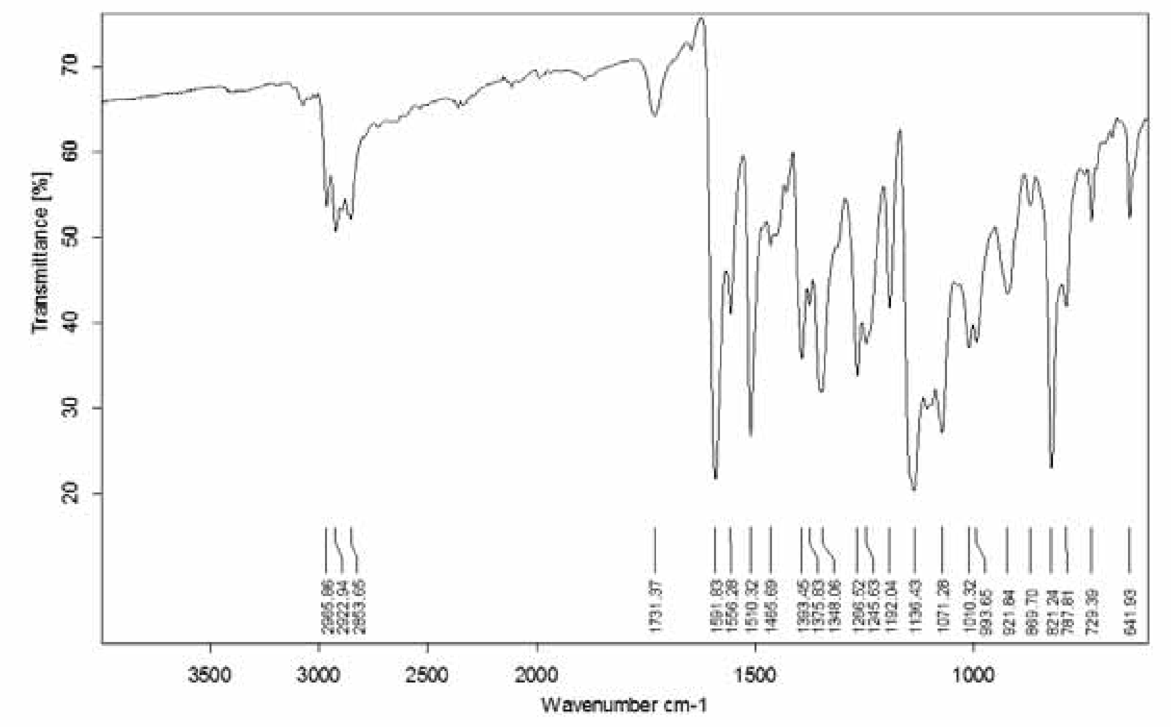

IR (ATR)

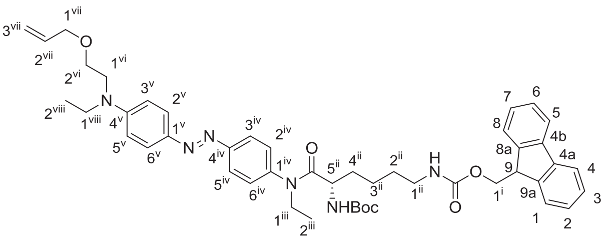

74

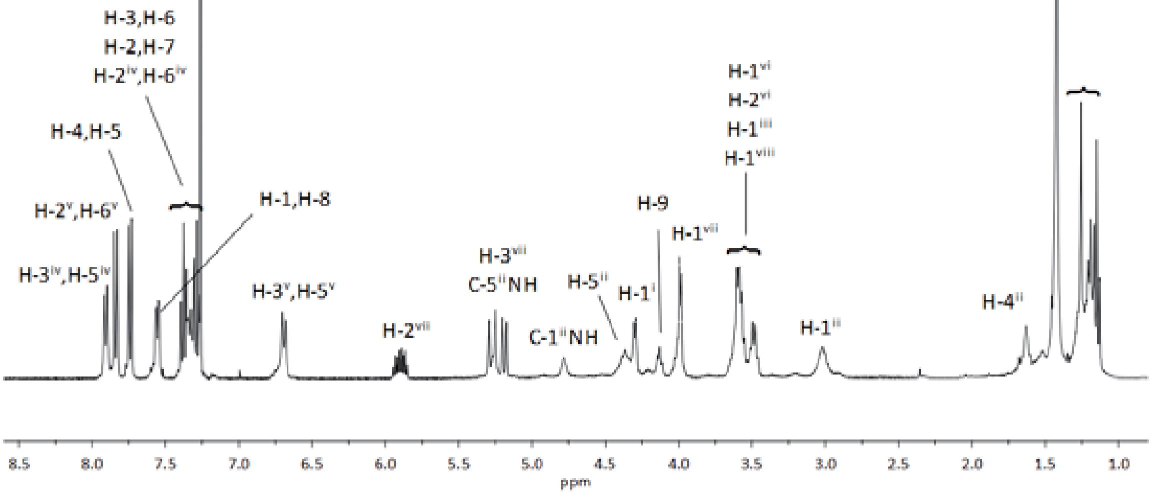

^{1}**H-NMR** (400 MHz, $CDCl_3$)

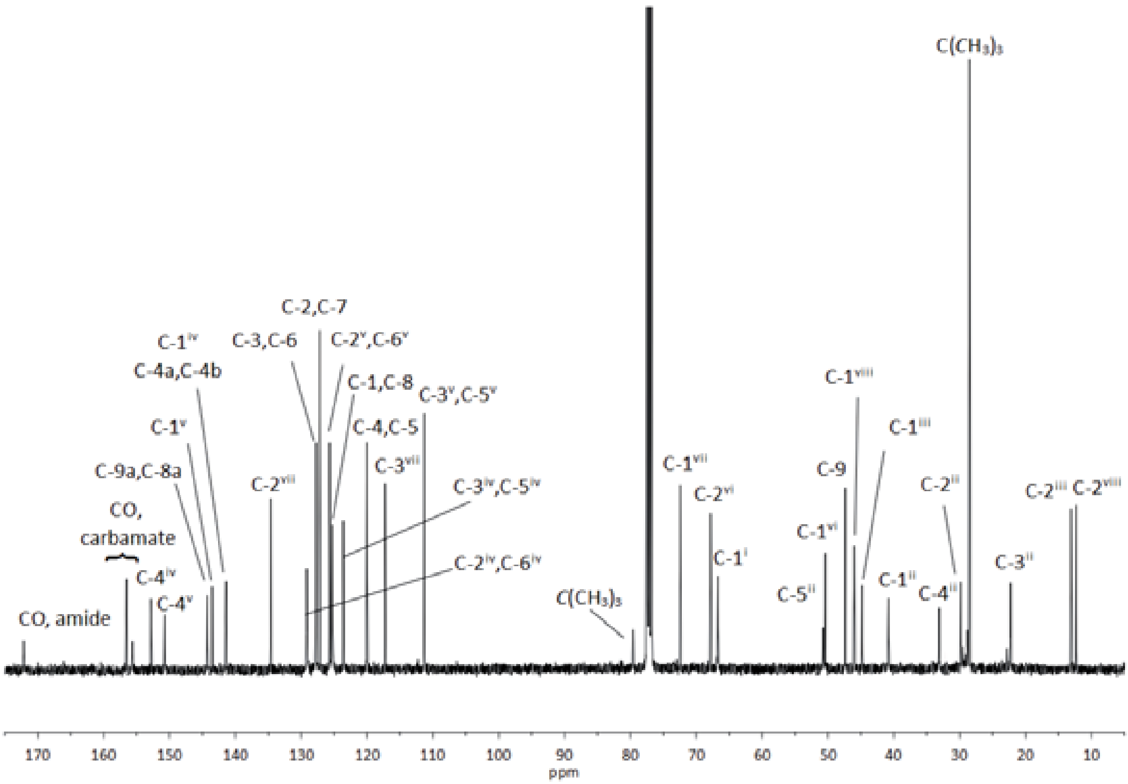

^{13}**C-NMR** (100.6 MHz, $CDCl_3$)

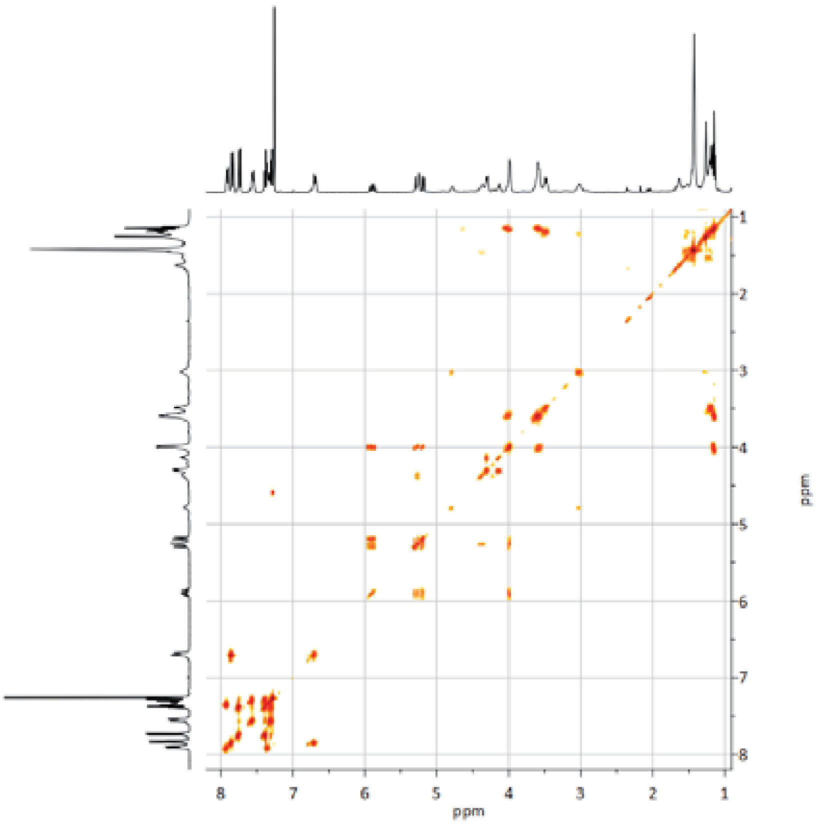

COSY (400 MHz, $CDCl_3$)

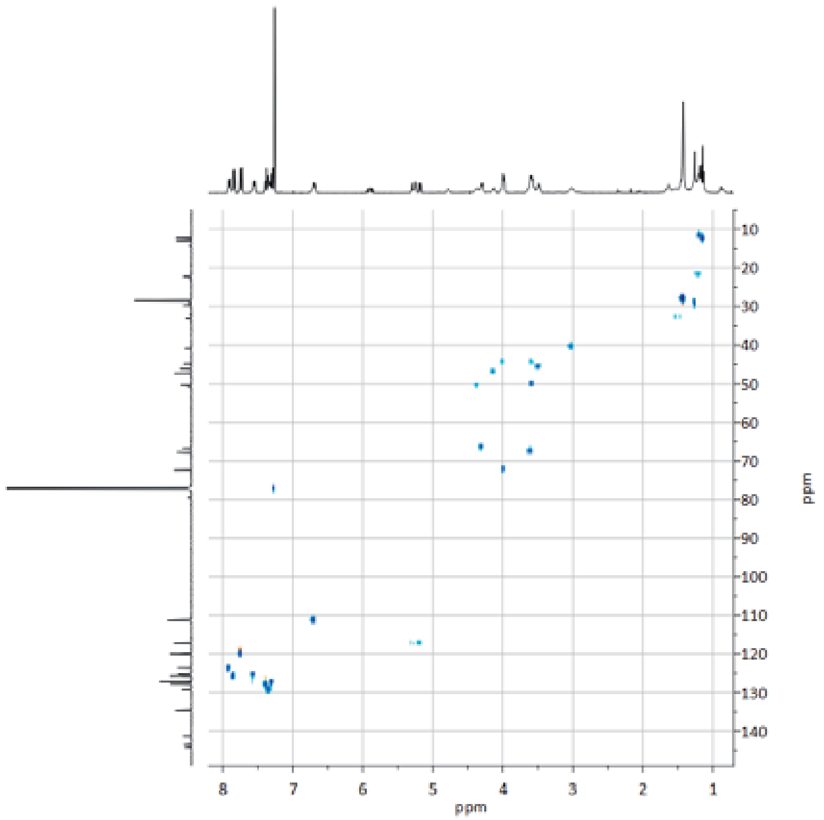

HSQC (400 MHz, $CDCl_3$)

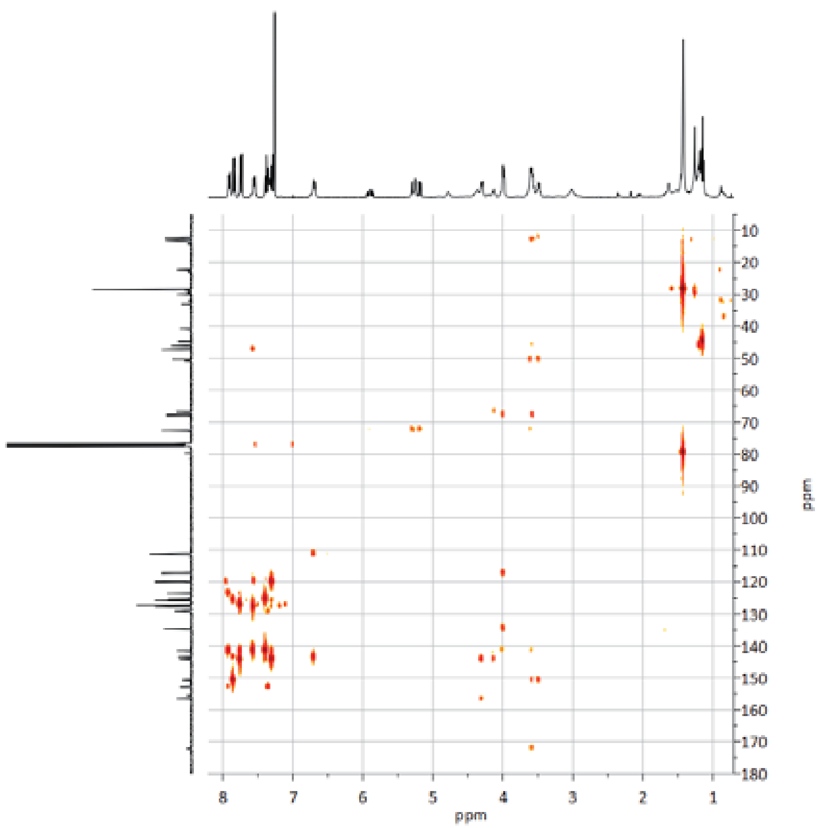

HMBC (400 MHz, $CDCl_3$)

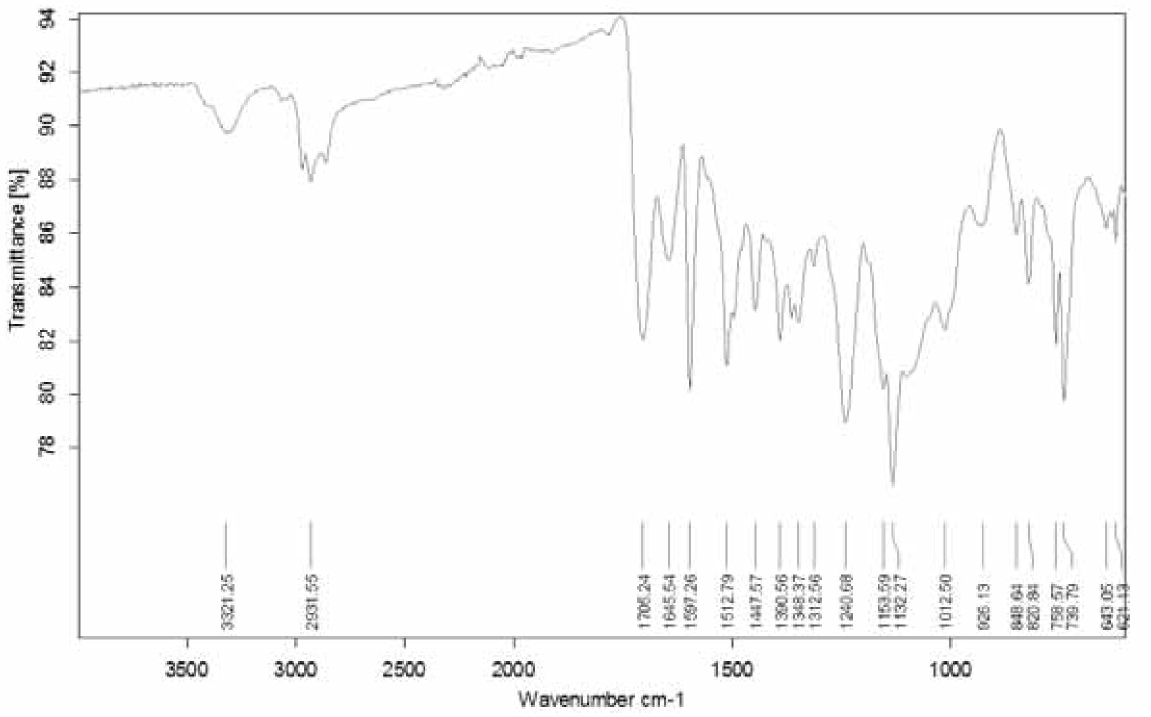

IR (ATR)

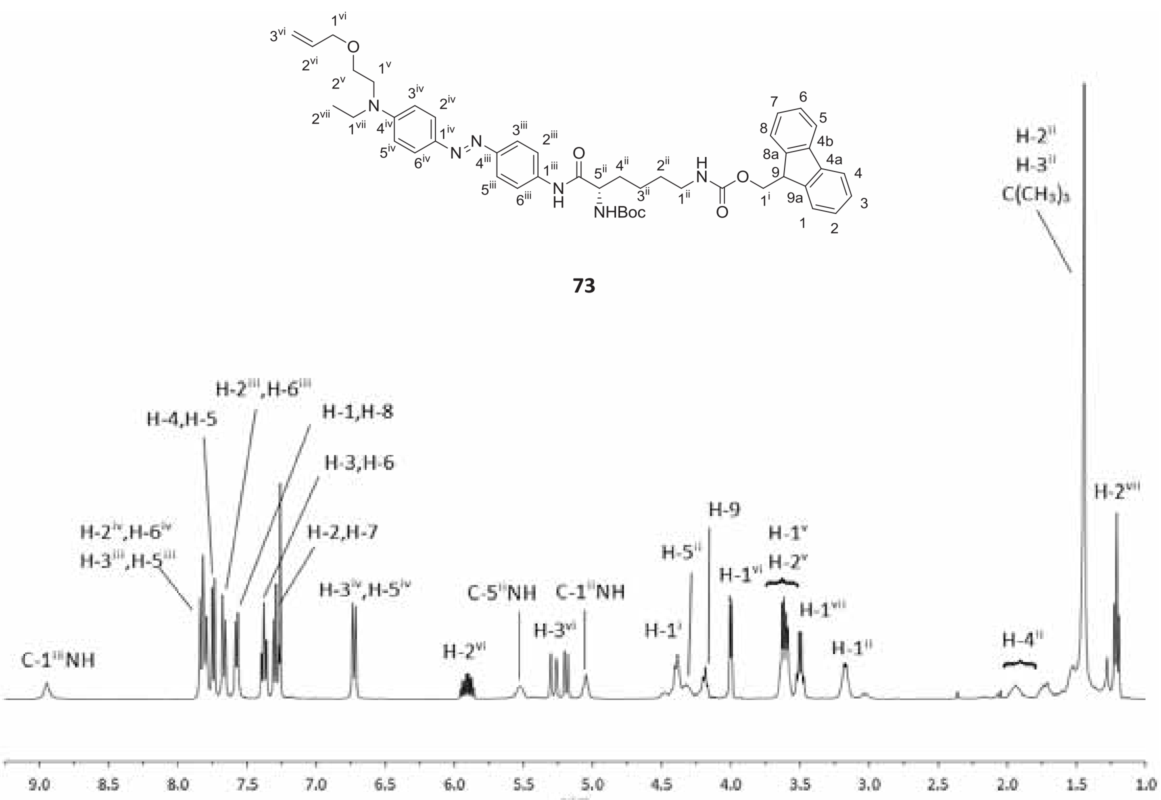

^{1}H-NMR (400 MHz, $CDCl_3$)

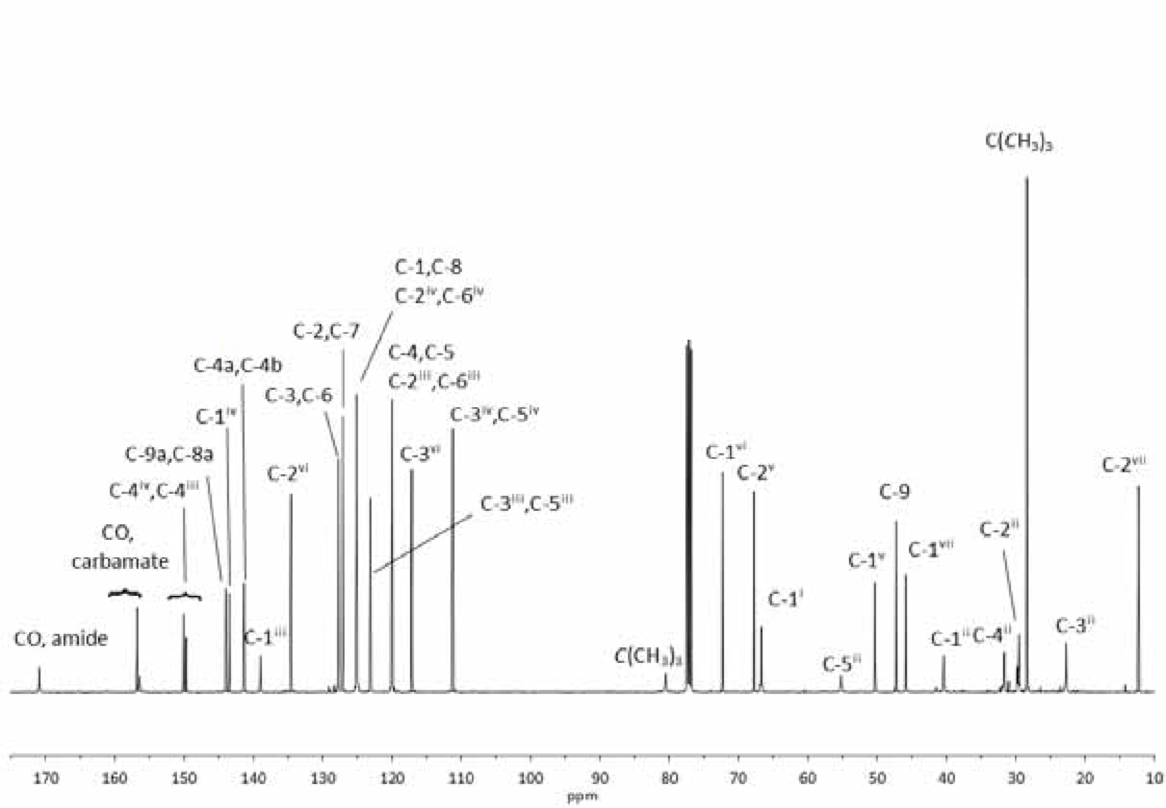

^{13}C-NMR (100.6 MHz, CDCl$_3$)

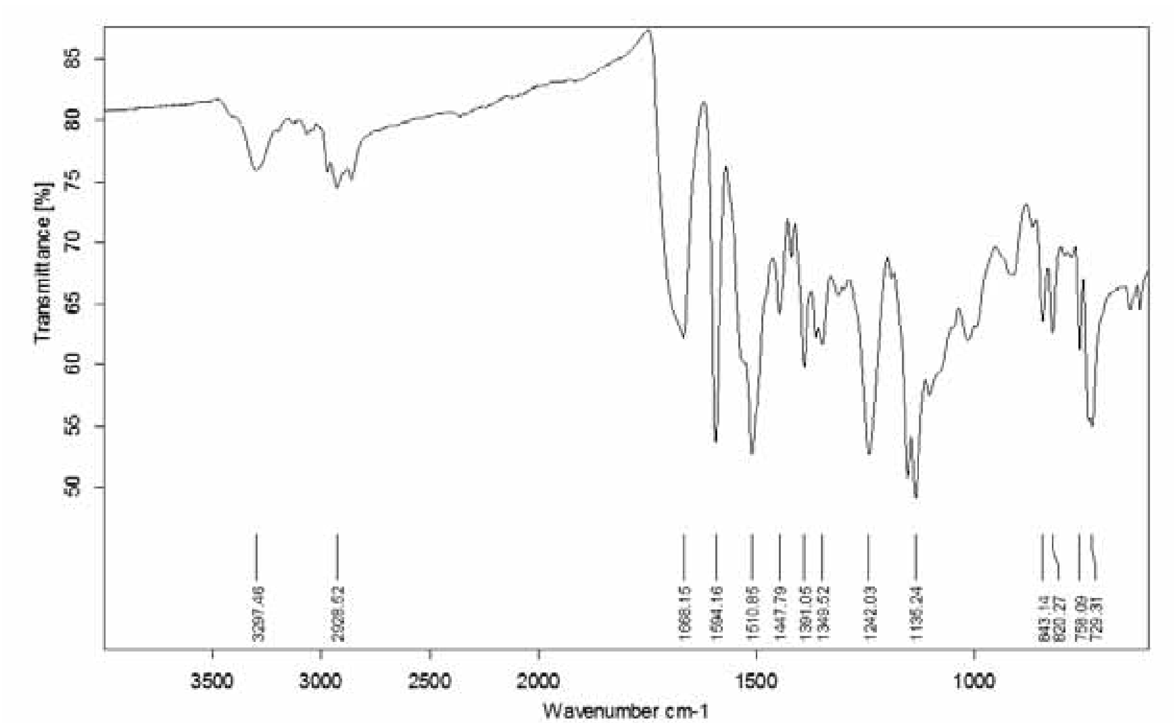

IR (ATR)

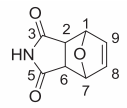

89

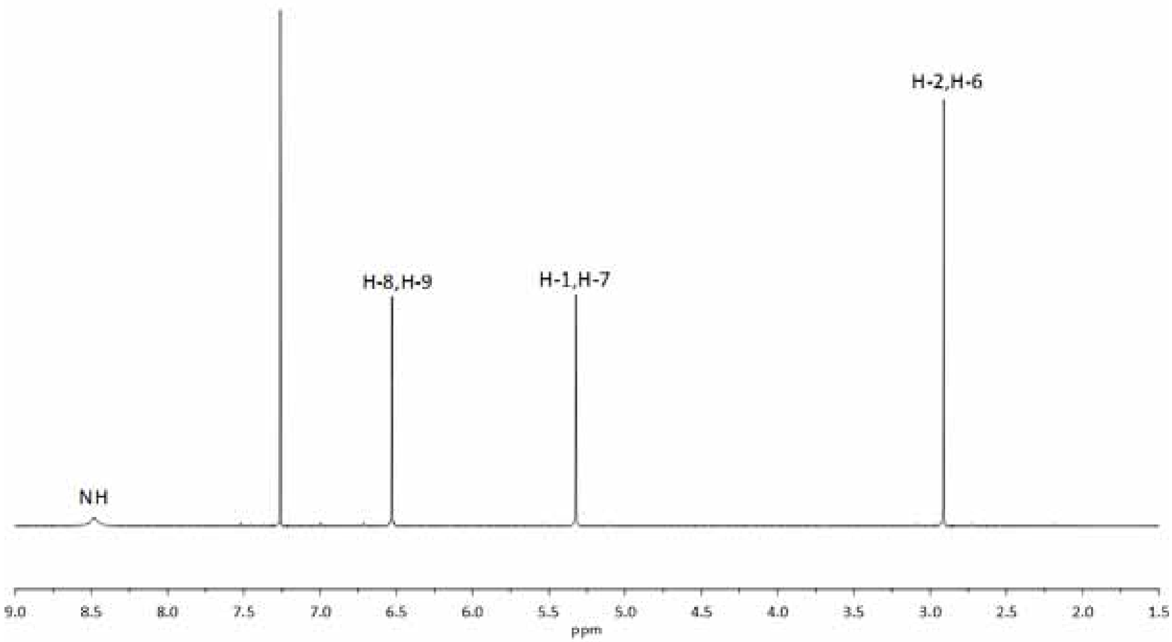

^{1}H-NMR (400 MHz, $CDCl_3$)

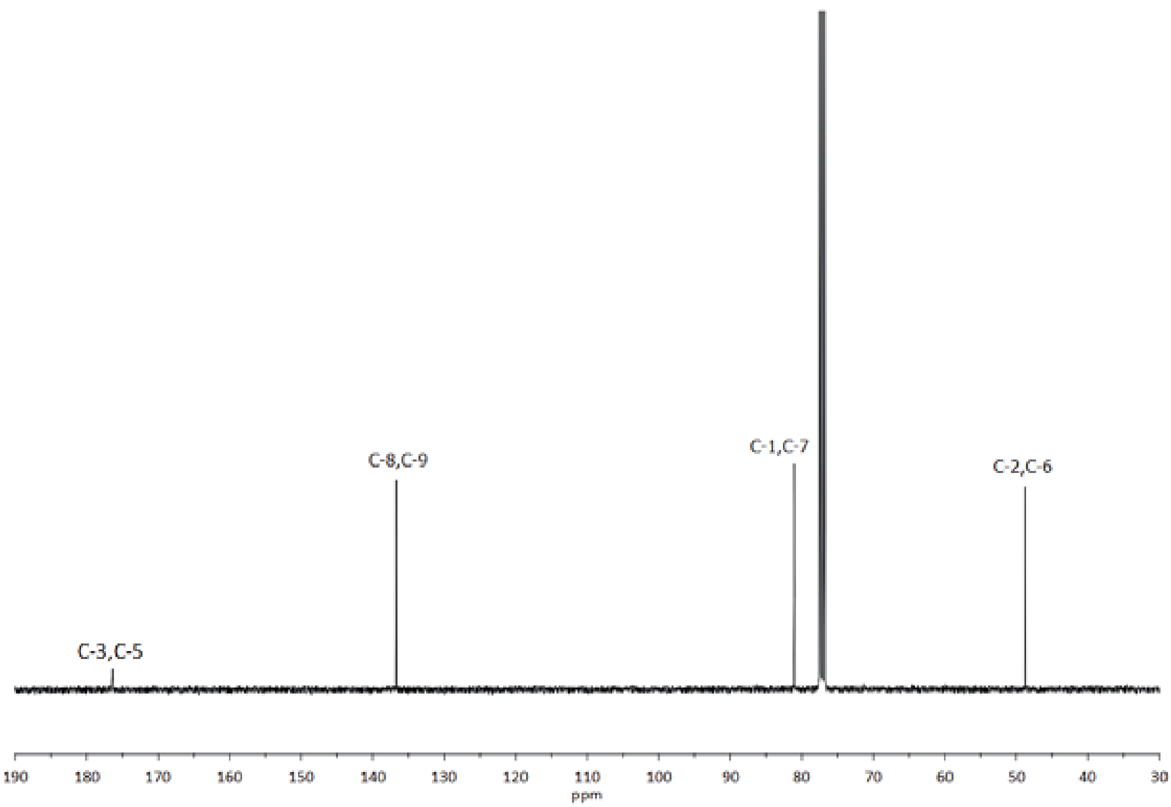

^{13}C-NMR (100.6 MHz, $CDCl_3$)

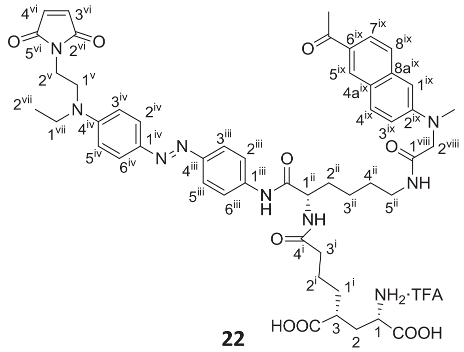

22

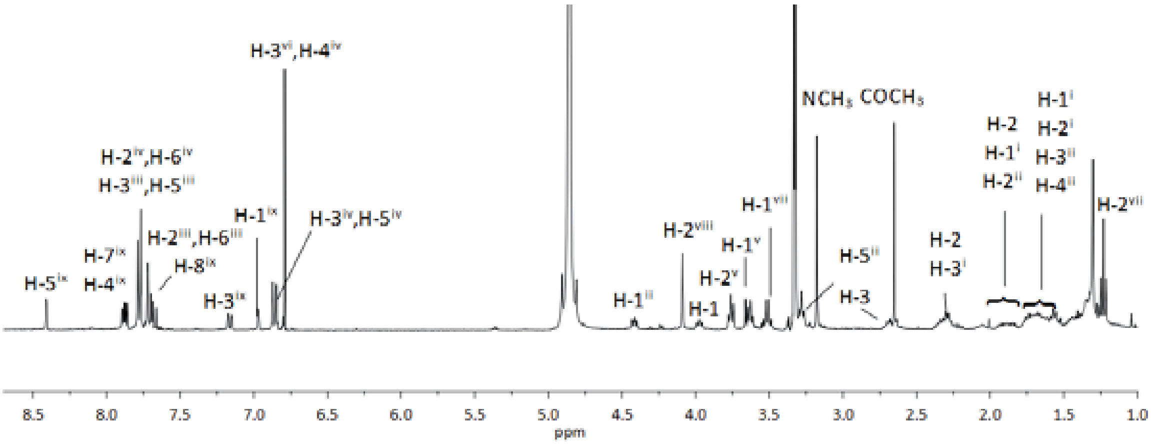

^{1}H-NMR (400 MHz, MeOH-d_4)

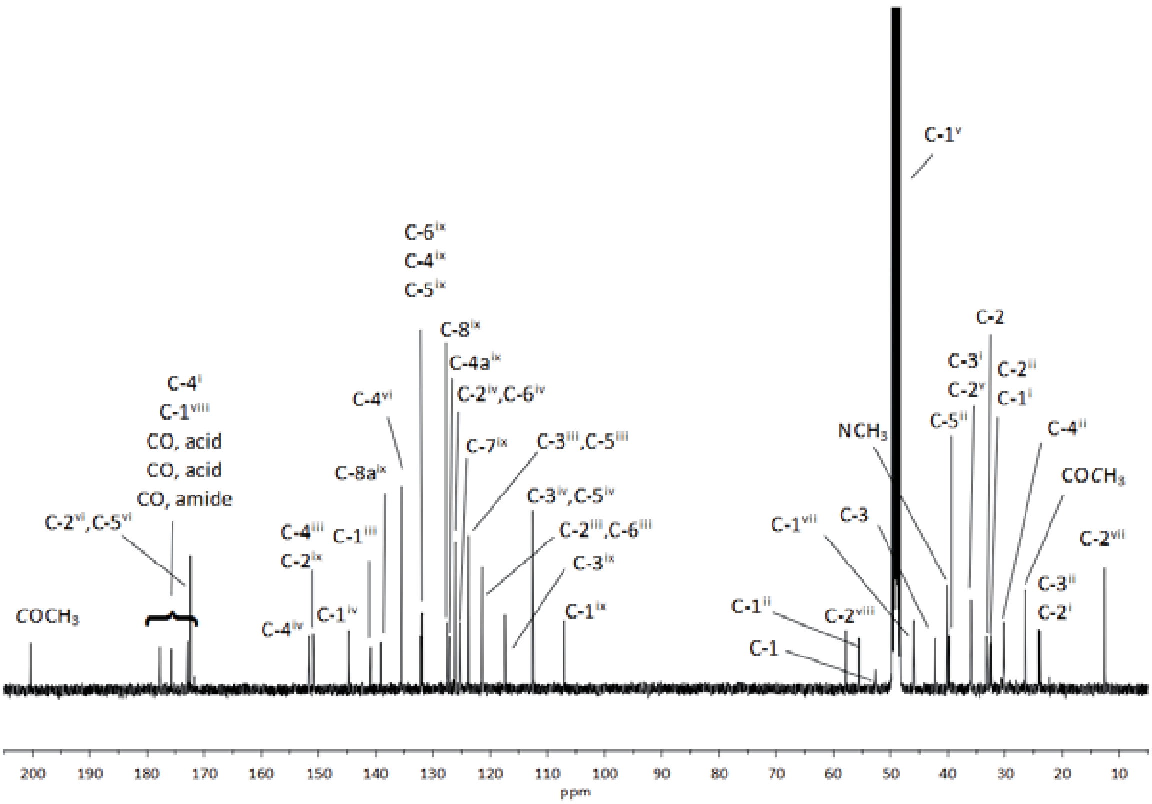

^{13}C-NMR (100.6 MHz, MeOH-d_4)

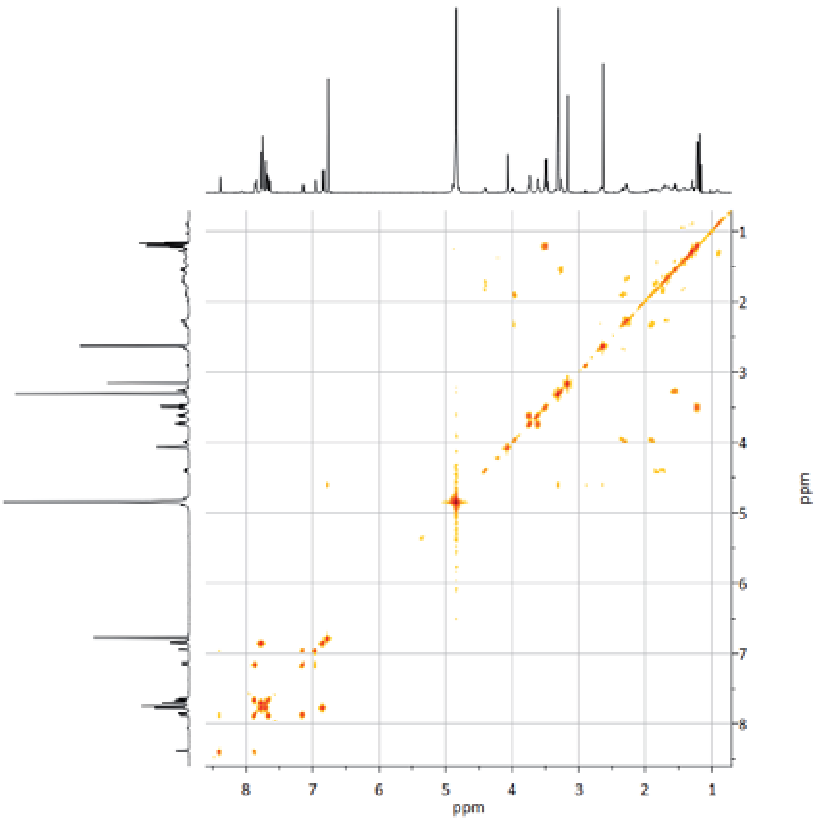

COSY (400 MHz, MeOH-d_4)

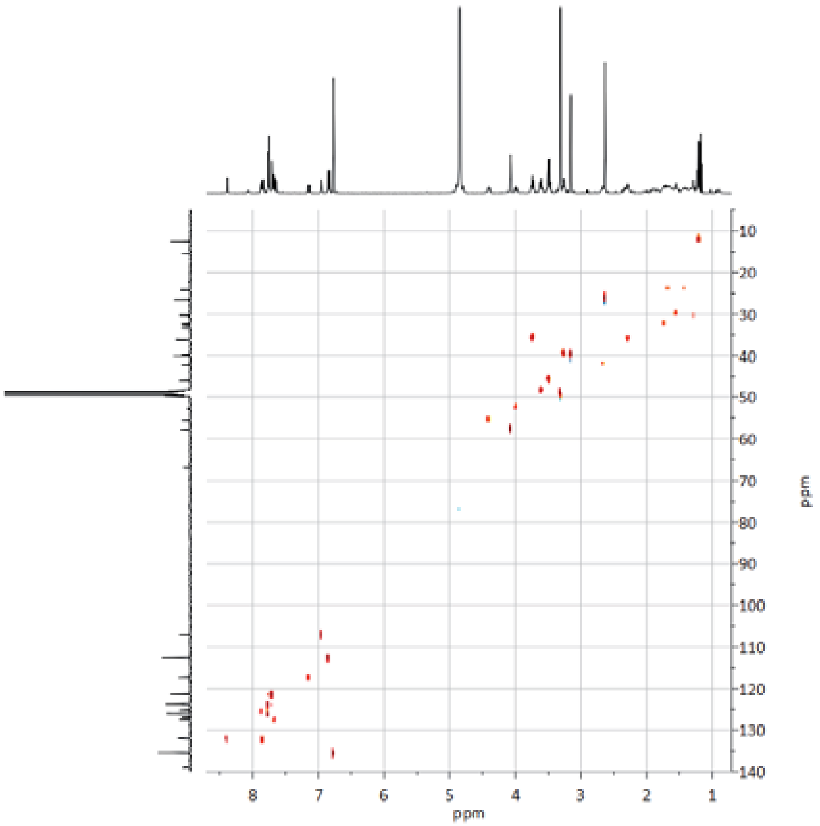

HSQC (400 MHz, MeOH-d_4)

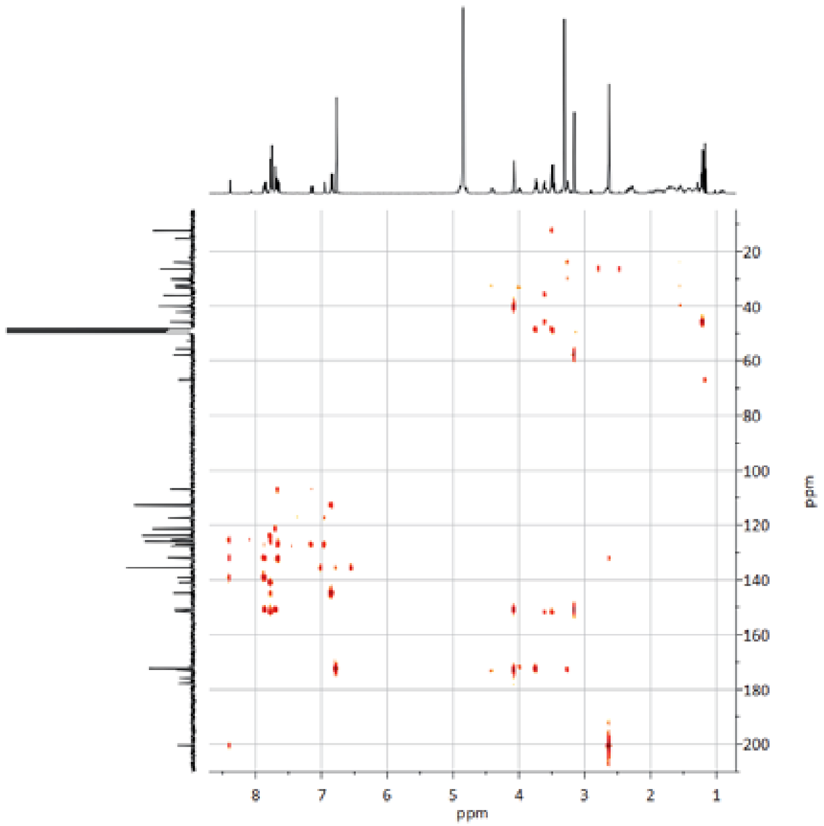

HMBC (400 MHz, MeOH-d_4)

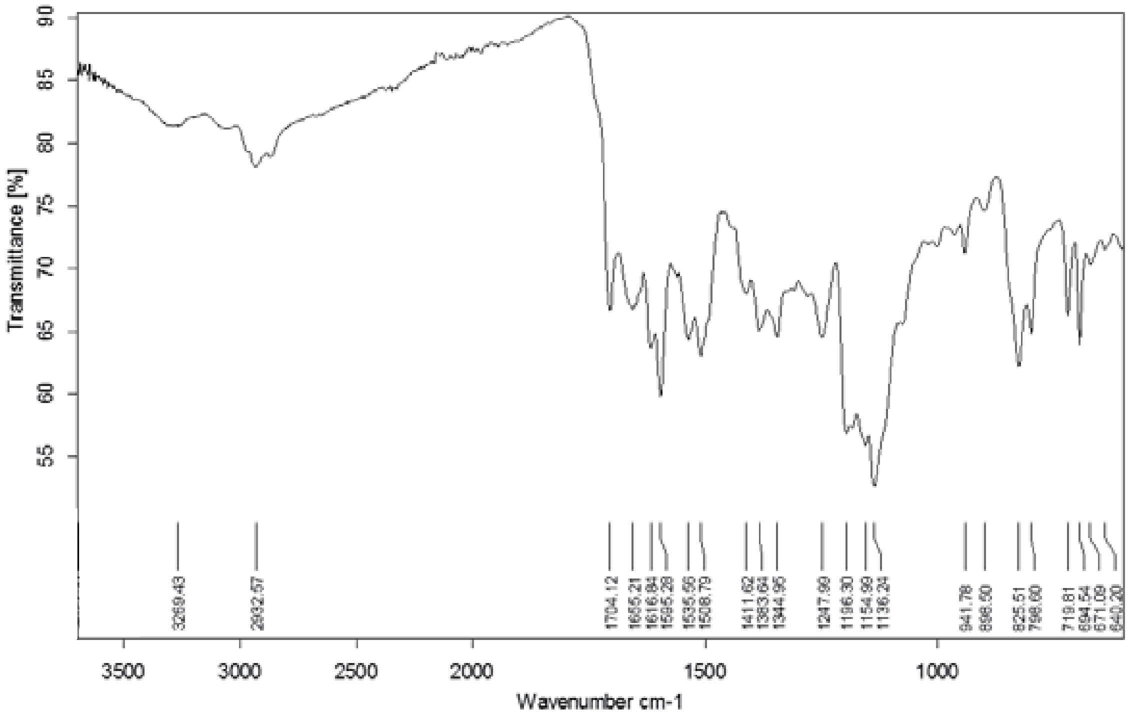

IR (ATR)

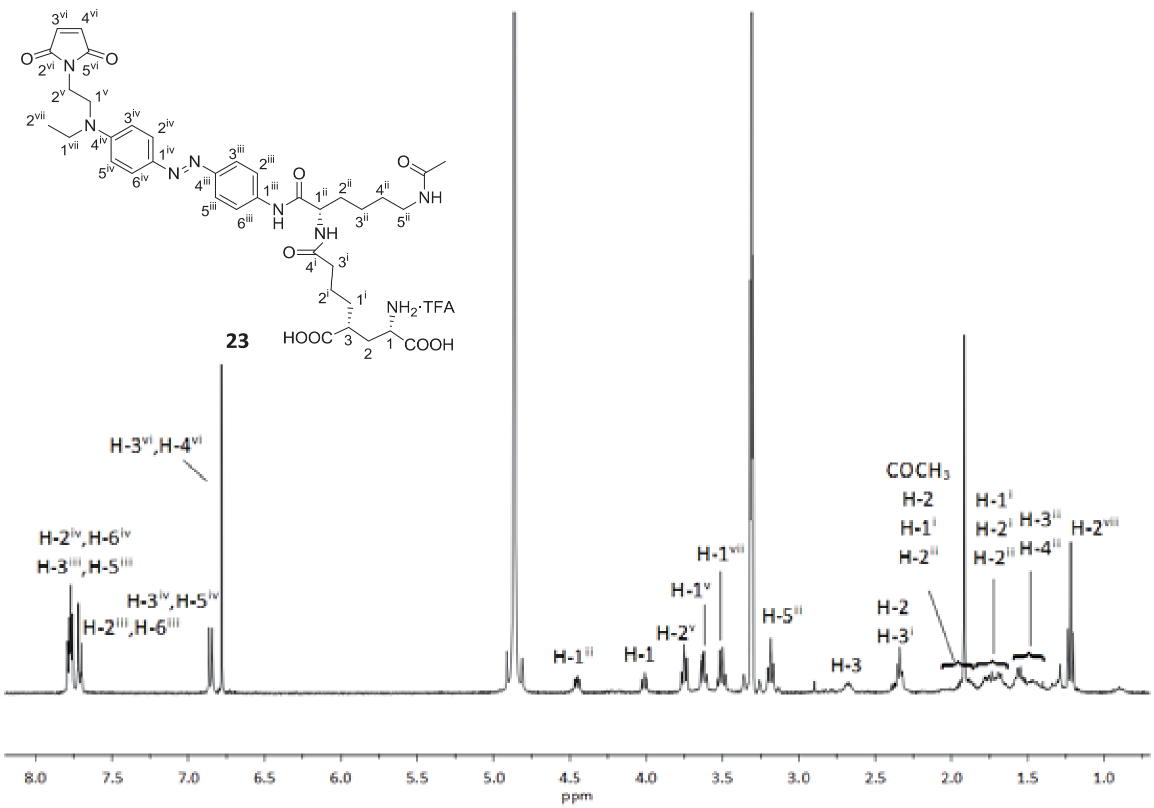

^{1}**H-NMR** (400 MHz, MeOH-d_4)

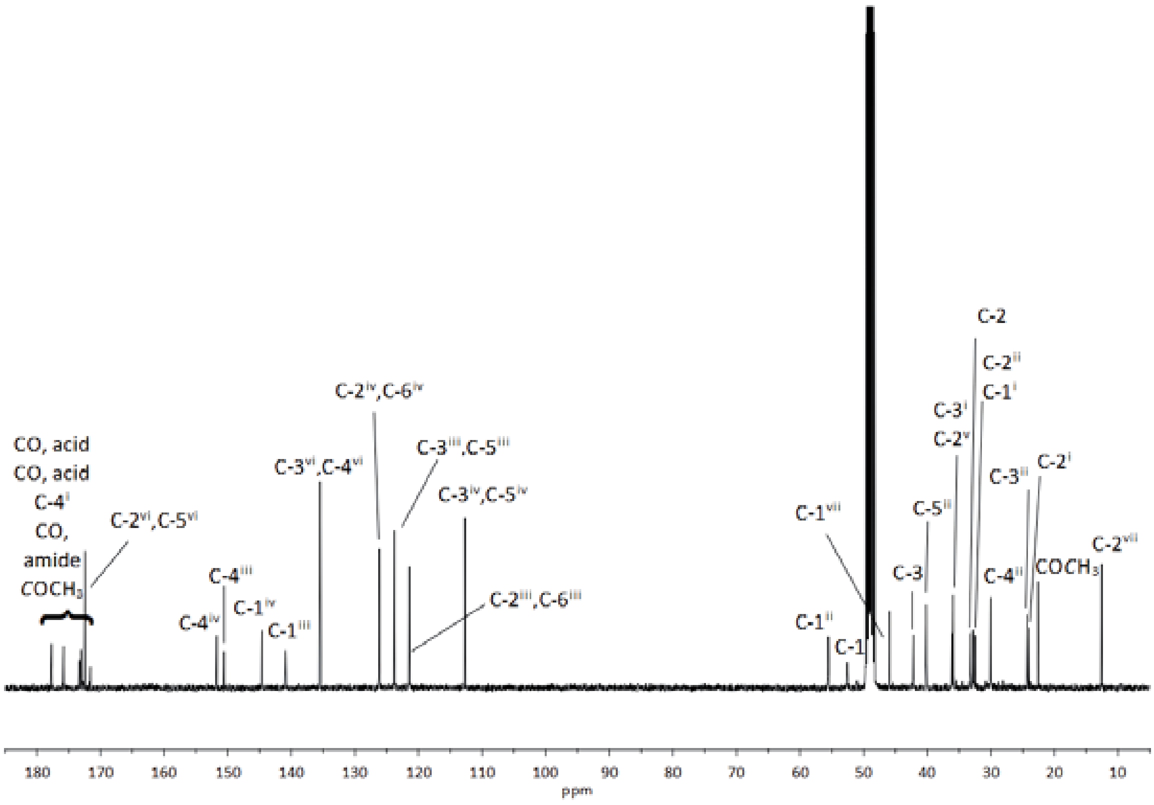

^{13}**C-NMR** (100.6 MHz, MeOH-d_4)

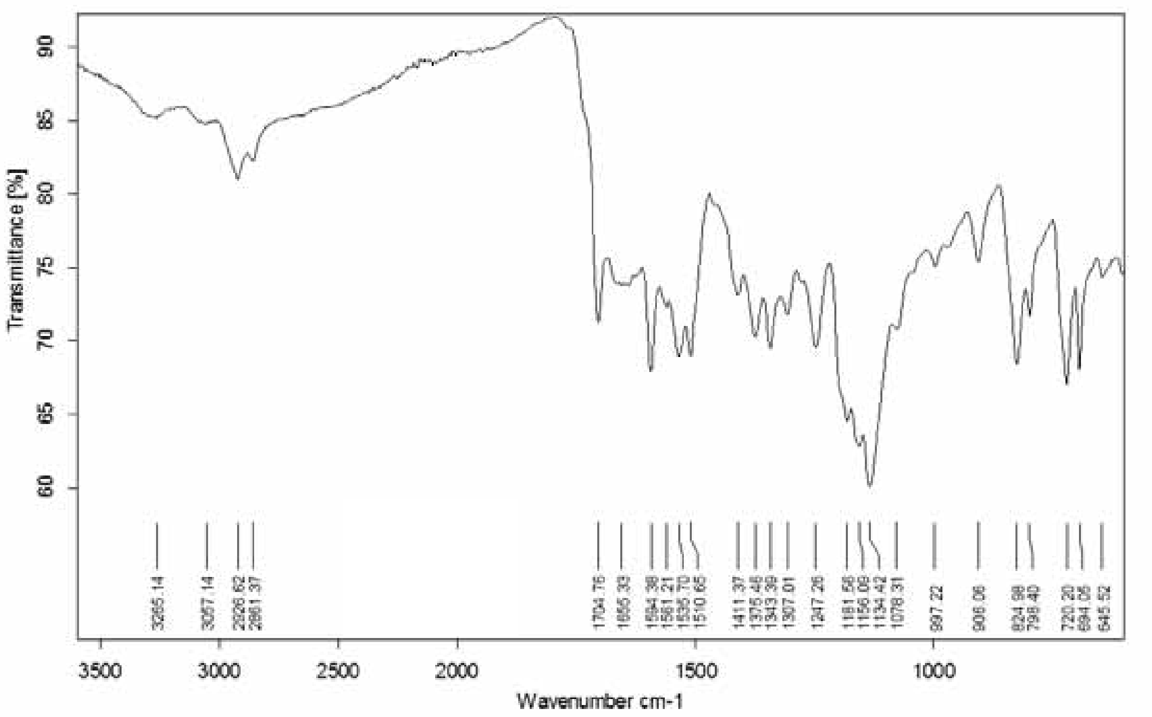

IR (ATR)

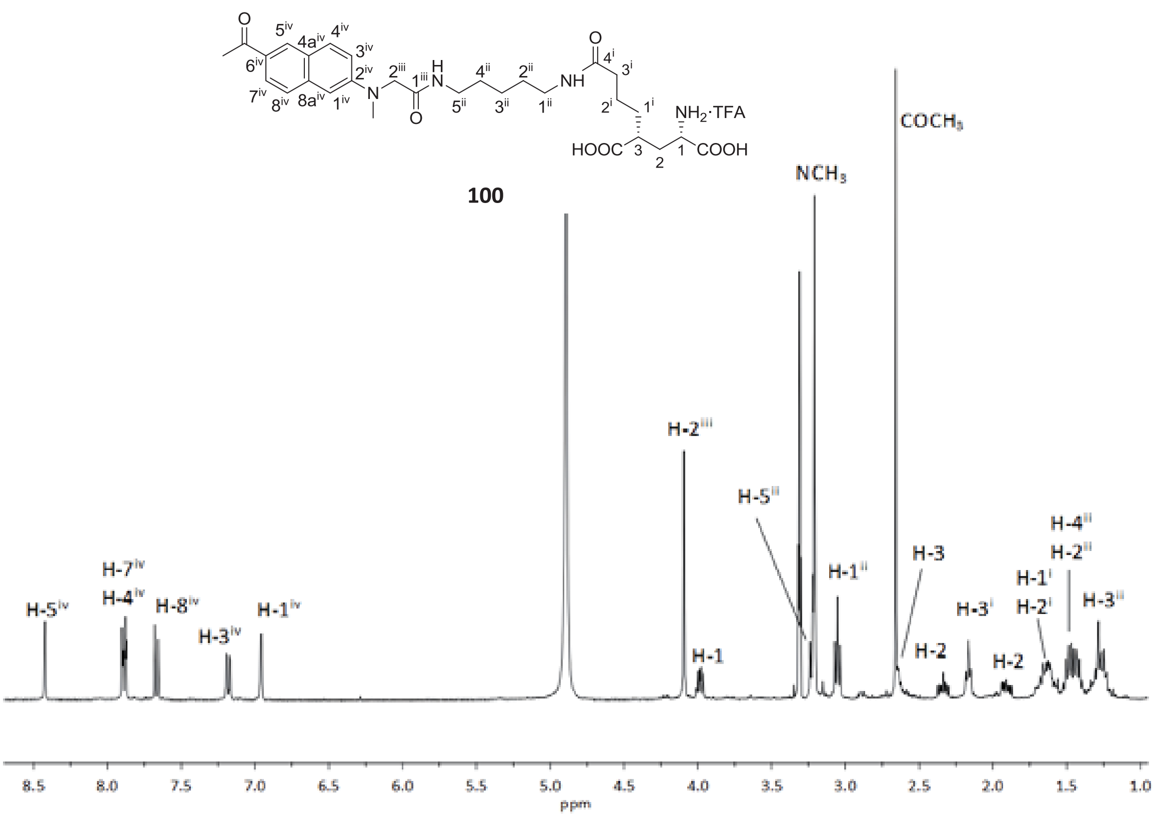

^{1}H-NMR (400 MHz, MeOH-d$_4$)

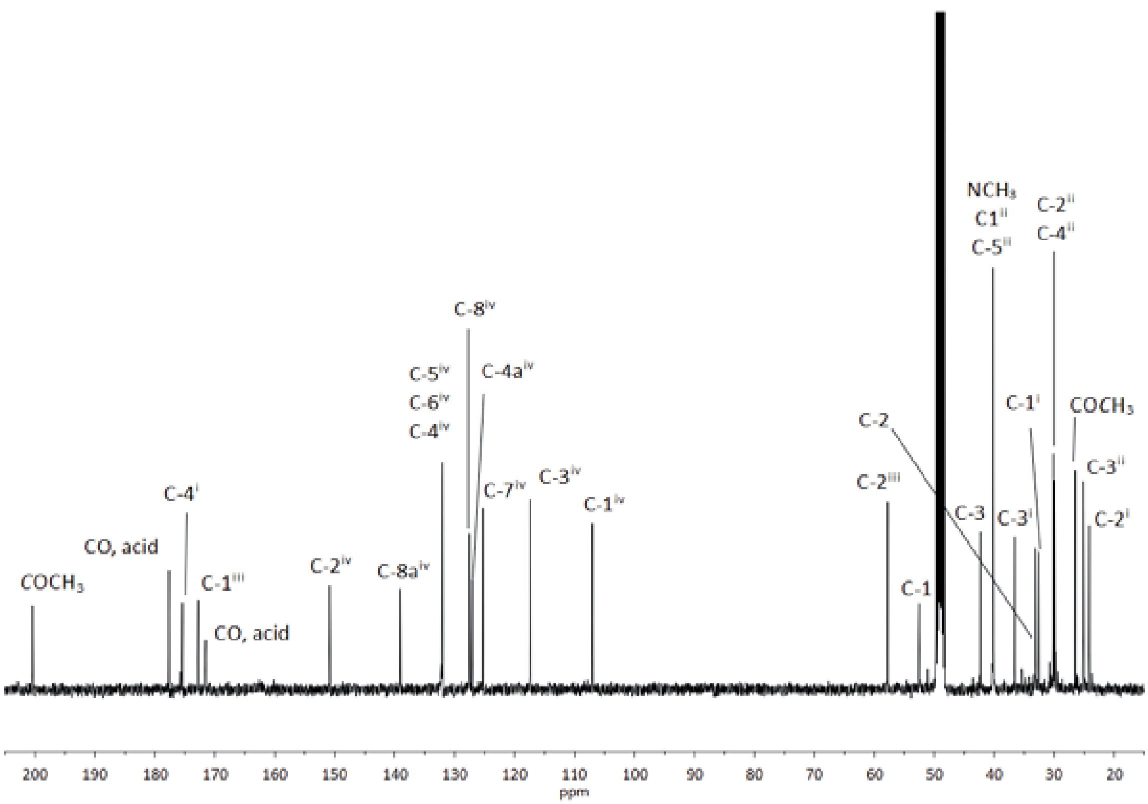

^{13}**C-NMR** (100.6 MHz, MeOH-d_4)

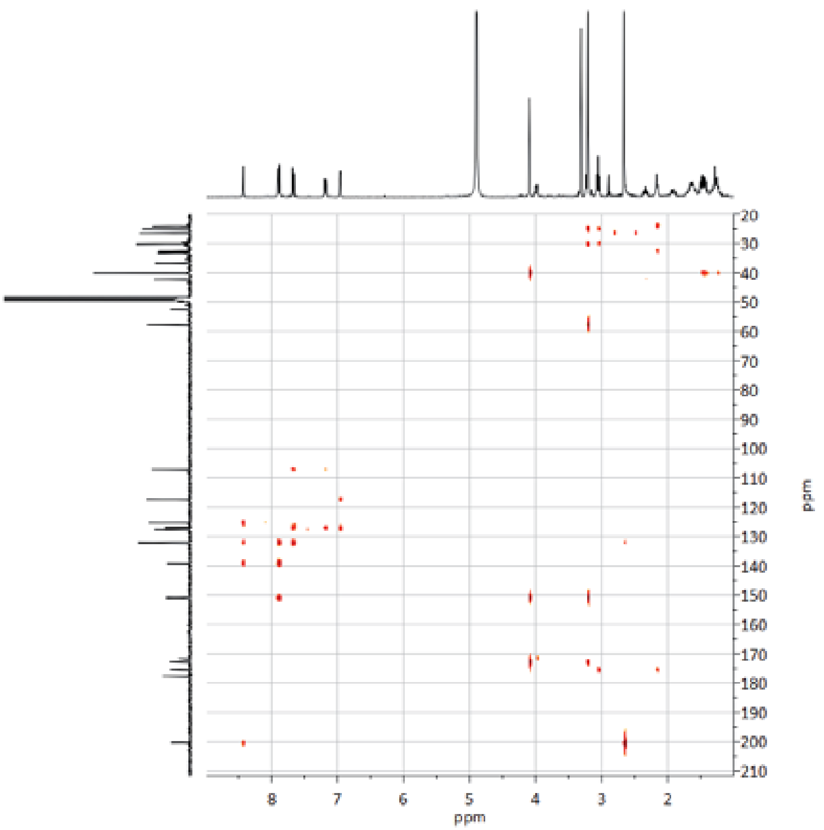

HMBC (400 MHz, MeOH-d_4)

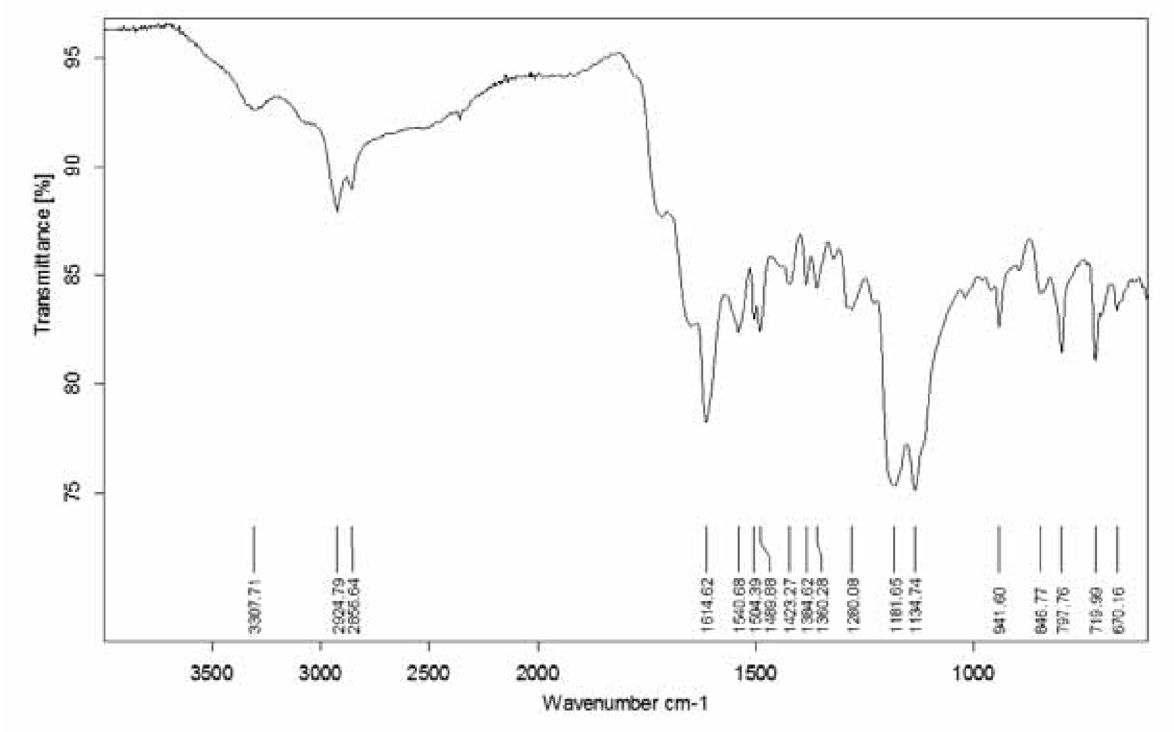
Transmittance [%]
95
90
85
80
75
3307,71
2924,79
2856,64
1614,62
1540,68
1504,39
1489,88
1423,27
1384,62
1360,28
1280,08
1181,65
1134,74
941,60
846,77
797,76
719,99
670,16
3500
3000
2500
2000
1500
1000
Wavenumber cm-1

IR (ATR)

Universitat Autònoma de Barcelona
Facultat de Ciències
Departament de Química

New Azobenzene-based Photoswitches for Two-Photon Optical Control of Neuronal Receptors

Spectral Appendices

Marta Gascón Moya

Ph.D. Thesis

Ph.D. in Chemistry

Supervisors:
Dr. Ramon Alibés Arqués
Dr. Felix Busqué Sánchez
Dr. Jordi Hernando Campos

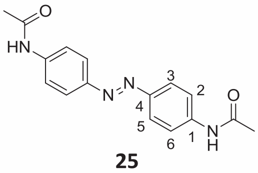

25

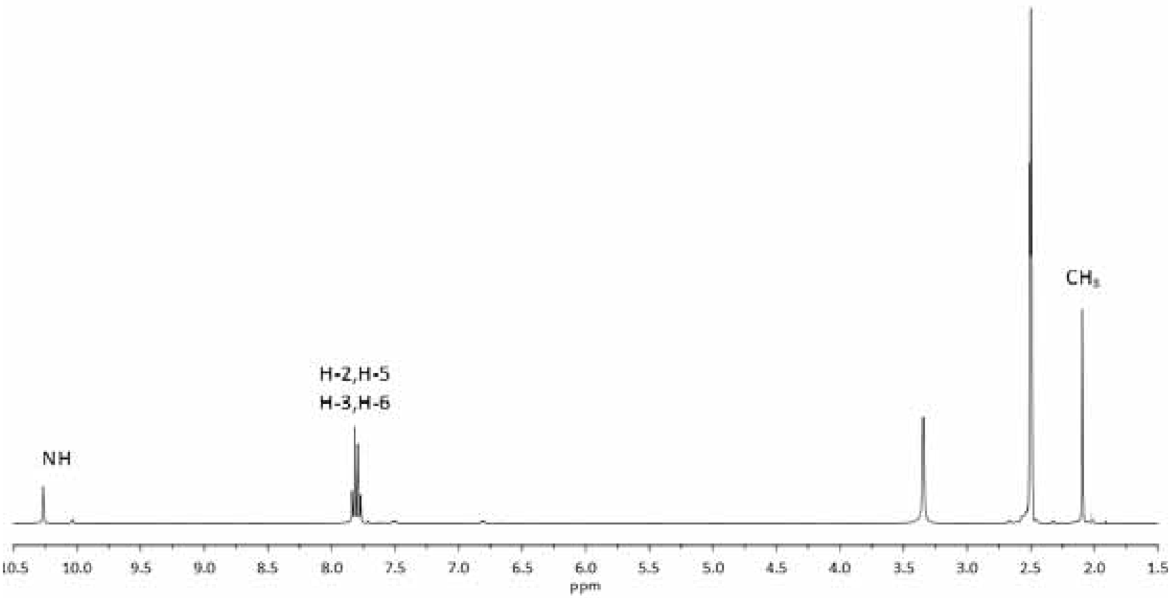

^{1}H-NMR (400 MHz, DMSO-d_6)

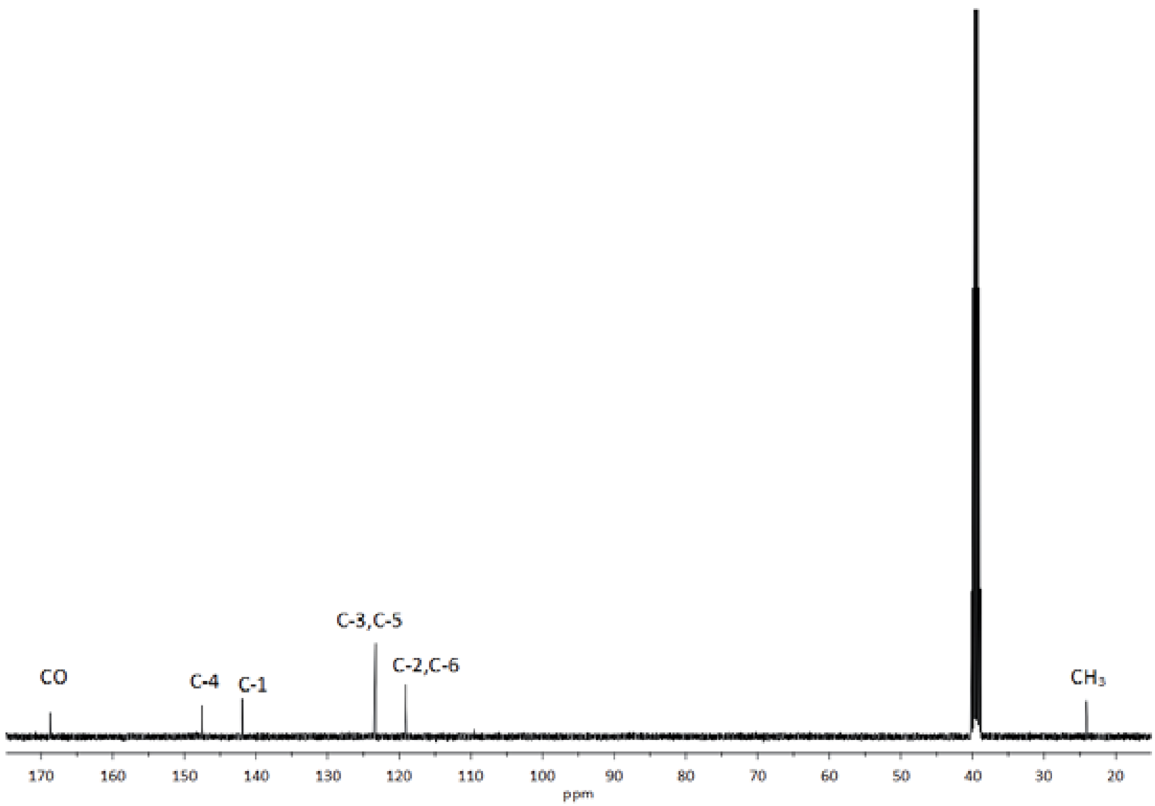

^{13}C-NMR (100.6 MHz, DMSO-d_6)

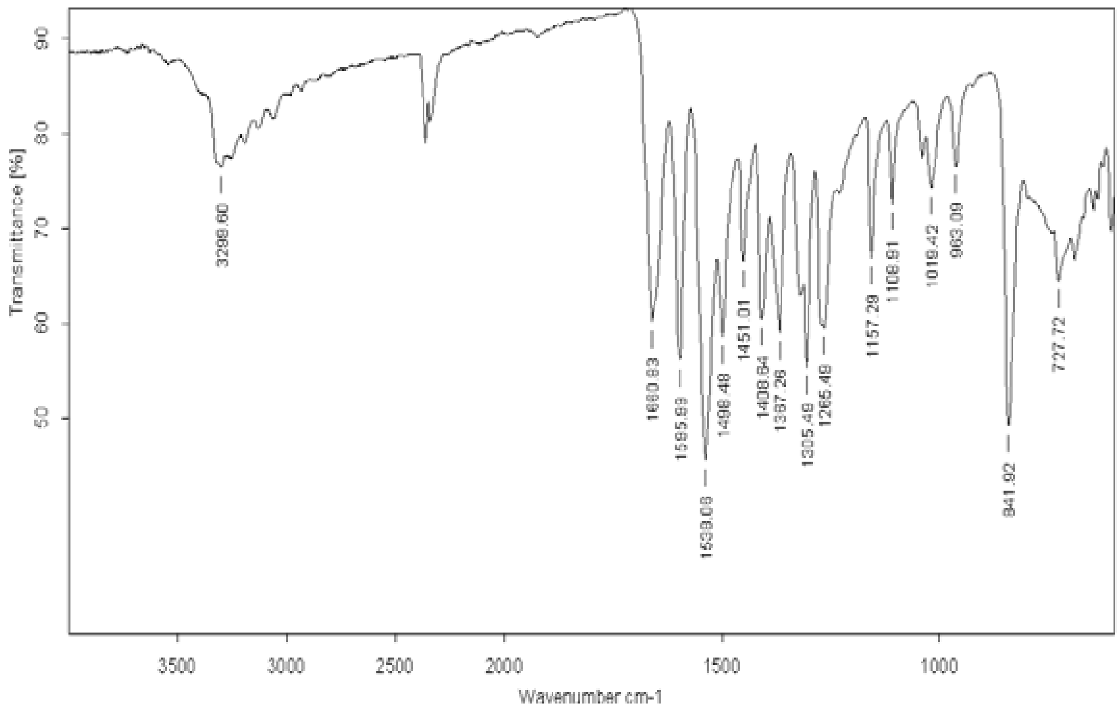

IR (ATR)

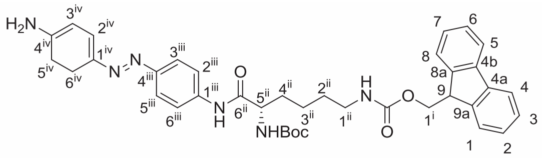

29

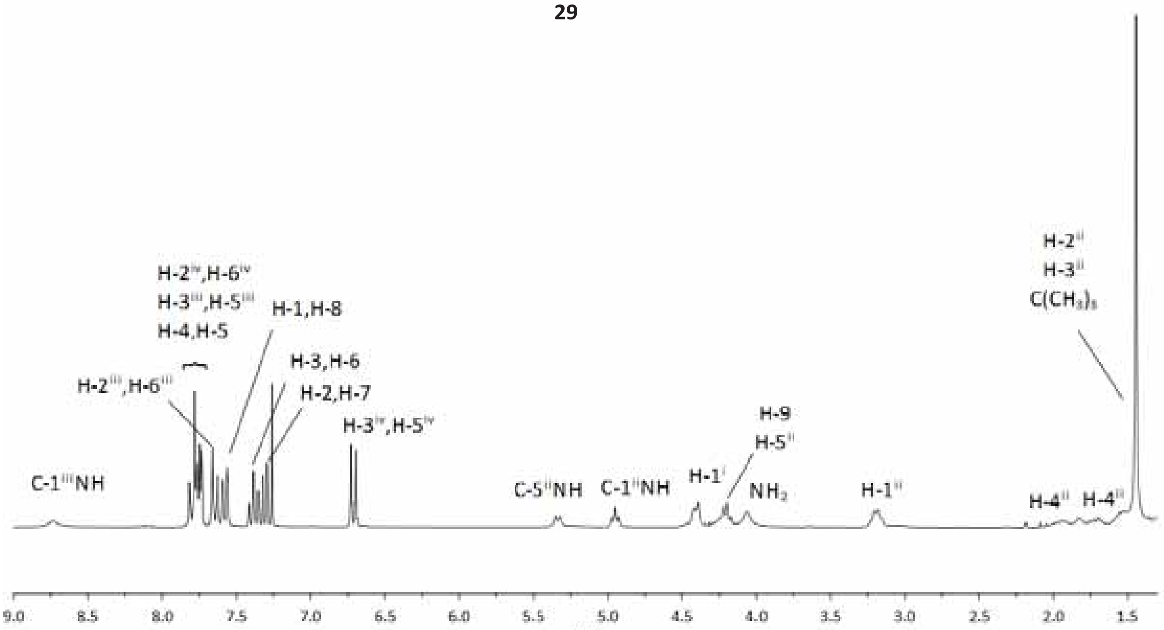

^{1}H-NMR (250 MHz, CDCl$_3$)

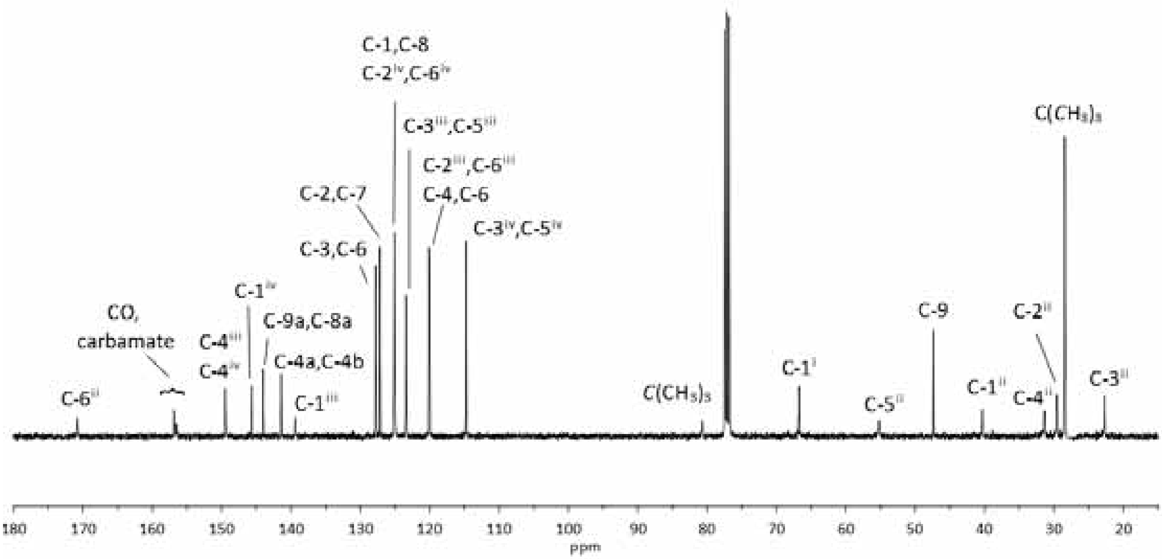

^{13}C-NMR (100.6 MHz, $CDCl_3$)

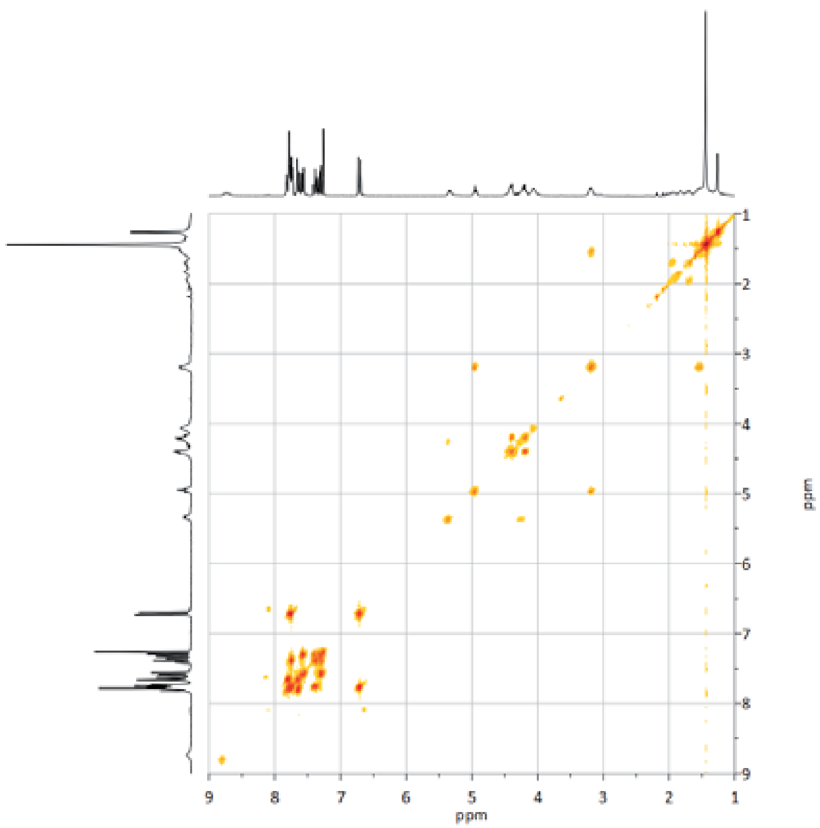

COSY (360 MHz, $CDCl_3$)

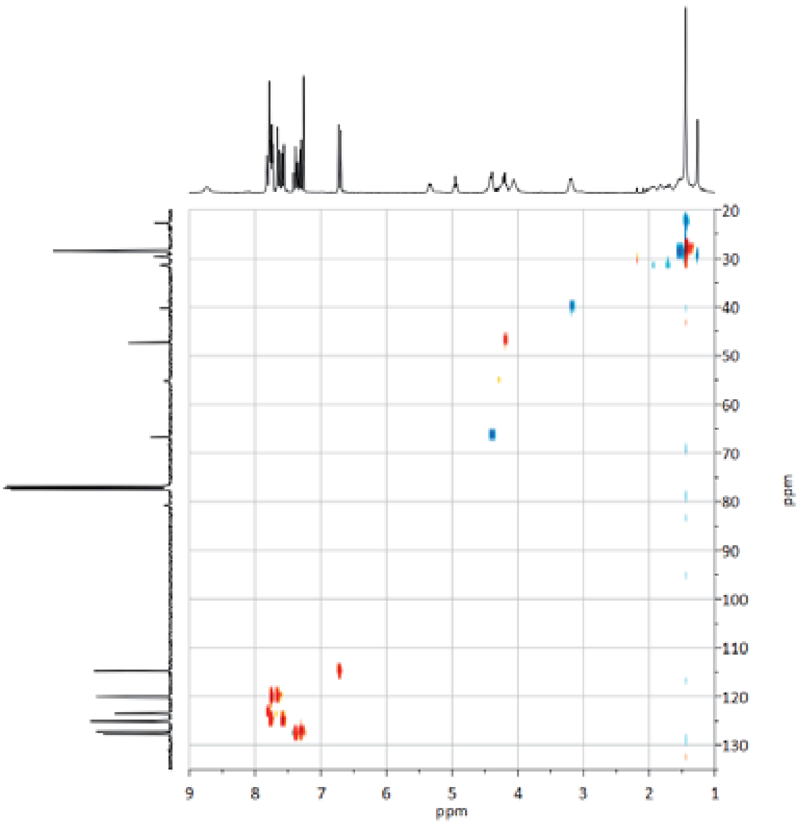

HSQC (400 MHz, $CDCl_3$. CH, CH_3: blue,CH_2: red)

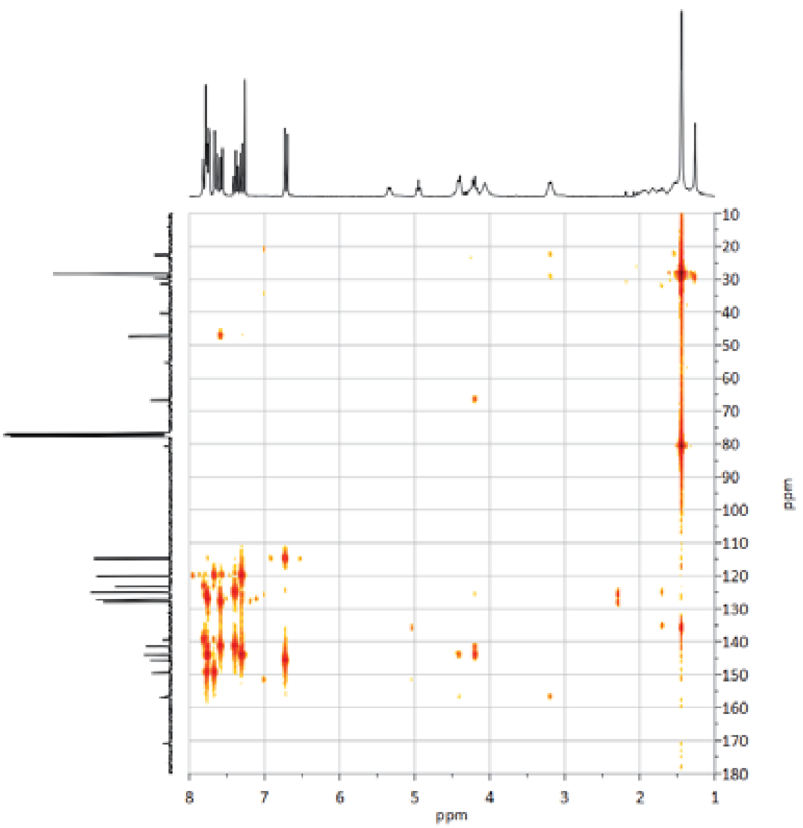

HMBC (400 MHz, $CDCl_3$)

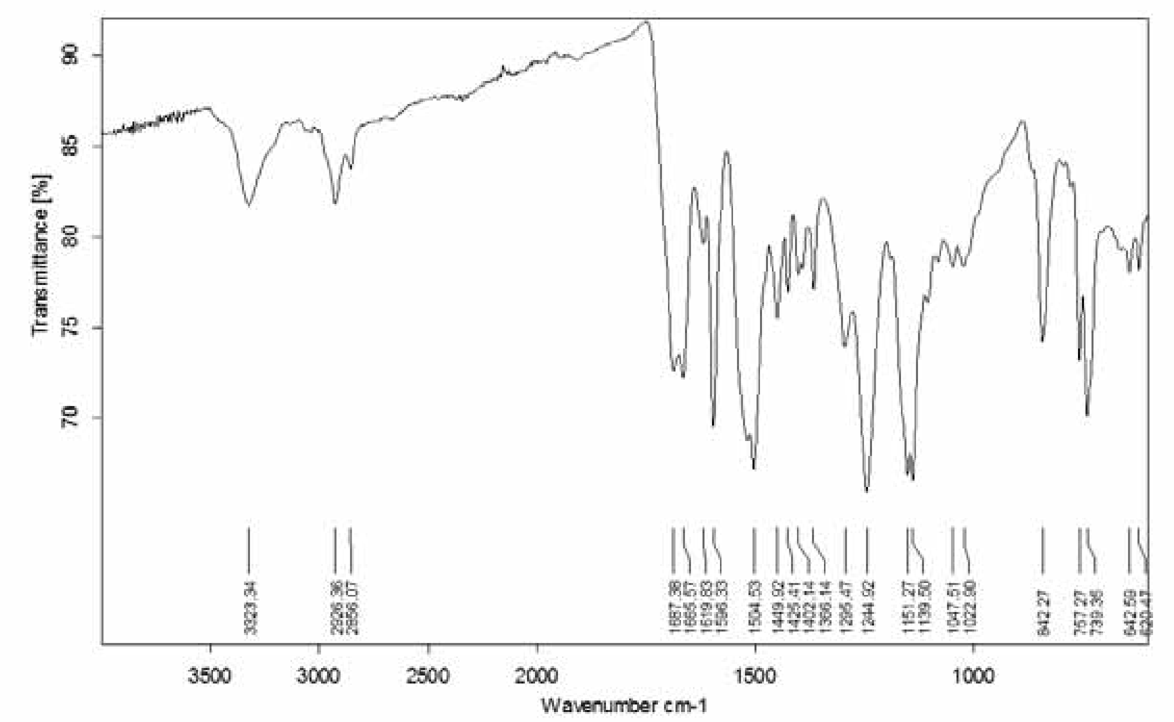

IR (ATR)

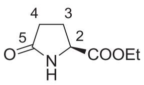

38

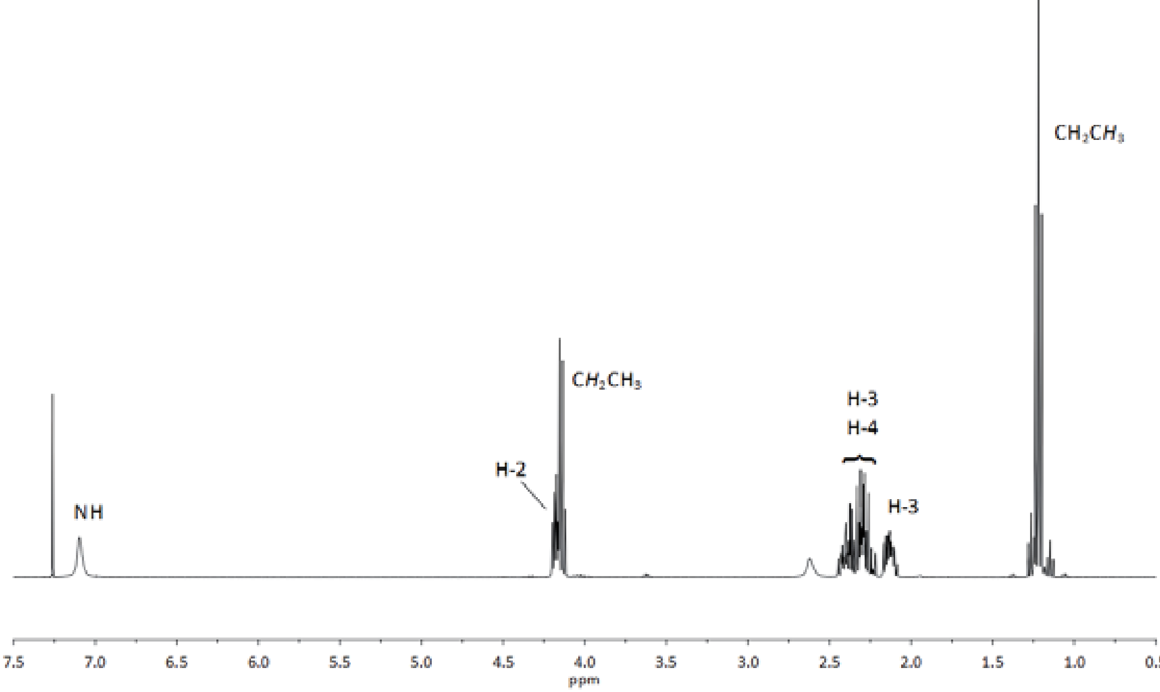

^{1}H-NMR (400 MHz, $CDCl_3$)

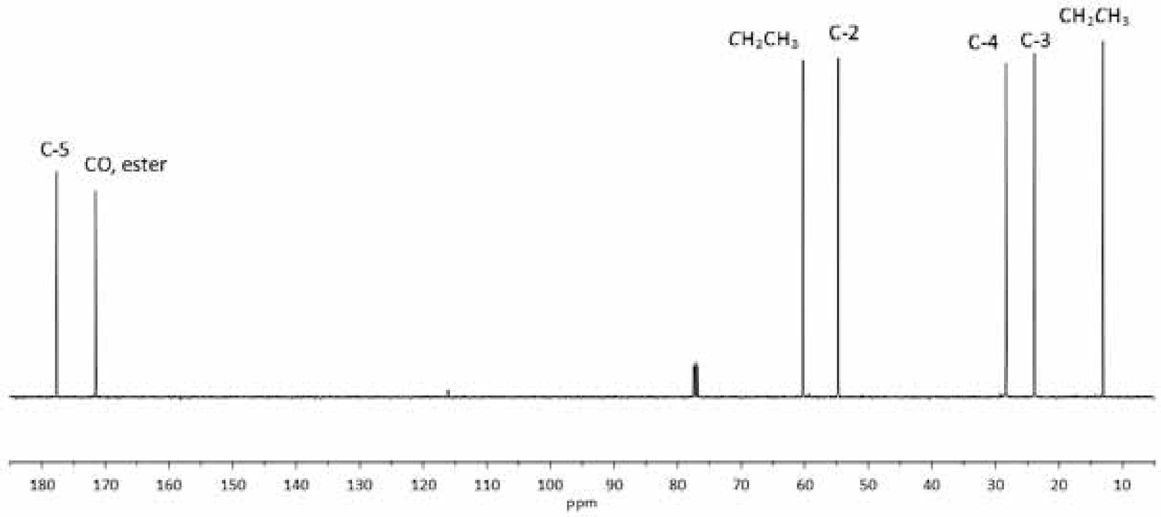

^{13}C-NMR (100.6 MHz, $CDCl_3$)

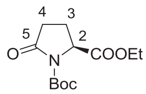

39

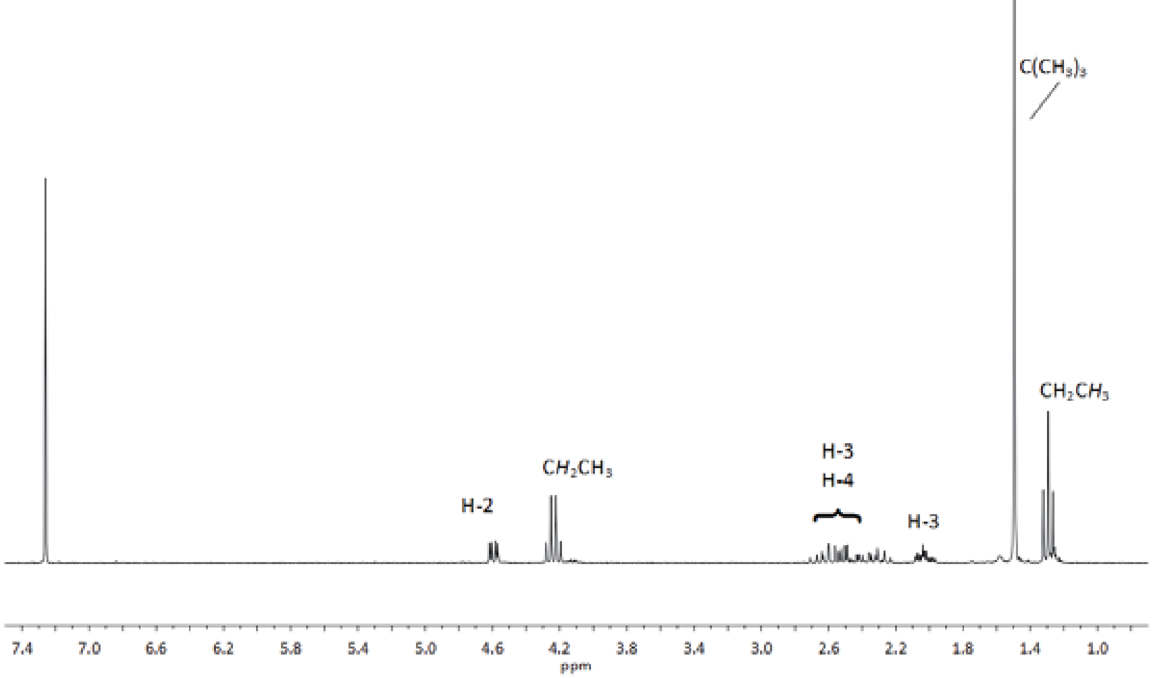

^{1}H-NMR (250 MHz, $CDCl_3$)

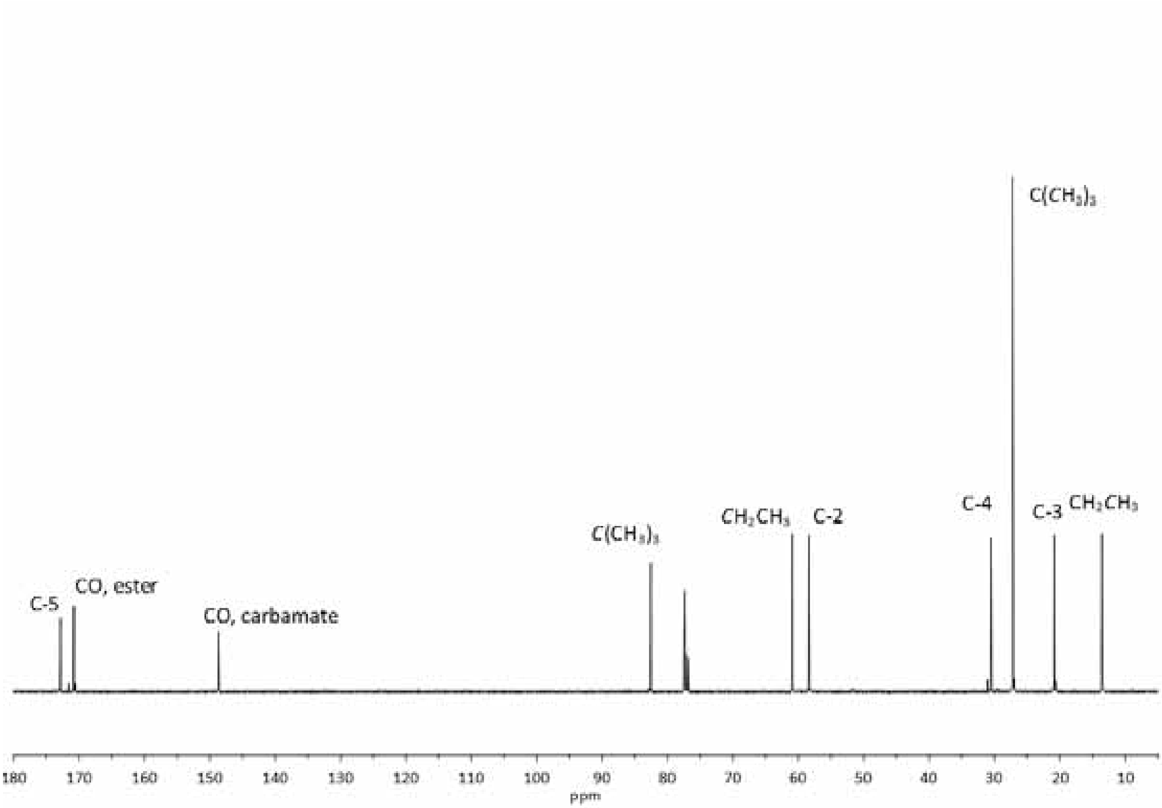

^{13}C-NMR (100.6 MHz, $CDCl_3$)

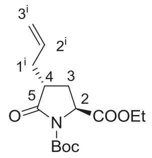

(4*R*)-**40**

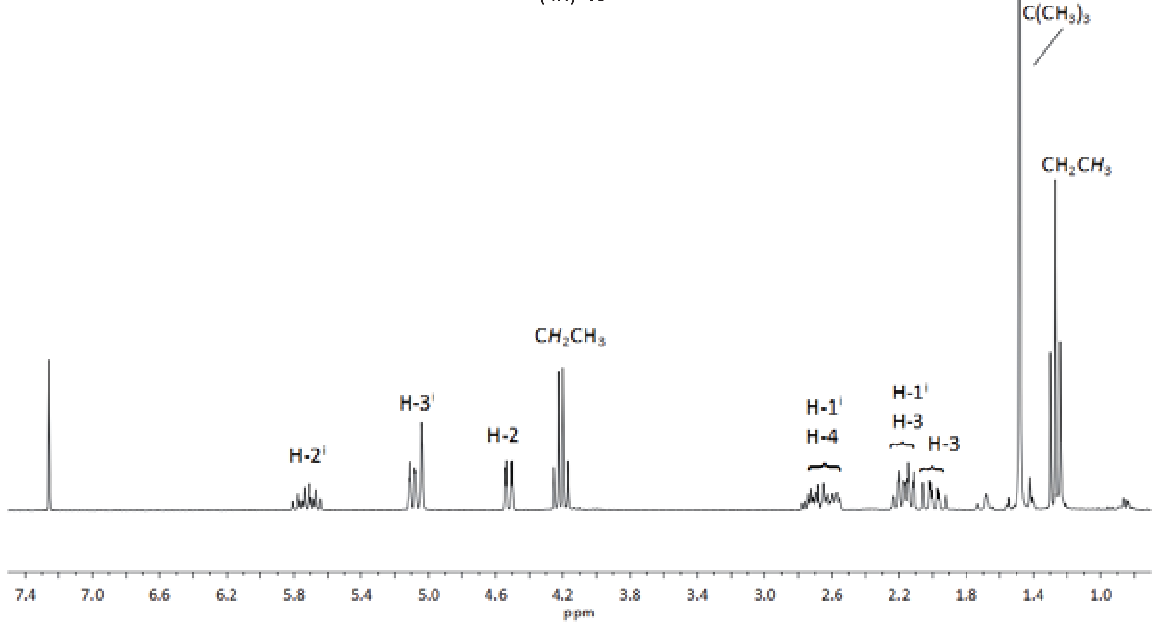

^{1}H-NMR (250 MHz, $CDCl_3$)

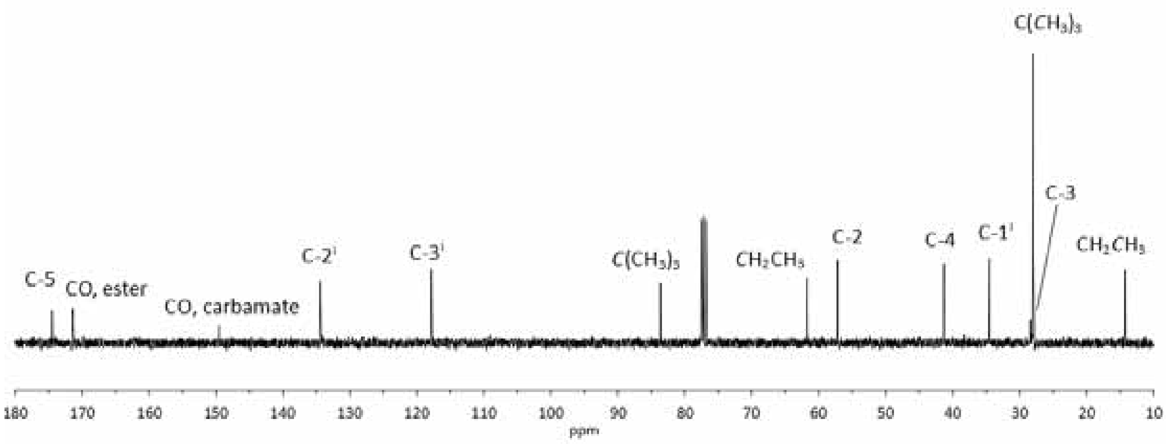

^{13}C-NMR (90 MHz, $CDCl_3$)

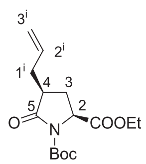

(4*S*)-**40**

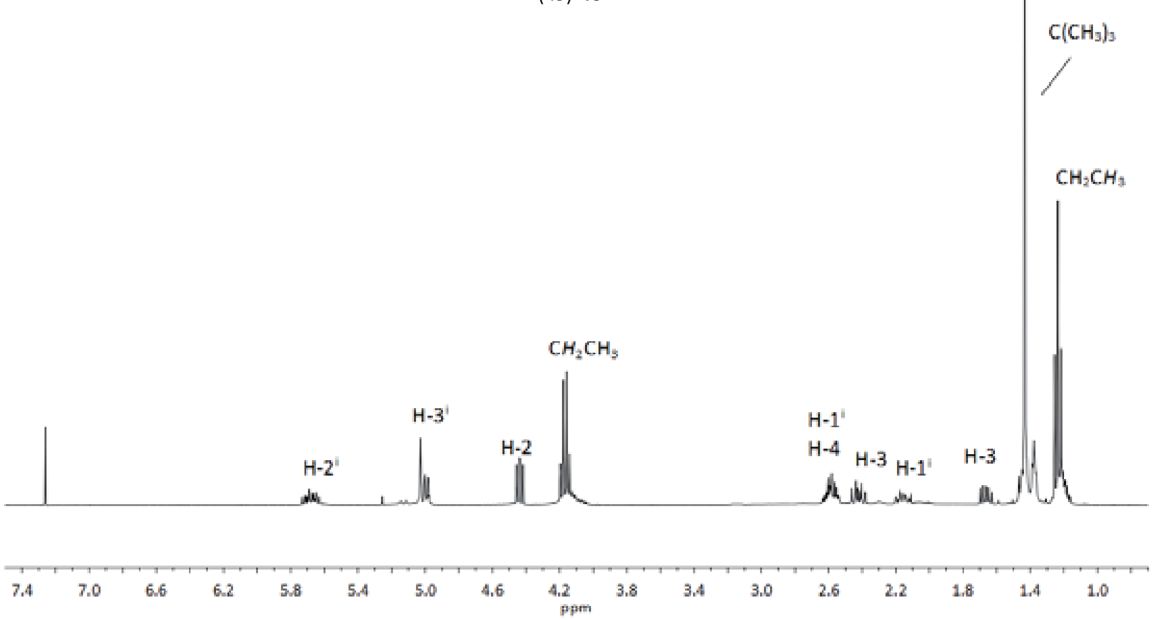

^{1}H-NMR (400 MHz, $CDCl_3$)

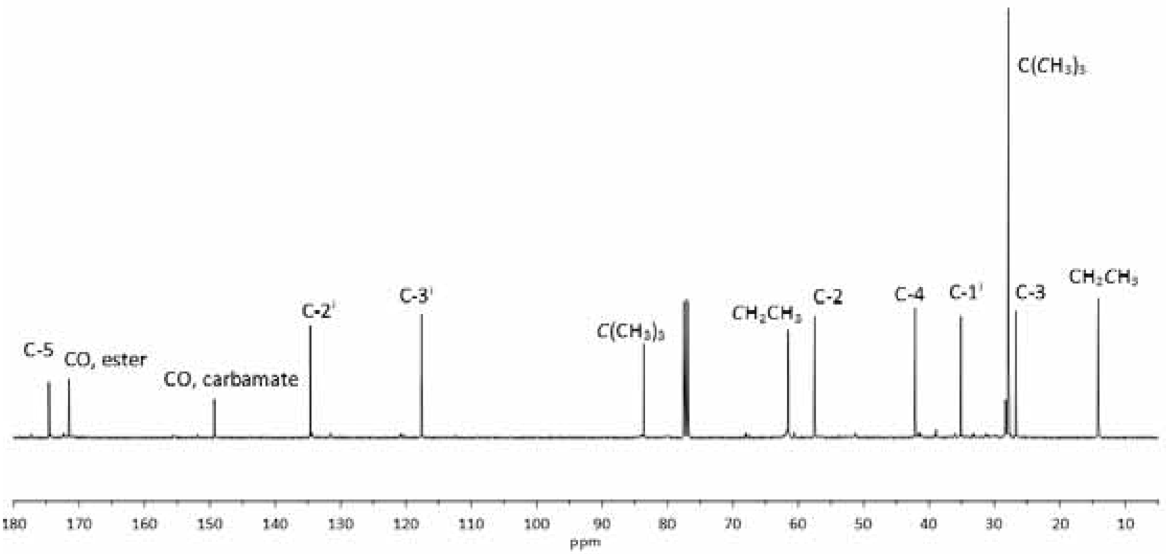

^{13}C-NMR (100.6 MHz, $CDCl_3$)

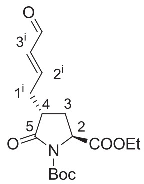

41

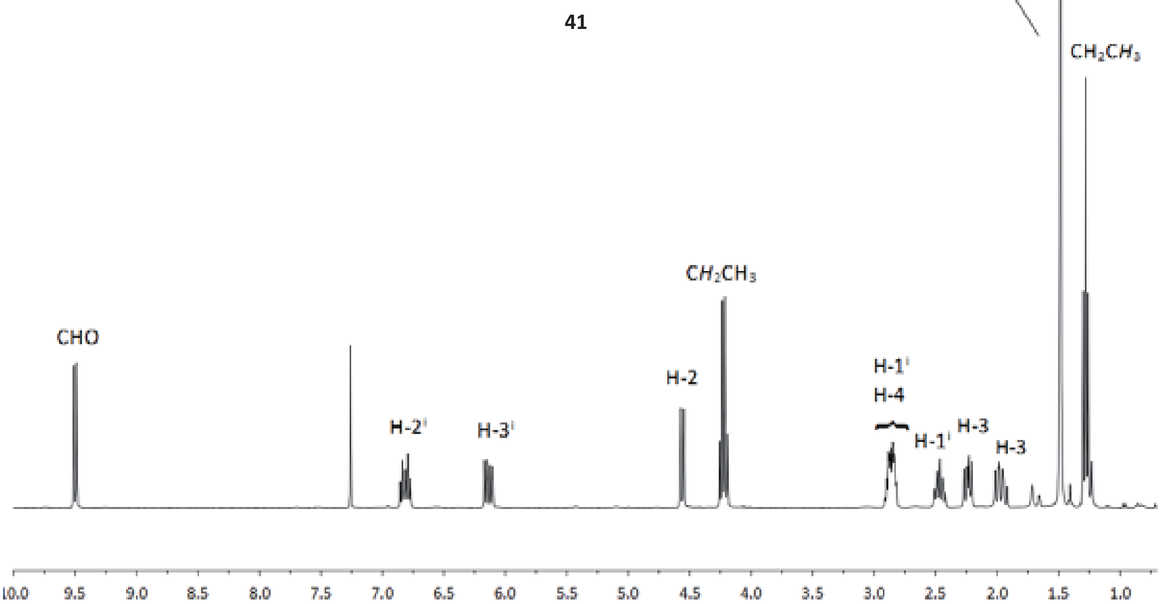

^{1}H-NMR (360 MHz, $CDCl_3$)

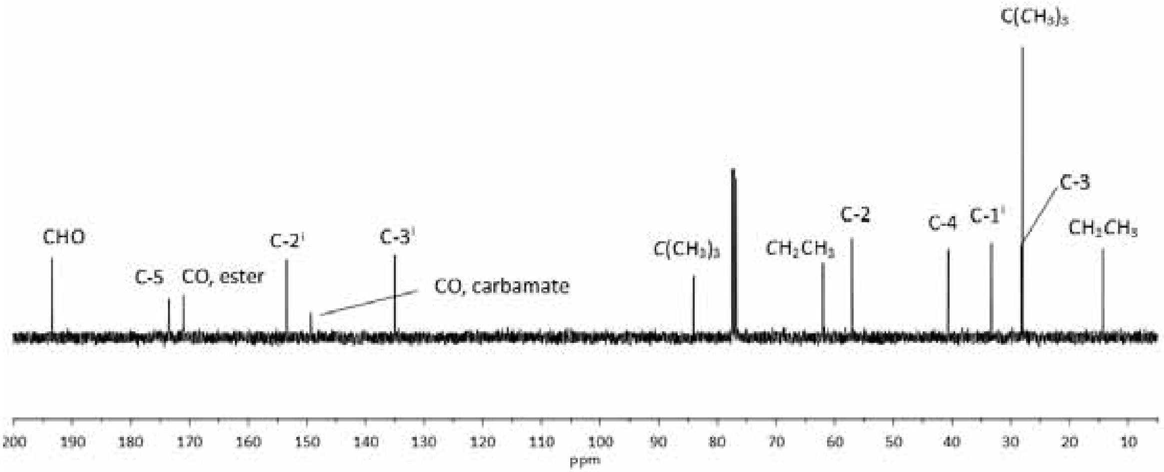

^{13}C-NMR (90 MHz, $CDCl_3$)

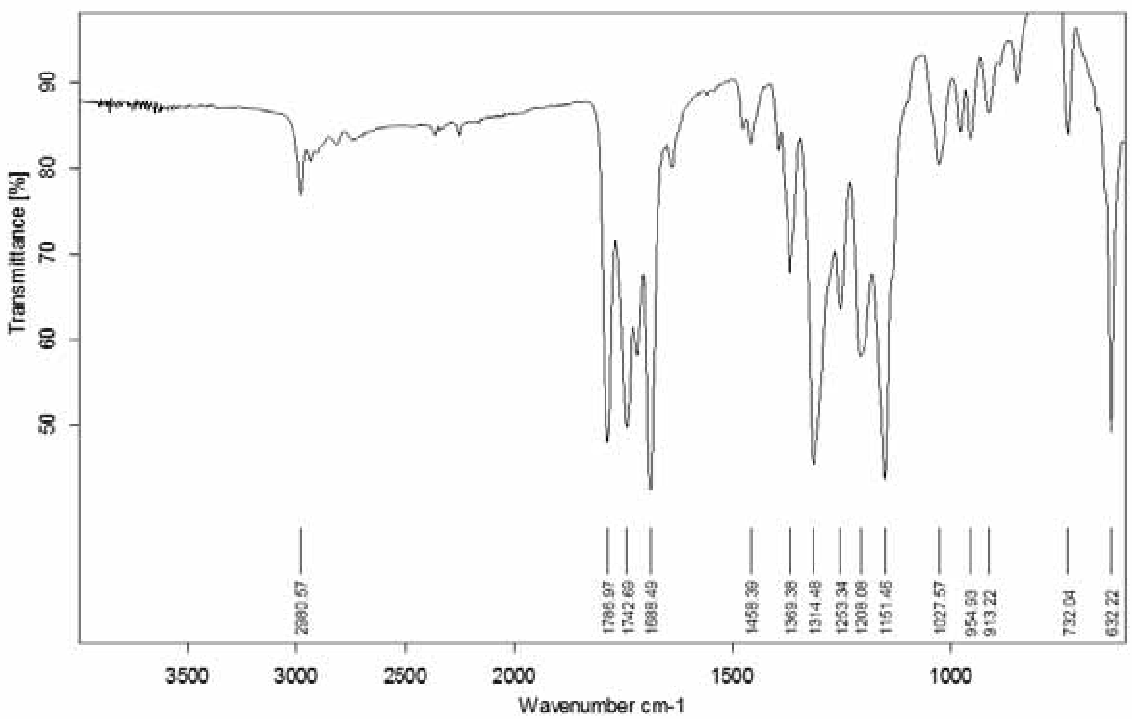

IR (ATR)

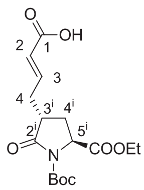

42

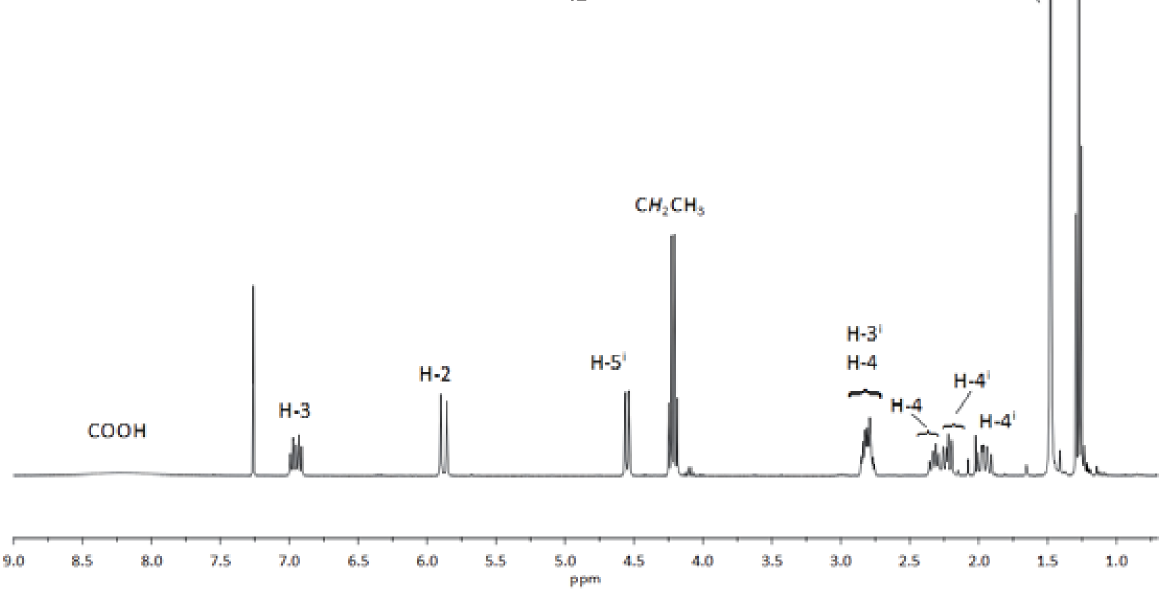

^{1}H-NMR (360 MHz, $CDCl_3$)

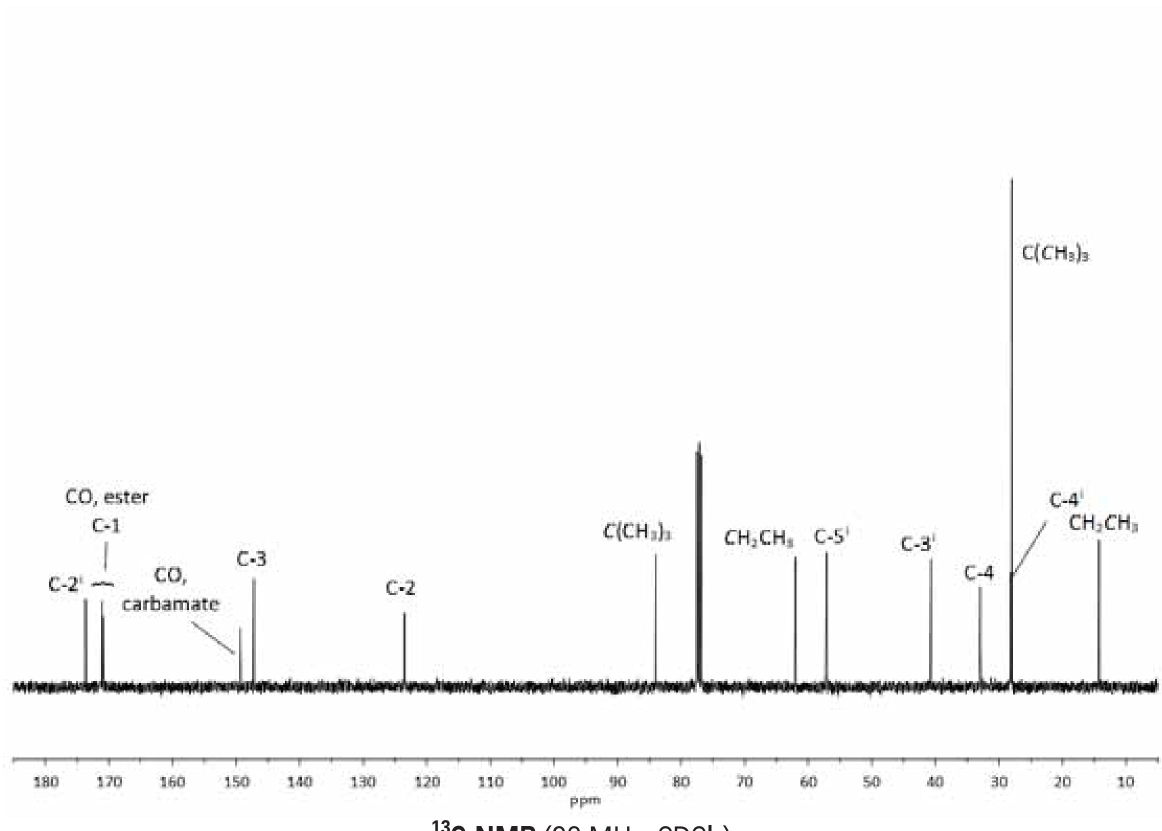

^{13}C-NMR (90 MHz, $CDCl_3$)

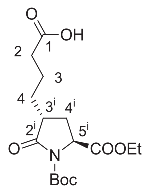

43

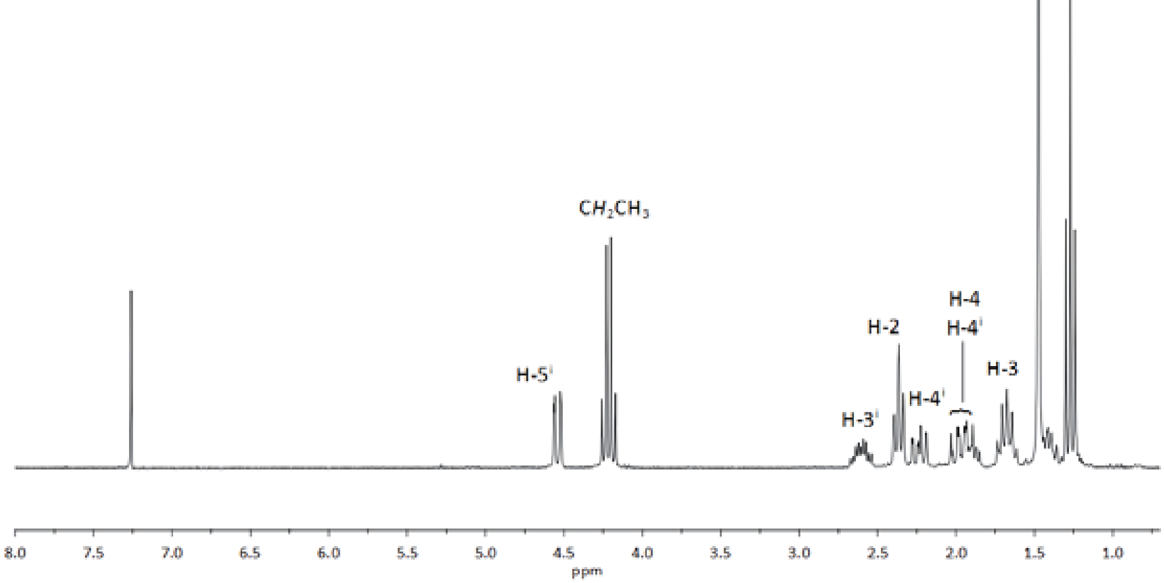

^{1}H-NMR (250 MHz, $CDCl_3$)

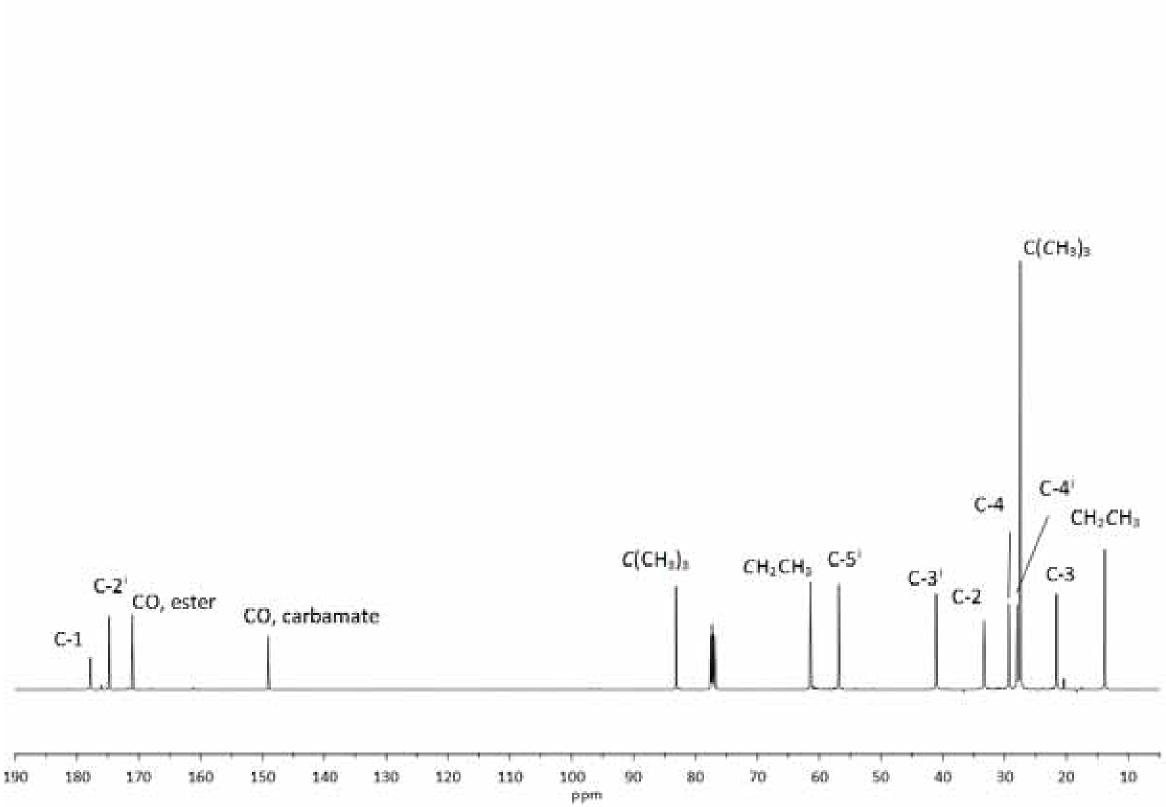

^{13}C-NMR (90 MHz, $CDCl_3$)

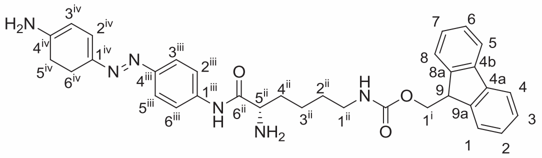

44

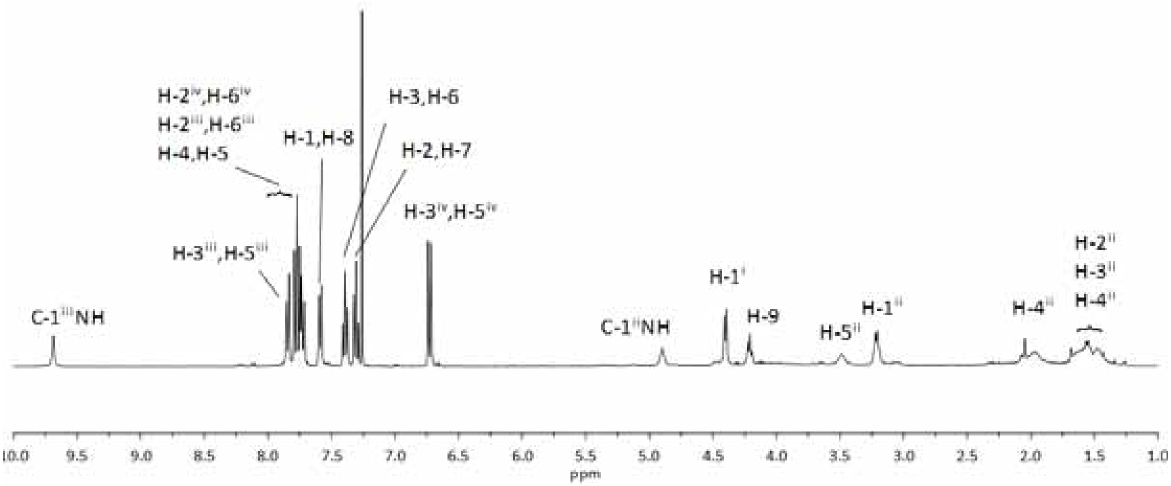

^{1}H-NMR (400 MHz, $CDCl_3$)

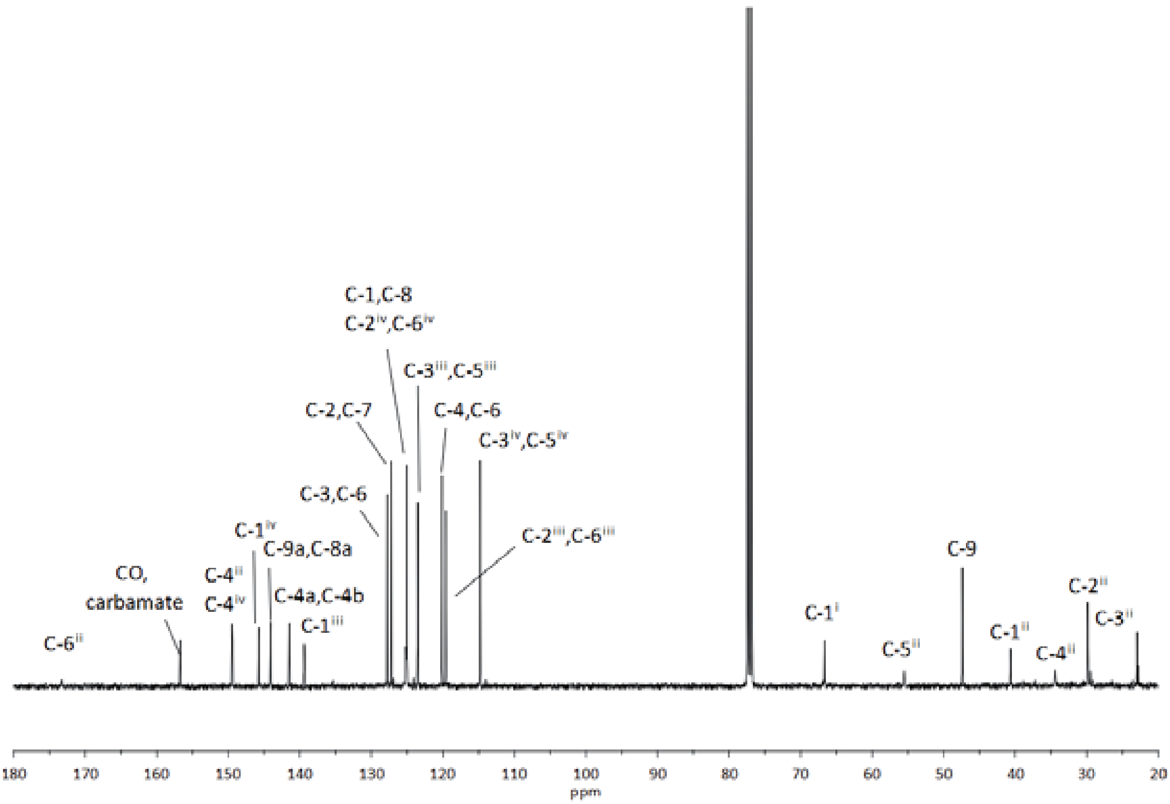

^{13}C-NMR (100.6 MHz, $CDCl_3$)

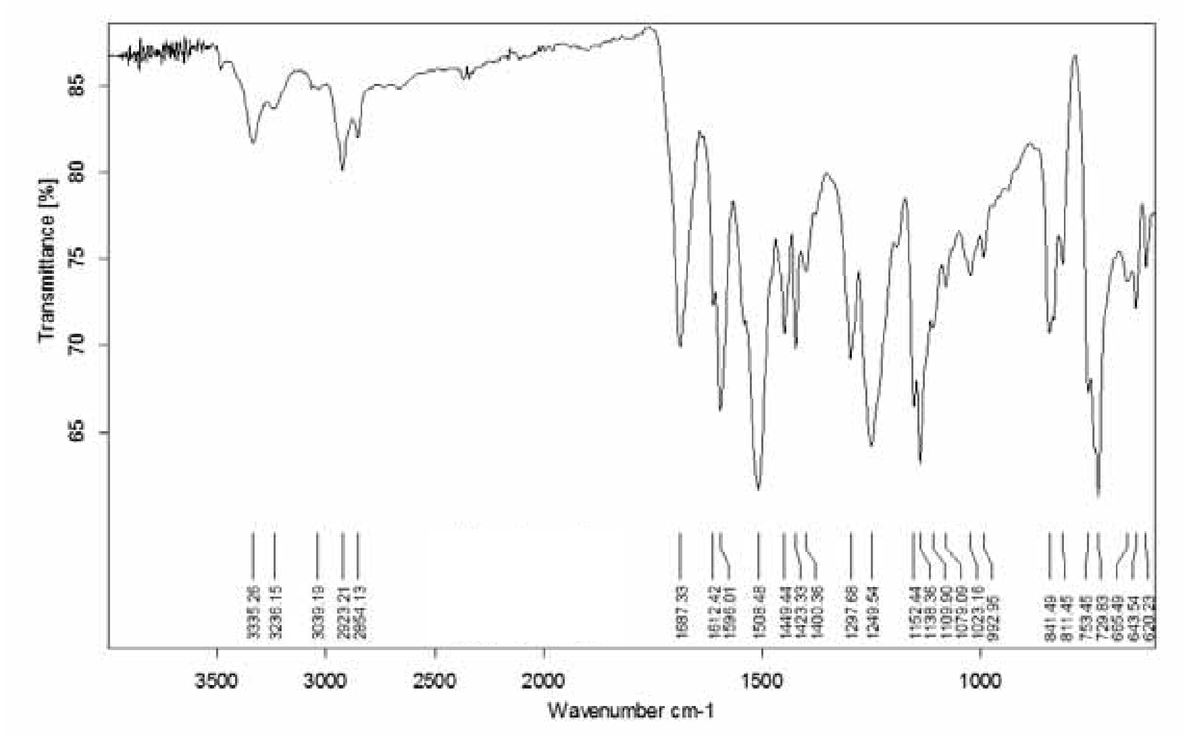

IR (ATR)

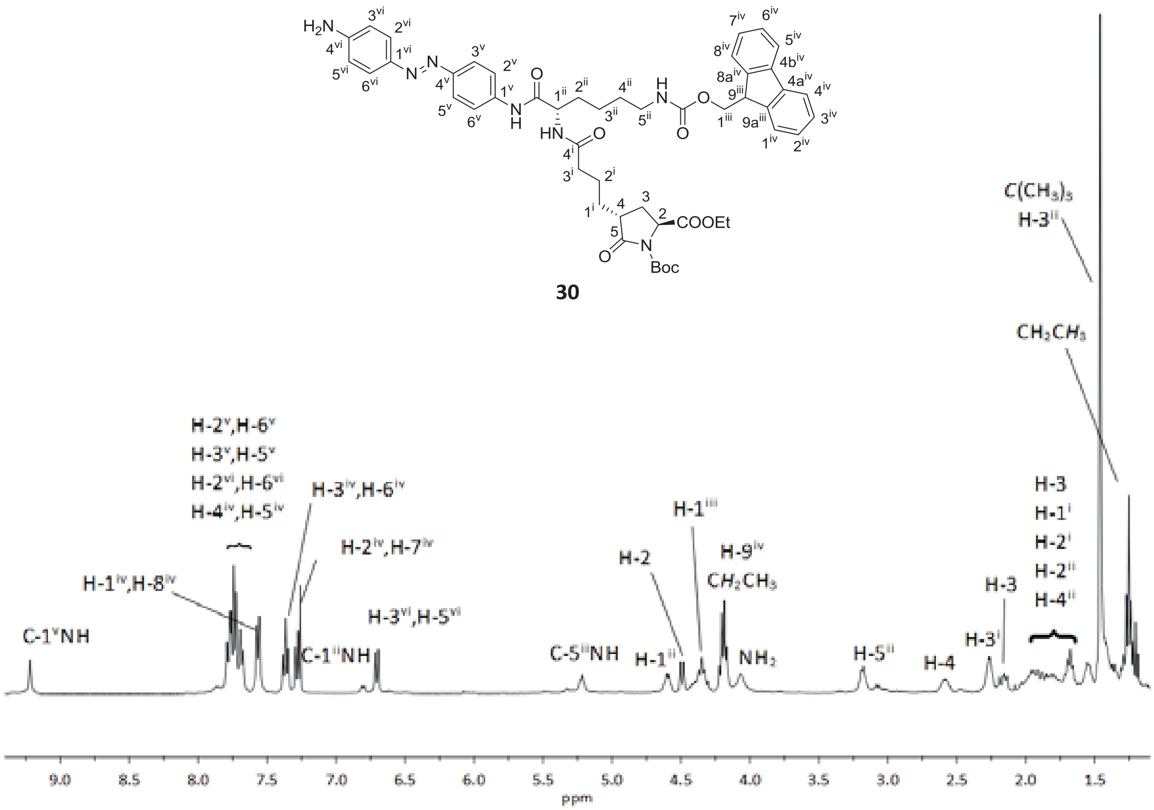

30

^{1}H-NMR (400 MHz, $CDCl_3$)

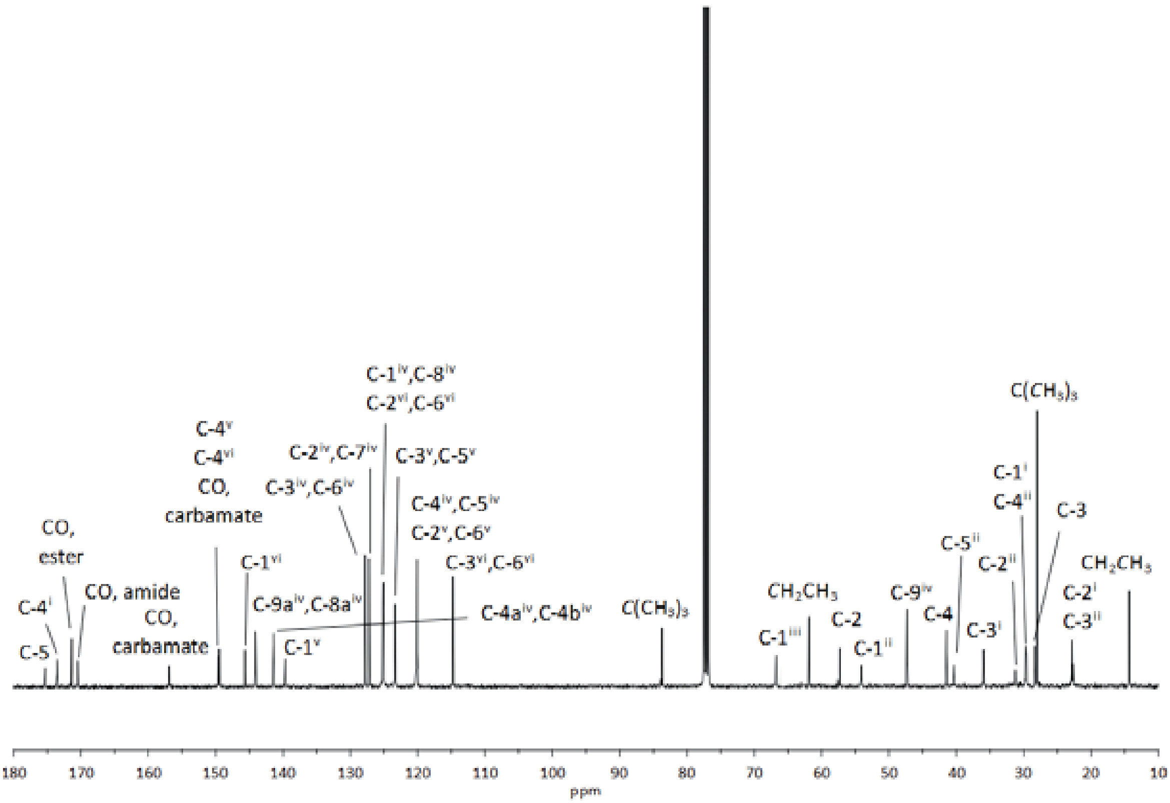

^{13}**C-NMR** (100.6 MHz, $CDCl_3$)

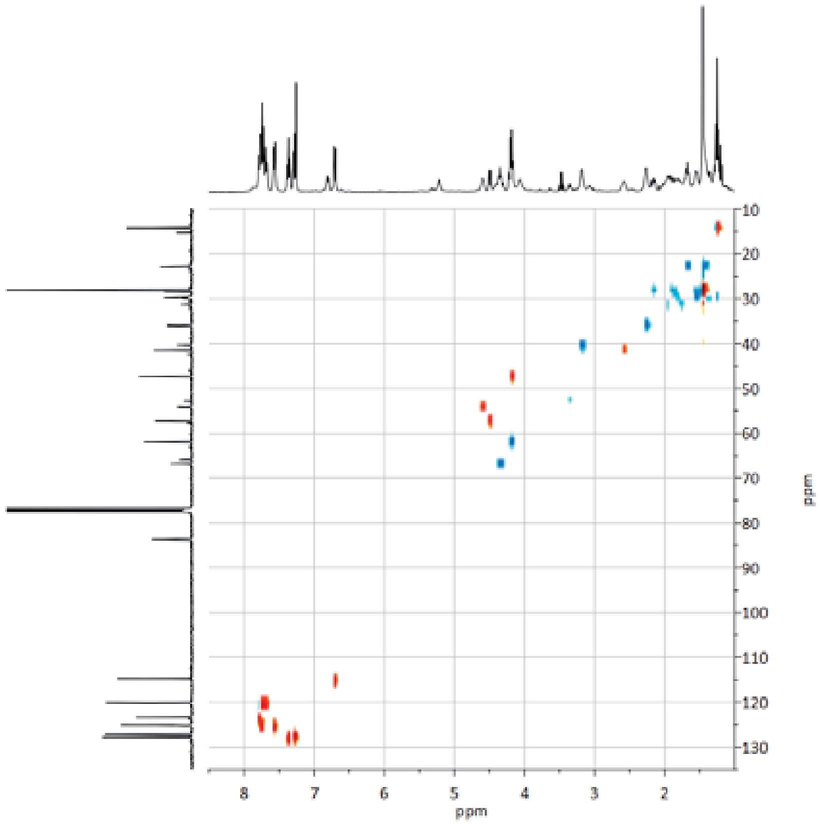

HSQC (400 MHz, $CDCl_3$. CH, CH_3: blue,CH_2: red)

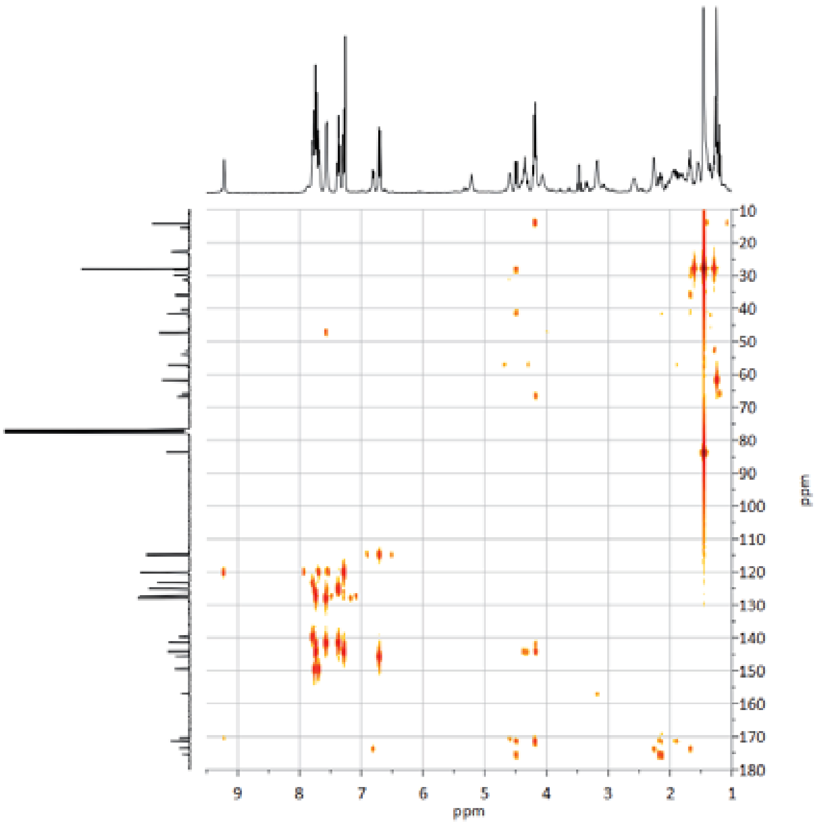

HMBC (400 MHz, $CDCl_3$)

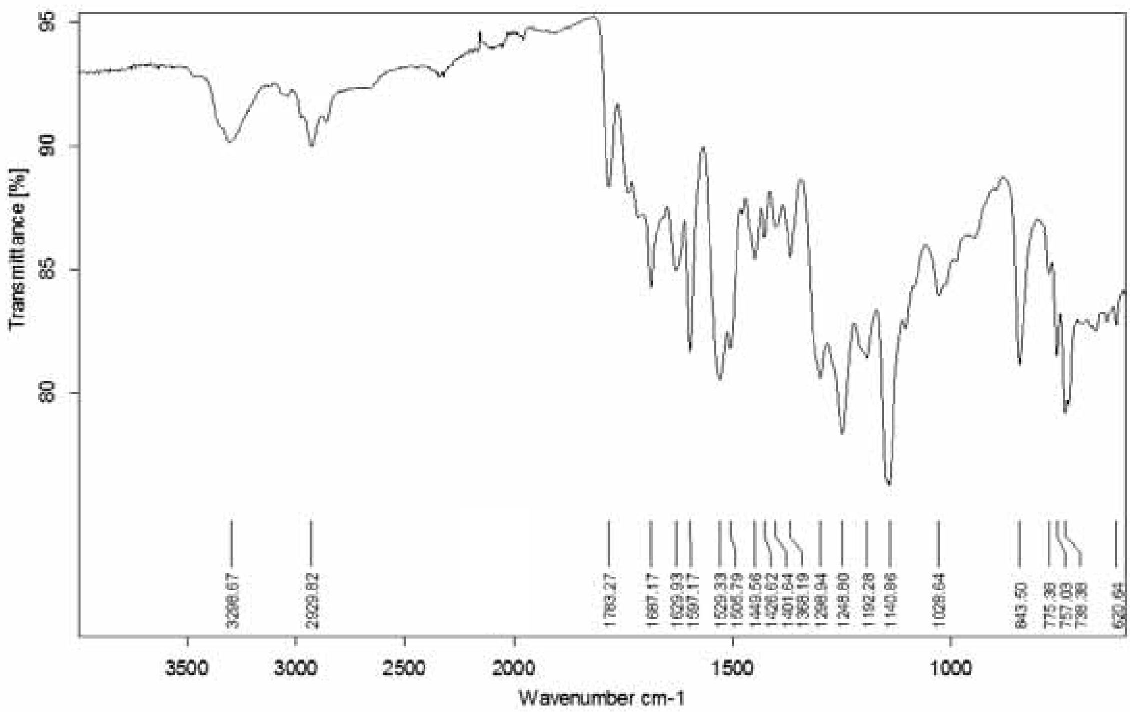

IR (ATR)

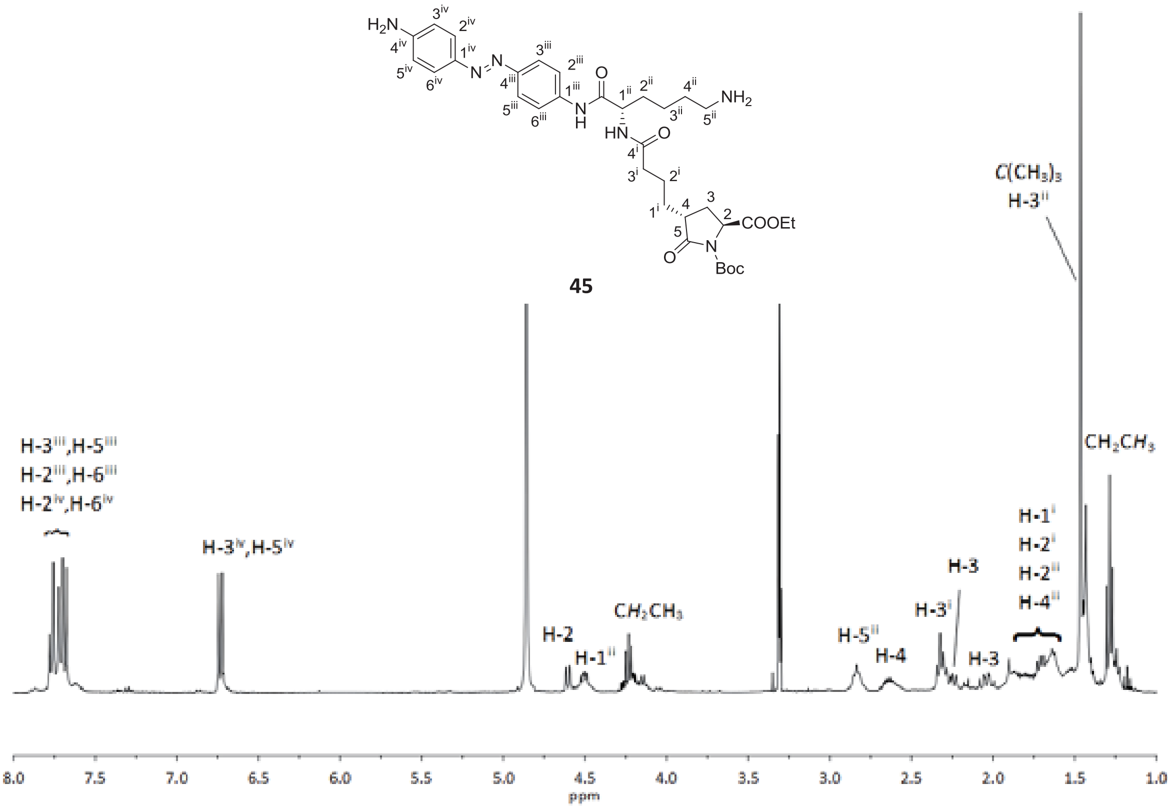

^{1}H-NMR (400 MHz, MeOH-d_4)

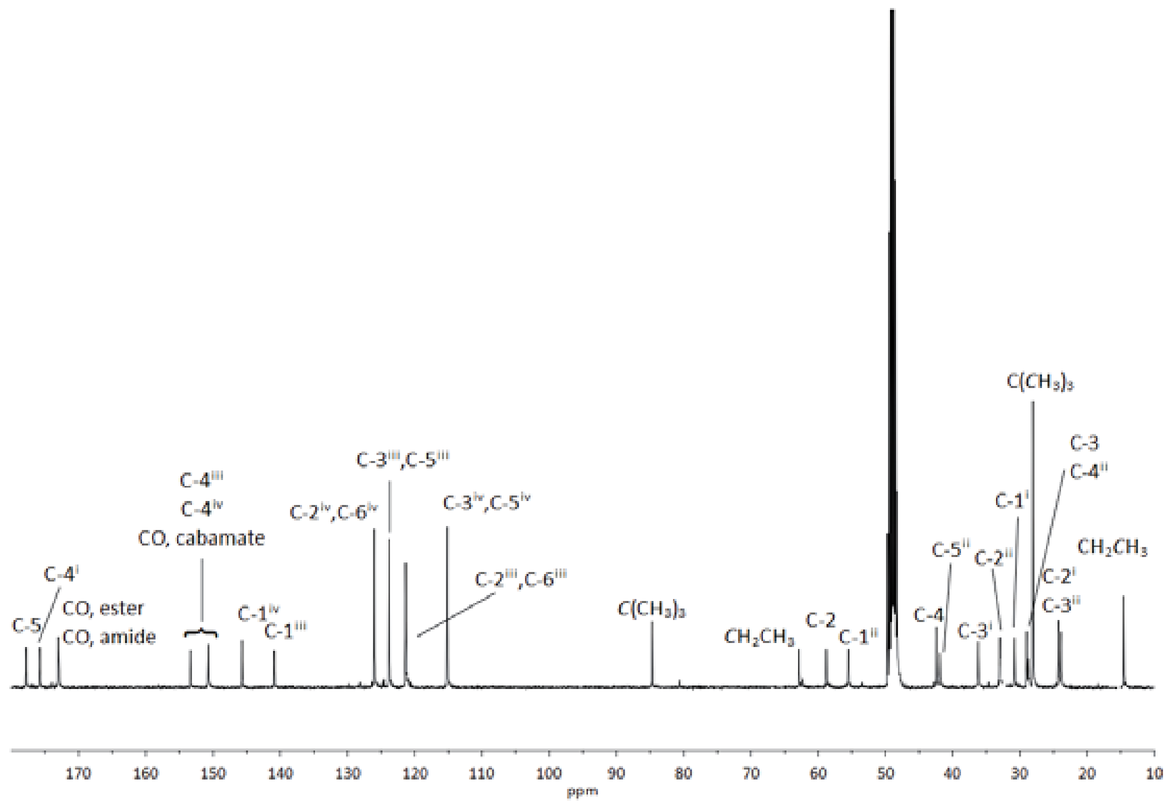

^{13}C-NMR (100.6 MHz, MeOH-d_4)

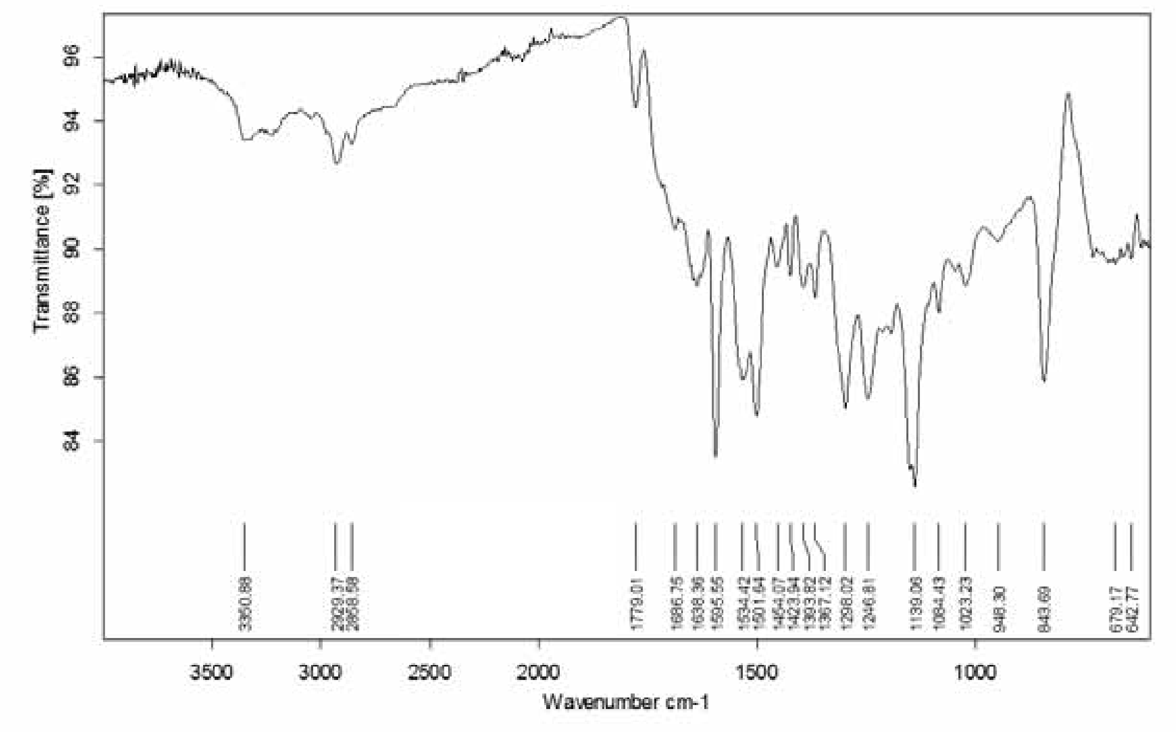

IR (ATR)

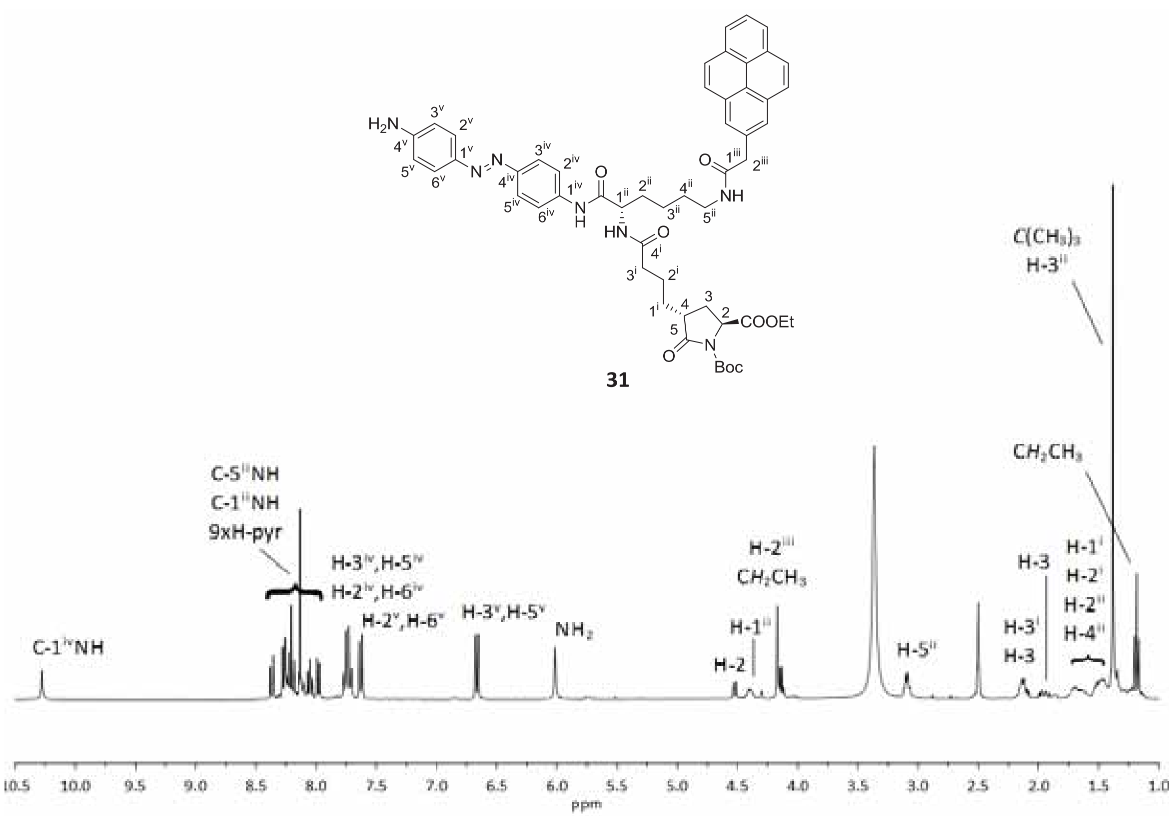

^{1}H-NMR (400 MHz, DMSO-d$_6$)

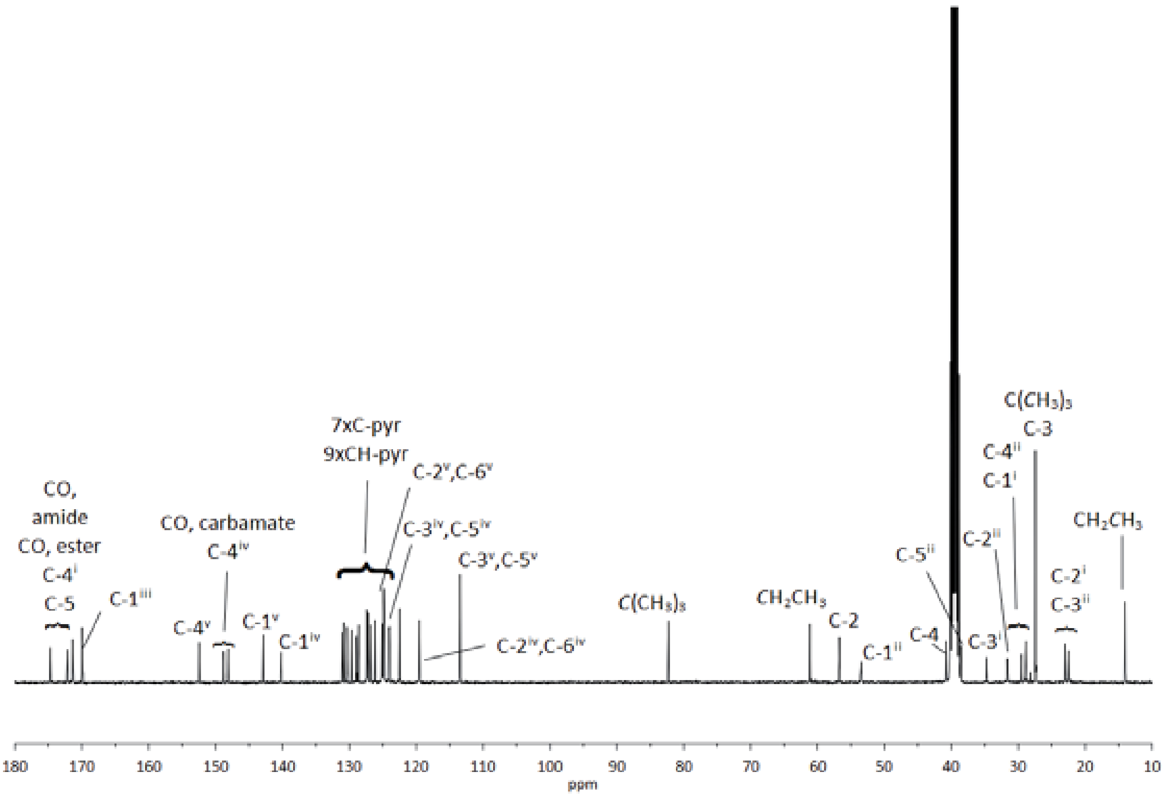

^{13}C-NMR (100.6 MHz, DMSO-d$_6$)

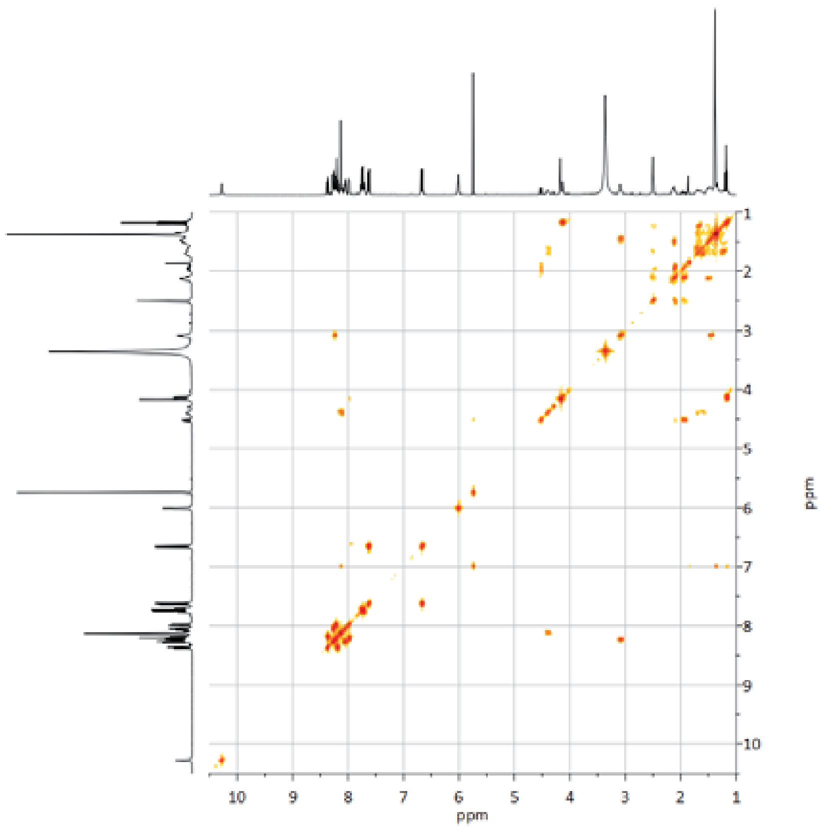

COSY (400 MHz, DMSO-d$_6$)

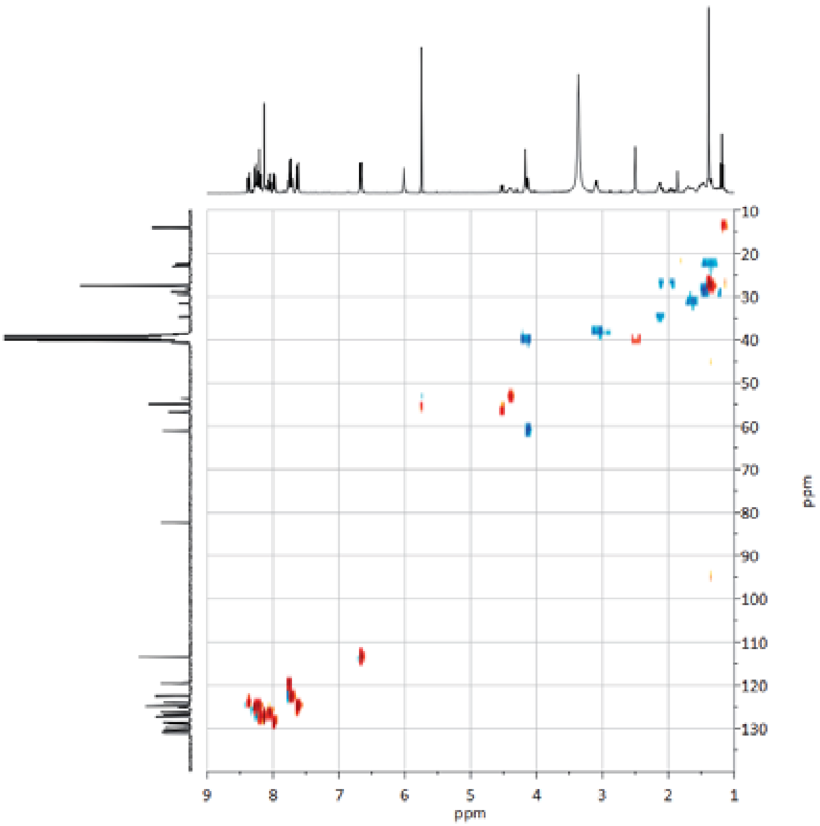

HSQC (400 MHz, DMSO-d_6, CH, CH_3: blue, CH_2: red)

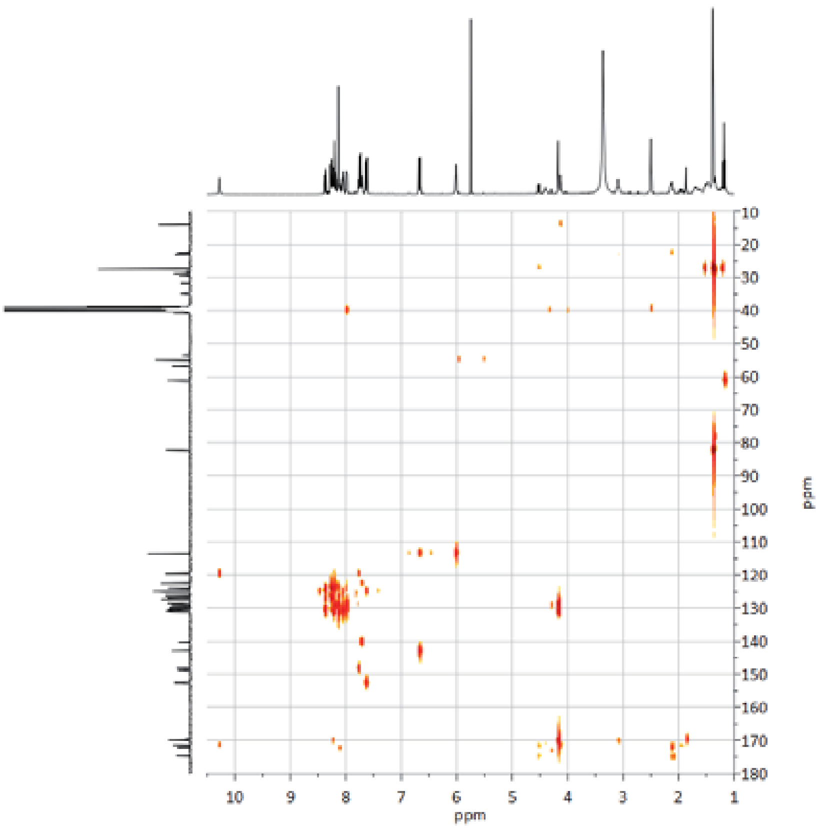

HMBC (400 MHz, DMSO-d_6)

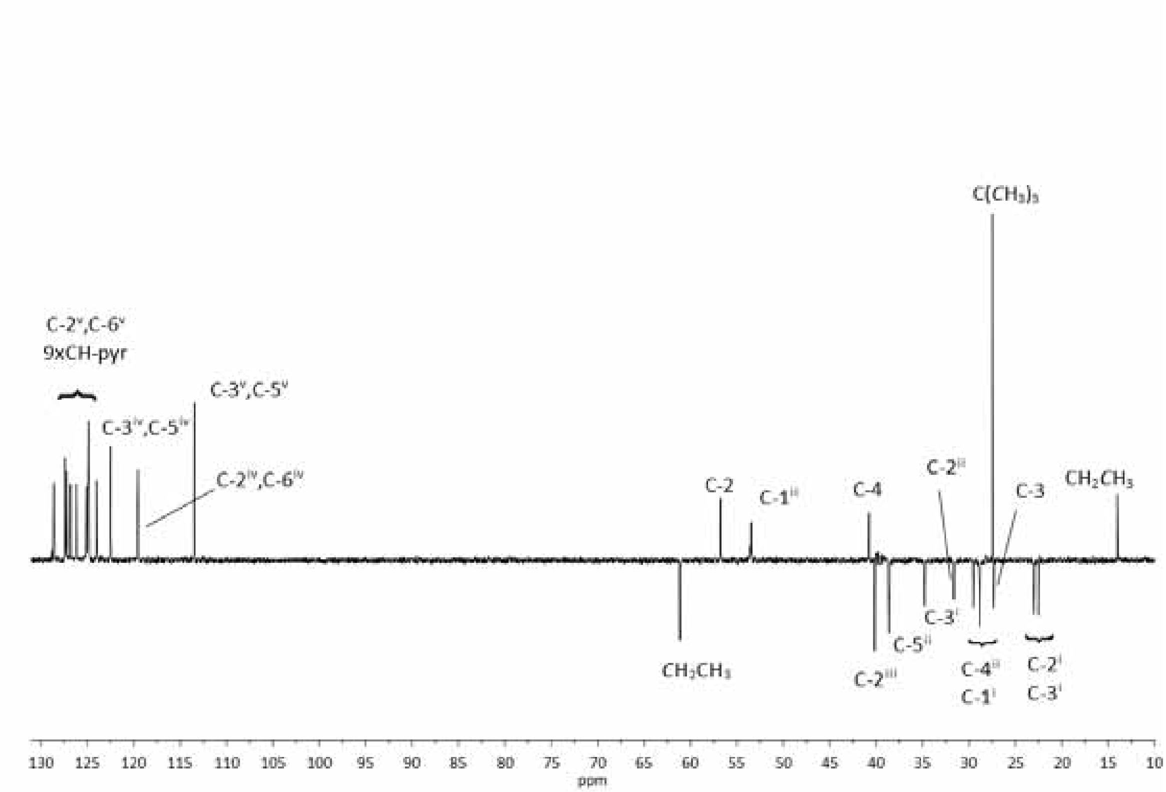

DEPT 135 (100.6 MHz, DMSO-d$_6$)

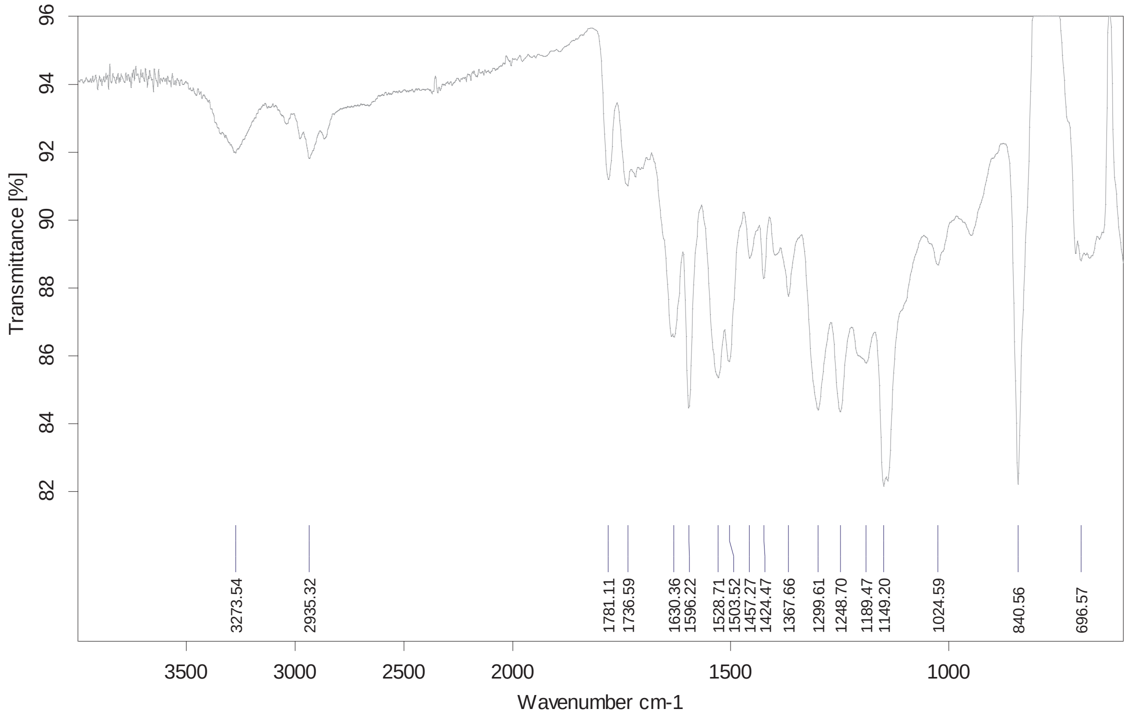

IR (ATR)

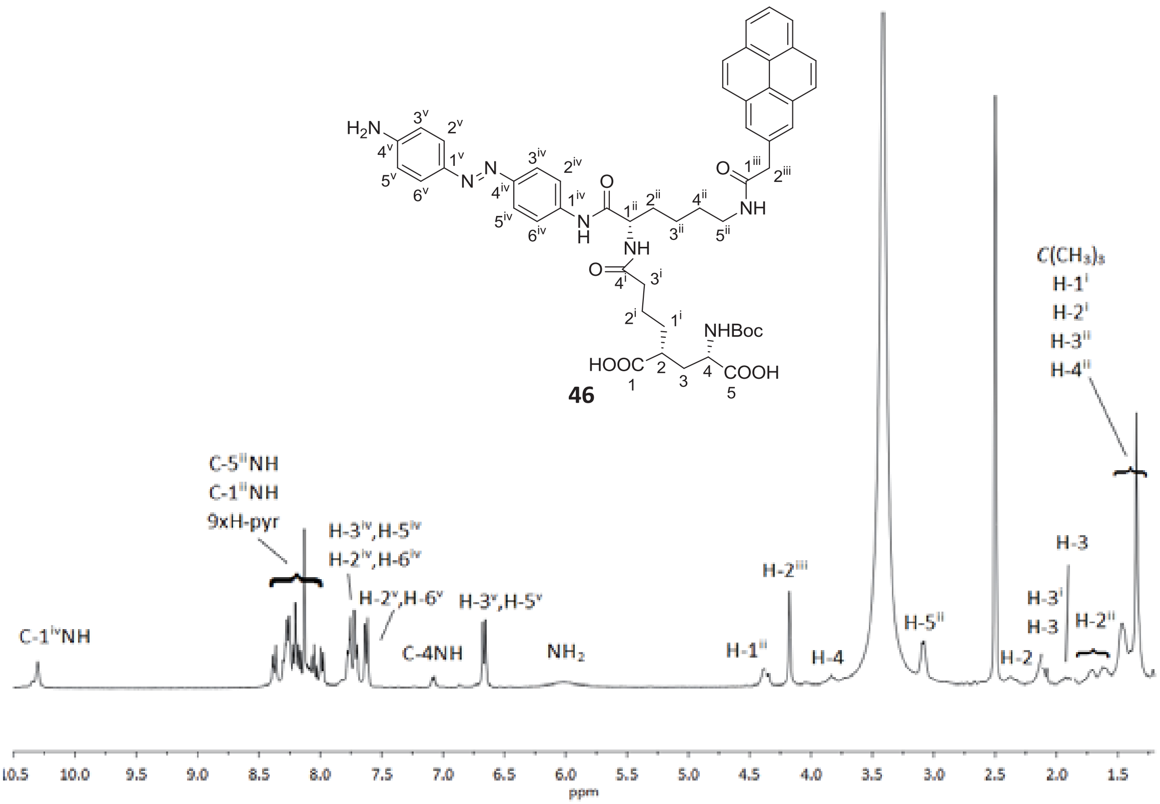

^{1}**H-NMR** (400 MHz, DMSO-d$_6$)

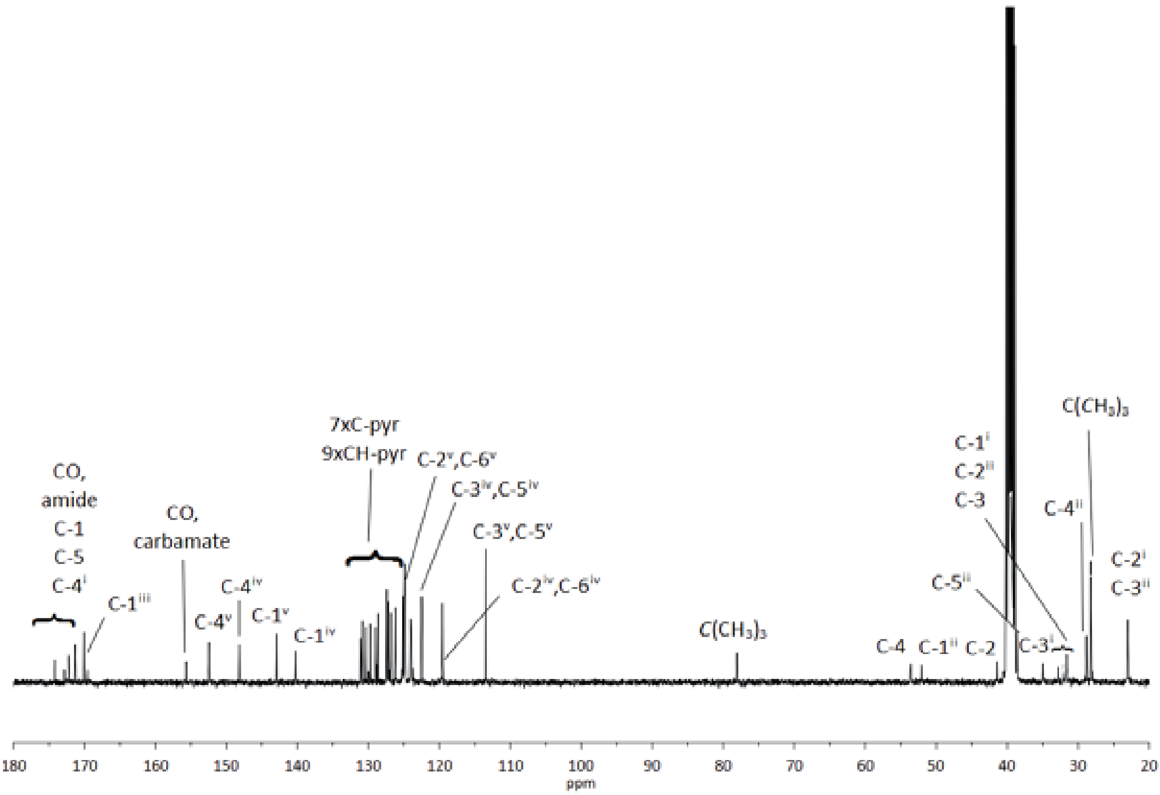

^{13}**C-NMR** (100.6 MHz, DMSO-d$_6$)

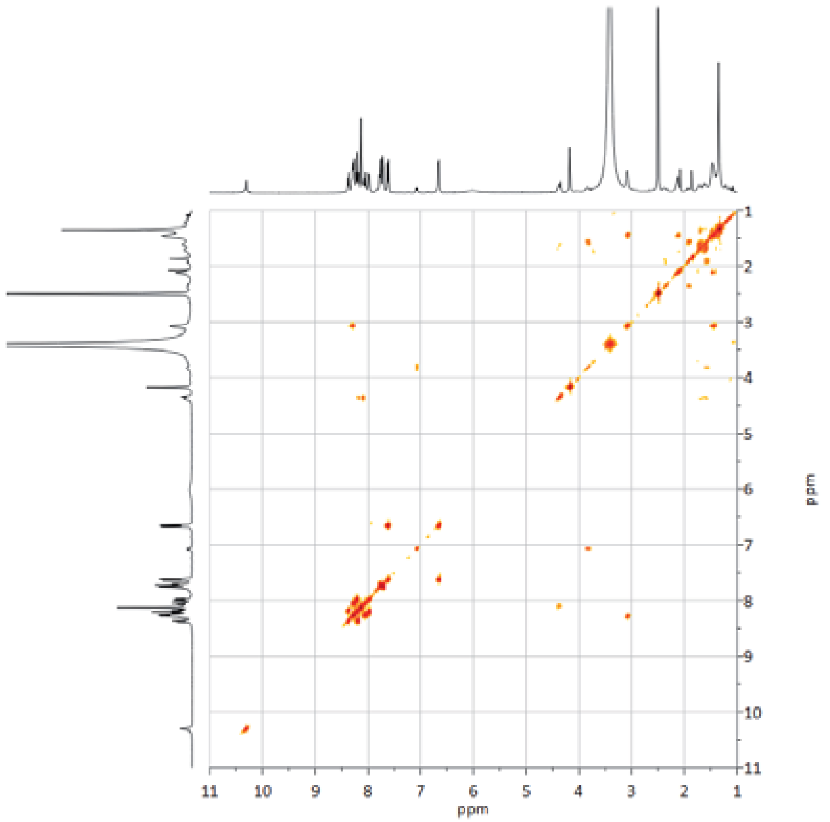

COSY (400 MHz, DMSO-d_6)

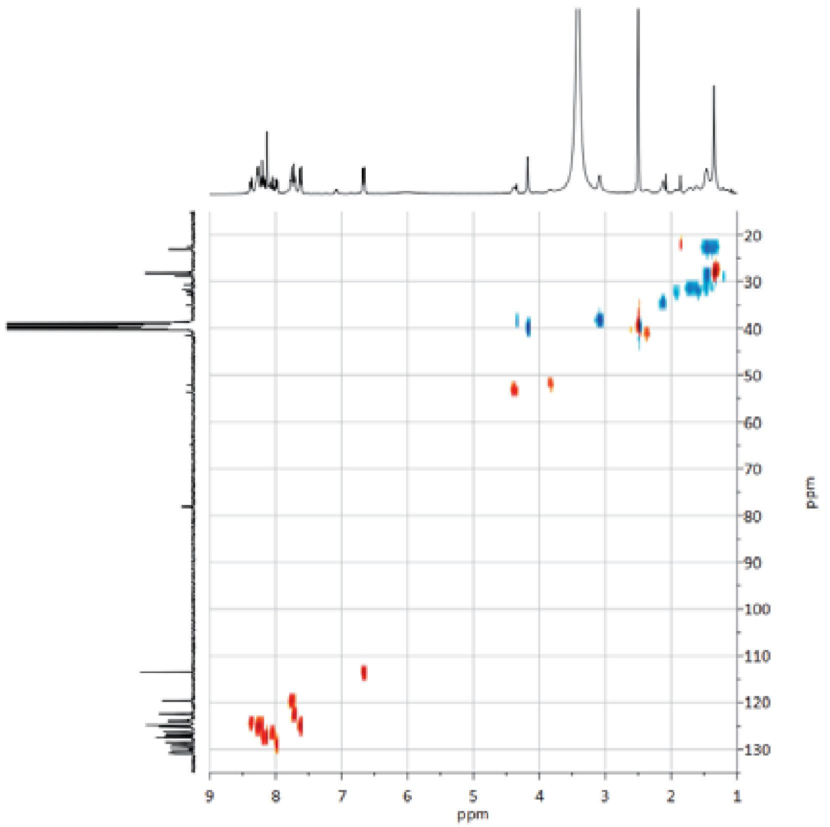

HSQC (400 MHz, DMSO-d_6. CH, CH_3: blue, CH_2: red)

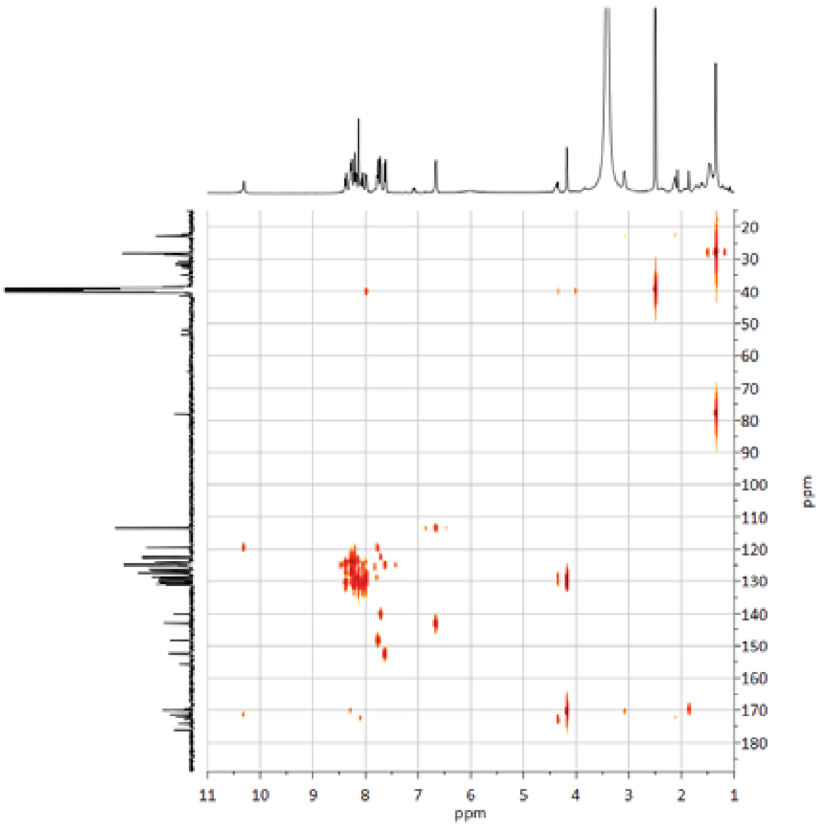

HMBC (400 MHz, DMSO-d_6)

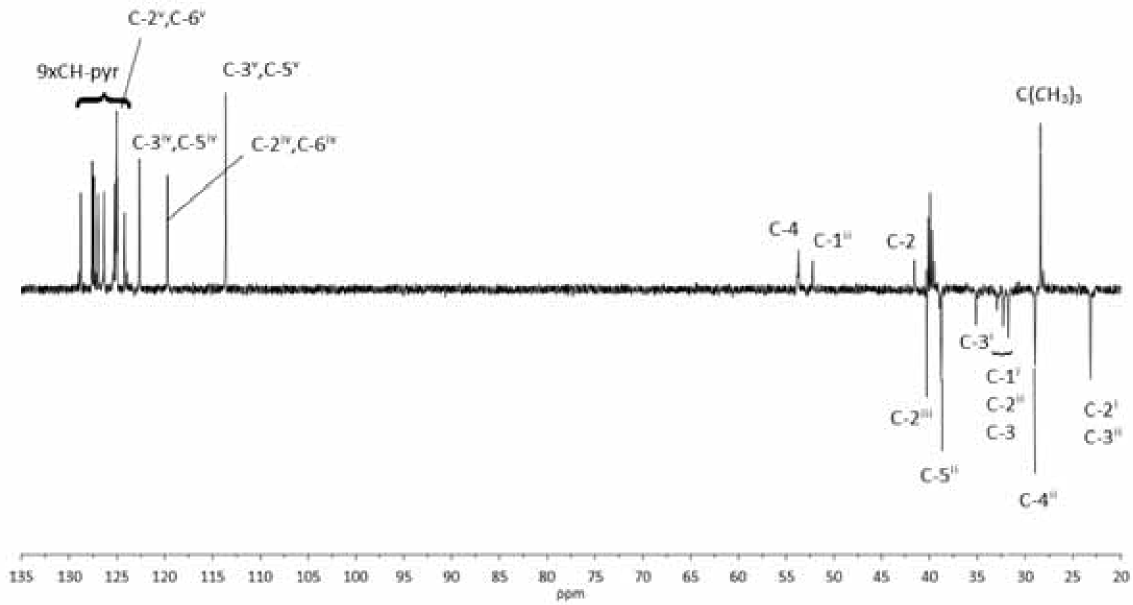

DEPT 135 (100.6 MHz, DMSO-d_6)

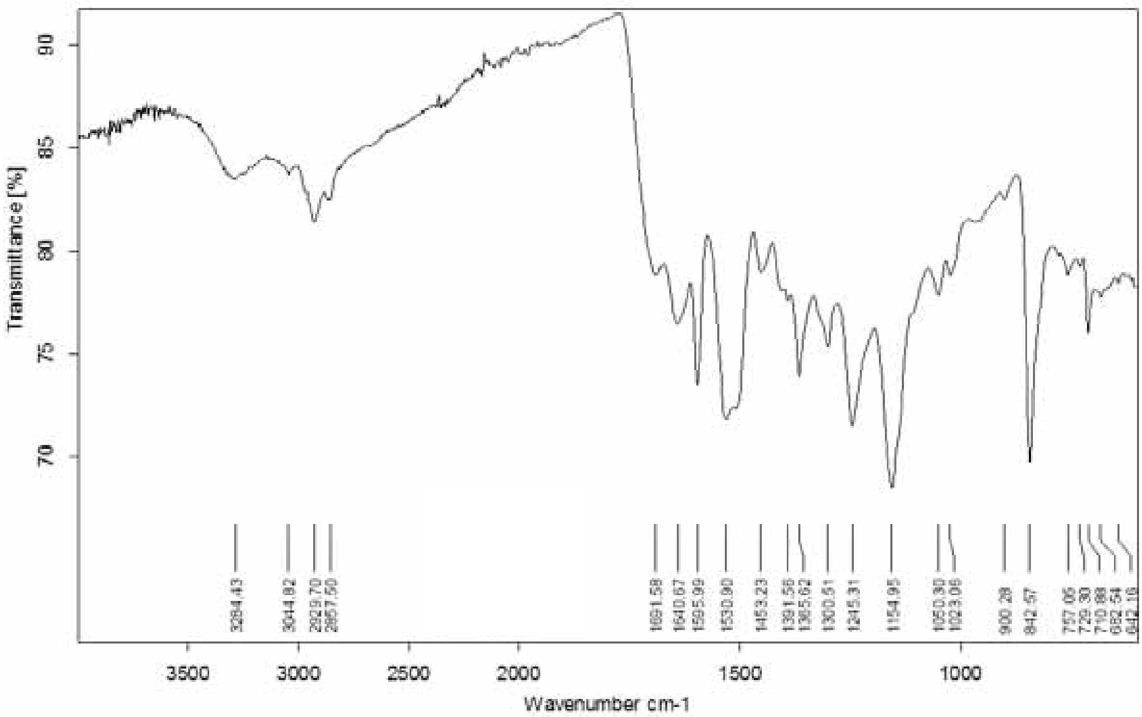

IR (ATR)

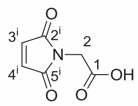

49

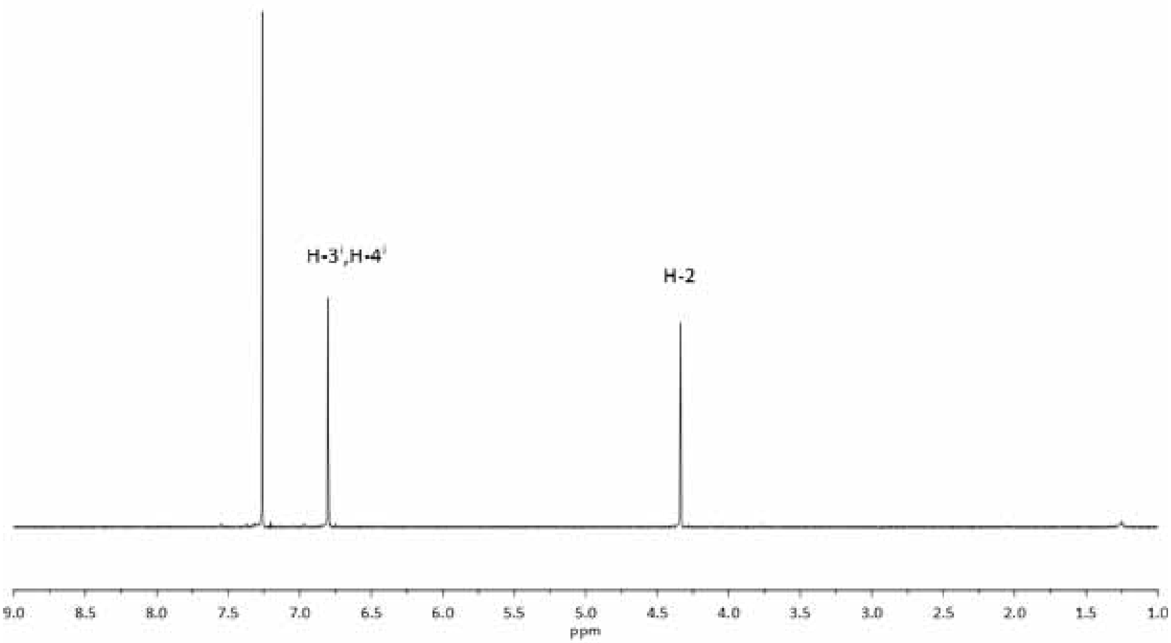

^{1}H-NMR (360 MHz, $CDCl_3$)

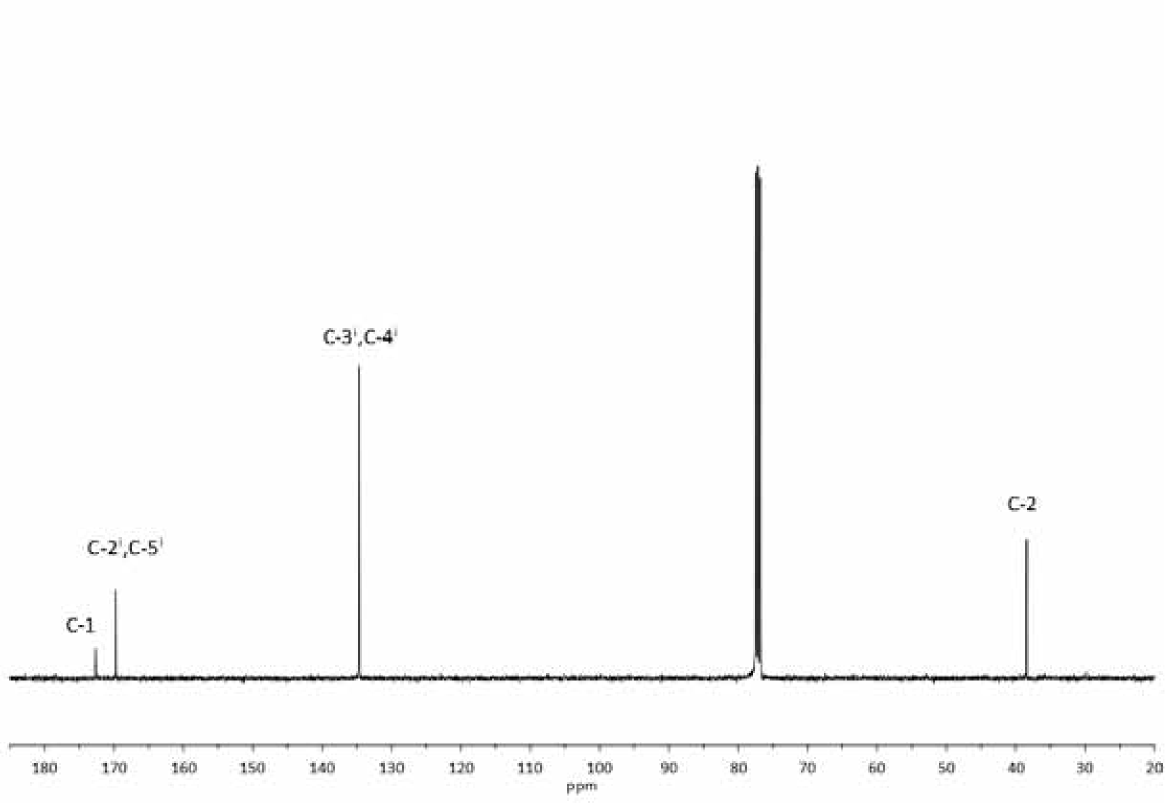

^{13}C-NMR (100.6 MHz, $CDCl_3$)

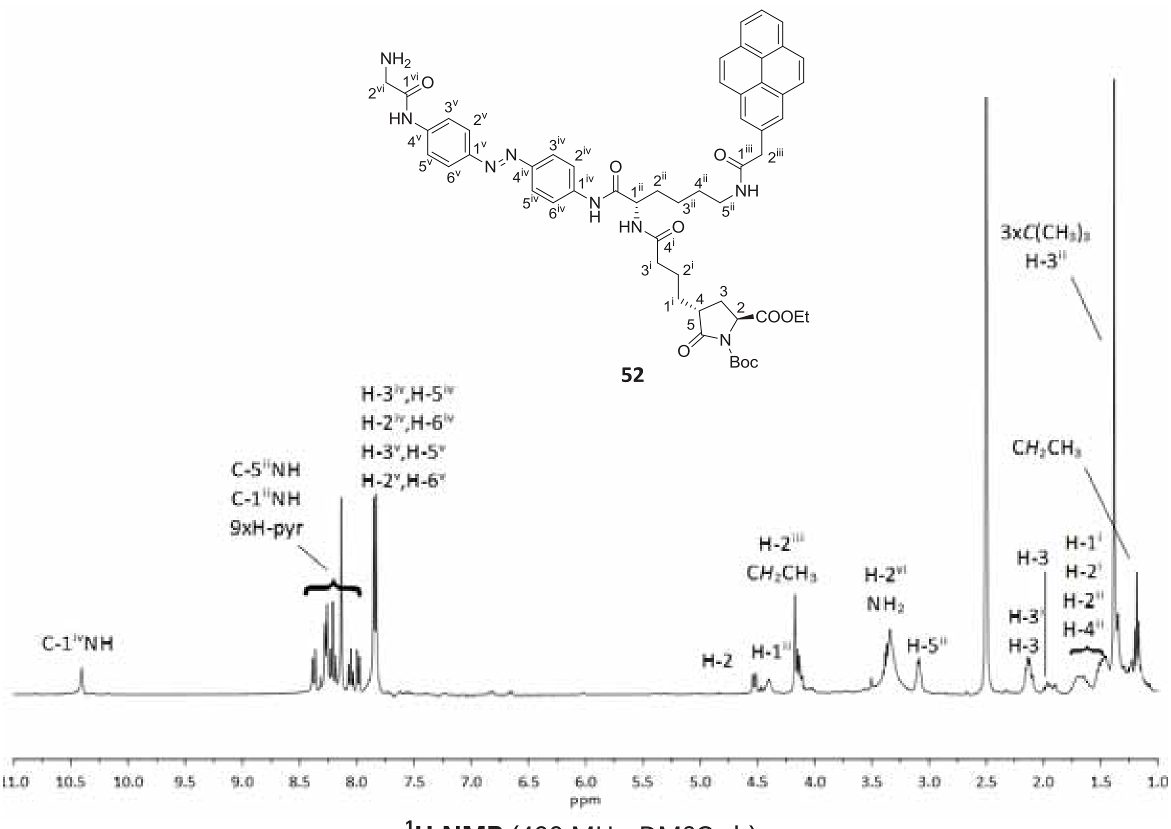

^{1}H-NMR (400 MHz, DMSO-d_6)

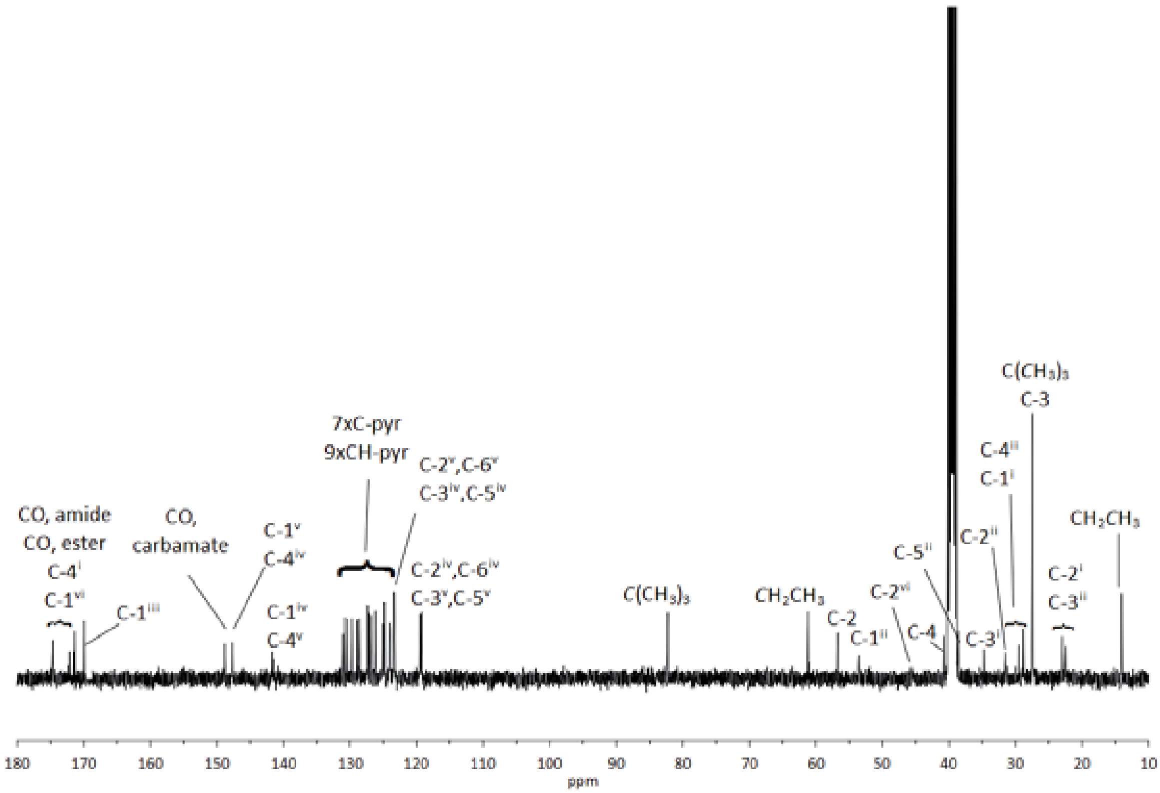

^{13}**C-NMR** (100.6 MHz, DMSO-d$_6$)

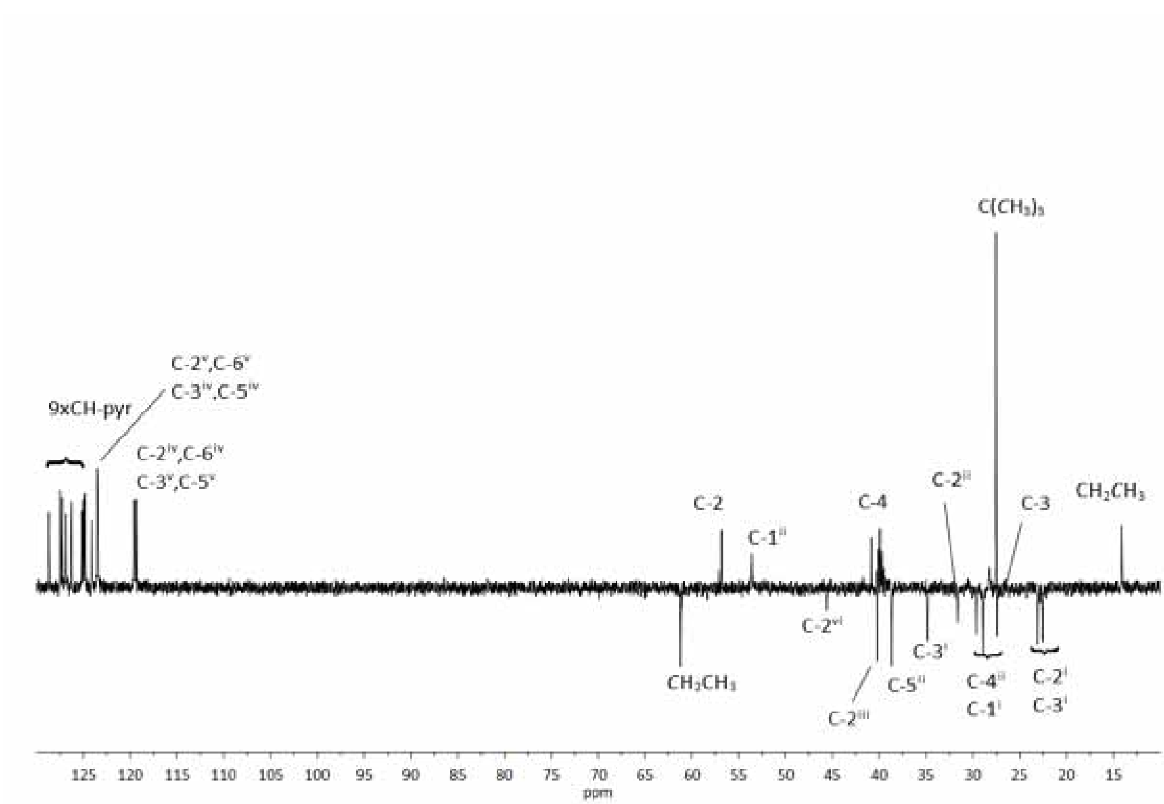

DEPT 135 (100.6 MHz, DMSO-d$_6$)

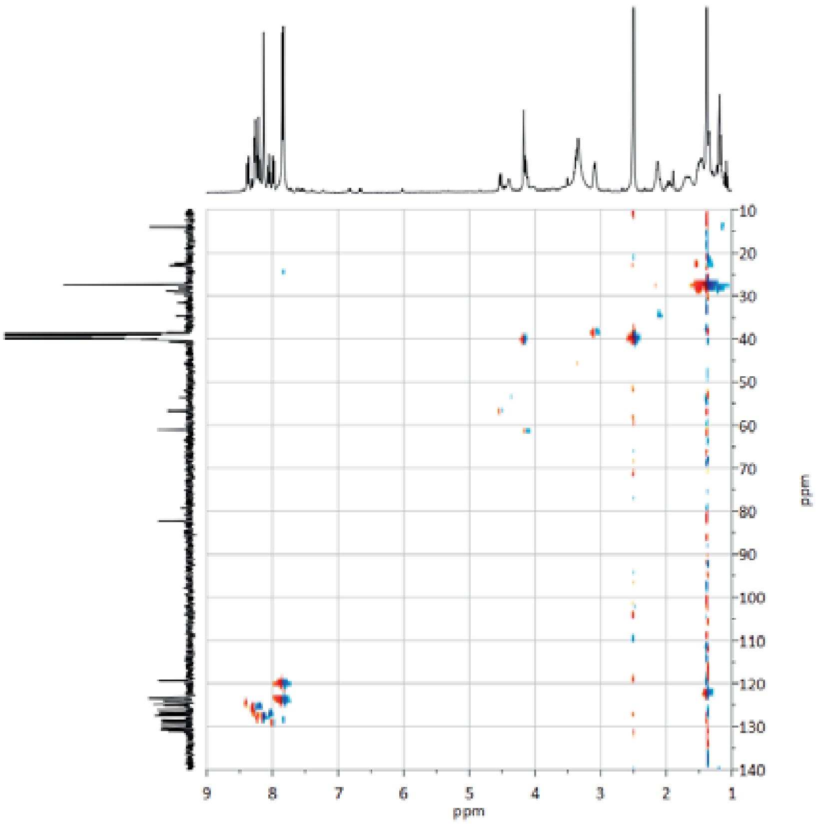

HSQC (400 MHz, DMSO-d_6)

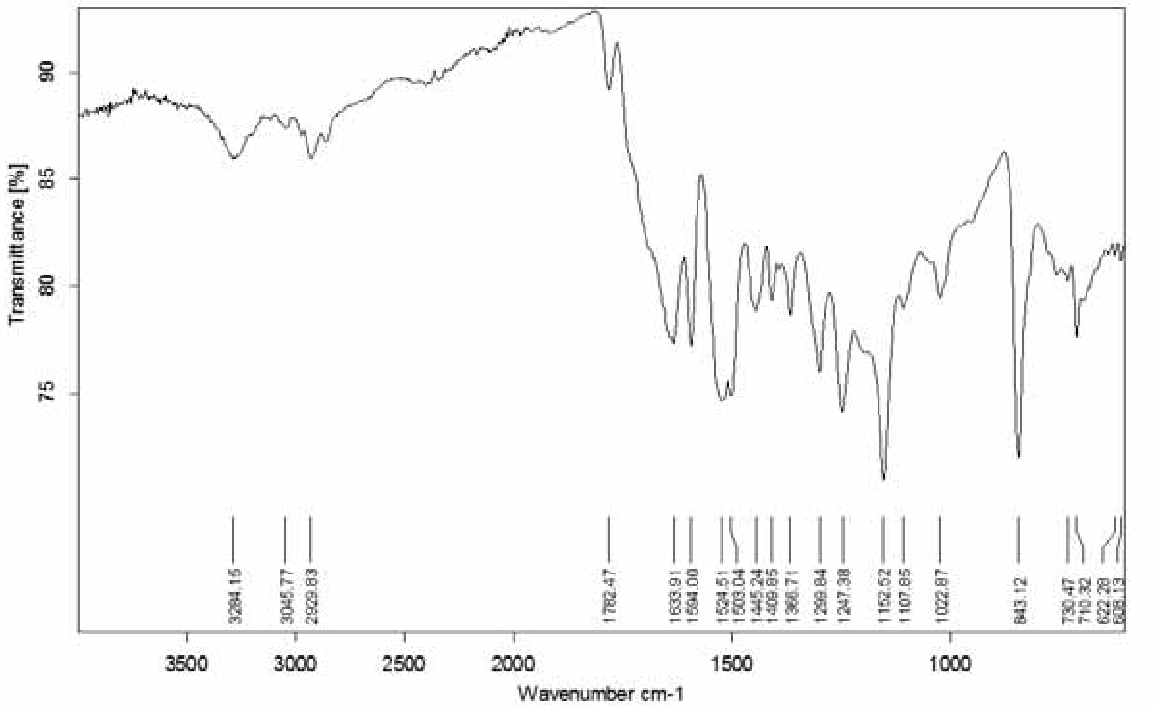

IR (ATR)

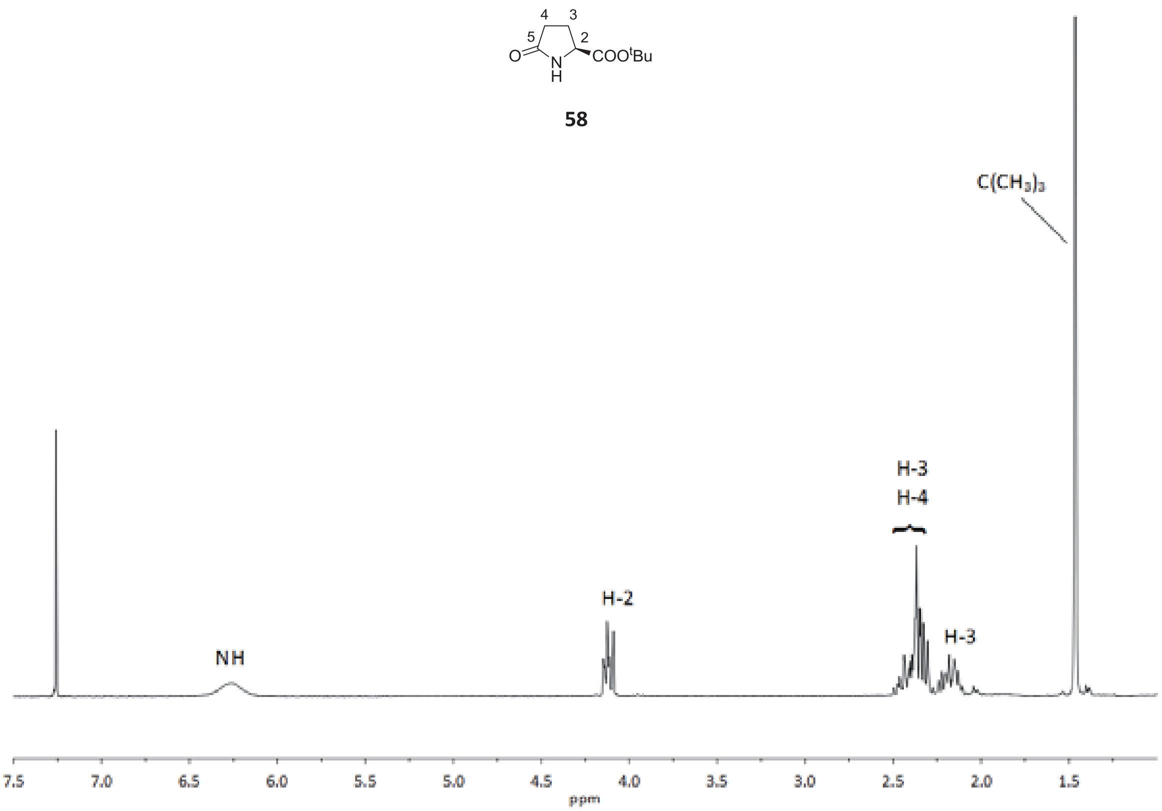

^{1}H-NMR (250 MHz, $CDCl_3$)

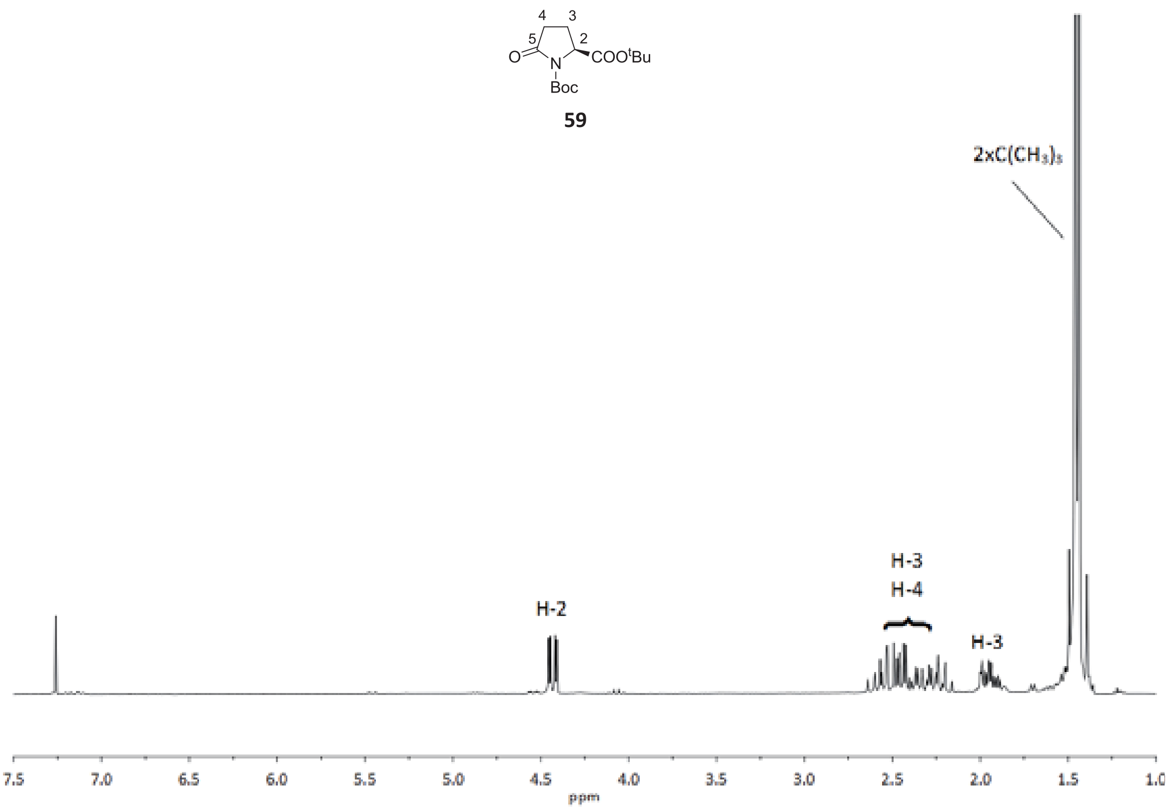

^{1}H-NMR (250 MHz, $CDCl_3$)

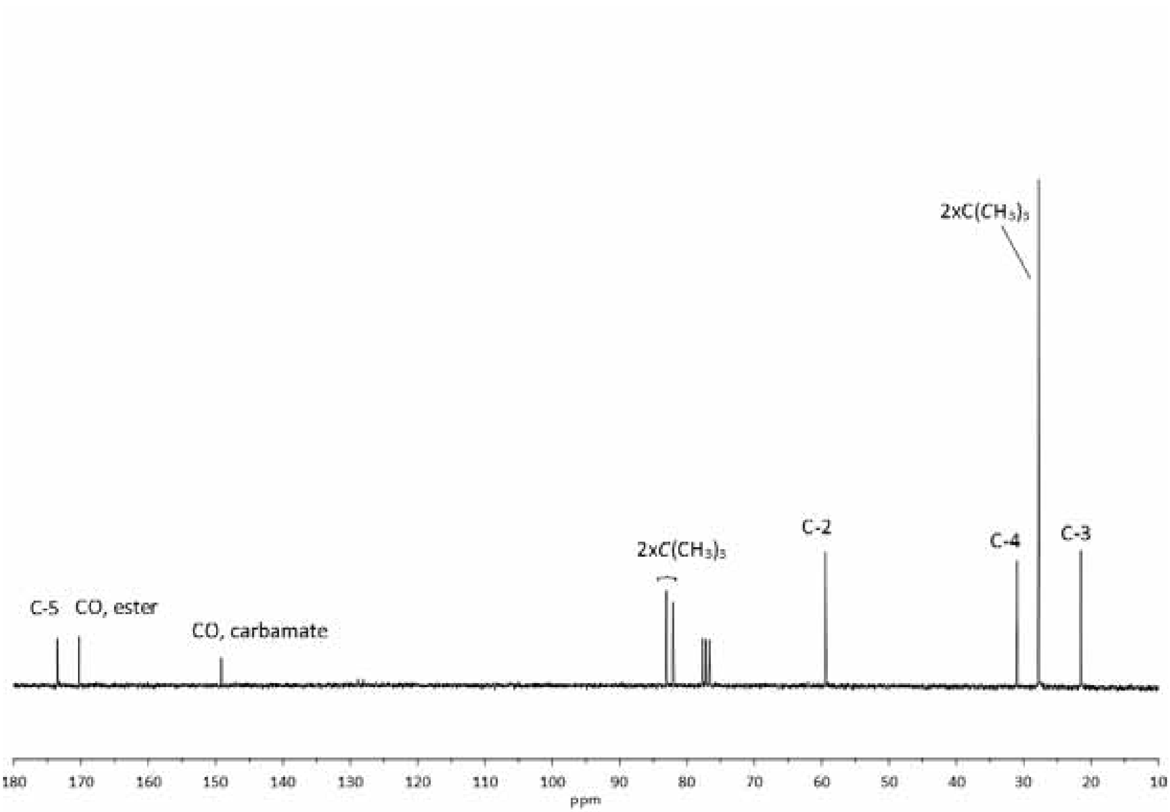

^{13}C-NMR (62.5 MHz, $CDCl_3$)

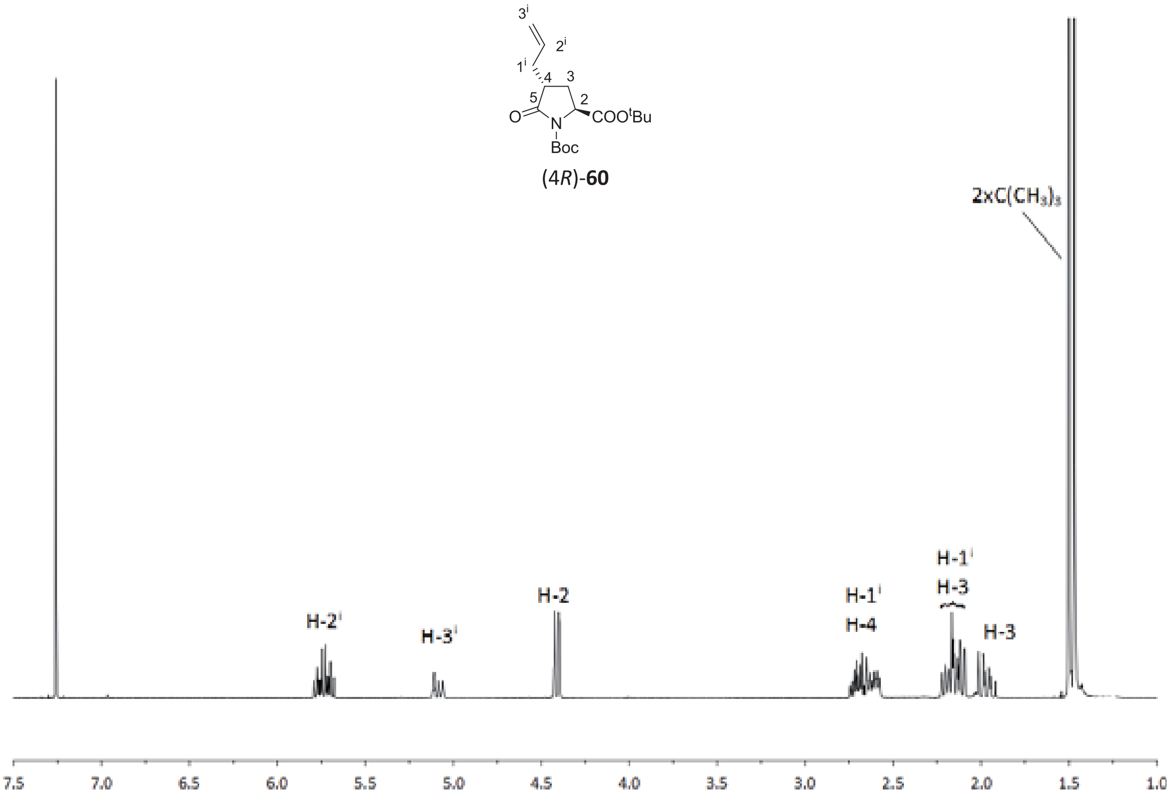

^{1}H-NMR (360 MHz, $CDCl_3$)

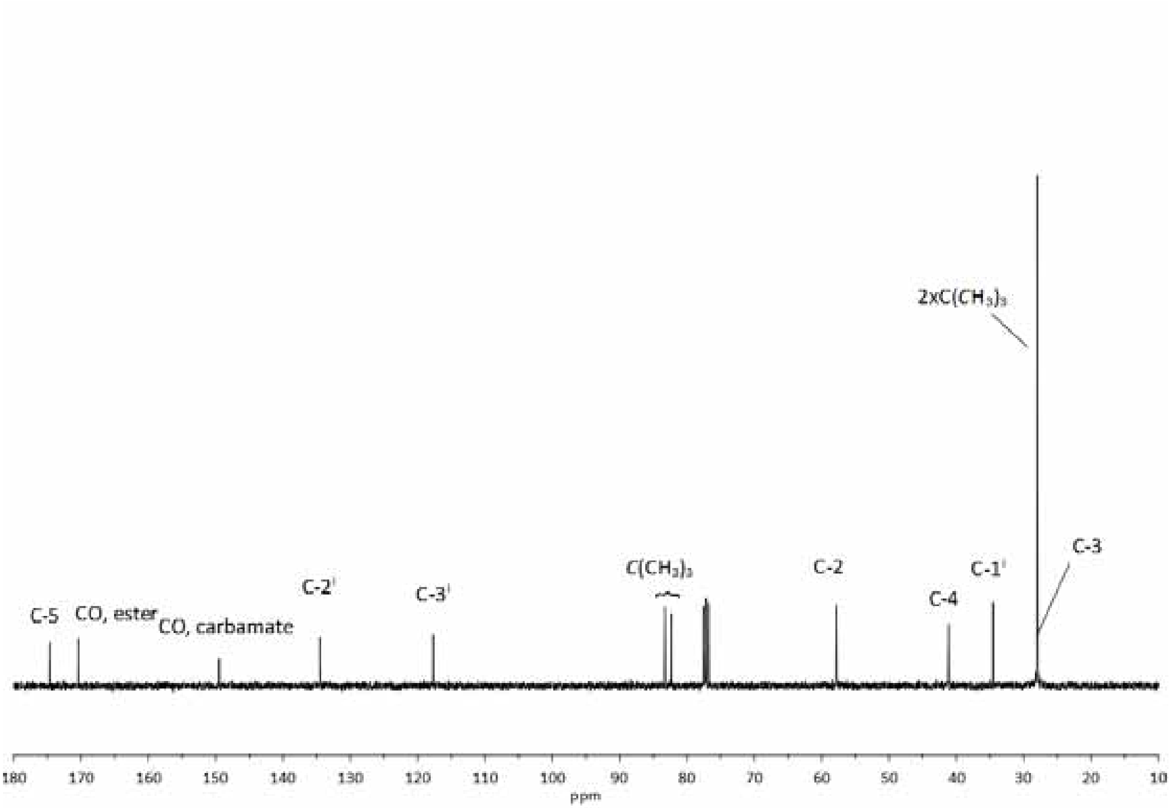

^{13}C-NMR (90 MHz, $CDCl_3$)

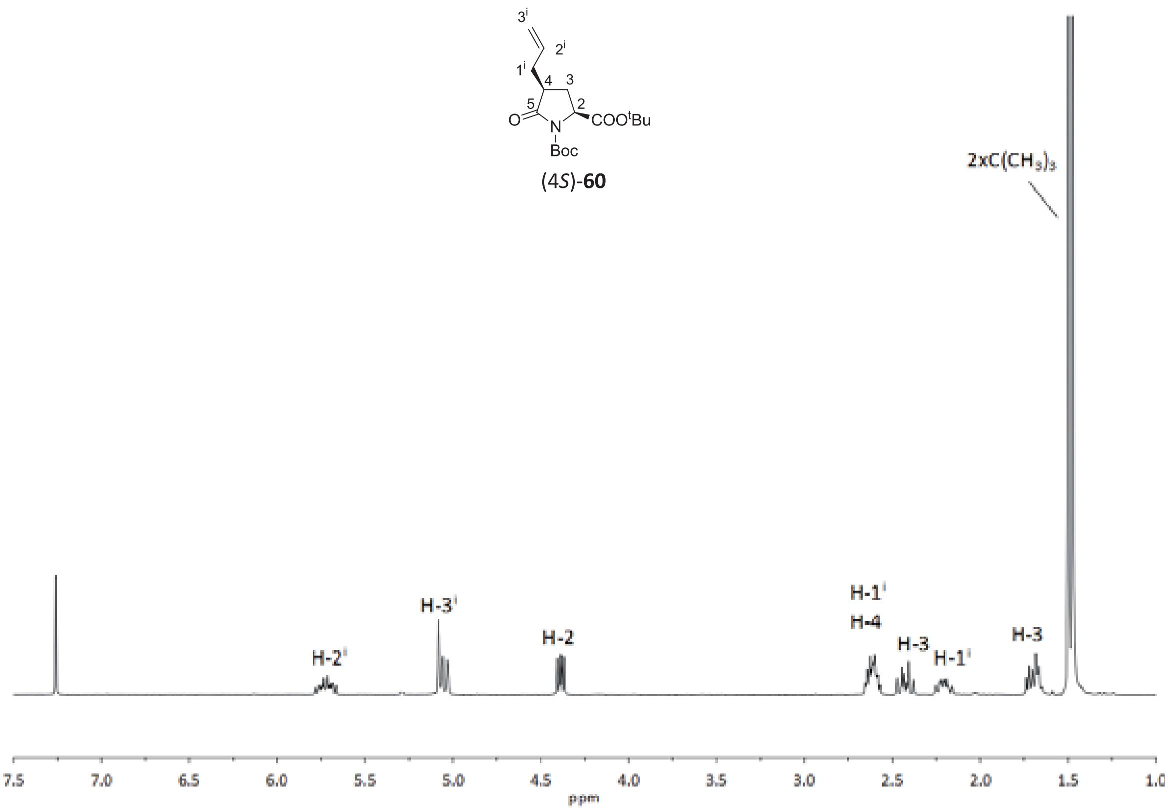

^{1}H-NMR (360 MHz, $CDCl_3$)

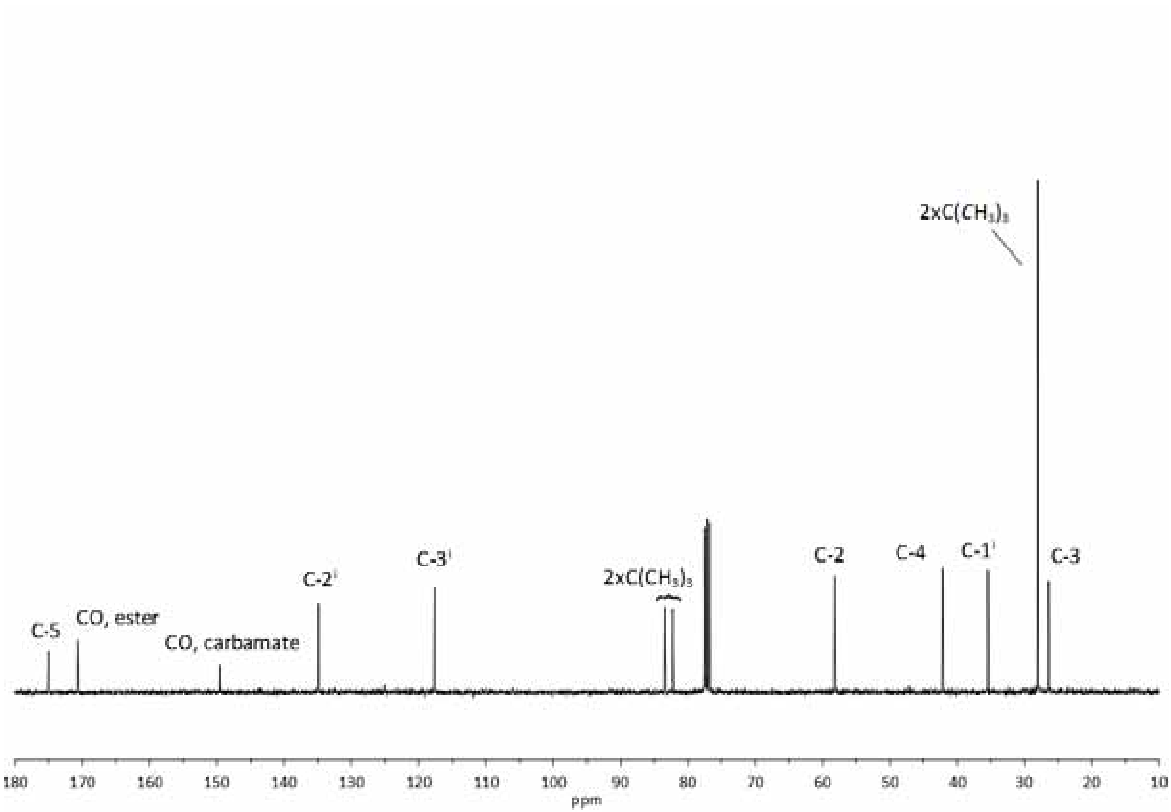

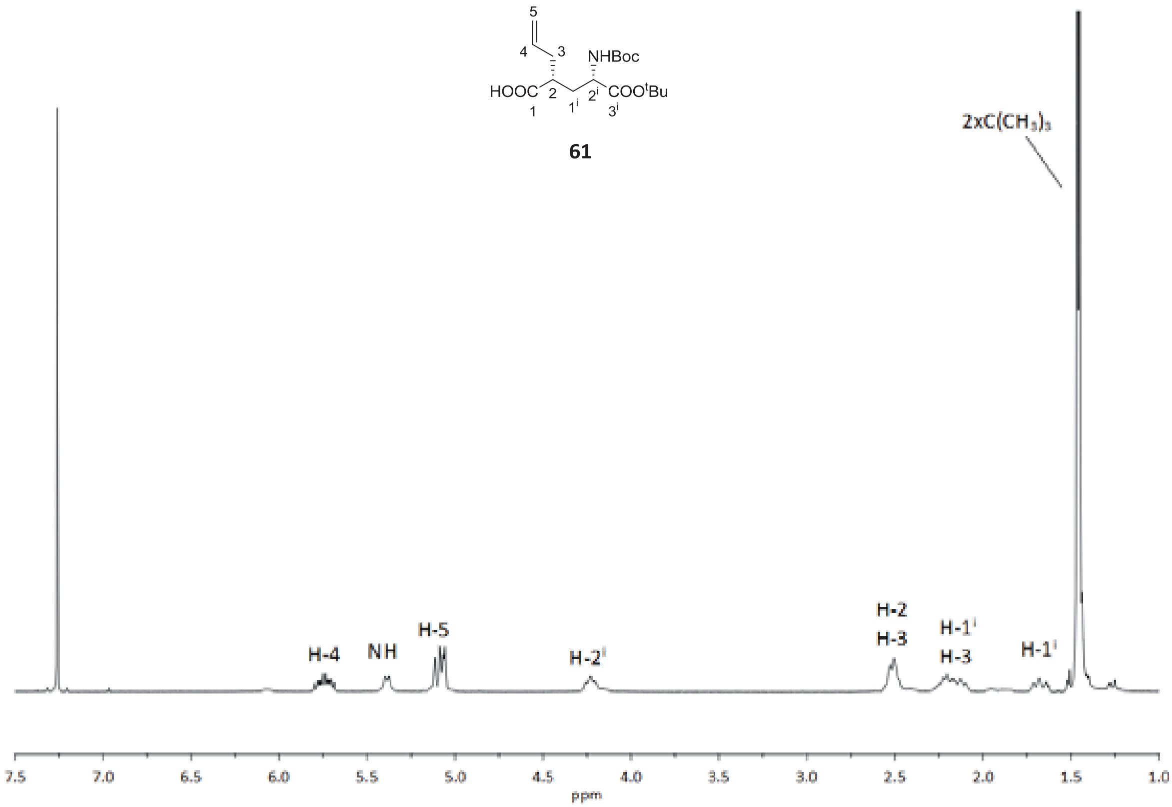

^{1}**H-NMR** (360 MHz, $CDCl_3$)

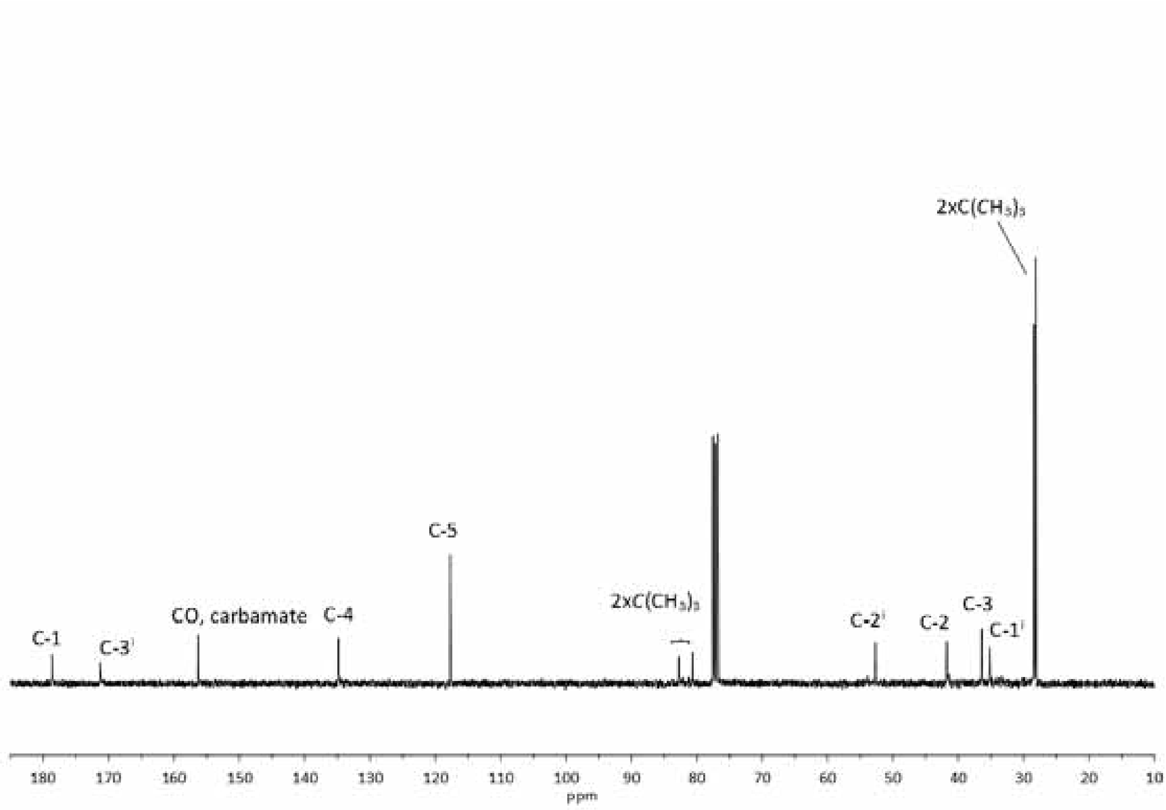

^{13}**C-NMR** (90 MHz, $CDCl_3$)

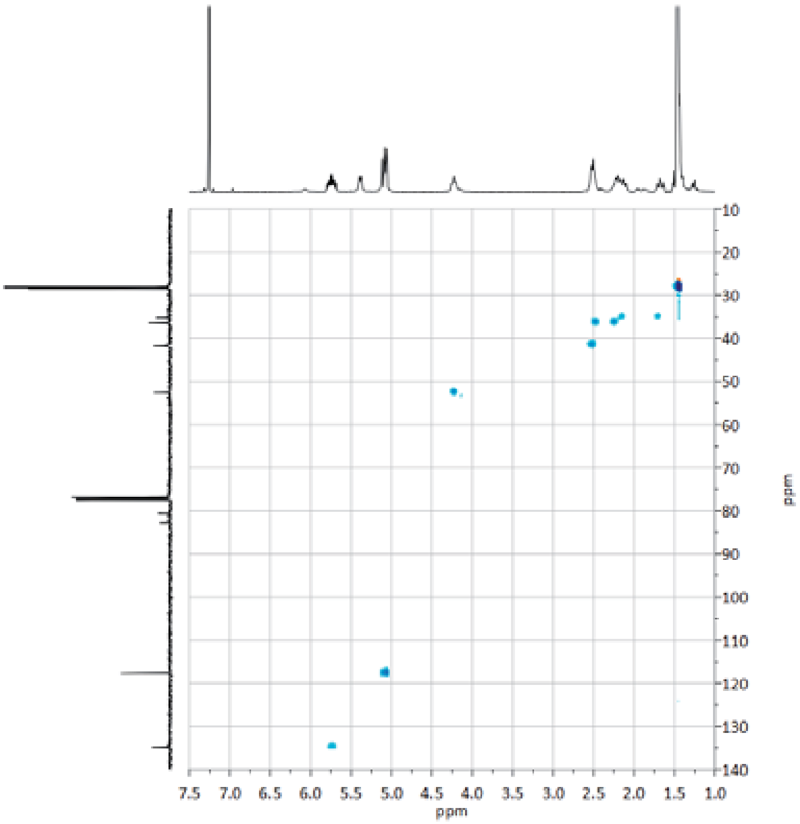

HSQC (360 MHz, $CDCl_3$)

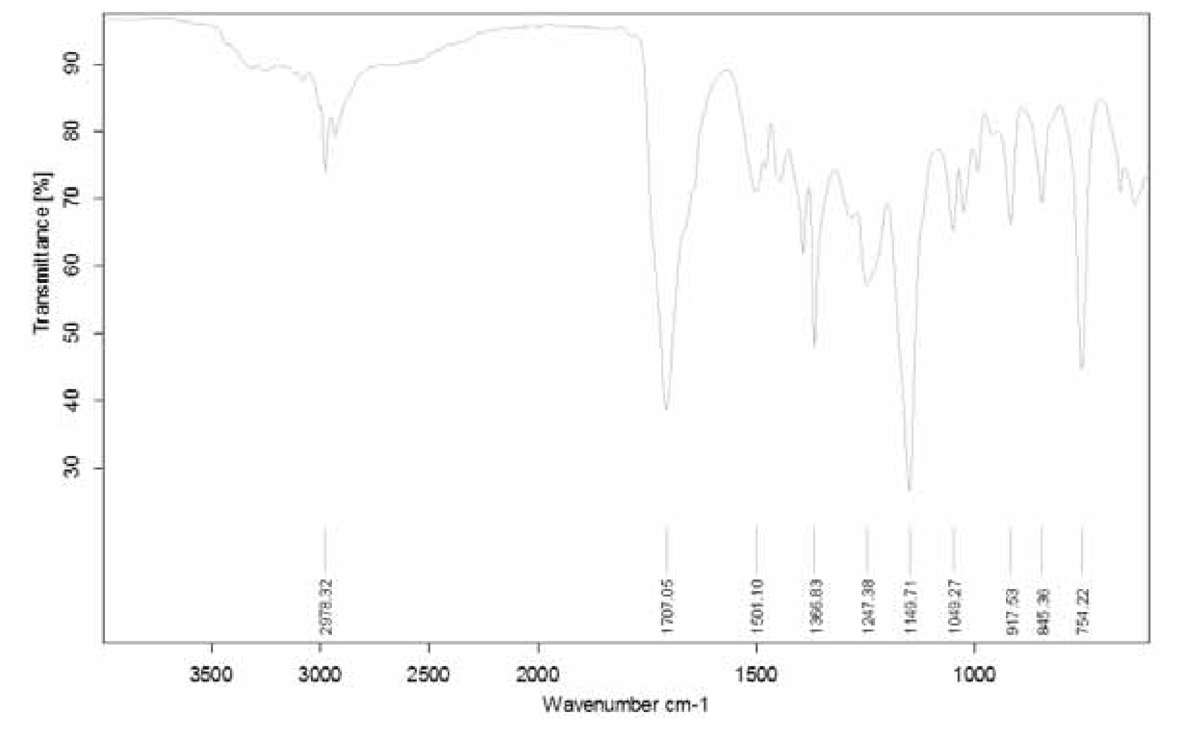

IR (ATR)

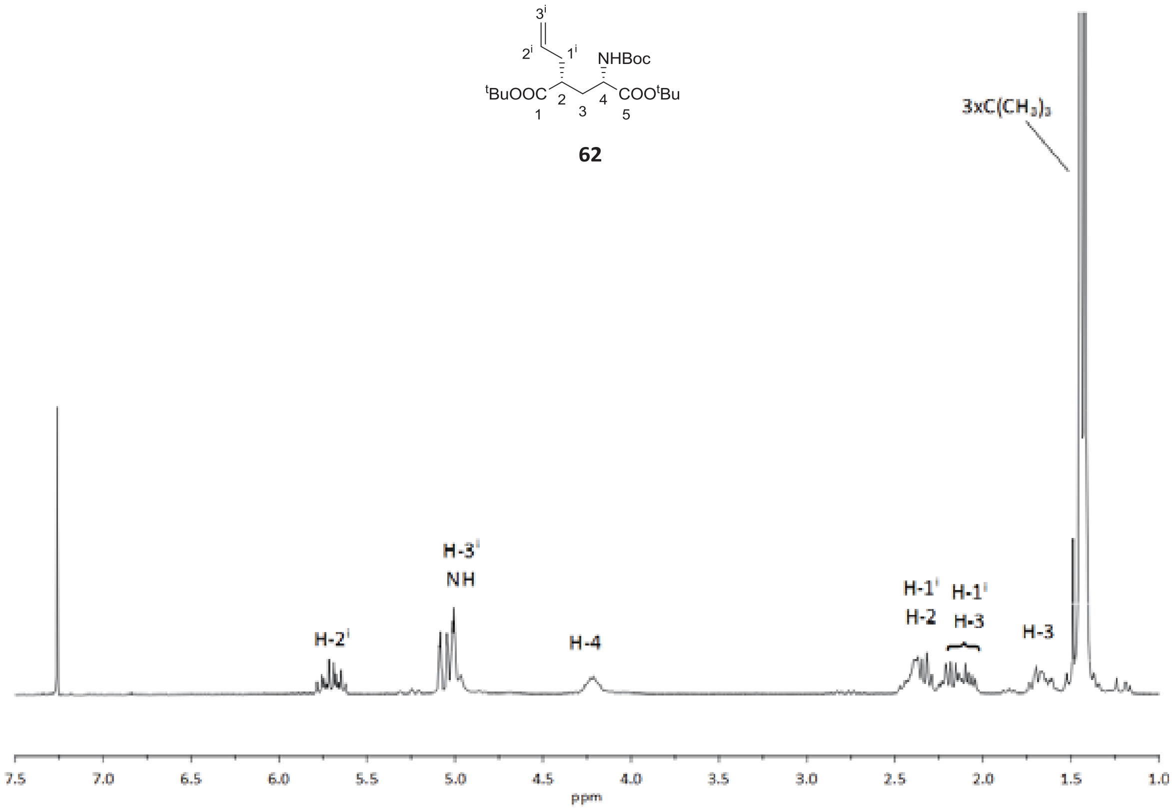

^{1}H-NMR (250 MHz, $CDCl_3$)

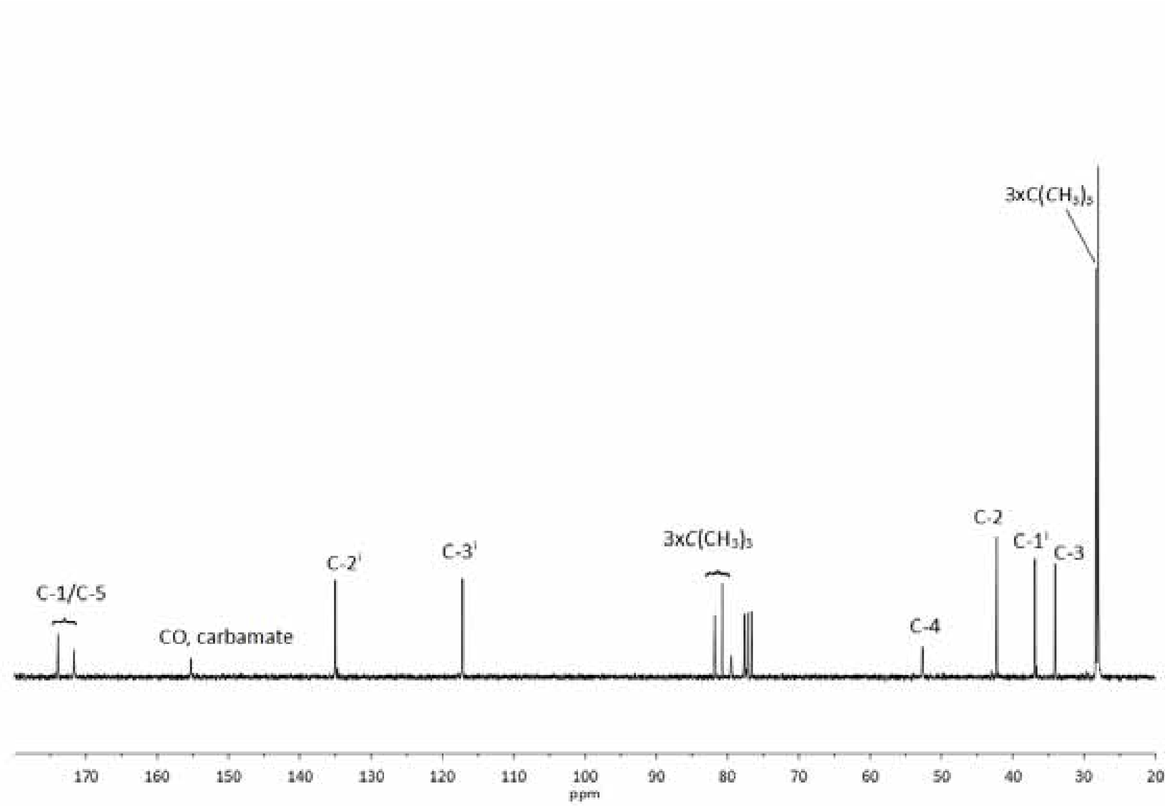

^{13}**C-NMR** (62.5 MHz, $CDCl_3$)

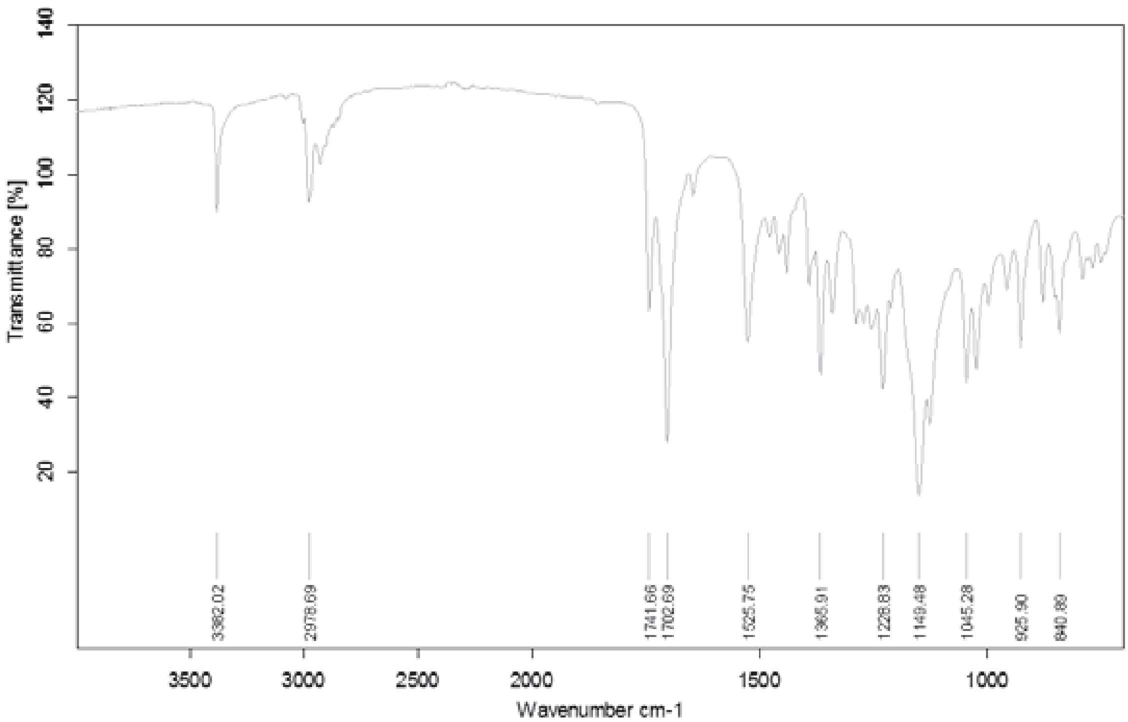

IR (ATR)

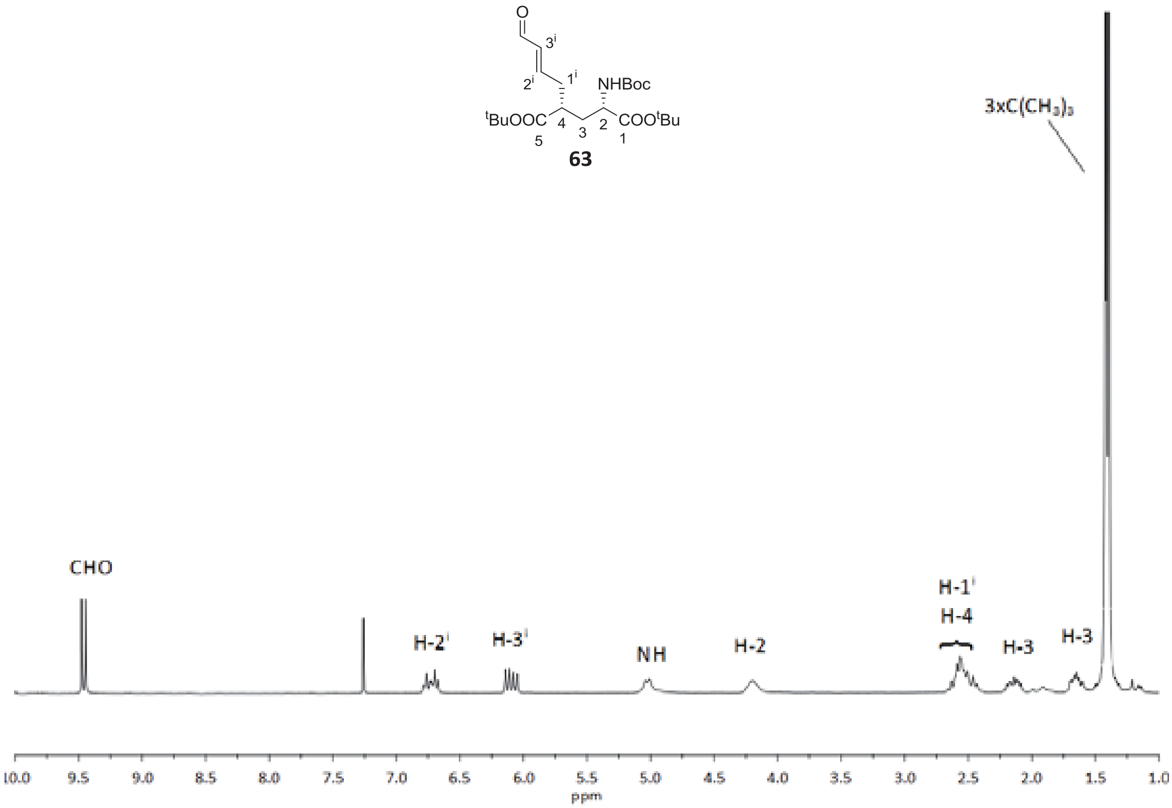

^{1}H-NMR (250 MHz, $CDCl_3$)

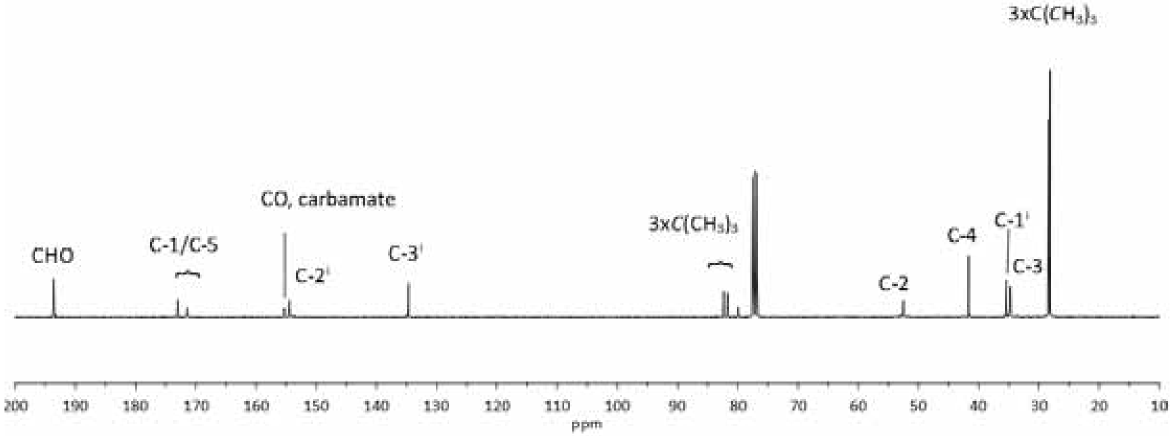

^{13}C-NMR (90 MHz, $CDCl_3$)

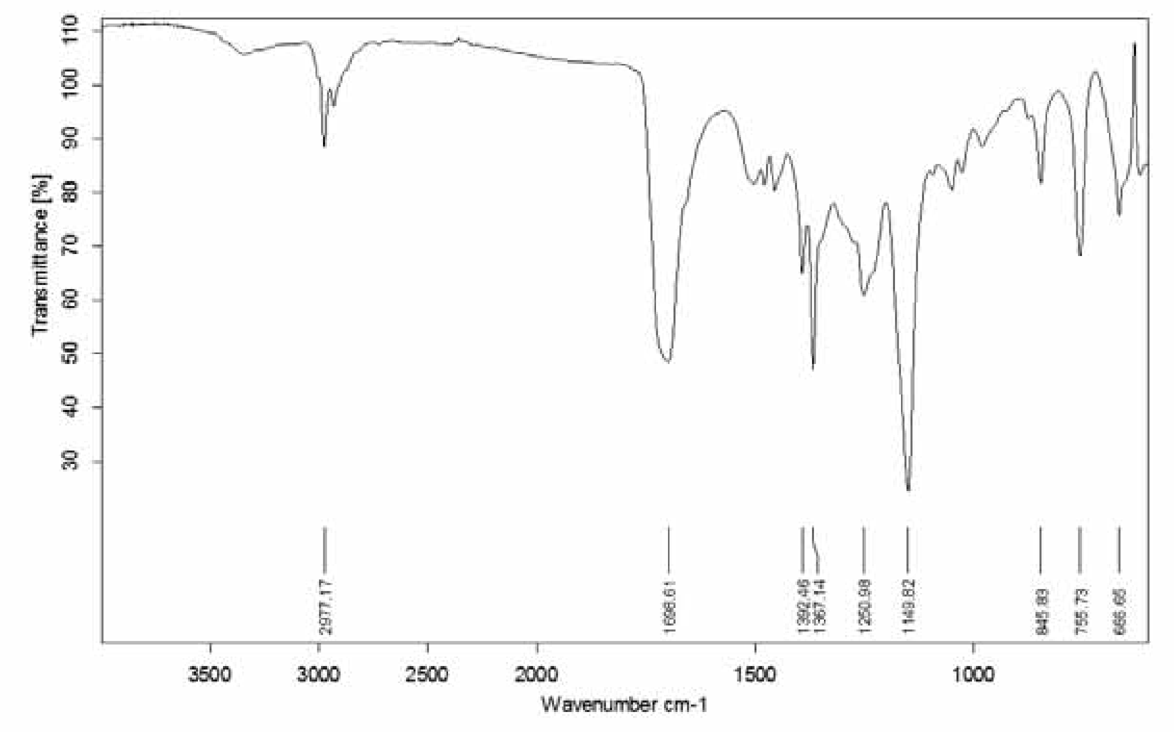

IR (ATR)

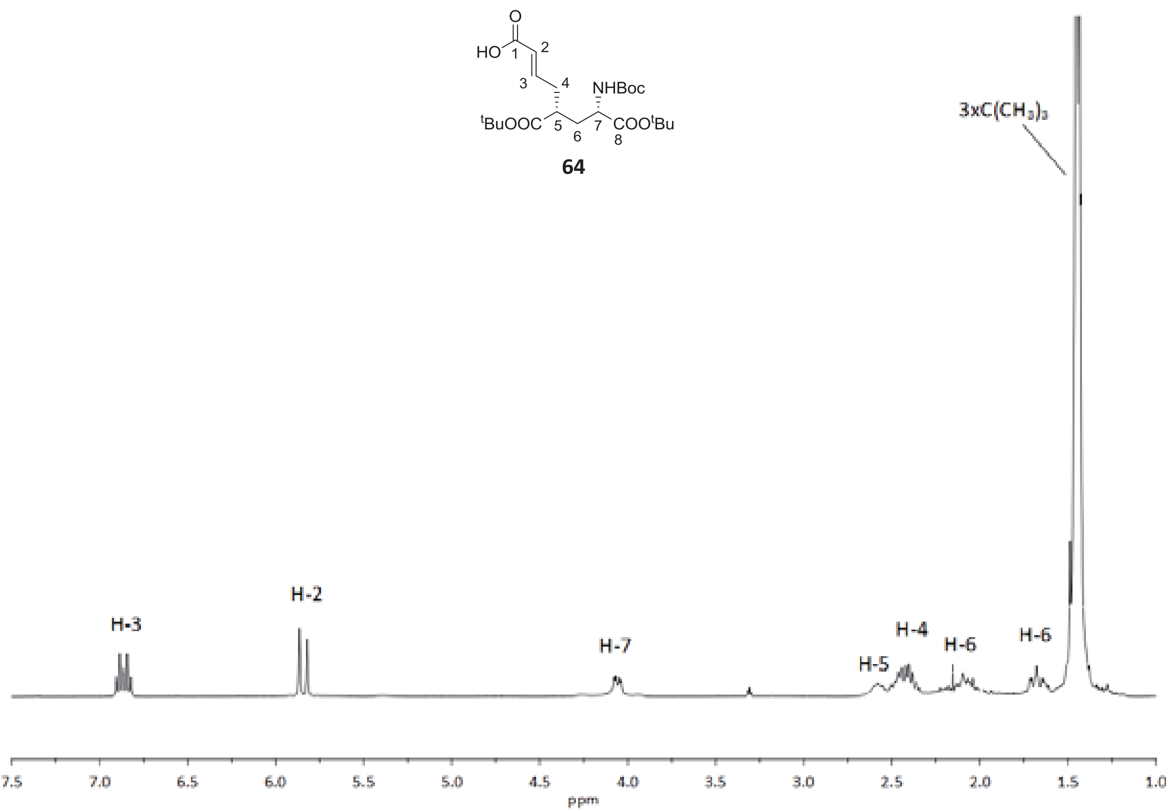

64

^{1}H-NMR (360 MHz, MeOH-d$_4$)

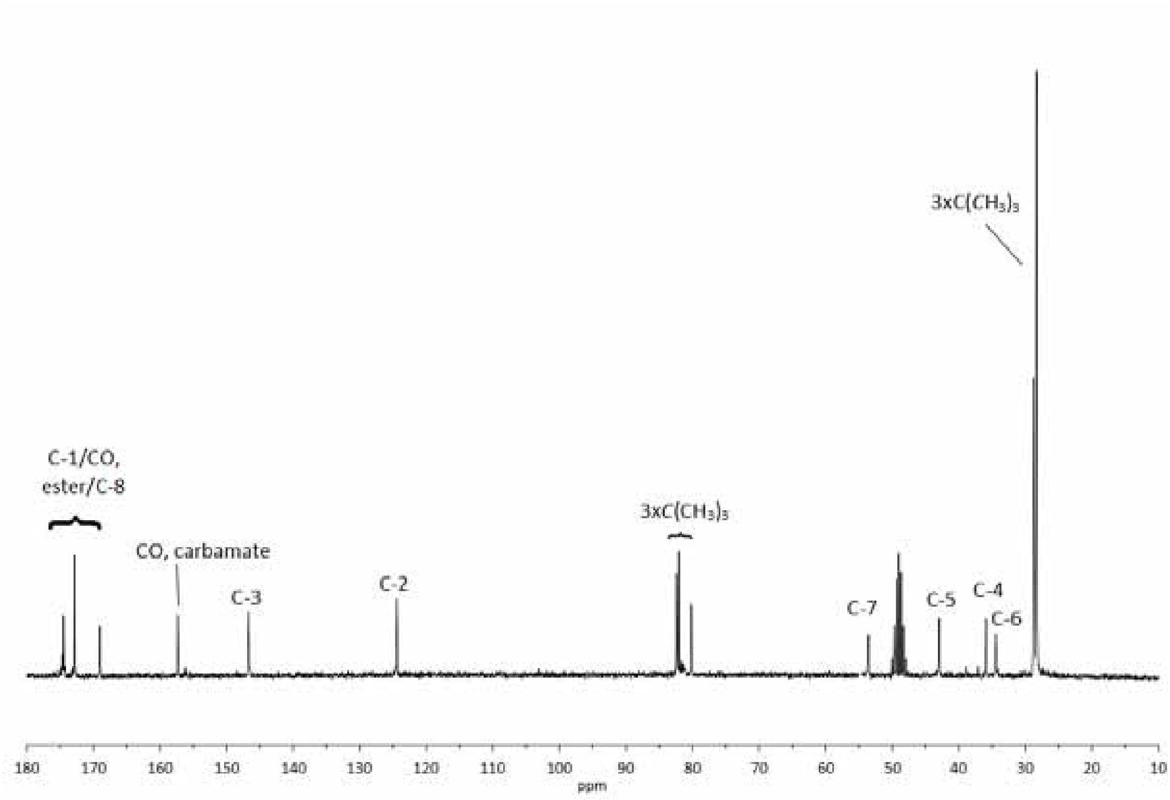

^{13}C-NMR (62.5 MHz, MeOH-d_4)

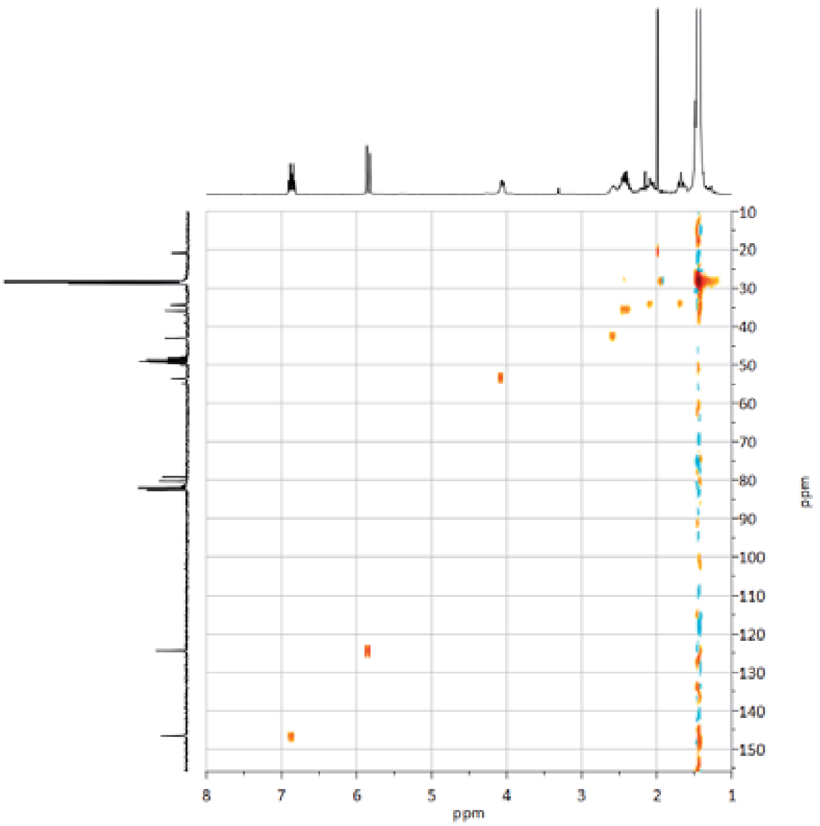

HSQC (400 MHz, MeOH-d_4)

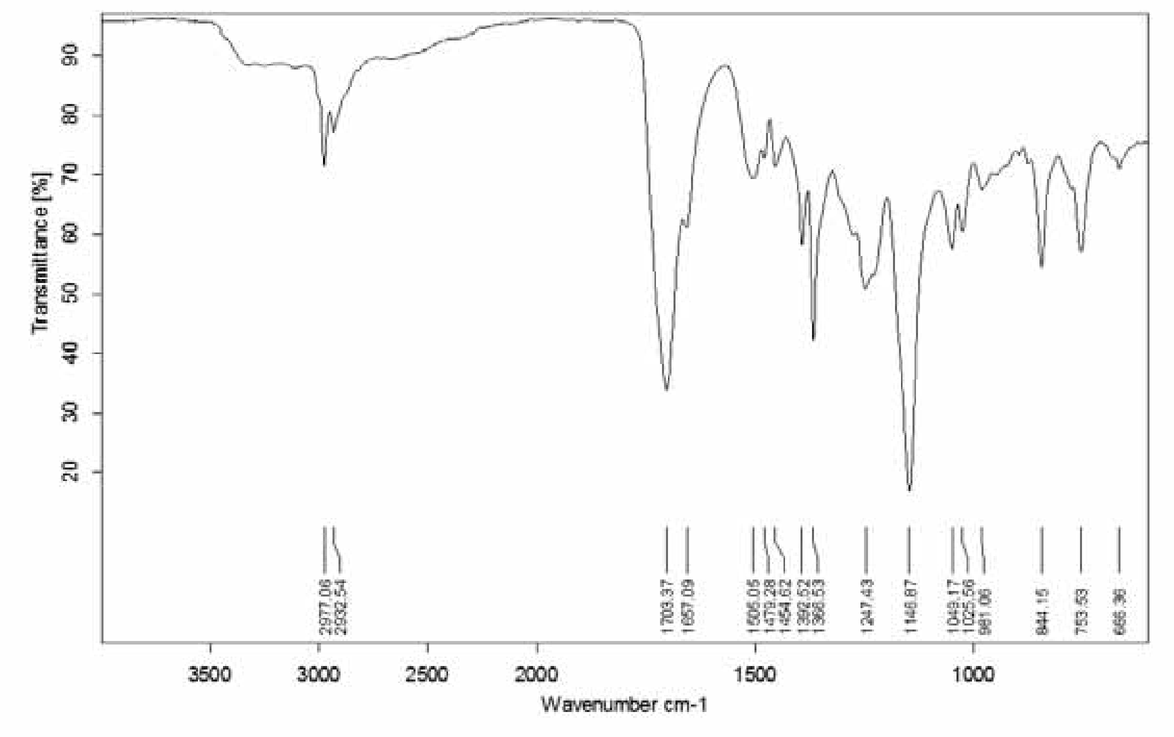

IR (ATR)

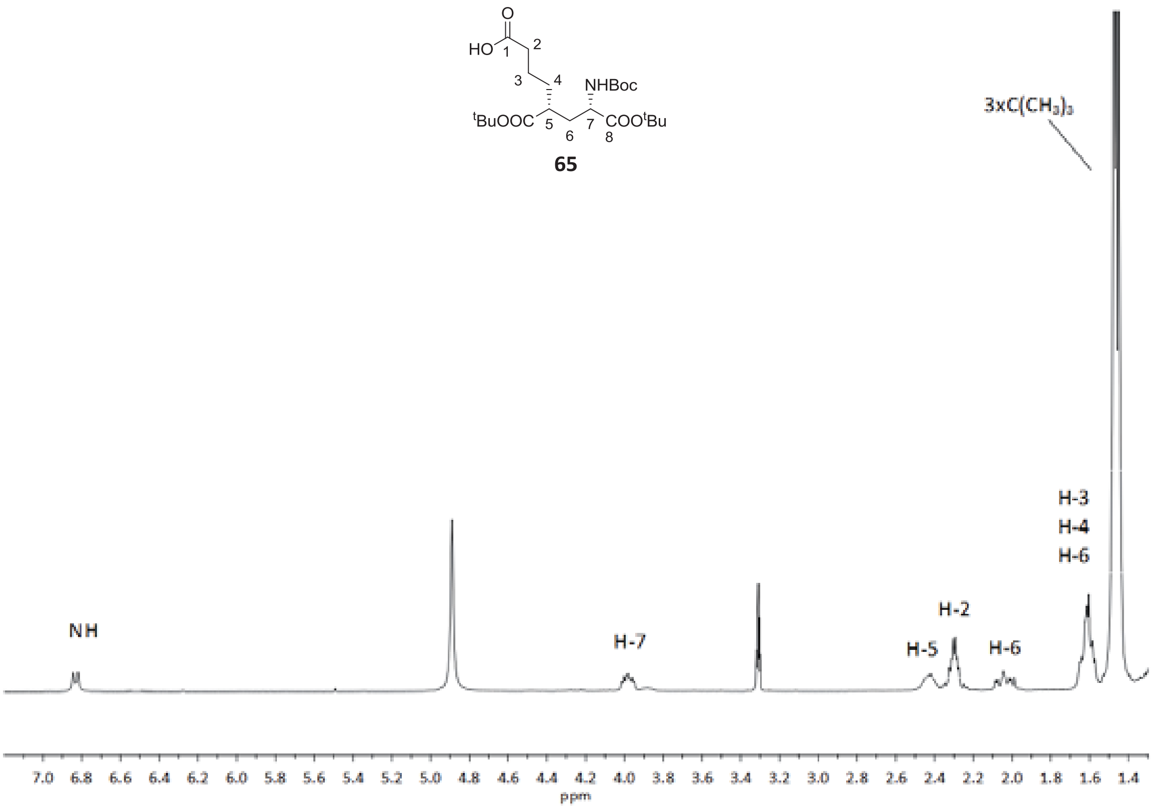

^{1}H-NMR (360 MHz, MeOH-d$_4$)

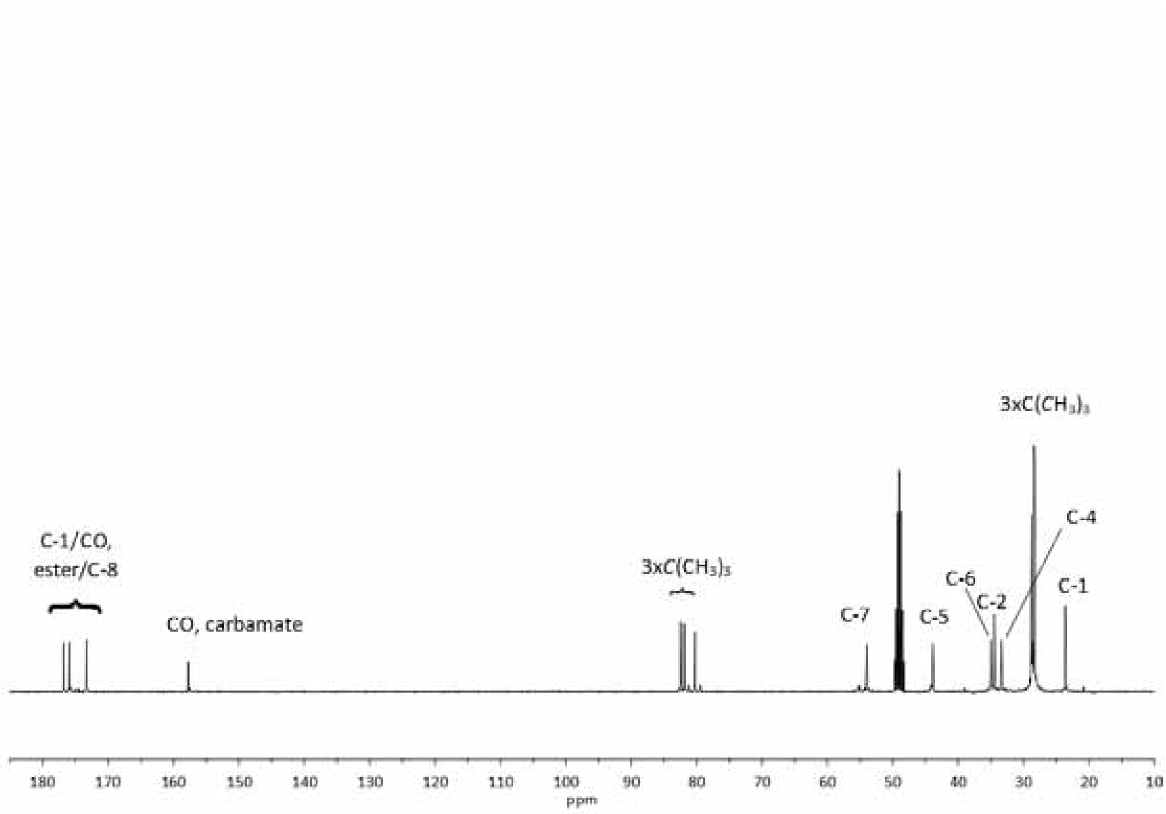

^{13}C-NMR (90 MHz, MeOH-d$_4$)

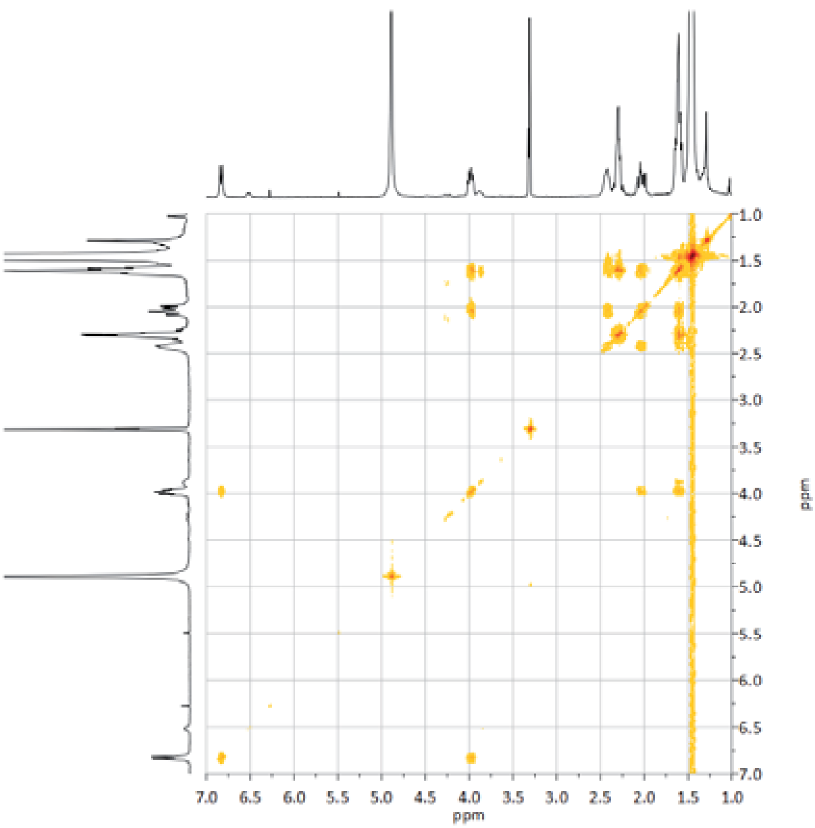

COSY (360 MHz, MeOH-d$_4$)

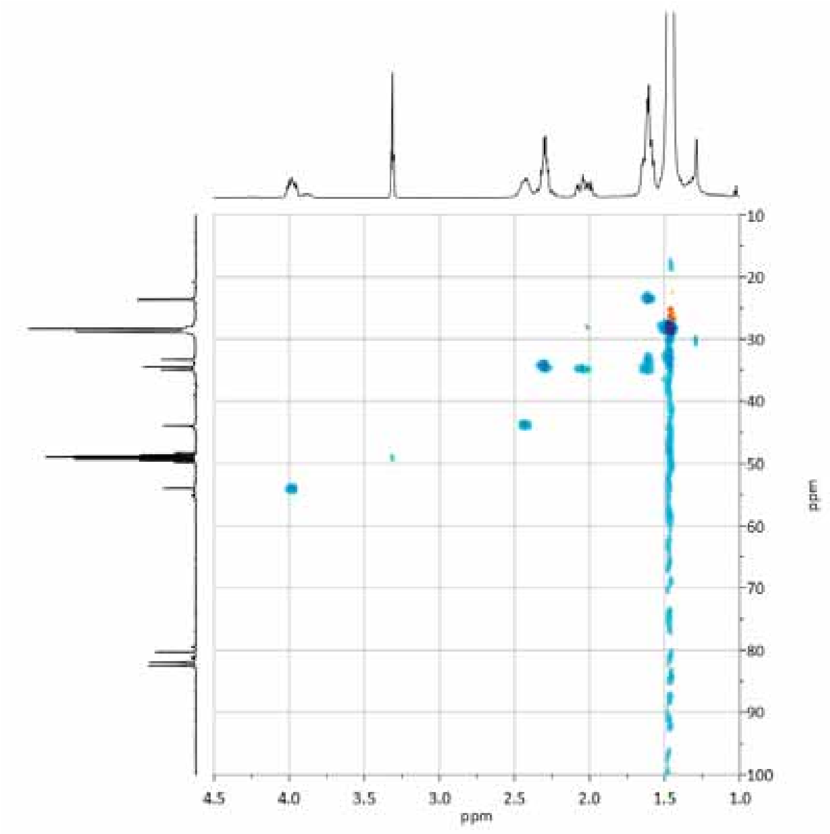

HSQC (360 MHz, MeOH-d_4)

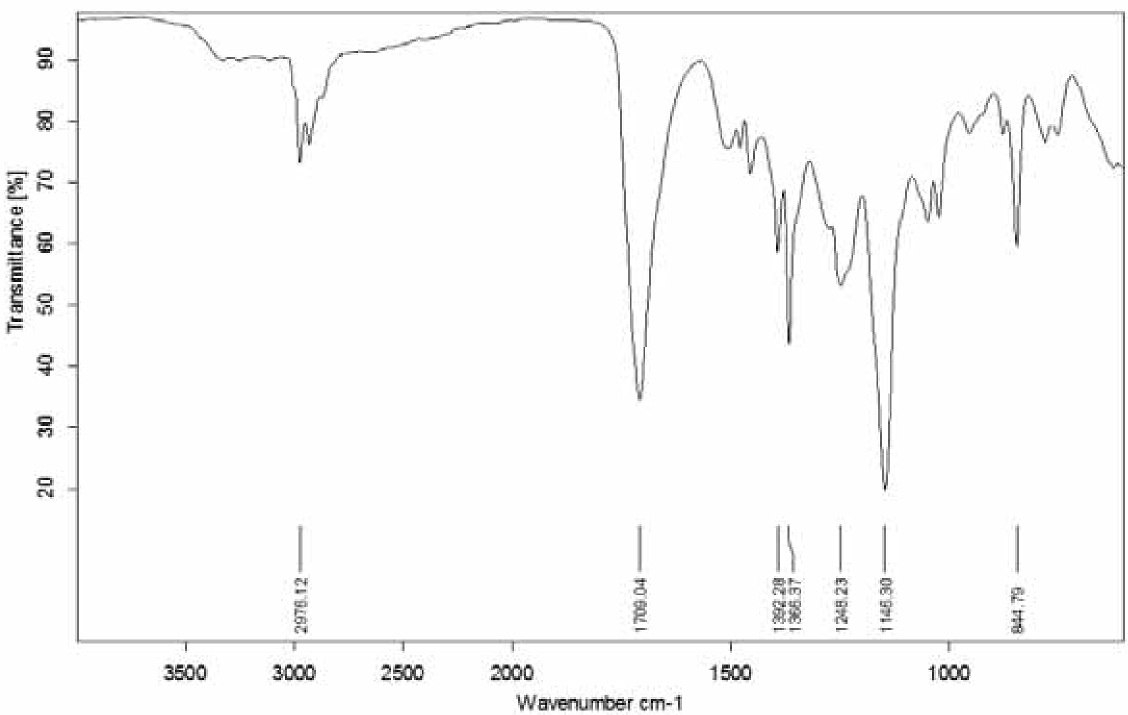

IR (ATR)

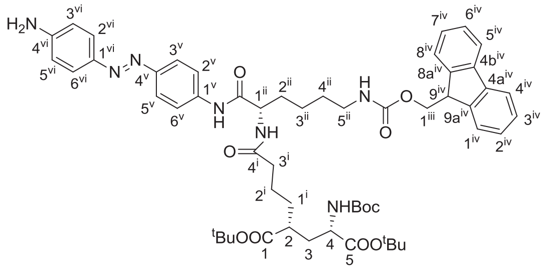

56

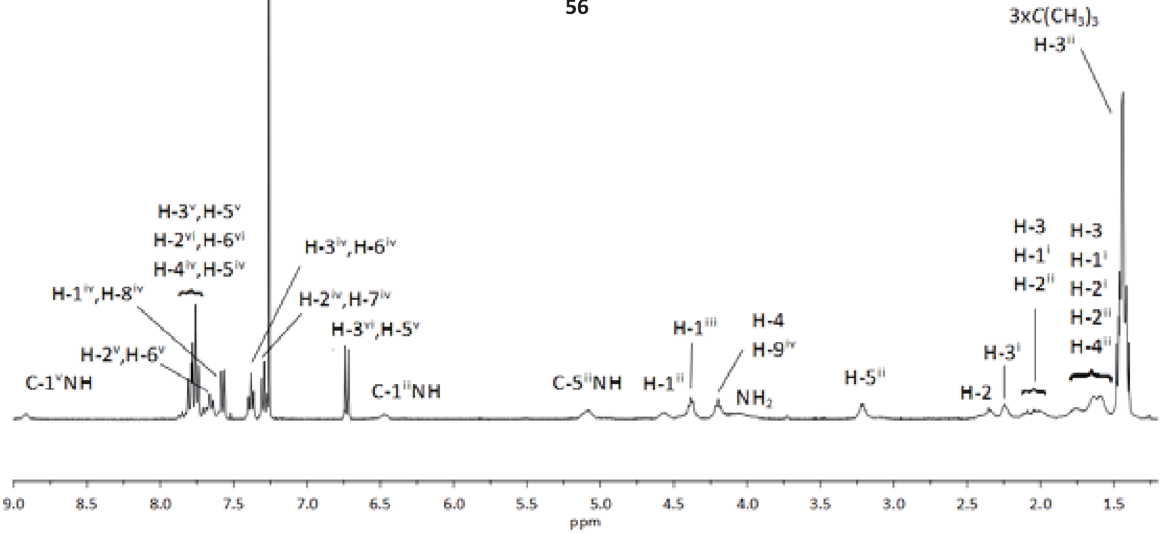

^{1}H-NMR (400 MHz, $CDCl_3$)

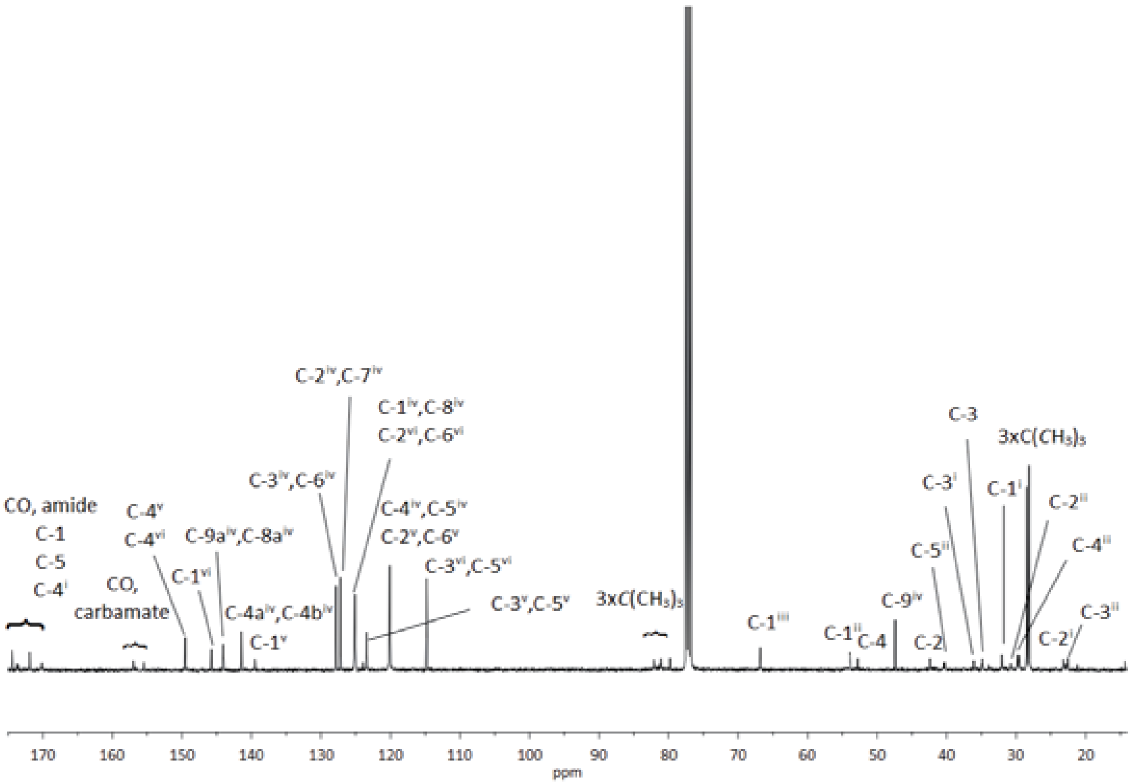

^{13}C-NMR (100.6 MHz, $CDCl_3$)

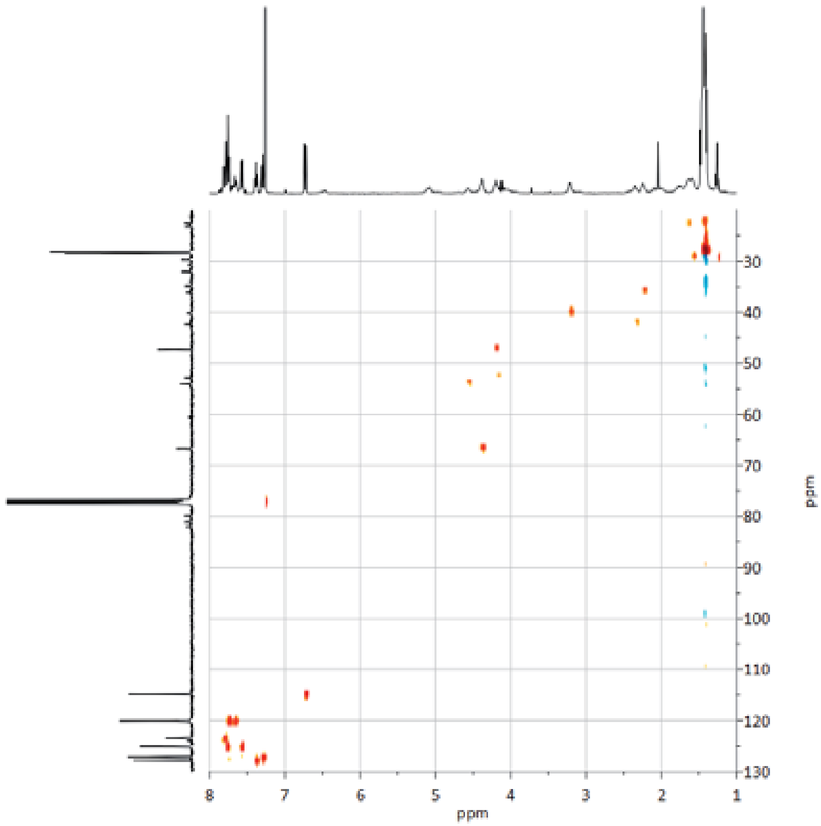

HSQC (400 MHz, $CDCl_3$. CH, CH_3: blue,CH_2: red)

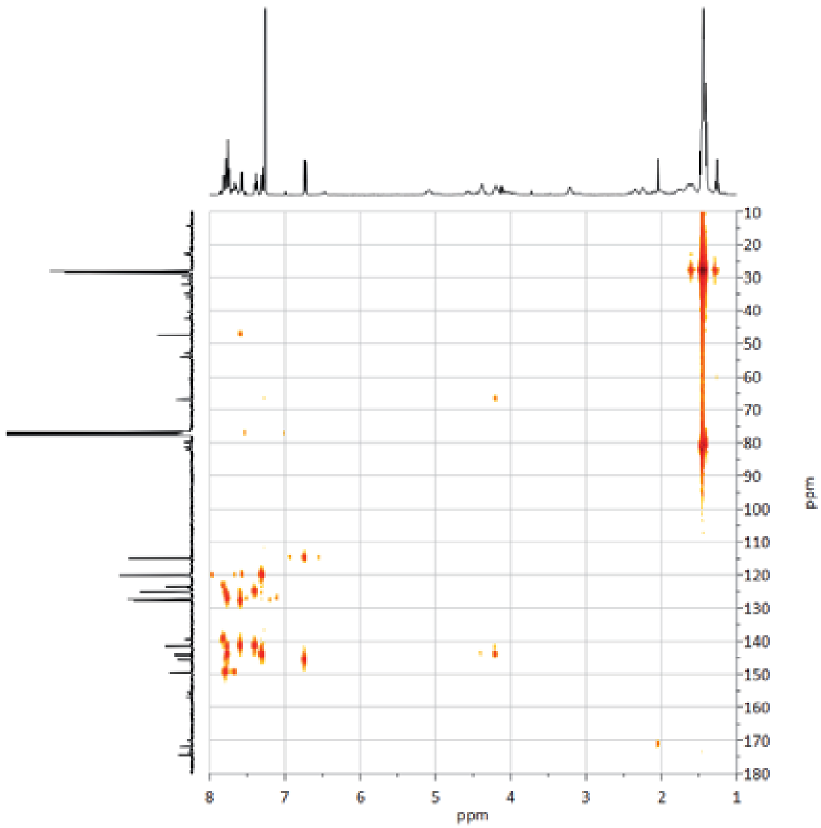

HMBC (400 MHz, $CDCl_3$)

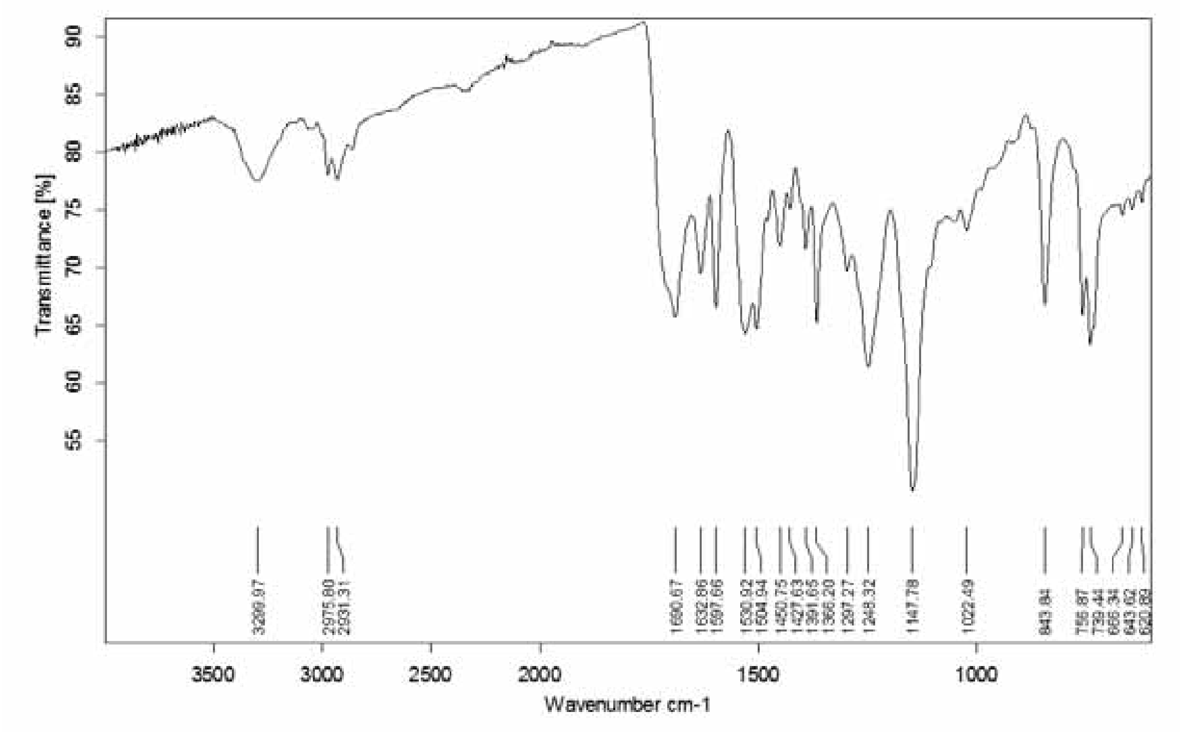

IR (ATR)

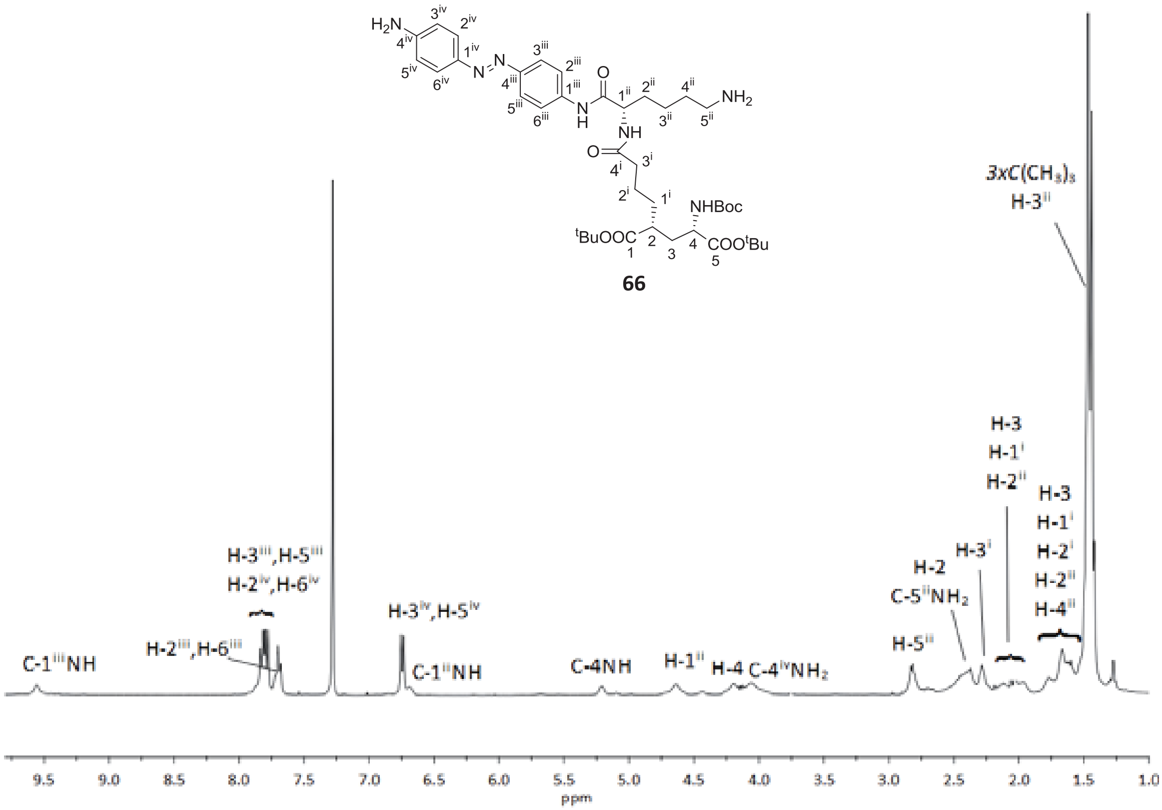

^{1}H-NMR (400 MHz, $CDCl_3$)

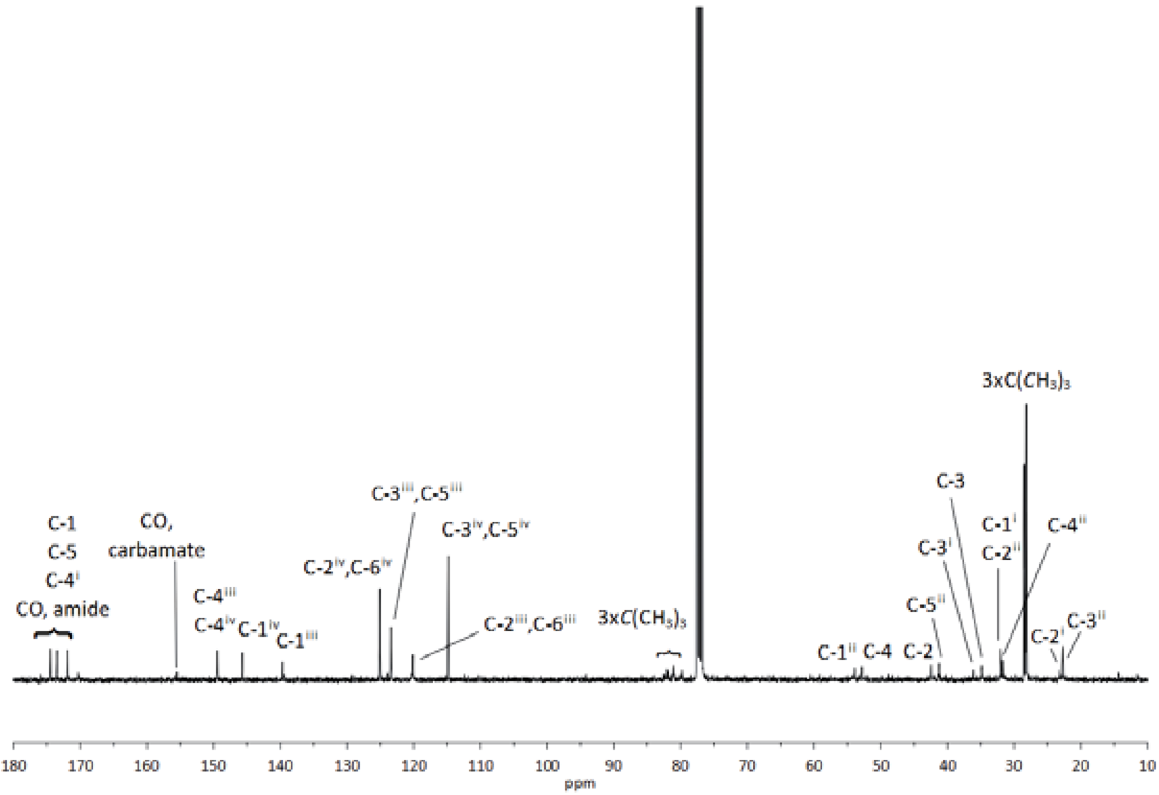

^{13}C-NMR (100.6 MHz, $CDCl_3$)

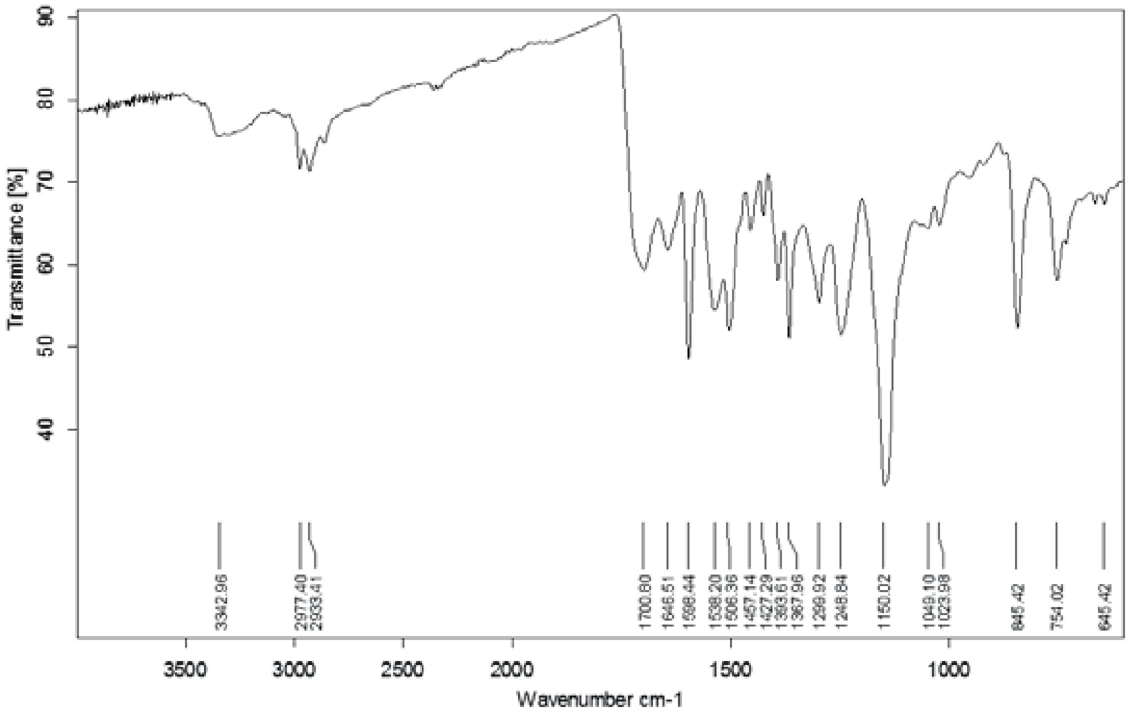

IR (ATR)

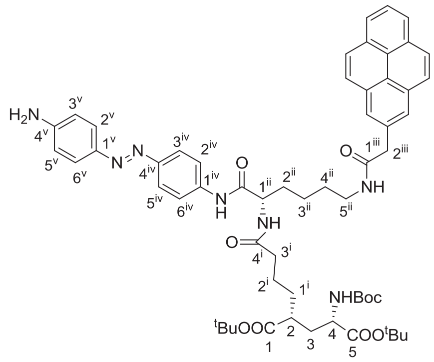

57

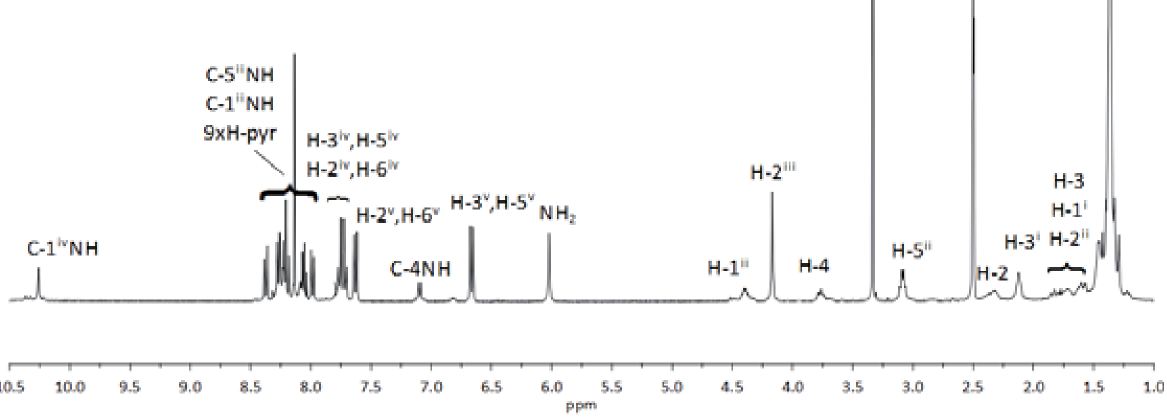

¹H-NMR (400 MHz, DMSO-d$_6$)

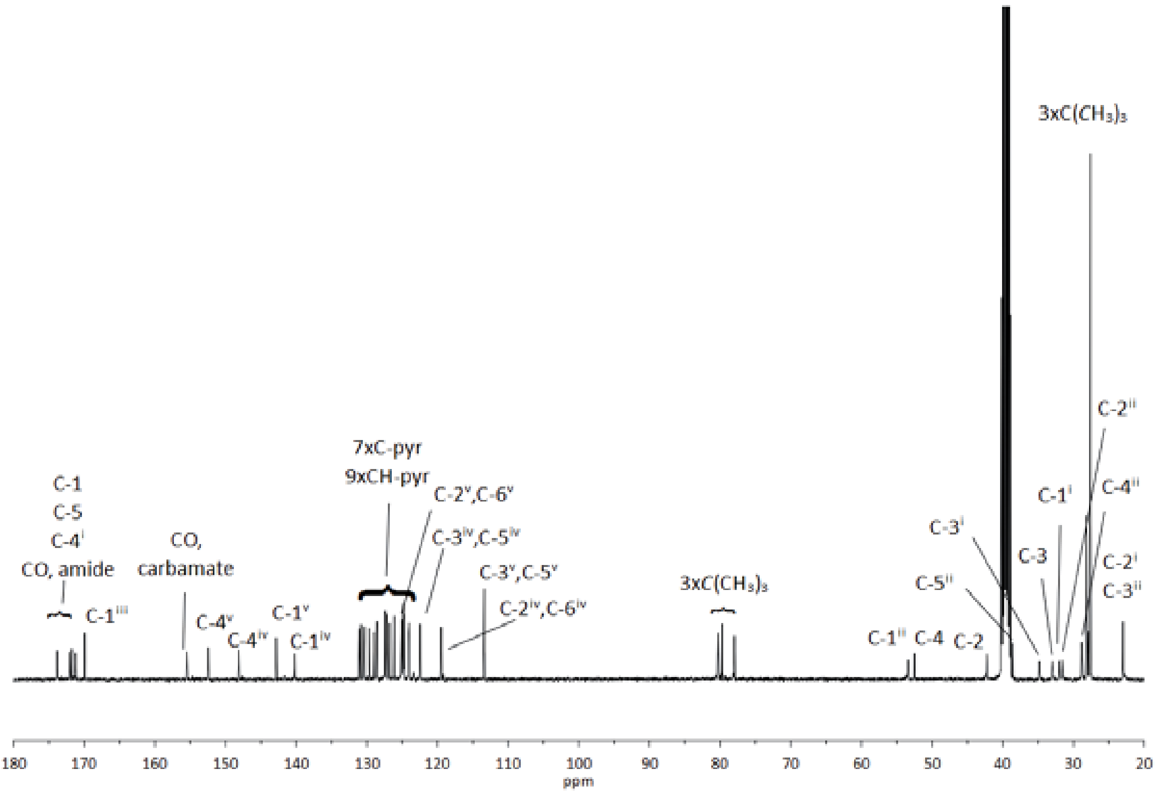

¹³C-NMR (100.6 MHz, DMSO-d$_6$)

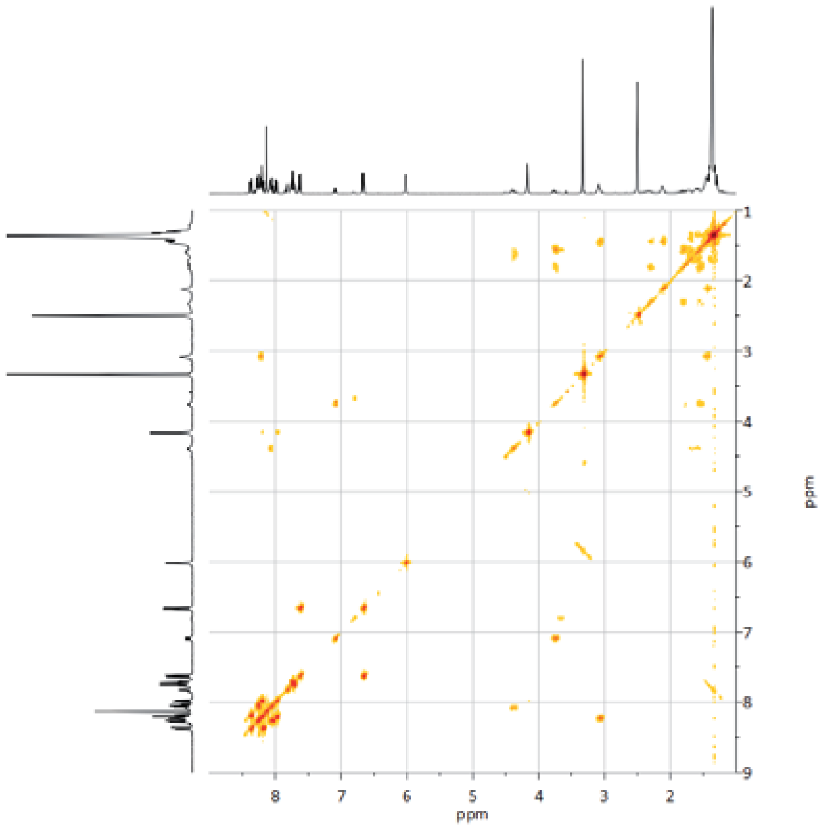

COSY (400 MHz, DMSO-d_6)

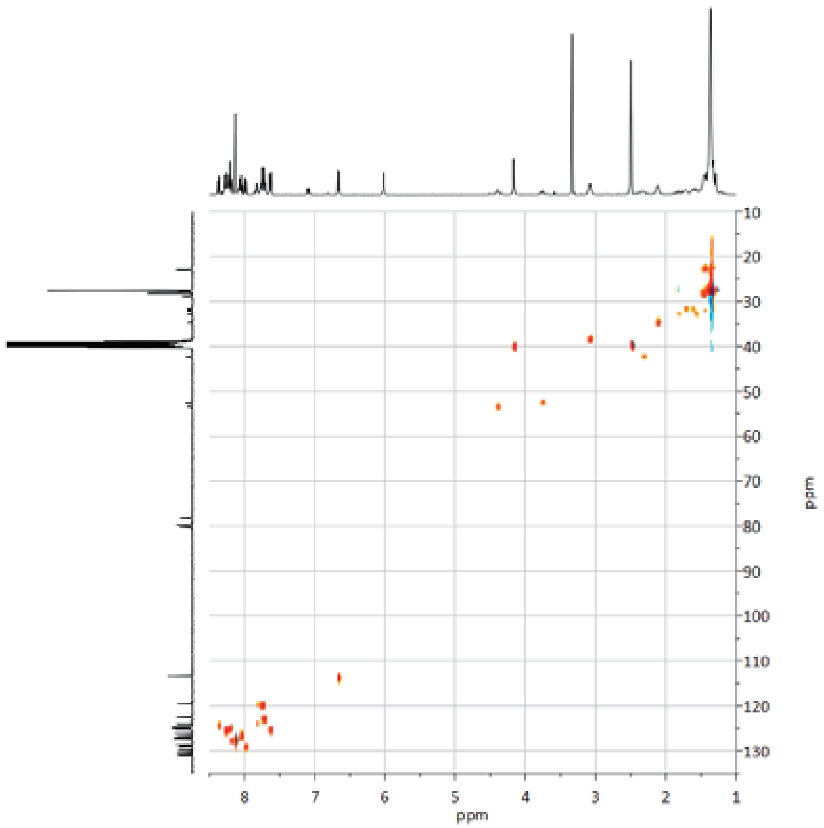

HSQC (400 MHz, DMSO-d_6)

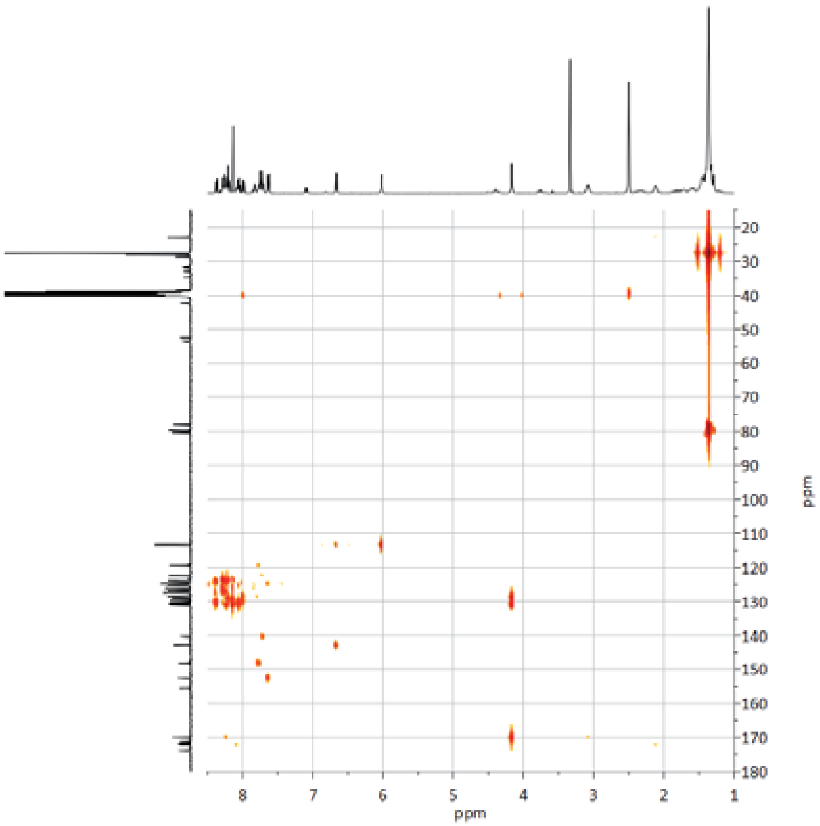

HMBC (400 MHz, DMSO-d_6)

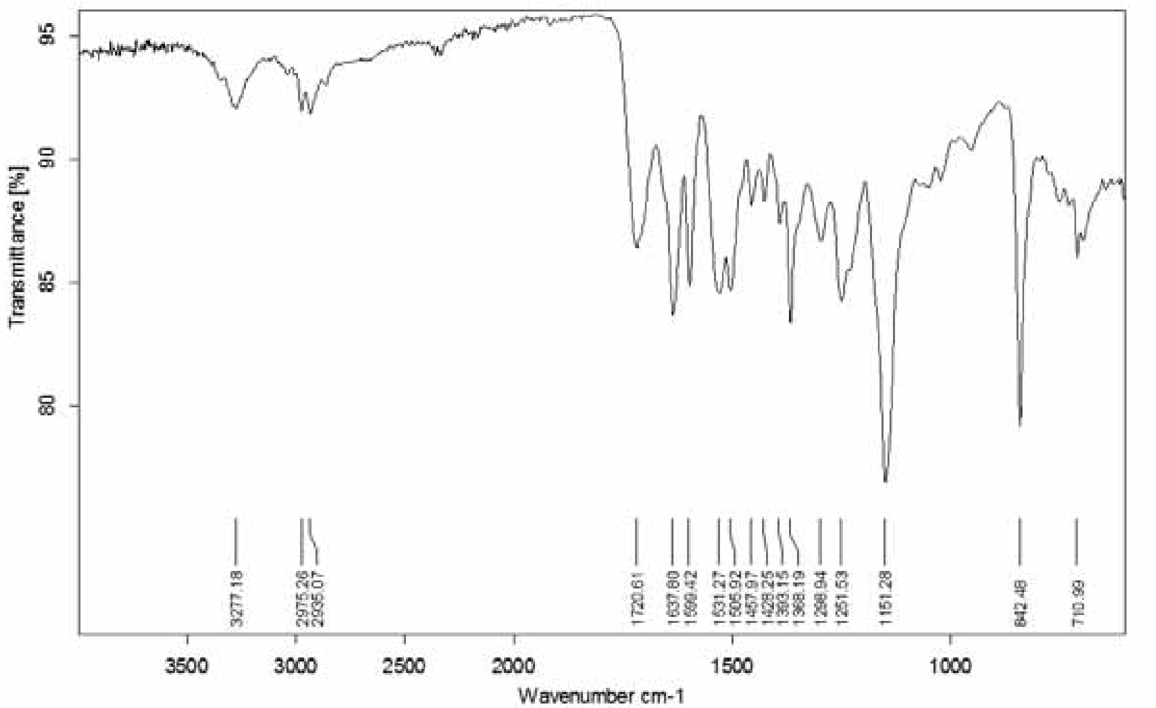

IR (ATR)

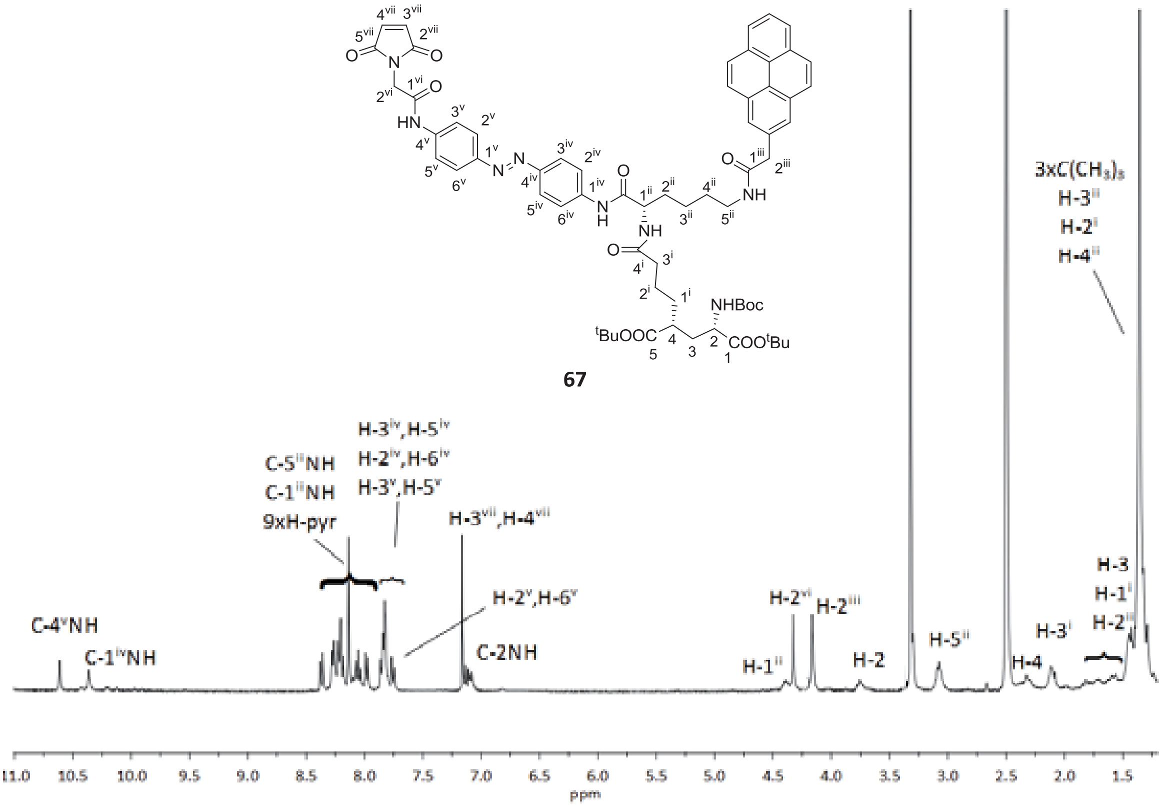

^{1}**H-NMR** (400 MHz, DMSO-d$_6$)

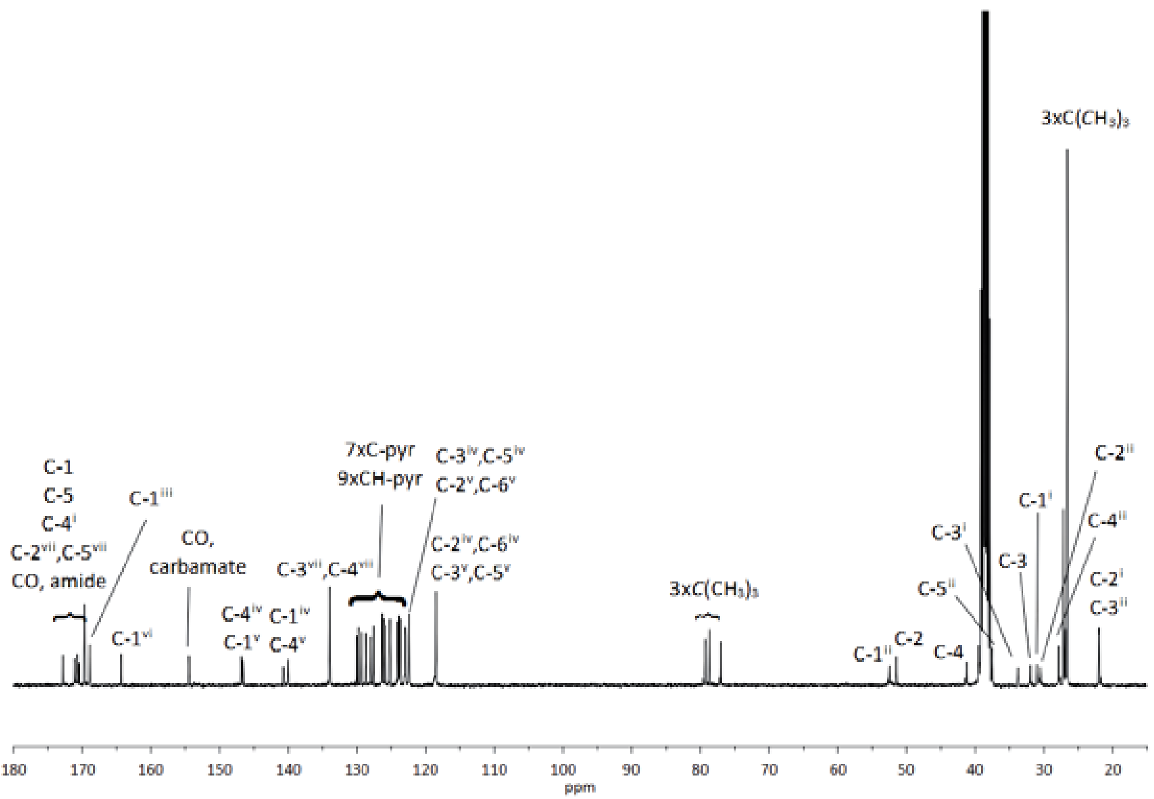

^{13}**C-NMR** (100.6 MHz, DMSO-d$_6$)

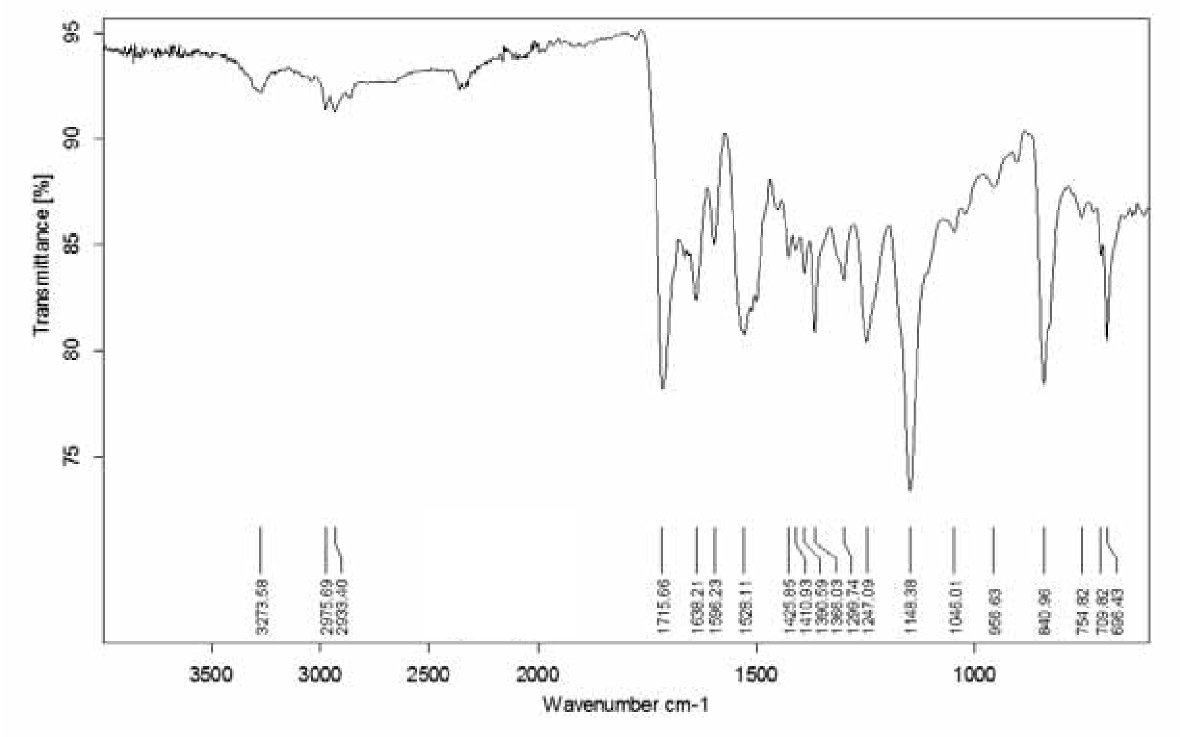

IR (ATR)

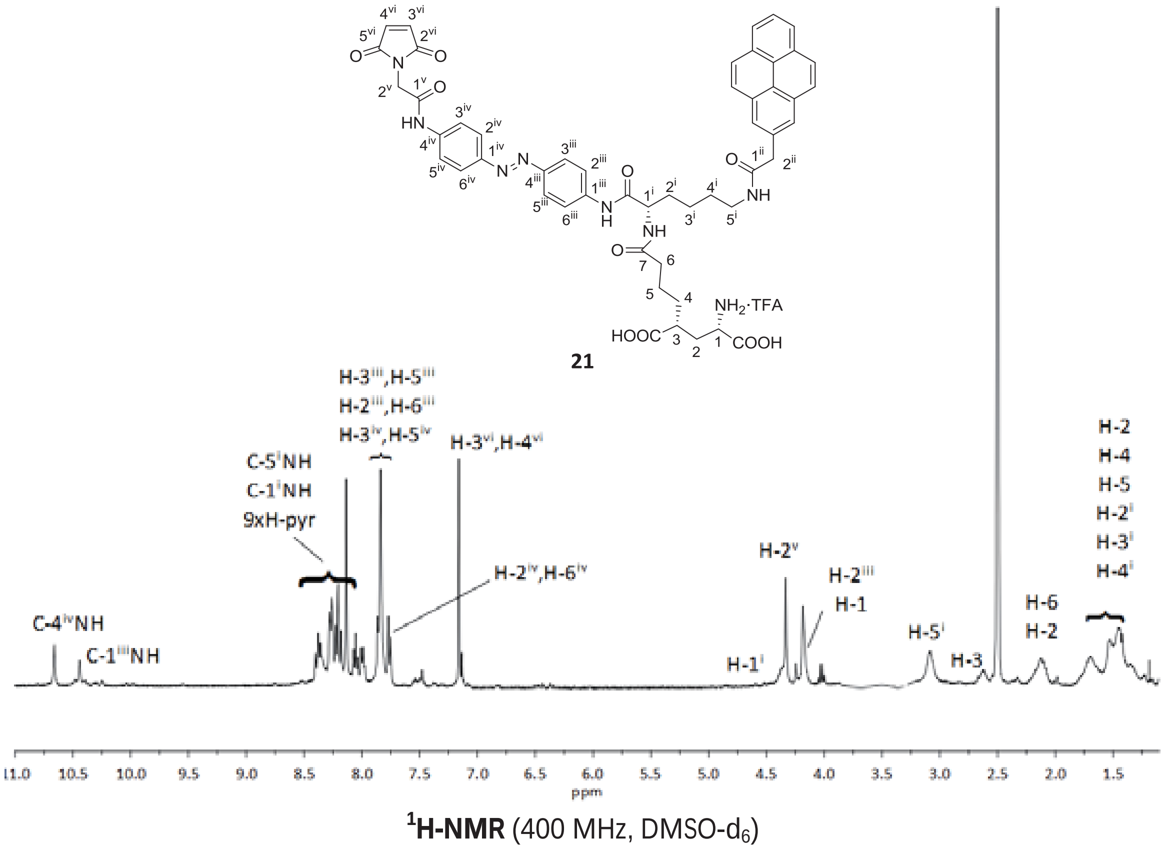

^{1}**H-NMR** (400 MHz, DMSO-d_6)

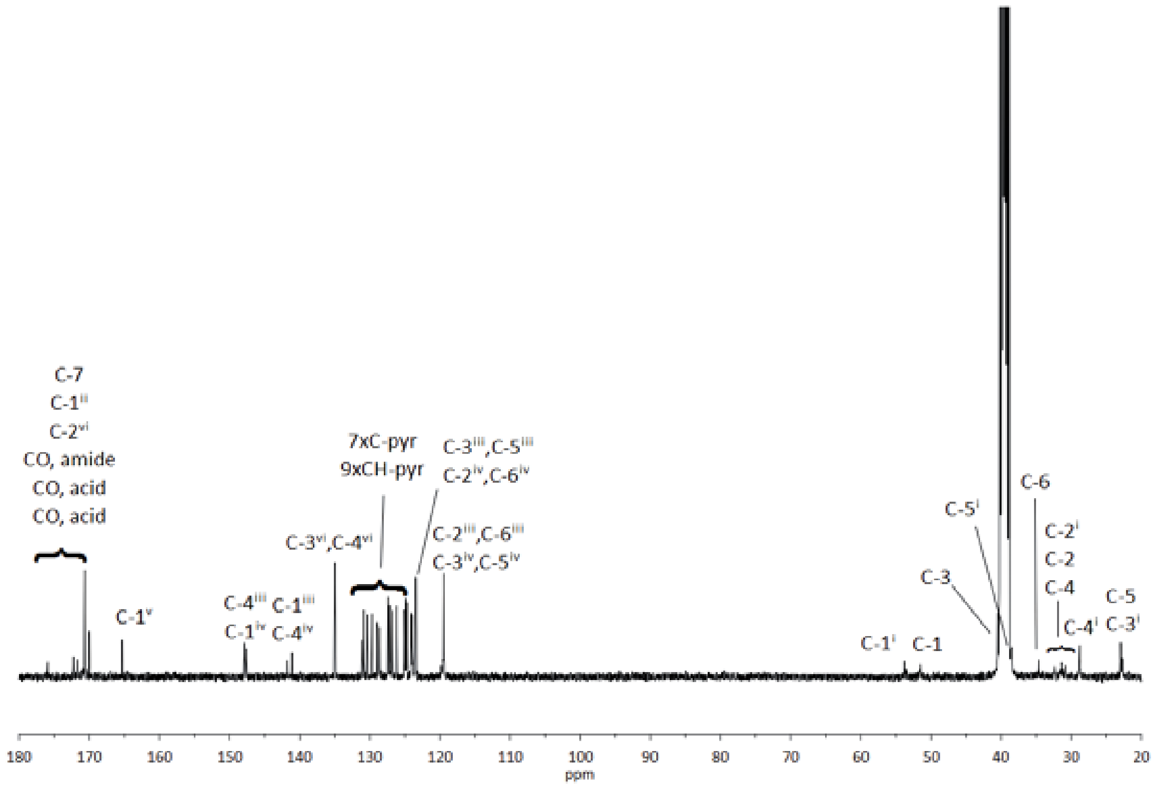

^{13}C-NMR (100.6 MHz, DMSO-d$_6$)

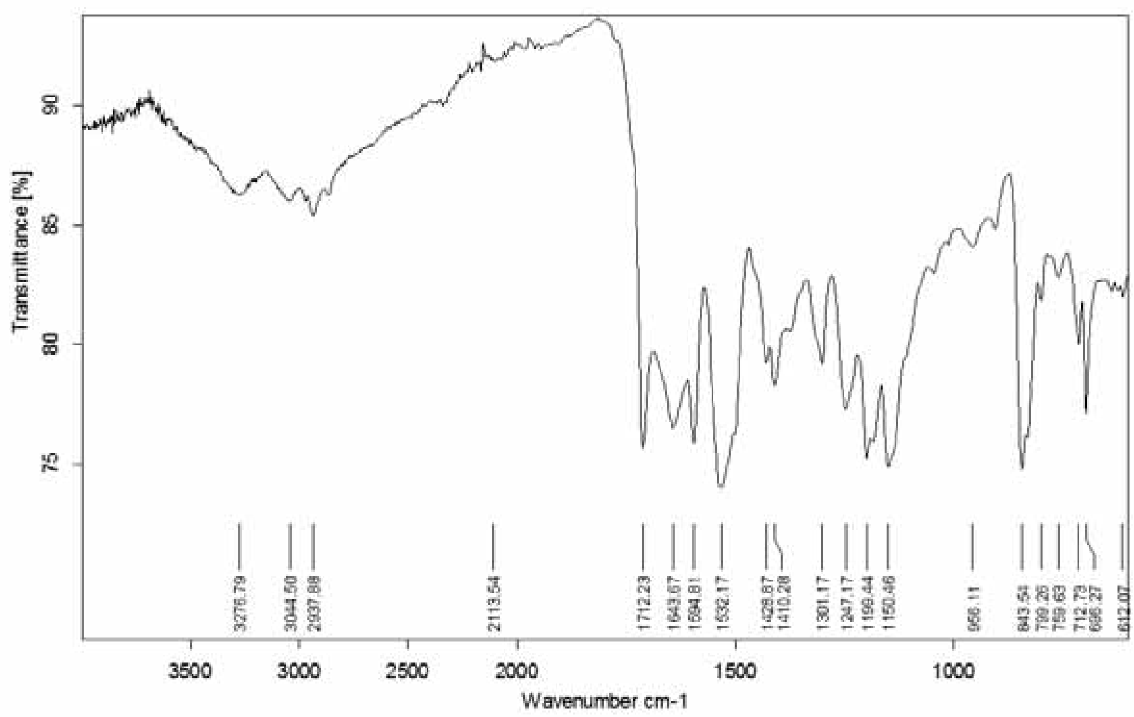

IR (ATR)

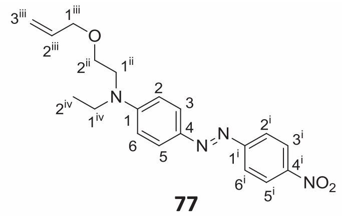

77

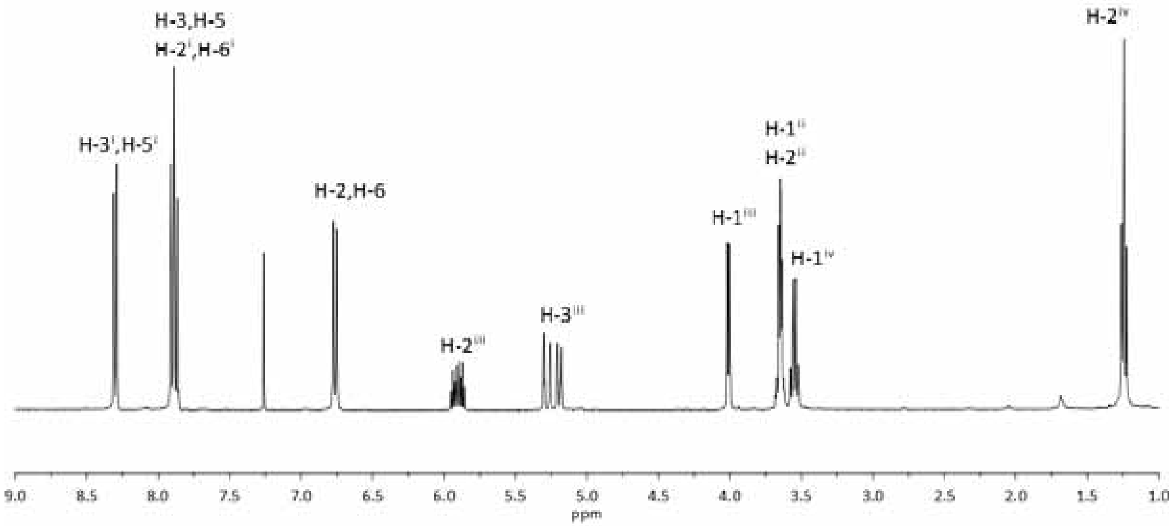

^{1}H-NMR (400 MHz, $CDCl_3$)

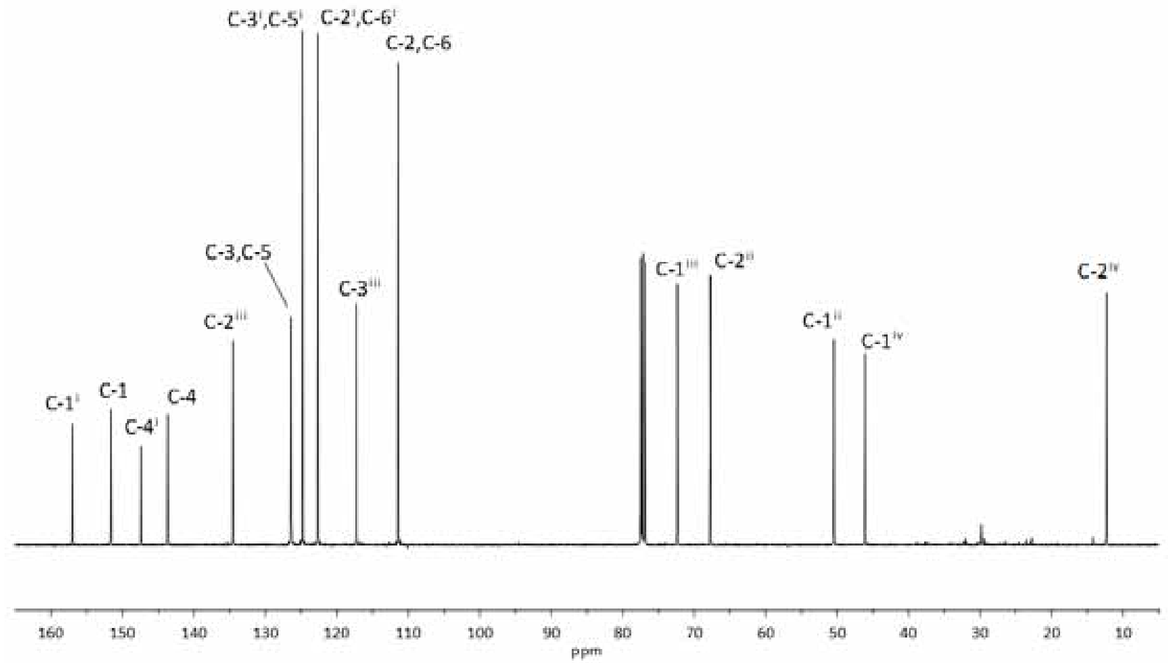

^{13}C-NMR (100.6 MHz, $CDCl_3$)

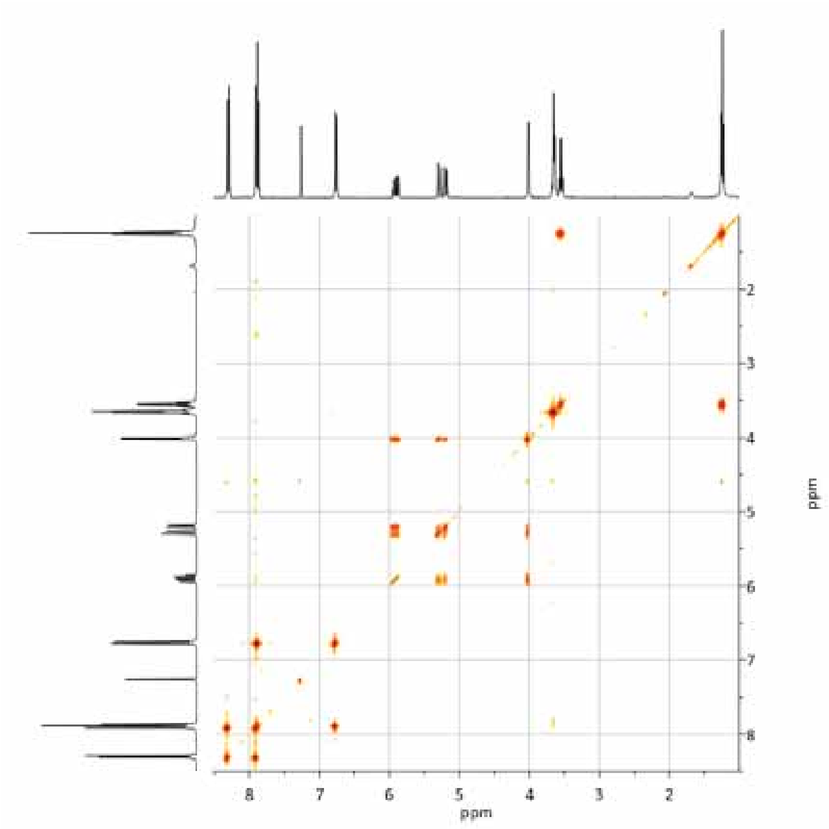

COSY (400 MHz, $CDCl_3$)

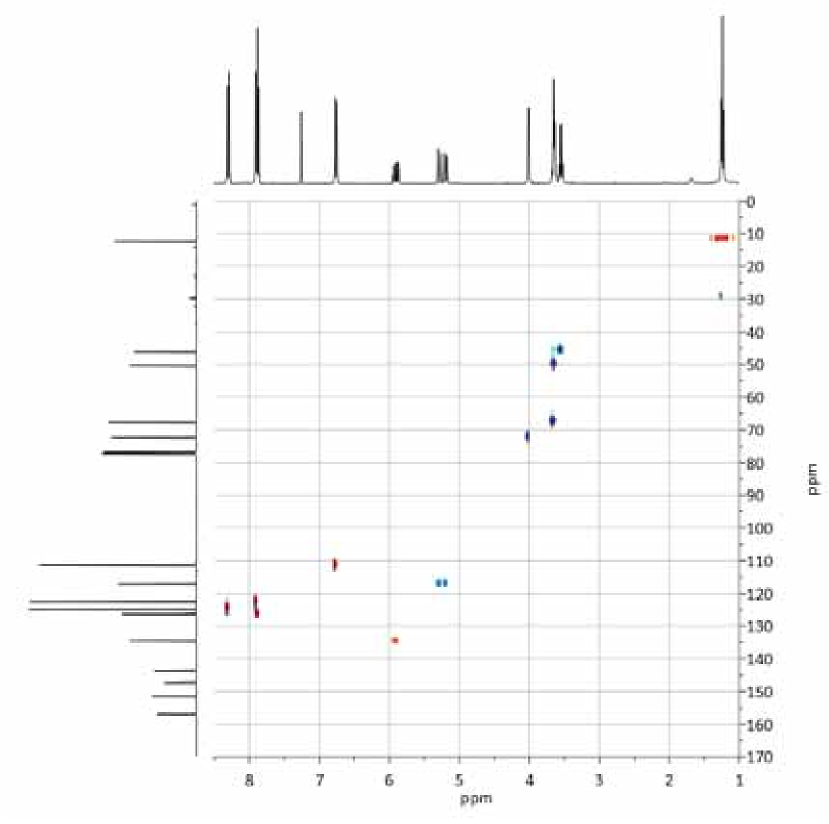

HSQC (400 MHz, $CDCl_{3.}$ CH, CH_3: blue,CH_2: red)

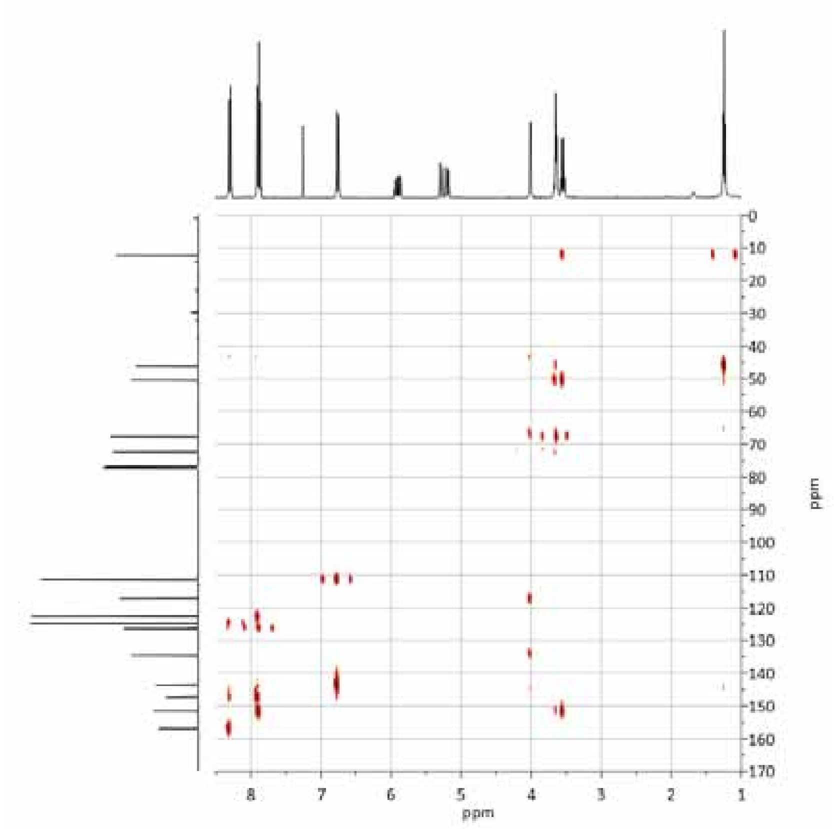

HMBC (400 MHz, $CDCl_3$)

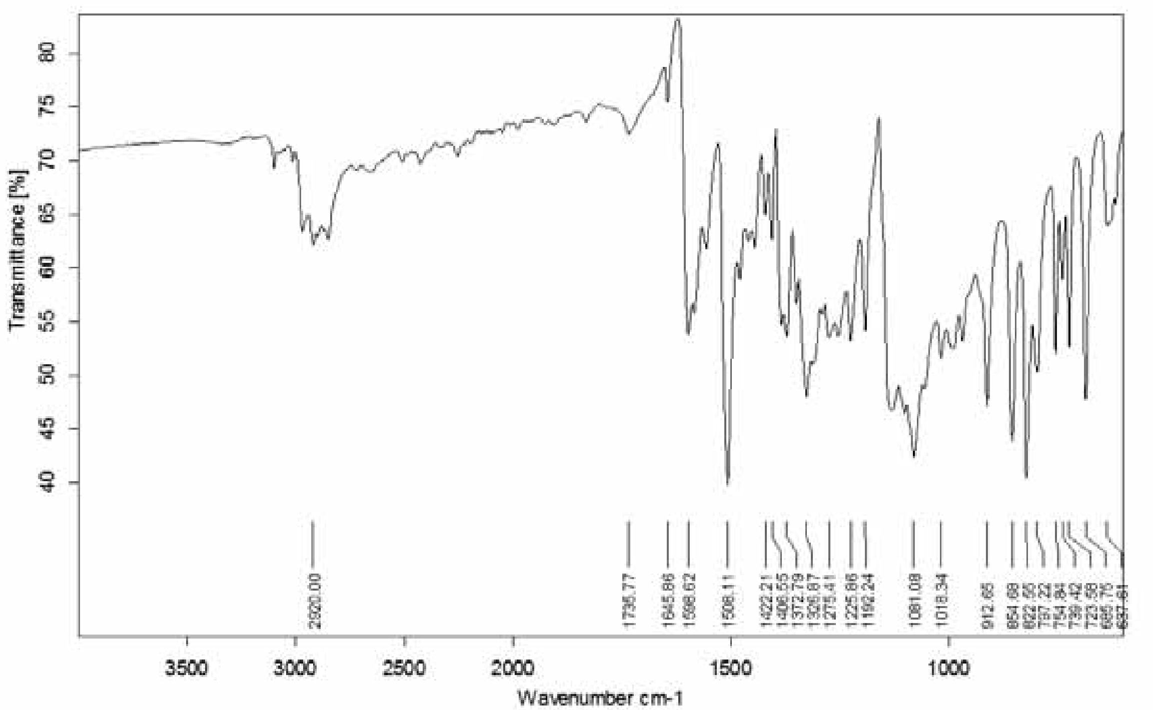

IR (ATR)

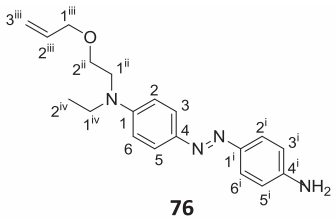

76

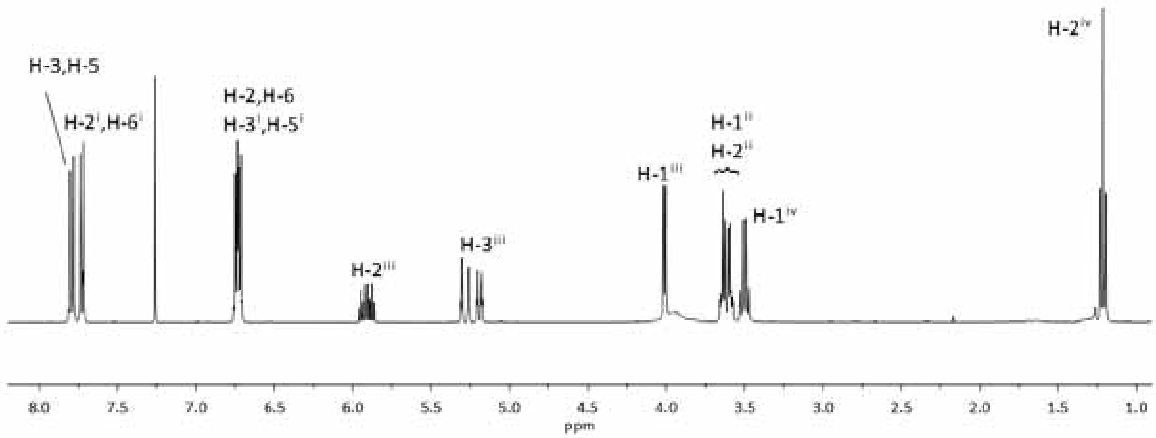

^{1}H-NMR (400 MHz, $CDCl_3$)

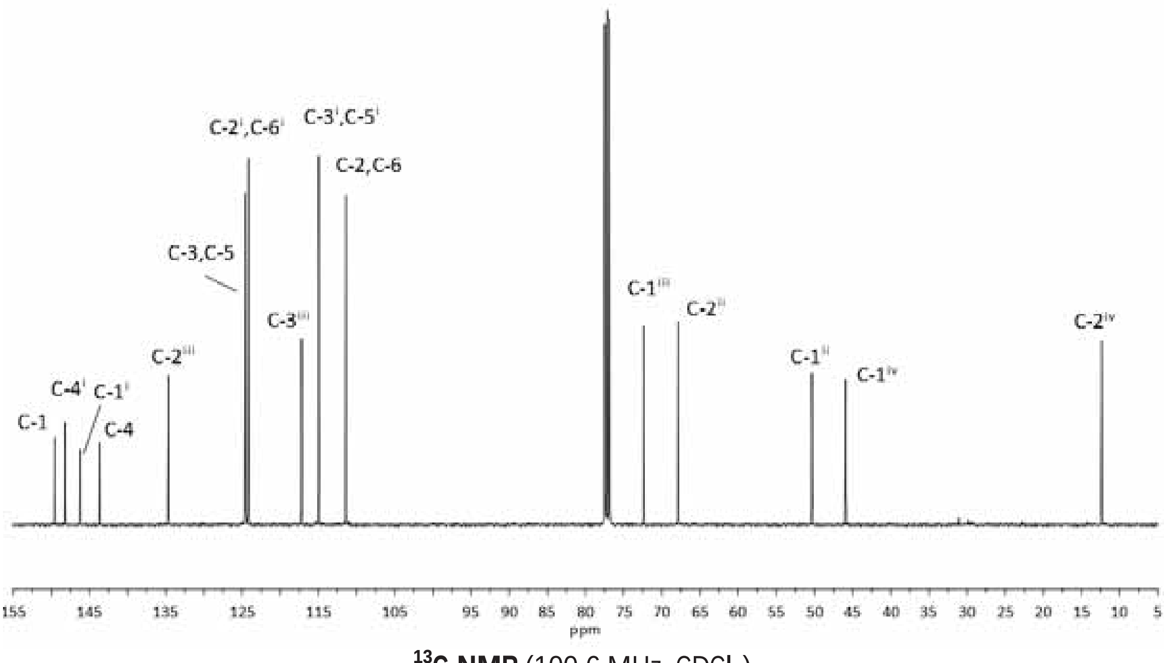

^{13}C-NMR (100.6 MHz, $CDCl_3$)

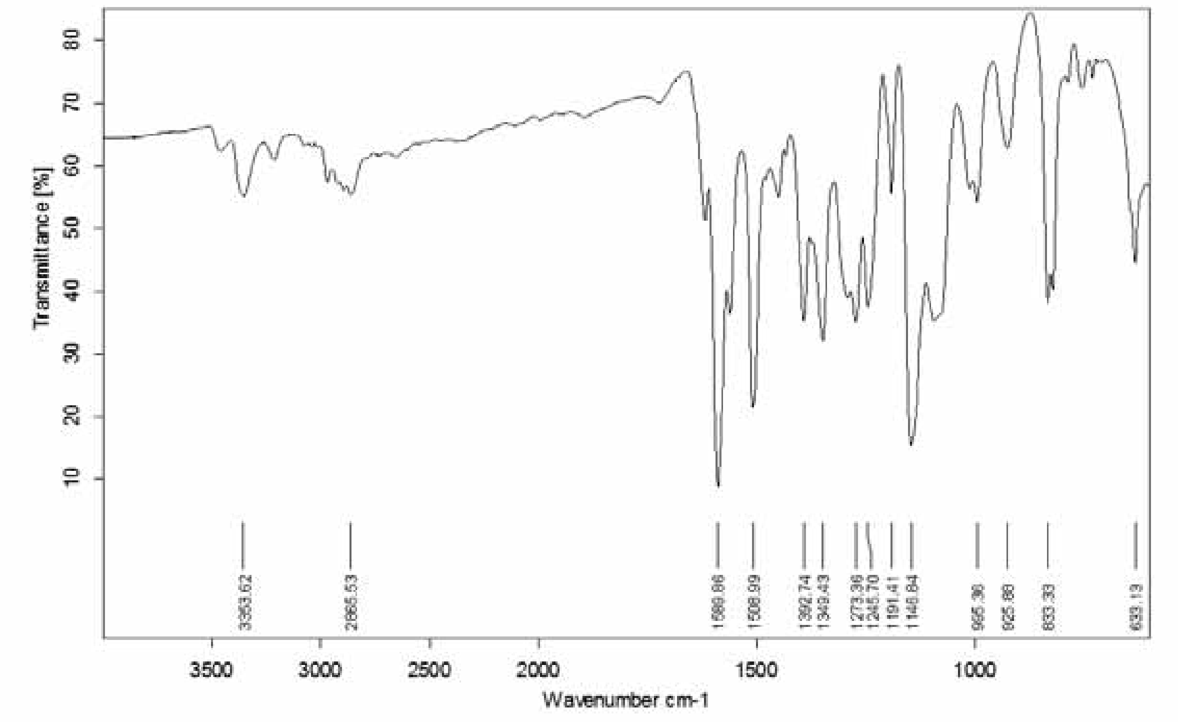

IR (ATR)

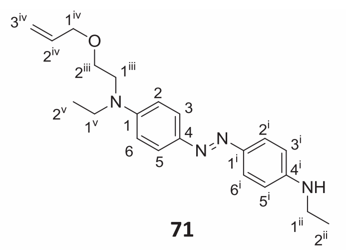

71

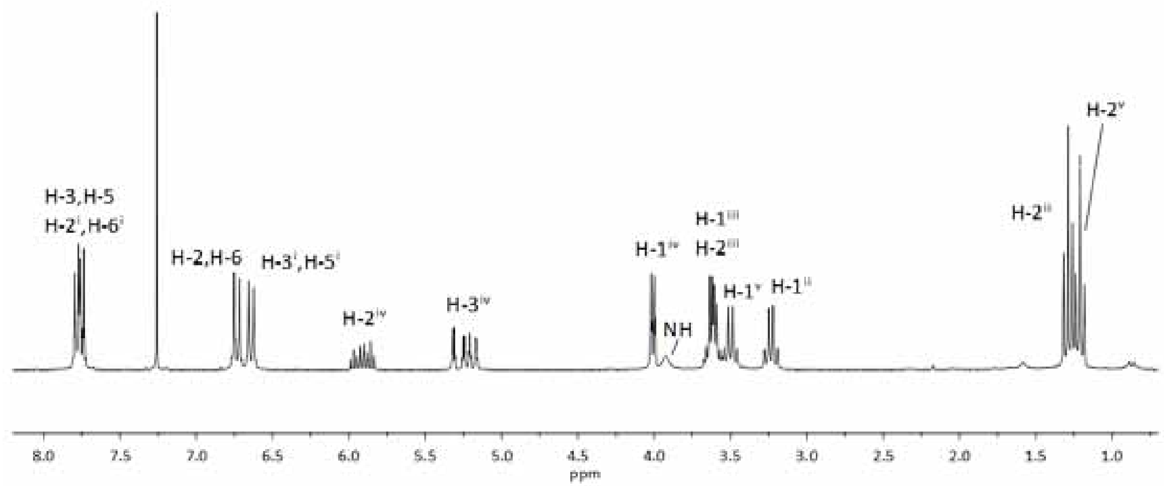

^{1}H-NMR (250 MHz, $CDCl_3$)

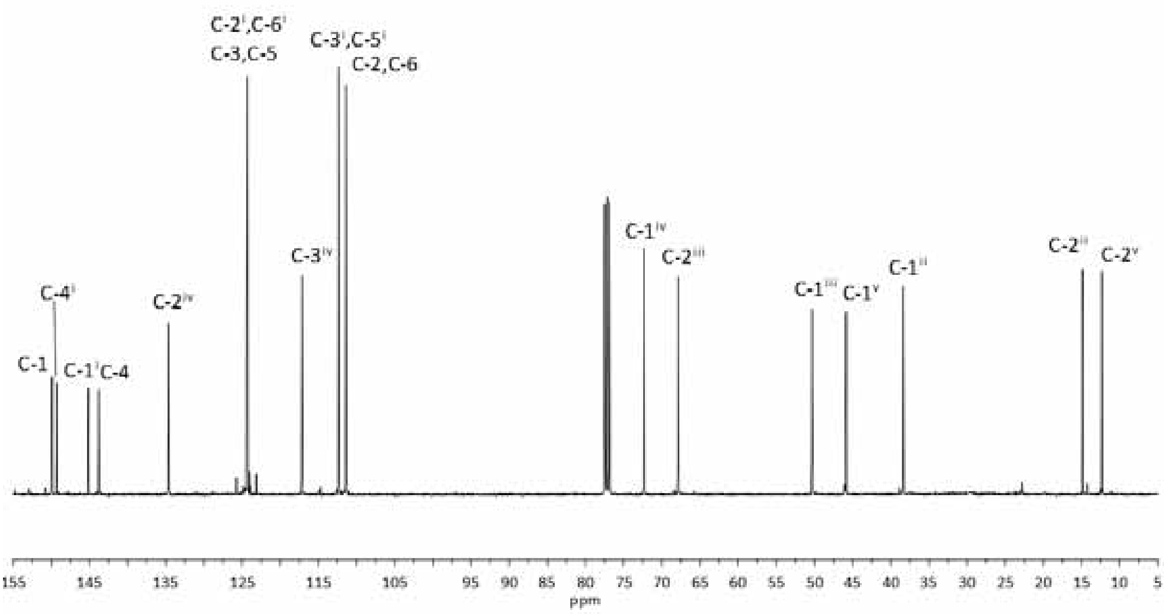

^{13}**C-NMR** (100.6 MHz, $CDCl_3$)

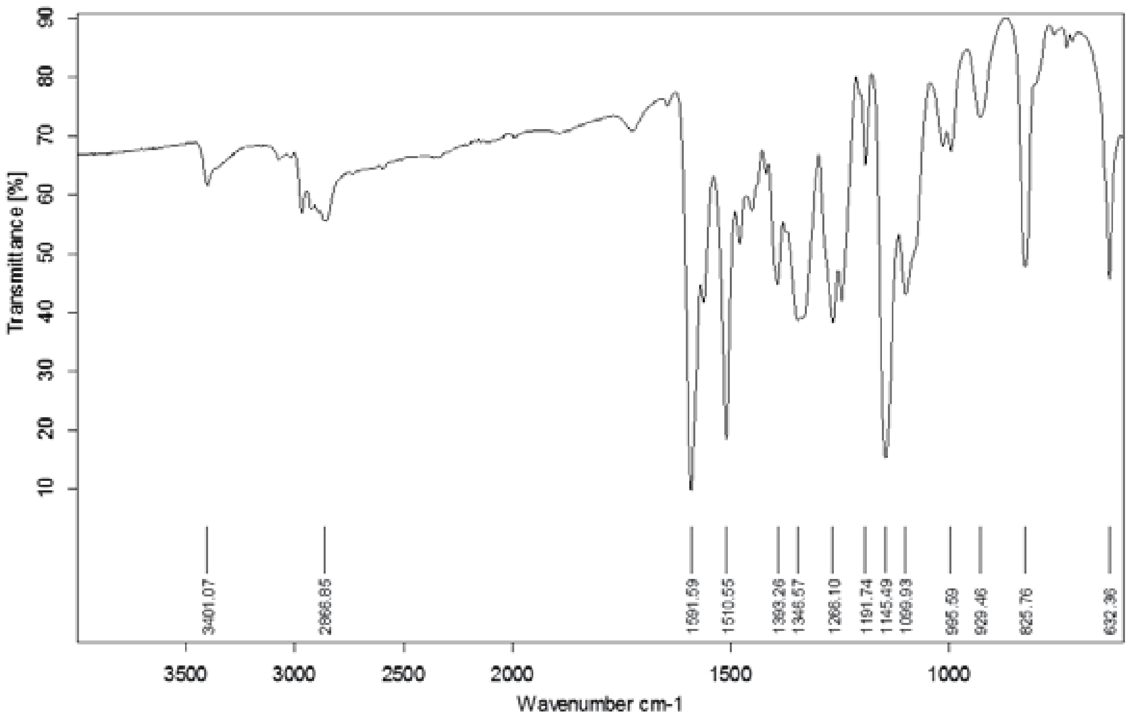

IR (ATR)

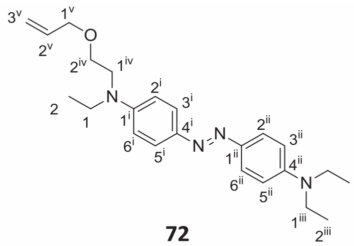

72

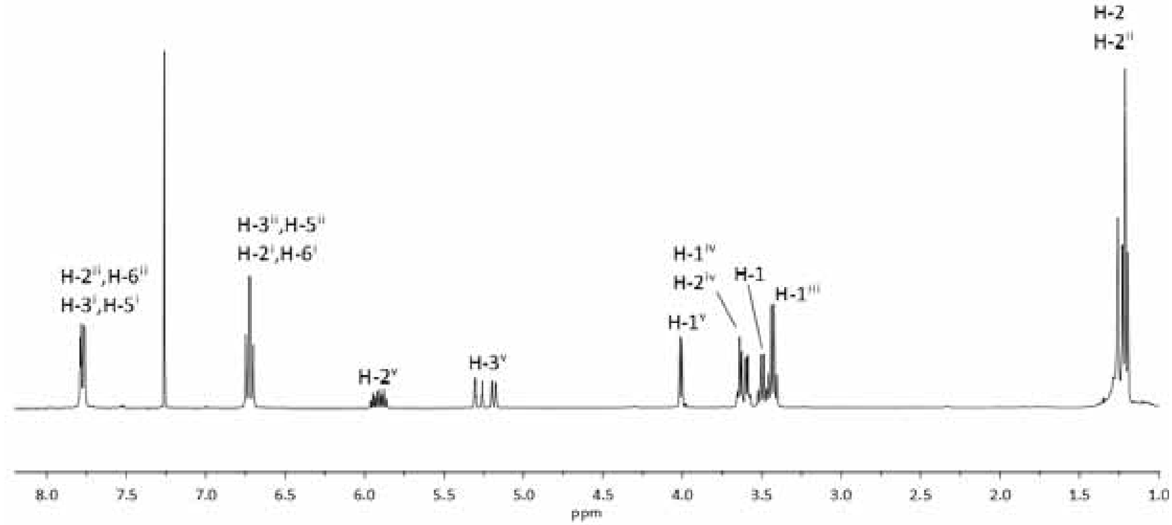

^{1}H-NMR (400 MHz, $CDCl_3$)

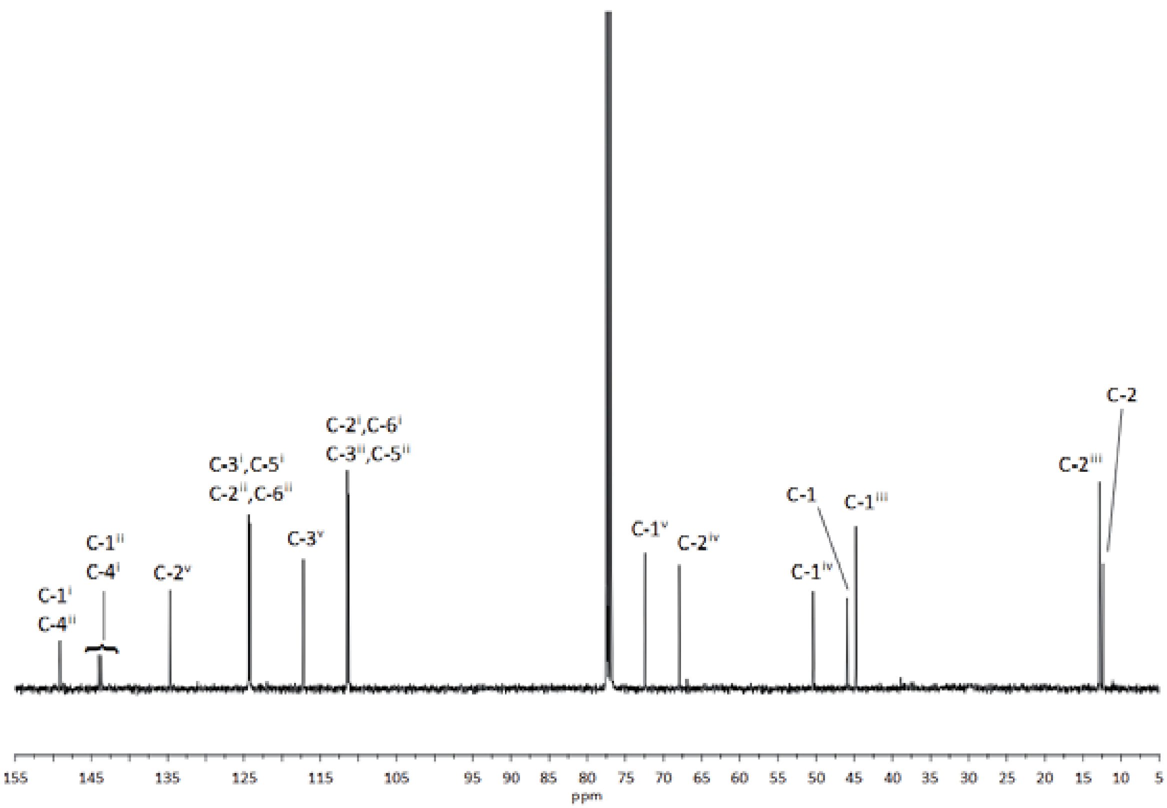

^{13}C-NMR (100.6 MHz, $CDCl_3$)

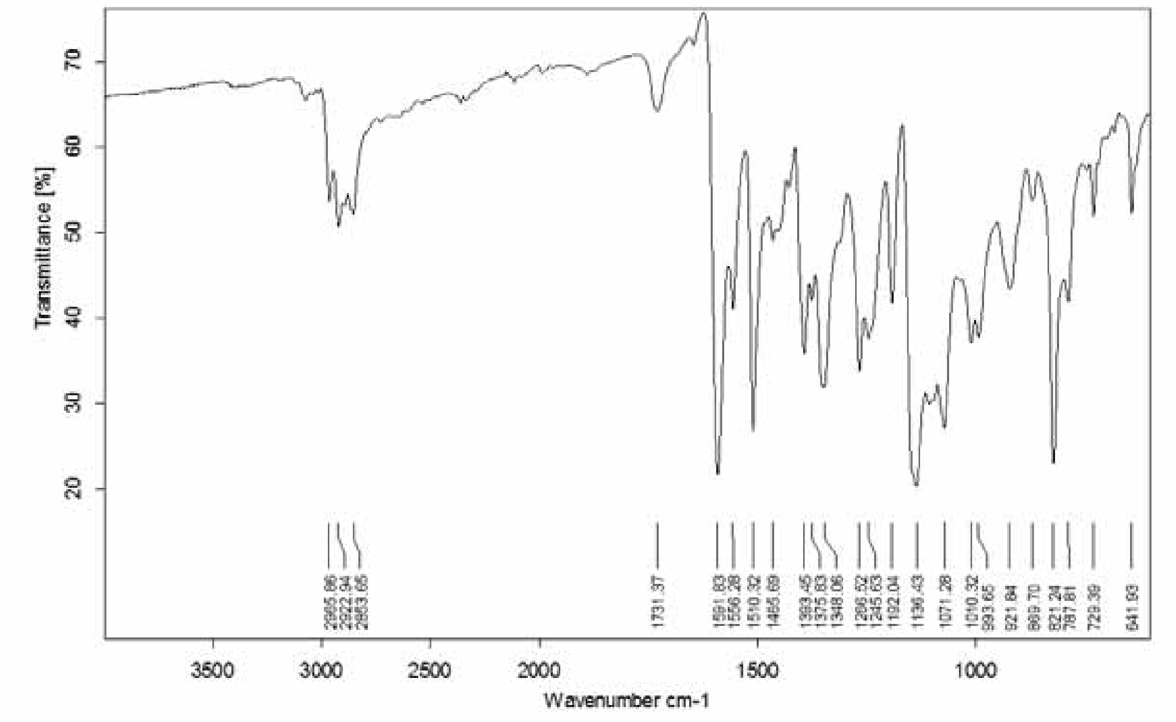

IR (ATR)

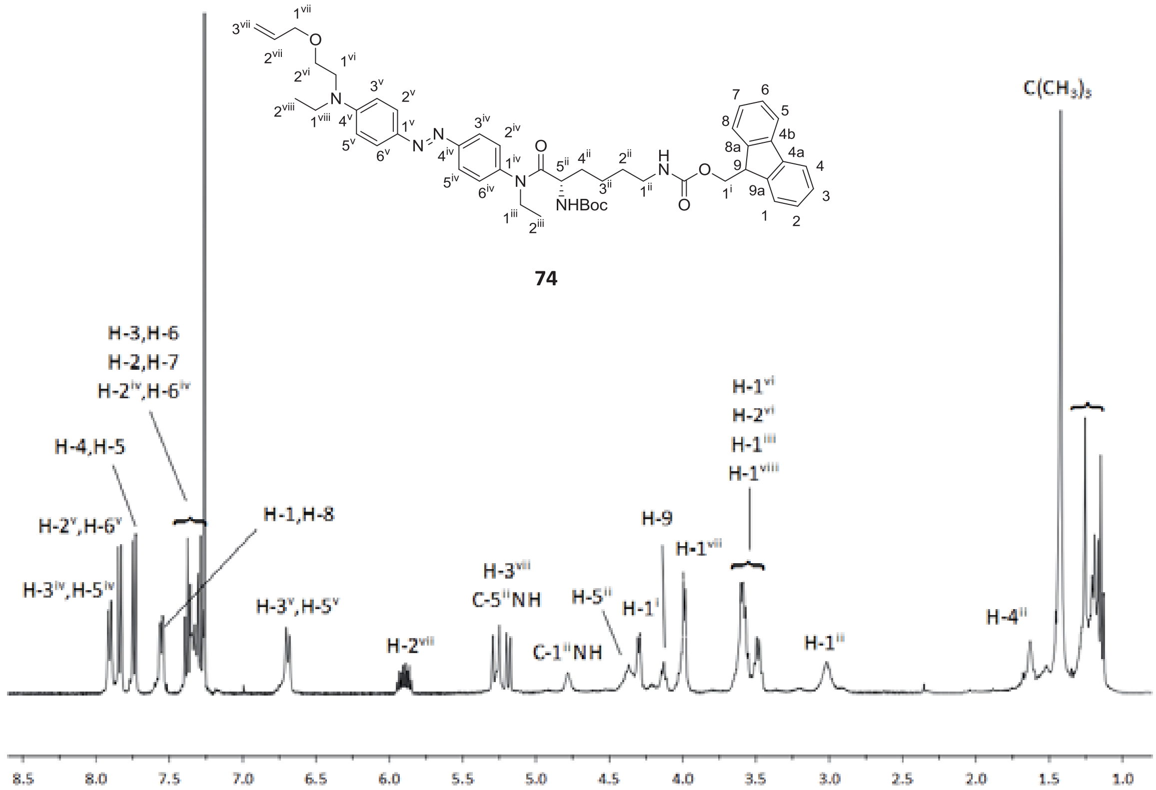

^{1}H-NMR (400 MHz, $CDCl_3$)

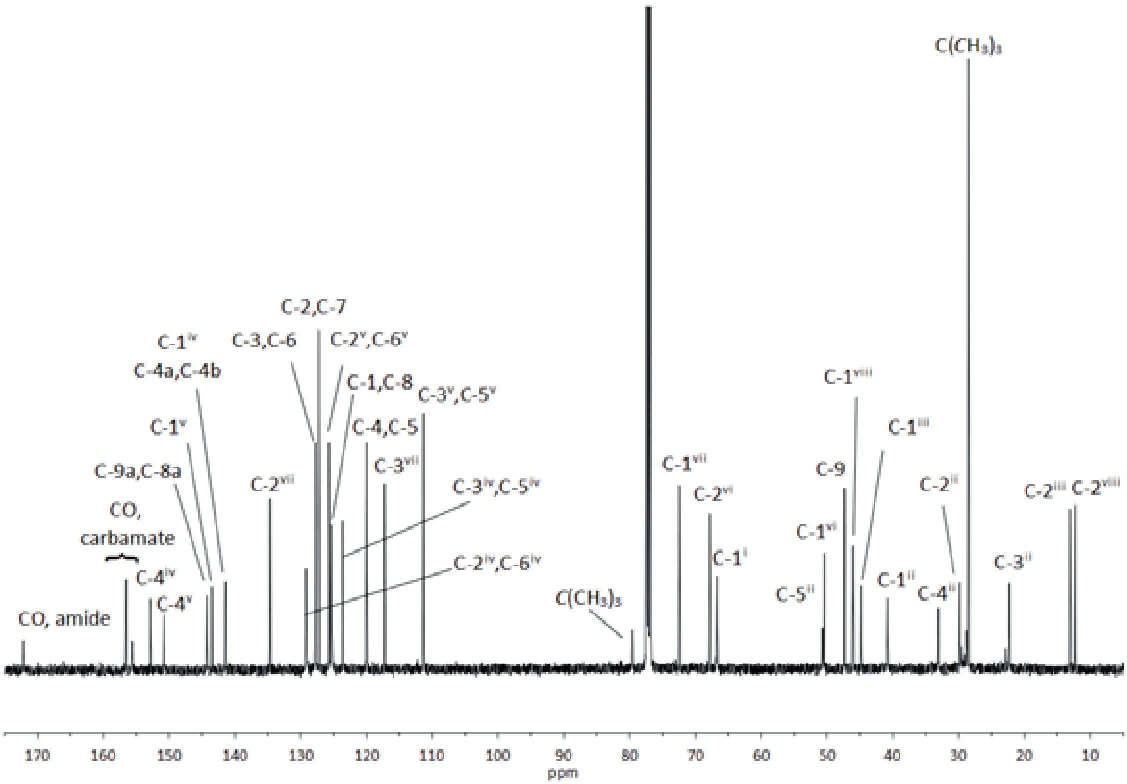

^{13}**C-NMR** (100.6 MHz, $CDCl_3$)

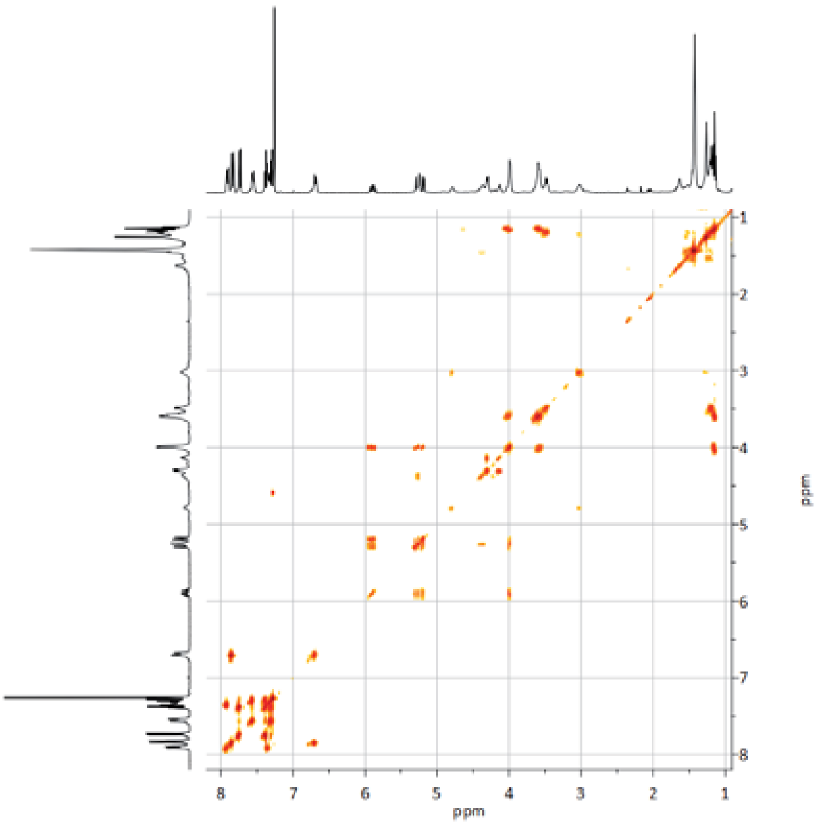

COSY (400 MHz, $CDCl_3$)

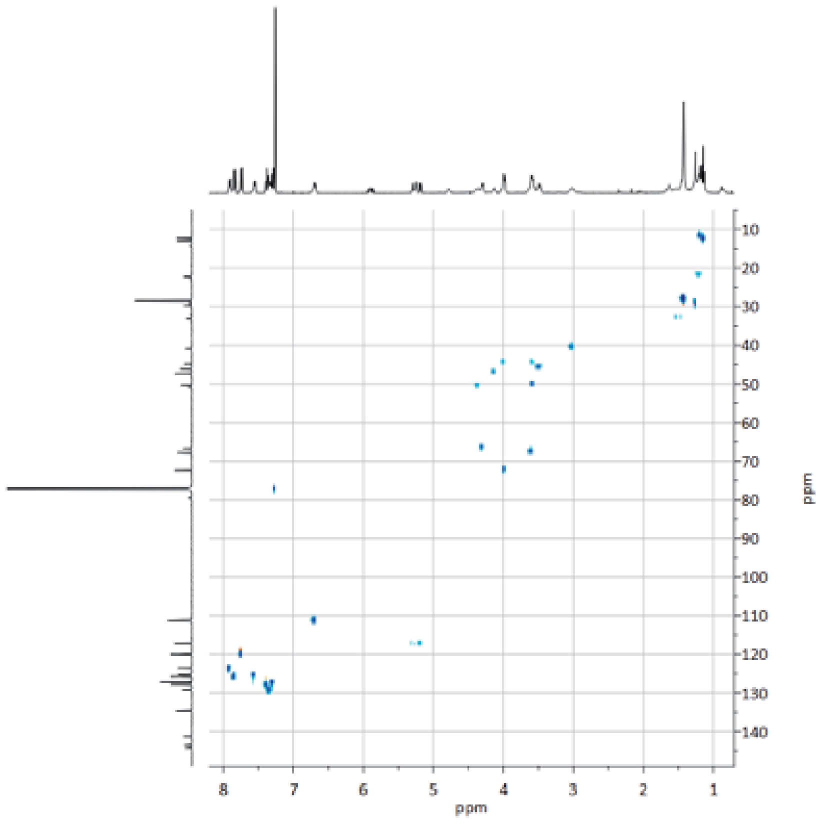

HSQC (400 MHz, $CDCl_3$)

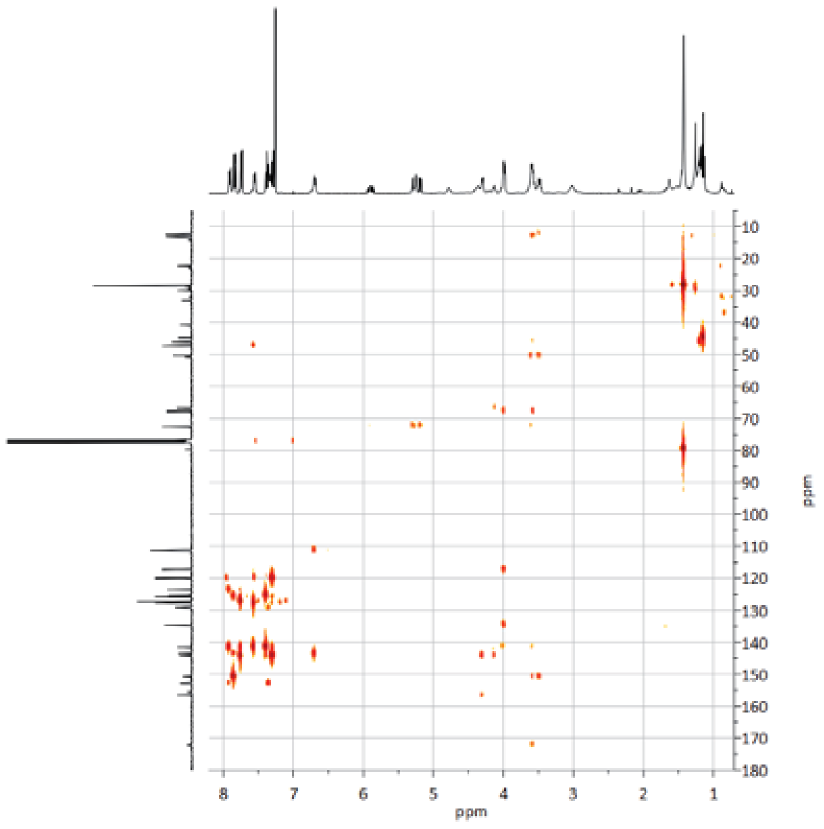

HMBC (400 MHz, $CDCl_3$)

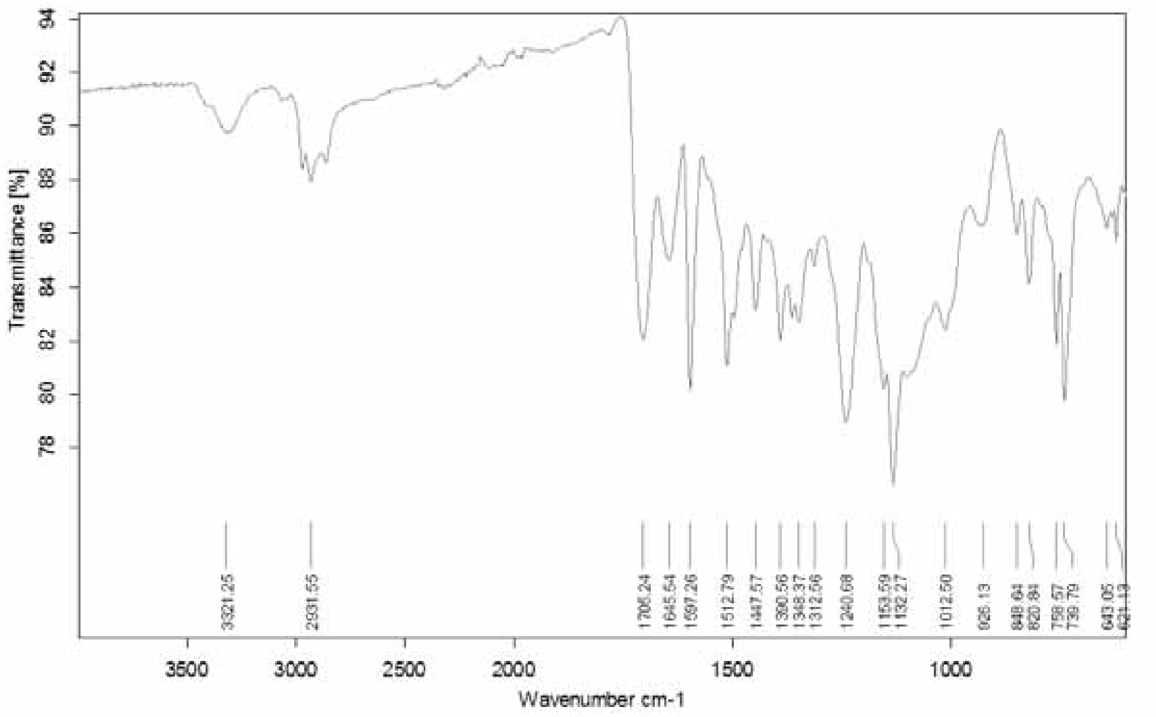

IR (ATR)

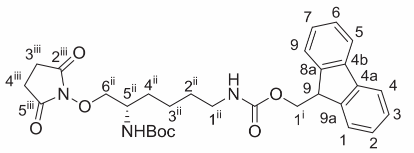

78

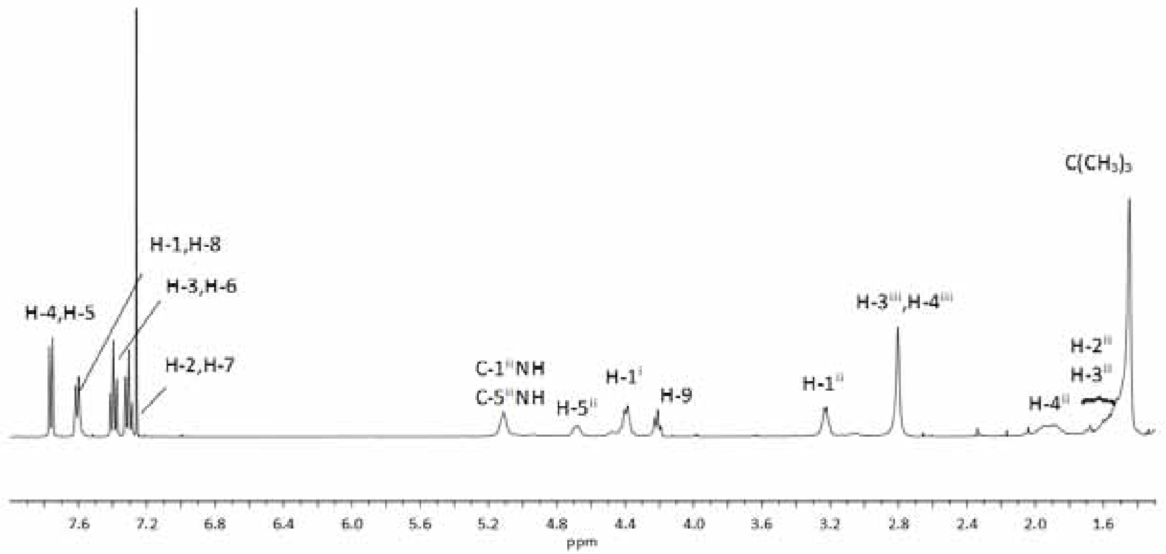

^{1}H-NMR (400 MHz, $CDCl_3$)

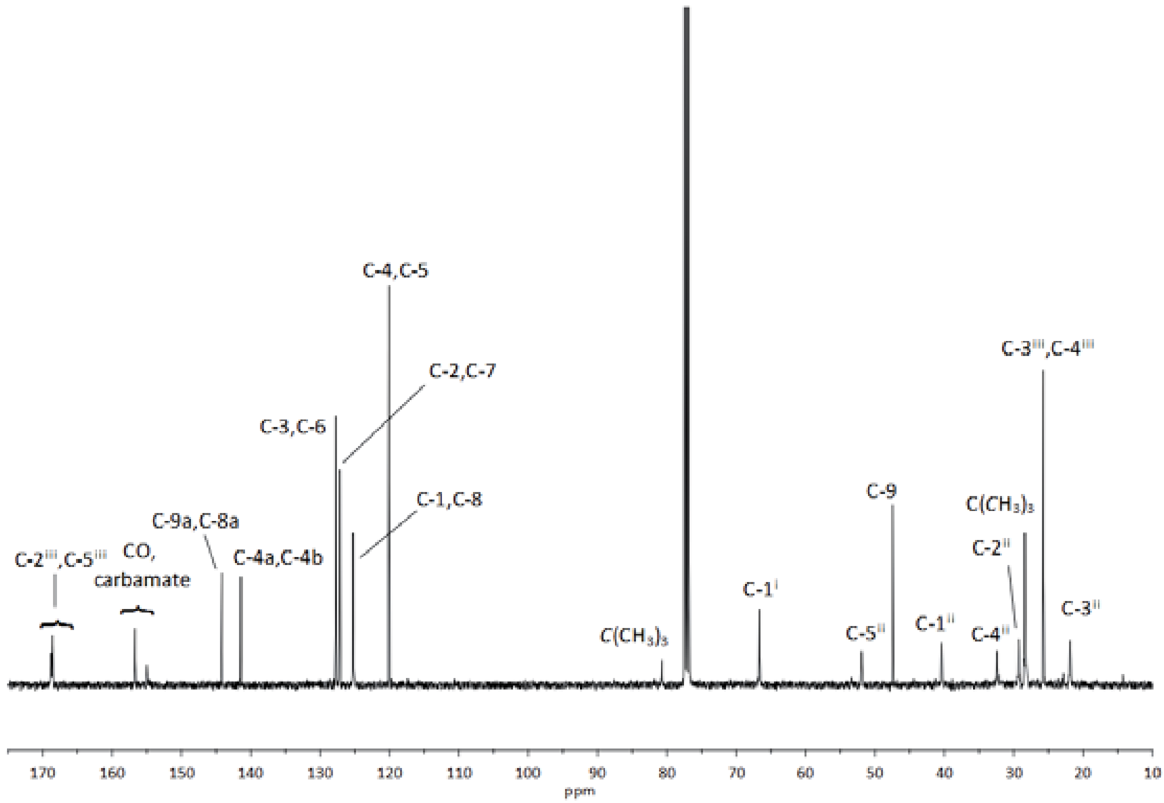

^{13}C-NMR (100.6 MHz, $CDCl_3$)

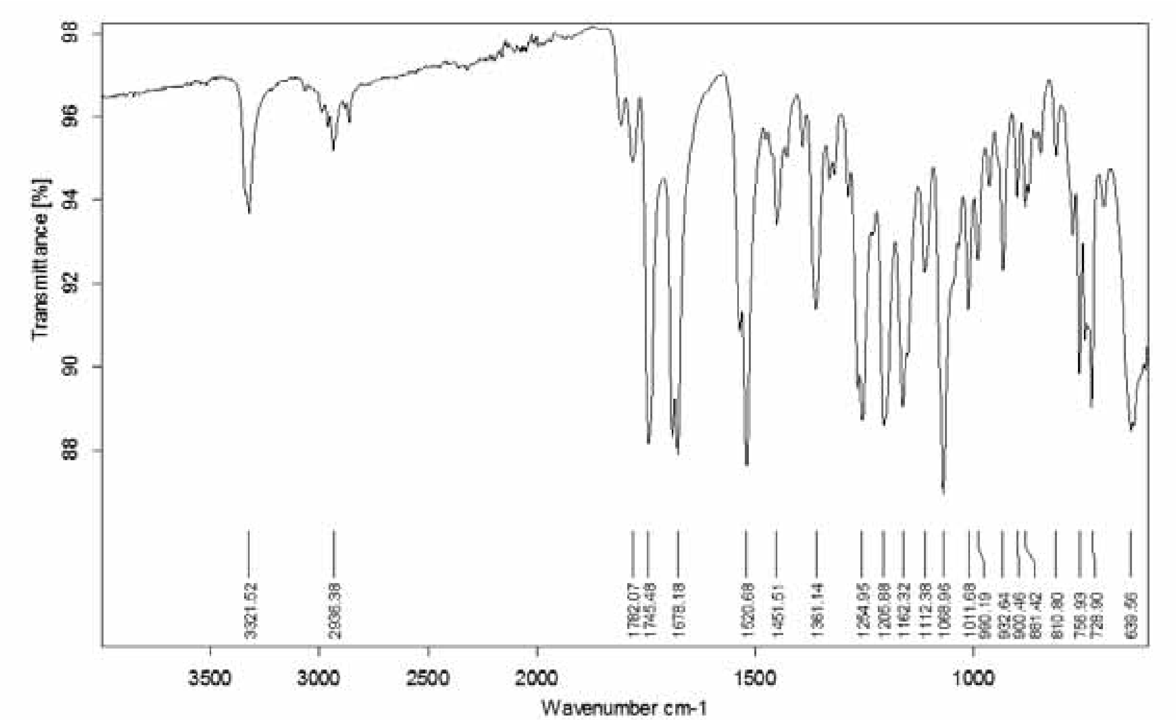

IR (ATR)

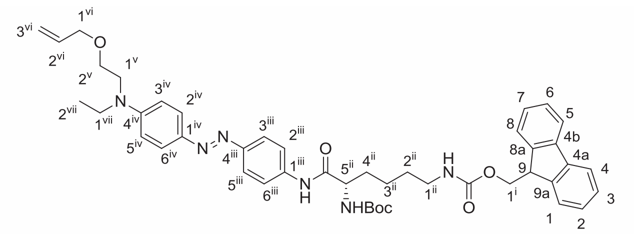

73

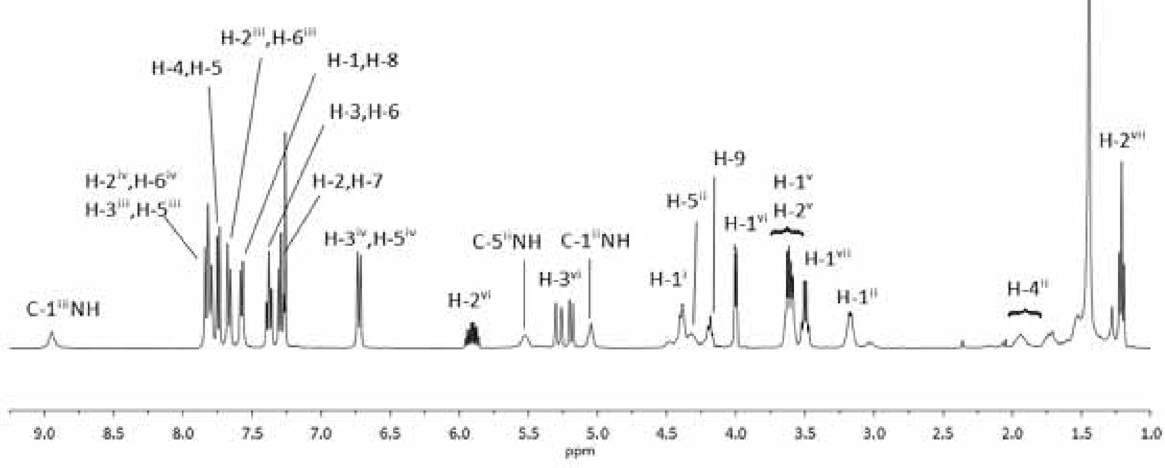

^{1}H-NMR (400 MHz, $CDCl_3$)

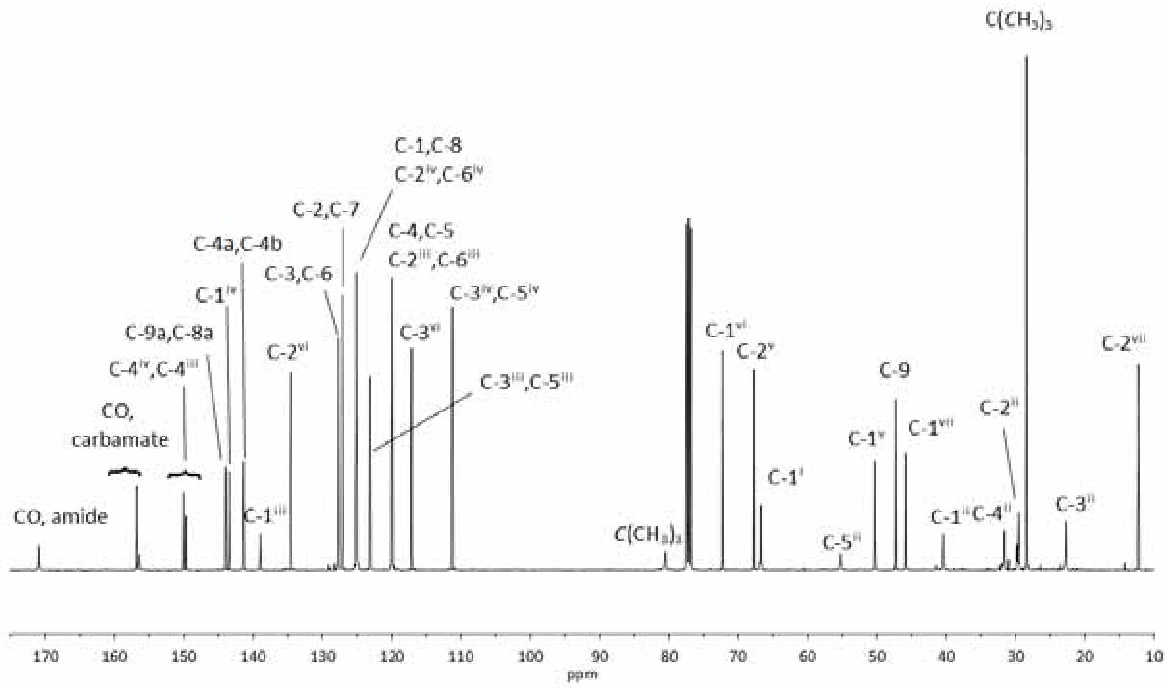

^{13}C-NMR (100.6 MHz, $CDCl_3$)

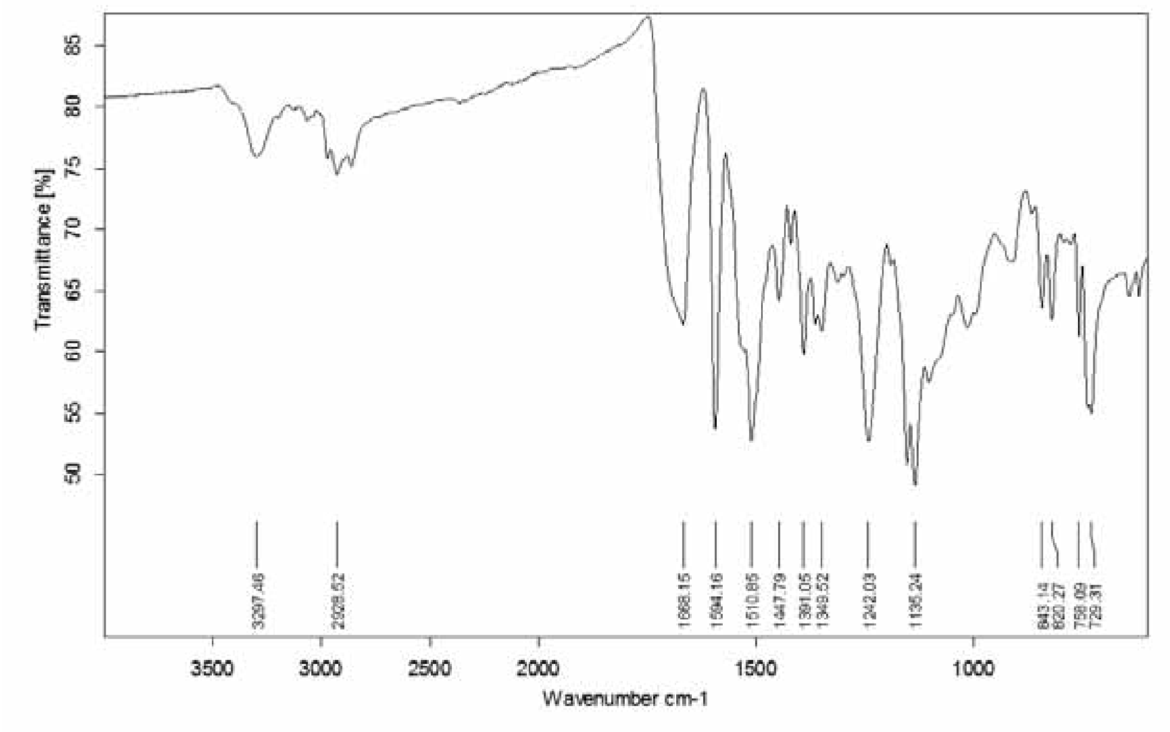

IR (ATR)

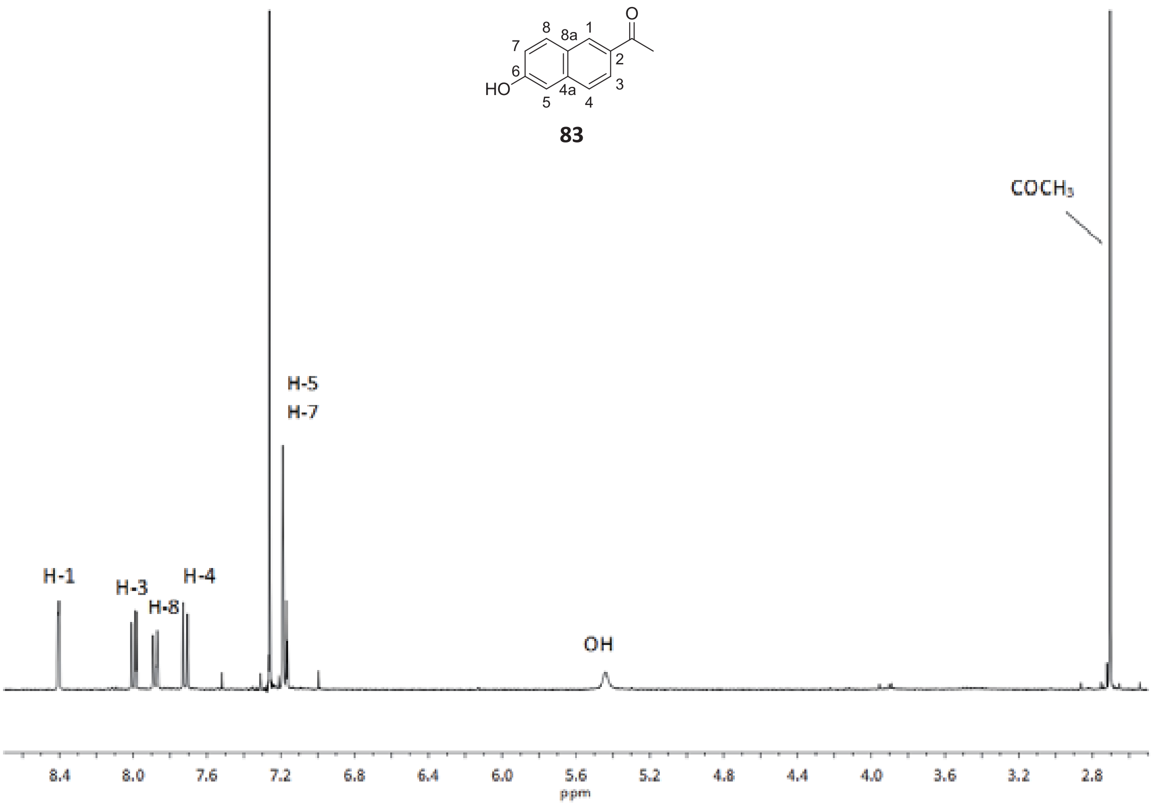

^{1}H-NMR (400 MHz, $CDCl_3$)

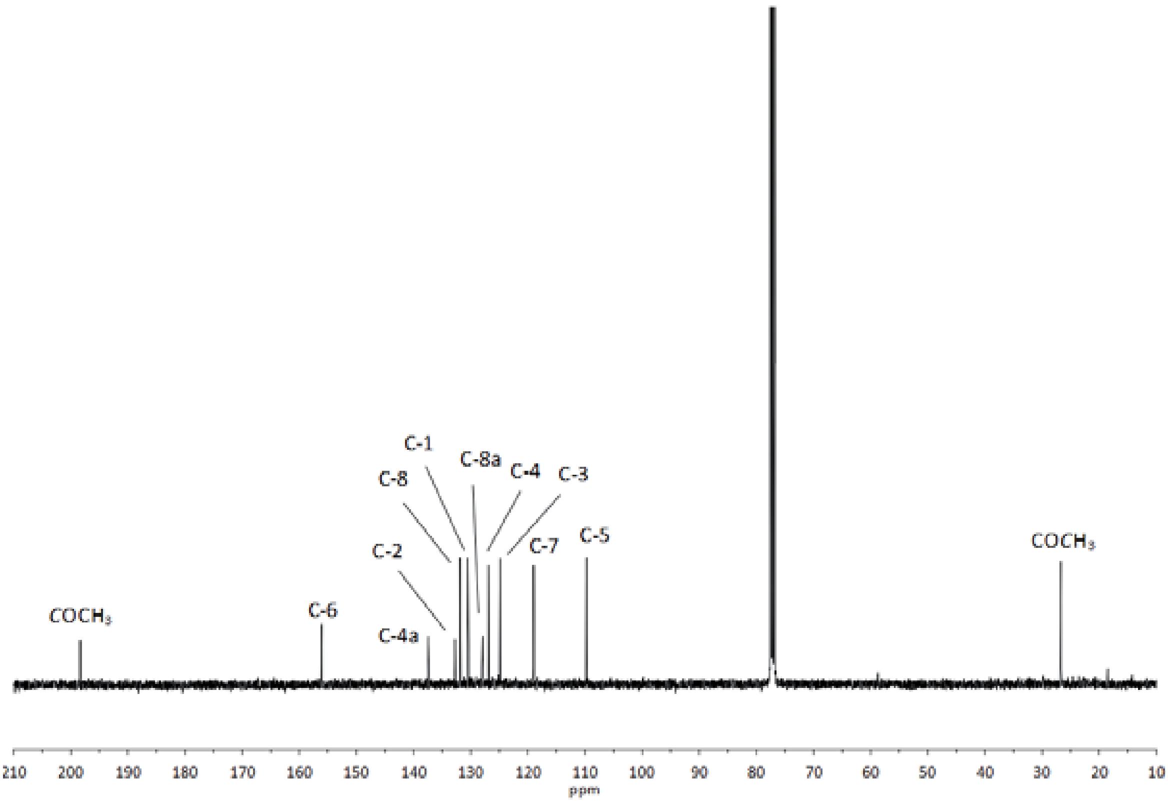

^{13}C-NMR (100.6 MHz, $CDCl_3$)

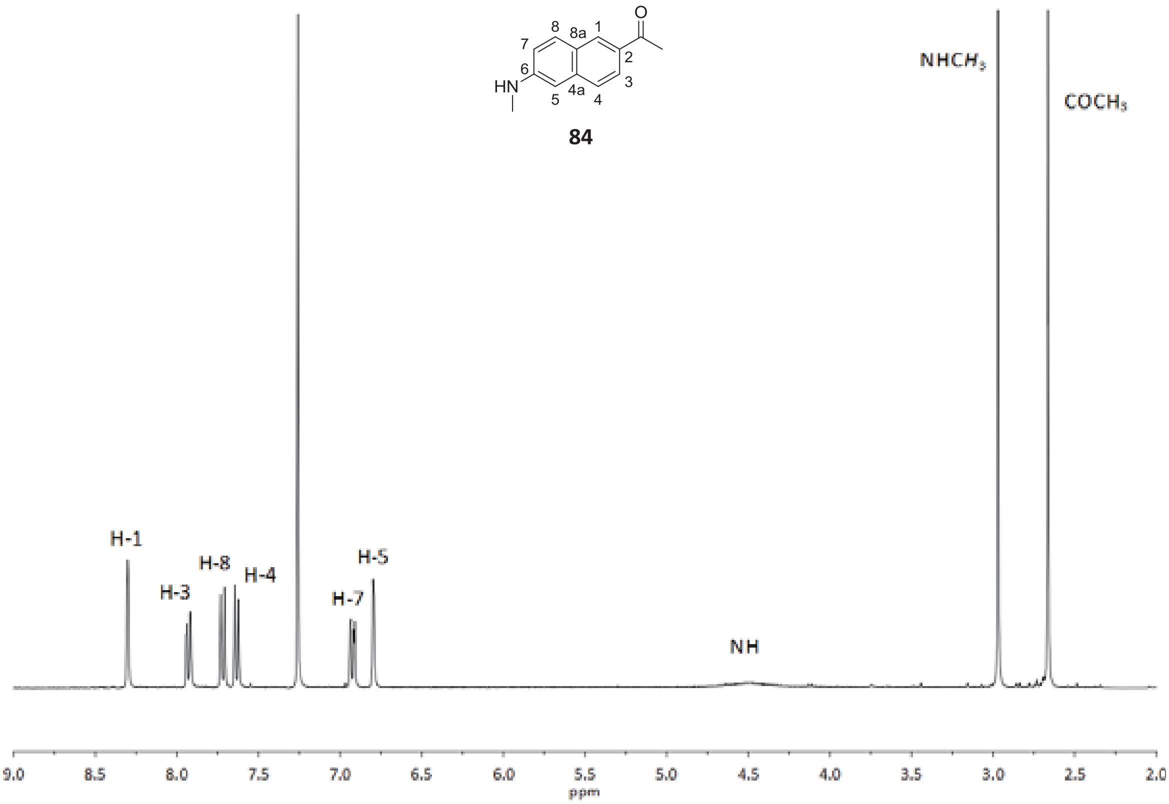

^{1}H-NMR (360 MHz, $CDCl_3$)

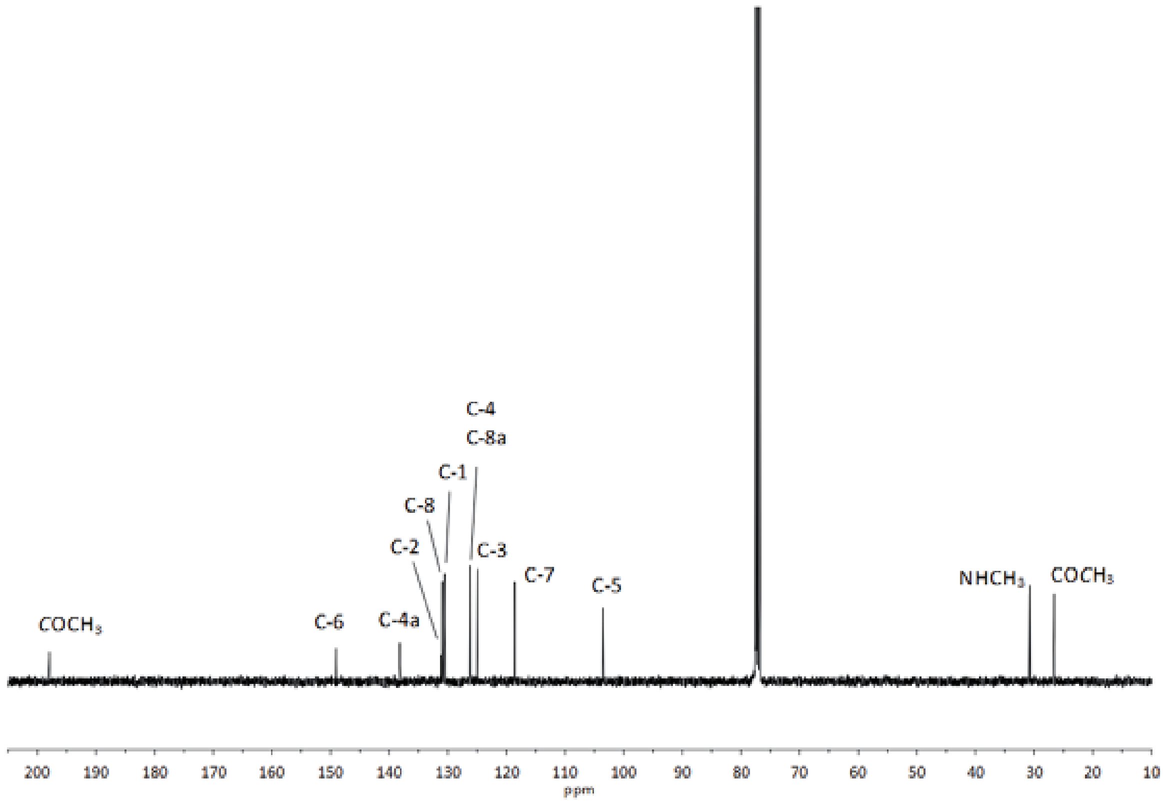

^{13}C-NMR (90 MHz, $CDCl_3$)

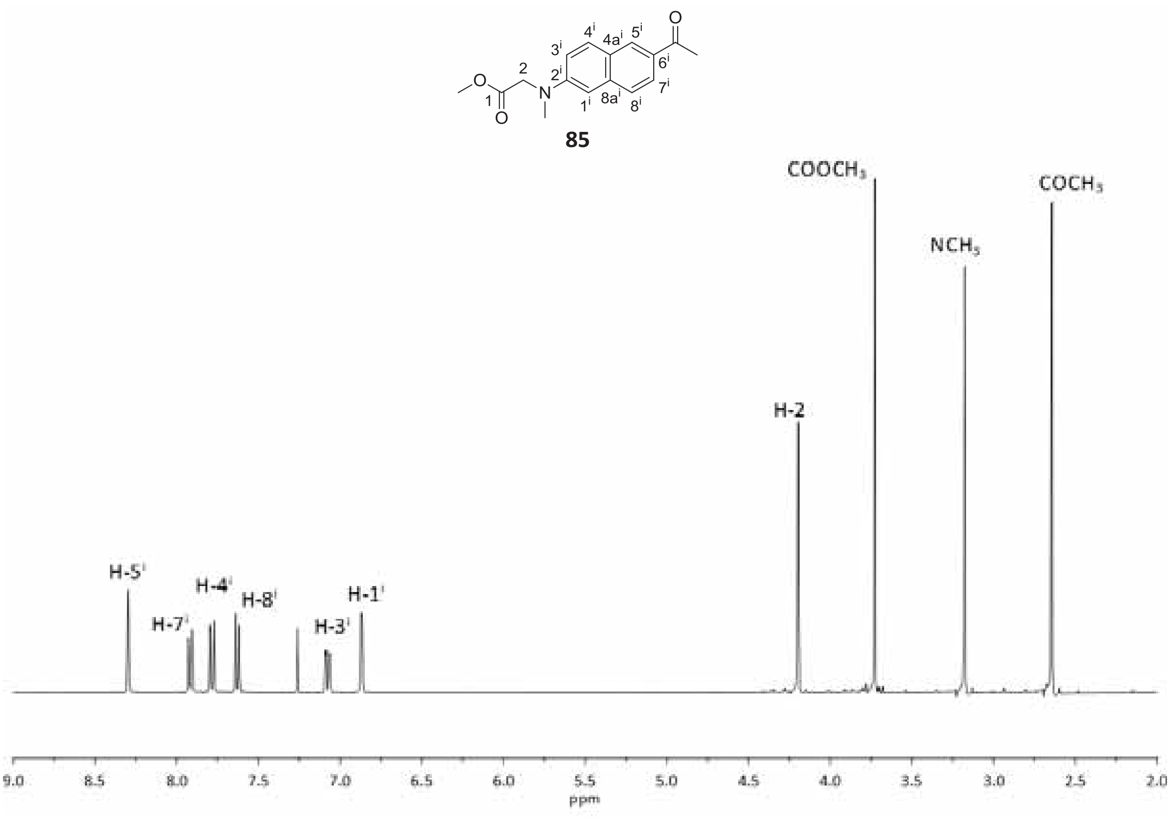

^{1}H-NMR (400 MHz, $CDCl_3$)

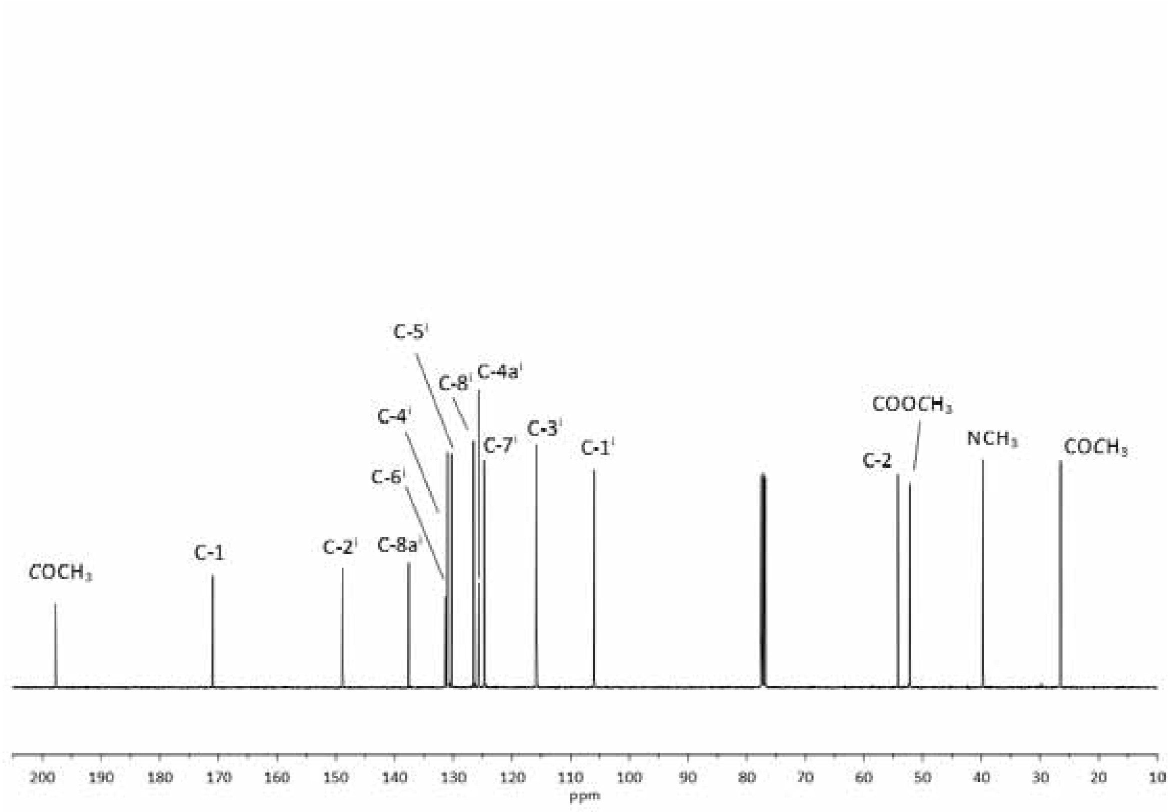

^{13}**C-NMR** (100.6 MHz, $CDCl_3$)

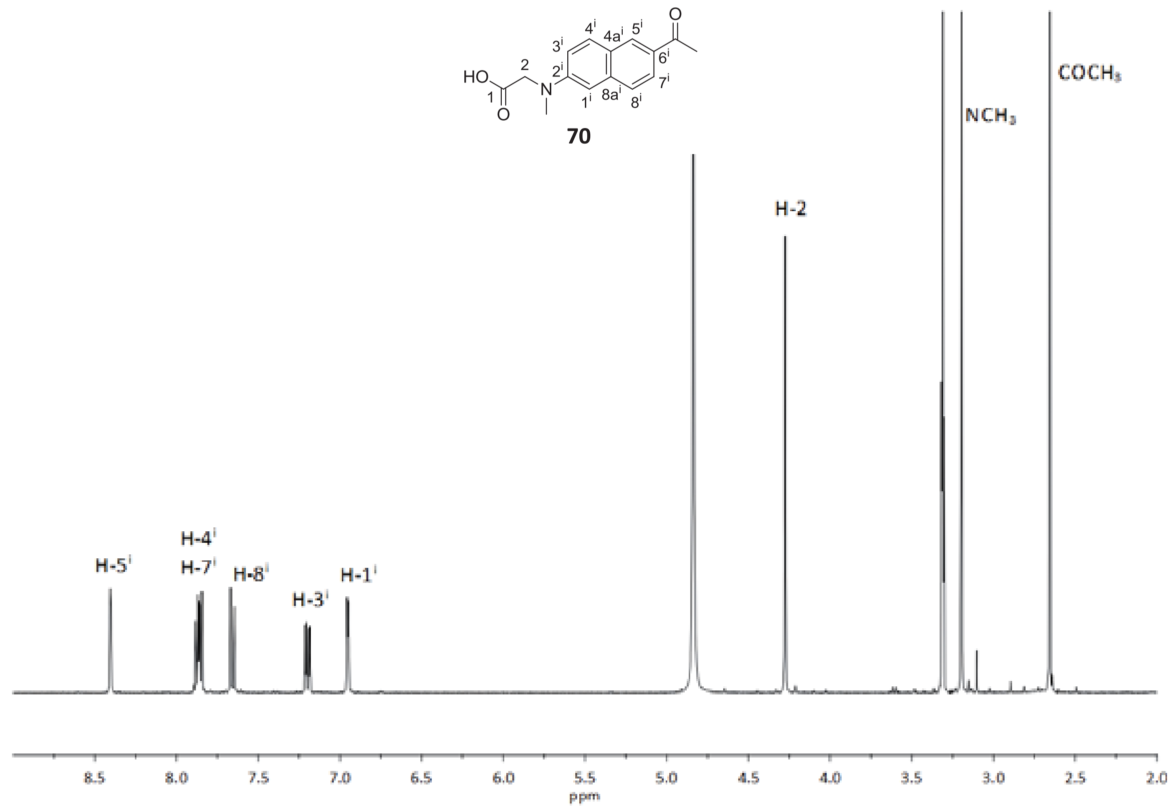

^{1}**H-NMR** (400 MHz, MeOH-d_4)

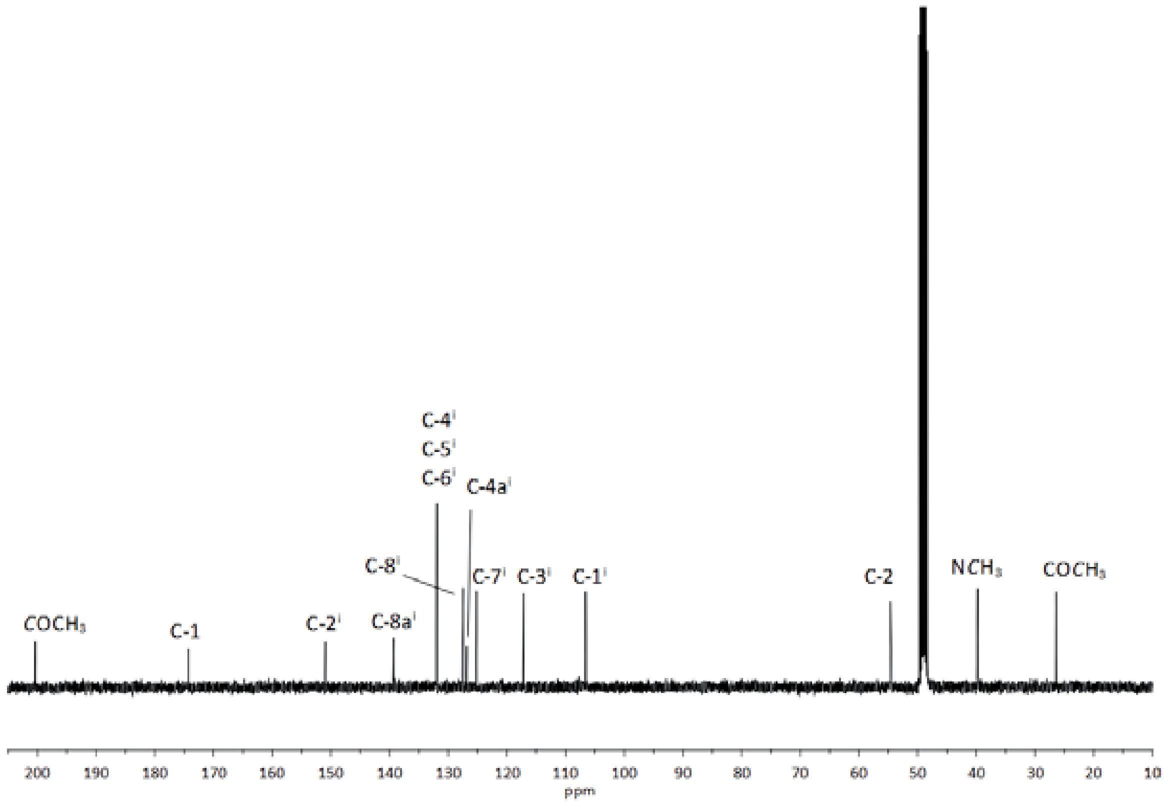

^{13}C-NMR (100.6 MHz, MeOH-d$_4$)

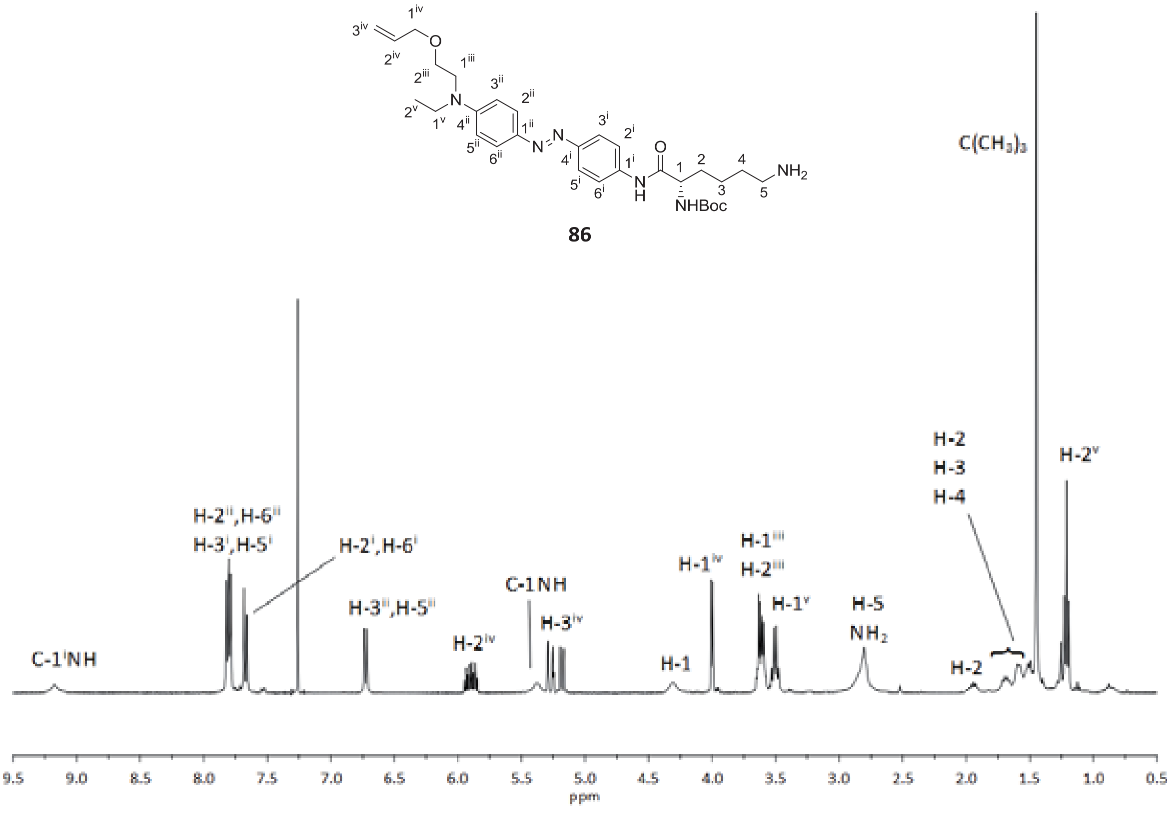

^{1}H-NMR (400 MHz, CDCl$_3$)

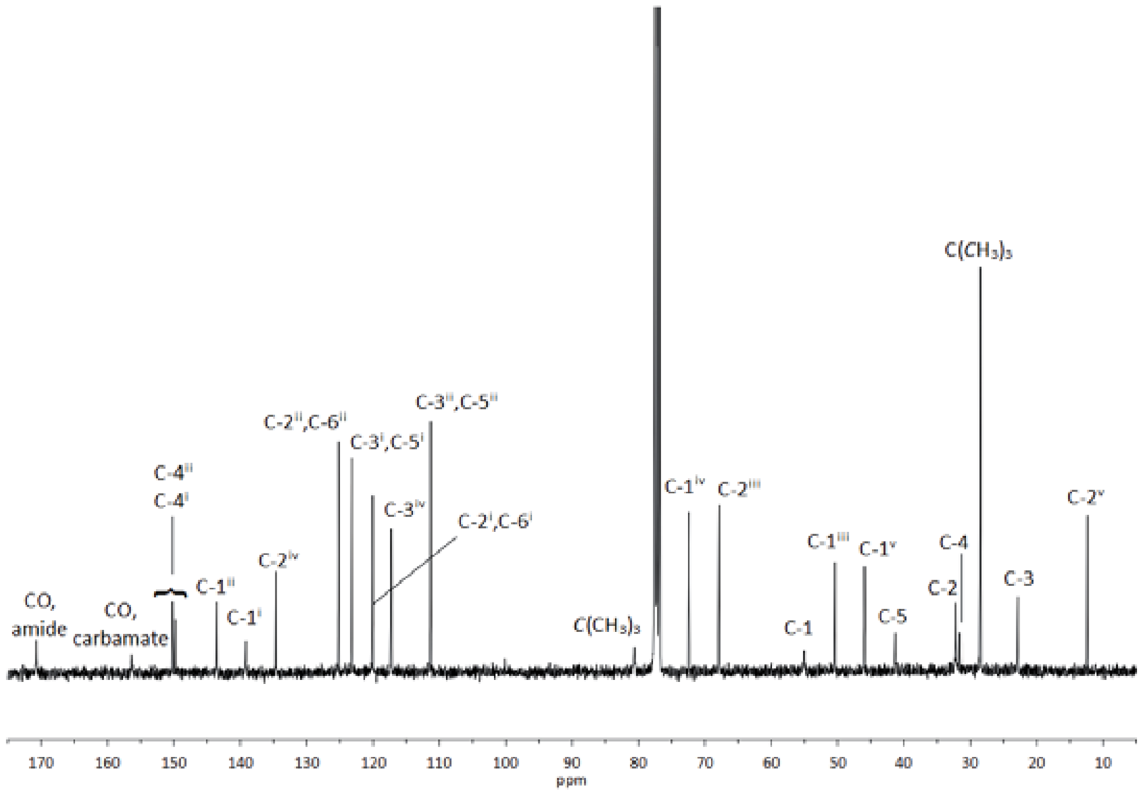

^{13}**C-NMR** (100.6 MHz, $CDCl_3$)

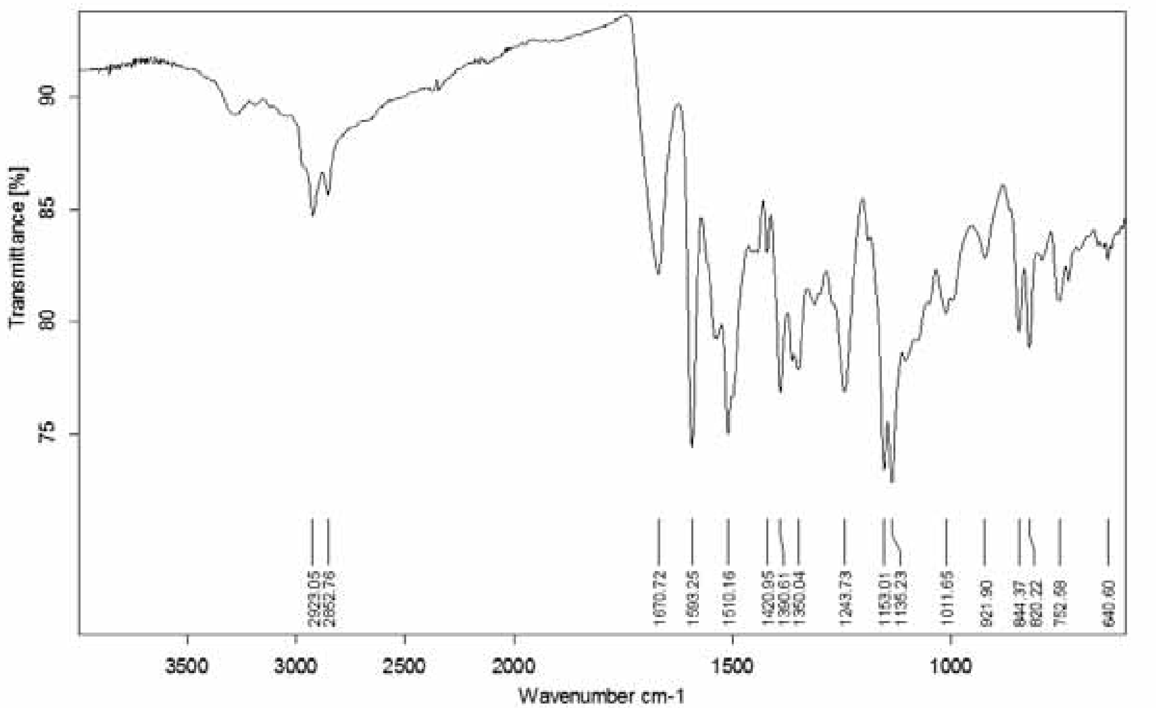

IR (ATR)

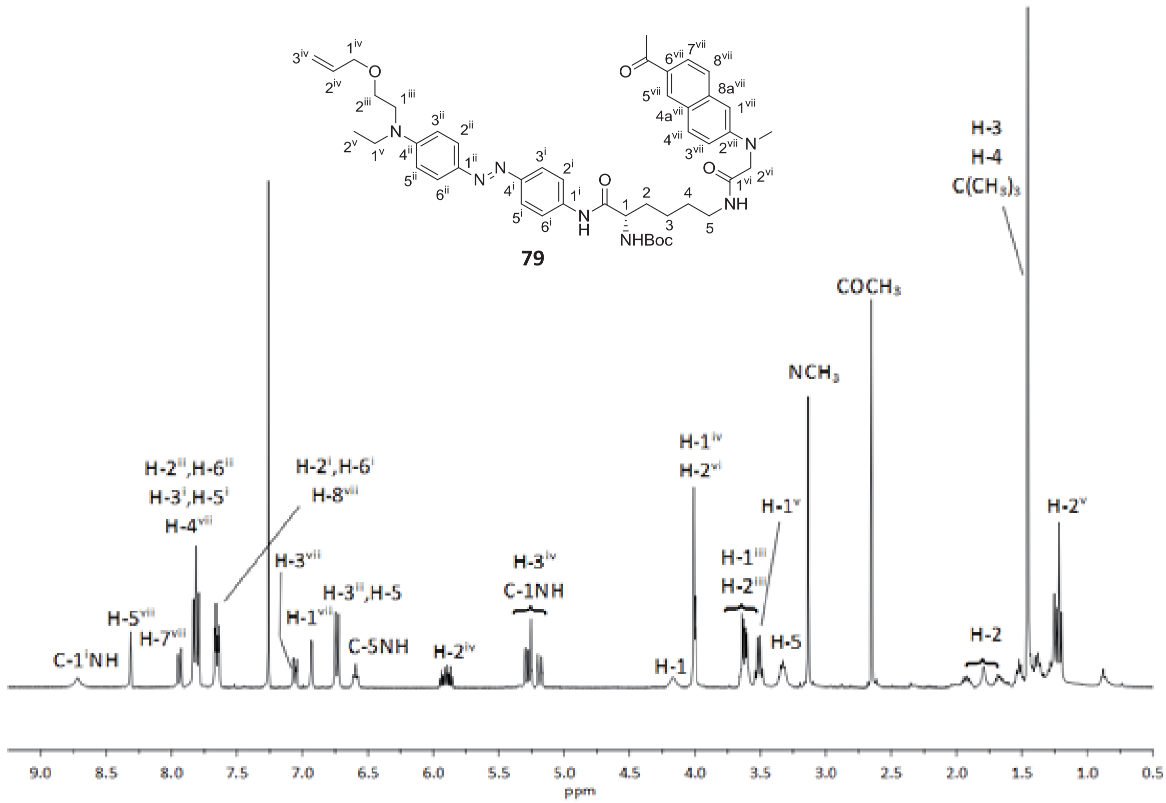

^{1}**H-NMR** (400 MHz, CDCl$_3$)

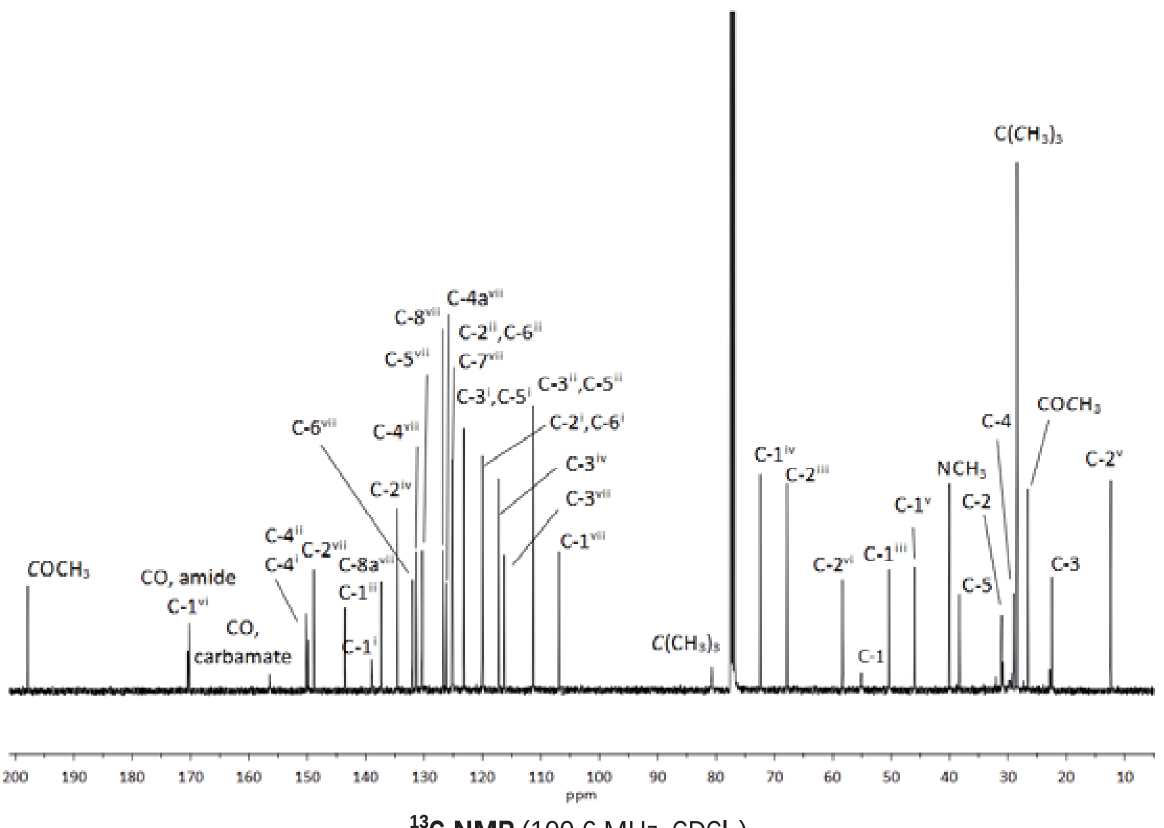

^{13}**C-NMR** (100.6 MHz, CDCl$_3$)

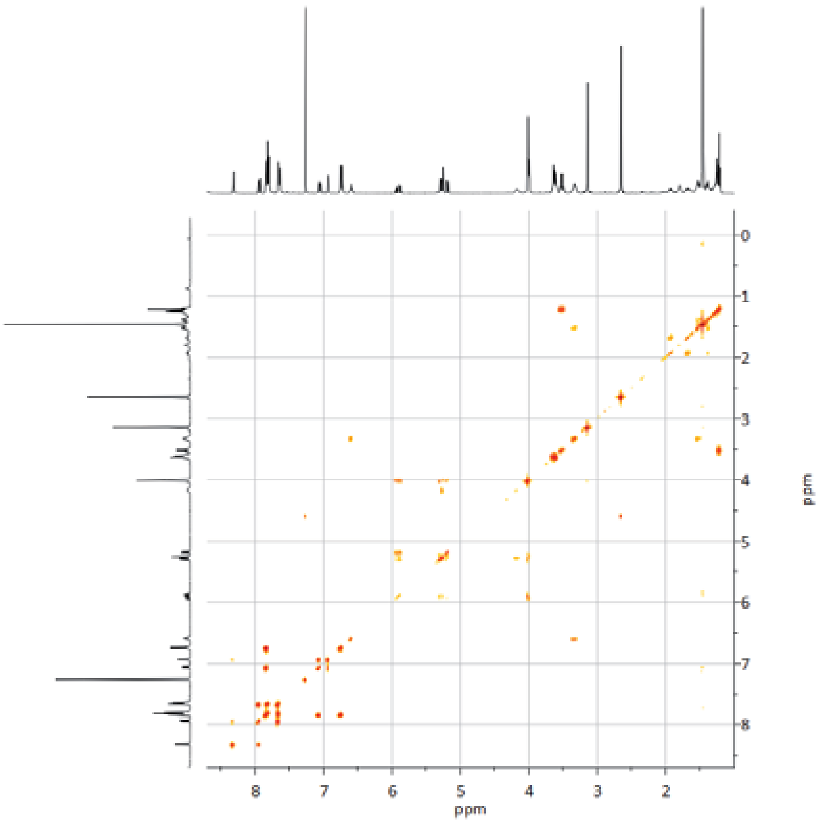

COSY (400 MHz, $CDCl_3$)

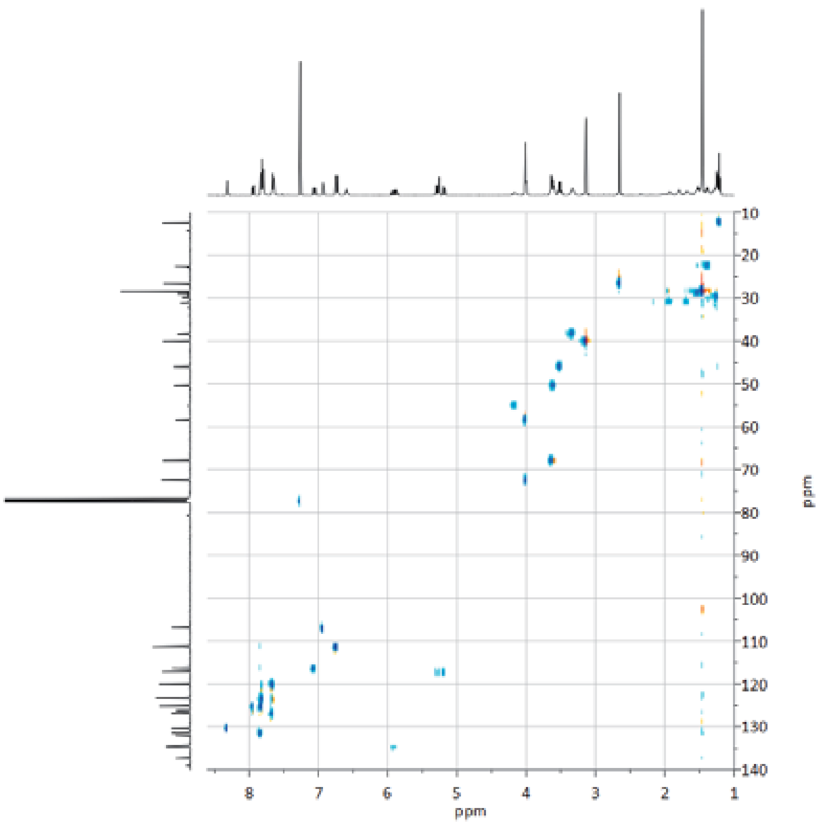

HSQC (400 MHz, $CDCl_3$)

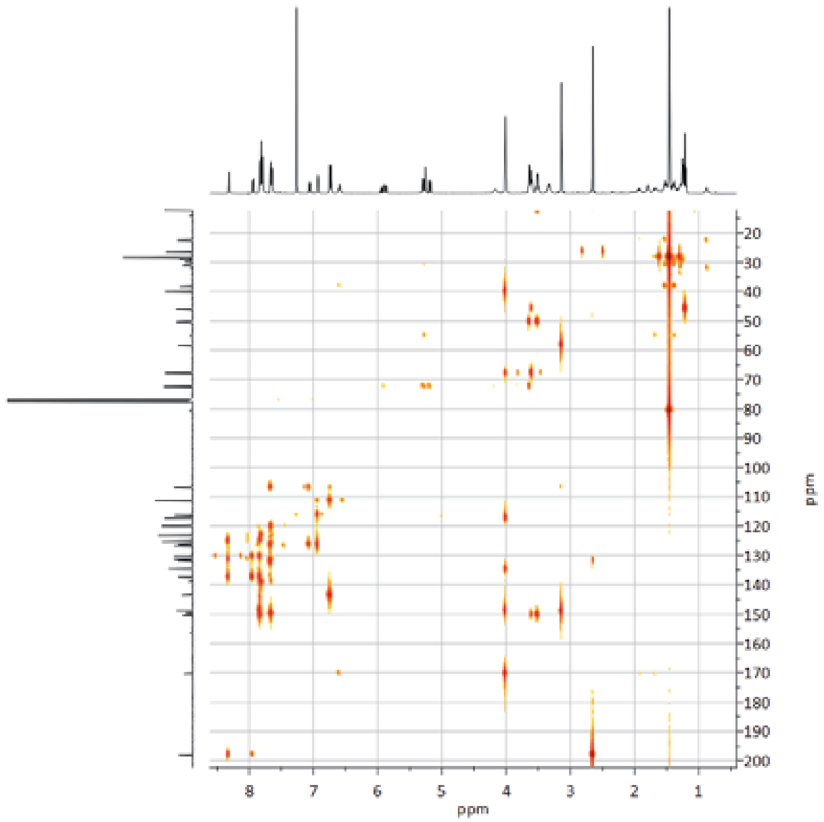

HMBC (400 MHz, $CDCl_3$)

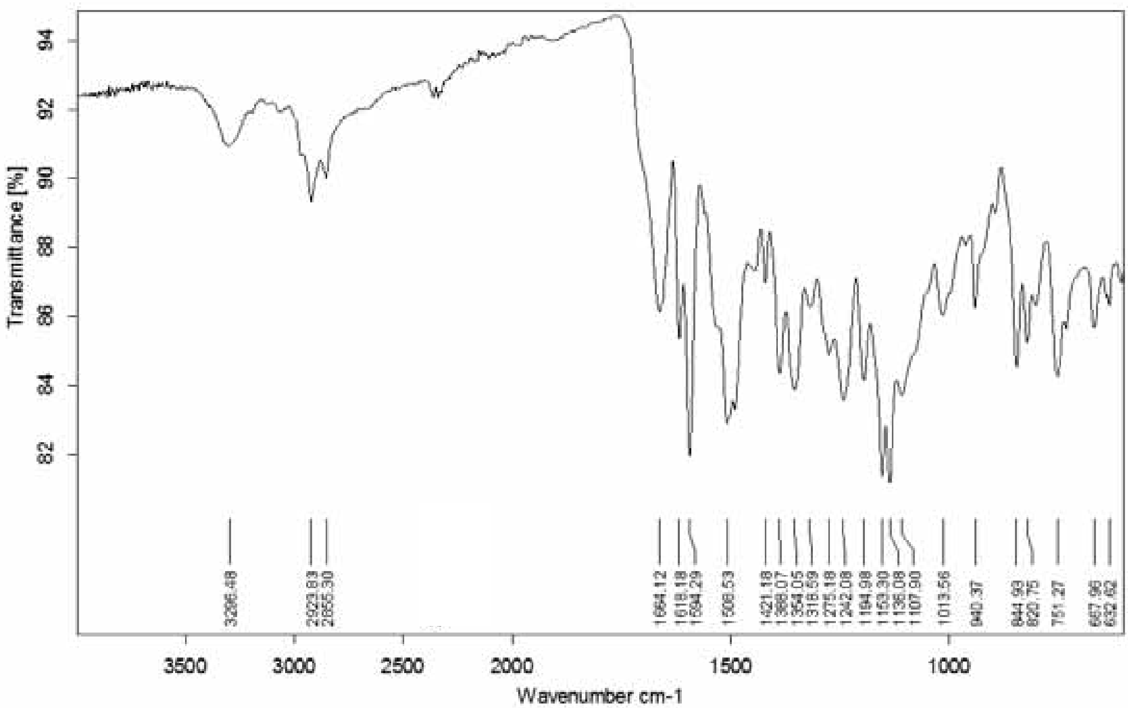

IR (ATR)

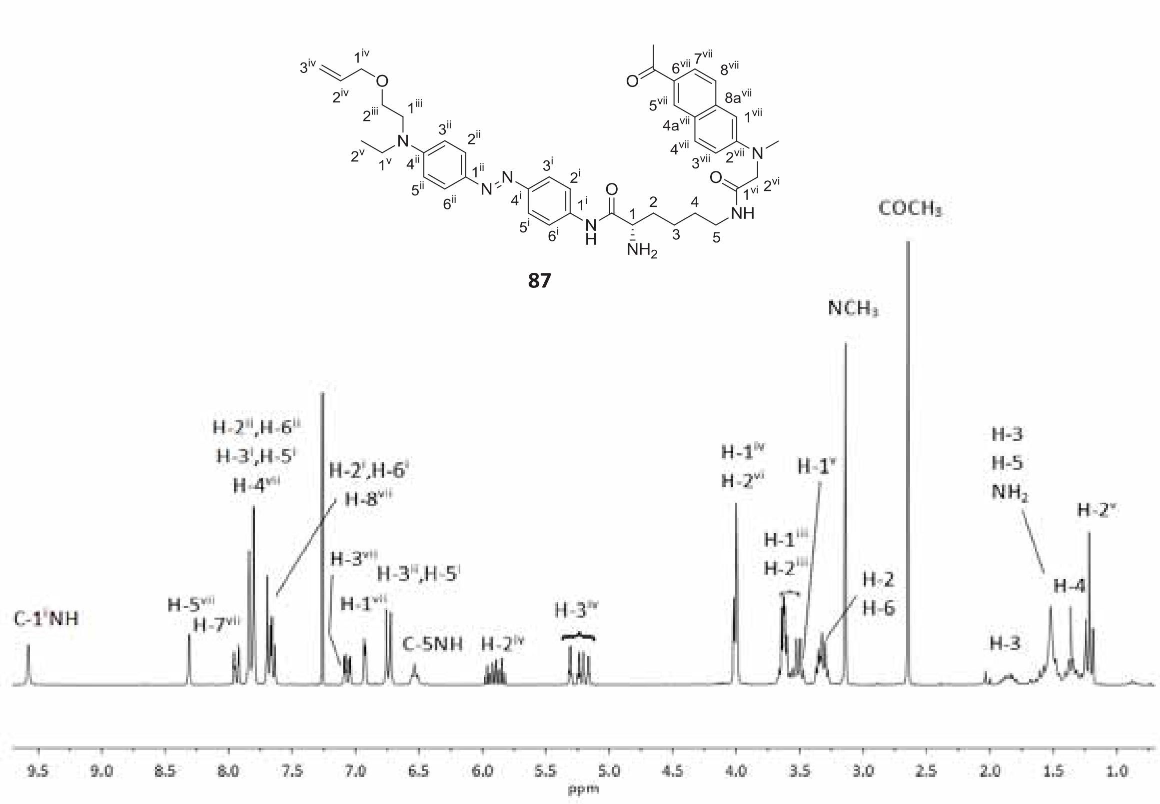

¹H-NMR (250 MHz, $CDCl_3$)

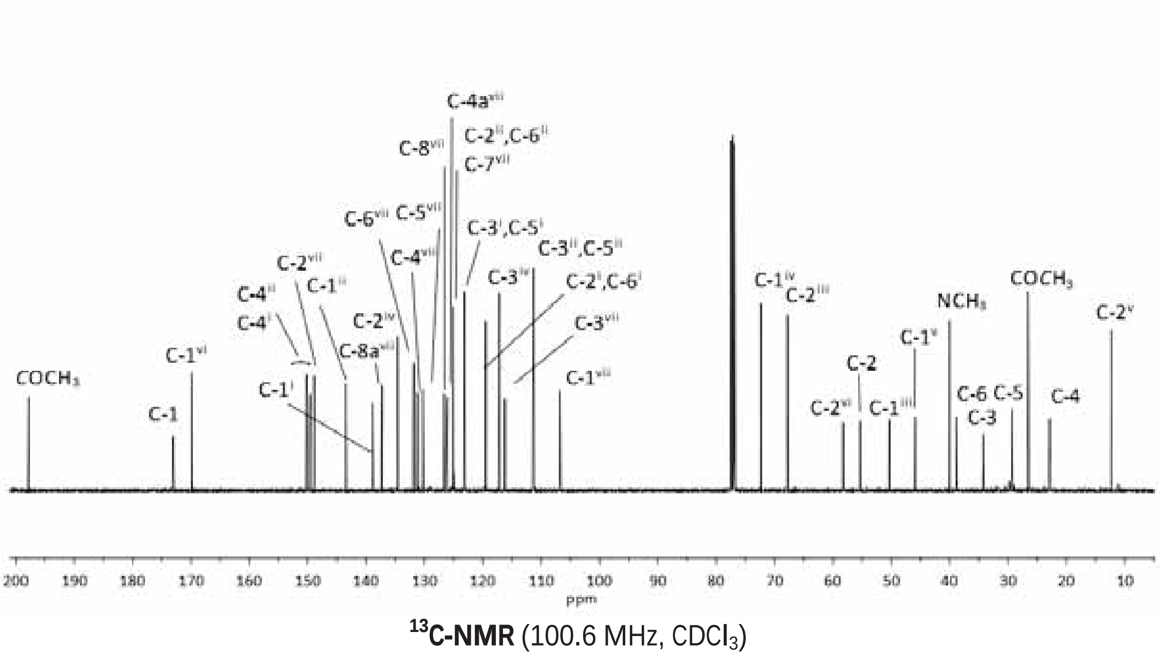

¹³C-NMR (100.6 MHz, $CDCl_3$)

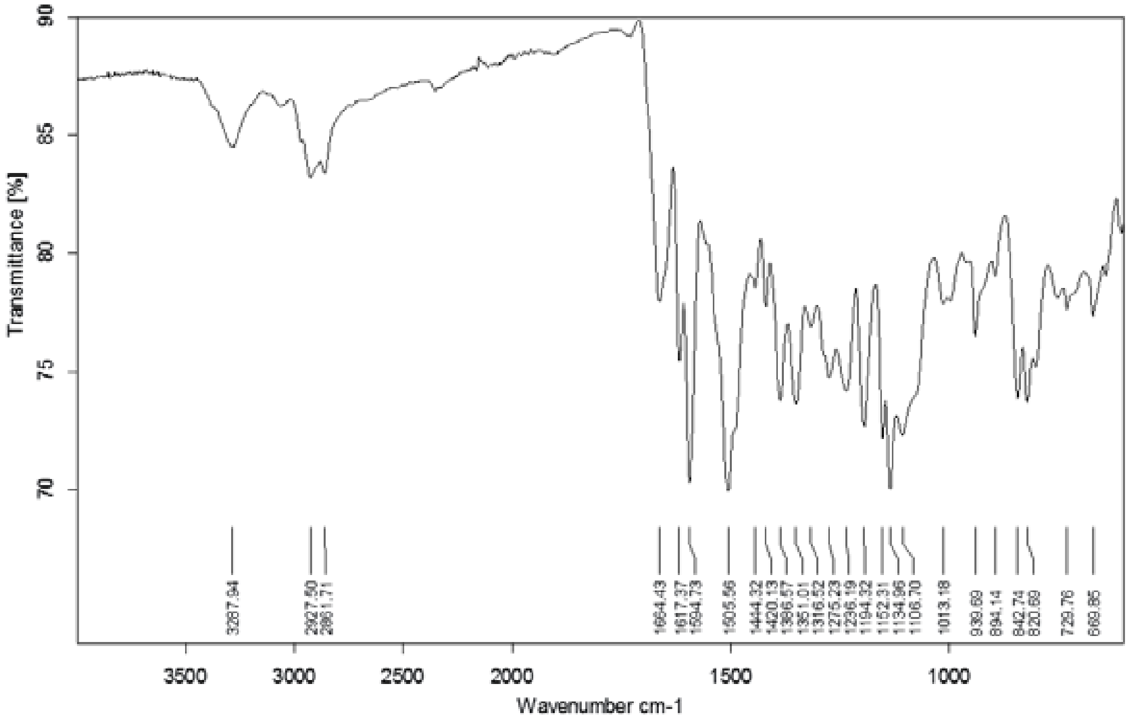

IR (ATR)

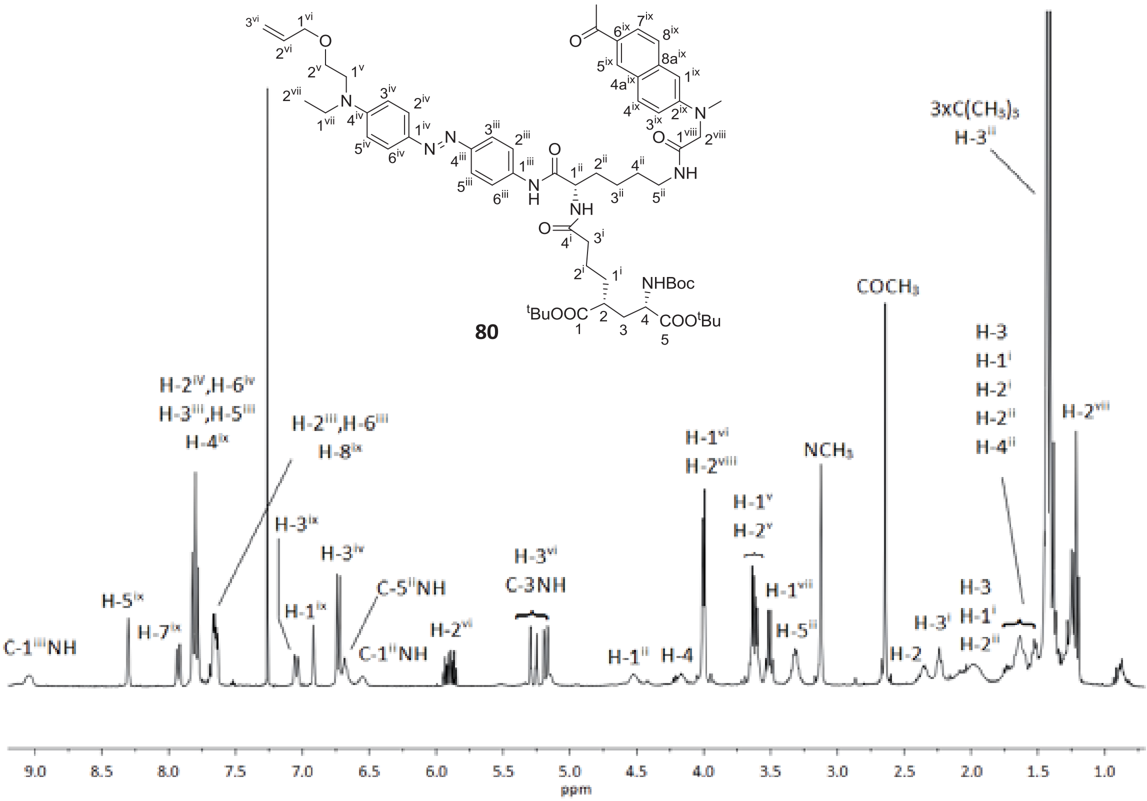

^{1}H-NMR (400 MHz, $CDCl_3$)

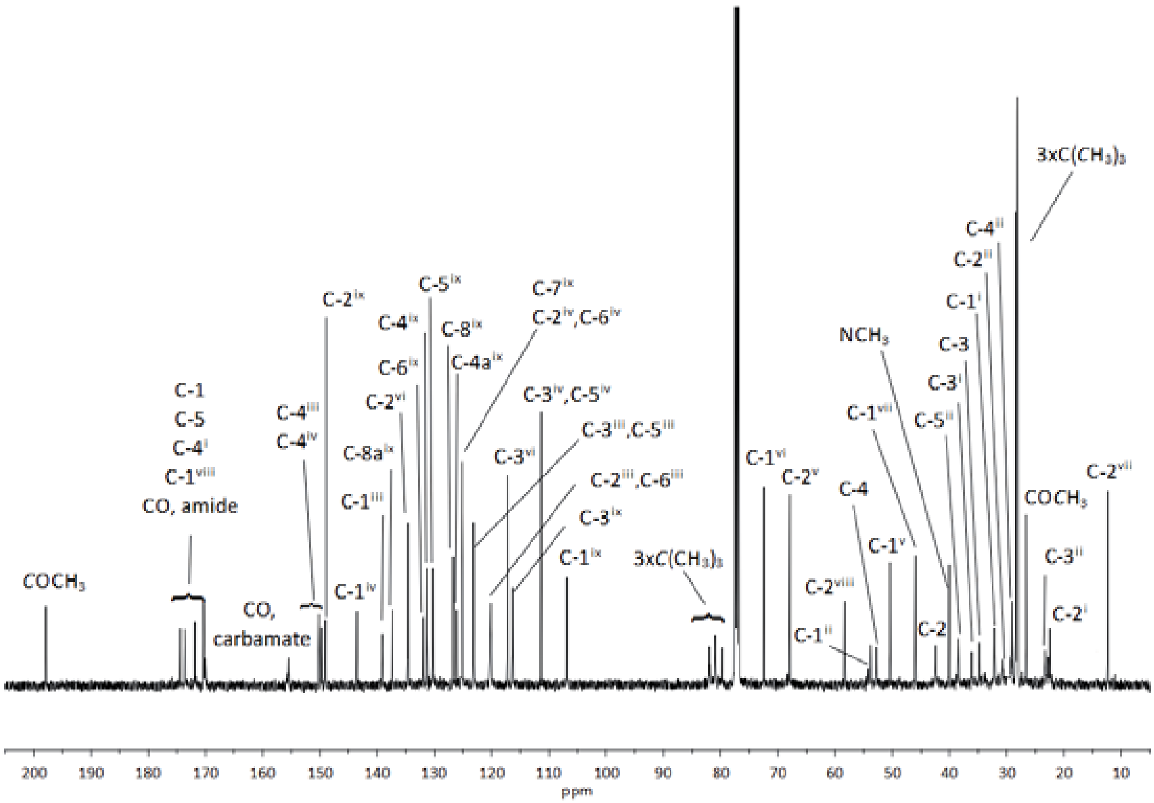

^{13}C-NMR (100.6 MHz, $CDCl_3$)

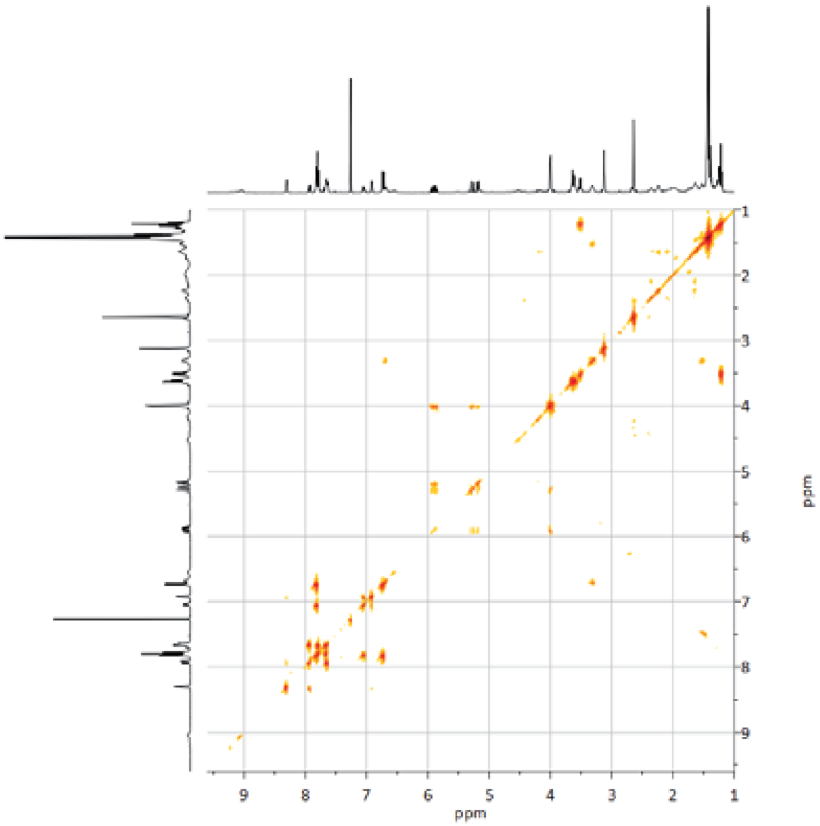

COSY (400 MHz, $CDCl_3$)

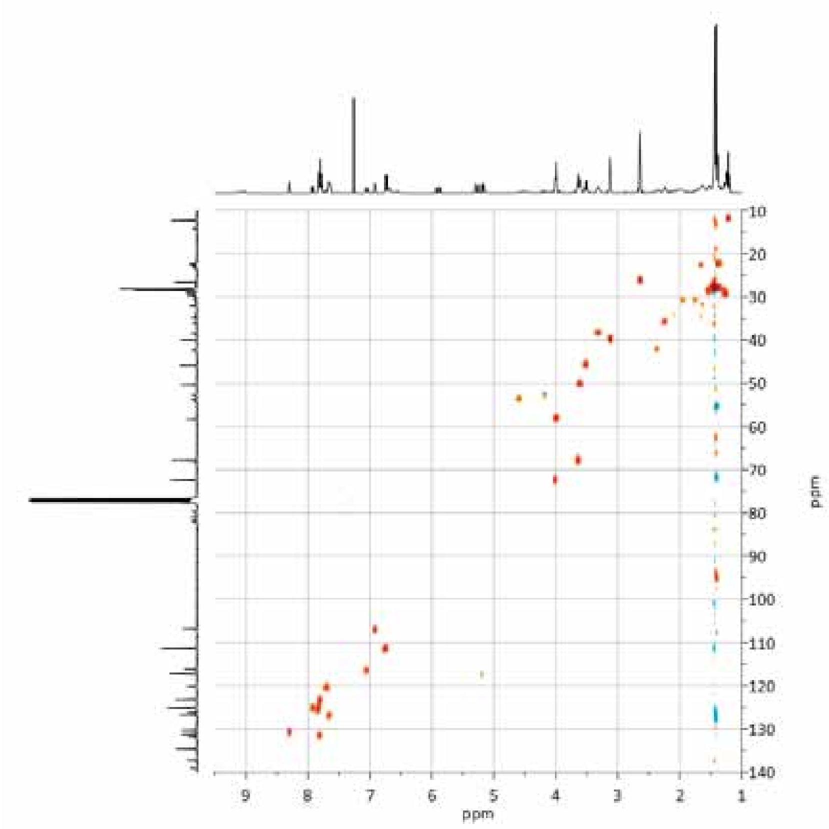

HSQC (400 MHz, $CDCl_3$)

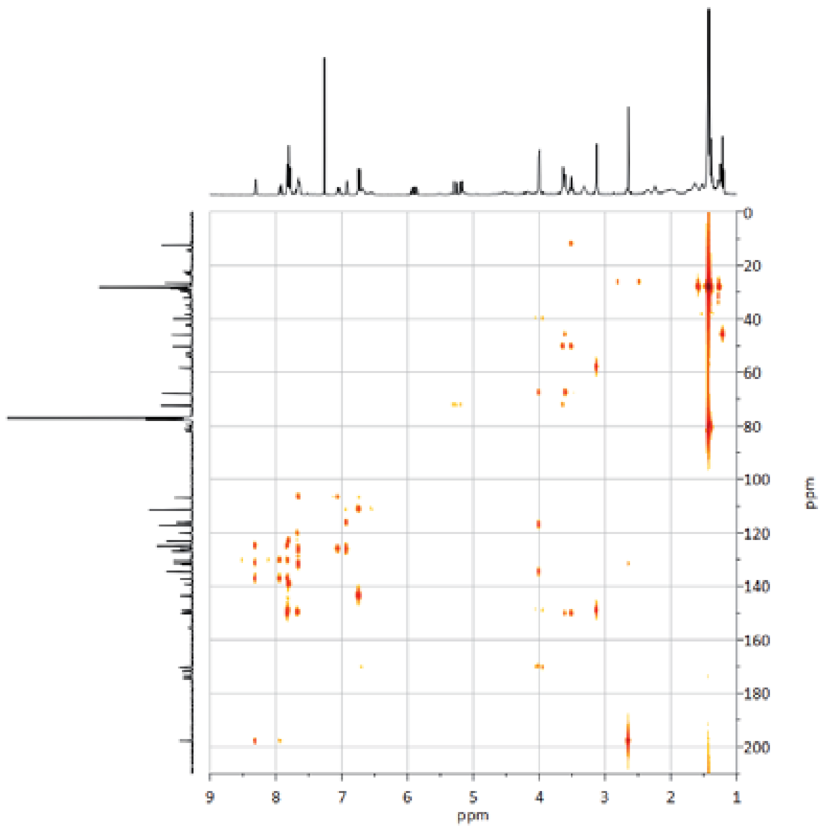

HMBC (400 MHz, $CDCl_3$)

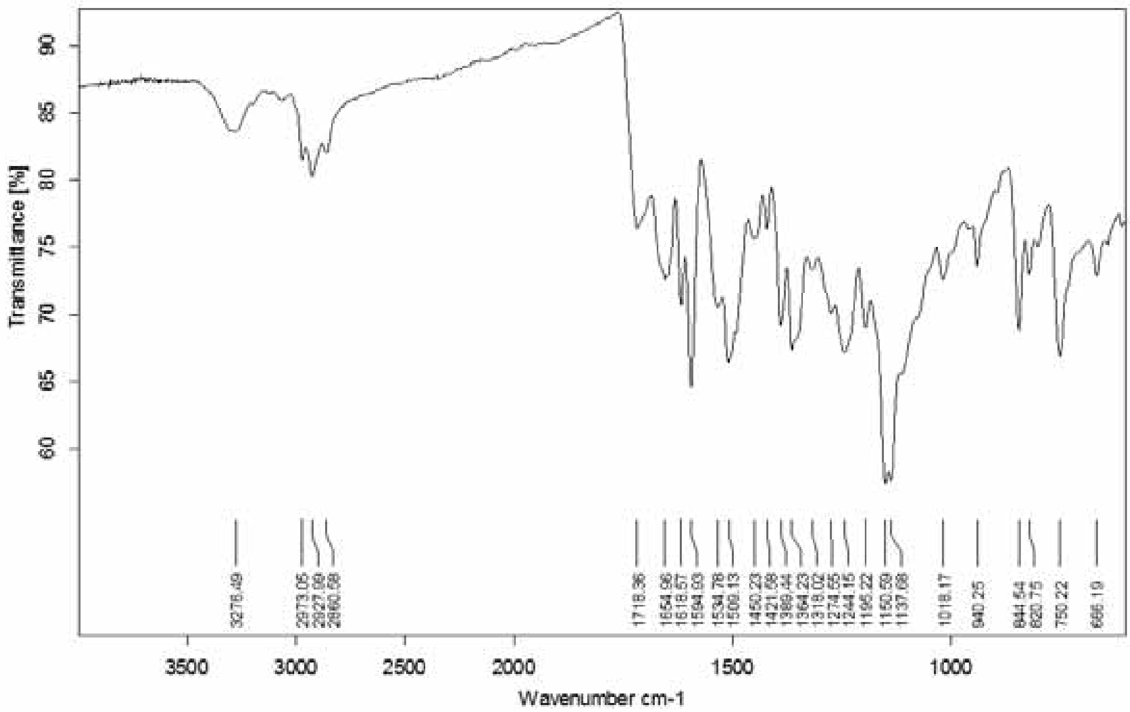

IR (ATR)

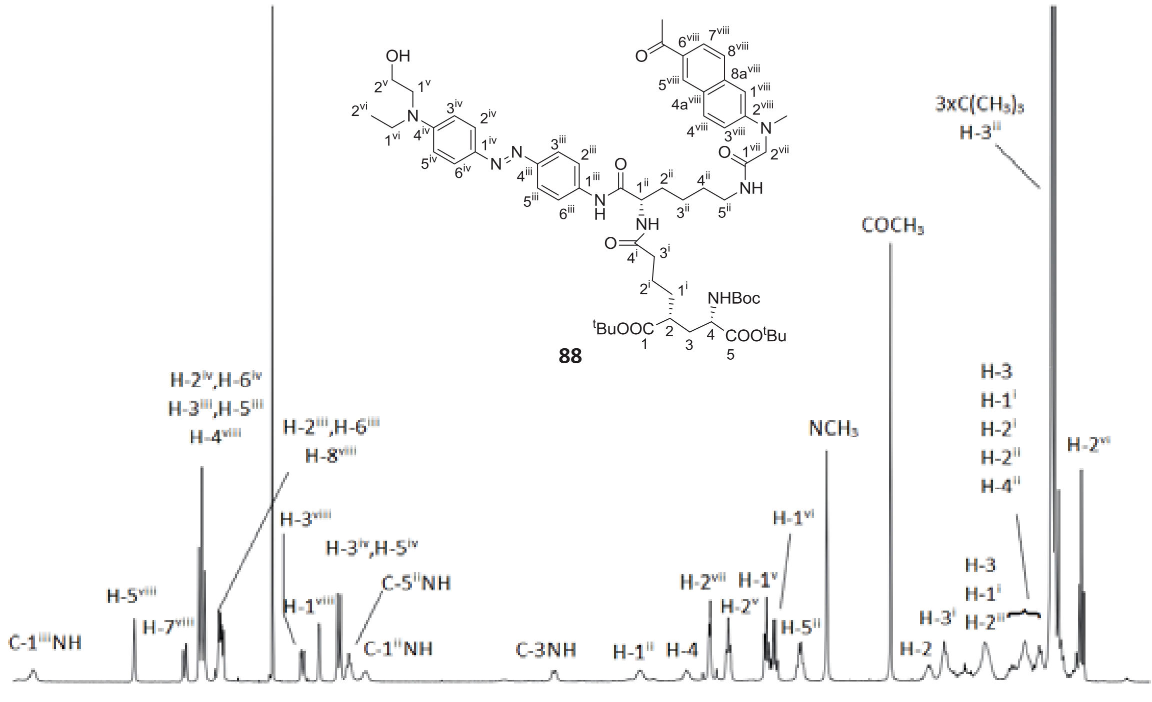

^{1}H-NMR (400 MHz, $CDCl_3$)

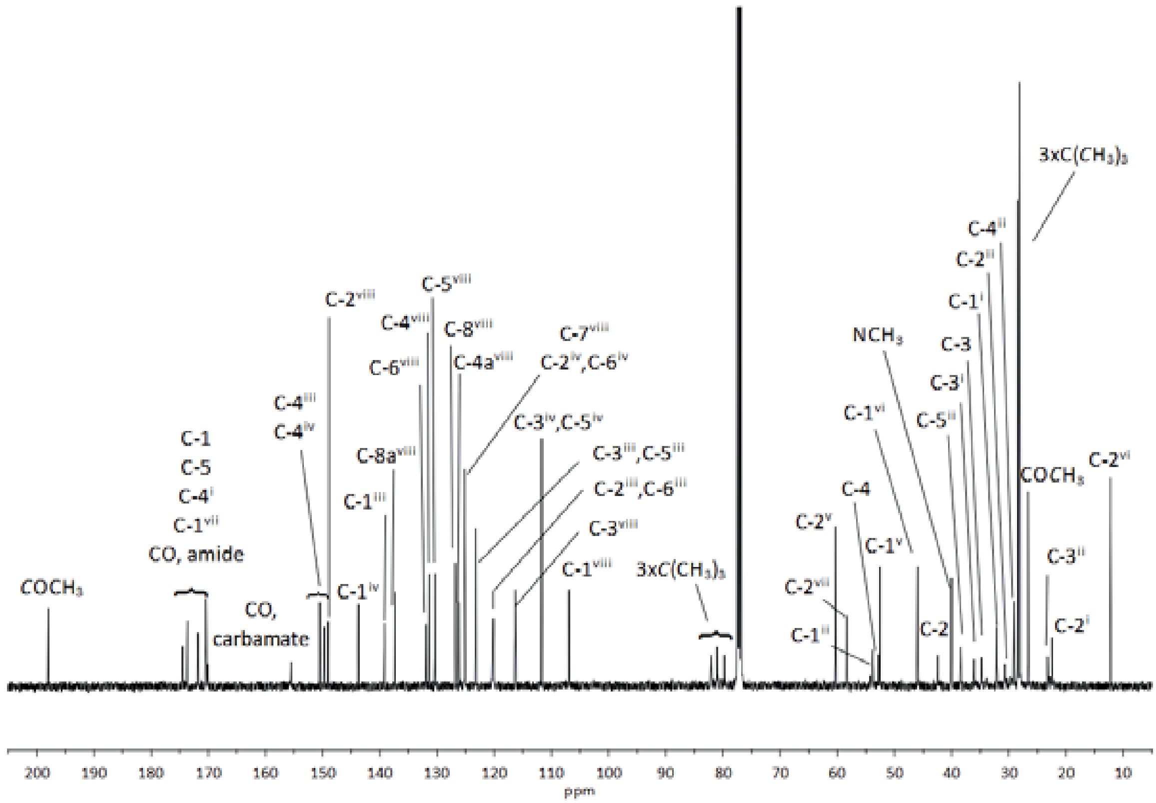

^{13}C-NMR (100.6 MHz, CDCl$_3$)

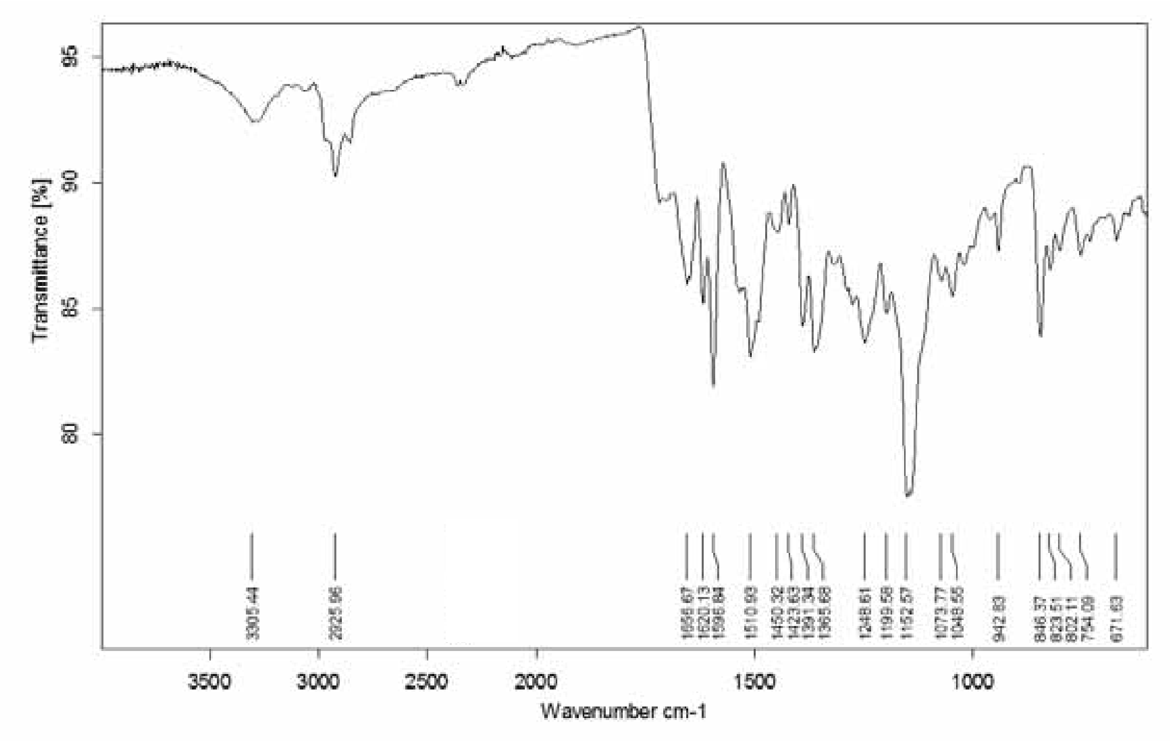

IR (ATR)

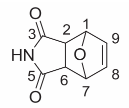

89

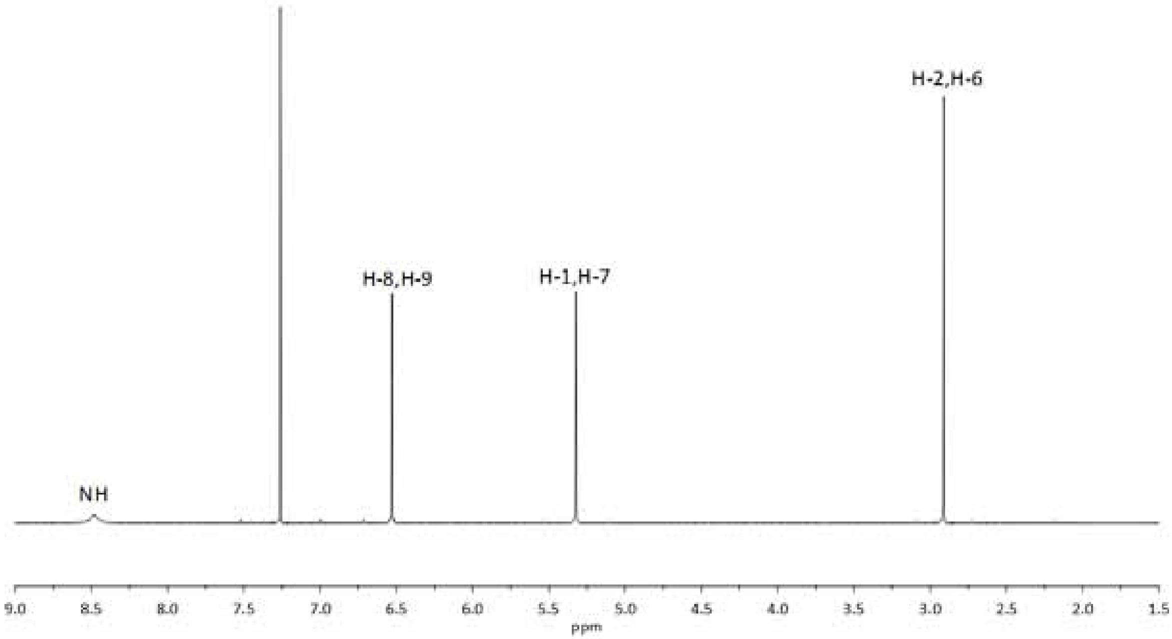

^{1}H-NMR (400 MHz, $CDCl_3$)

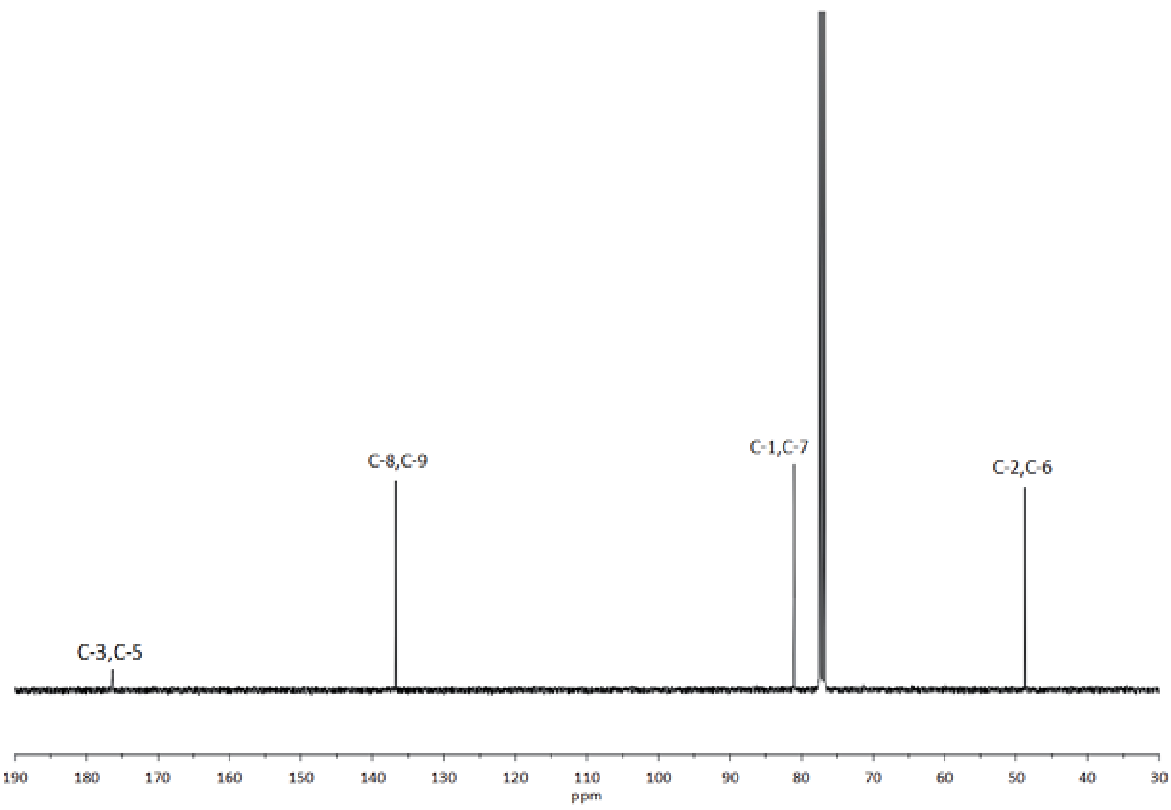

^{13}C-NMR (100.6 MHz, $CDCl_3$)

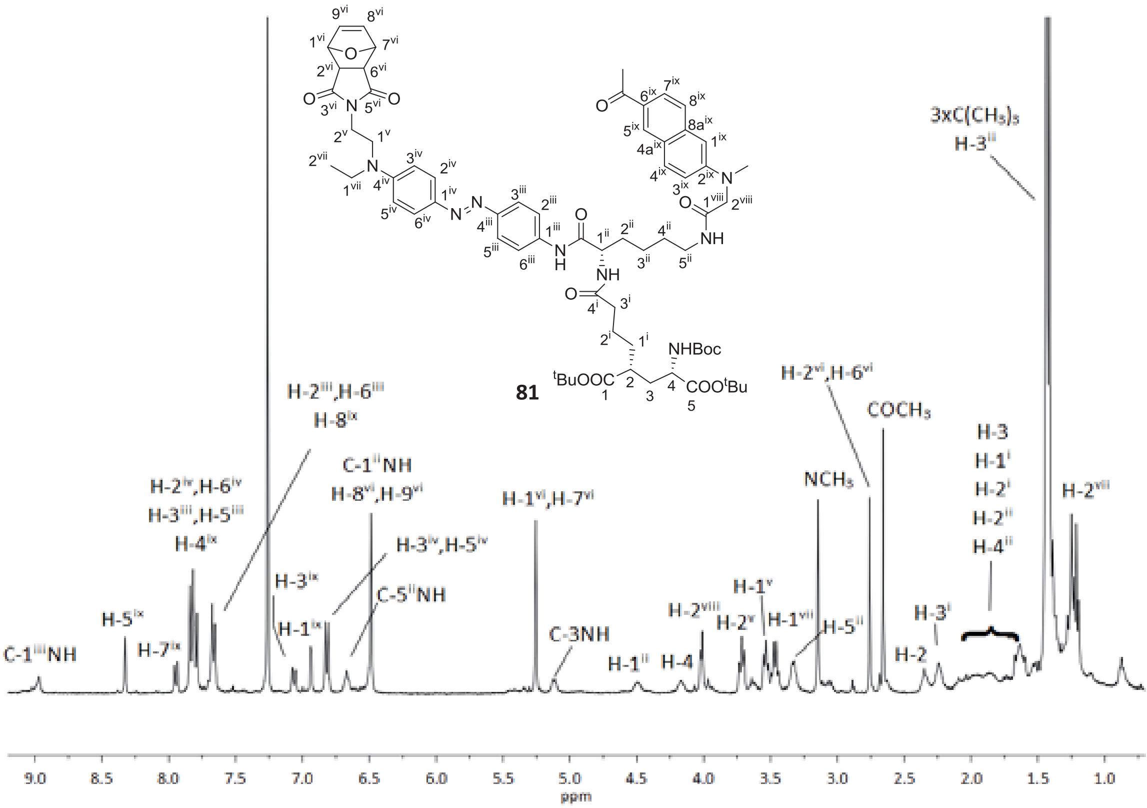

^{1}**H-NMR** (400 MHz, $CDCl_3$)

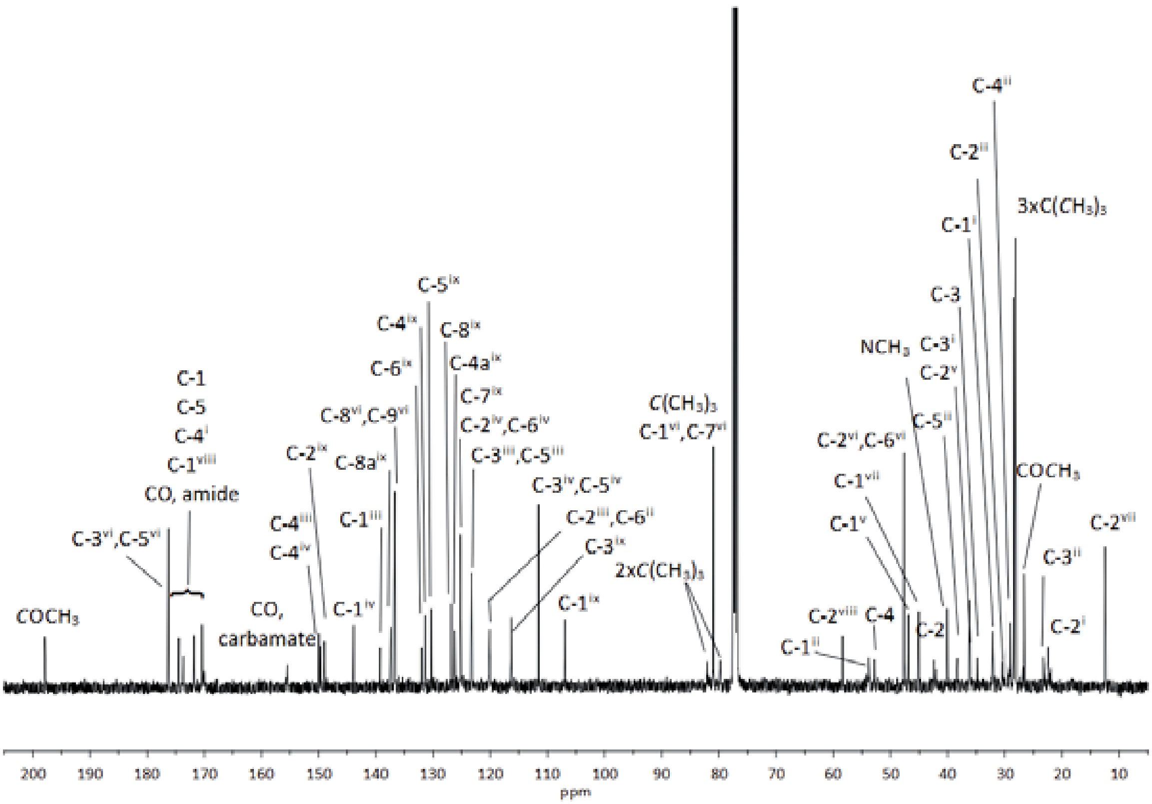

^{13}**C-NMR** (100.6 MHz, $CDCl_3$)

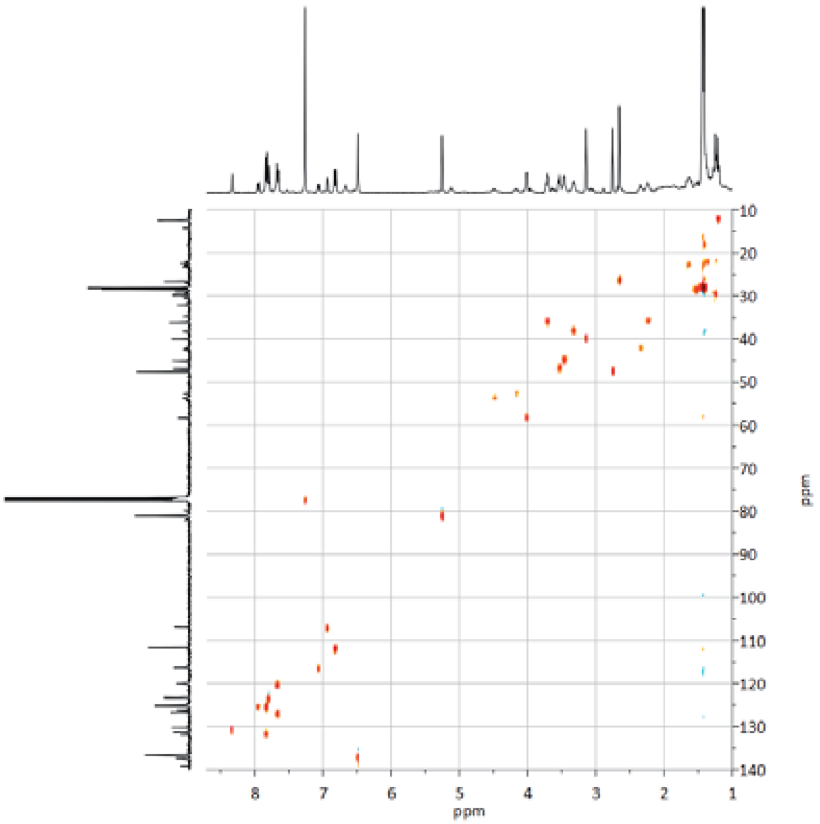

HSQC (400 MHz, $CDCl_3$)

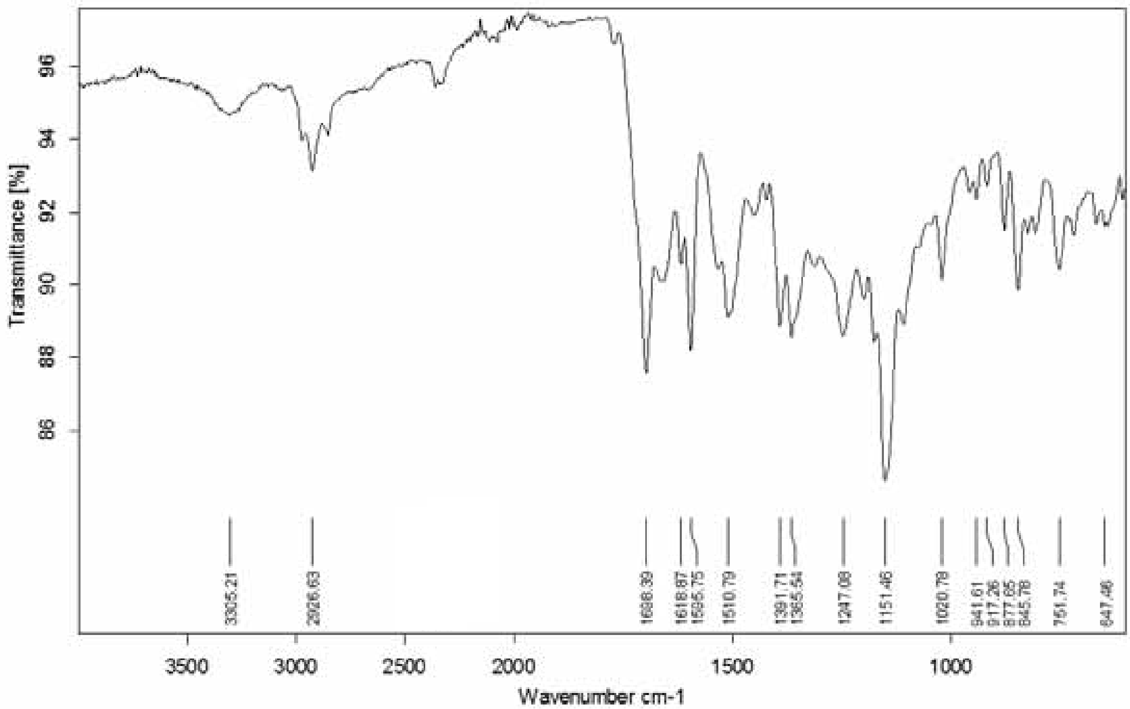

IR (ATR)

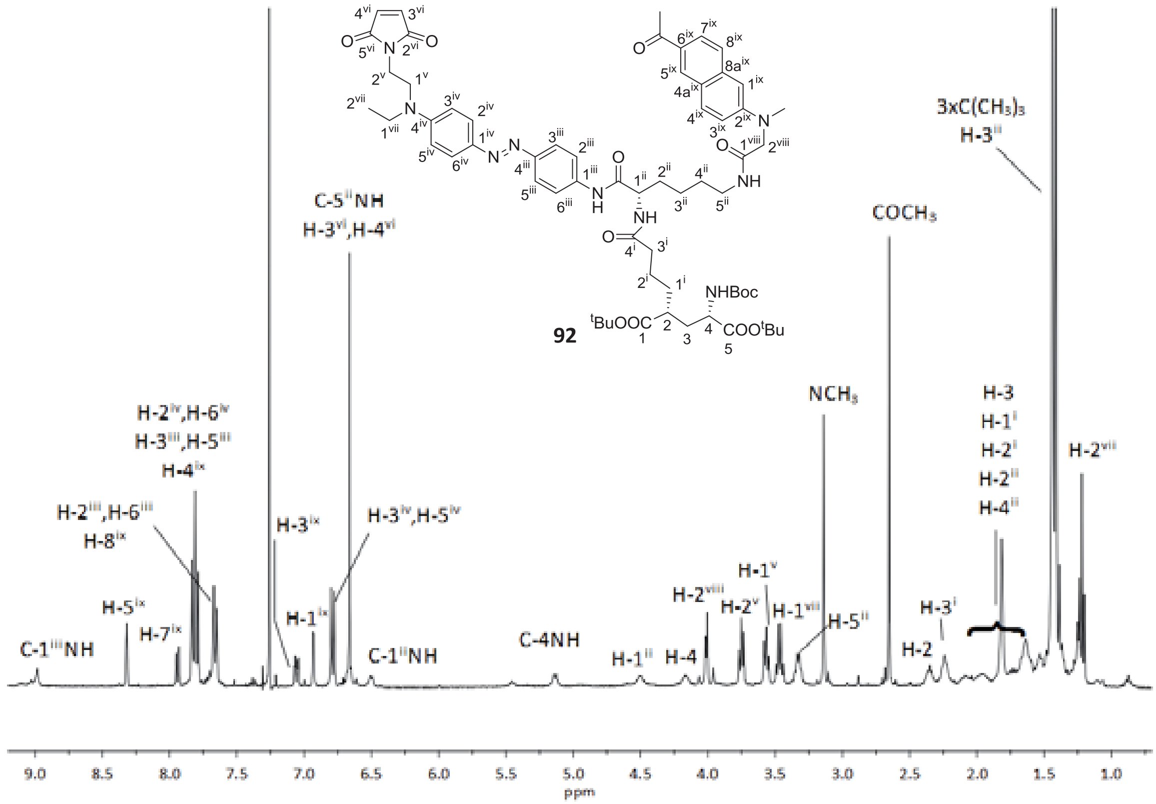

^{1}**H-NMR** (400 MHz, CDCl$_3$)

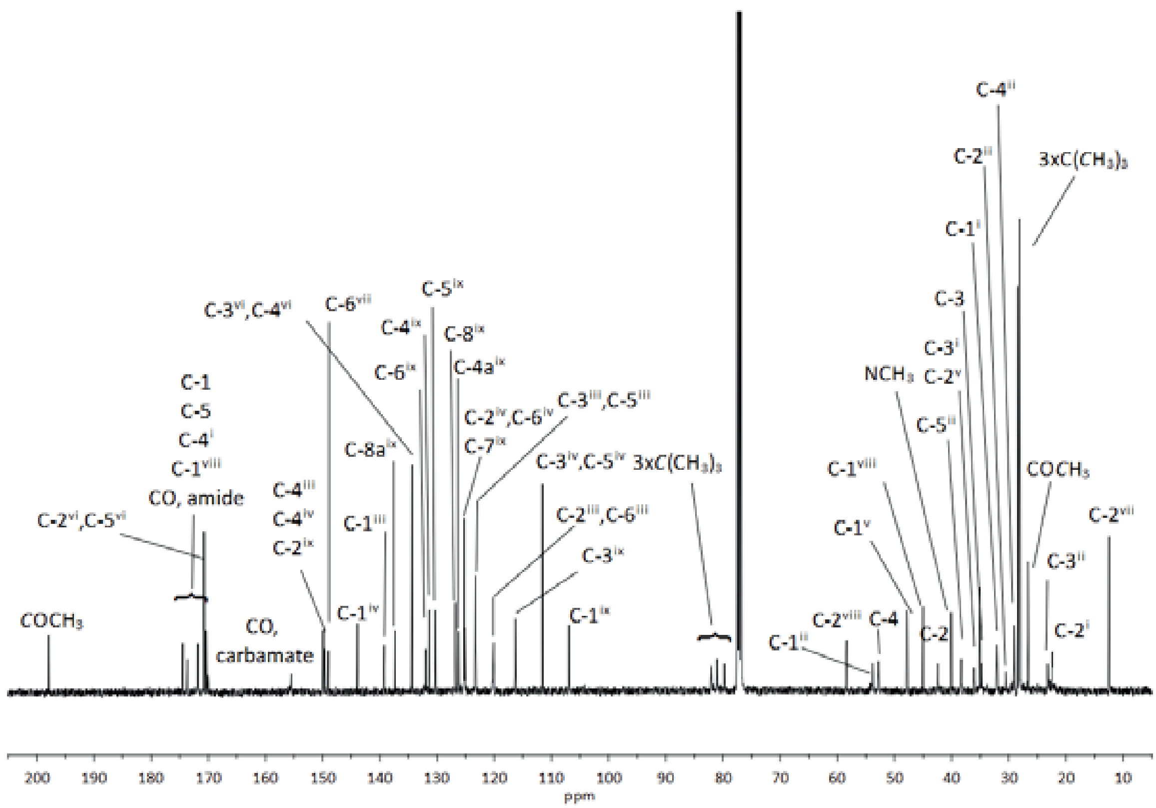

^{13}**C-NMR** (100.6 MHz, CDCl$_3$)

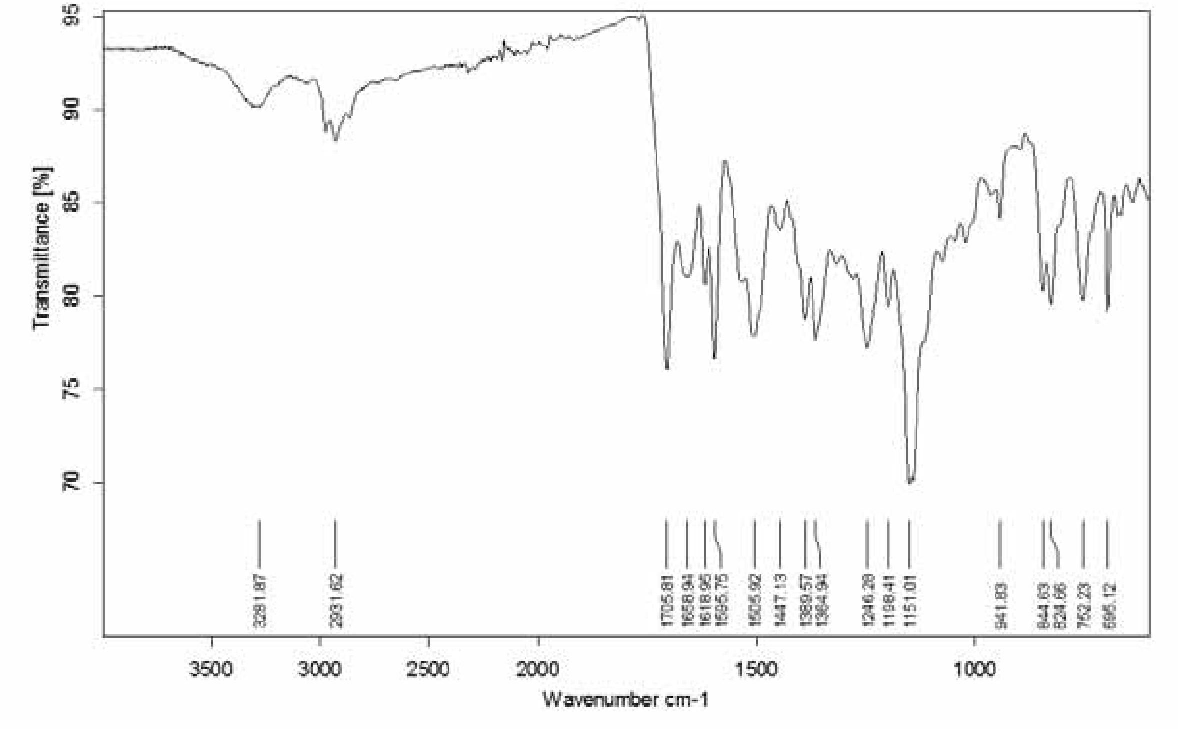

IR (ATR)

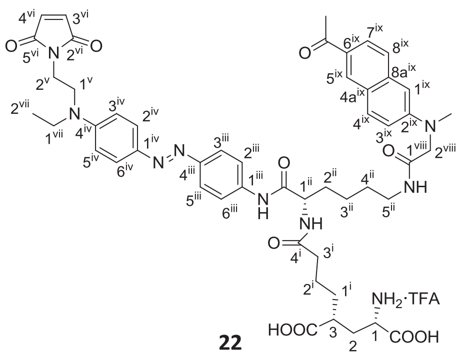

22

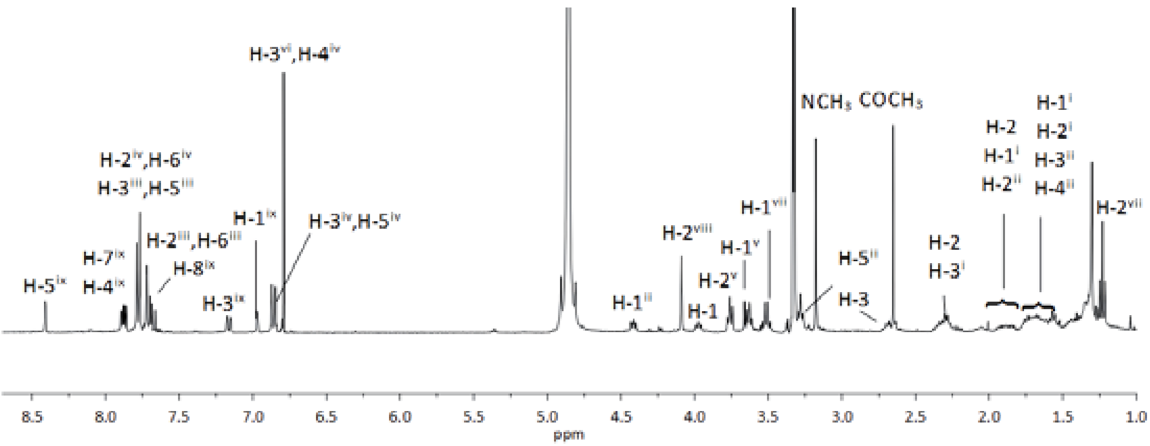

^{1}H-NMR (400 MHz, MeOH-d$_4$)

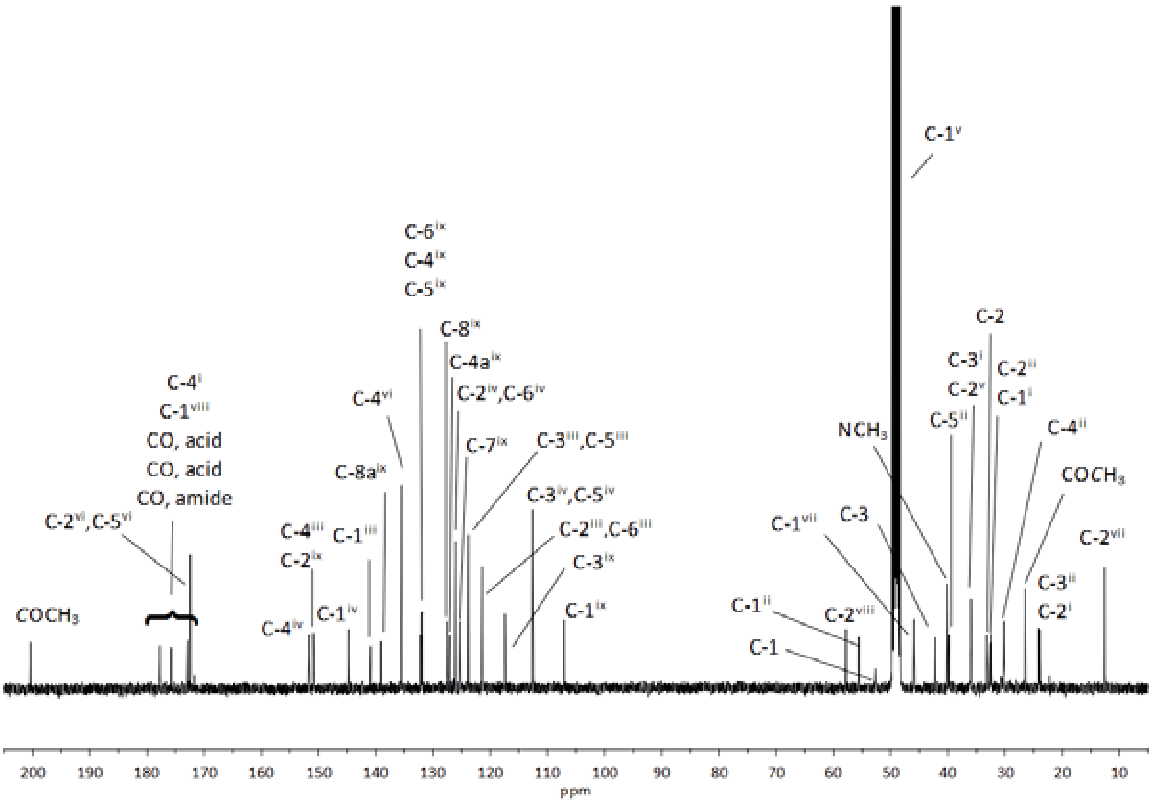

^{13}C-NMR (100.6 MHz, MeOH-d_4)

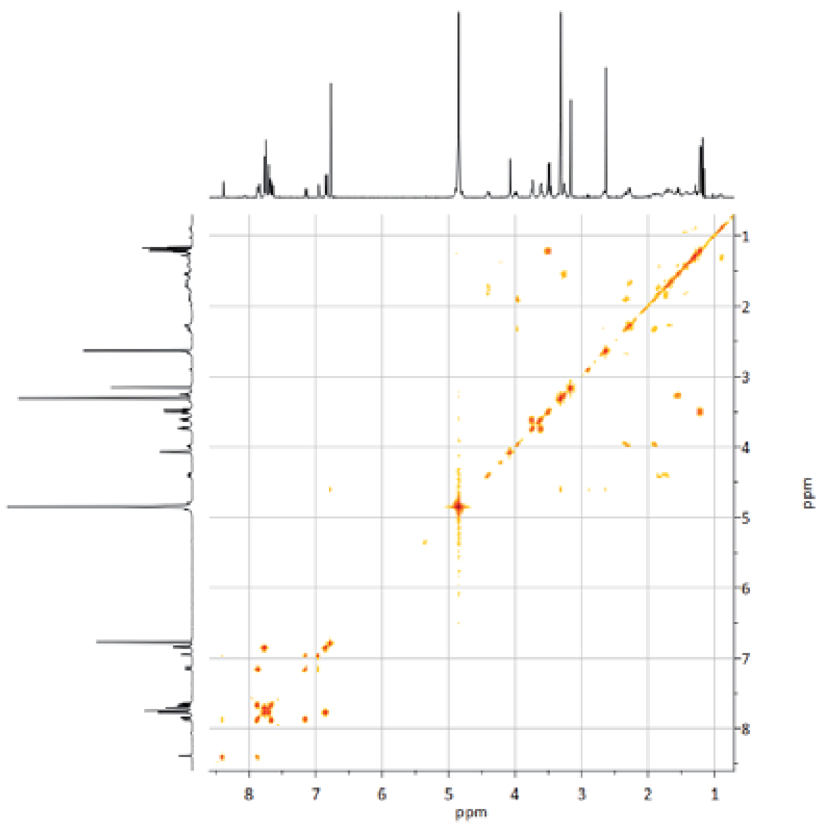

COSY (400 MHz, MeOH-d_4)

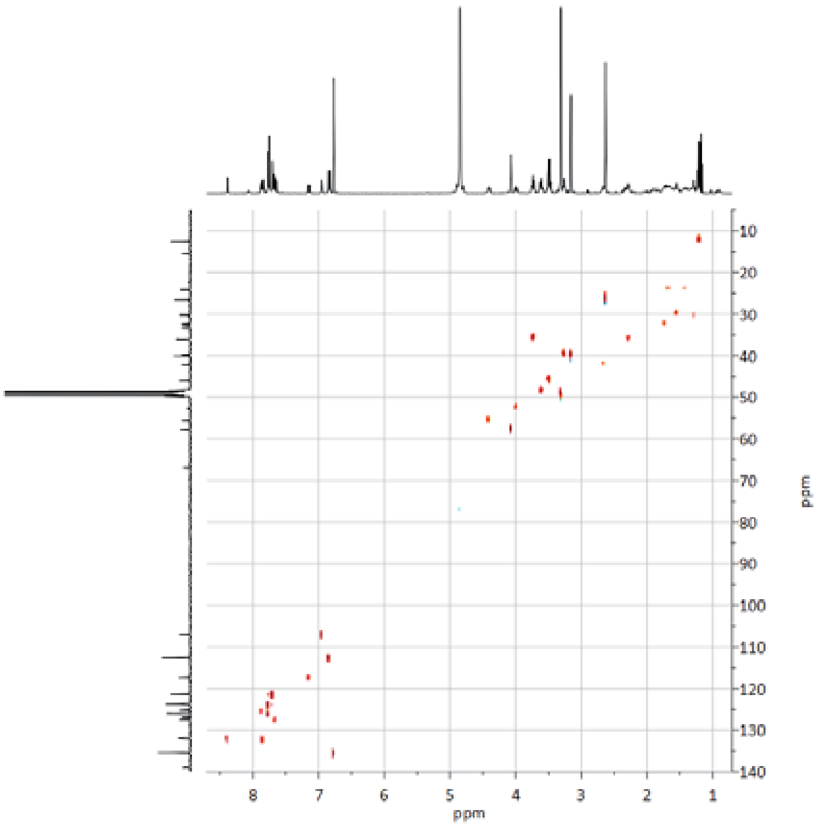

HSQC (400 MHz, MeOH-d4)

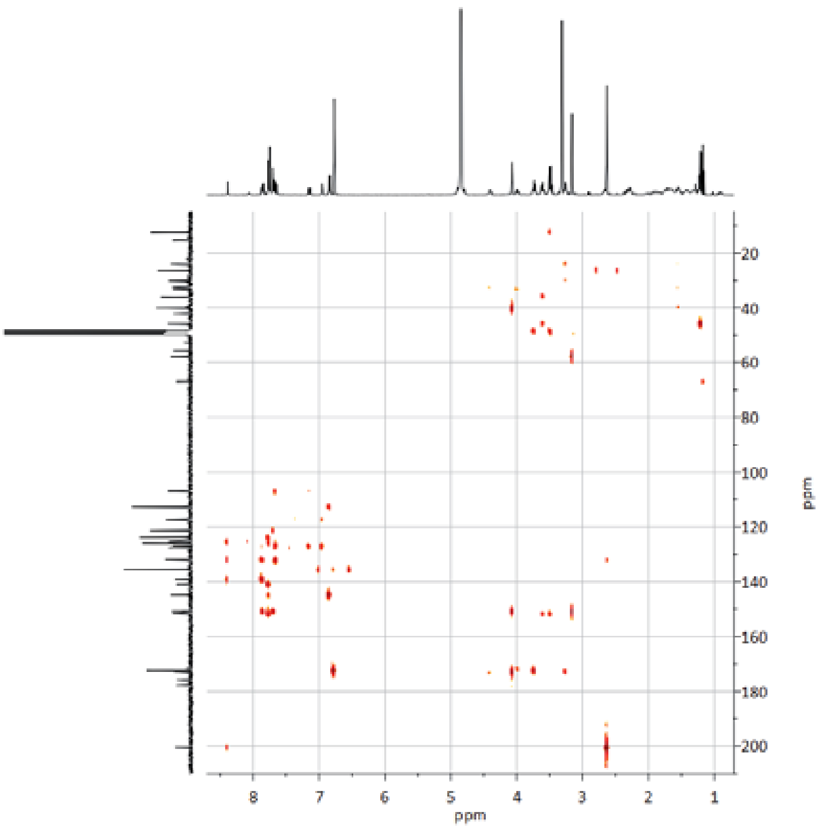

HMBC (400 MHz, MeOH-d4)

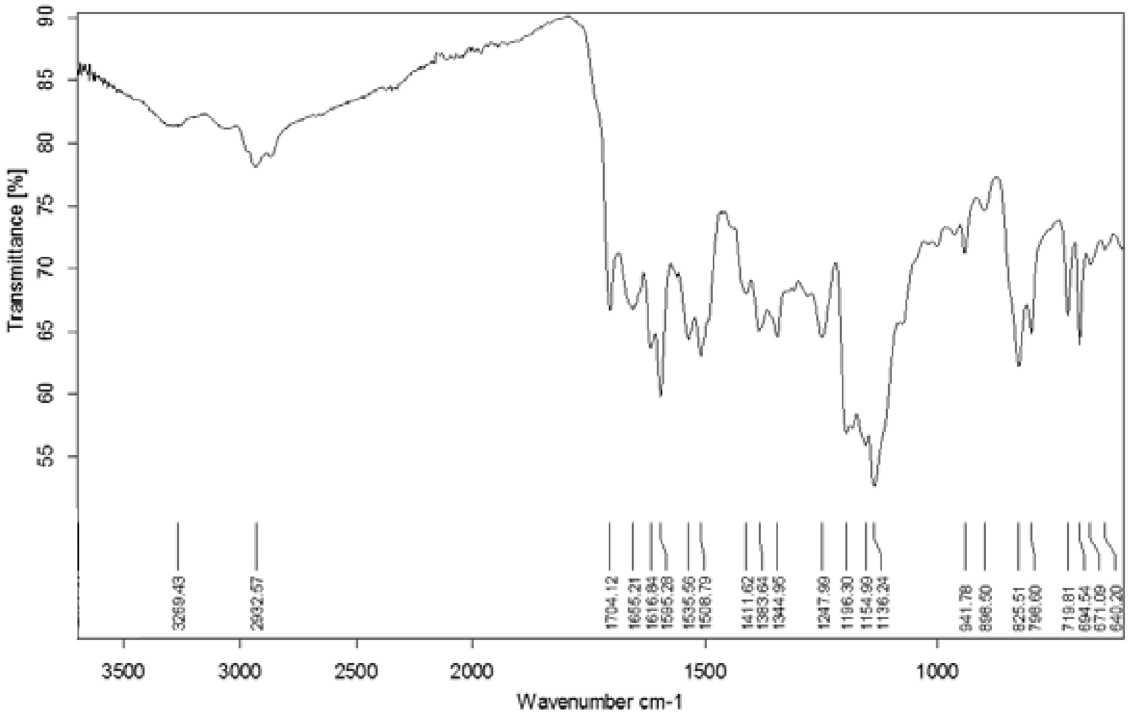

IR (ATR)

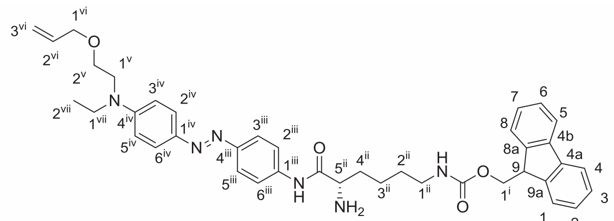

96

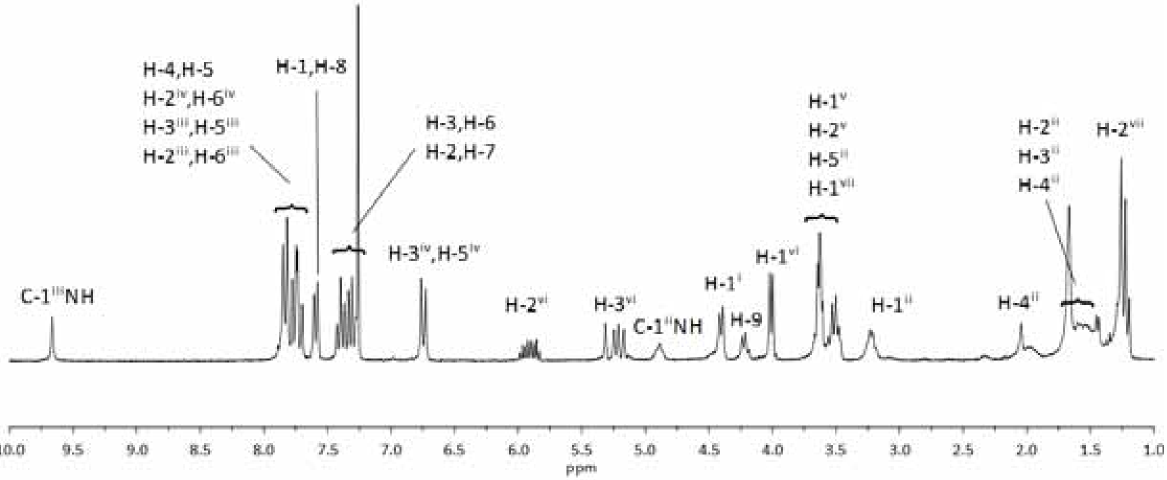

^{1}H-NMR (250 MHz, $CDCl_3$)

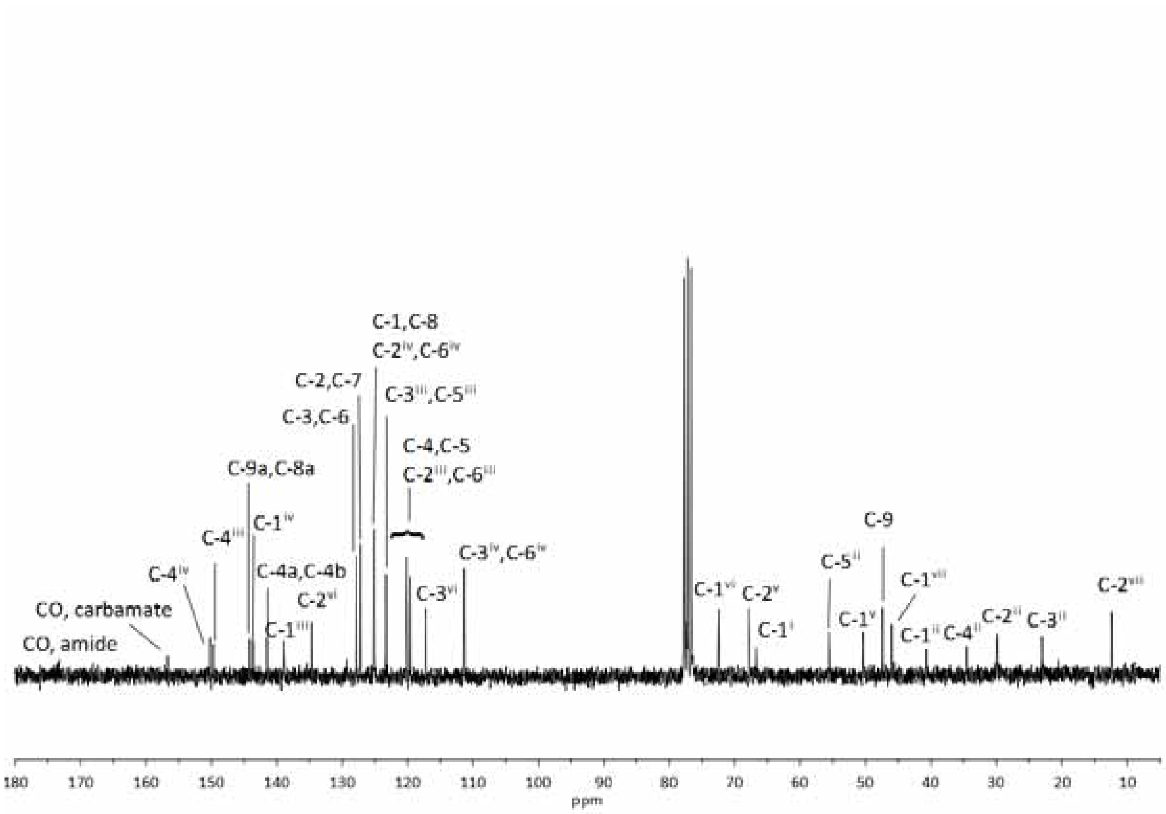

^{13}C-NMR (62.5 MHz, $CDCl_3$)

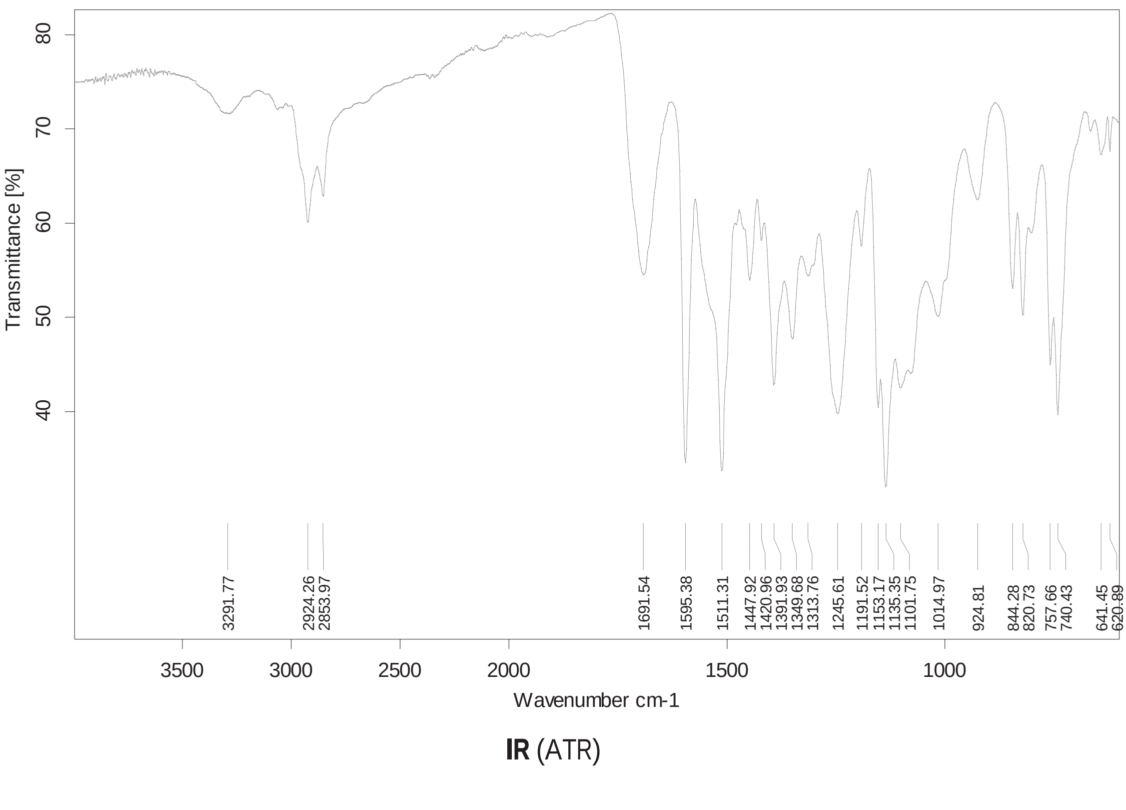

IR (ATR)

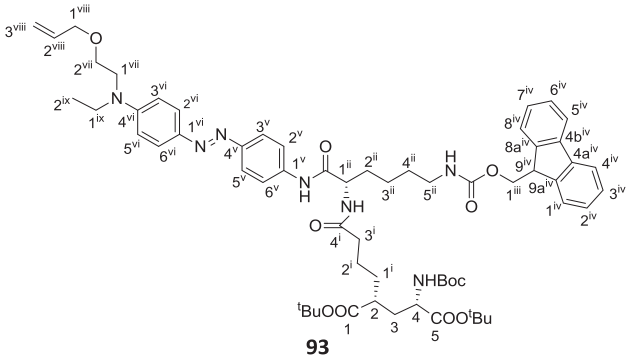

93

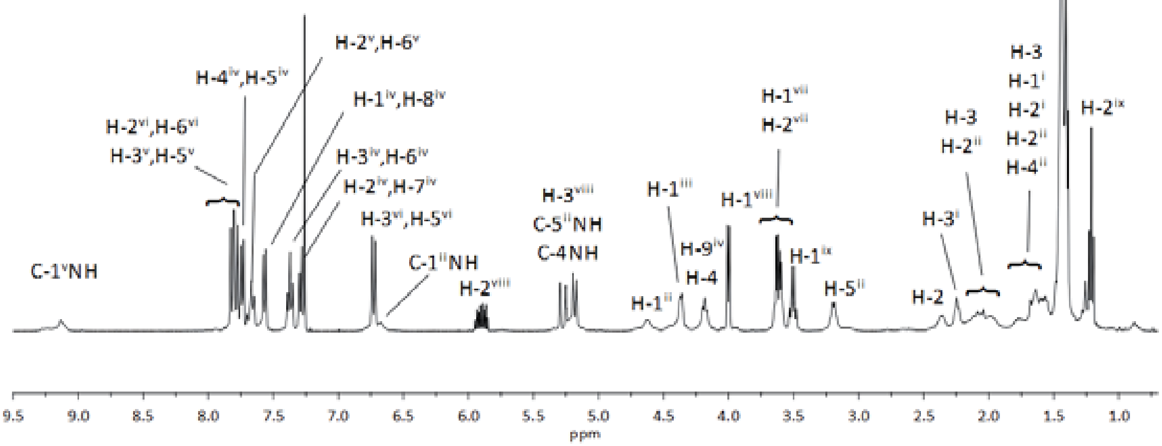

^{1}H-NMR (400 MHz, $CDCl_3$)

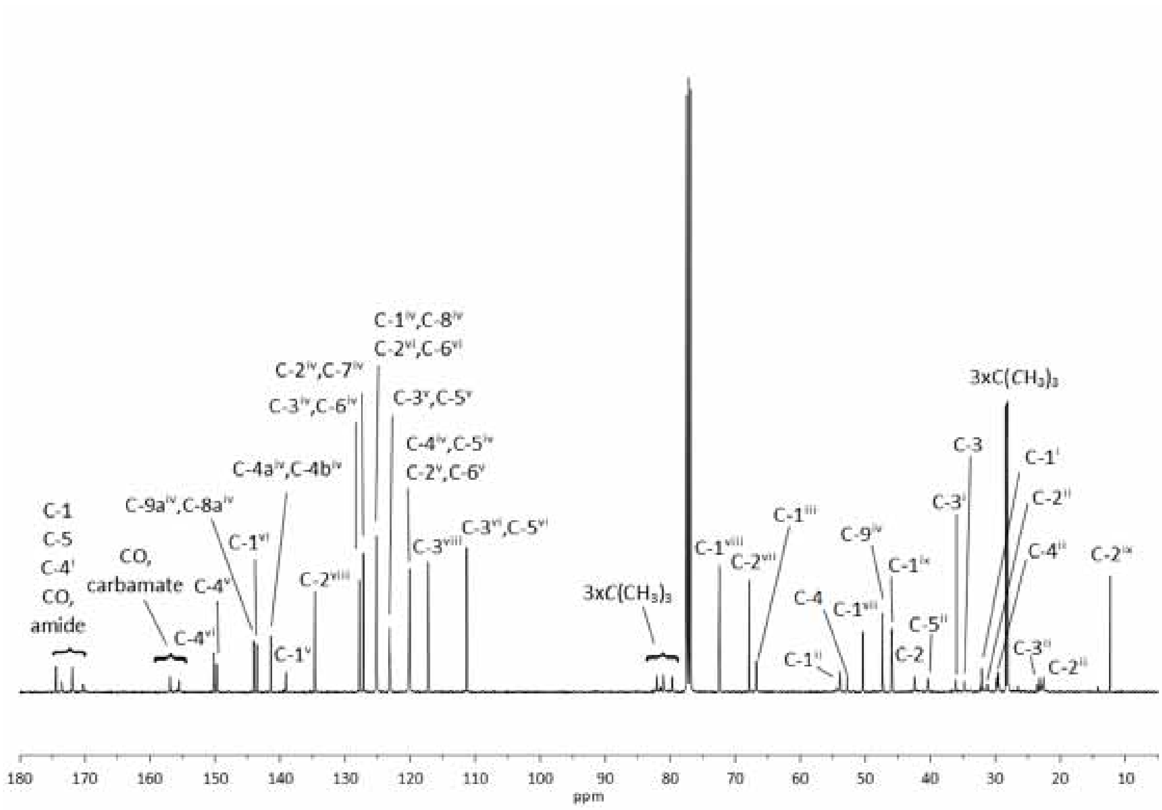

^{13}C-NMR (100.6 MHz, $CDCl_3$)

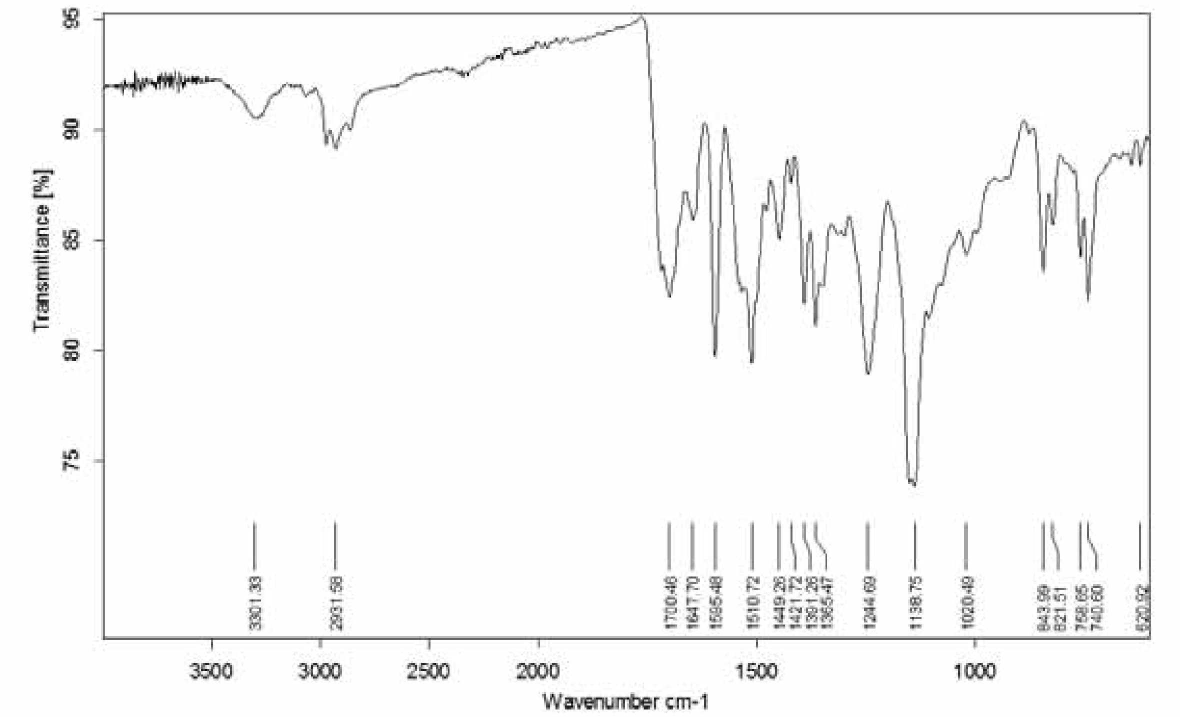

IR (ATR)

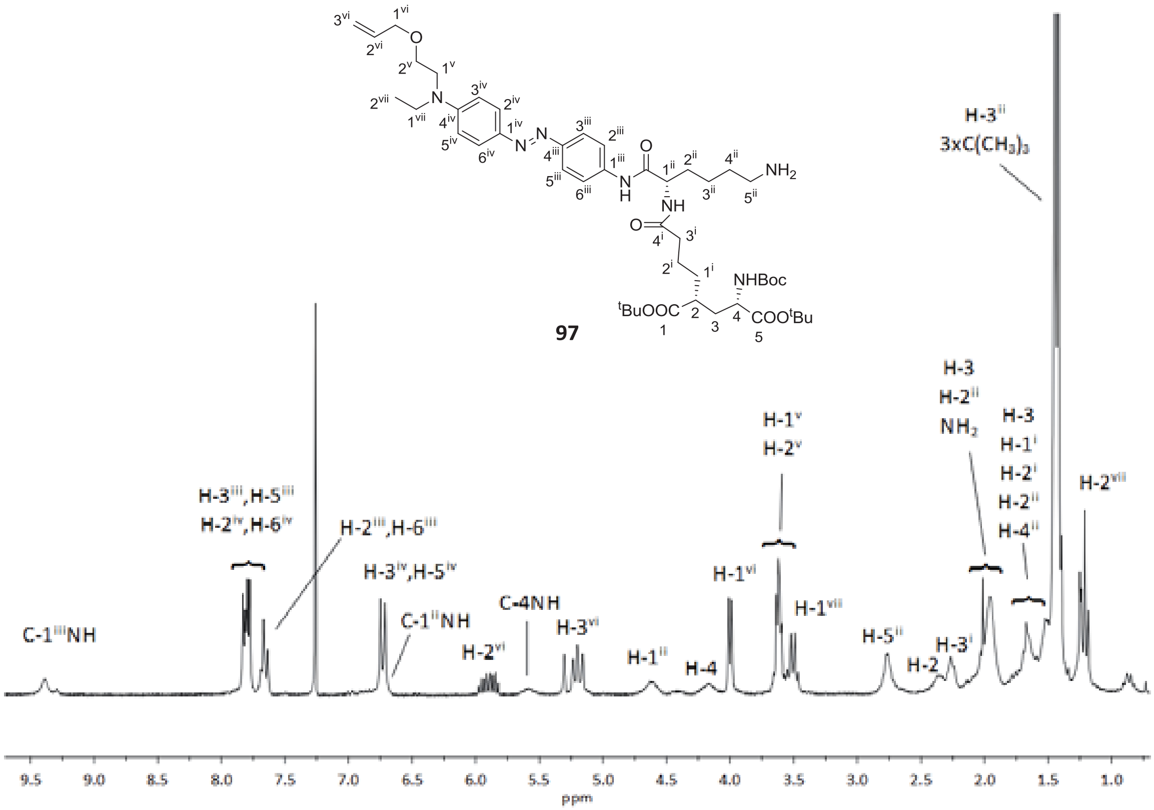

^{1}H-NMR (250 MHz, $CDCl_3$)

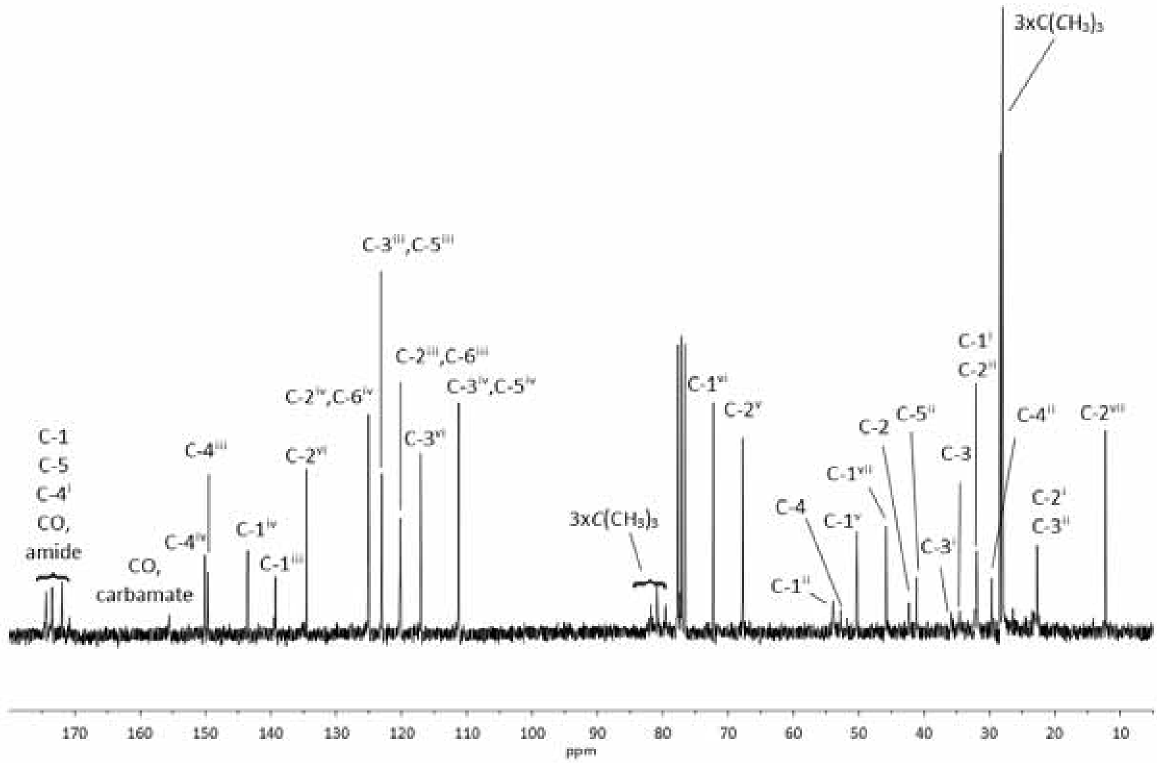

^{13}C-NMR (62.5 MHz, $CDCl_3$)

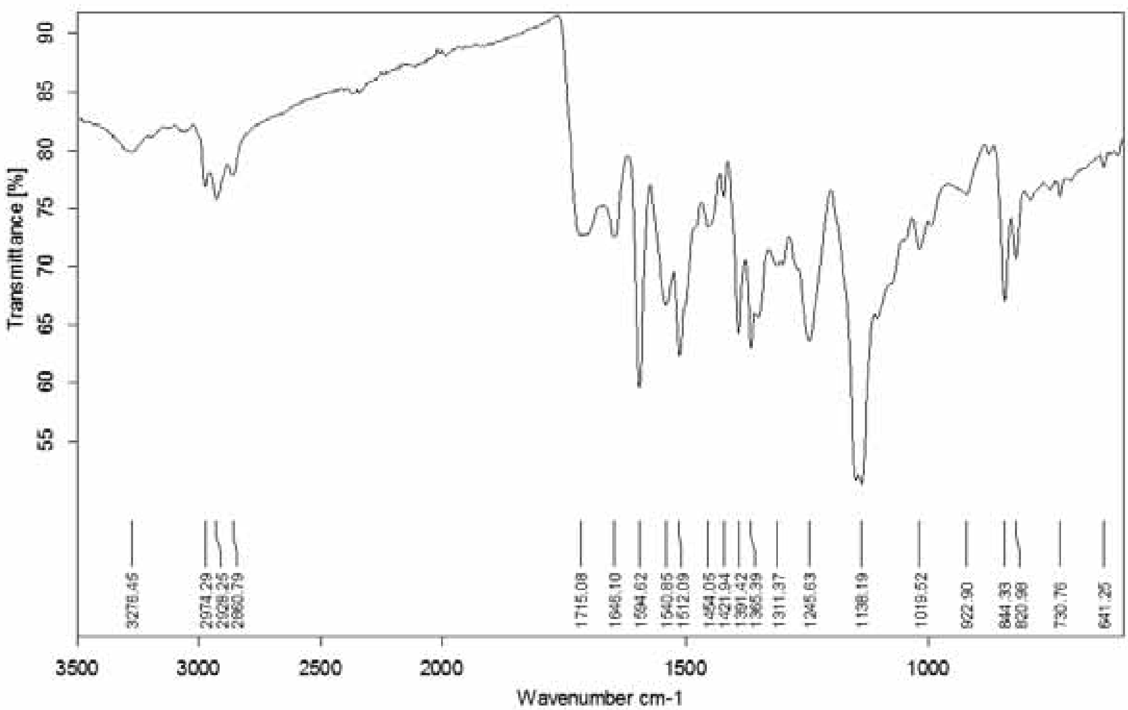

IR (ATR)

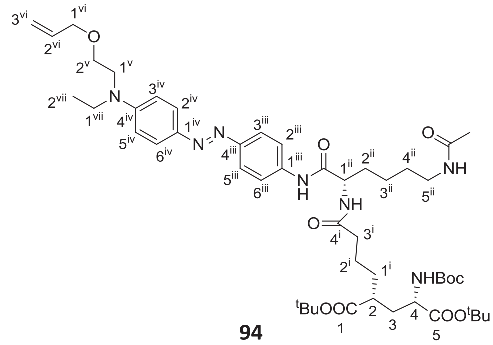

94

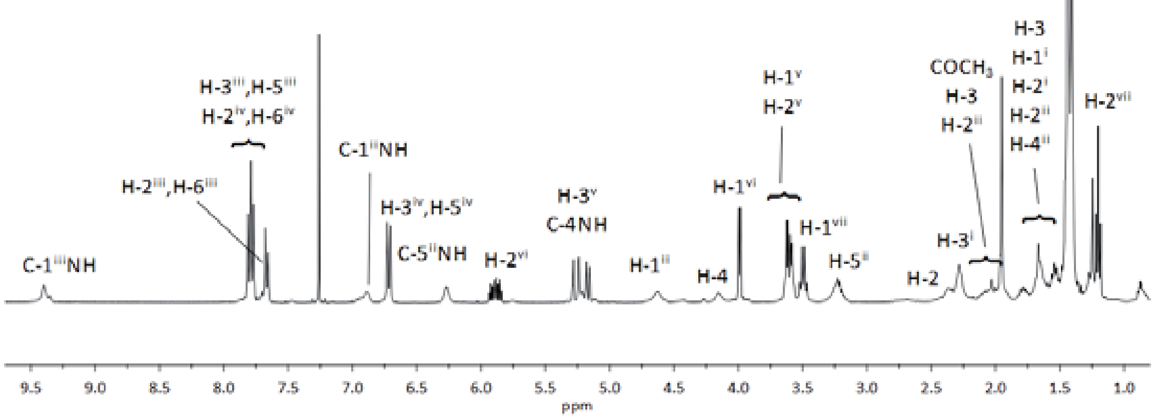

^{1}H-NMR (400 MHz, $CDCl_3$)

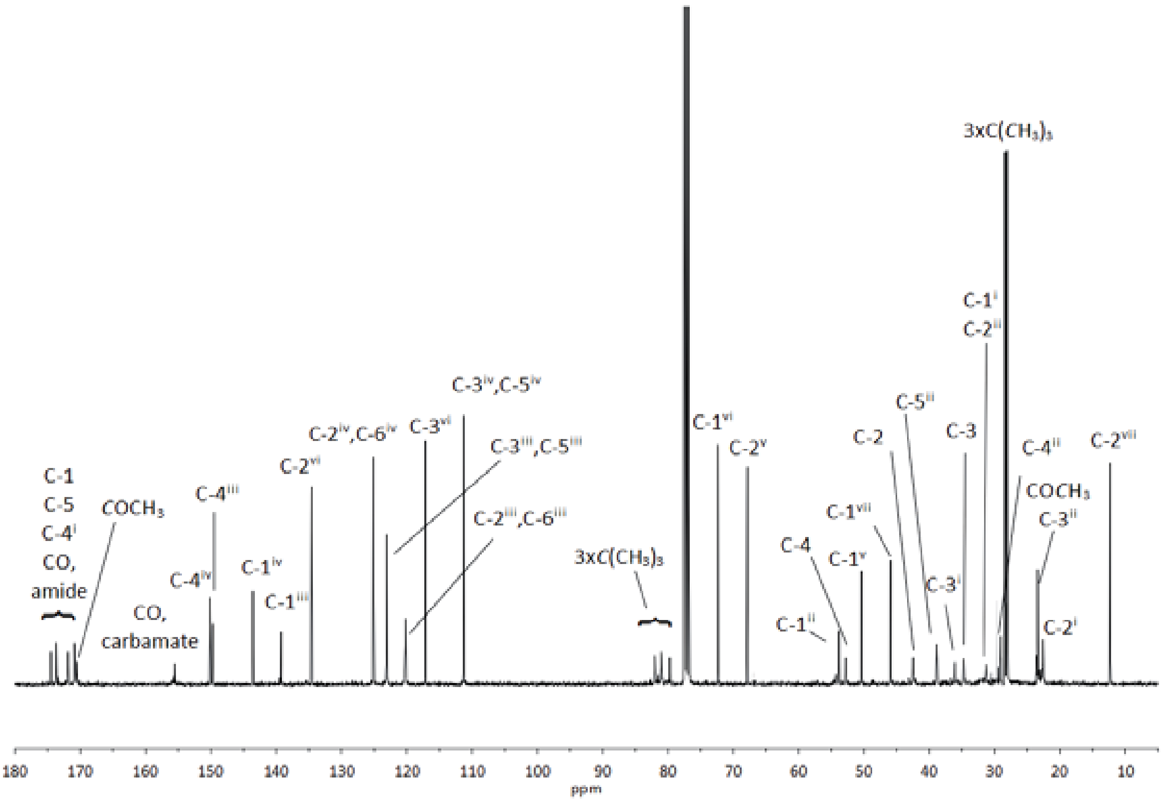

^{13}C-NMR (100.6 MHz, $CDCl_3$)

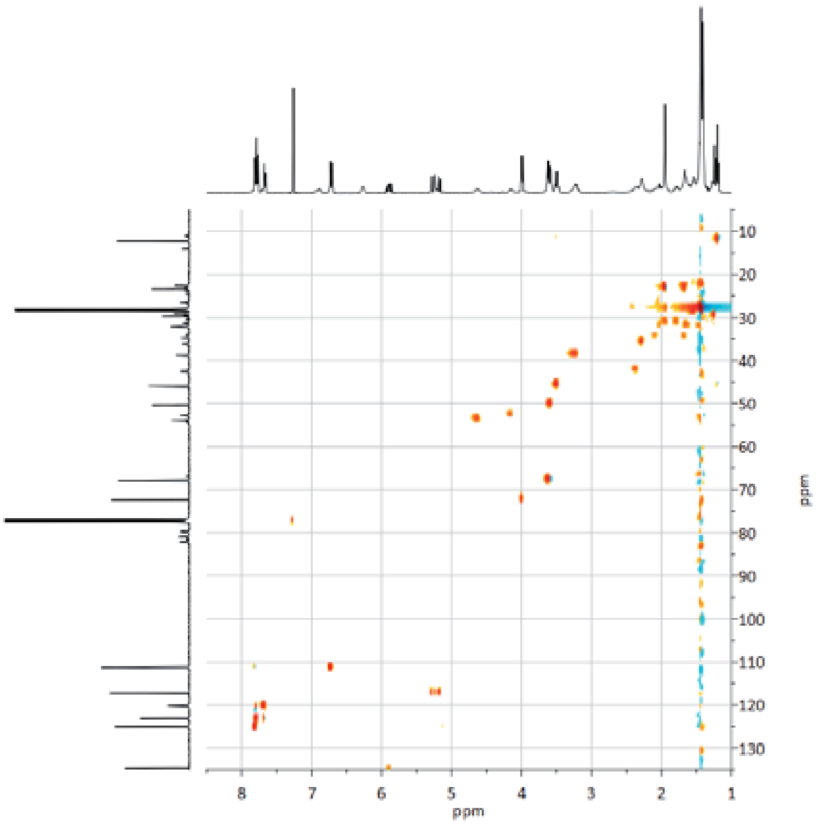

HSQC (400 MHz, $CDCl_3$)

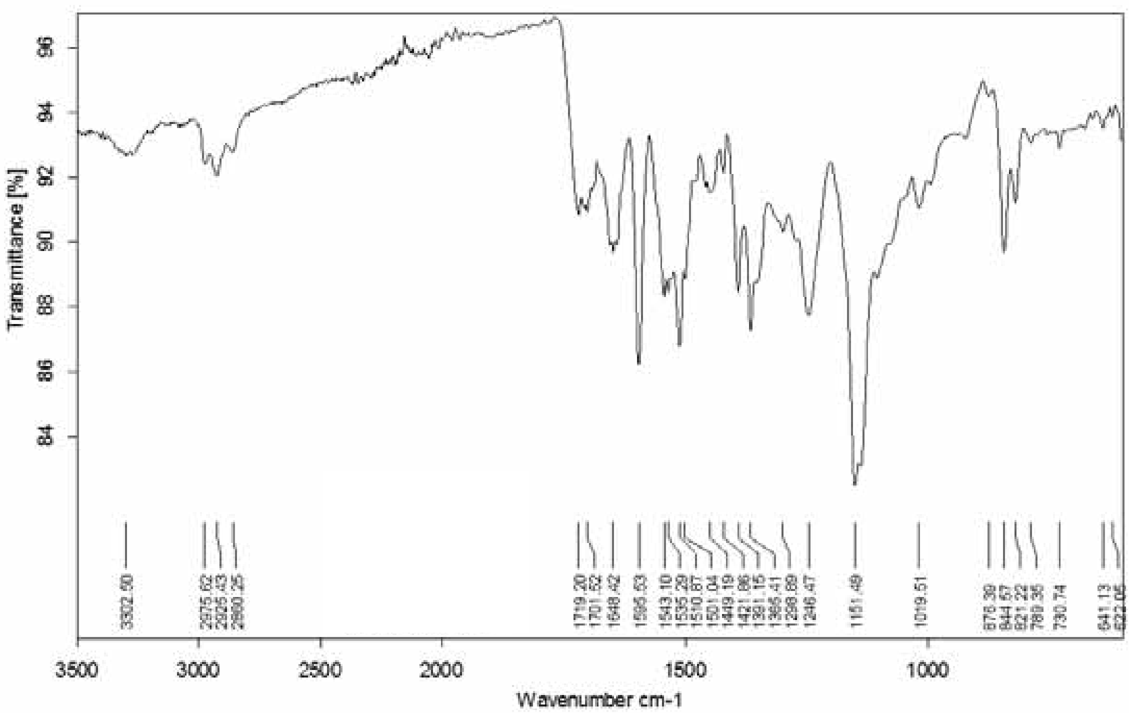

IR (ATR)

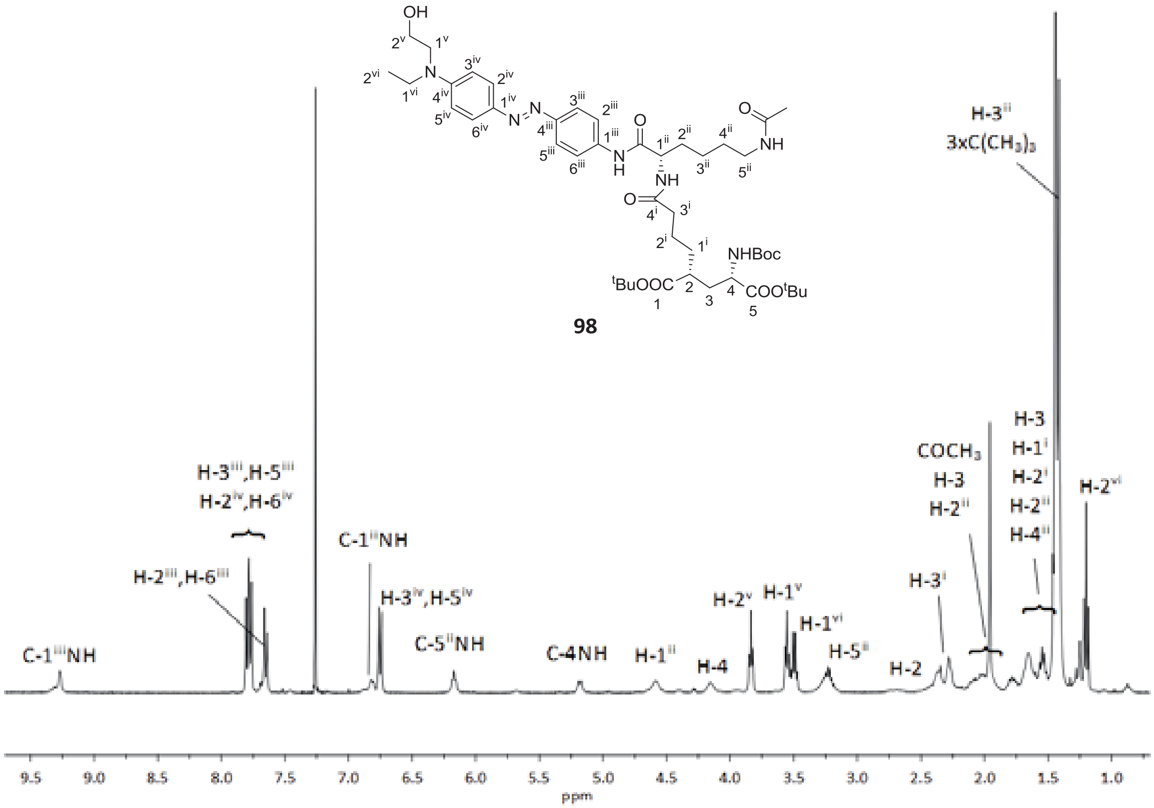

^{1}H-NMR (400 MHz, $CDCl_3$)

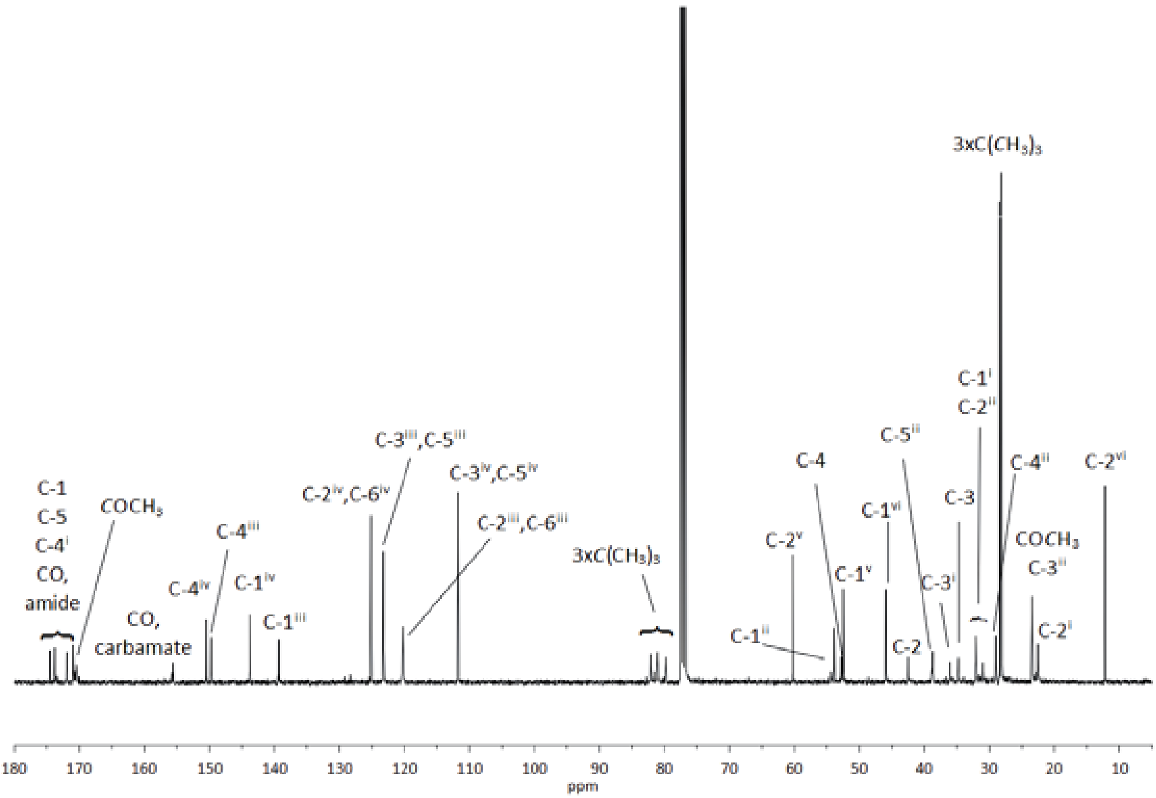

^{13}C-NMR (100.6 MHz, $CDCl_3$)

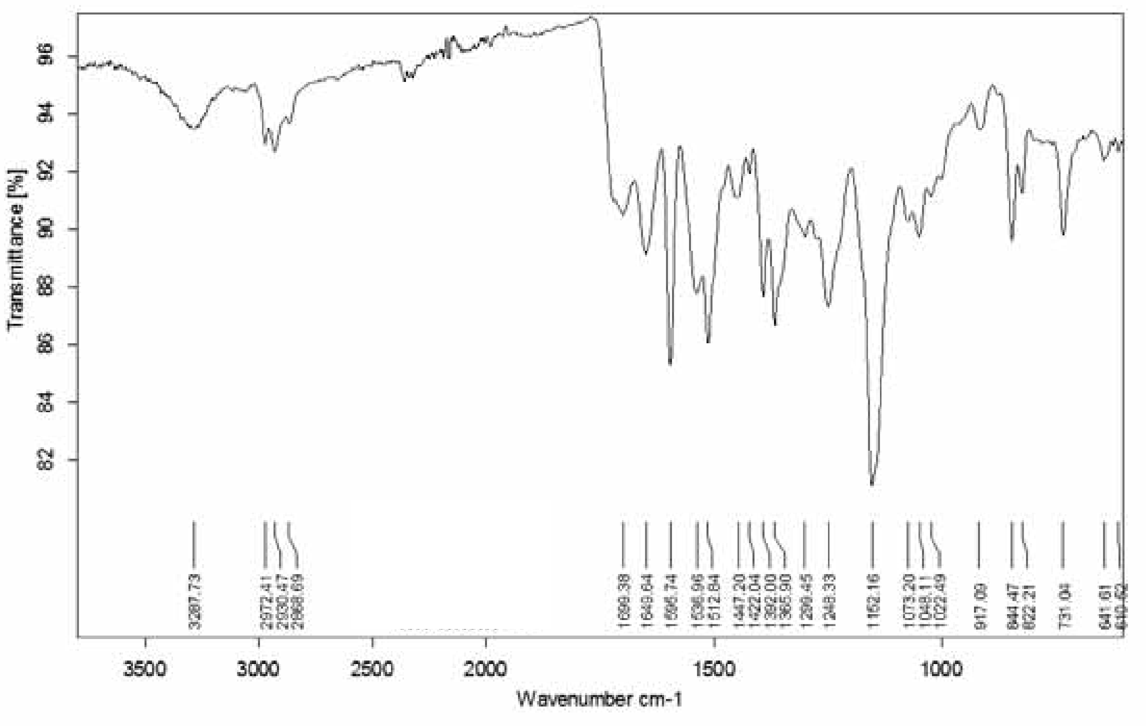

IR (ATR)

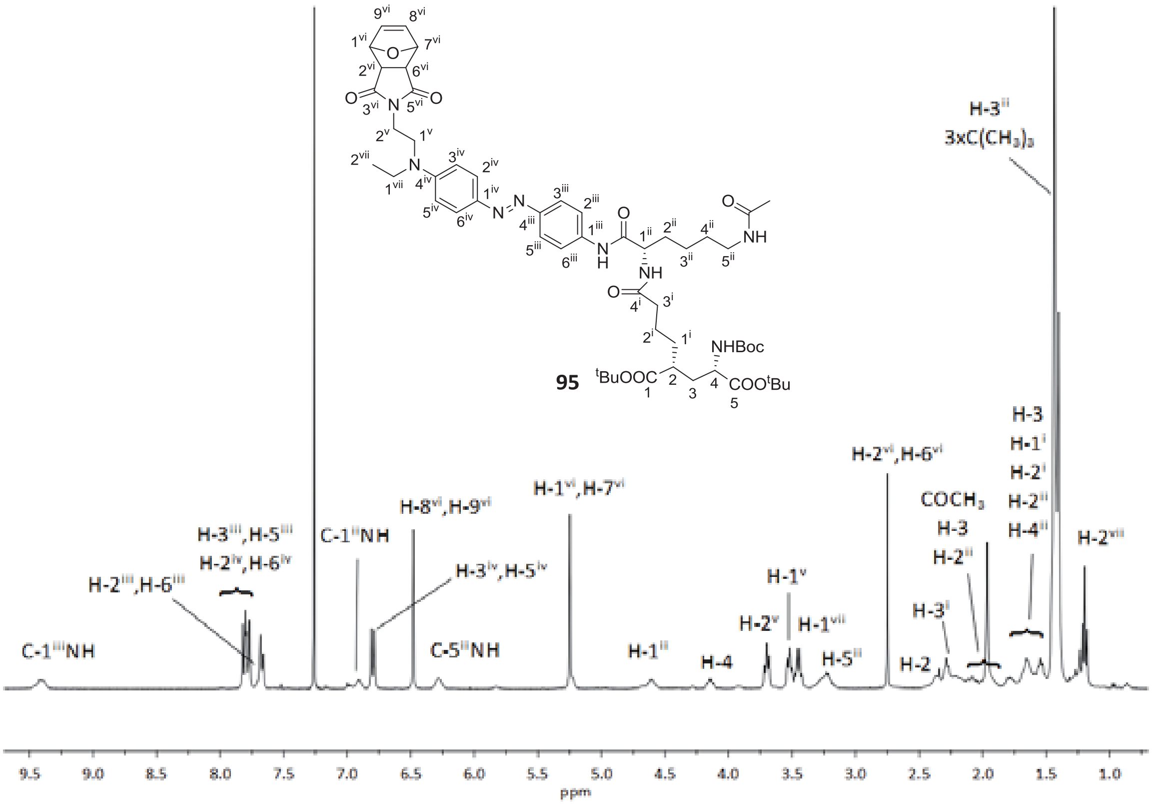

^{1}H-NMR (400 MHz, $CDCl_3$)

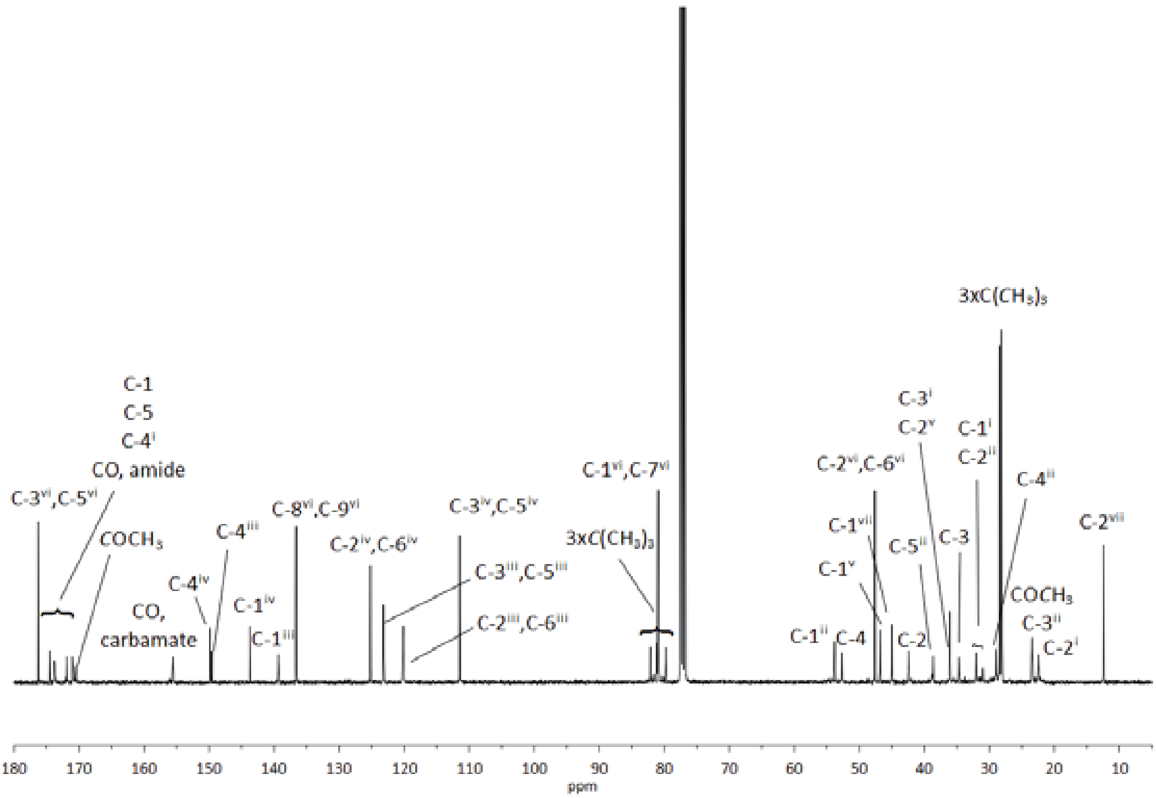

^{13}**C-NMR** (100.6 MHz, $CDCl_3$)

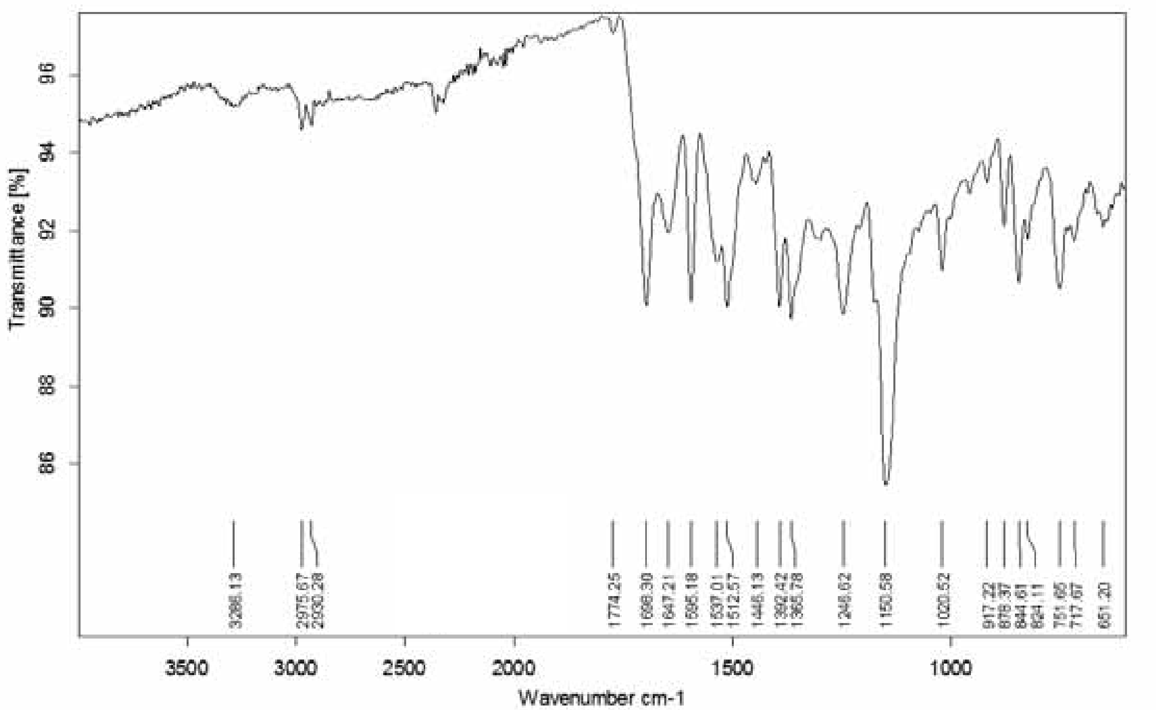

IR (ATR)

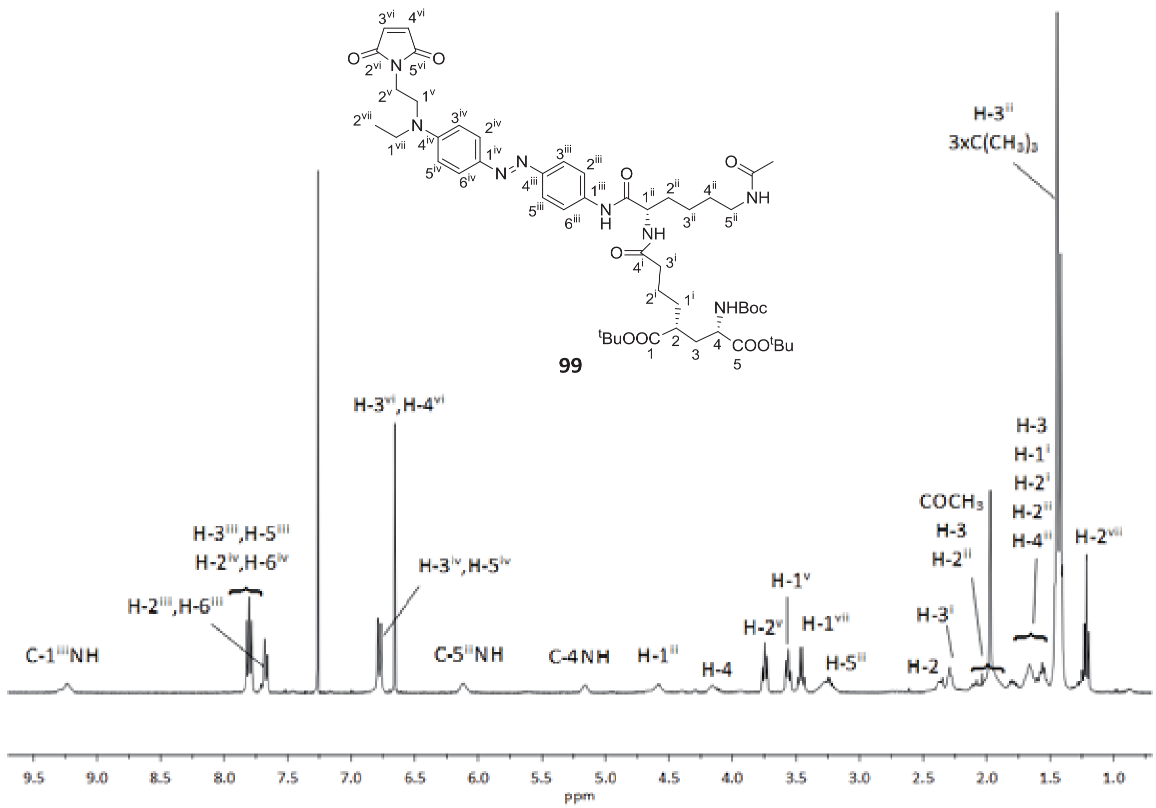

^{1}H-NMR (400 MHz, $CDCl_3$)

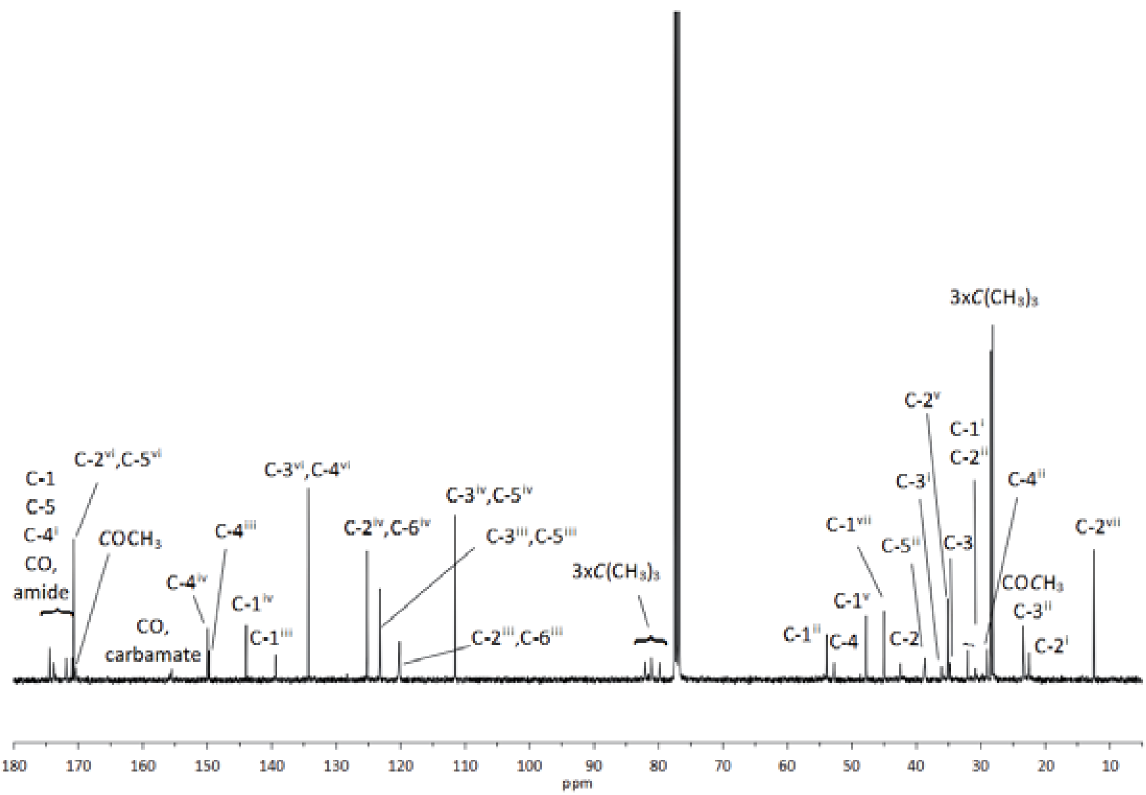

^{13}C-NMR (100.6 MHz, $CDCl_3$)

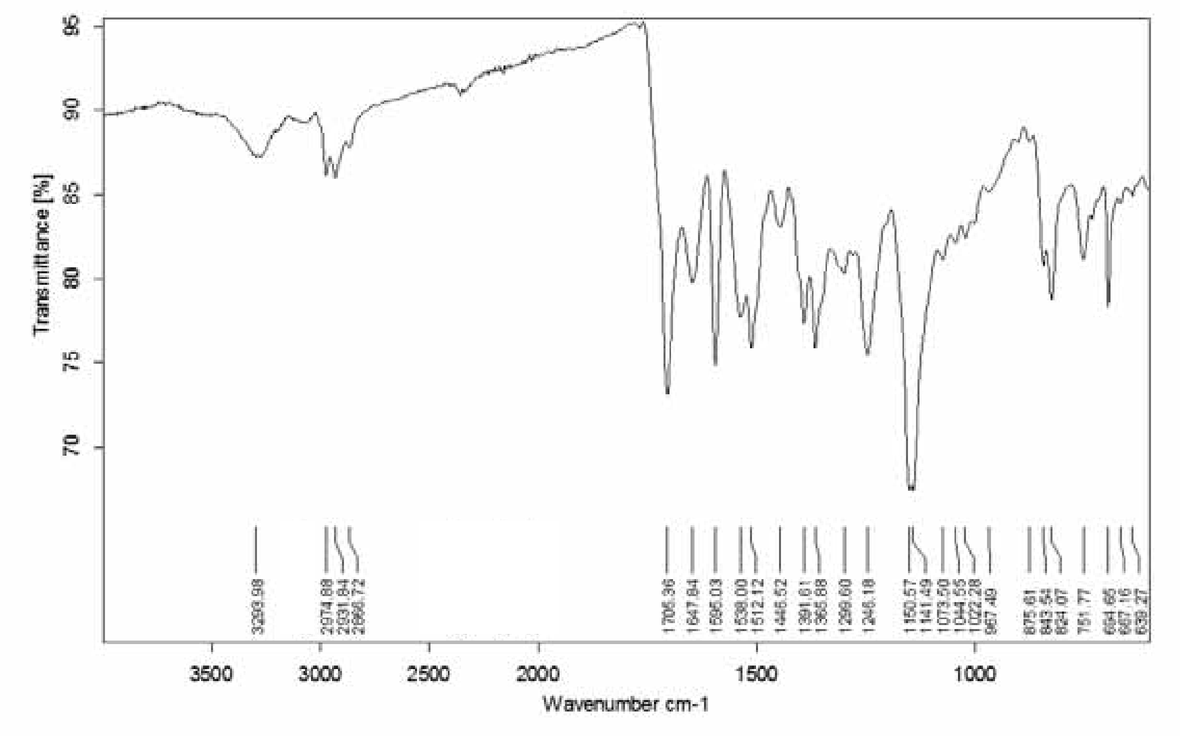

IR (ATR)

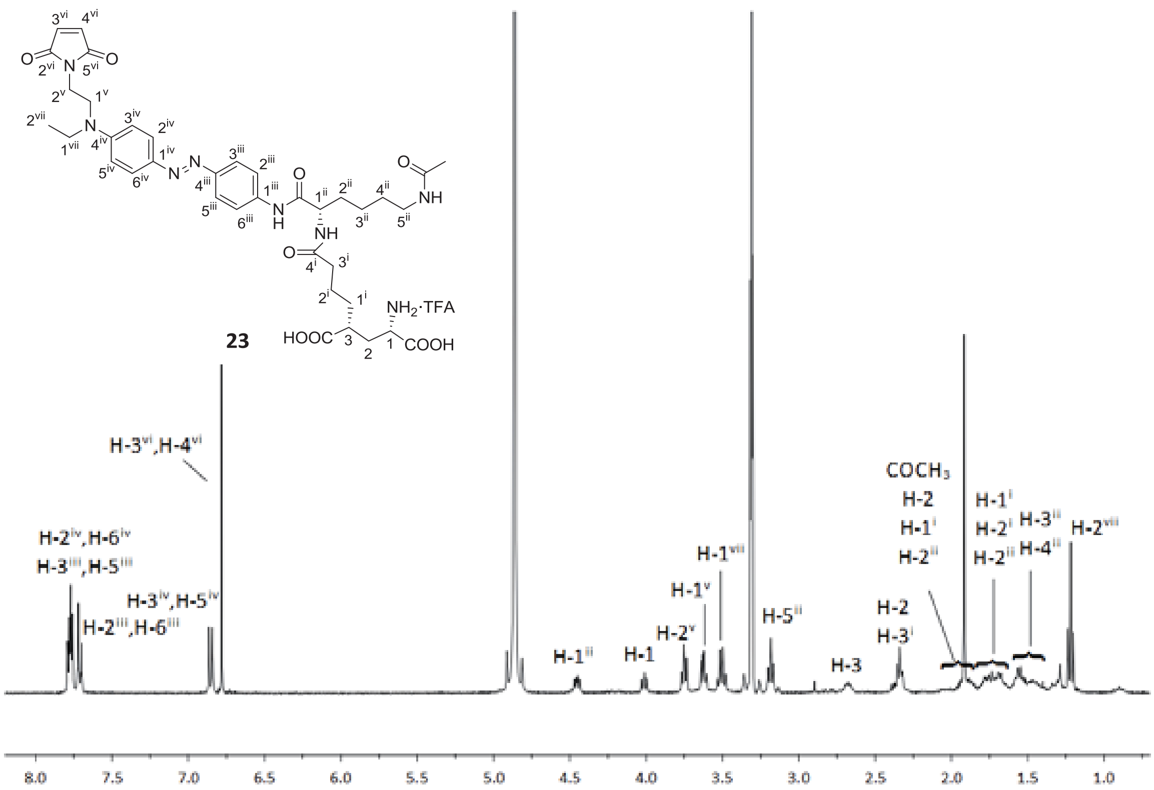

^{1}**H-NMR** (400 MHz, MeOH-d$_4$)

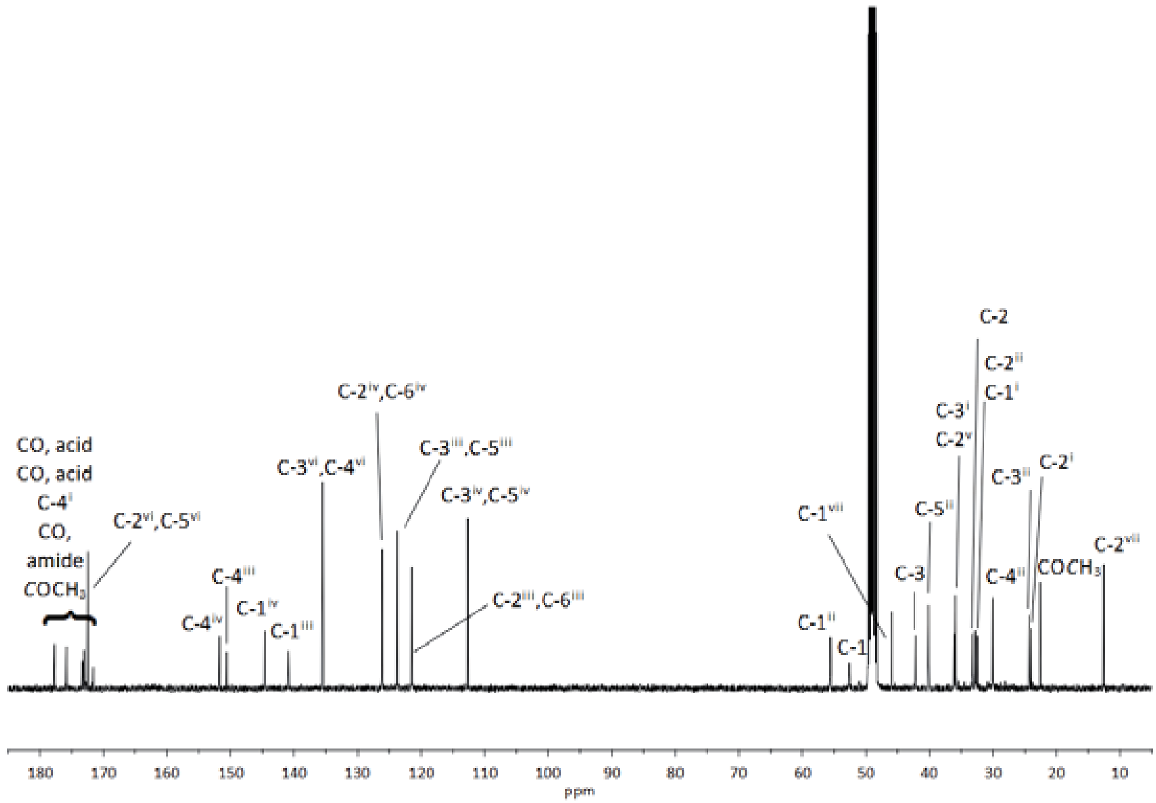

^{13}C-NMR (100.6 MHz, MeOH-d$_4$)

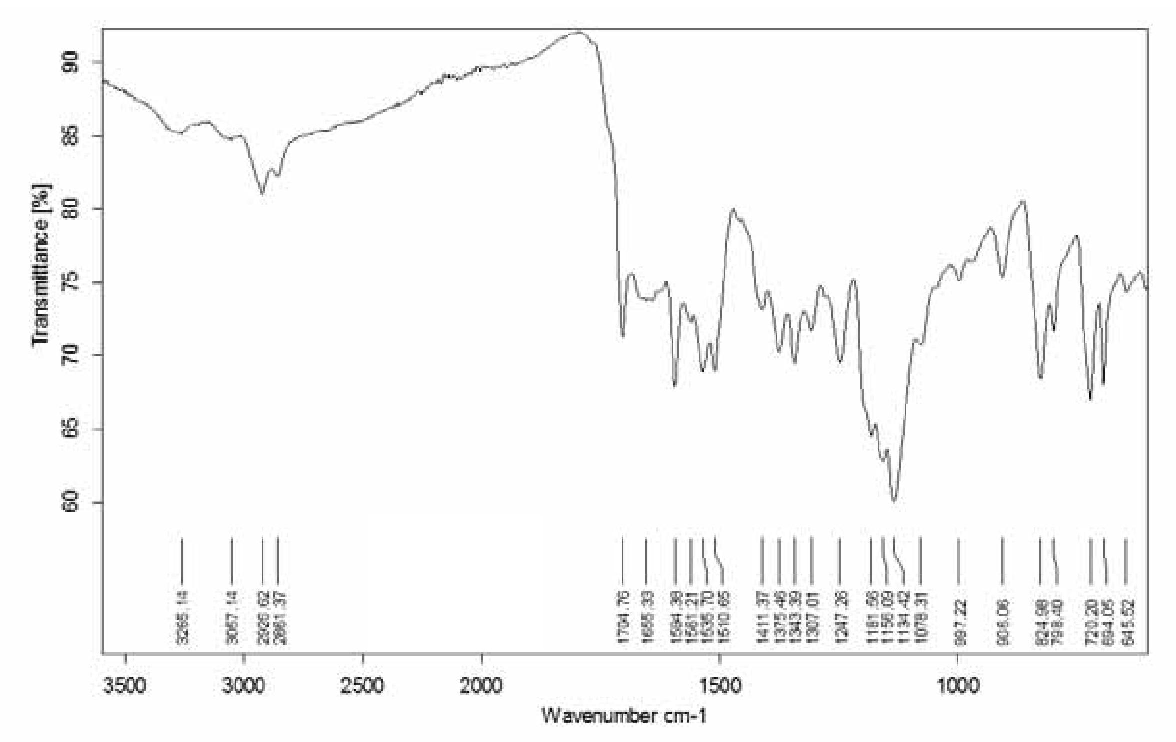

IR (ATR)

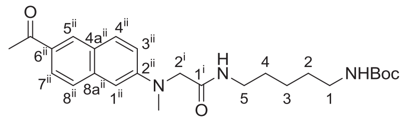

102

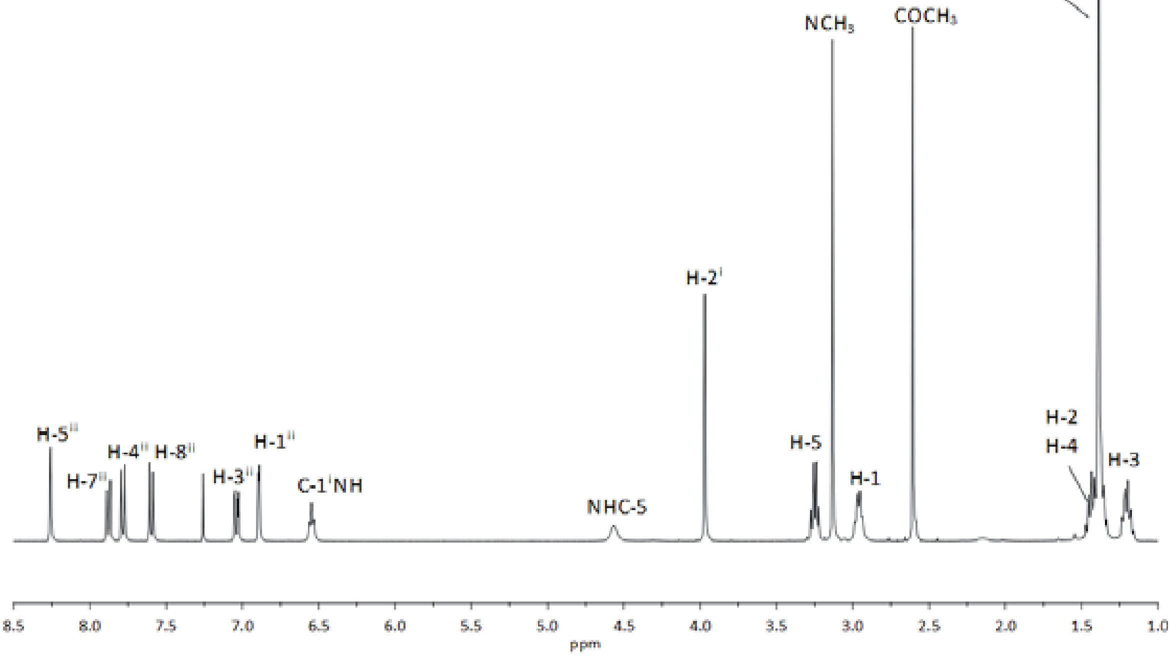

^{1}H-NMR (400 MHz, $CDCl_3$)

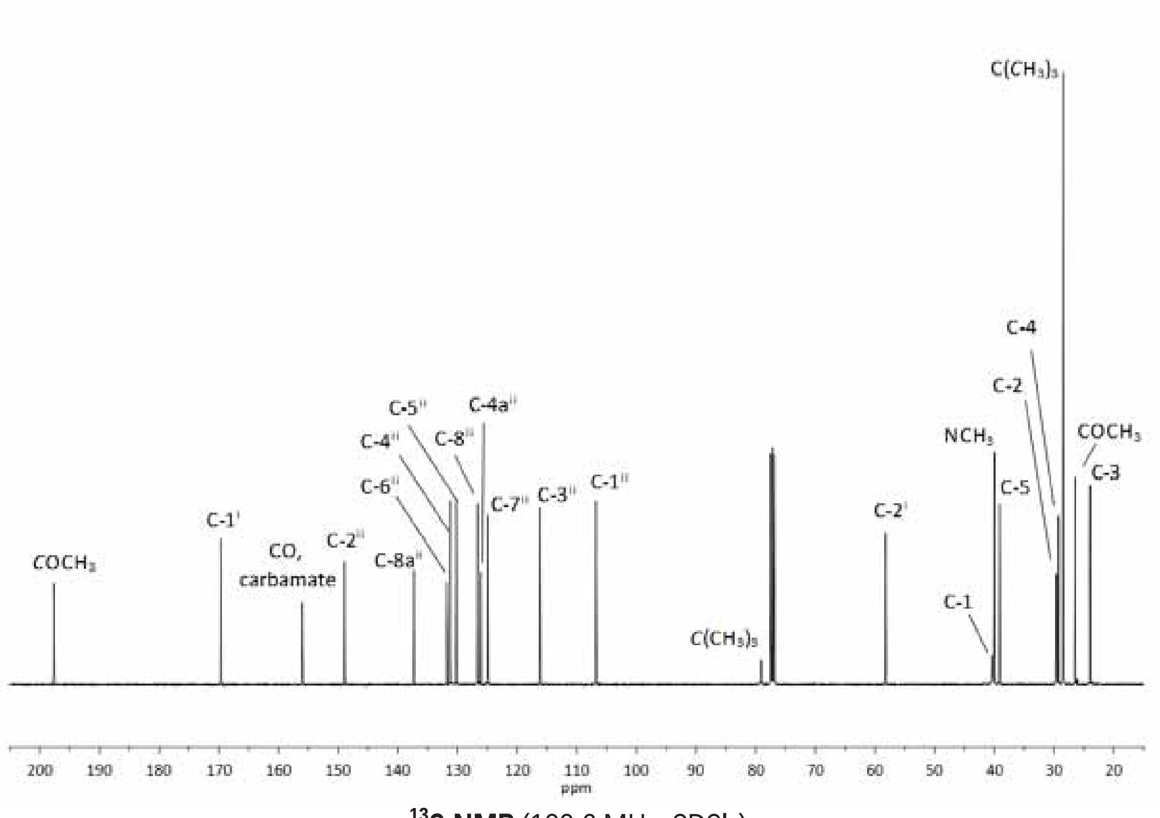

^{13}C-NMR (100.6 MHz, $CDCl_3$)

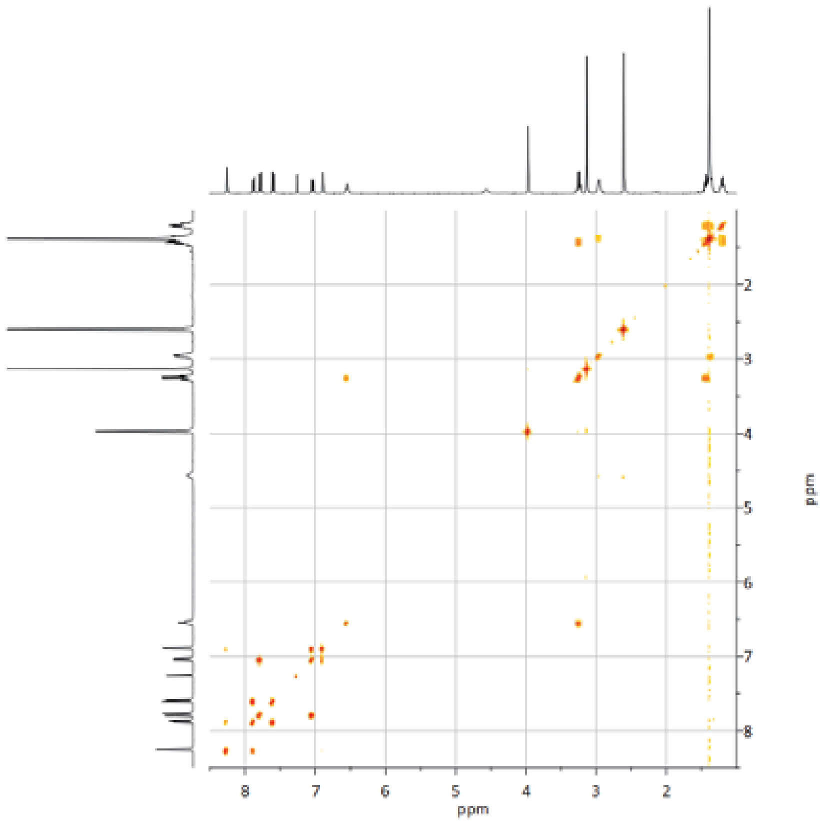

COSY (400 MHz, $CDCl_3$)

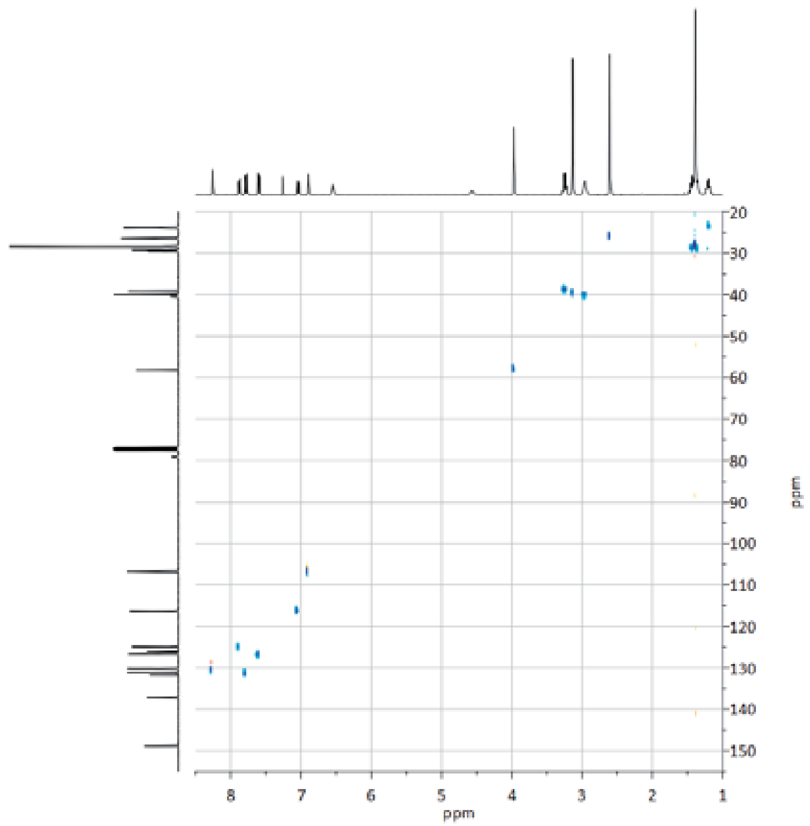

HSQC (400 MHz, $CDCl_3$)

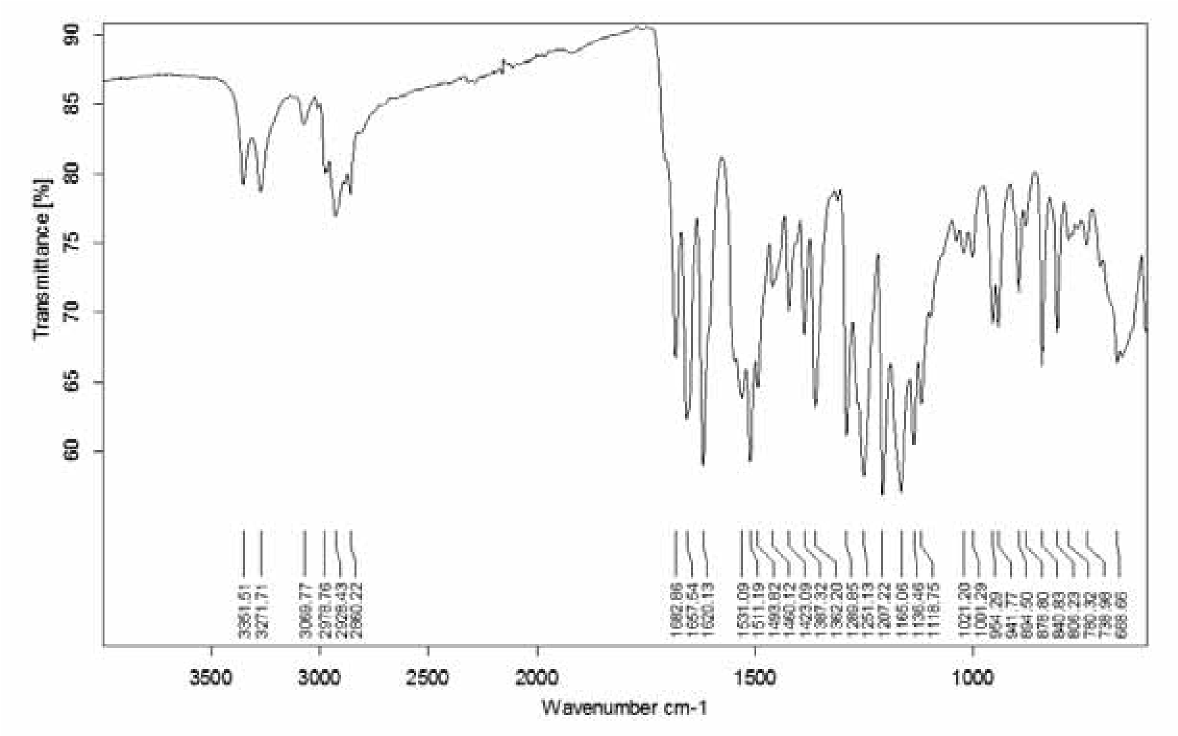

IR (ATR)

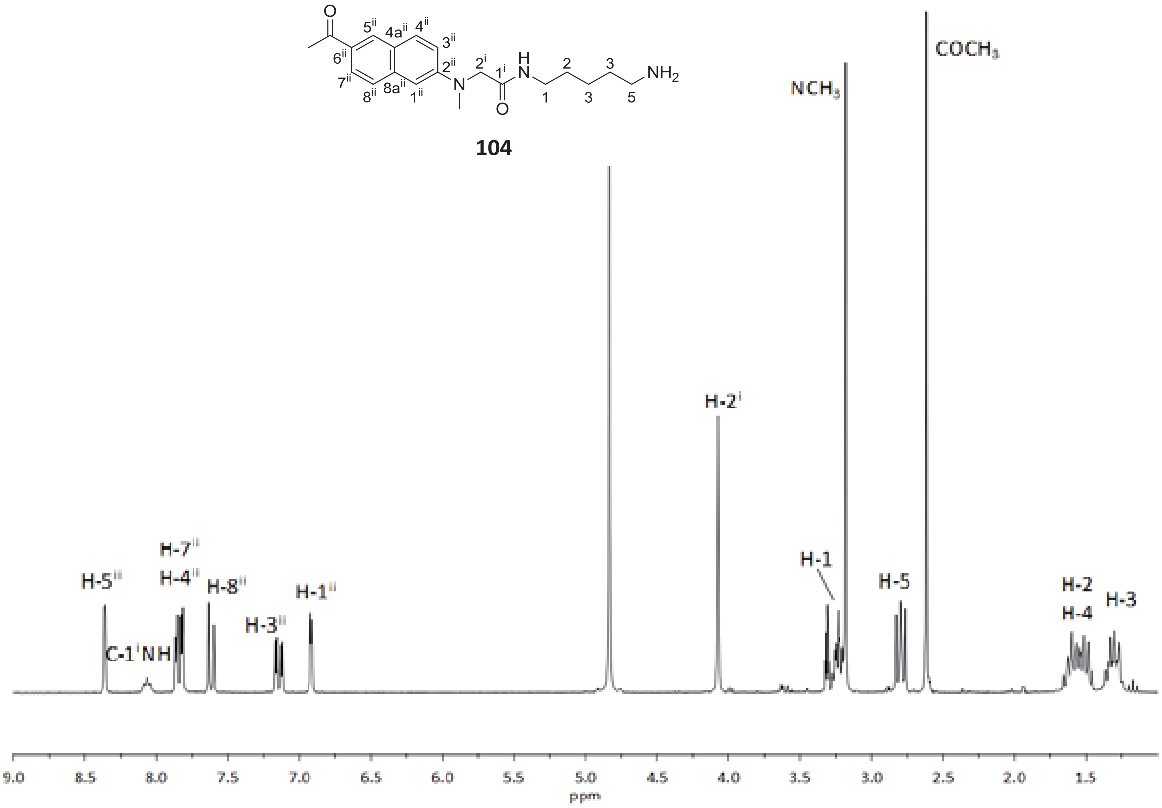

^{1}H-NMR (250 MHz, MeOH-d_4)

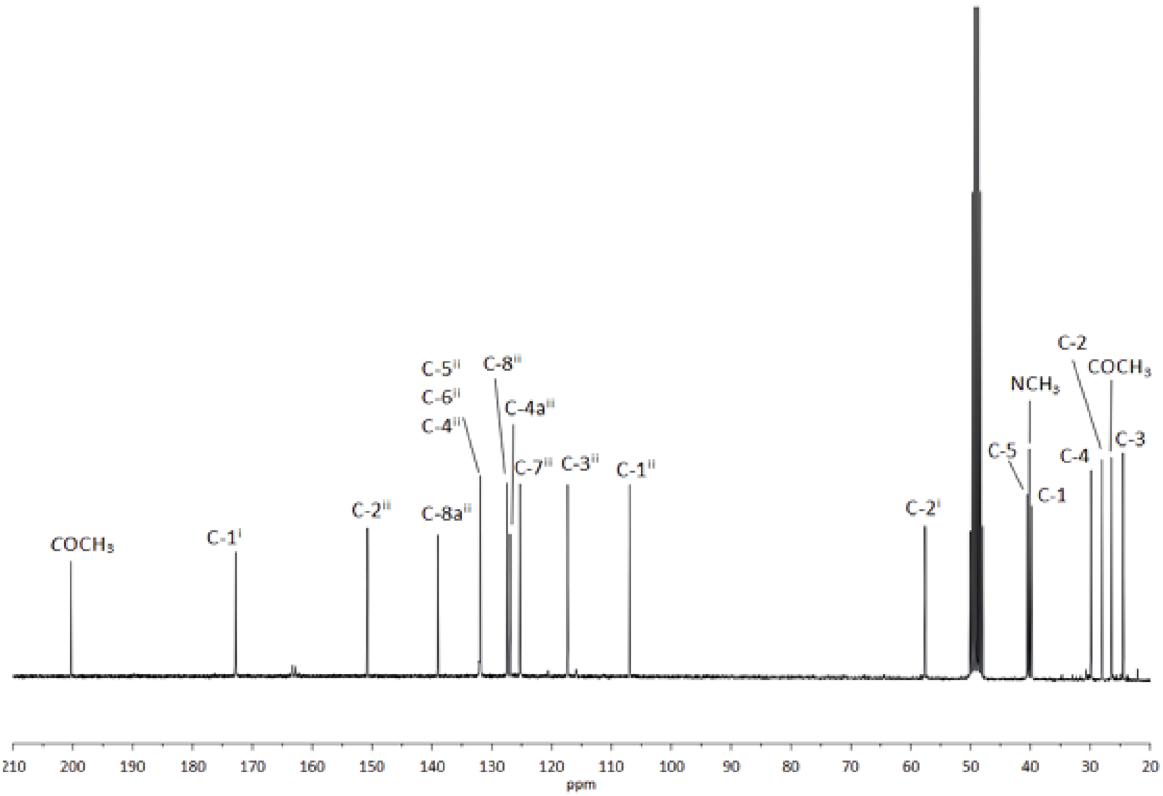

^{13}C-NMR (62.5 MHz, MeOH-d_4)

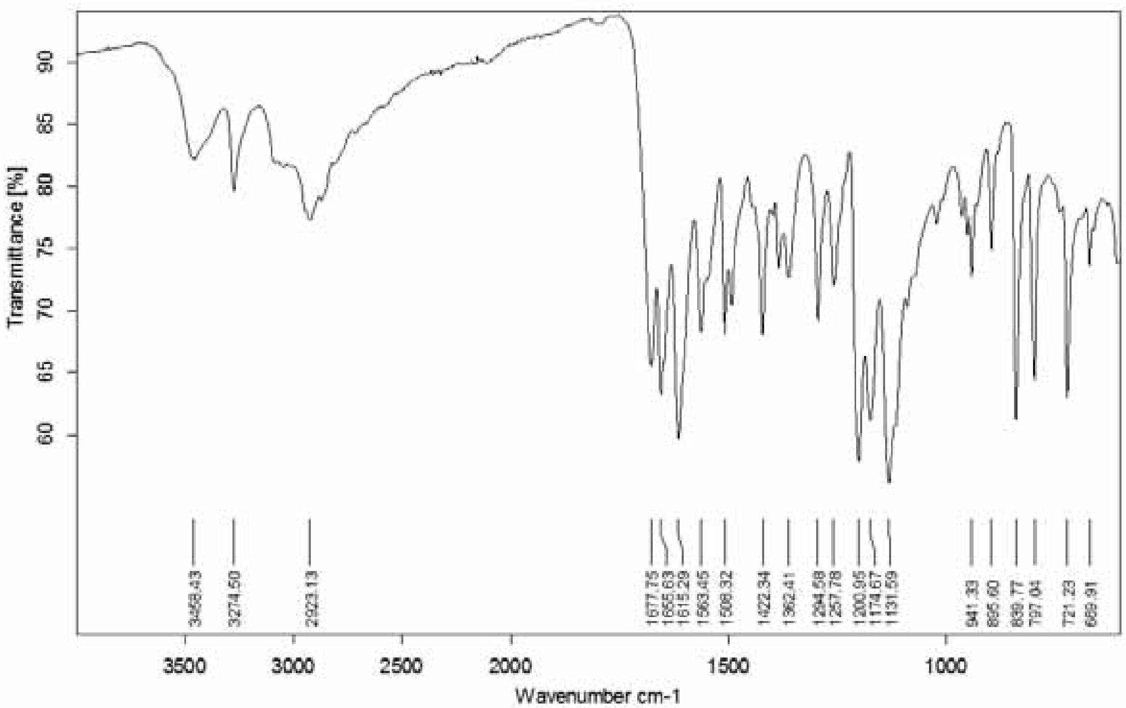

IR (ATR)

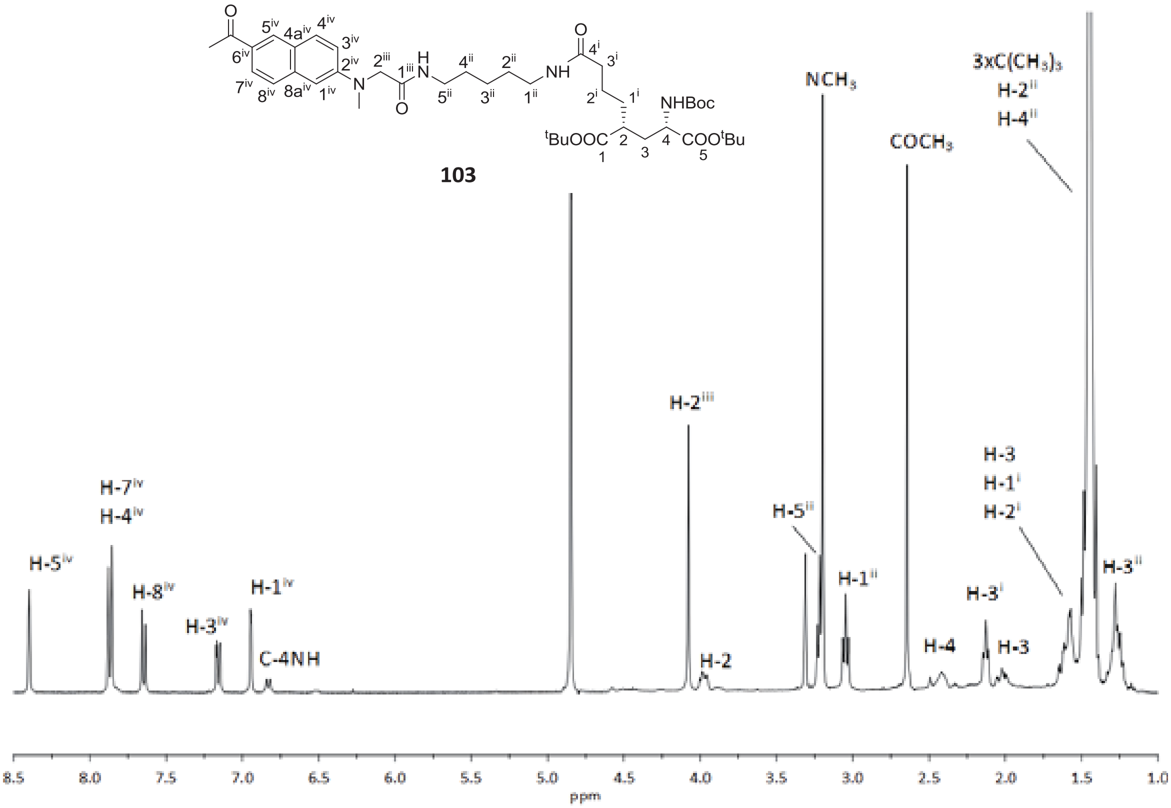

103

^{1}**H-NMR** (400 MHz, MeOH-d_4)

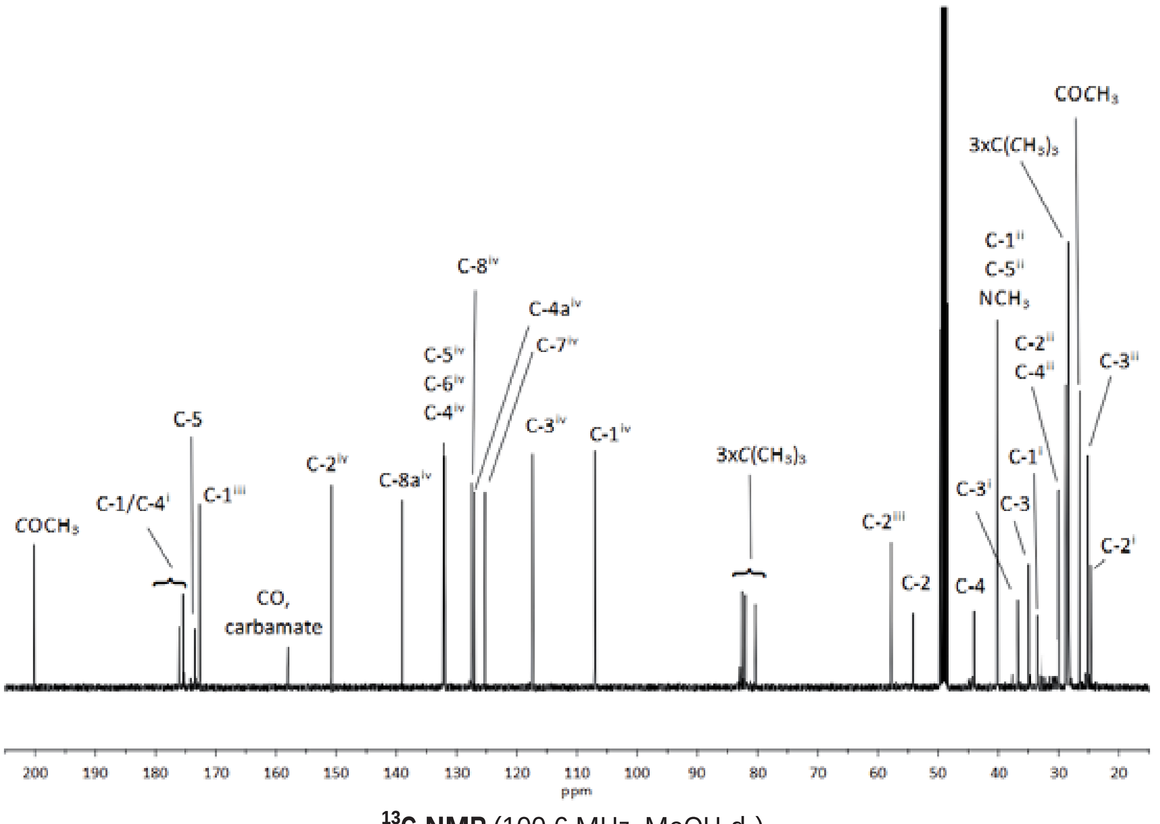

^{13}**C-NMR** (100.6 MHz, MeOH-d_4)

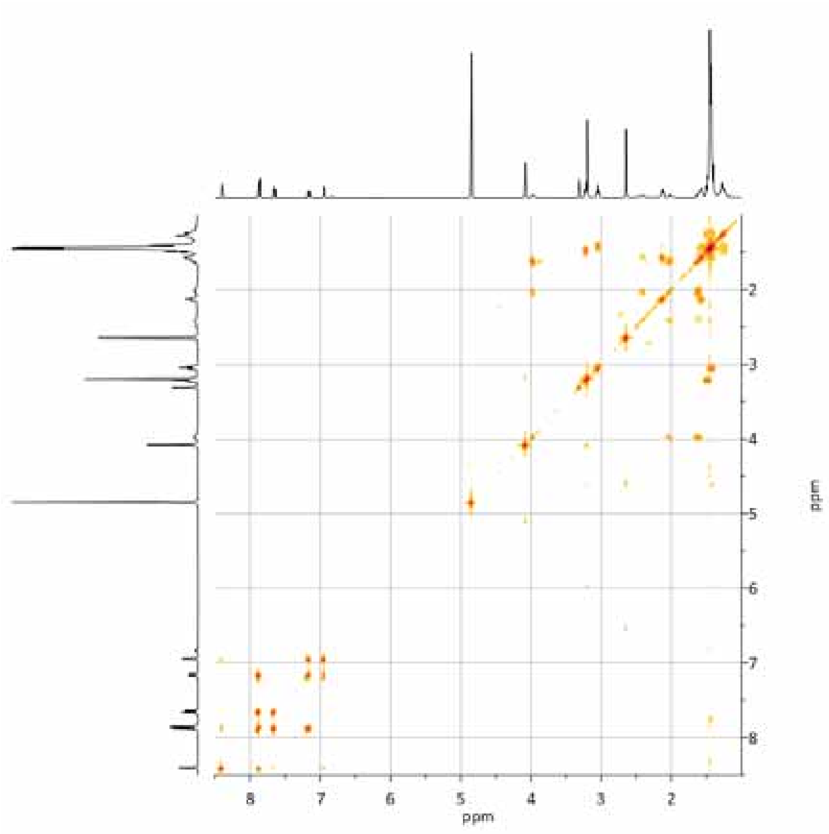

COSY (400 MHz, MeOH-d$_4$)

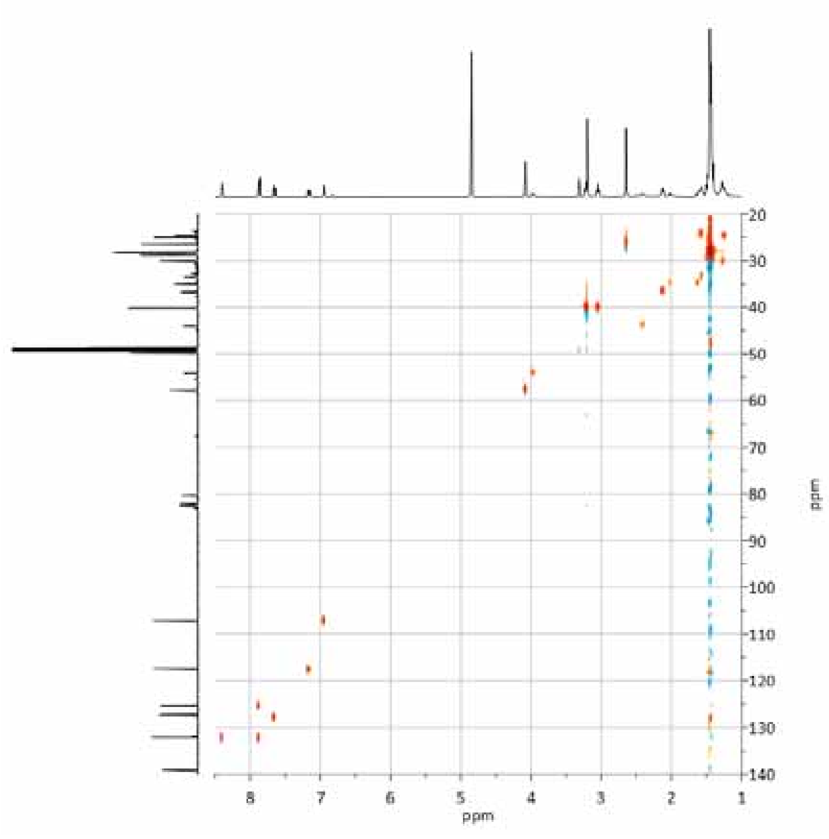

HSQC (400 MHz, MeOH-d$_4$)

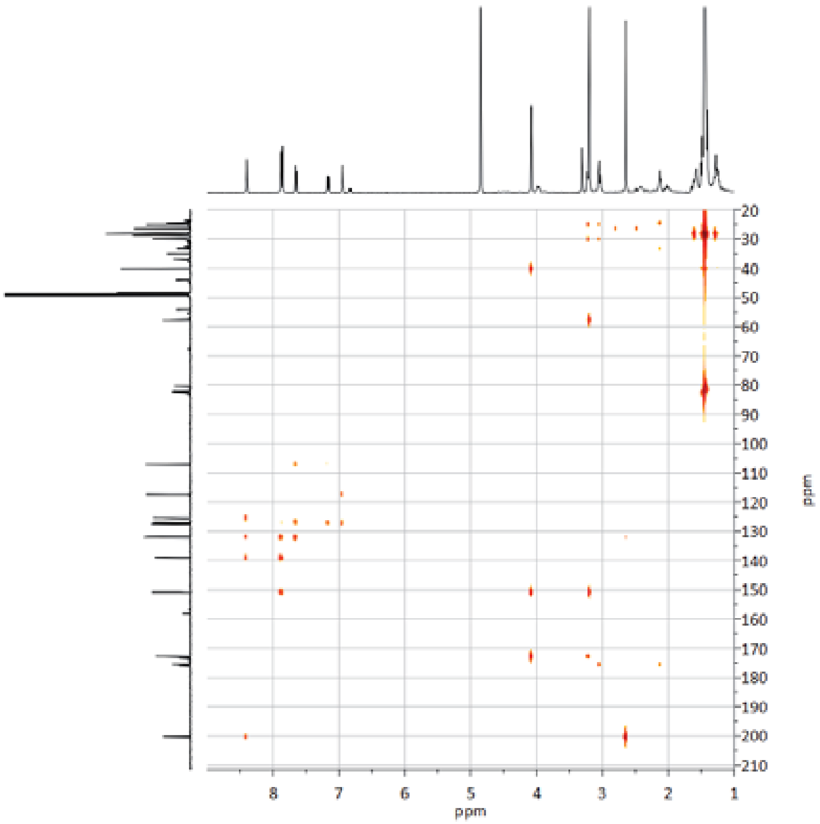

HMBC (400 MHz, MeOH-d_4)

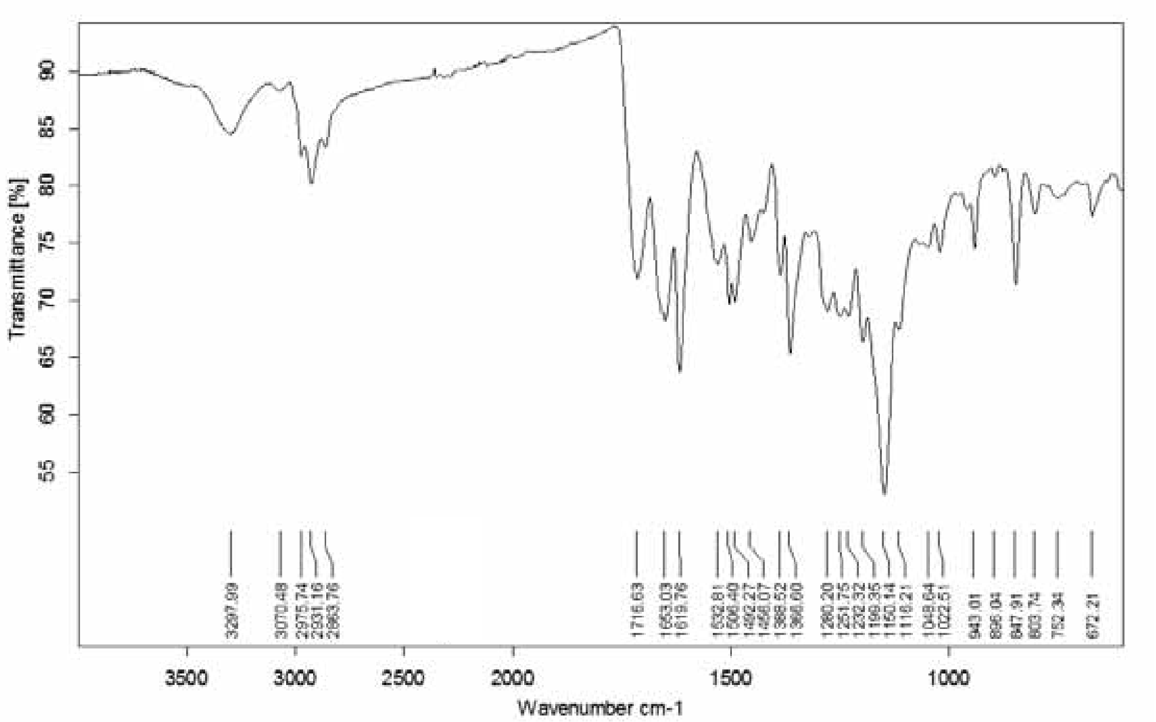

IR (ATR)

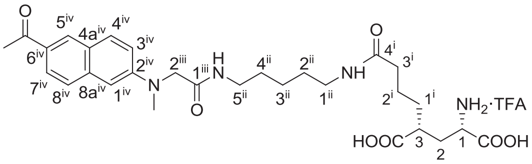

100

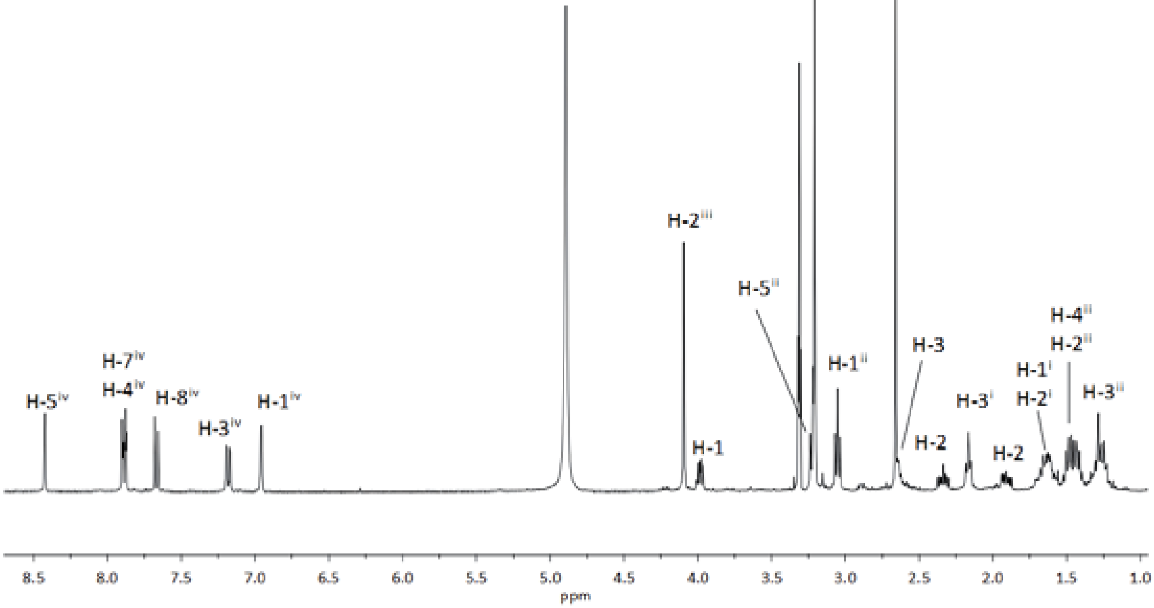

^{1}**H-NMR** (400 MHz, MeOH-d$_4$)

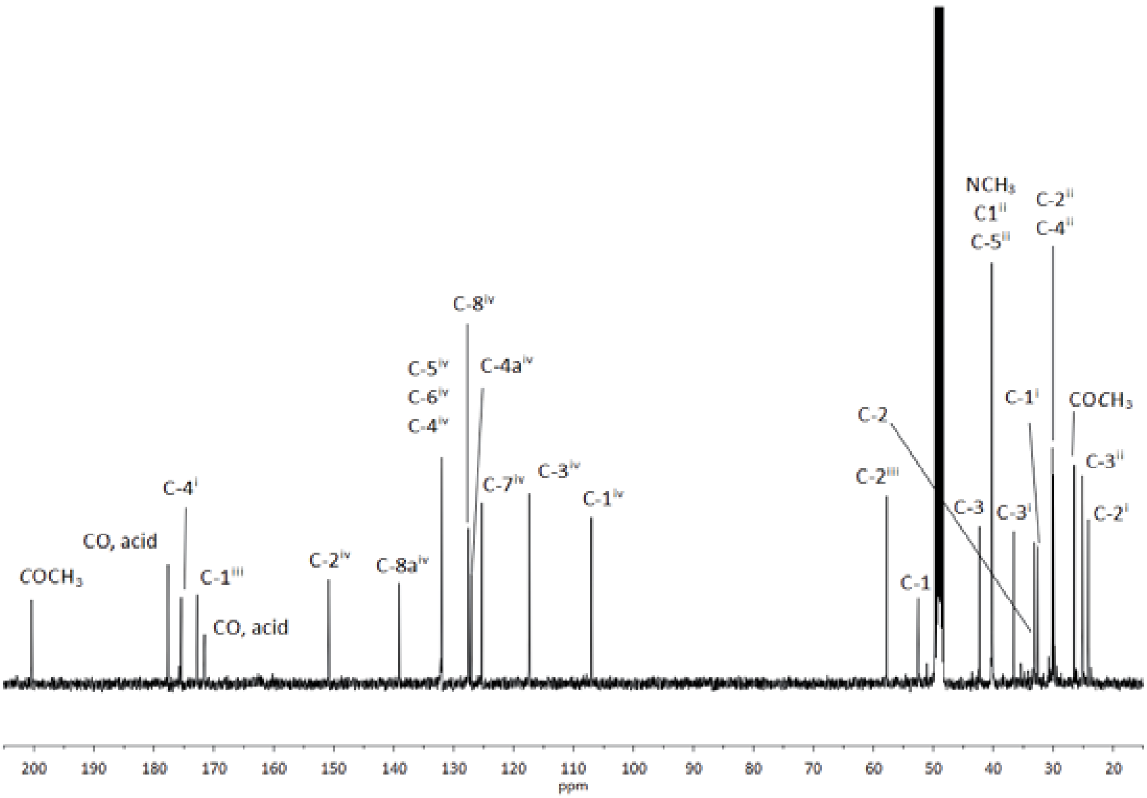

^{13}**C-NMR** (100.6 MHz, MeOH-d$_4$)

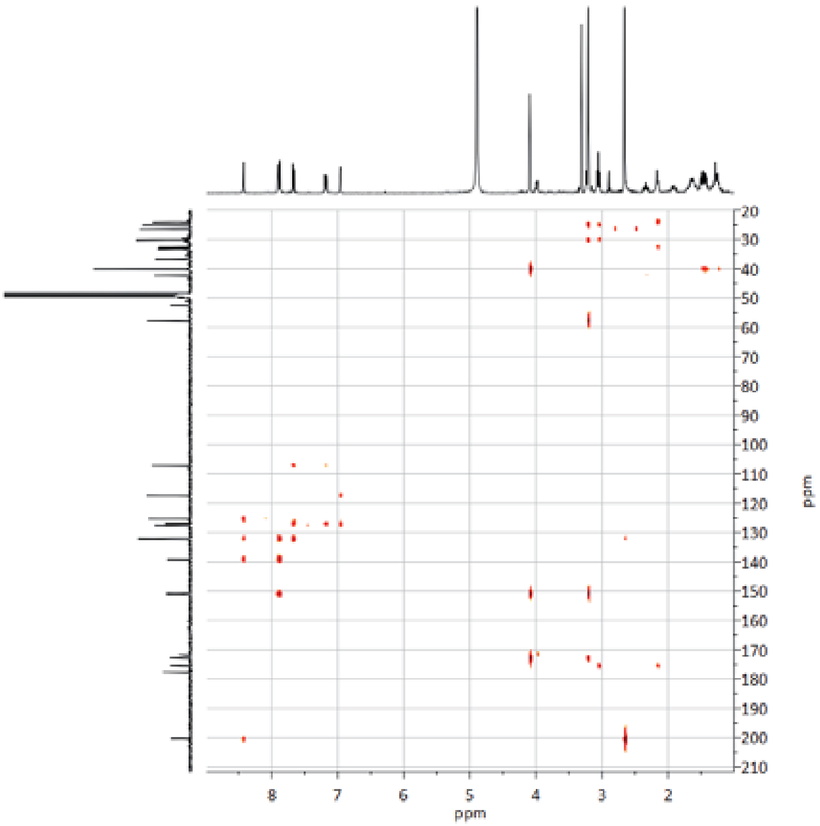

HMBC (400 MHz, MeOH-d_4)

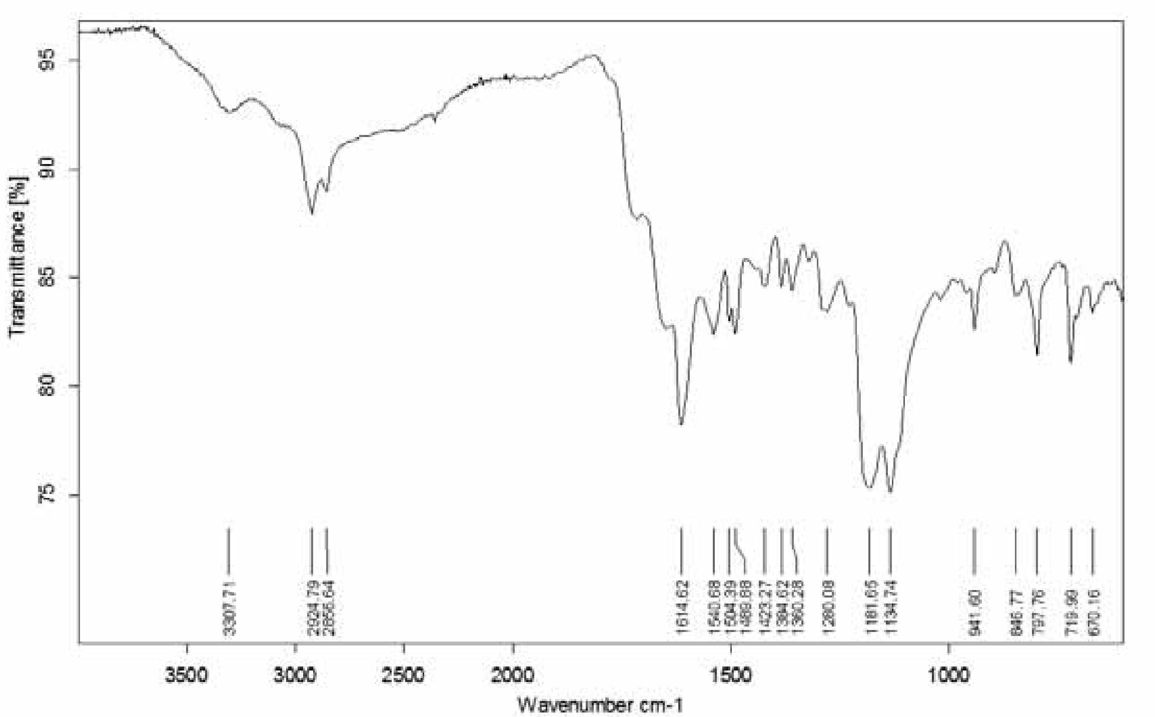

IR (ATR)